EMERGING INFECTIOUS DISEASES®

U.S. CENTERS FOR DISEASE CONTROL AND PREVENTION

Malaria and Other Vectorborne Diseases

April 2026

Andrea Marrapodi, Gregorio Pampinella, and Daniele Tozzi, *Mural portrait of Giovanni Battista Grassi*, 2018. Aerosol paint and pigments on exterior concrete wall. 30 m × 20.8 m. From *Lessons from the Past, Challenges for the Future* (Hall of Fame of Science). National Institute for Infectious Diseases "Lazzaro Spallanzani," Rome, Italy. Reproduced with permission of the artists.

Pages 477–674

EMERGING INFECTIOUS DISEASES

A Peer-Reviewed Journal Tracking and Analyzing Disease Trends

EDITOR IN CHIEF
Matthew J. Kuehnert

ASSOCIATE EDITORS

Charles Ben Beard
Fort Collins, Colorado, USA
Ermias Belay
Atlanta, Georgia, USA
David M. Bell
Atlanta, Georgia, USA
Sharon Bloom
Atlanta, Georgia, USA
Richard S. Bradbury
Townsville, Queensland, Australia
Corrie Brown
Athens, Georgia, USA
Adam Cohen
Atlanta, Georgia, USA
Benjamin J. Cowling
Hong Kong, China
Paul V. Effler
Perth, Western Australia, Australia
Anthony Fiore
Atlanta, Georgia, USA
David O. Freedman
Birmingham, Alabama, USA
Isaac Chun-Hai Fung
Statesboro, Georgia, USA
Shawn Lockhart
Atlanta, Georgia, USA
Alexandre Macedo de Oliveira
Atlanta, Georgia, USA
Nina Marano
Atlanta, Georgia, USA
Martin I. Meltzer
Atlanta, Georgia, USA
J. Glenn Morris, Jr.
Gainesville, Florida, USA
Patrice Nordmann
Fribourg, Switzerland
W. Clyde Partin, Jr.
Atlanta, Georgia, USA
Johann D.D. Pitout
Calgary, Alberta, Canada
Ann Powers
Fort Collins, Colorado, USA
Pierre E. Rollin
Atlanta, Georgia, USA
Frederic E. Shaw
Atlanta, Georgia, USA
David E. Swayne
Athens, Georgia, USA
Neil M. Vora
New York, New York, USA
David H. Walker
Galveston, Texas, USA
J. Scott Weese
Guelph, Ontario, Canada

Books and Other Media Editor
Nkuchia M. M'ikanatha
Harrisburg, Pennsylvania, USA

*Associate Editors are also members of our Editorial Board.

EDITORIAL BOARD

Sridhar Basavaraju
Atlanta, Georgia, USA
Barry J. Beaty
Fort Collins, Colorado, USA
Isaac Benowitz
Augusta, Maine, USA
Martin J. Blaser
New York, New York, USA
Andrea Boggild
Toronto, Ontario, Canada
Christopher Braden
Atlanta, Georgia, USA
Catherine M. Brown
Jamaica Plain, Massachusetts, USA
Charles H. Calisher
Fort Collins, Colorado, USA
Arturo Casadevall
New York, New York, USA
Kenneth G. Castro
Atlanta, Georgia, USA
Gerardo Chowell
Atlanta, Georgia, USA
Michel Drancourt
Marseille, France
Jan Felix Drexler
Berlin, Germany
Christian Drosten
Berlin, Germany
Clare A. Dykewicz
Atlanta, Georgia, USA
Kathleen Gensheimer
Phippsburg, Maine, USA
Rachel Gorwitz
Atlanta, Georgia, USA
Patricia M. Griffin
Decatur, Georgia, USA
Duane J. Gubler
Singapore
David L. Heymann
London, UK
Barbara Javor
San Diego, California, USA
Keith Klugman
Seattle, Washington, USA
Ajit P. Limaye
Seattle, Washington, USA
John S. Mackenzie
Perth, Western Australia, Australia
Joel Montgomery
Lilburn, Georgia, USA
David Morens
Bethesda, Maryland, USA
Frederick A. Murphy
Bethesda, Maryland, USA
Kristy O. Murray
Atlanta, Georgia, USA
Norbert Nowotny
Vienna, Austria, and Dubai, United Arab Emirates
Stephen M. Ostroff
Silver Spring, Maryland, USA
Christopher D. Paddock
Atlanta, Georgia, USA
John Papp
Atlanta, Georgia, USA
David A. Pegues
Philadelphia, Pennsylvania, USA
Philip M. Polgreen
Iowa City, Iowa, USA
Mario Raviglione
Milan, Italy, and Geneva, Switzerland
David Relman
Palo Alto, California, USA
Sarah G. H. Sapp
Atlanta, Georgia, USA
David Safronetz
Winnipeg, Manitoba, Canada
William Schaffner
Nashville, Tennessee, USA
Tom Schwan
Hamilton, Montana, USA
Wun-Ju Shieh
Taipei, Taiwan
Rosemary Soave
New York, New York, USA
Kathrine R. Tan
Atlanta, Georgia, USA
Phillip Tarr
St. Louis, Missouri, USA
Kenneth L. Tyler
Aurora, Colorado, USA

Editor in Chief Emeritus
D. Peter Drotman, Atlanta, Georgia, USA

Managing Editor Emeritus
Byron Breedlove, Atlanta, Georgia, USA

Founding Editor in Chief
Joseph E. McDade, Rome, Georgia, USA

STAFF

Managing Editor
Lesli Mitchell, Atlanta, Georgia, USA

Technical Writer-Editors
Shannon O'Connor, Team Lead; Dana Dolan, Amy J. Guinn, Jill Russell, Jude Rutledge, Cheryl Salerno, Bryce Simons

Production, Graphics, and Information Technology Staff
Reginald Tucker, Team Lead; William Hale, Tae Kim, Barbara Segal

Communications/Social Media
Candice Hoffmann, Team Lead; Patricia A. Carrington-Adkins, Heidi Floyd Argumedo

Journal Administrators
J. McLean Boggess, Claudia Johnson

Editorial Assistant
Nell Stultz

Peer Review Coordinator
Sasha Ruiz

Emerging Infectious Diseases is published monthly by the Centers for Disease Control and Prevention, 1600 Clifton Rd NE, Mailstop H16-2, Atlanta, GA 30329-4018, USA. Telephone 404-639-1960; email eideditor@cdc.gov

The conclusions, findings, and opinions expressed by authors contributing to this journal do not necessarily reflect the official position of the U.S. Department of Health and Human Services, the Public Health Service, the Centers for Disease Control and Prevention, or the authors' affiliated institutions. Use of trade names is for identification only and does not imply endorsement by any of the groups named above. All material published in *Emerging Infectious Diseases* is in the public domain and may be used and reprinted without special permission; proper citation, however, is required.
Use of trade names is for identification only and does not imply endorsement by the Public Health Service or by the U.S. Department of Health and Human Services.

EMERGING INFECTIOUS DISEASES is a registered service mark of the U.S. Department of Health and Human Services (HHS).

EMERGING INFECTIOUS DISEASES®

Malaria and Other Vectorborne Diseases **April 2026**

On the Cover

Andrea Marrapodi, Gregorio Pampinella, and Daniele Tozzi, *Mural portrait of Giovanni Battista Grassi, 2018.* Aerosol paint and pigments on exterior concrete wall. From Lessons from the Past, Challenges for the Future (Hall of Fame of Science). National Institute for Infectious Diseases "Lazzaro Spallanzani," Rome, Italy. Reproduced with permission of the artists.

About the Cover p. 669

Synopses

Medscape EDUCATION ACTIVITY

Research

EMERGING INFECTIOUS DISEASES®
April 2026

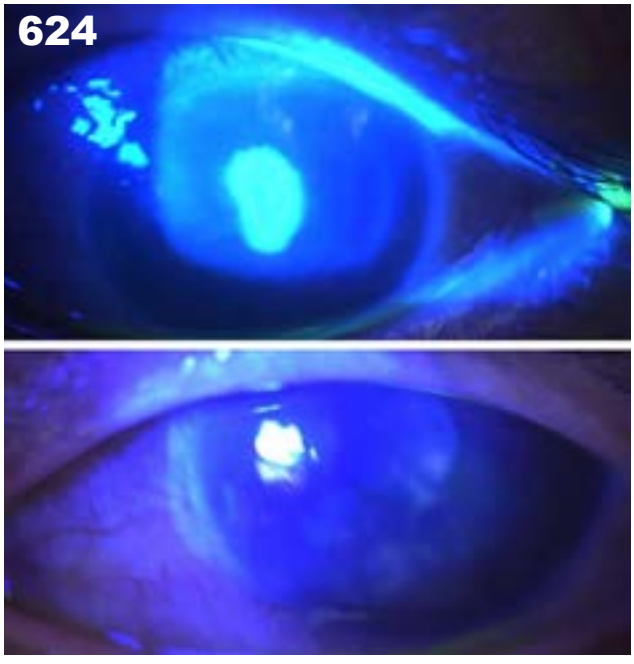

Dispatches

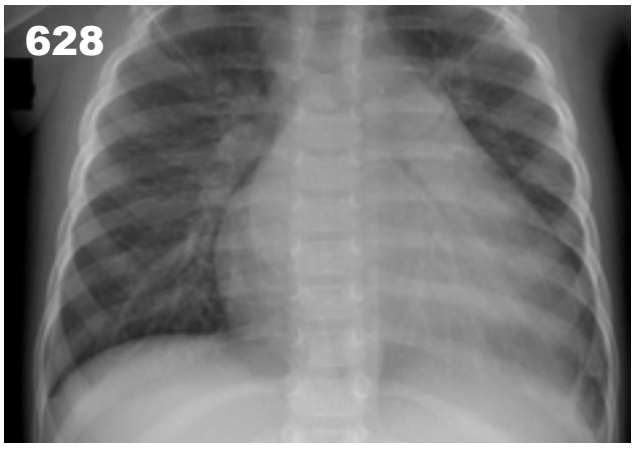

EMERGING INFECTIOUS DISEASES®
April 2026

Another Dimension

Research Letters

Photo Quiz

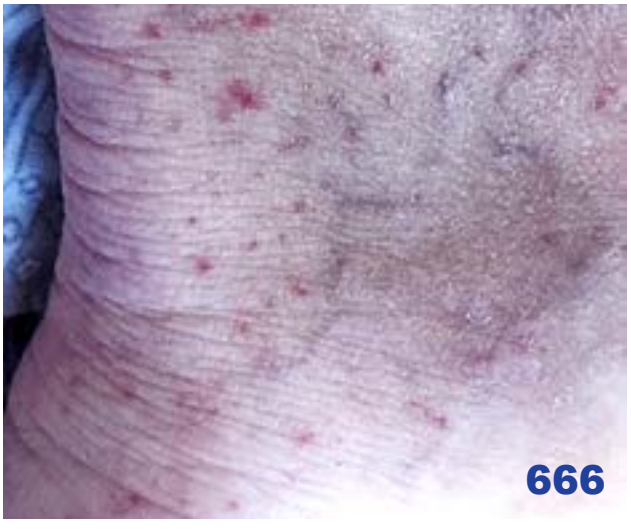

About the Cover

Etymologia

Correction

Vol.31 No.4

Some of the summary data included in Appendix 2 was incorrect in Foodborne Illness Acquired in the United States—Major Pathogens, 2019

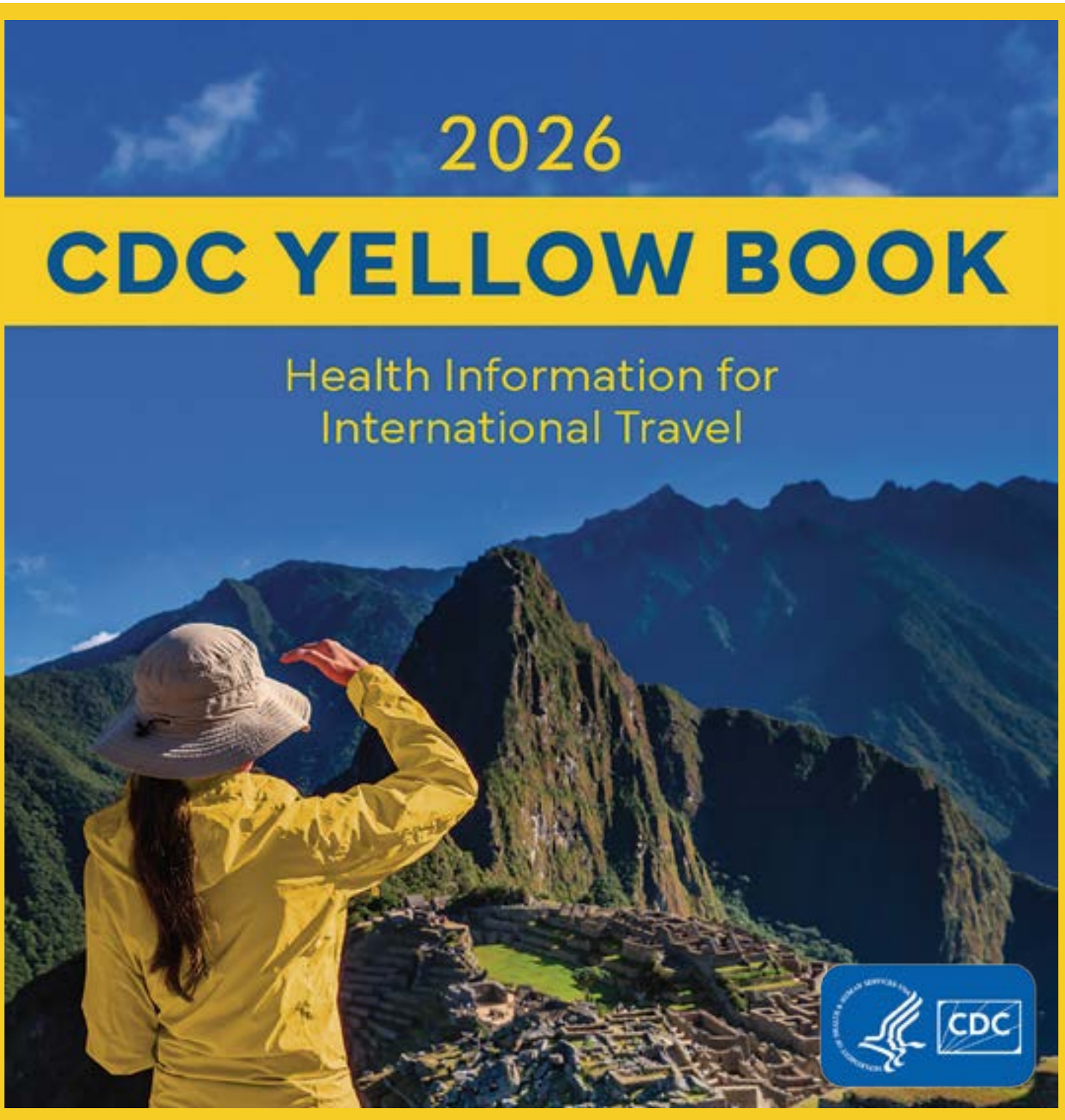

Launch of CDC Yellow Book 2026– A Trusted Travel Medicine Resource

CDC is pleased to announce the launch of the **CDC Yellow Book 2026**. The CDC Yellow Book is a resource containing the U.S. government's travel medicine recommendations and has been trusted by the travel medicine community for over 50 years. Healthcare professionals can use the print and digital versions to find the most up-to-date travel medicine information to better serve their patients' healthcare needs.

The CDC Yellow Book is available online now at www.cdc.gov/yellowbook and in print starting in June 2025 through Oxford University Press and other major online booksellers.

Pediatric Meningoencephalitis Cluster Caused by Snowshoe Hare Virus, Whistler, British Columbia, Canada, 2024

Faisal Ali, Miguel Imperial, Muhammad Morshed, David M. Goldfarb, Jonathan B. Gubbay, Catherine A. Hogan, Rohit Vijh, Ellie N. Andres, Marta Jaeckel, Jaskiran Sajan, Heidi Wood, Alyssia Robinson, Jennifer Tam

In support of improving patient care, this activity has been planned and implemented by Medscape, LLC and Emerging Infectious Diseases. Medscape, LLC is jointly accredited with commendation by the Accreditation Council for Continuing Medical Education (ACCME), the Accreditation Council for Pharmacy Education (ACPE), and the American Nurses Credentialing Center (ANCC), to provide continuing education for the healthcare team.

Medscape, LLC designates this Journal-based CME activity for a maximum of 1.00 ***AMA PRA Category 1 Credit(s)™***. Physicians should claim only the credit commensurate with the extent of their participation in the activity.

Successful completion of this CME activity, which includes participation in the evaluation component, enables the participant to earn up to 1.0 MOC points in the American Board of Internal Medicine's (ABIM) Maintenance of Certification (MOC) program. Participants will earn MOC points equivalent to the amount of CME credits claimed for the activity. It is the CME activity provider's responsibility to submit participant completion information to ACCME for the purpose of granting ABIM MOC credit.

All other clinicians completing this activity will be issued a certificate of participation. To participate in this journal CME activity: (1) review the learning objectives and author disclosures; (2) study the education content; (3) take the post-test with a 75% minimum passing score and complete the evaluation at https://www.medscape.org/qna/processor/77072?showStandAlone=true&isAspenArticle=true; and (4) view/print certificate. For CME questions, see page 672.

NOTE: It is the policy of Medscape Education to avoid the mention of brand names or specific manufacturers in accredited educational activities. However, trade and manufacturer names in this activity are provided in an effort to provide clarity. The use of brand or manufacturer names should not be viewed as an endorsement by Medscape of any specific product or manufacturer.

Release date: April 10, 2026; Expiration date: April 10, 2027

Learning Objectives

Upon completion of this activity, participants will be able to:

- Describe the clinical presentation of snowshoe hare virus (SSHV) infection
- Assess the laboratory analysis for SSHV infection
- Analyze outcomes of SSHV meningoencephalitis among patients in the current study
- Identify cerebrospinal fluid findings associated with SSHV meningoencephalitis

CME Editor

Amy J. Guinn, BA, MA, Technical Writer/Editor, Emerging Infectious Diseases. *Disclosure: Amy J. Guinn, BA, MA, has no relevant financial relationships.*

CME Author

Charles P. Vega, MD, Health Sciences Clinical Professor of Family Medicine, University of California, Irvine School of Medicine, Irvine, California. *Disclosure: Charles P. Vega, MD, has the following relevant financial relationships: served as consultant or advisor for: Boehringer Ingelheim; Exact Sciences; GlaxoSmithKline.*

Authors

Faisal Ali, MBChB; Miguel Imperial, MD, MHSc; Muhammad Morshed, PhD; David M. Goldfarb, MD; Jonathan B. Gubbay, MBBS, MMedSc; Catherine A. Hogan, MD; Rohit Vijh, MD, MPH; Ellie N. Andres, MPH, CPH; Marta Jaeckel, BSc, BTech, CPHI(C); Jaskiran Sajan, BTech, CPHI(C); Heidi Wood, PhD; Alyssia Robinson; Jennifer Tam, BSc(Pharm), MD, MHPE.

Snowshoe hare virus (SSHV) is an arbovirus in the California serogroup known to circulate throughout Canada and northern latitudes of the United States. The clinical spectrum of SSHV infection ranges from asymptomatic or mild febrile illness to neuroinvasive disease; neuroinvasive disease occurs more often in children and young adults. We describe a cluster of confirmed and probable SSHV meningoencephalitis cases in 3 children from Whistler, British Columbia, Canada, in the summer of 2024. We highlight the shared epidemiology, clinical manifestations, serologic diagnostic methods, and outcomes for the cases. All 3 children acquired the infection locally and made a full recovery. This case series suggests underrecognized SSHV infection prevalence that warrants enhanced surveillance and review of existing diagnostic algorithms. California serogroup viruses, including SSHV, should be recognized as a potential cause of neuroinvasive disease in North America during mosquito season, particularly when initial diagnostic testing is inconclusive.

Snowshoe hare virus (SSHV) is an arthropodborne California serogroup virus (CSGV) of the genus *Orthobunyavirus* (*1*,*2*). SSHV was first isolated from a snowshoe hare (*Lepus americanus*) in Montana, USA, in 1958 and is primarily found across Canada and the northern latitudes of the United States (*2*). The virus is maintained in an enzootic cycle between small mammals, particularly snowshoe hares but also rabbits (*Oryctolagus* and *Sylvilagus* spp.), squirrels (*Sciurus* spp.), chipmunks (*Tamias* and *Neotamias* spp.), and other rodents, and mosquito vectors, primarily *Aedes* and *Culiseta* spp. mosquitoes (*1*,*2*). SSHV transmission typically occurs during mosquito season (May–September in North America) through blood meal bites (*3*), and the incubation period is ≈3–7 days (*2*).

Most SSHV infections in humans are asymptomatic or cause mild illness, but the virus can lead to severe neuroinvasive disease, especially in children and young adults. Symptoms of SSHV infection can range from febrile illness to meningoencephalitis (*2*). Despite its potential for high rates of illness, SSHV infections are likely underdiagnosed and underreported.

SSHV infection diagnosis is challenging because clinical manifestations are nonspecific and often mimic those of other viral infections. The National Microbiology Laboratory in Canada offers molecular and serologic testing for SSHV and Jamestown Canyon virus (JCV), the 2 most common CSGVs that are known to circulate in Canada. Although reverse transcription PCR (RT-PCR) can differentiate between the CSGVs, it has lower sensitivity because of the low and transient viremia in immunocompetent persons, particularly at the stage of illness when they tend to be hospitalized. Serology is more sensitive, but IgM to CSGVs like SSHV and JCV cross-react when tested by ELISA. Most case definitions for a confirmed case of CSGV incorporate the comparison of acute and convalescent serum neutralizing antibody titers by a plaque reduction neutralizing assay (PRNT), generally requiring a change of ≥4-fold (*2*,*4*–*6*). We describe a cluster of 3 pediatric meningoencephalitis cases caused by SSHV infection in Whistler, British Columbia, Canada, during July–August 2024.

Cases

In summer 2024, three pediatric patients were admitted to British Columbia's pediatric tertiary hospital with cerebrospinal fluid (CSF) culture-negative meningoencephalitis. The 3 patients had similar clinical manifestations, lived in the same geographic area (Whistler, BC, Canada), had symptom onset dates within 1 week of each other (Figure), and had negative initial testing on first-tier and targeted infectious diseases workups.

When the treating clinicians recognized an epidemiologic link among the 3 cases, they alerted public health and expanded the diagnostic approach after patients clinically improved and were discharged. We obtained written consent to describe cases from all 3 patients' guardians.

Case 1

In late July 2024, a 12-year-old girl with no underlying conditions was seen in the emergency department with a 3-day history of severe, bilateral, pulsatile headache and associated photophobia and phonophobia and a 1-day history of abdominal pain and emesis. She was presumed to have a migraine and discharged home with regular analgesia.

The next day, day 5 after symptom onset, she arrived at the British Columbia Children's Hospital (BCCH) emergency department with worsening headaches waking her from sleep. She was afebrile and had an unremarkable neurologic examination

Author affiliations: University of British Columbia, Vancouver, British Columbia, Canada (F. Ali, M. Imperial, M. Morshed, D.M. Goldfarb, J.B. Gubbay, C.A. Hogan, R. Vijh, J. Tam); Children's & Women's Health Centre of British Columbia, Vancouver (F. Ali, M. Imperial, D.M. Goldfarb, J.B. Gubbay, J. Tam); British Columbia Centre for Disease Control, Vancouver (M. Morshed, C.A. Hogan); Vancouver Coastal Health Public Health Surveillance Unit, Vancouver (R. Vijh, E.N. Andres, M. Jaeckel, J. Sajan); National Microbiology Laboratory, Public Health Agency of Canada, Winnipeg, Manitoba, Canada (H. Wood, A. Robinson)

DOI: https://doi.org/10.3201/eid3204.251392

with no focal neurologic deficits, but her headache intensified throughout the day, and she was admitted to the hospital for further management.

Head computed tomography (CT) without contrast, CT venogram, and brain magnetic resonance imaging (MRI) were performed to assess for space-occupying lesions or sinus venous thrombosis. Results from those scans were unremarkable. On day 6 after symptom onset, clinicians performed a lumbar puncture (LP), which revealed an elevated opening pressure at 33.4 cm H_2O (reference range 11.5–25 cm H_2O). During LP, clinicians also collected a cerebrospinal fluid (CSF) sample. CSF analysis revealed an elevated nucleated cell count (NCC) of 250 × 10^6 cells/L (reference range ≤10 × 10^6 cells/L) (Table). She was treated empirically with ceftriaxone, vancomycin, and acyclovir after the LP.

CSF and blood cultures were negative, as was a BioFire Meningitis/Encephalitis CSF Panel (bioMérieux, https://www.biomerieux.com). CSF nucleic acid amplification test (NAAT) for Epstein-Barr virus (EBV) was also negative. Serologic tests for *Treponema pallidum*, Lyme disease, *Bartonella henselae*, *Toxoplasma gondii*, and West Nile virus (WNV) were nonreactive. EBV serology was IgM reactive but IgG nonreactive. Acyclovir and vancomycin were subsequently discontinued after 48 hours.

The patient continued to show clinical improvement and was discharged home after completing a 10-day course of ceftriaxone for culture-negative meningitis. On the day of discharge, she was doing well with only mild residual headaches. Repeat serology 6 weeks after initial serology was nonreactive for EBV IgM and IgG, suggesting a false-positive initial IgM result.

We performed retrospective testing for CSGV, and those results were most consistent with SSHV infection on the basis of higher SSHV than JCV neutralizing antibody titers, although not a ≥4-fold increase in titers (Table). The result of RT-PCR for CSGV was negative on serum collected on day 8 after symptom onset, but insufficient residual CSF was available to perform further CSGV RT-PCR. Those serology findings supported a diagnosis of probable SSHV meningoencephalitis. The patient was seen for follow-up 3 months after discharge, and her symptoms continued to improve.

Case 2

In early August 2024, a 3-year-old girl with history of strabismus and mild hypoxic ischemic encephalopathy with a single focal seizure 1 year earlier was admitted to the emergency department with 3 hemiclonic focal seizures and subsequent Todd's paresis after a 4-day history of fever and decreased energy. She was treated with seizure medications and transferred to BCCH for further management.

At admission to BCCH, she was empirically treated with acyclovir. Two EEGs had abnormal findings; the first noted a focal electroclinical seizure with onset from the right posterior quadrant corresponding with left hand twitching, and the second showed posterior quadrant slowing. She defervesced by day 3 of admission and had 1 additional seizure on day 7 of hospitalization. Over the next few days, her parents reported that she was having visual hallucinations, such as seeing rainbows and seeing the room filled with water, as well as balance and speech difficulties.

Clinicians performed an LP on day 11 after symptom onset, and CSF analysis revealed a slightly elevated NCC at 12 × 10^6 cells/L (Table). An MRI of the brain showed abnormal signal in the right perirolandic cortex, right insular cortex, and bilateral thalami, with scattered areas of sulcal

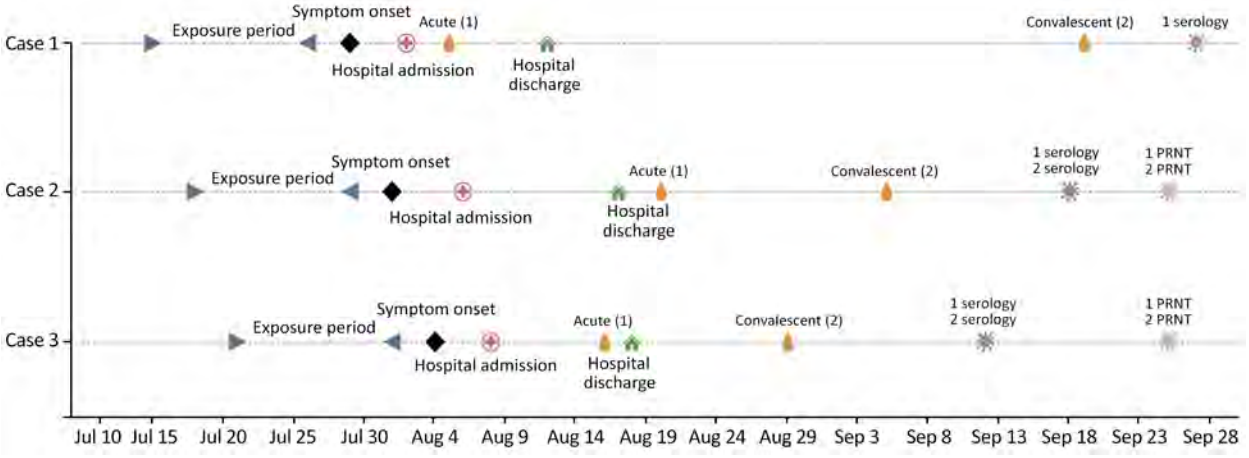

Figure. Chronological timeline of pediatric meningoencephalitis cases caused by snowshoe hare virus, Whistler, British Columbia, Canada, 2024. PRNT, plaque reduction neutralization test.

Table. Clinical and demographic characteristics of patients in cluster of pediatric meningoencephalitis cases caused by snowshoe hare virus, Whistler, British Columbia, Canada, 2024*

Characteristics	Case 1	Case 2	Case 3
Patient age, y/sex	12/F	3/F	2/M
Clinical manifestations	5-d history of headaches, neck stiffness, photophobia, and emesis; afebrile	4-d history of fever and decreased energy; multiple hemiclonic focal seizures and subsequent Todd's paresis on day 4 of illness	5-d history of fever, lethargy, and vomiting; bradycardia at admission
Medical history	No underlying conditions	History of mild hypoxic ischemic encephalopathy and previous seizure	Premature birth at 29 weeks' gestation
Acute CSGV serology	8 d after symptom onset	5 d after symptom onset	13 d after symptom onset
IgM immunoassay			
SSHV	Reactive	Reactive	Reactive
JCV	Reactive	Nonreactive	Reactive
PRNT			
SSHV	1:1,280	1:80	1:2,560
JCV	1:640	1:40	1:640
Convalescent CSGV serology	6 wks after acute serology	4 wks after acute serology	2 wks after acute serology
IgM immunoassay			
SSHV	Reactive	Reactive	Reactive
JCV	Reactive	Reactive	Reactive
PRNT			
SSHV	1:640	1:2,560	1:1,280
JCV	1:320	1:640	1:640
CSF testing†	6 d after symptom onset	11 d after symptom onset	6 d after symptom onset
NCC, × 10^6 cells/L (% lymphocytes)	250 (74)	12 (74)	112 (38); 51% neutrophils‡
Glucose, mmol/L	4.0	3.0	3.6
Protein, g/L	0.66	0.31	0.36
Head and brain imaging			
CT	Unremarkable	ND	Unremarkable
MRI	Unremarkable	Abnormal signal in the right perirolandic cortex, right insular cortex and bilateral thalami, with scattered areas of sulcal enhancement	ND

*CSF, cerebrospinal fluid; CSGV, California serogroup virus; CT, computed tomography; JCF, Jamestown Canyon virus; MRI, magnetic resonance imaging; NCC, nucleated cell count; ND, not done; PRNT, plaque reduction neutralization test; SSHV, snowshoe hare virus.
†Reference ranges: NCC ≤10 × 10^6 cells/L; glucose 2.8–4.4 mmol/L; protein 0.14–0.42 g/L.
‡Reference <6%.

enhancement. Results of CSF and blood cultures were negative. Results of BioFire Meningitis/Encephalitis CSF Panel performed on CSF samples and BioFire Respiratory 2.1 Panel (both bioMérieux) performed on nasopharyngeal swab samples were both negative. CSF 16S rRNA gene PCR result was also negative. Serologic tests for Lyme disease, cytomegalovirus, EBV, *Toxoplasma gondii*, *Bartonella henselae*, WNV, *Leptospira* spp., and *Rickettsia rickettsii* were nonreactive. Results of herpes simplex virus PCR of CSF samples, cryptococcal antigen tests of CSF and serum samples, and *Leptospira* blood and urine NAAT tests were also negative.

Acyclovir was subsequently discontinued after the negative herpes virus PCR. The patient remained hospitalized for 12 days and was subsequently discharged to home with regular seizure medications after clinical improvement but with lingering balance and speech issues. The patient was seen for follow-up 3 months after discharge with a resolution of symptoms and no further seizures.

We performed retrospective testing for CSGV using acute and convalescent serologies, which demonstrated a 32-fold rise in SSHV PRNT titers (Table), meeting the criteria for SSHV infection. RT-PCR for CSGV was negative on serum collected on day 5 of symptoms. Insufficient residual CSF was available to perform CSGV RT-PCR testing.

Case 3

In August 2024, a 2-year-old boy with a history of premature birth at 29 weeks' gestation was taken to his local emergency department with a 5-day history of fever, lethargy, and vomiting. On examination, he was febrile, lethargic, and bradycardic. Clinicians administered an intravenous fluid bolus, obtained blood cultures, and treated him empirically with ceftriaxone and acyclovir, then transferred him to BCCH for further management.

A CT head scan at BCCH showed unremarkable results, and an LP on day 6 of symptom onset demonstrated an elevated NCC of 112 × 10^6 cells/L (Table).

Cultures of blood and CSF were negative. BioFire Meningitis/Encephalitis CSF Panel performed on CSF samples, BioFire Respiratory 2.1 Panel performed on nasopharyngeal swab samples, and BioFire Gastrointestinal Panel of stool samples (all bioMérieux) all had negative results. Serum cryptococcal antigen, *Leptospira* blood and urine NAAT, WNV serology, and *Rickettsia rickettsii* serologic test were negative. CSF 16S rRNA gene PCR result was also negative. An ECG and an echocardiogram showed borderline corrected QT prolongation and no abnormalities in cardiac anatomy.

The patient returned to his baseline and was defervescent by day 3 of admission. Acyclovir was discontinued within 48 hours, and he completed a 10-day course of ceftriaxone for culture-negative meningitis before he was discharged home. The patient was seen for follow-up 3 months later and was doing well.

We performed retrospective testing for CSGV using acute and convalescent serologies (Table). Those findings were most consistent with SSHV infection given the higher SSHV neutralizing antibody titers compared with JCV. Although we observed only a 2-fold change in SSHV titers between the acute and convalescent samples, that result could be because the acute CSGV serology was obtained 13 days after symptom onset. Furthermore, JCV titers did not change between acute and convalescent phases. Insufficient residual CSF samples were available to perform CSGV RT-PCR.

Public Health Investigation

Informed of the 3 cases, public health authorities launched a public health investigation. Whistler is a mountain resort municipality in British Columbia, known for extensive year-round outdoor activities, and has millions of visitors annually. All 3 case-patients spent time outdoors and were frequently exposed to wooded areas during hikes, camping activities, and evening outdoor activities. All case-patients had experienced a mosquito bite. Parents reported multiple possible exposure locations, but only 1 neighborhood in Whistler was common to all 3 cases during the exposure windows. That information supported targeted vector surveillance during the subsequent mosquito season.

In response to the cluster, regional public health released an update asking clinicians to report cases of encephalitis for which no pathogen was identified and that occurred during the 2024 mosquito season. That update resulted in identification of an additional adult case in a person who also resided in Whistler and initially had autoimmune encephalitis diagnosed. A residual banked CSF sample and acute serum sample and a convalescent serum sample collected in collaboration with the patient's physician confirmed SSHV infection. That patient's treatment for the presumed autoimmune encephalitis was discontinued.

Furthermore, regional public health initiated an epidemiologic and environmental investigation during the 2025 mosquito season. That investigation included a small-scale mosquito surveillance pilot project in the same area to characterize local mosquito species and test them for potential pathogens like SSHV (*7*).

Discussion

We describe a cluster of 3 cases of confirmed and probable pediatric SSHV meningoencephalitis from Whistler, British Columbia, Canada, during July–August 2024. All 3 cases had serologic evidence of recent CSGV infection most consistent with SSHV. All had a median symptom duration of 5 (range 4–5) days before hospital admission. None required intensive care unit admission, and all recovered fully.

A previously reported cluster occurred in Quebec, Canada, in 1978, and involved 2 brothers with SSHV infection (*8*). In our cluster, diagnostic workup for CSGV was initiated only after initial investigations for meningoencephalitis were nondiagnostic and the treating clinicians recognized a possible epidemiologic link between the cases, spurring additional laboratory and public health investigations.

Our case series also highlights the variabilities in signs and symptoms and CSF findings in SSHV disease. Although pediatric viral meningoencephalitis typically includes lymphocytic predominance in CSF and variable protein and glucose levels, our small case series showed some variation. Two patients demonstrated lymphocytic predominance, but 1 had a slight neutrophilic predominance (Table). All 3 had CSF glucose levels within the reference range and protein levels within the reference range or slightly elevated. That variability is consistent with previous case reports of CSGV meningoencephalitis, which have also noted neutrophilic pleocytosis in CSF (*9*). Those results could be related to the timing of CSF sample collection relative to symptom onset because CSF samples obtained early in viral meningoencephalitis can exhibit a neutrophilic predominance.

The 3 cases in this study further highlight the complexity of diagnosing CSGV. None of the patients were positive for CSGV by RT-PCR from serum, reflecting known lower RT-PCR sensitivity. Exhaustive testing for the initial infectious disease workup left no residual CSF samples for retrospective RT-PCR, highlighting the need for an early high index of clinical suspicion.

However, 1 patient met the diagnostic criteria for confirmed CSGV infection on the basis of serologic testing, and the other 2 were probable cases with a strong epidemiologic link (Appendix, https://wwwnc.cdc.gov/EID/article/32/4/25-1392-App1.pdf).

Using paired serum samples typically requires a ≥4-fold increase in neutralizing antibodies to the specific virus PRNT titers in the convalescent serum sample to confirm acute infection because 2-fold changes can reflect assay variability (*5*). Detection of CSGV IgM by ELISA in a single serum sample is insufficient for diagnosis because those results might reflect prior infection or cross-reactivity within CSGVs. The high CSGV seroprevalence in Canada, estimated at up to 20%–30% depending on the region, further complicates interpretation of a single serum result because persistence of IgM for several months after infection has been described for both SSHV and JCV (*4*,*10*–*12*).

All 3 patients exhibited detectable IgM against both SSHV and JCV by ELISA. However, paired acute and convalescent PRNT titers indicated SSHV as the most likely causative agent. Case-patient 1 had a 2-fold decrease in SSHV PRNT titers over 6 weeks, but those titers were consistently higher than JCV titers, which also decreased by 2-fold. Case-patient 2 had a 32-fold rise in SSHV PRNT titers over 4 weeks, meeting the case definition for SSHV infection. Case-patient 3 had a 2-fold decrease in SSHV PRNT titers over 2 weeks and no change in JCV titers; the relatively higher initial SSHV titers compared with static JCV titers supported SSHV as the more likely virus. Of note, 2 of the patients had decreases in SSHV neutralizing antibody titers in convalescent serum samples compared with acute serum samples, which is opposite of expected results. However, patient 1 had initial serology collected at day 8 after symptom onset and patient 3 had initial serology collected at day 13 after symptom onset, in contrast to patient 2, who had initial serology collected at day 5 after symptom onset. The relatively delayed acute serum sample collection for patients 1 and 3 demonstrated higher initial SSHV titers than that of patient 2, likely reflecting a more established serologic response that would be expected later in the infection. Those findings highlight the importance of paired acute and convalescent serologic testing at the appropriate time interval and PRNT confirmation in diagnosing SSHV/CSGV infections. However, the strong epidemiologic link between the 3 cases strengthens the SSHV diagnosis in the 2 patients who might not have met the definition requiring a ≥4-fold rise in neutralizing antibodies from acute versus convalescent titers.

Few reports of neuroinvasive disease caused by SSHV are in the literature, even though seroprevalence studies in animals and humans would suggest relatively high rates of exposure in at least some geographic regions of North America, where positive CSGV serology ranges from 18% to 75% (*10*–*12*). For example, a serologic survey of snowshoe hares in the greater Yellowstone National Park area during 2009–2012 found SSHV seroprevalence rates ranging from 18% to 48% depending on the year, mirroring previous findings from Canada and Alaska in the 1960s that reported CSGV seroprevalence of 20%–75% in snowshoe hares (*13*). A 2015–2016 human serosurvey in New Brunswick, Canada, revealed that 31% of serum samples had CSGV antibodies, and further PRNT testing indicated that 26% of single-virus exposures were JCV and only 2% were SSHV (*14*). However, serology might not be able to definitively distinguish between those 2 CSGVs (*15*). Furthermore, 49.8% of encephalitis-associated cases in Canada have no diagnosed cause (*9*). Taken together, those findings suggest that SSHV-associated neuroinvasive disease is likely underdiagnosed and underreported in North America. Thus, identification of 4 confirmed neuroinvasive cases of SSHV infection in such a short timeframe and small geographic region has substantial clinical and public health implications.

One hypothesis for this cluster is that a higher than usual SSHV prevalence in the mosquito population that season led to a relatively high rate of exposure in the human population, resulting in detection of more neuroinvasive disease. Climate change could affect the distribution of CSGV hosts and, more crucially, the arthropod vectors (*16*). Limited empiric evidence has shown that warming temperatures can increase the winter survival of viruses in mosquitoes and, hence, the rate of transovarial transmission of viruses within those mosquitoes (*17*,*18*). SSHV infectivity also has been shown to be higher in mosquitoes incubated at higher temperatures (*11*). Furthermore, SSHV continues to be isolated from commonly captured mosquito species in Canada, typically *Aedes* spp., which are abundant and widespread (*10*,*14*). Those factors could lead to increased SSHV transmission in endemic regions and a broader distribution of the virus and its vectors.

Of note, >200 human cases of SSHV and JCV infection have been documented across Canada since 2006, and ≈70% of those were confirmed as JCV infections (*2*). However, our cluster of cases might indicate a shifting trend toward a higher SSHV prevalence in some parts of the country. That shift might reflect changes in virus circulation or vector or host distribution or could be attributed to improved serologic testing. That shift also potentially explains why our case series was among pediatric patients because most

symptomatic SSHV infections have been identified in children, but symptomatic JCV infections have been more frequently identified in adults (*2*,*10*,*19*). Future public health surveillance of mosquitoes for CSGV as well as updated seroprevalence studies could help substantiate that hypothesis. More studies are needed to delineate the true incidence of SSHV infections in North America.

Conclusions

This case series suggests an underrecognized incidence of SSHV infection that warrants enhanced future surveillance and review of existing diagnostic algorithms. In addition, many jurisdictions have no active mosquito surveillance, and the cases we describe highlight the need to reinvest in such surveillance to clarify risks for SSHV infection among humans. Clinicians in North America should consider CSGV, including SSHV, as a potential cause of neuroinvasive disease during mosquito season, particularly when initial diagnostic testing is inconclusive.

J.B.G. is a paid consultant scientific editor for GIDEON Informatics, Inc. (https://www.gideononline.com), which is unrelated to this article.

About the Author

Dr. Ali is a pediatric infectious diseases fellow at the University of British Columbia, Vancouver, British Columbia, Canada. His research interests include congenital infections and medical education.

References

1. Walker ED, Yuill TM. Snowshoe hare virus: discovery, distribution, vector and host associations, and medical significance. J Med Entomol. 2023;60:1252–61. https://doi.org/10.1093/jme/tjad128
2. Drebot MA. Emerging mosquito-borne bunyaviruses in Canada. Can Commun Dis Rep. 2015;41:117–23. https://doi.org/10.14745/ccdr.v41i06a01
3. Jansen S, Höller P, Helms M, Lange U, Becker N, Schmidt-Chanasit J, et al. Mosquitoes from Europe are able to transmit snowshoe hare virus. Viruses. 2024;16:222. https://doi.org/10.3390/v16020222
4. Canadian Network for Public Health Intelligence. Detection of IGM antibodies directed towards snowshoe hare virus by ELISA [cited 2025 Sep 12]. https://cnphi.canada.ca/gts/reference-diagnostic-test/5384
5. Canadian Network for Public Health Intelligence. Detection of antibodies directed towards snowshoe hare virus by PRNT [cited 2025 Sep 12]. https://cnphi.canada.ca/gts/reference-diagnostic-test/5385
6. Canadian Network for Public Health Intelligence. Molecular detection of snowshoe hare virus by reverse transcriptase PCR (RT-PCR)—guide to services [cited 2025 Sep 12]. https://cnphi.canada.ca/gts/reference-diagnostic-test/5383
7. Vancouver Coastal Health. New pilot project to study mosquito population in Sea to Sky region [cited 2026 Jan 20]. https://www.vch.ca/en/news/new-pilot-project-study-mosquito-population-sea-sky-region
8. Fauvel M, Artsob H, Calisher CH, Davignon L, Chagnon A, Skvorc-Ranko R, et al. California group virus encephalitis in three children from Quebec: clinical and serologic findings. Can Med Assoc J. 1980;122:60–2, 64.
9. Kulkarni MA, Lecocq AC, Artsob H, Drebot MA, Ogden NH. Epidemiology and aetiology of encephalitis in Canada, 1994–2008: a case for undiagnosed arboviral agents? Epidemiol Infect. 2013;141:2243–55. https://doi.org/10.1017/S095026881200252X
10. Goff G, Whitney H, Drebot MA. Roles of host species, geographic separation, and isolation in the seroprevalence of Jamestown Canyon and snowshoe hare viruses in Newfoundland. Appl Environ Microbiol. 2012;78:6734–40. https://doi.org/10.1128/AEM.01351-12
11. Buhler KJ, Dibernardo A, Pilfold NW, Harms NJ, Fenton H, Carriere S, et al. Widespread exposure to mosquitoborne California serogroup viruses in Caribou, Arctic fox, red fox, and polar bears, Canada. Emerg Infect Dis. 2023;29:54–63. https://doi.org/10.3201/eid2901.220154
12. Sampasa-Kanyinga H, Lévesque B, Anassour-Laouan-Sidi E, Côté S, Serhir B, Ward BJ, et al. Zoonotic infections in communities of the James Bay Cree territory: an overview of seroprevalence. Can J Infect Dis Med Microbiol. 2013;24:79–84. https://doi.org/10.1155/2013/370321
13. Tyers D, Zimmer J, Lewandowski K, Hennager S, Young J, Pappert R, et al. Serologic survey of snowshoe hares (*Lepus americanus*) in the greater Yellowstone area for brucellosis, tularemia, and snowshoe hare virus. J Wildl Dis. 2015;51:769–73. https://doi.org/10.7589/2015-01-021
14. Mincer J, Materniak S, Dimitrova K, Wood H, Iranpour M, Dibernardo A, et al. Jamestown Canyon and snowshoe hare virus seroprevalence in New Brunswick. J Assoc Med Microbiol Infect Dis Can. 2021;6:213–20. https://doi.org/10.3138/jammi-2021-0009
15. Evans AB, Peterson KE. Cross reactivity of neutralizing antibodies to the encephalitic California serogroup orthobunyaviruses varies by virus and genetic relatedness. Sci Rep. 2021;11:16424. https://doi.org/10.1038/s41598-021-95757-2
16. Snyman J, Snyman LP, Buhler KJ, Villeneuve CA, Leighton PA, Jenkins EJ, et al. California serogroup viruses in a changing Canadian Arctic: a review. Viruses. 2023;15:1242. https://doi.org/10.3390/v15061242
17. Lequime S, Paul RE, Lambrechts L. Determinants of arbovirus vertical transmission in mosquitoes. PLoS Pathog. 2016;12:e1005548. https://doi.org/10.1371/journal.ppat.1005548
18. Bergren NA, Kading RC. The ecological significance and implications of transovarial transmission among the vector-borne bunyaviruses: a review. Insects. 2018;9:173. https://doi.org/10.3390/insects9040173
19. Meier-Stephenson V, Drebot MA, Dimitrova K, DiQuinzio M, Fonseca K, Forrest D, et al. Case series of Jamestown Canyon virus infections with neurologic outcomes, Canada, 2011–2016. Emerg Infect Dis. 2024;30:874–81. https://doi.org/10.3201/eid3005.221258

Address for correspondence: Jennifer Tam, BC Children's Hospital, 4480 Oak St, Vancouver, BC V5Z 4H4, Canada; email: jennifer.tam@cw.bc.ca

Ecologic Investigative Strategies to Determine Human Plague Exposure Sites, United States, 1991–2018

Rebecca J. Eisen, Lynn M. Osikowicz, Erik Foster

Plague is a rare but potentially life-threatening fleaborne zoonotic disease caused by *Yersinia pestis*. Public health agencies in the United States use multiple concurrent epidemiologic and ecologic strategies to determine *Y. pestis* exposure sites. We reviewed 196 plague case files from 1991–2018 to describe effort and yield of implemented strategies. All files included an epidemiologic component, and 71% were followed up with environmental investigations. Environmental samples were collected for laboratory testing in 88% of investigations. The percentages of investigations yielding laboratory evidence of local transmission varied from 28% for testing live-trapped rodents to 50% for pet serology. We suggest that collection and laboratory testing of samples should be prioritized when epidemiologic investigations implicate potential exposure in an unusual setting, in areas where many people could be at risk of exposure to *Y. pestis*, or in situations where prevention activities extend beyond educational outreach and incur greater costs.

Plague is a rare but potentially life-threatening fleaborne zoonotic disease caused by the bacterium *Yersinia pestis*. Early diagnosis and effective antimicrobial treatment improve survival of plague infections (*1*). Awareness by the public and medical community of local *Y. pestis* transmission is critical to preventing plague cases and improving outcomes of infections (*2*,*3*). In the United States, plague is a nationally notifiable condition; healthcare providers and laboratories report plague cases to state and local health departments who then report confirmed and probable cases to the Centers for Disease Control and Prevention (CDC). Public health agencies promptly investigate cases and notify the public and healthcare providers of their occurrence. Along with those timely notifications, public health agencies encourage prevention measures (e.g., avoiding areas where plague epizootics have been detected, removing food and harborage for rodents in and around homes, avoiding handling sick or dead animals, and protecting people and pets from fleas), make recommendations on flea control or limiting access to public spaces undergoing active *Y. pestis* transmission, promote early medical care-seeking behavior if plague is suspected, and keep the medical community apprised of diagnosis and treatment guidelines (*2*,*4*–*7*). Accurately identifying when and where exposures to *Y. pestis* occur is central to effectively targeting this messaging.

In consultation or in collaboration with CDC, state and local public health departments follow up on human plague cases to determine where exposures to *Y. pestis* likely occurred and to identify ongoing risk. Place and mode of exposure are inferred from interviews with case patients or their close contacts on the basis of information provided about where the case-patient spent time before onset of symptoms, contact with sick or dead animals, or reports of flea or insect bites. To more definitively identify where *Y. pestis* is circulating in zoonotic hosts, environmental investigations are conducted at locations where the case-patient reportedly spent time within the expected incubation period. Such investigations range in complexity and quality of information gathered. Visual inspections of potential exposure sites are conducted to look for known risk factors (e.g., presence of food and harborage for rodents, evidence of rodent die-offs, and presence of free-roaming pets). Other strategies aim to collect specimens for laboratory testing to detect the presence of *Y. pestis* or provide serologic evidence of prior exposure to *Y. pestis* in pets, wildlife, or fleas (*2*,*8*–*10*). Such field methods include collecting blood from pets and information on any recent travel, searching for and collecting animal carcasses, swabbing animal burrows for host-seeking fleas, and live-trapping rodents and collecting their blood and infesting fleas. Finding laboratory evidence of *Y. pestis*

Author affiliation: Centers for Disease Control and Prevention, Fort Collins, Colorado, USA

DOI: https://doi.org/10.3201/eid3204.251357

at a potential exposure site increases confidence in the exposure site determination and is often beneficial when economically impactful decisions are made to prevent future cases (*4*).

To describe effort and yield of implemented ecologic strategies for plague, we reviewed CDC-maintained plague case files from 1991–2018. Our aim was to summarize when and where persons were exposed to *Y. pestis* in the United States, examine how often various investigative strategies were used to determine exposure sites, explore how often each of the methods aimed at collecting specimens for testing yielded laboratory evidence of current or prior *Y. pestis* transmission, and identify changes in public health practices related to exposure site determination.

Methods

CDC maintains a list of human plague cases and supplemental information reported to the US Public Health Service (1900–1946) and CDC (1947–present). Epidemiologic trends derived from those files from 1900–2012 were reported previously (*6*). Common environmental exposures identified in case files from 1970–1991 have also been reported (*11*). We reviewed case files from 1991–2018 with an emphasis on the investigative strategies used to determine exposure locations. Although plague case reporting continued after 2018, we ended our review in 2018 to eliminate detecting time-limited changes in behavior or public health practices attributable to the coronavirus pandemic. At least 2 of the authors reviewed each case file to extract information on month of symptoms onset; state, county, and location of exposure (peridomestic or away from a home environment); and noted recreational or occupational exposures. Supplementary information on environmental investigations was not collected systematically. We noted whether each case file contained information on conducting site visits, carcass collections, burrow swabbing to collect host-seeking fleas, live-trapping of small mammals to collect blood samples and ectoparasites, and blood collection from pets for serologic testing. When plague-positive laboratory testing was noted in the files, we recorded which sample types tested positive. We described categorical data derived from case files as counts or percentages of case files. We used contingency table analyses to compare counts between categories (JMP Statistical Software, https://www.jmp.com). Animal procedures for CDC investigations from 2009 onward were reviewed and approved by the Institutional Animal Care and Use Committee of the CDC Division of Vector-Borne Diseases, National Center for Emerging and Zoonotic Infectious Diseases.

Results

During 1991–2018, a total of 196 human plague cases were reported to CDC. A median of 5.5 cases was reported per year, with as few as 1 case or as many as 17 cases reported in a year (Figure 1). Reported exposures occurred in 13 states: New Mexico (92 cases), Colorado (39 cases), Arizona (22 cases), California (14 cases), Oregon (9 cases), Utah (7 cases), Wyoming (3 cases), Idaho (2 cases), Nevada (2 cases), Oklahoma (2 cases), Illinois (1 laboratory acquired infection), Montana (1 case), and Texas (1 case); the state of exposure was not determined for 1 case. Most case-patients (85%) were reportedly exposed to *Y. pestis* in southwestern states, including New Mexico (47%), Colorado (19%), and Arizona (11%), or in California (7%). Onset of symptoms was reported in April–October for 91% (n = 179) of cases. Most exposures were determined to have occurred in and around a home (peridomestic exposures) (68%, n = 133). Of the 47 (24%) case-patients exposed to *Y. pestis* away from a home setting, 36 were associated with recreational activities (e.g., camping, hiking, jogging, or hunting), and 10 were considered occupational exposures (e.g., veterinary medical professionals [n = 4], wildlife biologists and trappers [n = 5], or laboratorian [n = 1]). Subcounty level exposure sites were not determined for 16 (8%) cases. Most cases reported from New Mexico (74 cases, 80%), Colorado (28 cases, 71%), and Arizona (13 cases, 59%) were categorized as peridomestic exposures. In contrast, only 36% of California cases (5 cases) were categorized as peridomestic exposure; 50% (7 cases) were exposed away from the home, and exposure location was not determined for 14% (2 cases) of California cases.

State and local health departments conducted environmental investigations to determine exposure sites and to assess ongoing risk of exposure to *Y. pestis*. Findings of environmental investigations were documented in 140 case files (71%); CDC assisted in the field with 44 (31%) of these investigations (Figure 1). We noted a sharp decline in environmental investigations conducted in the most recent decade (χ^2 = 15.85; p<0.001) (Figure 1). Cumulatively from 1991–2008, environmental investigations were conducted for 80% (111) of 139 cases. By contrast, from 2009–2018, environmental investigations were conducted for only 51% of cases (29 of 57 cases). CDC's involvement in field activities declined significantly in the most recent decade compared with the prior decades (χ^2 = 18.05; p<0.001) (Figure 1). CDC assisted state and local health departments in the field with 39% (44) of 111 environmental investigations during 1991–2008, compared with assisting with only 1 of 29 environmental investigations during 2009–2018.

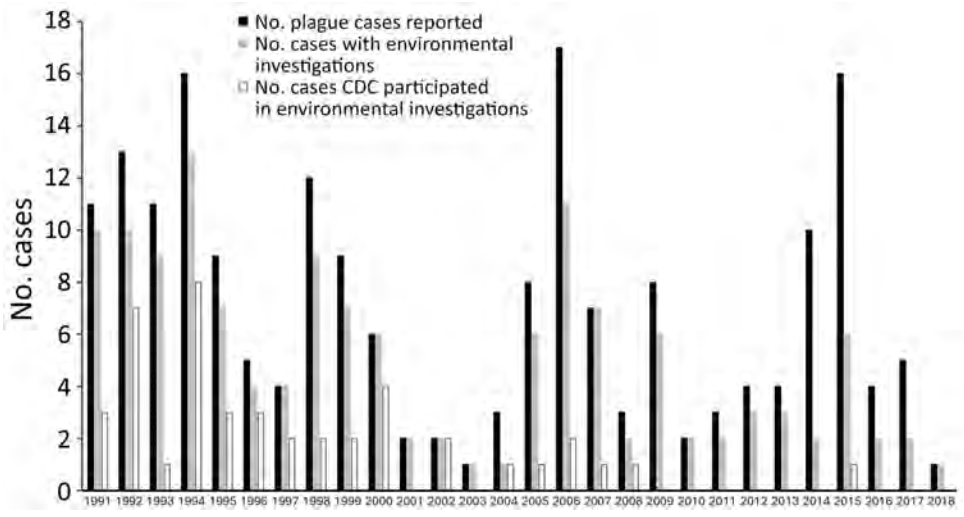

Figure 1. Reported plague cases and associated environmental investigations per year, United States, 1991–2018. The Centers of Disease Control and Prevention staff assisted state and local health departments in the field on a portion of case investigations.

No environmental investigations were recorded for 56 (29%) of 196 cases. Among the 140 (71%) case files with accompanying information on environmental investigations, 136 (97%) reported visiting potential exposure sites and conducting observational risk assessments (e.g., looking for signs of rodent activity/inactivity, availability of food and harborage for rodents). The 4 cases lacking information on site visits were associated with animal exposures in which case files indicated animals or animal carcasses were tested, but no additional information on site observations was provided. Among the observational studies conducted in 136 cases, 51 (38%) noted signs of rodent die-offs.

A total of 123 (63%) of 196 case files (88% of 140 case files noting environmental investigations) indicated use of ≥1 method to obtain samples for laboratory testing (e.g., small mammal trapping to collect blood and flea samples, burrow swabbing to collect host-seeking fleas, carcass collection, or blood collection from pets) (Figure 2). Plague positive samples were detected for 82 (67%) of 123 cases for which methods were used to collect samples for laboratory testing. A total of 85 (61%) of 140 case files with investigations included evidence of live-trapping of small mammals; among those, rodents or their infesting fleas tested positive for *Y. pestis* in 24 (28%) of the case investigations. Seventy-four (53%) case files indicated blood was collected from pets (cats or dogs) for serologic testing; among those, 37 (50%) investigations yielded seropositive results. Attempts to collect host-seeking fleas from rodent burrows were noted in 64 (46%) case files; among them, 24 (38%) investigations yielded plague positive fleas. Fifty-seven (41%) case files reported attempts to collect animal carcasses, of which 27 (47%) yielded laboratory evidence of *Y. pestis*. We believe this report is likely an underestimate of the actual effort to find carcasses because the notation of carcass searches was not systematic. When carcasses were found, they were noted in the files. However, a few instances reported looking for but not finding carcasses.

Compared with other methods that yield samples for laboratory testing (burrow swabbing, carcass collection, or collection of blood from pets), live-trapping small mammals and collecting their blood and infesting fleas and testing the resulting samples is the most time consuming and financially costly. We sought to determine the yield from those efforts. Most environmental investigations used multiple methods to collect environmental samples for testing (59%, 83 of 140 case files). Among the 24 cases where blood or fleas derived from live-trapping yielded plague positive laboratory results (17 case files with seropositive rodents, 10 with *Y. pestis* detected in infesting fleas; 3 case files in which both sample types were positive), 16 (67%) yielded positive laboratory results from other methods as well (e.g., pet serum, carcasses, or fleas collected from burrows). Only 8 environmental investigations (<10% of 82 cases with laboratory evidence for determining exposure sites) provided laboratory support for local transmission of *Y. pestis* based solely on live-trapping (i.e., other environmental samples did not yield positive laboratory testing results).

Fifty case files included laboratory evidence implicating various wildlife taxa in local *Y. pestis* transmission. Laboratory evidence included direct detection or serologic detection of *Y. pestis* in live trapped rodents or direct detection in infesting or host-seeking fleas, or direct detection of *Y. pestis* from animal carcasses. Most files (80%, n = 40 files) identified a single taxon exposed to *Y. pestis*; 9 files identified *Y. pestis* in 2 taxa and 1 file identified 3 infected taxa. Ground squirrels (40%, n = 20 files) and prairie dogs (24%, n = 12) were the

most common taxa implicated in local transmission. Other infected taxa included *Peromyscus* mice (18%, n = 9 files), woodrats (16%, n = 8 files), rabbits (12%, n = 6 files), chipmunks or bobcats (4%, n = 2 files), and a mountain lion and a tree squirrel (2%, n = 1 file).

Discussion

Most (71%) human plague cases reported for 1991–2018 were followed up with environmental investigations to determine exposure locations. However, we found a major decline in environmental investigations in the most recent decade evaluated. In that decade, exposure sites for plague cases were mostly inferred solely on the basis of case histories. When environmental investigations were conducted, observational risk assessments were almost always conducted. Nearly two thirds of case files also contained information indicating that methods were used to collect environmental samples for laboratory testing; among those cases, two thirds of field investigations yielded laboratory support for recent or ongoing *Y. pestis* transmission at the site investigated. Determinations of exposure sites were supported by laboratory evidence of *Y. pestis* in environmental samples in 42% of 196 reviewed case files.

Each investigative strategy has advantages and challenges. To overcome those challenges, multiple methods were often deployed within each environmental investigation to obtain environmental samples for testing. Small mammal trapping was the most noted method in case files, followed by blood collection from pets, collection of host-seeking fleas from rodent burrows, and collection of carcasses. Of note, those are rough estimates that depict broad trends in effort and yield. Notation of environmental investigation data within case files was not systematic or complete. Nonetheless, our review indicated that live-trapping was the method least likely to yield laboratory evidence of recent (rodent serology) or ongoing (direct detection in infesting fleas) *Y. pestis* transmission; only 28% of cases including live-trapping yielded laboratory evidence of *Y. pestis*. By contrast, nearly half of case files that included either pet serologic testing or direct detection of *Y. pestis* in collected carcasses yielded laboratory support for recent local transmission. Live-trapping of rodents is the most labor-intensive and costly strategy used in environmental investigations, and it rarely provides unique support for local plague transmission. In situations where plague activity was detected in live-trapped rodents or their infesting fleas, carcasses, host-seeking fleas, or pet serum often provided additional evidence of *Y. pestis* transmission. Because of the relatively low yield and more labor-intensive effort of live-trapping, the method might only be beneficial in unusual outbreaks.

Most human plague cases reported in the United States are associated with epizootic activity (*2*,*6*,*11*,*12*). During plague epizootics, fleaborne *Y. pestis* spreads rapidly among susceptible mammalian hosts, often ground squirrels and prairie dogs. As large numbers of rodents die from plague infection, their associated fleas seek alternative bloodmeal sources, including feeding on humans and their pets (*2*,*13*–*15*). Carnivores, lagomorphs, and other mammalian hosts are often exposed to *Y. pestis*, particularly during epizootic periods, through direct contact with infected rodents or exposure to their infectious fleas. Susceptibility among nonrodent hosts varies widely (*14*,*15*). The high mortality rate among rodents and other mammalian hosts explains the high success rate in detecting *Y. pestis* in carcasses found during case investigations. Although carcass testing yielded a high percentage of positive samples, finding carcasses can be difficult in some settings where scavengers remove carcasses or where carcasses are obstructed by vegetation, burrows, or other obstacles (*8*,*16*,*17*). This difficulty in finding carcasses is reflected in the low percentage of investigations that collect carcasses. Because carnivores and scavengers are exposed to rodents and their fleas over large areas, serologic testing of wild and domestic carnivores has proven to be effective in detection of prior exposures to *Y. pestis* in animals that survive infections (*18*–*22*). Monitoring seroprevalence in carnivores and scavengers is more commonly implemented as a surveillance strategy, rather than response. Some rodent species show a heterogeneous response to infection; that is, some rodents die from infection, but others survive

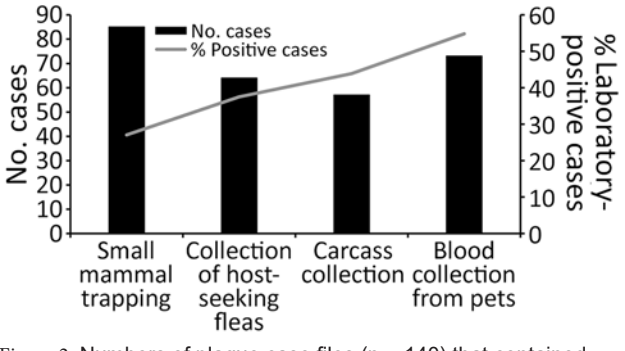

Figure 2. Numbers of plague case files (n = 140) that contained records of environmental investigations and noted using methods intended to collect laboratory testing samples, United States, 1991–2018. Methods included small mammal trapping (n = 85 cases), collection of pet serum (n = 73 cases), burrow swabbing to collect host-seeking fleas (n = 64 cases), or carcass collection (n = 57 cases). Percentages of cases where laboratory evidence of *Y. pestis* transmission was recorded in case files are shown for each sample acquisition method. Visual assessments were conducted for 136 cases (data not shown).

and seroconvert (*13*,*14*). Live-trapping capitalizes on detecting the small percentage of animals that were exposed to *Y. pestis*, survived infection, and seroconverted (*4*,*23*,*24*). Direct detection of *Y. pestis* in rodent blood or tissues is not conducted routinely because active infections in susceptible rodents are often fatal, reducing the odds of capturing a live infected rodent (*13*,*25*). Success in detecting plague activity in live-trapped rodent samples is dependent on the timing and location of trapping relative to the spread of *Y. pestis* in rodent communities, trapping effort, the composition of the rodent community, and the susceptibility or resistance to *Y. pestis* of species captured also influences the likelihood of capturing seropositive animals (*4*,*16*,*23*,*24*,*26*). Collecting and testing host-seeking fleas is often useful in detecting *Y. pestis* in fleas that have fled their dead or dying hosts, but success is dependent upon detecting a recent die-off and finding rodent burrows in the affected area. Although prevalence of *Y. pestis* in fleas is elevated during epizootics, even during active epizootics, prevalence of *Y. pestis* infection in fleas is often low (*23*,*26*,*27*).

Although fleaborne transmission remains the most common mode of *Y. pestis* transmission to humans, direct contact with infectious animals or animal carcasses is also a major mode of animal-to-human transmission (*2*,*6*,*11*,*28*–*30*). In recent decades, case investigations revealed that most plague case-patients were exposed to *Y. pestis* in the peridomestic environment in rural or semi-rural parts of the southwestern United States (*5*,*6*,*29*,*31*), where availability of food and harborage for rodents in the home environment is a known risk factor (*29*,*32*). Such food resources increase the chances of bringing potentially infectious rodents and their fleas into the home environment where they pose a risk to humans directly (flea bites, direct contact with infected animal carcasses) or indirectly (exposure to sick pets that were exposed to *Y. pestis* in and around the home). Cats are acutely susceptible to plague, and bites, scratches, or exposure to respiratory droplets of plague-infected cats pose a major hazard to humans. Veterinary staff and care takers treating sick cats are at elevated risk of plague infection (*28*,*33*,*34*). Although dogs exposed to *Y. pestis* can show clinical signs of plague infection, illness is often less severe in dogs compared with cats (*33*). Nonetheless, plague-infected dogs are implicated in direct transmission to humans (*35*,*36*). More often, pet dogs serve as phoretic hosts, bringing potentially infectious fleas into the home environment and sleeping in the same bed as a dog was identified as a major risk factor for plague (*37*,*38*). Humans spend a considerable amount of time in the same risk environments as their pets, but pets are usually more likely to come into direct contact with infected rodents and their fleas. As a result, pet serology is an effective means of identifying potential exposure sites in case investigations. However, pets (particularly dogs) often travel with humans and therefore collecting travel histories for the pets is essential to discerning exposure locations on the basis of pet serology alone.

The percentage of cases that led to public health agencies conducting environmental investigations declined sharply in the most recent decade evaluated. The reasons for this decline are not entirely clear, but we believe it coincided with changes in the World Health Organization's International Health Regulations (IHR; https://apps.who.int/gb/bd/pdf_files/IHR_2014-2022-2024-en.pdf), staffing at public health agencies, and competing priorities including responding to more common emerging vectorborne disease threats. Under the previous version of the IHR, published in 1969, all human plague cases required reporting to the World Health Organization. Under the updated IHR (2005), implemented in 2007, notification to the World Health Organization is required only for unexpected events that present a risk for international spread (*39*). After decades of conducting epidemiologic and environmental investigations of plague cases in the United States, geographic and behavioral risk factors are well characterized (*2*,*5*,*6*,*11*,*25*,*31*). Because of that knowledge, usual exposures in western states associated with outdoor activities, noted flea bites, or direct contact with sick or dead animals can be inferred through case histories alone.

Detecting *Y. pestis* in environmental samples builds confidence in determining locations of exposure and assessing ongoing transmission risk. Use of multiple concurrent environmental investigative strategies has proven effective in providing laboratory evidence of local *Y. pestis* transmission; however, the individual components have associated costs. It is worth scrutinizing the precision and accuracy of environmental data needed to inform public health action relative to the resources expended to obtain supportive environmental data. Most often, prevention focuses on educating the public and healthcare community of plague risk and prevention strategies. The exact location and extent of epizootic transmission might not be needed for such outreach, unless a plague case occurs in a densely populated setting. In instances where many people are at risk for exposure to *Y. pestis*, public health entities might recommend vector control or limiting site access (*4*,*16*). Laboratory evidence of ongoing transmission provides support for those decisions. Moreover, environmental sampling provides baseline data that can be used to assess the effectiveness of vector control efforts. We suggest that environmental

investigations, particularly collection of samples for laboratory testing, should be prioritized when epidemiologic investigations indicate potential exposure in an unusual setting, in areas where large populations could be at risk for exposure to *Y. pestis*, or in situations where prevention activities extend beyond educational outreach and incur greater costs.

Acknowledgments

We thank state and local health departments for providing supplemental information on environmental investigations to CDC and the Epidemiology and Surveillance Team in the Bacterial Diseases Branch, Division of Vector-Borne Diseases, National Center for Emerging and Zoonotic Infectious Diseases, CDC, for maintaining records of plague case investigations.

About the Author

Dr. Eisen is a research biologist and lead of the Entomology and Ecology Team in the Bacterial Diseases Branch, Division of Vector-Borne Diseases, National Center for Emerging and Zoonotic Infectious Diseases, Centers for Disease Control and Prevention, in Fort Collins, Colorado. Her research interests include understanding how plague and tickborne pathogens are maintained in enzootic cycles and applying that information to design and evaluate strategies to prevent human infections.

References

1. Kugeler KJ, Mead PS, Campbell SB, Nelson CA. Antimicrobial treatment patterns and illness outcome among United States patients with plague, 1942–2018. Clin Infect Dis. 2020;70(Suppl 1):S20–6. https://doi.org/10.1093/cid/ciz1227
2. Barnes AM. Surveillance and control of bubonic plague in the United States. Symp Zool Soc Lond. 1982;50:237–70.
3. Dennis DT, Mead PS. Plague. In: Guerrant RL, Walker DH, Weller PF, editors. Tropical infectious diseases. Philadelphia: Elsevier; 2009. p. 471–481.
4. Danforth M, Novak M, Petersen J, Mead P, Kingry L, Weinburke M, et al. Investigation of and response to 2 plague cases, Yosemite National Park, California, USA, 2015. Emerg Infect Dis. 2016;22:2045–53. https://doi.org/10.3201/eid2212.160560
5. Gage KL, Dennis DT, Tsai TF. Prevention of plague: recommendations of the Advisory Committee on Immunization Practices. MMWR Recomm Rep. 1996; 45(RR-14):1–15.
6. Kugeler KJ, Staples JE, Hinckley AF, Gage KL, Mead PS. Epidemiology of human plague in the United States, 1900–2012. Emerg Infect Dis. 2015;21:16–22. https://doi.org/10.3201/eid2101.140564
7. Nelson CA, Fleck-Derderian S, Cooley KM, Meaney-Delman D, Becksted HA, Russell Z, et al. Antimicrobial treatment of human plague: a systematic review of the literature on individual cases, 1937–2019. Clin Infect Dis. 2020;70(Suppl 1):S3–10. https://doi.org/10.1093/cid/ciz1226
8. Baltazard M, Davis DH, Devignat R, Girard G, Gohar MA, Kartman L, et al. Recommended laboratory methods for the diagnosis of plague. Bull World Health Organ. 1956; 14:457–509.
9. California Department of Public Health. California compendium of plague control. 2021 [cited 2025 Sep 1]. https://www.cdph.ca.gov/Programs/CID/DCDC/CDPH%20Document%20Library/CAPlagueCompendium.pdf
10. Stark HE, Hudson BW, Pittman B. Plauge epidemiology. Atlanta: Center for Disease Control, US Department of Health and Welfare, Public Health Service; 1966.
11. Craven RB, Maupin GO, Beard ML, Quan TJ, Barnes AM. Reported cases of human plague infections in the United States, 1970–1991. J Med Entomol. 1993;30:758–61. https://doi.org/10.1093/jmedent/30.4.758
12. Eskey CR, Haas VH. Plague in the western part of the United States. 1940 [cited 2025 Sep 1]. https://www.cabidigitallibrary.org/doi/full/10.5555/19412900475
13. Eisen RJ, Gage KL. Adaptive strategies of *Yersinia pestis* to persist during inter-epizootic and epizootic periods. Vet Res. 2009;40:1. https://doi.org/10.1051/vetres:2008039
14. Gage KL, Kosoy MY. Natural history of plague: perspectives from more than a century of research. Annu Rev Entomol. 2005;50:505–28. https://doi.org/10.1146/annurev.ento.50.071803.130337
15. Meyer KF. The known and the unknown in plague. Am J Trop Med. 1942;22:9–36. https://doi.org/10.4269/ajtmh.1942.s1-22.9
16. Davis RM, Smith RT, Madon MB, Sitko-Cleugh E. Flea, rodent, and plague ecology at Chuchupate Campground, Ventura County, California. J Vector Ecol. 2002;27:107–27.
17. Boone A, Kraft JP, Stapp P. Scavenging by mammalian carnivores on prairie dog colonies: implications for the spread of plague. Vector Borne Zoonotic Dis. 2009;9:185–90. https://doi.org/10.1089/vbz.2008.0034
18. Brown HE, Ettestad P, Reynolds PJ, Brown TL, Hatton ES, Holmes JL, et al. Climatic predictors of the intra- and inter-annual distributions of plague cases in New Mexico based on 29 years of animal-based surveillance data. Am J Trop Med Hyg. 2010;82:95–102. https://doi.org/10.4269/ajtmh.2010.09-0247
19. Carlson CJ, Bevins SN, Schmid BV. Plague risk in the western United States over seven decades of environmental change. Glob Change Biol. 2022;28:753–69. https://doi.org/10.1111/gcb.15966
20. Chomel BB, Jay MT, Smith CR, Kass PH, Ryan CP, Barrett LR. Serological surveillance of plague in dogs and cats, California, 1979–1991. Comp Immunol Microbiol Infect Dis. 1994;17:111–23. https://doi.org/10.1016/0147-9571(94)90036-1
21. Rust JH Jr, Cavanaugh DC, O'Shita R, Marshall JD Jr. The role of domestic animals in the epidemiology of plague. I. Experimental infection of dogs and cats. J Infect Dis. 1971;124:522–6. https://doi.org/10.1093/infdis/124.5.522
22. Rust JH Jr, Miller BE, Bahmanyar M, Marshall JD Jr, Purnaveja S, Cavanaugh DC, et al. The role of domestic animals in the epidemiology of plague. II. Antibody to *Yersinia pestis* in sera of dogs and cats. J Infect Dis. 1971; 124:527–31. https://doi.org/10.1093/infdis/124.5.527
23. Kosoy M, Reynolds P, Bai Y, Sheff K, Enscore RE, Montenieri J, et al. Small-scale die-offs in woodrats support long-term maintenance of plague in the US southwest. Vector Borne Zoonotic Dis. 2017;17:635–44. https://doi.org/10.1089/vbz.2017.2142
24. Stapp P, Salkeld DJ, Eisen RJ, Pappert R, Young J, Carter LG, et al. Exposure of small rodents to plague

during epizootics in black-tailed prairie dogs. J Wildl Dis. 2008;44:724–30. https://doi.org/10.7589/0090-3558-44.3.724
25. Link VB. A history of plague in United States of America. Public Health Monogr. 1955;26:1–120.
26. Thiagarajan B, Bai Y, Gage KL, Cully JF Jr. Prevalence of *Yersinia pestis* in rodents and fleas associated with black-tailed prairie dogs (*Cynomys ludovicianus*) at Thunder Basin National Grassland, Wyoming. J Wildl Dis. 2008;44:731–6. https://doi.org/10.7589/0090-3558-44.3.731
27. Hammond TT, Liebman KA, Payne R, Pigage HK, Padgett KA. Plague epizootic dynamics in chipmunk fleas, Sierra Nevada Mountains, California, USA, 2013–2015. Emerg Infect Dis. 2020;26:801–4. https://doi.org/10.3201/eid2604.190733
28. Gage KL, Dennis DT, Orloski KA, Ettestad P, Brown TL, Reynolds PJ, et al. Cases of cat-associated human plague in the Western US, 1977–1998. Clin Infect Dis. 2000;30:893–900. https://doi.org/10.1086/313804
29. Mann JM, Martone WJ, Boyce JM, Kaufmann AF, Barnes AM, Weber NS. Endemic human plague in New Mexico: risk factors associated with infection. J Infect Dis. 1979;140:397–401. https://doi.org/10.1093/infdis/140.3.397
30. Wong D, Wild MA, Walburger MA, Higgins CL, Callahan M, Czarnecki LA, et al. Primary pneumonic plague contracted from a mountain lion carcass. Clin Infect Dis. 2009;49:e33–8. https://doi.org/10.1086/600818
31. Eisen RJ, Enscore RE, Biggerstaff BJ, Reynolds PJ, Ettestad P, Brown T, et al. Human plague in the southwestern United States, 1957–2004: spatial models of elevated risk of human exposure to *Yersinia pestis*. J Med Entomol. 2007;44:530–7. https://doi.org/10.1093/jmedent/44.3.530
32. Schotthoefer AM, Eisen RJ, Kugeler KJ, Ettestad P, Reynolds PJ, Brown T, et al. Changing socioeconomic indicators of human plague, New Mexico, USA. Emerg Infect Dis. 2012;18:1151–4. https://doi.org/10.3201/eid1807.120121
33. Orloski KA, Lathrop SL. Plague: a veterinary perspective. J Am Vet Med Assoc. 2003;222:444–8. https://doi.org/10.2460/javma.2003.222.444
34. Oyston PC, Williamson D. Plague: infections of companion animals and opportunities for intervention. Animals (Basel). 2011;1:242–55. https://doi.org/10.3390/ani1020242
35. Runfola JK, House J, Miller L, Colton L, Hite D, Hawley A, et al.; Centers for Disease Control and Prevention. Outbreak of human pneumonic plague with dog-to-human and possible human-to-human transmission—Colorado, June–July 2014. MMWR Morb Mortal Wkly Rep. 2015;64:429–34.
36. Schaffer PA, Brault SA, Hershkowitz C, Harris L, Dowers K, House J, et al. Pneumonic plague in a dog and widespread potential human exposure in a veterinary hospital, United States. Emerg Infect Dis. 2019;25:800–3. https://doi.org/10.3201/eid2504.181195
37. Gould LH, Pape J, Ettestad P, Griffith KS, Mead PS. Dog-associated risk factors for human plague. Zoonoses Public Health. 2008;55:448–54. https://doi.org/10.1111/j.1863-2378.2008.01132.x
38. Meyer KF. The ecology of plague. Medicine (Baltimore). 1942;21:143–74. https://doi.org/10.1097/00005792-194205010-00002
39. World Health Organization. Manual for plague surveillance, diagnosis, prevention and control. 2024 [cited 2025 Sep 1]. https://www.who.int/publications/i/item/9789240090422

Address for correspondence: Rebecca J. Eisen, Centers for Disease Control and Prevention, 3156 Rampart Rd, Mailstop P02, Fort Collins, CO 80521, USA; email: dyn2@cdc.gov

EID Podcast

Telework during Epidemic Respiratory Illness

The COVID-19 pandemic has caused us to reevaluate what "work" should look like. Across the world, people have converted closets to offices, kitchen tables to desks, and curtains to videoconference backgrounds. Many employees cannot help but wonder if these changes will become a new normal.

During outbreaks of influenza, coronaviruses, and other respiratory diseases, telework is a tool to promote social distancing and prevent the spread of disease. As more people telework than ever before, employers are considering the ramifications of remote work on employees' use of sick days, paid leave, and attendance.

In this EID podcast, Dr. Faruque Ahmed, an epidemiologist at CDC, discusses the economic impact of telework.

Visit our website to listen:
https://go.usa.gov/xfcmN

EMERGING INFECTIOUS DISEASES®

Circulation Patterns, Genetic Diversity, and Public Health Implications of Enterovirus D68, Europe, 2014–2024

Cristina Andrés, Ignasi Prats-Méndez, Sofie Midgley, Natasa Berginc, Alejandra González-Sánchez, Caroline Klint Johannesen, Andrés Antón, Patricia Nadal-Barón, Thea K. Fischer, Heli Harvala, Kimberley S.M. Benschop

Enterovirus D68 (EV-D68) represents a continuing public health concern, given its association with severe respiratory illness and neurologic complications. In this study, we analyzed EV-D68 circulation and genetic evolution during 2014–2024 using data from 18 countries in Europe. Of 61,297 enterovirus-positive specimens, molecular detection and viral protein 1 sequencing identified 3,541 (6%) EV-D68 cases. A biennial circulation pattern was observed; detection rates ranged from 9% in 2014 to 0.9% in 2019. The pattern was disrupted in 2020 because of measures implemented in response to the COVID-19 pandemic, but then notable increases occurred in 2021 (14%), 2022 (10.7%), and 2024 (20.6%). Subgenogroups B3 (59.8%) and A2/D (28.0%) were predominant; A2/D reemerged as dominant in 2024. Mutation analyses revealed changes in antigenic regions. Our findings underscore the persistent adaptation and resurgence of EV-D68 after COVID-19. Continued genomic surveillance is essential to monitor transmission patterns caused by antigenic changes.

Enterovirus D68 (EV-D68), a nonpolio enterovirus of the *Picornaviridae* family, has attracted attention because of its potential to cause severe respiratory illness and neurologic complications, particularly in children. First isolated in 1962, EV-D68 was sporadically detected until outbreaks in 2010 revealed its capacity for widespread transmission (*1*–*4*). Moreover, several clades (A–D) and subclades (A1, A2/D, B1, B2, B3, and C) have been described (*5*). Subsequent studies have also demonstrated that EV-D68 exhibits a cyclical pattern of circulation and a biennial recurrence (*6*,*7*), which continued until the COVID-19 pandemic, when the incidence of seasonal respiratory viruses was disrupted.

The ongoing circulation of EV-D68 poses a challenge for public health because outbreaks frequently coincide with increased rates of hospitalization for respiratory distress and, occasionally, cases of acute flaccid myelitis (AFM) (8). The neuropathogenic properties of the virus have been linked to specific amino acid residues. In particular, Leser et al. (9) recently identified 4 amino acid substitutions in the VP1 gene (I553L, D554N, A650T, and K835E) that are associated with neurovirulence in mice. Several recent studies have shown that neutralizing antibody responses to EV-D68 increase with age and that infection with 1 clade can generate cross-reactive immunity against other clades, providing key insights into population immunity and transmission dynamics (10–12).

Despite improvements in surveillance efforts, comprehensive analysis of EV-D68 circulation patterns and the elucidation of viral features remains limited. This study provides a summary of trends

Author affiliations: Vall d'Hebron Hospital Universitari, Vall d'Hebron Institut de Recerca (VHIR), Vall d'Hebron Barcelona Hospital Campus, Barcelona, Spain (C. Andrés, I. Prats-Méndez, A. González-Sánchez, A. Antón, P. Nadal-Barón); Statens Serum Institut, Copenhagen, Denmark (S. Midgley); National Laboratory of Health, Environment and Food, Laboratory for Polio, Ljubljana, Slovenia (N. Berginc); Nordsjællands Hospital, Hillerød, Denmark (C.K. Johannesen, T.K. Fischer); Centro de Investigación Biomédica en red de Enfermedades Infecciosas CIBERINFEC, Instituto Carlos III, Madrid, Spain (A. Antón); University of Copenhagen, Copenhagen (T.K. Fischer); National Health Service Blood and Transplant, London, UK (H. Harvala); University of Oxford, Oxford, UK (H. Harvala); Turku University Central Hospital, Turku, Finland (H. Harvala); University of Turku, Turku (H. Harvala); National Institute for Public Health and the Environment, Bilthoven, the Netherlands (K.S.M. Benschop)

DOI: https://doi.org/10.3201/eid3204.251022

in EV-D68 circulation in Europe during 2014–2024, particularly focusing on prevalence, genetic diversity, and potential public health implications.

Methods

Data Collection

We obtained epidemiologic and molecular data from the passive and hospital-based surveillance systems (enterovirus, influenza-like illness, or acute flaccid paralysis [AFP]) of various institutions affiliated with the European Non-Poliovirus Enterovirus Network through a data collection form (Appendix Table 1, https://wwwnc.cdc.gov/EID/article/32/4/25-1022-App1.pdf) and other studies (*1*,*3*,*13*–*16*). Specimens from patients with symptoms suggestive of an enterovirus-related acute respiratory infection or neurologic illness (meningitis, AFP, or myelitis) were tested for virological confirmation according to case definition (*17*). Information regarding the samples that were tested and subsequently identified as EV-D68 was gathered during October 2014–December 2024. We also extracted demographics and clinical data from previous published works (*1*,*3*,*13*–*16*). Institutional Review Board approval (PR(AG)419/2023) was obtained from the Hospital Universitari Vall d'Hebron Clinical Research Ethics Committee.

Enterovirus Detection and Characterization

We conducted enterovirus detection using different real-time multiplex RT-PCRs (Table 1) (*34*). We subjected the partial viral protein (VP) 1 or the complete genome to sequencing for enterovirus typing (*35*) and genomic annotation of all enterovirus-positive specimens, as previously reported (*1*–*3*,*33*,*36*–*38*) (Table 1). We conducted further molecular characterization of EV-D68 by phylogenetic analyses using IQ-TREE multicore version 2.4.0 (Model Finder) (*39*) to define the genetic clades (Appendix Figure 1). References used for EV-D68 phylogeny at clade level are according to the following GenBank accession numbers: A1, KT959173; A2/D, F726085, KT959178, KU242683, and KY358058; B1, KP745751; B2, KP745768; B3, KT711083, KT803593, KU982558, and KY385886. In addition, we analyzed amino acid substitutions within antigenic epitopes of the VP1 protein, specifically the BC-loop (positions 642–655) and DE-loop (positions 692–698), and other areas recently linked to neuropathogenesis (*9*) using the Data Explorer module in MEGA6 (*40*). Numbering of amino acid positions in translated nucleotide sequences are relative to the Fermon strain (GenBank accession no. AY426531) and clinical isolate U.S./IL/14-18952 (GenBank accession no. KM851230) for the sequence annotation of immunogenicity and neuropathogenic sites. We determined the frequency of amino acid residues per antigenic site using EV-D68 A2/D and B3 clades, compared between prepandemic (2014–2019), pandemic (2020–2022), and postpandemic (2023–2024) periods, and plotted with Weblogo 3 (*41*). We compiled GenBank accession numbers of sequences used from the previously published studies and newly generated sequences (Appendix Table 2).

Results

EV-D68 Circulation through Europe

During October 2014–December 2024, a total of 61,297 specimens from 50 institutions across 18 countries in Europe (Table 1) were laboratory-confirmed as enterovirus. A total of 3,541 (6%) of 61,297 were identified as EV-D68; of those, 2,339 (66%) were further genetically characterized based on the VP1 sequence (n = 2,057) or complete genome (n = 282). Subgenogroups B3 (1,398 [59.8%]) and A2/D (654 [28.0%]) were overall the most prevalent, followed by B2 (202 [8.6%]), B1 (71 [3.0%]), and A1 (14 [0.6%]) (Figure 1; Appendix Figure 1). EV-D68 was predominantly collected from persons with acute respiratory infection symptoms, primarily children; incidence among adolescents and adults (>15 years of age) increased during 2024 (Tables 2, 3).

In Europe, EV-D68 circulation was predominantly observed during even years (9% in 2014, 6.3% in 2016, 4.4% in 2018), although circulation was disrupted in 2020 because of the implementation of preventive measures for SARS-CoV-2 (Figure 2). Nevertheless, we observed a notable upsurge in EV-D68 cases in 2021 (14.0%) across multiple countries (Figure 2). We also observed subsequent circulation in 2022 (10.7%) and during the 2024 season (20.6%). Although fewer cases were detected in 2023 (2.8%), the numbers were still substantially higher than in the low-circulation years before the pandemic (1.1% in 2015, 0.2% in 2017, and 0.9% in 2019) (Figure 2). Regardless of the changing epidemiology of EV-D68 over the years, we observed further levels of predominance of the EV-D68 clades over the study period (Figure 1). Although B3 prevailed in 2015 and 2016, A2/D dominated in 2017; both subgenogroups cocirculated in 2018. B3 was dominant again in the following years but decreased in 2024, when A2/D was the dominant subgenogroup (82.1%) (Figure 1).

Table 1. Details of participant countries in study of circulation patterns, genetic diversity, and public health implications of EV-D68 circulation, Europe, 2014–2024

Country	No. institutions	Screening methods	Sequencing method references	No. EV-D68 positive/no. enterovirus positive (%)†
Austria	1	NA	(*18*)	7/625 (1)
Belgium	2	Feces: enterovirus PCR on GI-TAC assay; respiratory samples: enterovirus PCR and EV-D68 PCR on respiratory TAC assay; others: in-house enterovirus PCR; CSF: FilmArray panel (BioFired Diagnostics, https://www.biofiredx.com)	NA	158/3,281 (5)
Bulgaria	1	Cell culture and inhouse enterovirus PCR	NA	0/61 (0)
Croatia	1	NA	NA	9/1,066 (1)
Czech Republic	1	Cell culture and in-house enterovirus PCR	NA	0/310 (0)
Denmark	1	In-house enterovirus and RV PCR (*19*)	(*18*)	293/6,204 (5)
Estonia	1	NA	NA	0/27 (0)
Finland	3	In-house enterovirus and RV PCR	(*18*)	100/1,177 (8)
France	1	In-house enterovirus, rhinovirus, and EV-D68 PCR (*20*)	(*18*)	549/10,111 (5)
Germany	4	In-house enterovirus and RV PCR	(*21*)	46/3,237 (1)
Hungary	1	In-house enterovirus PCR (*22*)	(*18*)	0/112 (0)
Iceland	1	In-house enterovirus and EV-D68 PCR (*23*,*24*)	(*25*,*26*)	13/219 (6)
Ireland	1	Respiratory samples: Luminex NxTAG Respiratory Panel (EV/RV) (Diasorin, https://www.diasorin.com); enterovirus (*18*) and in-house EV-D68 PCR	(*18*)	6/552 (1)
Italy	2	Allplex Respiratory Panel (Seegene, https://www.seegene.com) and in-house enterovirus and EV-D68 PCR (*27*,*28*)	(*18*)	129/1,696 (8)
Latvia	1	NA	NA	0/104 (0)
Lithuania	1	NA	NA	0/22 (0)
Luxembourg	1	NA	NA	1/346 (0)
Netherlands	8	In-house enterovirus and EV-D68 PCR (*13*, *29*, *30*)	(*18*)	236/5,747 (4)
Norway	2	In-house enterovirus and EV-D68 PCR (*31*)	(*18*)	89/1,048 (8)
Poland	1	NA	NA	0/159 (0)
Portugal	1	Allplex Respiratory Panel (Seegene)	NA	23/95 (24)
Romania	1	NA	NA	9/9 (100)
Slovakia	1	NA	NA	0/130 (0)
Slovenia	3	In-house enterovirus and EV-D68 PCR (*23*)	(*18*)	119/1,502 (8)
Spain	4	Respiratory: Allplex Respiratory Panel (Seegene); feces and CSF: RealCycle EV/hPeV detection (Progenie) and Allplex Meningitis V2 Panel (Seegene)	(*18*, *32*, *33*)	1,354/9,721 (14)
Sweden	1	Allplex Respiratory Panel (Seegene) and in-house enterovirus and EV-D68 PCR (*27*)	(*18*)	234/4,188 (6)
United Kingdom	4	In-house enterovirus and EV-D68 PCR	(*18*); Colindale reference laboratory sequencing	166/9,548 (2)
Total	50			3,541/61,297 (6)

*CSF, cerebrospinal fluid; EV-D68, enterovirus D68; GI-TAC, Gastrointestinal TaqMan Array Card; hPeV, human parechovirus; NA, not applicable.
†Studies used in number of enterovirus-positive specimens: (*1*,*3*,*13*–*16*).

Mutation Analyses of EV-D68 Strains

Immunogenic Epitopes

We have provided the frequency of amino acid changes detected at antigenic sites (BC- and DE-loops) of EV-D68 strains in prepandemic, pandemic, and postpandemic periods (Figure 3), as well as the complete mutation analysis of *VP1* gene per year and per clade (Appendix Figures 2, 3). We observed a clear change in amino acid diversity in both A2/D (Appendix Figure 2) and B3 (Appendix Figure 3) clades during the 2 periods. Positions 647 and 650 in the BC-loop exhibited the greatest degree of variation compared with other sites in both clades (Figure 3). Within the A2/D clade, prepandemic sequences were predominantly characterized by glutamic acid at position 647 (E647) and valine at position 650 (V650). Although the isoleucine at position 650 (I650) dominated until 2016, a transition to valine (V650) was observed in 2017 and 2018; the detection rate during 2019 was 50% (Appendix Figure 2). Conversely, during the pandemic and postpandemic era (2020–2024), we observed a marked shift in residue predominance. Glycine at position 647 (G647) and isoleucine at position 650 (I650)

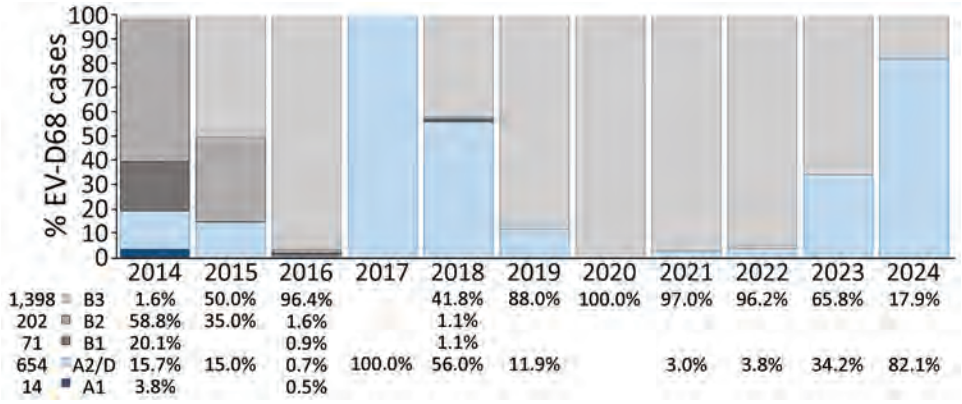

Figure 1. Yearly percentage and global distribution of EV-D68 cases, by clade, in study of circulation patterns, genetic diversity, and public health implications of EV-D68 circulation, Europe, 2014–2024. Numbers at bottom left indicate total numbers of cases by clade during the study period. EV-D68, enterovirus D68.

became the dominant residues, largely replacing the prepandemic amino acids and indicating a substantial change in the antigenic landscape of the BC-loop (Figure 3; Appendix Figures 2, 4). Regarding the B3 clade, prepandemic sequences exhibited a high predominance of alanine at both position 647 (A647) and 650 (A650). In the aftermath of 2020, those residues underwent a substantial replacement by threonine at both positions (T647 and T650), which subsequently became predominant in postpandemic B3 sequences. In addition, within the DE-loop, position 695 exchange of amino acids before and after the pandemic (from S695 to N695) also indicates antigenic drift in this loop (Figure 3; Appendix Figures 3, 4).

Neurovirulent Epitopes

We further investigated the genetic diversity of the recently identified neurovirulence-associated markers within the *VP1* gene (I553L, D554N, A650T, and K835E) (Table 4; Appendix Figure 4) (*9*). In the context of the A2/D clade, we observed no substantial changes among prepandemic, pandemic, and postpandemic periods; we observed neurovirulent amino acid changes at L553 and E835 and a glutamic acid at position 554 predominantly identified, in contrast to position 650, which was described previously as changing from a valine to an isoleucine (Table 4). With regard to the B3 clade, L553 was only identified in 2014, albeit in 1 sequence, whereas E554 was only identified in 2023–2024 in a shift from D to E. As described previously, we observed an apparent change to the neurovirulent threonine at position 650 (T650). In addition to A2/D, the neurovirulent glutamic acid at position 835 (E835) was detected throughout the decade (Table 4).

Discussion

This study offers a comprehensive overview of the circulation of EV-D68 across Europe over a decade, emphasizing its prevalence, seasonality, and evolution. Our findings underscore the persistent adaptation and resurgence of EV-D68 in the postpandemic era.

Our analysis revealed a biennial seasonal pattern of EV-D68 activity and a pronounced prevalence during even years. That pattern is consistent with the findings of previous studies that have documented similar biennial trends in North America (*42*) and Europe (*3*,*33*,*36*,*38*). The interruption of the pattern in 2020 corroborates findings from other investigations that reported a reduced circulation of respiratory pathogens during the COVID-19 pandemic because of the implementation of preventive measures against SARS-CoV-2 (*43*). The resurgence of EV-D68 in 2021 and the subsequent peaks in 2022 and 2024 lend further support to the hypothesis that relaxing public health restrictions led to the reestablishment of EV-D68 transmission chains. Whether transmission reverts to a biennial cycle and changes in genetic diversity remain will require continued surveillance. Moreover, the predominance of EV-D68–related respiratory infections, especially in children, is cause for concern, particularly in the context of AFM. Although initial epidemiologic studies indicated a temporal association between

Table 2. Age groups of case-patients available from study of circulation patterns, genetic diversity, and public health implications of enterovirus D68 circulation, Europe, 2014–2024*

	No. (%)			
Age group, y	2014	2015–2017	2018–2023	2024
<1	120 (**30.85**)	103 (**32.29**)	259 (21.48)	22 (4.37)
1–5	135 (**34.70**)	143 (**44.83**)	569 (**47.18**)	86 (17.10)
6–15	56 (14.40)	35 (10.97)	154 (12.77)	54 (10.74)
>15	78 (20.05)	38 (11.91)	224 (18.57)	341 (**67.79**)

*Bold indicates most affected populations.

EV-D68 outbreaks and AFM cases, subsequent neuropathological evidence demonstrating EV-D68 within anterior horn motor neurons has directly supported a causal relationship (*2*,*44*,*45*).

The high prevalence of EV-D68 in the 2024 season in some countries in Europe (20.6%) contrasts with earlier reports from the 2014 outbreak in Europe and United States, in which prevalence reached ≈9%–12% (*19*,*37*). That observation underscores the potential for variations in outbreak magnitude, which might be influenced by factors such as population immunity, viral evolution, public health interventions, and enhanced surveillance systems, particularly after the COVID-19 pandemic, which could have improved the detection of several respiratory viruses, such as EV-D68.

Genetic characterization of EV-D68 specimens revealed some replacements and dynamic genetic drifts in the predominance of subgenogroups B3 and A2/D over time, as has been reported in other regions and with similar yearly trends to this study (*36*,*46*,*47*). The exchange of clades might be associated with antigenic drift and immune selection pressures, which could have also driven the reemergence of A2/D as the dominant clade (82.1%) during 2024 with additional substitutions within the antigenic epitopes, as we observed. Moreover, that exchange could be related to differences in age distribution among B3- and A2/D-related cases, as previously described (*36*). During 2024, according to the available data, the ratio A2/D:B3 exhibited a higher prevalence among adults than in children (Table 2). That phenomenon could be attributed to immune evasion in adults, which is likely caused by changes in antigenic properties caused by mutations in antigenic epitopes, resulting in reduced neutralization by underlying neutralizing antibodies (*36*). Regarding that phenomenon, we observed amino acid changes within the *VP1* gene, particularly in the BC-loop and DE-loop in positions 647, 650 (A2/D and B3), and 695 (B3), which mirror mutations reported during earlier outbreaks (*36*,*47*).

Table 3. Clinical data available from cases in study of circulation patterns, genetic diversity, and public health implications of enterovirus D68 circulation, Europe, 2014–2024*

Symptom	Global no. (%)
Respiratory	657 (91.50)
Gastrointestinal	–
Neurologic	38 (5.29)
Hand, foot, and mouth disease/skin	–
Fever	14 (1.95)
Other	9 (1.25)

*Dash indicates there were no cases in which those symptoms were present.

Those changes could be associated with potential changes in viral fitness, neuropathogenesis, and immune evasion, as previously reported (*9*,*48*), or could represent an adaptive shift influencing receptor-binding properties and host-immune interactions (*49*). The significance of the identified changes, along with the changes seen over time in the BC-loop and DE-loop, require further investigations.

In addition to mutations in the VP1 region, changes outside the antigenic sites, such as the mice-neurovirulent E835 mutation, also deserve attention. E835 has been identified as a key factor in increasing neurotropism in mice, potentially promoting viral replication in motor neurons and enhancing retrograde axonal transport (*9*). In our series, E835 was mostly observed (instead of K835) in A2/D and B3. Also, the L553 mutation has been frequently reported in A2/D-related cases during the study period, which is also suspected to be a neurovirulence-related change in mice. Conversely, the B3 clade appears to have retained the isoleucine variant at this position, which is characterized as nonvirulent (*15*), yet we observed a shift to the neurovirulent threonine at position 650 after 2020. We observed a similar pattern at site 554, where there is a tendency to shift toward glutamic acid (E), another supposedly nonvirulent substitution seen in both the A2/D and B3 clades, although that residue position might also play a role in immune escape (*15*). The presumed neurovirulent genetic markers were identified in some A2/D- and B3-related cases in this study, but no increase in

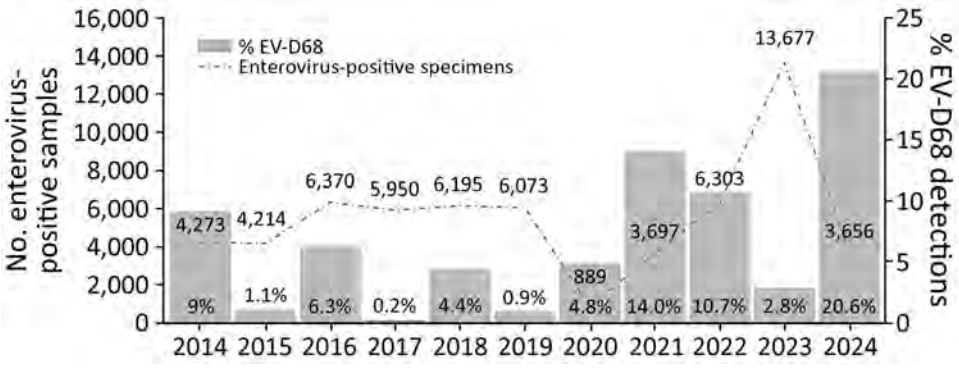

Figure 2. Yearly distribution of enterovirus-positive specimens and percentage of EV-D68–related infections in study of circulation patterns, genetic diversity, and public health implications of EV-D68 circulation, Europe, 2014–2024. EV-D68, enterovirus D68.

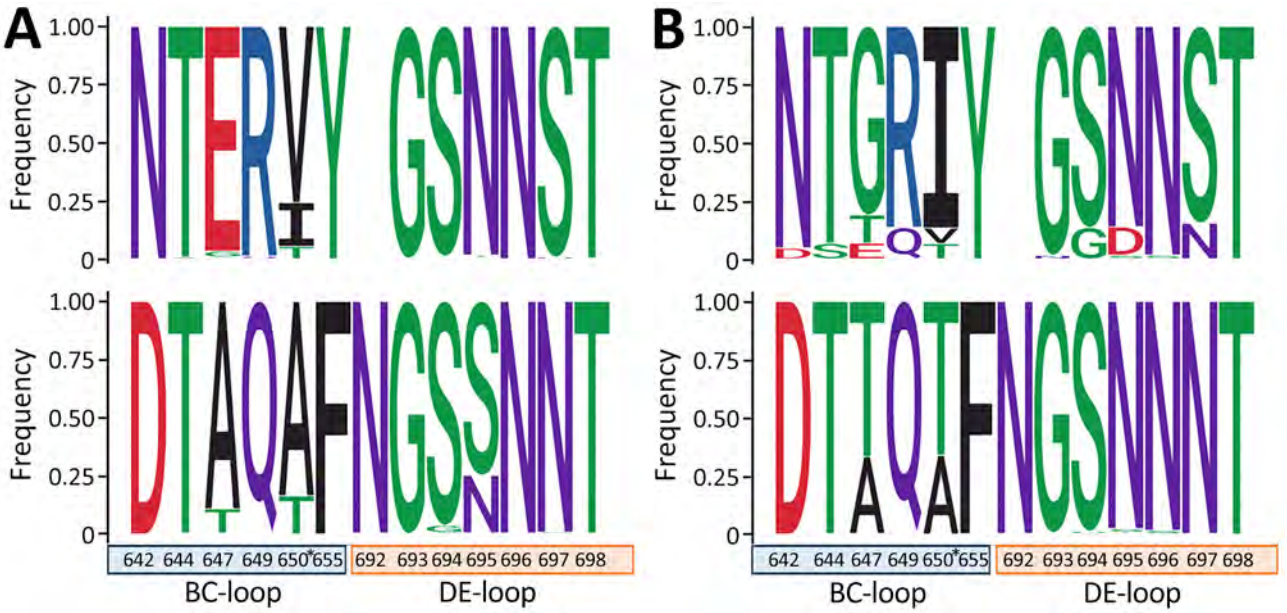

Figure 3. Frequency of amino acid changes within the antigenic epitopes of the viral protein 1 (BC- and DE-loops) in clades A2/D and B3 in study of circulation patterns, genetic diversity, and public health implications of enterovirus D68 circulation, Europe, 2014–2024. A) Amino acid changes in the prepandemic period (2014–2019) in clade A2/D (top) and clade B3 (bottom); B) changes during pandemic and postpandemic periods (2020–2024) in clade A2/D (top) and clade B3 (bottom). Amino acids are colored according to their chemistry. Numbering is related to complete enterovirus D68 genome. Asterisks indicate position 650, also related to neurovirulence in mice. Image was created with WebLogo 3 (*41*).

AFM-related cases was detected (*8*). Further research is required to ascertain whether those mutations or combinations of them are associated with severe clinical outcomes.

Of note, the emergence of SARS-CoV-2 coincided with increased mutational events on EV-D68, suggesting that competition with other respiratory pathogens during the pandemic might have driven such gradual changes (*50*). The circulation of new lineages that might have acquired an evolutionary advantage, possibly through immune evasion mechanisms (changes within antigenic epitopes), could then explain the predominance of the A2/D subgenogroup in 2024. Given the biennial epidemic cycles of EV-D68 and its apparent resurgence after the COVID-19 pandemic, global genomic monitoring is increasingly needed to identify emerging variants that could result in

Table 4. Amino acid changes within mice-neurovirulent-related sites (553, 554, 650, and 835) in clades A2/D and B3 in study of circulation patterns, genetic diversity, and public health implications of enterovirus D68 circulation, Europe, 2014–2024*

			EV-D68 complete genome numeration									
			553	554	650	835			553	554	650	835
			VP1 region						VP1 region			
	No. sequences		1	2	BC† 98	283	No. sequences		1	2	BC† 98	283
Year	(WG)	Clade	I	D	A	K	(WG)	Clade	I	D	A	K
2014	49	A2/D	L	E	I	E	5	B3	L/V	•	•	E
2015	3	A2/D	–	–	I	–	10 (2)	B3	•	•	•	E
2016	3 (1)	A2/D	L	E	I	E	424 (10)	B3	•	•	•	E
2017	5	A2/D	–	–	V	E	–	B3	–	–	–	–
2018	209 (32)	A2/D	L	E	V	E	156 (43)	B3	•	•	•	E
2019	8 (4)	A2/D	L	E	V	E	59 (13)	B3	•	•	T	E
2020	–	A2/D	–	–	–	–	13 (8)	B3	•	•	T	E
2021	15 (3)	A2/D	L	E	I	E	481 (44)	B3	•	•	T	E
2022	6 (3)	A2/D	L	E	I/V	E	150 (65)	B3	•	•	T	E
2023	13 (5)	A2/D	L	E	I	E	25 (12)	B3	•	E	T	E
2024	343 (28)	A2/D	L	E	I	E	75 (9)	B3	•	E	T	E

0%–25% 26%–49% 50%–74% 75%–100%

*Percentages are based on partial (650) or whole (553, 554, and 835) genome sequences. Numbering is related to complete EV-D68 genomes. Dots indicate amino acid is the same as in reference sequence. Dashed line notes start of COVID-19 pandemic period. A, alanine; E, glutamic acid; EV-D68, enterovirus D68; I, isoleucine; I/V, isoleucine/valine; L, leucine; L/V, leucine/valine; T, threonine; WG, whole genome; –, no information on amino acid position.
†Refers to antigenic epitope BC-loop.

higher incidence and increased risk for neurologic complications. Resurgence shows an opportunity for targeted public health interventions, such as enhancing diagnostic capacity during anticipated peaks and promoting preventive measures.

Although this study provides valuable insights and is supported by both existing literature and recent findings, its first limitation is its reliance on laboratory-confirmed cases, which might potentially underestimate the true burden of EV-D68, because milder cases frequently go undiagnosed. In addition, although surveillance data might not be uniformly collected across Europe (and are largely unavailable at that level), the relevance of this study lies in the participation of 50 institutions from 18 countries in Europe. In addition, the limited number of fully genetically characterized cases might fail to capture the full diversity of circulating strains, at least during the 2024 season. Future studies should prioritize expanding genomic surveillance and integrating serologic data to better understand the effects of EV-D68 in both community and hospital populations, in relation to population-level immunity against this virus.

In conclusion, the reemergence of EV-D68 after the COVID-19 pandemic and its genetic evolution highlight current limitations that might pose a substantial public health challenge. An enhanced surveillance system based on real-time genomic monitoring of circulating viruses, coupled with a deeper understanding of the factors driving the evolution of this reemerging pathogen, is crucial to mitigating its impact.

Acknowledgments

We thank the European Society for Clinical Virology for hosting the European Non-Polio Enterovirus Network. We acknowledge all clinicians and technical staff participating in the European enterovirus/poliovirus surveillance programs in all participating laboratories and those who contributed to the collection, testing, and reporting of clinical and virological data presented in this study. We would specifically like to acknowledge Jeroen Cremer for sequencing all EV-D68 strains from the Netherlands and Lieuwe Roorda, Leo Smeets, and Thijs van de Laar for the additional 2024 EV-D68 sequence data from the Netherlands to complete the data collected over the study period.

This research was partially supported by Fondo de Investigación Sanitaria, Ministerio Español de Economía y Competitividad (grant no. FIS PI22/00023) and CIBER–Consorcio Centro de Investigación Biomédica en Red (CIBERINFEC, ISCIII–CIBER de Enfermedades Infecciosas), Instituto de Salud Carlos III, Ministerio de Ciencia e Innovación, and Unión Europea–NextGenerationEU.

During the preparation of this work, the authors used ChatGPT to improve readability and clarity. After using this tool, all authors reviewed and edited the content as needed and took full responsibility for the content of the publication.

About the Author

Dr. Andrés is a postdoctoral researcher at Respiratory Viruses Unit in the Microbiology Department of Hospital Univeristari Vall d'Hebron. Her research interests are the epidemiology and molecular characterization of viruses, especially influenza viruses, enteroviruses, rhinoviruses, and coronaviruses.

References

1. Benschop KS, Albert J, Anton A, Andrés C, Aranzamendi M, Armannsdóttir B, et al. Re-emergence of enterovirus D68 in Europe after easing the COVID-19 lockdown, September 2021. Euro Surveill. 2021;26:2100998. https://doi.org/10.2807/1560-7917.ES.2021.26.45.2100998
2. Simoes MP, Hodcroft EB, Simmonds P, Albert J, Alidjinou EK, Ambert-Balay K, et al. Epidemiological and clinical insights into the enterovirus D68 upsurge in Europe 2021–2022 and emergence of novel B3-derived lineages, ENPEN Multicentre Study. J Infect Dis. 2024;230:e917–28. https://doi.org/10.1093/infdis/jiae154
3. Andrés C, Vila J, Creus-Costa A, Piñana M, González-Sánchez A, Esperalba J, et al. Enterovirus D68 in hospitalized children, Barcelona, Spain, 2014–2021. Emerg Infect Dis. 2022;28:1327–31. https://doi.org/10.3201/eid2807.220264
4. Messacar K, Tyler KL. Enterovirus D68-associated acute flaccid myelitis: rising to the clinical and research challenges. JAMA. 2019;321:831–2. https://doi.org/10.1001/jama.2019.1016
5. Tokarz R, Firth C, Madhi SA, Howie SRC, Wu W, Sall AA, et al. Worldwide emergence of multiple clades of enterovirus 68. J Gen Virol. 2012;93:1952–8. https://doi.org/10.1099/vir.0.043935-0
6. Messacar K, Pretty K, Reno S, Dominguez SR. Continued biennial circulation of enterovirus D68 in Colorado. J Clin Virol. 2019;113:24–6. https://doi.org/10.1016/j.jcv.2019.01.008
7. Andrés C, Vila J, Gimferrer L, Piñana M, Esperalba J, Codina MG, et al. Surveillance of enteroviruses from paediatric patients attended at a tertiary hospital in Catalonia from 2014 to 2017. J Clin Virol. 2019;110:29–35. https://doi.org/10.1016/j.jcv.2018.11.004
8. Helfferich J, Calvo C, Alpeter E, Andrés C, Antón A, Aubart M, et al. Acute flaccid myelitis in Europe between 2016 and 2023: indicating the need for better registration. Euro Surveill. 2025;30:2400579. https://doi.org/10.2807/1560-7917.ES.2025.30.21.2400579
9. Leser JS, Frost JL, Wilson CJ, Rudy MJ, Clarke P, Tyler KL. VP1 is the primary determinant of neuropathogenesis in a

mouse model of enterovirus D68 acute flaccid myelitis. J Virol. 2024;98:e0039724. https://doi.org/10.1128/jvi.00397-24
10. Pons-Salort M, Lambert B, Kamau E, Pebody R, Harvala H, Simmonds P, et al. Changes in transmission of enterovirus D68 (EV-D68) in England inferred from seroprevalence data. eLife. 2023;12:12. https://doi.org/10.7554/eLife.76609
11. Kamau E, Harvala H, Blomqvist S, Nguyen D, Horby P, Pebody R, et al. Increase in enterovirus D68 infections in young children, United Kingdom, 2006–2016. Emerg Infect Dis. 2019;25:1200–3. https://doi.org/10.3201/eid2506.181759
12. Karelehto E, Koen G, Benschop K, van der Klis F, Pajkrt D, Wolthers K. Enterovirus D68 serosurvey: evidence for endemic circulation in the Netherlands, 2006 to 2016. Euro Surveill. 2019;24:1800671. https://doi.org/10.2807/1560-7917.ES.2019.24.35.1800671
13. Poelman R, Schuffenecker I, Van Leer-Buter C, Josset L, Niesters HG, Lina B; ESCV-ECDC EV-D68 study group. European surveillance for enterovirus D68 during the emerging North-American outbreak in 2014. J Clin Virol. 2015;71:1–9. https://doi.org/10.1016/j.jcv.2015.07.296
14. de Schrijver S, Vanhulle E, Ingenbleek A, Alexakis L, Johannesen CK, Broberg EK, et al.; ENPEN Study Collaborators. Epidemiological and clinical insights into enterovirus circulation in Europe, 2018–2023: a multi-center retrospective surveillance study. J Infect Dis. 2025;232:e104–15. https://doi.org/10.1093/infdis/jiaf179
15. Hirvonen A, Johannesen CK, Simmonds P, Fischer TK, Harvala H, Benschop KSM, et al.; ENPEN study collaborators. Sustained circulation of enterovirus D68 in Europe in 2023 and the continued evolution of enterovirus D68 B3-lineages associated with distinct amino acid substitutions in VP1 protein. J Clin Virol. 2025;178:105785. https://doi.org/10.1016/j.jcv.2025.105785
16. Bubba L, Broberg EK, Jasir A, Simmonds P, Harvala H, Redlberger-Fritz M, et al.; Enterovirus study collaborators. Circulation of non-polio enteroviruses in 24 EU and EEA countries between 2015 and 2017: a retrospective surveillance study. Lancet Infect Dis. 2020;20:350–61. https://doi.org/10.1016/S1473-3099(19)30566-3
17. Harvala H, Benschop KSM, Berginc N, Midgley S, Wolthers K, Simmonds P, et al.; On Behalf Of The Enpen Hospital-Based Surveillance Network. European Non-Polio Enterovirus Network: introduction of hospital-based surveillance network to understand the true disease burden of non-polio enterovirus and parechovirus infections in Europe. Microorganisms. 2021;9:1827. https://doi.org/10.3390/microorganisms9091827
18. Nix WA, Oberste MS, Pallansch MA. Sensitive, seminested PCR amplification of VP1 sequences for direct identification of all enterovirus serotypes from original clinical specimens. J Clin Microbiol. 2006;44:2698–704. https://doi.org/10.1128/JCM.00542-06
19. Midgley CM, Watson JT, Nix WA, Curns AT, Rogers SL, Brown BA, et al.; EV-D68 Working Group. Severe respiratory illness associated with a nationwide outbreak of enterovirus D68 in the USA (2014): a descriptive epidemiological investigation. Lancet Respir Med. 2015;3:879–87. https://doi.org/10.1016/S2213-2600(15)00335-5
20. Schuffenecker I, Mirand A, Josset L, Henquell C, Hecquet D, Pilorgé L, et al. Epidemiological and clinical characteristics of patients infected with enterovirus D68, France, July to December 2014. Euro Surveill. 2016;21. https://doi.org/10.2807/1560-7917.ES.2016.21.19.30226
21. Keeren K, Böttcher S, Diedrich S. Enterovirus Surveillance (EVSurv) in Germany. Microorganisms. 2021;9:2005. https://doi.org/10.3390/microorganisms9102005
22. Diedrich S, Driesel G, Schreier E. Sequence comparison of echovirus type 30 isolates to other enteroviruses in the 5′ noncoding region. J Med Virol. 1995;46:148–52. https://doi.org/10.1002/jmv.1890460212
23. Dierssen U, Rehren F, Henke-Gendo C, Harste G, Heim A. Rapid routine detection of enterovirus RNA in cerebrospinal fluid by a one-step real-time RT-PCR assay. J Clin Virol. 2008;42:58–64. https://doi.org/10.1016/j.jcv.2007.11.016
24. Bragstad K, Jakobsen K, Rojahn AE, Skram MK, Vainio K, Holberg-Petersen M, et al. High frequency of enterovirus D68 in children hospitalised with respiratory illness in Norway, autumn 2014. Influenza Other Respir Viruses. 2015;9:59–63. https://doi.org/10.1111/irv.12300
25. Oberste MS, Maher K, Kilpatrick DR, Flemister MR, Brown BA, Pallansch MA. Typing of human enteroviruses by partial sequencing of VP1. J Clin Microbiol. 1999;37:1288–93. https://doi.org/10.1128/JCM.37.5.1288-1293.1999
26. Oberste MS, Maher K, Kilpatrick DR, Pallansch MA. Molecular evolution of the human enteroviruses: correlation of serotype with VP1 sequence and application to picornavirus classification. J Virol. 1999;73:1941–8. https://doi.org/10.1128/JVI.73.3.1941-1948.1999
27. Piralla A, Girello A, Grignani M, Gozalo-Margüello M, Marchi A, Marseglia G, et al. Phylogenetic characterization of enterovirus 68 strains in patients with respiratory syndromes in Italy. J Med Virol. 2014;86:1590–3. https://doi.org/10.1002/jmv.23821
28. Piralla A, Girello A, Premoli M, Baldanti F. A new real-time reverse transcription-PCR assay for detection of human enterovirus 68 in respiratory samples. J Clin Microbiol. 2015;53:1725–6. https://doi.org/10.1128/JCM.03691-14
29. Benschop K, Molenkamp R, van der Ham A, Wolthers K, Beld M. Rapid detection of human parechoviruses in clinical samples by real-time PCR. J Clin Virol. 2008;41:69–74. https://doi.org/10.1016/j.jcv.2007.10.004
30. Jaramillo-Gutierrez G, Benschop KS, Claas EC, de Jong AS, van Loon AM, Pas SD, et al. September through October 2010 multi-centre study in the Netherlands examining laboratory ability to detect enterovirus 68, an emerging respiratory pathogen. J Virol Methods. 2013;190:53–62. https://doi.org/10.1016/j.jviromet.2013.02.010
31. Hayes A, Nguyen D, Andersson M, Antón A, Bailly JL, Beard S, et al. A European multicentre evaluation of detection and typing methods for human enteroviruses and parechoviruses using RNA transcripts. J Med Virol. 2020;92:1065–74. https://doi.org/10.1002/jmv.25659
32. Cabrerizo M, Echevarria JE, González I, de Miguel T, Trallero G. Molecular epidemiological study of HEV-B enteroviruses involved in the increase in meningitis cases occurred in Spain during 2006. J Med Virol. 2008;80:1018–24. https://doi.org/10.1002/jmv.21197
33. González-Sanz R, Taravillo I, Reina J, Navascués A, Moreno-Docón A, Aranzamendi M, et al. Enterovirus D68-associated respiratory and neurological illness in Spain, 2014–2018. Emerg Microbes Infect. 2019;8:1438–44. https://doi.org/10.1080/22221751.2019.1668243
34. Harvala H, Jasir A, Penttinen P, Pastore Celentano L, Greco D, Broberg E. Surveillance and laboratory detection for non-polio enteroviruses in the European Union/European Economic Area, 2016. Euro Surveill. 2017;22:16-00807. https://doi.org/10.2807/1560-7917.ES.2017.22.45.16-00807

35. Kroneman A, Vennema H, Deforche K, v d Avoort H, Peñaranda S, Oberste MS, et al. An automated genotyping tool for enteroviruses and noroviruses. J Clin Virol. 2011;51:121–5. https://doi.org/10.1016/j.jcv.2011.03.006
36. Hodcroft EB, Dyrdak R, Andrés C, Egli A, Reist J, García Martínez de Artola D, et al. Evolution, geographic spreading, and demographic distribution of enterovirus D68. PLoS Pathog. 2022;18:e1010515. https://doi.org/10.1371/journal.ppat.1010515
37. Bal A, Sabatier M, Wirth T, Coste-Burel M, Lazrek M, Stefic K, et al. Emergence of enterovirus D68 clade D1, France, August to November 2018. Euro Surveill. 2019; 24:1800699. https://doi.org/10.2807/1560-7917.ES.2019.24.3.1800699
38. Pellegrinelli L, Giardina F, Lunghi G, Uceda Renteria SC, Greco L, Fratini A, et al. Emergence of divergent enterovirus (EV) D68 sub-clade D1 strains, northern Italy, September to October 2018. Euro Surveill. 2019;24:1900090. https://doi.org/10.2807/1560-7917.ES.2018.24.7.1900090
39. Kalyaanamoorthy S, Minh BQ, Wong TKF, von Haeseler A, Jermiin LS. ModelFinder: fast model selection for accurate phylogenetic estimates. Nat Methods. 2017;14:587–9. https://doi.org/10.1038/nmeth.4285
40. Tamura K, Peterson D, Peterson N, Stecher G, Nei M, Kumar S. MEGA5: molecular evolutionary genetics analysis using maximum likelihood, evolutionary distance, and maximum parsimony methods. Mol Biol Evol. 2011;28:2731–9. https://doi.org/10.1093/molbev/msr121
41. Crooks GE, Hon G, Chandonia JM, Brenner SE. WebLogo: a sequence logo generator. Genome Res. 2004;14:1188–90. https://doi.org/10.1101/gr.849004
42. Messacar K, Abzug MJ, Dominguez SR. The emergence of enterovirus-D68. Microbiol Spectr. 2016;4:4.3.37. https://doi.org/10.1128/microbiolspec.EI10-0018-2016
43. Britton PN, Hu N, Saravanos G, Shrapnel J, Davis J, Snelling T, et al. COVID-19 public health measures and respiratory syncytial virus. Lancet Child Adolesc Health. 2020;4:e42–3. https://doi.org/10.1016/S2352-4642(20)30307-2
44. Messacar K, Asturias EJ, Hixon AM, Van Leer-Buter C, Niesters HGM, Tyler KL, et al. Enterovirus D68 and acute flaccid myelitis—evaluating the evidence for causality. Lancet Infect Dis. 2018;18:e239–47. https://doi.org/10.1016/S1473-3099(18)30094-X
45. Vogt MR, Wright PF, Hickey WF, De Buysscher T, Boyd KL, Crowe JE Jr. Enterovirus D68 in the anterior horn cells of a child with acute flaccid myelitis. N Engl J Med. 2022;386:2059–60. https://doi.org/10.1056/NEJMc2118155
46. Wang H, Diaz A, Moyer K, Mele-Casas M, Ara-Montojo MF, Torrus I, et al. Molecular and clinical comparison of enterovirus D68 outbreaks among hospitalized children, Ohio, USA, 2014 and 2018. Emerg Infect Dis. 2019;25:2055–63. https://doi.org/10.3201/eid2511.190973
47. Shi Y, Liu Y, Wu Y, Hu S, Sun B. Molecular epidemiology and recombination of enterovirus D68 in China. Infect Genet Evol. 2023;115:105512. https://doi.org/10.1016/j.meegid.2023.105512
48. Brown DM, Hixon AM, Oldfield LM, Zhang Y, Novotny M, Wang W, et al. Contemporary circulating enterovirus D68 strains have acquired the capacity for viral entry and replication in human neuronal cells. MBio. 2018;9:e01954-18. https://doi.org/10.1128/mBio.01954-18
49. Fall A, Abdullah O, Han L, Norton JM, Gallagher N, Forman M, et al. Enterovirus D68: genomic and clinical comparison of 2 seasons of increased viral circulation and discrepant incidence of acute flaccid myelitis—Maryland, USA. Open Forum Infect Dis. 2024;11:ofae656. https://doi.org/10.1093/ofid/ofae656
50. Dhanasekaran V, Sullivan S, Edwards KM, Xie R, Khvorov A, Valkenburg SA, et al. Human seasonal influenza under COVID-19 and the potential consequences of influenza lineage elimination. Nat Commun. 2022;13:1721. https://doi.org/10.1038/s41467-022-29402-5

Address for correspondence: Cristina Andrés, Respiratory Viruses Unit—Virology Section, Microbiology Department, Hospital Universitari Vall d'Hebron, Passeig Vall d'Hebron 119-129, 08035 Barcelona, Spain; email: cristina.andresverges@vallhebron.cat

Enhanced Detection of *Coccidioides* spp. Fungi from Environmental Samples Using Droplet Digital PCR

Jessica Paulette Segovia-Mota, Ricardo Eaton-González, Jimena Carrillo-Tripp, Meritxell Riquelme

Coccidioidomycosis (Valley fever), caused by *Coccidioides* spp. fungi, is a reemerging, neglected fungal disease endemic to arid and semiarid regions of the Americas. Environmental detection remains challenging because of spatial heterogeneity, seasonal variability, low DNA abundance, PCR inhibitors, and lack of standardized methods. We conducted environmental surveillance in Baja California, Mexico, an understudied region near the US–Mexico border, by collecting 74 soil samples from active rodent burrows across 5 locations. We evaluated droplet digital PCR (ddPCR) for *Coccidioides* detection and compared ddPCR with nested PCR targeting the internal transcribed spacer 1 region. ddPCR demonstrated greater sensitivity, detecting *Coccidioides* spp. DNA at all sampling sites, whereas nested PCR detected *Coccidioides* spp. DNA from only 1 site. Although additional work is required to rigorously quantify sensitivity and specificity, ddPCR could help identify *Coccidioides* environmental hotspots, thus enabling public health interventions, such as warning communities of areas that pose higher risk for infection.

Coccidioidomycosis, commonly known as Valley fever, has been increasingly reported across North, South, and Central America, pointing to its reemergence as a public health concern (*1*). Coccidioidomycosis is caused by 2 ascomycetous fungal species belonging to the genus *Coccidioides*: *C. immitis* and *C. posadasii* (*2*). *C. immitis* is primarily found in California, USA, whereas *C. posadasii* prevails in southern Arizona, New Mexico, and Texas, USA; parts of Central and South America (*2*–*4*); and several states in Mexico, including Sonora, Nuevo León, Coahuila, and Baja California. *Coccidioides* is considered one of North America's most concerning endemic mycoses (*5*–*7*).

Human *Coccidioides* infection occurs primarily through inhalation of airborne arthroconidia produced during the saprophytic phase (*8*). Spores easily disperse by wind and can remain viable for long periods in arid environments (*2*). Once inhaled, arthroconidia transform into parasitic spherules that, upon maturation, release endospores, which can remain in the lungs or disseminate systemically (*8*,*9*).

Despite high incidence rates of 150,000–350,000 cases annually in the United States (*10*), environmental detection of *Coccidioides* spp. fungi remains limited. Isolation of the fungi from soil is rare because of nontargeted sampling, limited understanding of the fungus' ecologic niche, interference from other microorganisms, and Biosafety Level 3 requirements associated with handling microbes that produce arthroconidia (*10*–*13*). Most environmental isolation attempts, including animal inoculation using soil-derived suspensions, have had low success rates (*7*,*12*).

Direct detection of *Coccidioides* spp. DNA from soil without prior fungal isolation has produced mixed results (*12*). Early studies analyzing 90 soil samples from active rodent burrows in semiarid regions of Baja California, Mexico, Valle de las Palmas (VDP) and San José de la Zorra (SJZ), used nested PCR targeting the internal transcribed spacer (ITS) 2 region (*6*). Although 32 (35.5%) samples tested positive, 13.33% were later confirmed as false-positive by BLAST analysis (*6*), reflecting high ITS2 sequence similarity among fungi and amplification of nontarget taxa. To improve specificity, Vargas-Gastélum et al. (*16*) designed primers targeting the ITS1 region. Using that approach, nested PCR identified *Coccidioides* spp. DNA in 27.5% (11/40) of soil samples, primarily

Author affiliations: Centro de Investigación Científica y Educación Superior de Ensenada (CICESE), Ensenada, Mexico (J.P. Segovia-Mota, J. Carrillo-Tripp, M. Riquelme); Facultad de Ciencias Marinas, Universidad Autónoma de Baja California, Ensenada (R. Eaton-González)

DOI: https://doi.org/10.3201/eid3204.251146

from rodent burrows (*16*). Consistent with previous studies (*14*,*15*,*17*,*18*), researchers observed higher detection rates in deeper rodent burrow soils than in surface samples (*16*), likely reflecting favorable microenvironmental conditions for fungal growth and the potential role of rodents as reservoir hosts (*2*,*9*,*15*,*19*).

A previous study using ELISA further evaluated exposure to *Coccidioides* spp. in wild rodents captured from VDP (*15*). That study detected coccidioidal antibodies in Eastern deer mice (*Peromyscus maniculatus*) and desert woodrats (*Neotoma lepida*) but not in San Diego pocket mice (*Chaetodipus fallax*) or Dulzura kangaroo rats (*Dipodomys simulans*), likely because of limited cross-reactivity of secondary antibodies with Heteromyidae species.

More recently, environmental detection of *Coccidioides* spp. fungi has advanced through development of the CocciEnv quantitative PCR (qPCR)–based assay, which targets a multicopy transposable element and provides high sensitivity and specificity in soil samples (*20*–*22*). Complementary molecular approaches, such as droplet digital PCR (ddPCR), offer additional advantages, including absolute quantification and increased tolerance to PCR inhibitors, enabling detection of low-abundance targets commonly encountered in environmental matrices (*23*). ddPCR partitions each reaction into thousands of droplets, each of which acts as an independent amplification reaction (*24*). Droplets are scored as negative or positive on the basis of target amplification, generating a digital readout from which target concentration is estimated by using Poisson statistics (*25*). That approach enables absolute quantification without the need for standard curves and has been shown to improve sensitivity compared with qPCR in multiple applications. For example, ddPCR outperformed qPCR in the detection of *Aspergillus* spp. fungi in human respiratory samples (*26*) and demonstrated superior sensitivity for detecting *Tilletia controversa* fungi teliospores in soil samples, achieving detection limits ≈100-fold lower than conventional PCR and several-fold lower than real-time PCR (*27*). For *Coccidioides* spp. fungi, ddPCR has previously been used to estimate copy numbers of multicopy transposon elements from DNA extracted from *Coccidioides* spp. isolates (*28*), supporting its potential as a complementary tool to qPCR-based and nested PCR–based assays for environmental surveillance. Considering those advantages, we assessed ddPCR for detecting *Coccidioides* spp. fungi in soils from previously identified *Coccidioides*–positive sites and to screen additional potentially endemic areas of Baja California identified as hotspots for *Coccidioides* spp. fungi in recent species distribution models (*29*).

Methods

Sampling Sites

We selected 5 sampling sites within VDP and SJZ on the basis of previous reports confirming *Coccidioides* spp. detection in soil (*6*,*29*). VDP, located ≈10 km southeast of Tijuana, included 3 sampling sites: Rancho Gilbert (RG), sampled on June 7, 2023, and Rancho Las Golondrinas (RLG) and Rancho Carrizo (RC), both sampled on May 16, 2024. SJZ, situated ≈32 km north of Ensenada, comprised the Community of San José de la Zorra (CSJZ) and Agua Escondida (AE), both sampled on July 2, 2024 (Figure 1).

We collected a total of 76 soil samples: 20 from RG, 12 from RLG, 18 from RC, 14 from CSJZ, and 12 from AE (Appendix 1 Table 1, https://wwwnc.cdc.gov/EID/article/32/4/25-1146-App1.xlsx). We directed sampling to active rodent burrows encountered during ≈2-hour sampling efforts at each site, guided by animal trails and visible evidence of small mammal activity. We used that strategy to maximize the likelihood of targeting ecologically relevant *Coccidioides* spp. microhabitats. We collected mixed soil samples from burrow entrances at a depth of 10–15 cm. We identified active burrows by the absence of cobwebs or vegetation obstructing the entrance and the presence of loose, uncompacted soil, indicating recent use. We collected ≈40 g of soil from each burrow and placed samples in sterile plastic jars. To prevent cross-contamination, we rinsed the sampling spoon with chlorine between sites. We used sterile gloves and face masks during sample handling as precautionary safety measures.

At each site, we recorded data using a standardized form, capturing information on global positioning system coordinates, temperature, wind speed, predominant vegetation (e.g., scrub, chaparral, forest, grassland, unvegetated or bare soil, or riparian), characteristics of the sampling site (e.g., burrow associated with or not associated with a rock or plant), soil texture (coarse, medium, fine), soil compaction (compact or uncompacted), and soil moisture condition (dry, wet, mixed). We also took panoramic site photographs and images of the specific burrow and collected sample.

DNA Extraction from Soil Samples

We used the DNeasy PowerSoil Pro Kit (QIAGEN, https://www.qiagen.com) to extract DNA from 250 mg of soil per extraction, following the manufacturer's protocol. We used the NanoDrop Lite spectrophotometer (Thermo Fisher Scientific, https://www.thermofisher.com) to assess DNA A260/A280

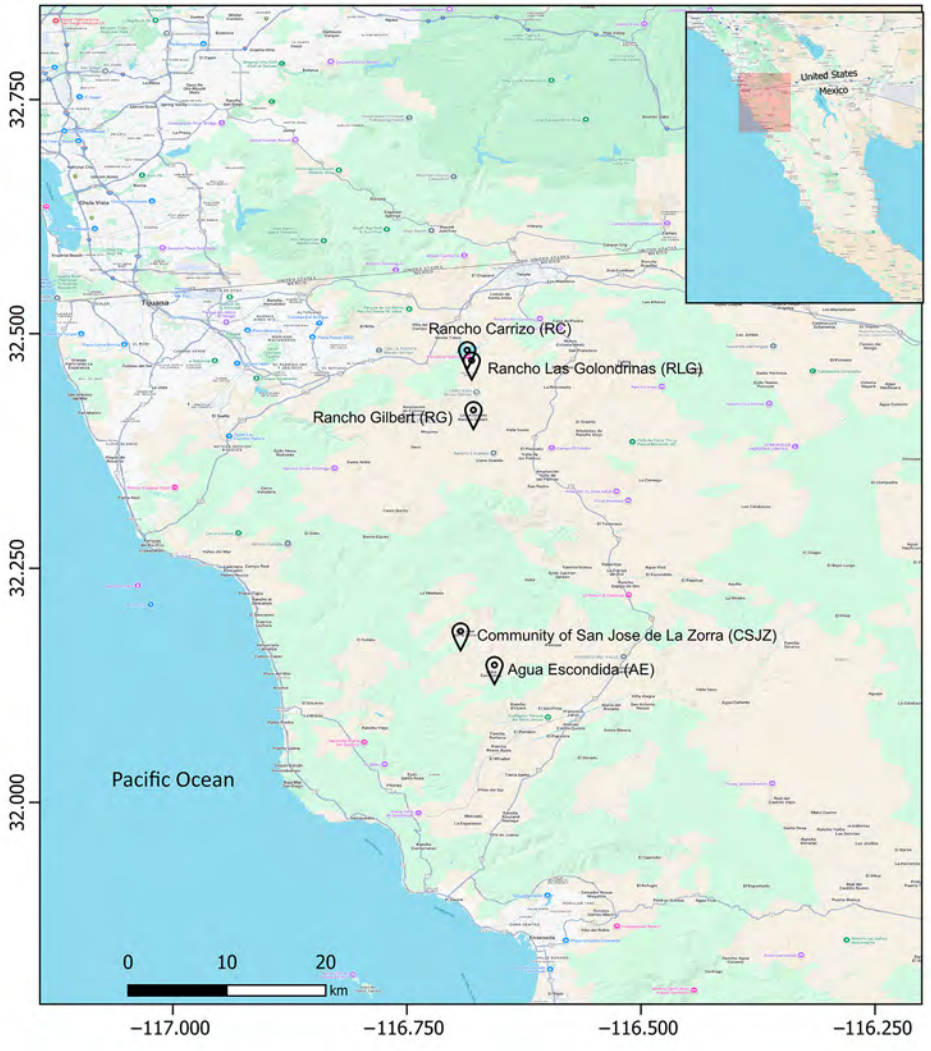

Figure 1. Locations of soil sampling sites from a study of enhanced detection of *Coccidioides* spp. fungi from environmental samples using droplet digital PCR, Baja California, Mexico. Rancho Gilbert was sampled on June 7, 2023; Rancho Las Golondrinas on May 16, 2024; Rancho Carrizo on May 16, 2024; and Community of San José de la Zorra and Agua Escondida on July 2, 2024. Inset shows location of study area at the US–Mexico border.

concentration and purity using 1 µL of sample. We verified DNA integrity by electrophoresis on a 1% agarose gel and normalized all DNA samples to a final concentration of 10 ng/µL.

Detection of *Coccidioides* spp. Fungi by Nested PCR

We used nested PCR to detect *Coccidioides* from DNA extracted from soil samples. The first PCR targeted the ITS1-5.8s–ITS2 region (≈900 bp) using primers NS1 and NLB4 (*14*,*30*). We used 0.48 ng of genomic DNA from *C. posadasii* (courtesy of Dr. Bridget Barker, Institute of Pathogens and Microbiomes, Northern Arizona University, USA) as a positive control and used HPLC-grade water (highly refined Type I ultrapure water used in high-performance liquid chromatography) as a negative control. We confirmed amplified products by electrophoresis on a 1% agarose gel. For the second round of amplification, we used a 1:10 dilution of the first PCR product. For that reaction, we used ITS1CF and ITS1CR primers to target the ITS1 region (≈120 bp) specific for *Coccidioides* spp. (*16*). We analyzed those products by electrophoresis on a 2% agarose gel. We purified positive amplicons by using a QIAquick Gel Extraction Kit (QIAGEN) and submitted amplicons to Eton Bioscience, Inc. (https://www.etonbio.com; San Diego, CA, USA), for sequencing. We manually curated sequencing results by using MEGA version 11.0.13 (https://www.megasoftware.net) and confirmed species identity via BLASTn searches against the National Center for Biotechnology Information nucleotide database (https://blast.ncbi.nlm.nih.gov).

Detection of *Coccidioides* spp. Fungi by ddPCR

We performed ddPCR on a QX200 Droplet Digital PCR system (Bio-Rad Laboratories, https://www.bio-rad.com) after optimizing primer concentrations and annealing temperatures. We adapted the same

primers used in the second nested PCR for ddPCR, following manufacturer guidelines, which recommend avoiding a G at the 5′ end, maintaining a GC content of 50%–60%, ending the 3′ end with a G or C, and avoiding primer dimer formation. Each 21-μL reaction contained 10.5 μL of QX200 ddPCR EvaGreen Supermix (Bio-Rad), 0.126 μL (60 nmol) each of forward (ITS1CF-EVA 5′-AAGTGGCGTCCGGCTGCG-CACCTCCCCCGCGG-3′) and reverse (ITS1CR-EVA 5′-ACGCCGCGCAAGGCGGGCGATCCCCGGC-3′) primers, 9.248 μL of Milli-Q grade water, and 1 μL (10 ng) of template DNA. We included 2 types of negative controls: a no template control (NTC) of HPLC-grade water, and a control of 28.8 ng of *Aspergillus fischeri* DNA as a template (provided by D. Martínez-Soto, CICESE, Ensenada, Mexico). We used 0.048 ng of *C. posadasii* DNA as a template in positive controls. We generated droplets by using a QX200 Droplet Generator (Bio-Rad), transferred droplets to a 96-well plate, sealed with aluminum foil using the PX1 PCR Plate Sealer (Bio-Rad), and processed in a C1000 Touch Thermal Cycler (Bio-Rad). The amplification program consisted of an initial cycle of enzyme activation at 95°C for 10 minutes, followed by 40 cycles of denaturation at 95°C for 30 seconds, annealing/extension at 70°C for 60 seconds, and stabilization at 4°C for 5 minutes, followed by inactivation at 90°C for 5 minutes. After amplification, we read the plate by using the QX200 Droplet Reader (Bio-Rad). We performed droplet analysis by using the QuantaSoft and QuantaSoft Analysis Pro software (Bio-Rad). We manually set the threshold to differentiate positive from negative droplets on the basis of negative controls. We reported the concentration of *Coccidioides* DNA in each sample in copies/μL, calculated from the fraction of positive droplets.

One of the 3 NTCs in the ddPCR run for RG samples had a positive drop above the threshold that corresponded to 0.0663 copies/μL. Another NTC of the 3 included in the ddPCR run for samples RC, RLG, AE, and CSJZ had a positive drop above the threshold that corresponded to 0.09 copies/μL. We determined those values were background noise. For each ddPCR run, we considered samples positive only if they exhibited a concentration ≥2-fold higher than the maximum background value observed in the NTCs.

Results

DNA Yield and Purity

The average A260/A280 ratio across all samples was 1.69, and DNA purity was consistently <1.8. Although lower than ideal, those values are acceptable for downstream molecular applications like PCR and ddPCR.

Nested PCR Results

Nested PCR detected *Coccidioides* spp. DNA in 5 (6.6%) of 76 soil samples, all from RG, representing 25% (5/20) of samples from that site (Table). Those positive samples (RG1, RG9, RG10, RG19, and RG20) exhibited amplicons within the expected size range of ≈120 bp (Figure 2). Sequencing and BLAST analysis confirmed all positive samples as *C. immitis*. In addition, nested PCR confirmed the positive control used throughout the experiments as *C. posadasii* (Appendix 2 Table 1, https://wwwnc.cdc.gov/EID/article/32/4/25-1146-App2.pdf).

ddPCR Results

In contrast to the nested PCR, the ddPCR identified 30 (39%) of 76 soil samples as *Coccidioides* spp.–positive (Table). For all ddPCR reactions, we successfully generated >10,000 droplets per sample (Figure 3; Appendix 1 Table 2), ensuring sufficient sensitivity and robustness. Among the negative controls used for the RG samples, 2 of the 3 NTC and both *A. fischeri* DNA controls showed no positive droplets (Figure 3). However, 1 NTC (NTC1) produced a single droplet above the fluorescence threshold (Appendix 1 Table 2), likely caused by minor contamination during sample handling. Similarly, we observed isolated single-droplet signals in 2 of the 3 NTCs for the other sample sets (RC, RLG, CSJZ, and AE). On the basis of those findings, we classified samples with only 1 positive droplet as negative. Positive samples ranged from 2 droplets (2.86 copies/20-μL well) to 238 droplets (332.67 copies/20-μL well).

Table. Comparison of nested PCR and ddPCR for detection of *Coccidioides* spp. fungi from environmental samples, Baja California, Mexico*

Location	Collection date	No. samples collected	No. (%) nested PCR–positive	No. (%) ddPCR-positive
Rancho Gilbert	2023 Jun 7	20	5 (25)	16 (80)
Rancho Carrizo	2024 May 16	18	0	5 (27.8)
Rancho Las Golondrinas	2024 May 16	12	0	1 (8.3)
San José de la Zorra	2024 Jul 2	14	0	5 (35.7)
Agua Escondida	2024 Jul 2	12	0	3 (25)
Total		76	5 (6.6)	30 (39.5)

*PCR targeted internal transcribe spacer 1 region of *Coccidioides*. ddPCR, digital droplet PCR.

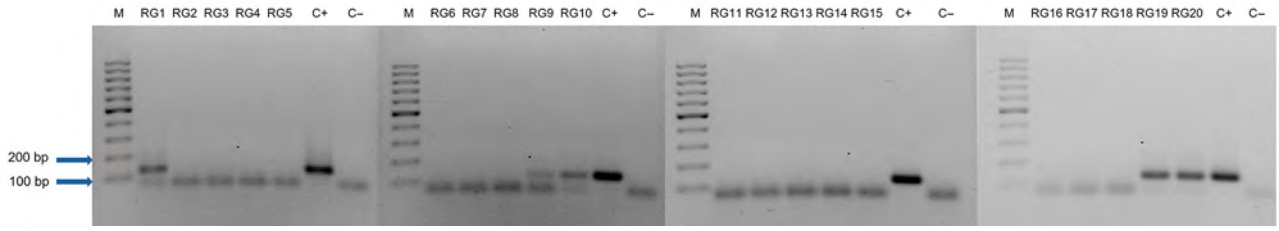

Figure 2. Nested PCR detection of *Coccidioides* spp. fungi DNA from environmental samples using droplet digital PCR, Baja California, Mexico. Agarose gel electrophoresis (2%) stained with ethidium bromide shows the results from nested PCR amplification of *Coccidioides* spp. internal transcribed spacer region from 20 DNA extracted from soil samples collected in RG, Baja California. Positive bands are ≈120 bp. Lanes: M, GeneRuler ladder (100-bp); RG1–RG20, DNA from soil samples; C+, positive control of 0.48 ng of *C. posadasii* DNA used as template; C–, negative control of highly refined Type I ultrapure (HPLC) water. RG, Rancho Gilbert.

Of the 20 samples from RG, 16 showed amplification with multiple positive droplets, indicating the presence of *Coccidioides* DNA (Table; Figure 3, panel A). The 5 samples identified as positive by nested PCR (RG1, RG9, RG10, RG19, and RG20) were also positive by ddPCR, confirming *Coccidioides* DNA. In addition, 11 other samples were also *Coccidioides*-positive by ddPCR, but samples RG4, RG8, RG11, and RG12 were negative by both nested PCR and ddPCR. In total, the ddPCR indicated an 80% detection rate for RG. Among the 18 samples from RC, which were all negative by nested PCR, 5 samples (RC1, RC5, RC8, RC10, and RC18) showed positive droplet amplification by ddPCR, yielding a positivity rate of 27.8% (Table; Figure 3, panel B). For RLG, only 1 (RLG4) of 12 samples tested positive by ddPCR (Figure 3, panel C), resulting in an 8.3% positivity rate. For the locality comprising CSJZ and AE, none of the 26 samples tested positive by nested PCR (Table; Figure 2). However, ddPCR detected *Coccidioides* spp. DNA in 8 of those samples (AE3, AE6, AE8, CSJZ2, CSJZ8, CSJZ10,

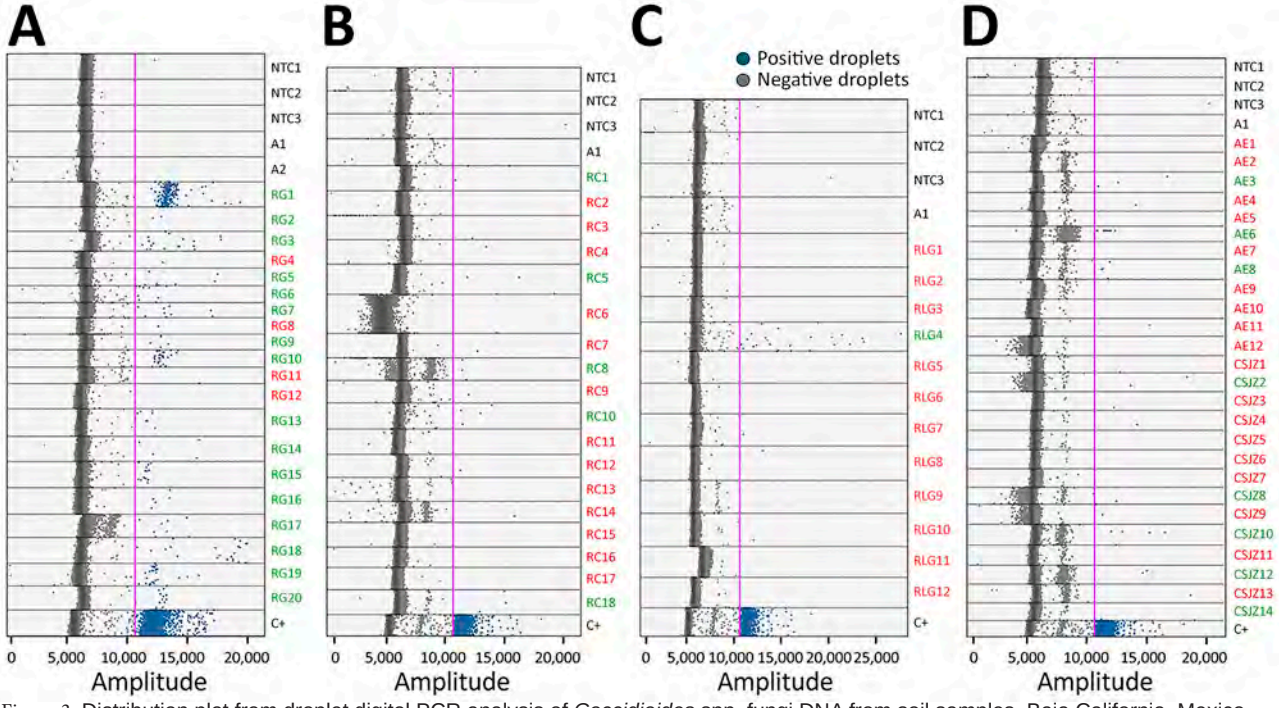

Figure 3. Distribution plot from droplet digital PCR analysis of *Coccidioides* spp. fungi DNA from soil samples, Baja California, Mexico. A) Samples from RG; B) samples from RC; C) samples from RLG; and D) samples from AE and Community of San José de la Zorra (CSJZ). The pink line represents the fluorescence threshold. Red text indicates negative sampling sites; green text indicates positive sampling sites. A1–2, negative templates of 28.8 ng of *Aspergillus fischeri* DNA; AE, Agua Escondida; C+, 0.048 ng of *C. posadasii* DNA used as positive template; CSJZ, Community of San José de la Zorra; NTC1–3, nontemplate controls of highly refined type I ultrapure (HPLC) water; RC, Rancho Carrizo; RG, Rancho Gilbert; RLG, Rancho las Golondrinas.

CSJZ12, and CSJZ14), resulting in an overall positivity rate of 30.7% for that locality (Figure 3, panel D; Figure 4).

Discussion

This study demonstrates that ddPCR is more sensitive than nested PCR for detecting *Coccidioides* spp. in environmental soil samples. ddPCR confirmed all nested PCR–positive samples from VDP and revealed additional positive samples in both VDP and SJZ, including areas previously considered *Coccidioides*-negative. Those findings highlight ddPCR's capacity to detect cryptic environmental reservoirs of *Coccidioides* spp. fungi.

Additional support for the higher sensitivity of ddPCR comes from the amount of *Coccidioides* spp. DNA template required for successful amplification. In contrast to nested PCR, ddPCR reactions required a 10-fold dilution of *Coccidioides* spp. DNA to avoid signal saturation and droplet overloading, indicating that DNA concentrations that are readily accommodated by nested PCR exceed the optimal dynamic range of ddPCR. The necessity for dilution underscores ddPCR's ability to detect and quantify low copy numbers of target DNA.

Our results are not intended to challenge the established CocciEnv qPCR-based method but rather to position ddPCR as a complementary molecular method for detecting *Coccidioides* spp. DNA in soil samples. Together, the 2 approaches highlight the advantage of aligning detection strategies with specific study objectives and suggest that ddPCR could complement existing qPCR-based surveillance tools rather than replace them.

Identification of *C. immitis* in the California–Baja California region is consistent with previous reports documenting the occurrence of both C. *immitis* and *C. posadasii* in northern Mexico (*4*,*16*,*31*–*33*). The coexistence of both species in that region was proposed in 2002 by Fisher et al. (*3*), when they described *C. posadasii* as distinct from the California population of *C. immitis* and documented the geographic distribution of both species across the southwestern United States and northern Mexico (*3*). Therefore, the BLAST results obtained in this study align with previous molecular and ecologic characterizations of *Coccidioides* spp. in this region.

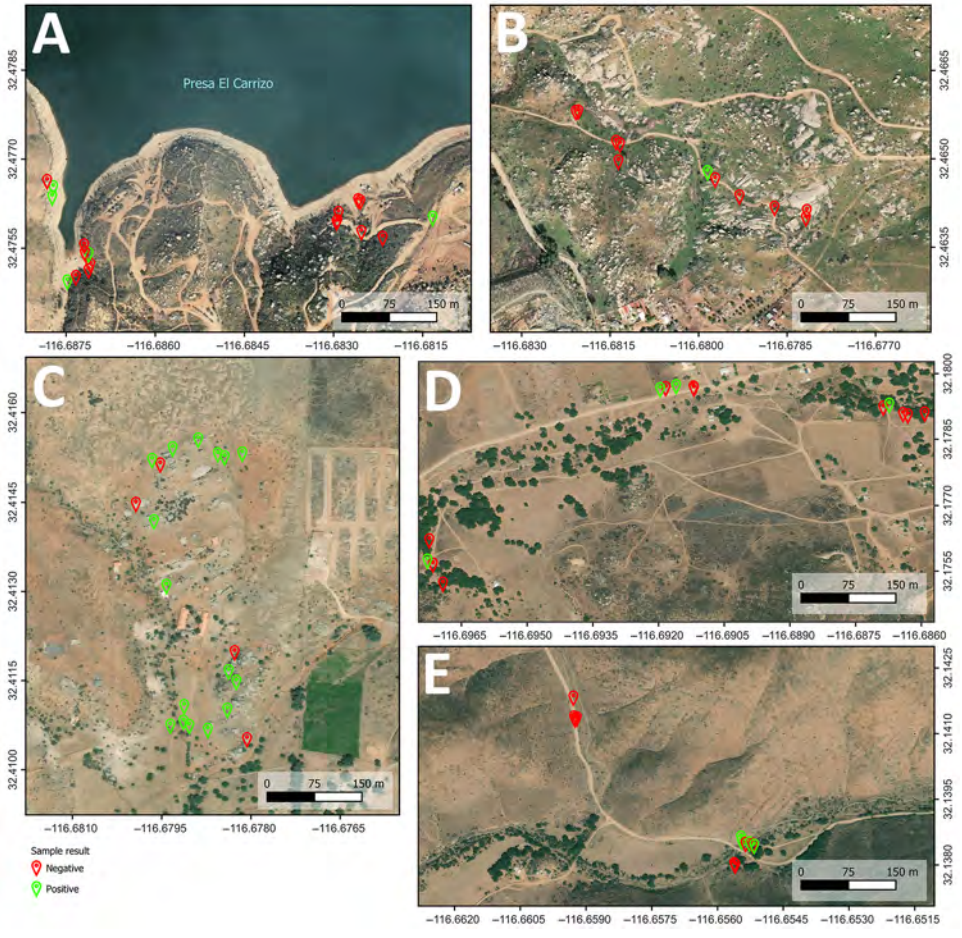

Figure 4. Negative and positive sites for enhanced detection of *Coccidioides* spp. fungi from environmental samples using droplet digital PCR, Baja California, Mexico. A) Rancho Carrizo; B) Rancho las Golondrinas; C) Rancho Gilbert; D) Community of San José de la Zorra; E) Agua Escondida.

The ability of ddPCR to detect low quantities of *Coccidioides* spp. DNA enabled us to expand the known distribution of *Coccidioides* fungi within the 2 locations studied. Nested PCR detected *Coccidioides* DNA in only 5 (6.5%) of 76 samples analyzed (all from VDP), but ddPCR confirmed those samples and detected 11 additional positive samples from VDP plus 19 additional samples from SJZ sampling locations, revealing a broader environmental range.

Previous studies using nested PCR with ITS2-targeting primers reported positivity rates of 74% in VDP and 10% in SJZ, with rodent burrow soil samples contributing to detection (*6*,*15*). Although all samples in our study were collected from active burrows, nested PCR with primers targeting ITS1 yielded lower detection rates of 25% in samples from VDP and none in samples from SJZ. Those discrepancies might reflect differences in sample size, temporal and environmental variability, or differences in primer selection and target regions (Appendix 1 Table 2). In addition, those discrepancies reinforce the need for highly sensitive detection methods, such as ddPCR, for pathogen surveillance in heterogeneous environments and for cryptic human and environmental pathogens, such as *Coccidioides* spp. fungi.

Of note, earlier studies used ITS2F and ITS2R primers (*6*,*15*), but our nested PCR protocol used the ITS1CF and ITS1CR primers developed by Vargas-Gastélum et al. (*16*). That approach enabled successful detection for *Coccidioides* spp. in 11 of 40 samples (*16*), including 9 from burrows, suggesting improved specificity for *Coccidioides* spp. using that primer set.

The ddPCR technique has previously demonstrated high sensitivity for detecting fungal pathogens such as *Pneumocystis*, *Aspergillus*, and *Cryptococcus* spp. fungi in immunocompromised patients in clinical settings (*34*). In this study, we demonstrated that ddPCR can be effectively used to directly extract DNA from soil samples to achieve sensitive and specific detection and quantification of *Coccidioides* spp. fungi in complex environmental matrices. By targeting the ITS1 region with primers optimized for ddPCR performance, our approach enabled reliable detection even when target DNA concentrations were extremely low or when PCR inhibitors (i.e., conditions that commonly limit the performance of conventional and real-time PCRs in environmental samples) were present. Those results highlight the usefulness of ddPCR as a robust tool for environmental surveillance of *Coccidioides* spp. Our findings build upon earlier work that used ddPCR to estimate the copy number of a multicopy transposon element by using DNA extracted from *Coccidioides* spp. isolates, in support of a nested qPCR (*28*). Although that study did not apply ddPCR directly to environmental DNA and encountered limitations related to reaction saturation because of the high copy number of the target (*28*), it provided a proof of concept for using ddPCR in *Coccidioides* molecular analyses. By extending ddPCR applications to soil-derived DNA and optimizing the assay for low-copy targets, our study complements and advances that prior work, demonstrating the feasibility and advantages of ddPCR for direct environmental detection and quantification of *Coccidioides* spp.

Although our ddPCR results showed clear positive results at each site, threshold determination is critical when working with environmental DNA. We manually set a fluorescence threshold to reduce false positives, excluding isolated droplets observed in negative controls. However, because of the complexity of soil matrices and the possibility of droplet misclassification or background fluorescence, sometimes referred to as the significant rainfall effect, a certain degree of false-positive results can be expected. That limitation is especially relevant because ddPCR does not permit sequencing of amplified products, which makes distinguishing true positives from potential artifacts difficult (*35*). To address that problem, we adopted a cautious interpretative approach, excluding samples with only a single droplet above the threshold. That approach minimizes overestimation, but it also raises the possibility of underreporting true positives. Nevertheless, those borderline cases could still represent genuine low-copy *Coccidioides* DNA, emphasizing the need for additional validation studies to refine ddPCR thresholds and improve specificity for environmental applications.

Most samples from AE, RC, RLG, and CSJZ showed low signal intensities, typically consisting of 2–4 positive droplets. Given the lack of technical replication, we cannot exclude the possibility that those represent false-positive samples, and we accordingly interpreted those results with caution. In contrast, sample RLG4 yielded a substantially higher signal of 26 positive droplets, providing stronger support for the presence of *Coccidioides* spp. DNA at the RLG site. That finding suggests that directed sampling with increased replication and sampling effort should be undertaken in RLG during future studies.

From a public health perspective, improved environmental *Coccidioides* detection is urgently needed amid increasing Valley fever incidence and expanding

pathogen distribution, possibly linked to climate change and land use transformations (*22*,*29*,*36*). Our study represents a foundational effort to apply ddPCR for environmental detection of *Coccidioides* spp. The results highlight the method's superior sensitivity over nested PCR and its potential for surveillance of environmental soil samples, particularly in vulnerable regions with similar ecologic characteristics, to uncover endemic areas previously undetected by conventional techniques. The enhanced sensitivity of ddPCR offers opportunities to improve spatial risk mapping, anticipate outbreak potential, and strengthen early detection strategies.

Although ddPCR entails a higher initial investment than conventional qPCR, for both instrumentation and reagents, that cost difference can be mitigated in high-throughput applications. Once equipment is in place, ddPCR becomes increasingly cost-competitive when processing large numbers of samples, particularly because it provides absolute quantification without the need for standard curves and exhibits high analytic sensitivity and run-to-run robustness. Workflows for ddPCR typically require greater technical expertise and slightly longer hands-on and processing times than qPCR. However, when assays are well optimized and performed by trained personnel, the increased sensitivity and quantitative precision of ddPCR can offset those costs by reducing the need for repeat testing and confirmatory analyses. Taken together, those features suggest that ddPCR represents a valuable and competitive option for large-scale environmental surveillance and diagnostic applications. Given its analytic robustness and sensitivity, ddPCR also has the potential to become a reference methodology in specialized clinical and environmental diagnostic laboratories, particularly for pathogens with low DNA abundance such as *Coccidioides*.

Although we created the distribution maps in this study on the basis of results from single ddPCR runs, those maps should be interpreted more generally as indicating whether a site represents a potential Valley fever hotspot, rather than as definitive or quantitative assessments of presence or absence of *Coccidioides* spp. fungi in each sampled point. As expected for environmental sampling of this organism, specific positive locations can vary across sampling times.

In conclusion, further research on ddPCR for *Coccidioides* detection using larger sample sets, additional molecular markers, and sequencing confirmation will be essential to improving detection accuracy and our understanding of *Coccidioides* spp. ecology in soil environments. Nonetheless, ddPCR could be an additional tool for detecting *Coccidioides* spp. across endemic, emerging, and reemerging regions, providing opportunities for more informed public health interventions, such as identifying high-risk environments, warning communities about areas with elevated exposure risk, and guiding occupational safety measures during soil-disturbing activities.

This article was preprinted at https://doi.org/10.1101/2025.08.10.669480.

Acknowledgments

We thank Ofelia Sastré and Jonatan Aguilar from UABC for technical help during the 2023 sampling and Ofelia Candolfi for providing the DNeasy PowerSoil ProKit from QIAGEN. We thank Dolores Camacho for technical assistance with nested PCR and Karen García, Idalia Montesinos, and Sócrates Avilés (Bio-Rad) for technical assistance with ddPCR.

We are grateful to the Consejo Nacional de Humanidades, Ciencias y Tecnologías (CONAHCYT) of Mexico for providing a scholarship to J.P.S.-M. and for project no. 316602 "Acquisition of equipment for the detection and characterization of environmental microbial agents and their response to climate change in northwestern Mexico," which allowed the purchase of the ddPCR equipment.

The authors declare the use of ChatGPT (OpenAI, https://chatgpt.com) during the preparation of this work to check grammar and improve readability and language of the work. After using this tool, the authors reviewed and edited the content as needed and take full responsibility for the content of the published article.

About the Author

Ms. Segovia-Mota is a biologist at Centro de Investigación Científica y Educación Superior de Ensenada (CICESE), Ensenada, Mexico. Her research interests include pathogenic fungi and their role in ecosystems and their potential effects on human health.

References

1. Kirkland TN, Fierer J. Coccidioidomycosis: a reemerging infectious disease. Emerg Infect Dis. 1996;2:192–9. https://doi.org/10.3201/eid0203.960305
2. Nguyen C, Barker BM, Hoover S, Nix DE, Ampel NM, Frelinger JA, et al. Recent advances in our understanding of the environmental, epidemiological, immunological, and clinical dimensions of coccidioidomycosis. Clin Microbiol Rev. 2013;26:505–25. https://doi.org/10.1128/CMR.00005-13
3. Fisher MC, Koenig GL, White TJ, Taylor JW. Molecular and phenotypic description of *Coccidioides posadasii* sp. nov.,

previously recognized as the non-California population of *Coccidioides immitis*. Mycologia. 2002;94:73–84. https://doi.org/10.1080/15572536.2003.11833250
4. Luna-Isaac JA, Muñiz-Salazar R, Baptista-Rosas RC, Enríquez-Paredes LM, Castañón-Olivares LR, Contreras-Pérez C, et al. Genetic analysis of the endemic fungal pathogens *Coccidioides posadasii* and *Coccidioides immitis* in Mexico. Med Mycol. 2014;52:156–66. https://doi.org/10.1093/mmy/myt005
5. Baptista Rosas RC, Riquelme M. The epidemiology of coccidioidomycosis in Mexico [in Spanish]. Rev Iberoam Micol. 2007;24:100–5. https://doi.org/10.1016/S1130-1406(07)70022-0
6. Baptista-Rosas RC, Catalán-Dibene J, Romero-Olivares AL, Hinojosa A, Cavazos T, Riquelme M. Molecular detection of *Coccidioides* spp. from environmental samples in Baja California: linking Valley fever to soil and climate conditions. Fungal Ecol. 2012;5:177–90. https://doi.org/10.1016/j.funeco.2011.08.004
7. Barker BM, Tabor JA, Shubitz LF, Perrill R, Orbach MJ. Detection and phylogenetic analysis of *Coccidioides posadasii* in Arizona soil samples. Fungal Ecol. 2012;5:163–76. https://doi.org/10.1016/j.funeco.2011.07.010
8. Kolivras KN, Comrie AC. Modeling Valley fever (coccidioidomycosis) incidence on the basis of climate conditions. Int J Biometeorol. 2003;47:87–101. https://doi.org/10.1007/s00484-002-0155-x
9. Taylor JW, Barker BM. The endozoan, small-mammal reservoir hypothesis and the life cycle of *Coccidioides* species. Med Mycol. 2019;57:S16–20. https://doi.org/10.1093/mmy/myy039
10. McCotter OZ, Benedict K, Engelthaler DM, Komatsu K, Lucas KD, Mohle-Boetani JC, et al. Update on the epidemiology of coccidioidomycosis in the United States. Med Mycol. 2019;57:S30–40. https://doi.org/10.1093/mmy/myy095
11. Georg LK, Ajello L, Gordon MA. A selective medium for the isolation of *Coccidioides immitis*. Science. 1951;114:387–9. https://doi.org/10.1126/science.114.2963.387.b
12. Greene DR, Koenig G, Fisher MC, Taylor JW. Soil isolation and molecular identification of *Coccidioides immitis*. Mycologia. 2000;92:406–10. https://doi.org/10.1080/00275514.2000.12061175
13. Baptista-Rosas RC, Hinojosa A, Riquelme M. Ecological niche modeling of *Coccidioides* spp. in western North American deserts. Ann N Y Acad Sci. 2007;1111:35–46. https://doi.org/10.1196/annals.1406.003
14. Baptista-Rosas RC, Riquelme M, Muñiz-Salazar R, Catalán-Dibene J, Zimbrón-Hernández MA, Meza-Ayala A, et al. Seroprevalence of antibodies against *Coccidioides* spp. in patients with initial clinical diagnosis of tuberculosis in Ensenada, Baja California, Mexico [in Spanish]. Enf Inf Microbiol. 2012;32:69–73.
15. Catalán-Dibene J, Johnson SM, Eaton R, Romero-Olivares AL, Baptista-Rosas RC, Pappagianis D, et al. Detection of coccidioidal antibodies in serum of a small rodent community in Baja California, Mexico. Fungal Biol. 2014;118:330–9. https://doi.org/10.1016/j.funbio.2014.01.006
16. Vargas-Gastélum L, Romero-Olivares AL, Escalante AE, Rocha-Olivares A, Brizuela C, Riquelme M. Impact of seasonal changes on fungal diversity of a semi-arid ecosystem revealed by 454 pyrosequencing. FEMS Microbiol Ecol. 2015;91:5. https://doi.org/10.1093/femsec/fiv044
17. Kollath DR, Teixeira MM, Funke A, Miller KJ, Barker BM. Investigating the role of animal burrows on the ecology and distribution of *Coccidioides* spp. in Arizona soils. Mycopathologia. 2020;185:145–59. https://doi.org/10.1007/s11046-019-00391-2
18. Radosevich M, Head J, Couper L, Weaver A, Camponuri S, Montoya L, et al. Characterizing the soil microbial community associated with the fungal pathogen *Coccidioides immitis*. J Fungi (Basel). 2025;11:309. https://doi.org/10.3390/jof11040309
19. Emmons CW, Ashburn LL. The isolation of *Haplosporangium parvum* spp. and *Coccidioides immitis* from wild rodents. Their relationship to coccidioidomycosis. Public Health Rep. 1942;57:1715–27. https://doi.org/10.2307/4584276
20. Bowers JR, Parise KL, Kelley EJ, Lemmer D, Schupp JM, Driebe EM, et al. Direct detection of *Coccidioides* from Arizona soils using CocciENV, a highly sensitive and specific real-time PCR assay. Med Mycol. 2019;57:246–55. https://doi.org/10.1093/mmy/myy007
21. Wagner R, Montoya L, Gao C, Head JR, Remais J, Taylor JW. The air mycobiome is decoupled from the soil mycobiome in the California San Joaquin Valley. Mol Ecol. 2022;31:4962–78. https://doi.org/10.1111/mec.16640
22. Wagner R, Montoya L, Head JR, Campo S, Remais J, Taylor JW. *Coccidioides* undetected in soils from agricultural land and uncorrelated with time or the greater soil fungal community on undeveloped land. PLoS Pathog. 2023;19:e1011391. https://doi.org/10.1371/journal.ppat.1011391
23. Wang D, Wang S, Du X, He Q, Liu Y, Wang Z, et al. ddPCR surpasses classical qPCR technology in quantitating bacteria and fungi in the environment. Mol Ecol Resour. 2022;22:2587–98. https://doi.org/10.1111/1755-0998.13644
24. Bio-Rad Laboratories, Inc. Droplet digital PCR applications guide, bulletin 6407 verB. Hercules (CA): The Laboratories; 2014.
25. Hindson BJ, Ness KD, Masquelier DA, Belgrader P, Heredia NJ, Makarewicz AJ, et al. High-throughput droplet digital PCR system for absolute quantitation of DNA copy number. Anal Chem. 2011;83:8604–10. https://doi.org/10.1021/ac202028g
26. Poh TY, Ali NABM, Chan LLY, Tiew PY, Chotirmall SH. Evaluation of droplet digital polymerase chain reaction (ddPCR) for the absolute quantification of *Aspergillus* species in the human airway. Int J Mol Sci. 2020;21:3043. https://doi.org/10.3390/ijms21093043
27. Liu J, Li C, Muhae-Ud-Din G, Liu T, Chen W, Zhang J, et al. Development of the droplet digital PCR to detect the teliospores of *Tilletia controversa* Kühn in the soil with greatly enhanced sensitivity. Front Microbiol. 2020;11:4. https://doi.org/10.3389/fmicb.2020.00004
28. Chow NA, Griffin DW, Barker BM, Loparev VN, Litvintseva AP. Molecular detection of airborne *Coccidioides* in Tucson, Arizona. Med Mycol. 2016;54:584–92. https://doi.org/10.1093/mmy/myw022
29. Ocampo-Chavira P, Eaton-Gonzalez R, Riquelme M. Of mice and fungi: *Coccidioides* spp. distribution models. J Fungi (Basel). 2020;6:320. https://doi.org/10.3390/jof6040320
30. Martin KJ, Rygiewicz PT. Fungal-specific PCR primers developed for analysis of the ITS region of environmental DNA extracts. BMC Microbiol. 2005;5:28. https://doi.org/10.1186/1471-2180-5-28
31. Castañón-Olivares LR, Güereña-Elizalde D, González-Martínez MR, Licea-Navarro AF, González-González GM, Aroch-Calderón A. Molecular identification of *Coccidioides* isolates from Mexican patients. Ann N Y Acad Sci. 2007;1111:326–35. https://doi.org/10.1196/annals.1406.047

32. Barker BM, Litvintseva AP, Riquelme M, Vargas-Gastélum L. *Coccidioides* ecology and genomics. Med Mycol. 2019;57: S21–9. https://doi.org/10.1093/mmy/myy051
33. Kollath DR, Miller KJ, Barker BM. The mysterious desert dwellers: *Coccidioides immitis* and *Coccidioides posadasii*, causative fungal agents of coccidioidomycosis. Virulence. 2019;10:222–33. https://doi.org/10.1080/21505594.2019.1589363
34. Guo J, Tian W, Lin H, Hu L, Gao X, Xia J, et al. Analytical and clinical validation of multiplex droplet digital PCR assay for detecting pathogenic fungal infection in lungs. Mycology. 2024;15:110–9. https://doi.org/10.1080/21501203.2023.2296941
35. Kiselinova M, Pasternak AO, De Spiegelaere W, Vogelaers D, Berkhout B, Vandekerckhove L. Comparison of droplet digital PCR and seminested real-time PCR for quantification of cell-associated HIV-1 RNA. PLoS One. 2014;9:e85999. https://doi.org/10.1371/journal.pone.0085999
36. Howard MH, Sayes CM, Giesy JP, Li Y. Valley fever under a changing climate in the United States. Environ Int. 2024;193:109066. https://doi.org/10.1016/j.envint. 2024.109066

Address for correspondence: Meritxell Riquelme, Department of Microbiology, Centro de Investigación Científica y de Educación Superior de Ensenada, Ctra. Ensenada-Tijuana No. 3918, Ensenada 22860, Mexico; email: riquelme@cicese.mx

The Public Health Image Library

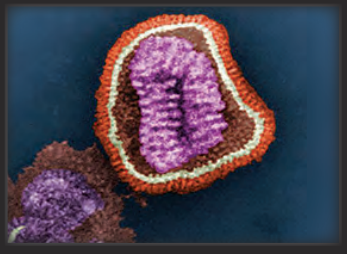
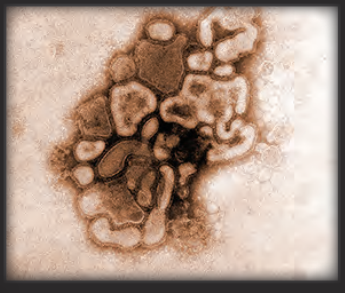
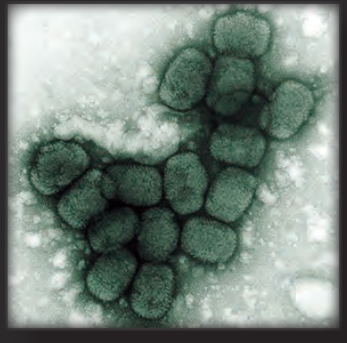



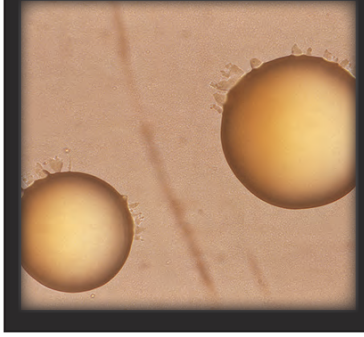
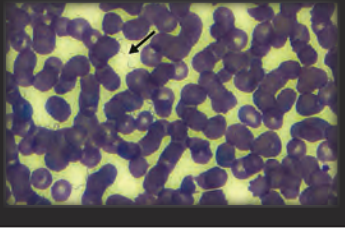

The Public Health Image Library (PHIL), Centers for Disease Control and Prevention, contains thousands of public health–related images, including high-resolution (print quality) photographs, illustrations, and videos.

PHIL collections illustrate current events and articles, supply visual content for health promotion brochures, document the effects of disease, and enhance instructional media.

PHIL images, accessible to PC and Macintosh users, are in the public domain and available without charge.

Visit PHIL at: http://phil.cdc.gov

Evaluation of Effectiveness of Autocidal Gravid Ovitraps for Preventing Zika Virus Infection, Puerto Rico, USA

Zachary J. Madewell, Sandra J. Kiplagat, India Kellum, Matthew J. Lozier, Olga Lorenzi, Janice Perez-Padilla, Freddy A. Medina, Jorge L. Muñoz-Jordán, Laura E. Adams, Gabriela Paz-Bailey, Stephen H. Waterman, Roberto Barrera, Tyler M. Sharp

Aedes aegypti mosquitoes drive arboviral outbreaks in tropical regions. Zika virus (ZIKV), linked to congenital and neurologic complications, caused a major outbreak in Puerto Rico, USA, in 2016, infecting ≈26% of the population. Autocidal gravid ovitraps (AGOs), pesticide-free devices targeting gravid *Ae. aegypti* mosquitoes, have been shown to reduce transmission of another arbovirus, chikungunya. During March–May 2017, we conducted a household-based serosurvey in 4 demographically similar communities in southeastern Puerto Rico, 2 with long-term AGO deployment (≈85% coverage) and 2 without, to assess effects of AGOs on ZIKV transmission. Among 271 participants ≥5 years of age, ZIKV seroprevalence was much lower in intervention than nonintervention communities (9.6% vs. 20.0%). Protective effects were strongest among older adults, larger households (≥4 persons), and persons spending more time at home. Although study design and measurement limitations could limit generalizability of results, our findings support AGOs as sustainable nonchemical tools for reducing ZIKV infections.

Throughout the Americas, dengue virus (DENV), chikungunya virus (CHIKV), and Zika virus (ZIKV), transmitted by *Aedes aegypti* mosquitoes, cause periodic outbreaks (*1*,*2*). Those arboviruses often cocirculate, overwhelming health systems in tropical regions (*1*–*3*). During a 2015–2016 epidemic, ZIKV gained global attention for its links to congenital Zika syndrome, microcephaly, and Guillain-Barré syndrome (*4*). In Puerto Rico, USA, >71,000 suspected cases and >39,000 laboratory-confirmed ZIKV infections were reported during that period (*5*,*6*).

Conventional *Aedes* spp. mosquito control strategies, such as insecticide spraying, habitat removal, and community education, face growing limitations. Insecticide resistance is widespread, spraying is costly and labor-intensive, and sustained community engagement for source reduction is often difficult to maintain (*7*,*8*). Those challenges have spurred interest in alternative tools, such as the autocidal gravid ovitrap (AGO), a pesticide-free device developed by the Centers for Disease Control and Prevention (CDC) to attract and trap gravid female *Ae. aegypti* mosquitoes (*9*). Once inside the AGO, mosquitoes are unable to escape, reducing breeding populations without chemical insecticides. AGOs require infrequent maintenance and have sustained effects when deployed at scale (*8*,*10*).

Long-term community AGO deployment has been shown to reduce *Ae. aegypti* mosquito densities by up to 80% (*11*–*13*). During the 2014–2015 chikungunya outbreak in Puerto Rico, communities using AGOs had lower mosquito densities and 5-fold lower CHIKV infection rates, suggesting that AGOs can meaningfully disrupt arbovirus transmission (*14*). Although CHIKV and ZIKV share a vector, differences in epidemic timing, asymptomatic infection rates, and behavioral responses might influence intervention effectiveness. AGO effectiveness for reducing ZIKV infection risk has not been well studied. Given the possible severe outcomes from ZIKV infection, evaluating the protective effect of AGOs is critical for informing public health strategies.

Although no confirmed ZIKV infections have been reported in Puerto Rico since 2019, competent

Author affiliations: Centers for Disease Control and Prevention, San Juan, Puerto Rico, USA (Z.J. Madewell, S.J. Kiplagat, I. Kellum, M.J. Lozier, O. Lorenzi, J. Perez-Padilla, F.A. Medina, J.-L. Muñoz-Jordán, L.E. Adams, G. Paz-Bailey, S.H. Waterman, R. Barrera, T.M. Sharp); US Public Health Service Commissioned Corps, Rockville, Maryland, USA (L.E. Adams, T.M. Sharp)

DOI: https://doi.org/10.3201/eid3204.251206

mosquito vectors and risk for reintroduction persist. In 2024, Puerto Rico experienced its first major dengue outbreak in >10 years, in which >6,000 confirmed cases and 11 deaths occurred (*15*–*17*). That outbreak underscores the ongoing threat of mosquitoborne viruses, their substantial economic burden, and the need for sustainable control strategies (*18*,*19*). We evaluated the effectiveness of AGOs in reducing ZIKV infection and *Ae. aegypti* mosquito abundance in Puerto Rico by comparing ZIKV seroprevalence and mosquito abundance between communities with and without AGOs.

Methods

Study Setting

We conducted this study in 4 communities already participating in a long-term entomologic trial in the Salinas and Guayama municipalities on Puerto Rico's southeastern coast. In 2015, the population of Salinas was 30,114 and the population of Guayama was 43,700; both had population densities of 434–672 persons per square mile (*13*). Both municipalities have young (median age ≈36 years) populations, ≈15% of whom are ≥65 years of age (*13*). The municipalities also have near equal sex distribution, and >50% of households are below the poverty line (*13*).

Community-level data showed that the 4 study sites were small, semiurban neighborhoods with comparable population sizes, household densities, and occupancy rates (Appendix Table 1, https://wwwnc.cdc.gov/EID/article/32/4/25-1206-App1.pdf). Average household size was 2.6–3.6 persons. Most homes were single-story with patios or gardens, and architecture and climate were similar across sites. All communities had piped water and waste removal services, including sewer or septic coverage depending on location (*9*,*13*,*20*). Those indicators support baseline demographic and infrastructural comparability of intervention and nonintervention sites.

The 2 intervention communities (La Margarita, Villodas) are geographically buffered by vegetation or roads (200–500 meters), reducing mosquito movement from adjacent areas (*20*). The nonintervention communities (Arboleda, La Playa) without AGOs are embedded in larger urban zones. Although not randomized, we selected sites that were demographically and environmentally comparable on the basis of census and field data (*13*,*21*). All 4 sites have had continuous mosquito surveillance since 2012. Prior analyses confirmed that differences in *Ae. aegypti* mosquito abundance between intervention and nonintervention areas emerged only after trap deployment (*14*,*22*). Consistent with prior evaluations, we observed similar female *Ae. aegypti* mosquito abundance during the predeployment baseline period, October–December 2011, in the original paired communities of La Margarita and Villodas (Appendix Figure 1). A CHIKV serosurvey in those sites found no systematic demographic or household-level differences (*13*). Other community-based serosurveys in Puerto Rico have shown consistent ZIKV, DENV, and CHIKV seroprevalence patterns, and variation was driven more by age and household factors than geography (*23*,*24*). Together, those findings confirmed sustained reductions in *Ae. aegypti* mosquitoes in intervention areas and limited underlying differences, supporting the inference that observed ZIKV effects were unlikely to reflect underlying community characteristics (*13*,*20*,*25*).

AGO Intervention

AGOs attract and capture gravid female *Ae. aegypti* mosquitoes (*9*,*10*,*20*). Each household in intervention communities received 3 traps, maintained every 2 months by trained staff. Deployment began during 2011–2013 and ultimately covered ≈85% of households. Previous studies documented that intervention communities experienced marked and sustained reductions in *Ae. aegypti* mosquito abundance compared with nonintervention sites (*21*). Weekly entomologic surveillance using sentinel AGOs provided data on *Ae. aegypti* mosquito abundance, which we linked to participant infection status (*9*,*20*,*26*) (Appendix).

Study Design and Sampling

We conducted a cross-sectional, community-based serosurvey during March–May 2017 to assess ZIKV infection among residents in the 4 communities. We conducted the serosurvey 6–9 months after peak ZIKV transmission in Puerto Rico during August 2016 to capture infections from the outbreak period. The survey overlapped with the seasonal arbovirus activity trough (March–April), when incident infections are uncommon (*17*). Therefore, IgM detection in this survey reflects infections acquired during the 2016 epidemic rather than new infections occurring at the time of sampling. Although the serosurvey was conducted in 2017, analysis and reporting were delayed because of competing public health response priorities and the time required for data harmonization, quality assurance, and linkage to longitudinal entomologic surveillance.

For sampling, we used a stratified random design, assigning a unique identifier to each residential

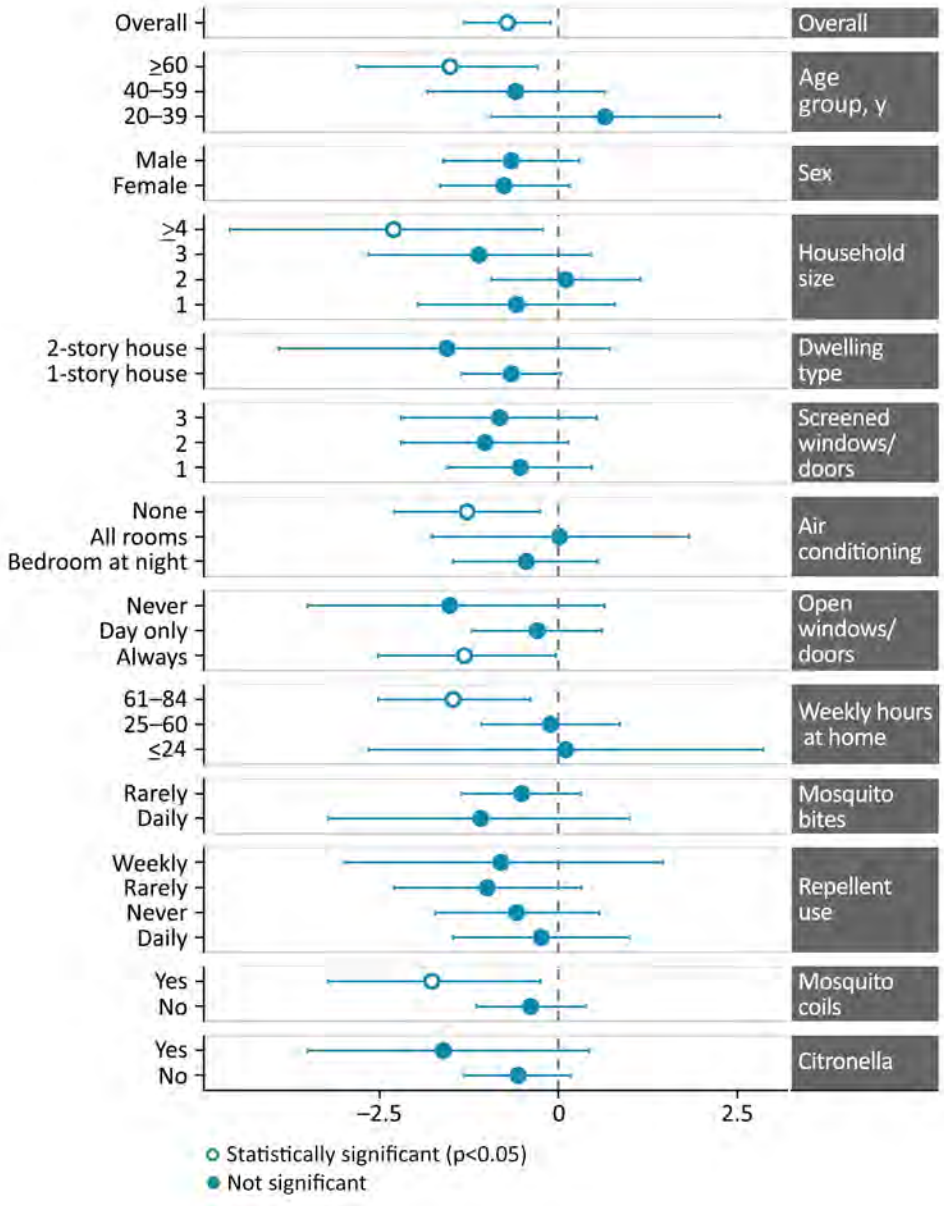

Figure 1. Adjusted prevalence ratios for ZIKV seropositivity by demographic and behavioral characteristic among participants in an evaluation of effectiveness of autocidal gravid ovitraps for preventing Zika virus infection, Puerto Rico, USA. Values left of 0 (corresponding to adjusted prevalence ratio <1) indicate lower ZIKV seroprevalence in intervention communities. log-adjusted prevalence ratios show statistically significant (p<0.05) overall seroprevalence reduction, and specific reductions among older adults (≥60 years of age), participants in larger households (≥4 persons), those without air conditioning, those who always kept windows or doors open, and those spending ≥61 hours/week at home. Use of mosquito coils was also associated with reduced ZIKV seropositivity in intervention areas. Error bars represent 95% CIs. ZIKV, Zika virus.

structure and randomly selecting households to achieve ≈28.5% coverage of the total population. We chose 28.5% coverage to balance statistical power with operational feasibility for household-based venous blood collection. The 28%–30% coverage target was successfully applied in prior arboviral serosurveys in the same study communities and yielded representative samples for demographic and household characteristics (*13*,*25*). Field teams visited each selected household up to 3 times to recruit participants. If a household was vacant or the head-of-household remained unavailable after 3 visits, we randomly replaced that household to meet enrollment targets.

Eligible participants included all residents ≥5 years of age who slept in the selected household for ≥4 of the previous 7 nights. We excluded children <5 years of age because of the difficulty of venous blood collection and ethical considerations of venipuncture in that age group. Although younger children can provide valuable information on recent arbovirus circulation in endemic settings, ZIKV was newly introduced in Puerto Rico in 2015–2016; thus, all age groups were susceptible, and infection risk was broadly distributed. Our primary aim was to assess community-level ZIKV infection prevalence across the general population after the epidemic, which we could accomplish by including participants ≥5

years of age. Participant selection was independent of household AGO presence; in intervention communities, households were neither included nor excluded based on whether AGOs were installed at that specific residence.

We obtained written informed consent from all adult participants. Persons 15–20 years of age provided written assent with parental or guardian permission, and children 5–14 years of age provided verbal assent with written parental or guardian permission. All participants provided blood specimens, regardless of reported symptoms, and completed structured questionnaires on demographic and housing characteristics, mosquito prevention practices, and recent illness history (Appendix). This study was reviewed and approved by the CDC Institutional Review Board (protocol no. 6800).

Laboratory Testing

Field teams collected venous blood specimens and transported specimens on the same day to the CDC Dengue Branch (Division of Vector-Borne Diseases, National Center for Emerging and Zoonotic Infectious Diseases) in San Juan, Puerto Rico. Upon arrival, we centrifuged samples to separate serum, then aliquoted and stored serum at –20°C until testing.

We tested serum specimens for ZIKV IgM by using the CDC Zika IgM antibody capture ELISA (Zika MAC-ELISA), following CDC instructions, and tested for DENV IgM by using the DENV Detect IgM capture ELISA (InBios International, Inc., https://inbios.com), following manufacturer instructions. The Zika MAC-ELISA has high sensitivity and specificity for recent ZIKV infection in dengue-endemic settings, although some cross-reactivity with other flaviviruses, particularly DENV, can occur (*27*,*28*). To minimize misclassification, our primary outcome defined ZIKV infection as ZIKV IgM–positive and DENV IgM–negative results, an approach supported by evaluations of the Zika MAC-ELISA showing that IgM reactivity is strongest for the homotypic virus in dengue-endemic settings (*27*). We also conducted a sensitivity analysis by including participants testing positive for ZIKV IgM, DENV IgM, or both. We did not test for DENV or ZIKV IgG because available assays show substantial cross-reactivity among ZIKV-exposed persons in dengue-endemic settings, limiting the usefulness of those assays for distinguishing prior ZIKV from prior DENV infection (*29*).

Statistical Analysis

We estimated prevalence ratios (PRs) for ZIKV infection by using Poisson regression with robust SEs, adjusting for age, sex, and time spent at home. We explored effect modification across demographic and household subgroups. Sensitivity analyses included broader arbovirus IgM outcomes and models incorporating entomologic data. We conducted all analyses in R version 4.4.2 (The R Project for Statistical Computing, https://www.r-project.org) (Appendix).

Results

Study Population

A total of 330 participants from 242 households completed the serosurvey: 71 households from Arboleda (nonintervention), 79 from La Margarita (intervention), 40 from La Playa (nonintervention), and 52 from Villodas (intervention). We selected households from among 1,228 total residential structures, of which 1,014 (82.6%) were occupied during enumeration (Appendix Figure 2). We prioritized household sampling by structures that participated in a prior 2015–2016 CHIKV serosurvey, then randomly selected replacement households to meet enrollment targets.

Of the 330 enrolled participants, we excluded 55 because of indeterminate serology results: 32 hemolyzed samples, 17 equivocal results, and 6 nonspecific results. We excluded another 4 participants who tested DENV IgM–positive. Thus, we included a total of 271 (82.1%) participants from 208 households: 65 households in Arboleda, 65 in La Margarita, 33 in La Playa, and 45 in Villodas. Among included participants, 136 (50.2%) lived in intervention communities and 135 (49.8%) lived in nonintervention communities. Participants' median age was 59 (IQR 46–69) years; 165 (60.9%) were female and 106 (39.1%) were male (Table 1; Appendix Table 2). Most had lived in their communities for >10 years, and household characteristics were similar between groups.

The secondary sensitivity analysis included an expanded sample of 297 participants with valid ZIKV or DENV IgM results, including those who were DENV IgM–positive. That population had similar demographic and household characteristics to the primary analytic sample (Appendix Table 3).

Baseline Characteristics

Characteristics among participants in intervention and nonintervention communities did not differ substantially, including for age, sex, number of household residents, and duration of residence (Table 1; Appendix Table 2). However, participants in nonintervention communities reported higher levels of mosquito exposure than participants in intervention

communities, including more frequent daily bites (24.6% vs. 8.1%; p = 0.004) and being bitten at home (79.3% vs. 66.9%; p = 0.031). Citronella use was more common in nonintervention areas (31.9% vs. 16.2%; p = 0.004), suggesting greater perceived or actual mosquito abundance or differing perceptions of citronella's effectiveness relative to other control methods. Other prevention behaviors, such as repellent or coil

Table 1. Characteristics of participants in an evaluation of effectiveness of autocidal gravid ovitraps for preventing Zika virus infection, Puerto Rico, USA*

Characteristics	Total, n = 271	Participant data		p value†
		Intervention, n = 136	Nonintervention, n = 135	
Age group, y, n = 267				0.283
<20	18 (6.7)	9 (6.7)	9 (6.8)	
20–39	31 (11.6)	19 (14.2)	12 (9.0)	
40–59	86 (32.2)	47 (35.1)	39 (29.3)	
≥60	132 (49.4)	59 (44.0)	73 (54.9)	
Median age, y (IQR)	59 (46–69)	59 (43–69)	60 (49–69)	0.324
Sex				0.242
F	165 (60.9)	88 (64.7)	77 (57.0)	
M	106 (39.1)	48 (35.3)	58 (43.0)	
Years in community, n = 269				0.244
0–19	104 (38.7)	56 (41.2)	48 (36.1)	
20–39	116 (43.1)	52 (38.2)	64 (48.1)	
≥40	49 (18.2)	28 (20.6)	21 (15.8)	
Median years (IQR) in community, n = 269	24 (12–35)	21 (13–35)	29 (12–34)	0.307
Acute illness with rash, fever, or joint pain since November 2015, n = 270				0.271
Y	58 (21.5)	25 (18.4)	33 (24.6)	
N	212 (78.5)	111 (81.6)	101 (75.4)	
Household characteristics				
No. persons in household				0.516
1	60 (22.1)	30 (22.1)	30 (22.2)	
2	101 (37.3)	47 (34.6)	54 (40.0)	
3	52 (19.2)	25 (18.4)	27 (20.0)	
≥4	58 (21.4)	34 (25.0)	24 (17.8)	
Median no. (IQR) persons in household	2 (2–3)	2 (2–3)	2 (2–3)	0.454
No. children <5 years of age				0.081
0	250 (92.3)	121 (89.0)	129 (95.6)	
1	17 (6.3)	13 (9.6)	4 (3.0)	
2	4 (1.5)	2 (1.5)	2 (1.5)	
Annual household income, USD, n = 238				0.059
<25,000	173 (72.7)	88 (73.3)	85 (72.0)	
26,000–50,000	46 (19.3)	18 (15.0)	28 (23.7)	
51,000–75,000	16 (6.7)	11 (9.2)	5 (4.2)	
>76,000	3 (1.3)	3 (2.5)	0 (0.0)	
Dwelling type				0.393
One-story house	248 (91.5)	122 (89.7)	126 (93.3)	
Two-story house	23 (8.5)	14 (10.3)	9 (6.7)	
No. screened windows/doors, n = 270				0.789
1	139 (51.5)	70 (51.9)	69 (51.1)	
2	87 (32.2)	45 (33.3)	42 (31.1)	
3	44 (16.3)	20 (14.8)	24 (17.8)	
Air conditioning use				0.312
In all rooms	42 (15.5)	18 (13.2)	24 (17.8)	
Only in bedroom at night	140 (51.7)	68 (50.0)	72 (53.3)	
None	89 (32.8)	50 (36.8)	39 (28.9)	
Frequency of open windows/doors				0.496
Always	96 (35.4)	46 (33.8)	50 (37.0)	
Only during the day	116 (42.8)	63 (46.3)	53 (39.3)	
Only at night	7 (2.6)	2 (1.5)	5 (3.7)	
Never	52 (19.2)	25 (18.4)	27 (20.0)	
Mosquito exposure				
Weekly hours at home				0.827
≤24	19 (7.0)	9 (6.6)	10 (7.4)	
25–60	91 (33.6)	48 (35.3)	43 (31.9)	
61–84	161 (59.4)	79 (58.1)	82 (60.7)	
Median weekly hours (IQR) at home	73 (42–84)	72 (42–84)	74 (44–84)	0.536

*Values are no. (%) except as indicated. Intervention communities had autocidal gravid ovitraps installed; nonintervention communities did not. IQR, interquartile range.

†χ^2 test was used for comparison of percentages, Fisher exact test was for comparison of categories with ≥1 value <5, and Mann-Whitney U test was used for medians.

use, were similar across groups. We observed similar patterns in the sensitivity analysis (Appendix Table 3).

ZIKV Seroprevalence

Overall, we detected recent ZIKV infection in 40 of the 271 participants, corresponding to 14.8% seroprevalence. Seroprevalence was much lower (9.6%, 13/136) in intervention communities than nonintervention communities (20.0%, 27/135). Overall crude PR was 0.48 (95% CI 0.26–0.89); after adjusting for confounders, the adjusted PR (aPR) was 0.49 (95% CI 0.27–0.90) (Figure 1; Appendix Table 4).

Lower ZIKV seroprevalence in intervention communities was consistent across most demographic and behavioral subgroups (Figure 1; Appendix Table 4). Among participants ≥60 years of age, seroprevalence was 5.1% in intervention and 23.3% in nonintervention communities (aPR 0.22 [95% CI 0.06–0.75]). We observed similar protective associations among participants in larger households (≥4 residents; aPR 0.10 [95% CI 0.01–0.81]), without air conditioning (aPR 0.28 [95% CI 0.10–0.78]), and those who used mosquito coils (aPR 0.17 [95% CI 0.04–0.78]), although subgroup sizes were small.

Among participants who always kept windows or doors open, those in intervention communities had lower seroprevalence than those in nonintervention communities (6.5% vs. 24.0%; aPR 0.27 [95% CI 0.08–0.97]). Similarly, those spending ≥61 hours/week at home in intervention areas had lower seroprevalence compared with those in nonintervention areas (5.1% vs. 22.0%). In intervention communities, predicted infection probability rose with time at home, peaking at 52 hours per week before declining (Appendix Figure 3). In contrast, infection probability in nonintervention communities increased steadily, peaking at 84 hours.

Among the 297 participants in the expanded sensitivity analysis, 41 (13.8%) tested ZIKV IgM–positive and 5 (1.7%) tested DENV IgM–positive (Appendix Tables 3, 4). Overall arbovirus seroprevalence remained much lower in intervention communities than in nonintervention communities (9.2% vs. 21.5%; aPR 0.44 [95% CI 0.24–0.78]) (Appendix Table 5). The strongest protective associations persisted among older adults (aPR 0.21 [95% CI 0.07–0.62]), participants without air conditioning (aPR 0.25 [95% CI 0.09–0.69]), and those in larger households (aPR 0.10 [95% CI 0.01–0.80]), supporting the robustness of the primary findings.

Perceptions of AGO Effectiveness

Among participants in intervention communities, 105/136 (77.2%) reported a reduction in household mosquito density related to AGOs. Few reported an increase (3.7%, n = 5) or no change (8.1%, n = 11) in mosquito density, and 11.0% (n = 15) were unsure or did not respond to that question.

ZIKV Seropositivity and Acute Febrile Illness

Among ZIKV-seropositive participants, 37.5% (15/40) reported experiencing an acute febrile illness since November 2015, compared with 18.7% (43/231) of ZIKV-seronegative participants (p = 0.014) (Table 2). Seropositive participants more frequently reported common Zika symptoms than seronegative participants, including rash (27.5% vs. 8.7%), fever (30.0% vs. 15.2%), and joint pain (32.5% vs. 16.5%) (p≤0.040). However, care-seeking (20.0% seropositive vs. 12.1% seronegative; p = 0.270) and hospitalization (2.5% seropositive vs. 0.4% seronegative; p = 0.682) were infrequent and did not differ significantly by serostatus.

Entomologic Trends and ZIKV Seropositivity Association

During the ZIKV epidemic, January 2016–May 2017, mean weekly *Ae. aegypti* mosquito abundance per surveillance trap was substantially lower in intervention than nonintervention communities (1.40 [95% CI 1.28–1.52] vs. 9.98 [95% CI 8.98–11.00] mosquitoes per trap) (Figure 2). In Poisson regression models adjusted for age category, sex, and hours spent at home, higher mosquito abundance was positively associated with ZIKV seropositivity. Each additional female mosquito captured per trap-week was associated with a 4% increase in ZIKV seropositivity risk at a 2-week lag (risk ratio [RR] 1.044 [95% CI 1.011–1.077]; p = 0.008) (Table 3). Associations at shorter lag times were similar in magnitude and reached statistical significance at a 1-week lag (RR 1.028 [95% CI 1.003–1.053]; p = 0.026), but not at 0 lag. Formal interaction tests provided no evidence that associations differed by intervention status (Appendix Table 6).

Discussion

In this community-based serosurvey, AGO deployment was associated with lower ZIKV seroprevalence and higher mosquito suppression in intervention communities compared with nonintervention communities. Residents in intervention communities had approximately half the ZIKV seroprevalence of residents in nonintervention communities. However, because we did not conduct a randomized evaluation and seroprevalence was measured 6–9 months after peak transmission, residual confounding and differential misclassification might have contributed

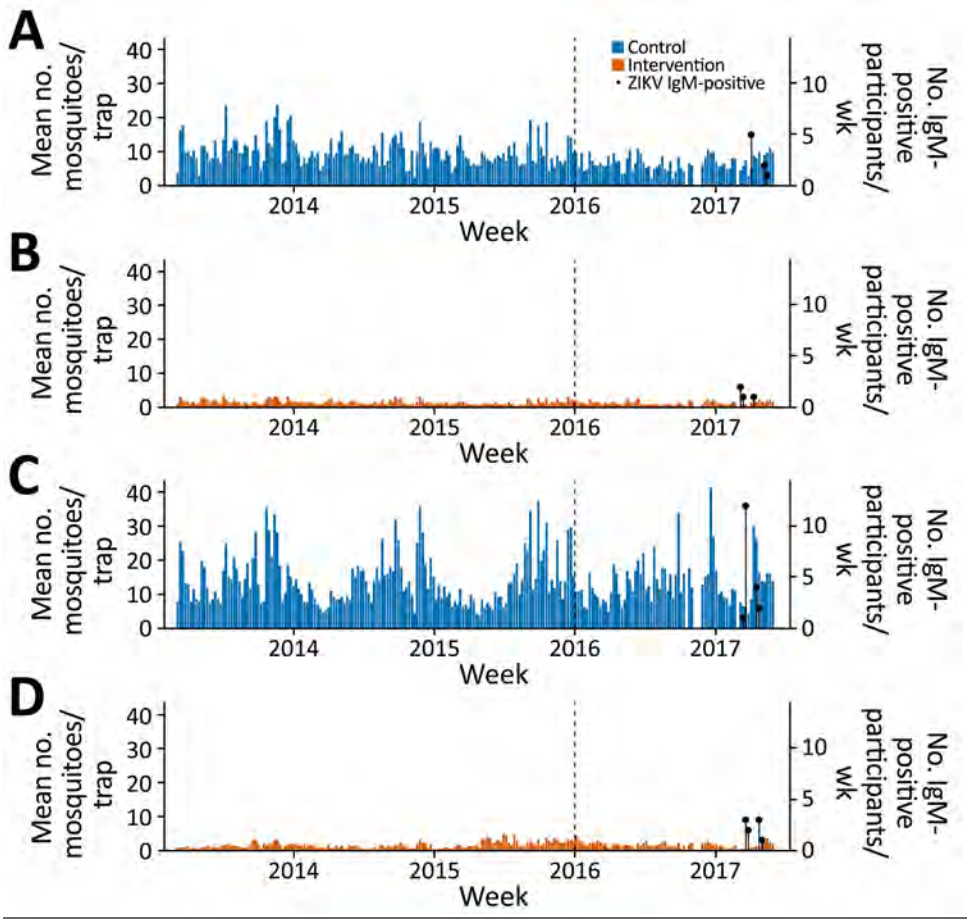

Figure 2. Weekly *Aedes aegypti* mosquito abundance from an evaluation of effectiveness of autocidal gravid ovitraps (AGOs) for preventing Zika virus infection, Puerto Rico, USA. Mean mosquito counts per surveillance trap are shown weekly for each of the 4 study communities: A) Arboleda; B) La Margarita; C) La Playa; D) Villodas. Intervention communities had AGOs. Black lollipop markers indicate the weekly number of ZIKV IgM–positive participants identified during the 2017 postepidemic serosurvey. Dashed vertical lines indicate first known ZIKV case in Puerto Rico on December 31, 2015. Mosquito abundance remained substantially lower in intervention communities throughout the epidemic period, aligning with the reduced ZIKV seroprevalence observed in those areas. Scales for the y-axes differ substantially to underscore patterns but do not permit direct comparisons. ZIKV, Zika virus.

to the observed difference. Associations appeared stronger in some subgroups (e.g., older adults, larger households, and participants spending more time at home), although subgroup estimates were imprecise and should be interpreted cautiously. Overall, these findings are consistent with, but do not establish, a protective association between AGOs and lower peridomestic vector exposure and arboviral infection risk (*30*).

Our findings build on research demonstrating sustained *Ae. aegypti* mosquito population reductions in the same communities where AGOs have been maintained for nearly a decade (*8*). Similar effects were observed in northern Mexico and North Carolina, where mass trapping reduced *Aedes* spp. mosquito abundance and shifted mosquito populations toward younger, less infectious females (*31*,*32*). During Puerto Rico's 2014–2015 chikungunya outbreak, CHIKV seroprevalence in AGO intervention areas was half that of nonintervention areas (*13*,*25*). This study extends that evidence to ZIKV, revealing a positive association between reduced mosquito abundance and seropositivity, particularly at a 2-week lag, consistent with the ZIKV incubation period (*33*). Our results also align with entomologic surveillance, which showed frequent ZIKV detection in *Ae. aegypti* mosquito pools from untreated sites but rarely in AGO communities during the 2016 epidemic (*14*). Even modest increases in vector density could elevate short-term infection risk, aligning with findings suggesting DENV transmission is unlikely when weekly female *Ae. aegypti* mosquito densities remain <4/trap (*30*). Stronger apparent protection among older persons and those spending more time at home is consistent with the peridomestic biting behavior of *Ae. aegypti* mosquitoes (*34*,*35*) and a household-level mechanism of protection (*18*). The lack of protection among younger adults might reflect increased mobility and mosquito exposure outside the home, which is concerning for pregnant women, who face increased risk for ZIKV complications. However, few participants in our study were pregnant, limiting our ability to directly assess those differences. If AGOs provide less protection for more mobile persons, complementary strategies, including personal protection, prenatal counseling, and risk messaging, might be needed during outbreaks.

Table 2. Reported acute febrile illness and symptom profiles among participants in an evaluation of effectiveness of autocidal gravid ovitraps for preventing Zika virus infection, Puerto Rico, USA*

Characteristics	Overall, n = 270†	ZIKV-positive, n = 40	ZIKV-negative, n = 230	p value‡
Acute febrile illness	58 (21.5)	15 (37.5)	43 (18.7)	0.014
Rash	31 (11.5)	11 (27.5)	20 (8.7)	0.002
Fever	47 (17.4)	12 (30.0)	35 (15.2)	0.040
Joint pain	51 (18.9)	13 (32.5)	38 (16.5)	0.030
Sought medical care for illness	36 (13.3)	8 (20.0)	28 (12.2)	0.275
Hospitalized for illness	2 (0.7)	1 (2.5)	1 (0.4)	0.684

*Values are no. (%). ZIKV, Zika virus.
†One ZIKV-negative participant with missing information on acute febrile illness and related symptom history was excluded from this table.
‡χ^2 test was used for comparison of percentages and Fisher exact test was for comparison of categories with ≥1 value <5.

Our results highlight the potential of nonchemical vector control tools to reduce arbovirus transmission. Other interventions have demonstrated reductions in mosquito densities, but few have shown population-level impacts on human infection (*36*,*37*). AGOs offer a pesticide-free, community-accepted alternative that requires infrequent maintenance and is well suited to semiurban settings where indoor mosquito biting is common and insecticide resistance limits traditional approaches (*18*). Compared with aerial spraying or *Wolbachia*-based bacterial releases, AGOs are less resource-intensive, but large-scale deployment would require sustained funding, logistical coordination, and public-sector capacity. The observed association with lower ZIKV infection supports continued evaluation of AGOs as part of integrated vector management.

The relationship between time spent at home and ZIKV risk differed by community type, and infection probability rose more steeply in nonintervention areas. That finding aligns with evidence that human mobility influences arboviral exposure and should be considered in intervention evaluations (*38*–*40*). We also observed protective associations among participants without air conditioning and those who kept windows or doors open, suggesting AGOs could be particularly beneficial in households with higher mosquito exposure. Mosquito coil use appeared beneficial in intervention communities, highlighting potential added value in combining AGOs with personal protection tools in integrated strategies.

The first limitation of this study is that sampling occurred 6–9 months after peak ZIKV transmission; thus, waning IgM might have underestimated cumulative incidence. However, ZIKV IgM can persist for ≥12–25 months; one study reported detectable IgM in >70% of ZIKV-infected persons at 12–19 months (*41*), suggesting that our survey likely captured most infections from the 2016 outbreak. Nonetheless, if infection timing differed systematically between community types, differential IgM detectability could have biased between-community comparisons (e.g., earlier infections in intervention communities could accentuate differences due to waning seroprevalence, whereas earlier infections in nonintervention communities would tend to attenuate differences). Second, all participants were sampled during the same period using the same protocol, but we cannot exclude temporal differences in infection timing as a contributor to observed differences in IgM seroprevalence. Third, we did not measure IgG, which would have provided information on baseline flavivirus seroprevalence. However, DENV transmission was minimal during the study period, as documented by passive and enhanced surveillance that reported no laboratory-confirmed dengue cases in 2017 (*3*,*16*), reducing the likelihood that cocirculating dengue or DENV-ZIKV cross-reactivity materially biased IgM results. In dengue-endemic settings, conventional DENV-like particle IgG assays show substantial cross-reactivity among ZIKV-exposed persons, limiting their specificity for distinguishing prior DENV versus ZIKV infection. In Puerto Rico, DENV and ZIKV are the only flaviviruses with sustained human transmission, and no ZIKV circulation was documented before the 2015–2016 epidemic. We selected demographically and environmentally comparable intervention and nonintervention communities, and longstanding entomologic surveillance and prior household-based

Table 3. Association between lagged *Aedes aegypti* female mosquito abundance and ZIKV IgM seropositivity in an evaluation of effectiveness of autocidal gravid ovitraps for preventing Zika virus infection, Puerto Rico, USA*

Lag, wks	Adjusted RR (95% CI)†	p value	p for interaction‡
0	1.028 (0.996–1.062)	0.091	0.115
1	1.028 (1.003–1.053)	0.026	0.776
2	1.044 (1.011–1.077)	0.008	0.400

*Reflects test for effect modification by community intervention status. RR, risk ratio; ZIKV, Zika virus.
†RRs were estimated by using Poisson regression with a log link and robust (sandwich) SEs. Lagged mosquito abundance was modeled as a continuous predictor (per +1 female per trap-week). Lags 0–2 represent mosquito abundance in the week of specimen collection (lag 0) and 1–2 weeks prior (lags 1–2). Adjusted models include age category, sex, and hours spent at home (community) categories.
‡Interaction p values are Wald tests from pooled models including a mosquito abundance × intervention status interaction term using robust standard errors.

serosurveys of CHIKV and DENV did not indicate large systematic differences between communities. Those data provide some reassurance that major imbalances in underlying immunity are not obvious; however, we cannot rule out meaningful community-level differences in baseline exposure risk or other unmeasured factors that might influence infection risk. Any residual flavivirus cross-immunity would be expected to be similar across communities and would tend to bias estimates toward the null, consistent with cohort data from Nicaragua showing that prior DENV infection reduced symptomatic ZIKV disease but did not alter overall ZIKV infection risk (symptomatic and inapparent combined) (*42*). Fourth, several self-reported indicators related to mosquito exposure differed by community type, but because we collected data on those indicators after AGOs were implemented for several years and after the epidemic, they cannot be interpreted as definitive baseline differences and might reflect intervention-related changes in exposure or reporting. As a nonrandomized community comparison, residual confounding from unmeasured differences between communities (e.g., fine-scale environmental conditions, housing characteristics, human mobility patterns, or uptake of personal protective behaviors) could partially or fully explain the observed seroprevalence differences. Finally, the modest sample size limited precision, particularly for subgroup estimates, so evidence of effect modification should be cautiously interpreted.

Despite those limitations, use of a validated ELISA, exclusion of DENV IgM–positive participants in the primary analysis, minimal DENV transmission during the study period, and consistent sensitivity analyses increase confidence that the observed association is not solely attributable to assay limitations. Most ZIKV-seropositive participants did not report illness or care-seeking, underscoring the value of serologic surveillance in capturing asymptomatic or unrecognized infections.

In conclusion, by linking entomologic control with human health outcomes, this study contributes to the evidence for sustained *Aedes* spp. mosquito vector control to reduce ZIKV transmission. Amid increasing arbovirus outbreaks and rising concerns about insecticide resistance, integrating AGOs into broader vector control programs could help close the gap between entomologic impact and human health benefit.

About the Author

Dr. Madewell is an epidemiologist with the Dengue Branch, Division of Vector-Borne Diseases, National Center for Emerging and Zoonotic Infectious Diseases, Centers for Disease Control and Prevention, in San Juan, Puerto Rico. His primary research interests include epidemiologic study and modeling of infectious diseases.

References

1. Paixão ES, Teixeira MG, Rodrigues LC. Zika, chikungunya and dengue: the causes and threats of new and re-emerging arboviral diseases. BMJ Glob Health. 2018;3:e000530. https://doi.org/10.1136/bmjgh-2017-000530
2. Patterson J, Sammon M, Garg M. Dengue, Zika and chikungunya: emerging arboviruses in the New World. West J Emerg Med. 2016;17:671–9. https://doi.org/10.5811/westjem.2016.9.30904
3. Madewell ZJ, Hernandez-Romieu AC, Wong JM, Zambrano LD, Volkman HR, Perez-Padilla J, et al. Sentinel enhanced dengue surveillance system—Puerto Rico, 2012–2022. MMWR Surveill Summ. 2024;73:1–29. https://doi.org/10.15585/mmwr.ss7303a1
4. Musso D, Gubler DJ. Zika virus. Clin Microbiol Rev. 2016;29:487–524. https://doi.org/10.1128/CMR.00072-15
5. Sharp TM, Quandelacy TM, Adams LE, Aponte JT, Lozier MJ, Ryff K, et al. Epidemiologic and spatiotemporal trends of Zika virus disease during the 2016 epidemic in Puerto Rico. PLoS Negl Trop Dis. 2020;14:e0008532. https://doi.org/10.1371/journal.pntd.0008532
6. Quandelacy TM, Healy JM, Greening B, Rodriguez DM, Chung KW, Kuehnert MJ, et al. Estimating incidence of infection from diverse data sources: Zika virus in Puerto Rico, 2016. PLOS Comput Biol. 2021;17:e1008812. https://doi.org/10.1371/journal.pcbi.1008812
7. Dusfour I, Vontas J, David JP, Weetman D, Fonseca DM, Corbel V, et al. Management of insecticide resistance in the major *Aedes* vectors of arboviruses: advances and challenges. PLoS Negl Trop Dis. 2019;13:e0007615. https://doi.org/10.1371/journal.pntd.0007615
8. Barrera R, Harris A, Hemme RR, Felix G, Nazario N, Muñoz-Jordan JL, et al. Citywide control of *Aedes aegypti* (Diptera: Culicidae) during the 2016 Zika epidemic by integrating community awareness, education, source reduction, larvicides, and mass mosquito trapping. J Med Entomol. 2019;56:1033–46. https://doi.org/10.1093/jme/tjz009
9. Barrera R, Amador M, Acevedo V, Caban B, Felix G, Mackay AJ. Use of the CDC autocidal gravid ovitrap to control and prevent outbreaks of *Aedes aegypti* (Diptera: Culicidae). J Med Entomol. 2014;51:145–54. https://doi.org/10.1603/ME13096
10. Mackay AJ, Amador M, Barrera R. An improved autocidal gravid ovitrap for the control and surveillance of *Aedes aegypti*. Parasit Vectors. 2013;6:225. https://doi.org/10.1186/1756-3305-6-225
11. Obregón JA, Ximenez MA, Villalobos EE, de Valdez MRW. Vector mosquito surveillance using Centers for Disease Control and Prevention autocidal gravid ovitraps in San Antonio, Texas. J Am Mosq Control Assoc. 2019;35:178–85. https://doi.org/10.2987/18-6809.1
12. Montenegro D, Martinez L, Tay K, Hernandez T, Noriega D, Barbosa L, et al. Usefulness of autocidal gravid ovitraps for the surveillance and control of *Aedes* (*Stegomyia*) *aegypti* (Diptera: Culicidae) in eastern Colombia. Med Vet Entomol. 2020;34:379–84. https://doi.org/10.1111/mve.12443
13. Sharp TM, Lorenzi O, Torres-Velásquez B, Acevedo V, Pérez-Padilla J, Rivera A, et al. Autocidal gravid ovitraps protect

humans from chikungunya virus infection by reducing *Aedes aegypti* mosquito populations. PLoS Negl Trop Dis. 2019;13:e0007538. https://doi.org/10.1371/journal.pntd.0007538
14. Barrera R, Amador M, Acevedo V, Beltran M, Muñoz JL. A comparison of mosquito densities, weather and infection rates of *Aedes aegypti* during the first epidemics of chikungunya (2014) and Zika (2016) in areas with and without vector control in Puerto Rico. Med Vet Entomol. 2019;33:68–77. https://doi.org/10.1111/mve.12338
15. Ware-Gilmore F, Rodriguez DM, Ryff, MPH K, Torres JM, Velez MP, Torres-Toro CT, et al. Dengue outbreak and response—Puerto Rico, 2024. MMWR Morb Mortal Wkly Rep. 2025;74:54–60. https://doi.org/10.15585/mmwr.mm7405a1
16. Rodriguez DM, Madewell ZJ, Torres JM, Rivera A, Wong JM, Santiago GA, et al. Epidemiology of dengue—Puerto Rico, 2010–2024. MMWR Morb Mortal Wkly Rep. 2024;73:1112–7. https://doi.org/10.15585/mmwr.mm7349a1
17. Thayer MB, Marzan-Rodriguez M, Torres Aponte J, Rivera A, Rodriguez DM, Madewell ZJ, et al. Dengue epidemic alert thresholds for surveillance and decision-making in Puerto Rico: development and prospective application of an early warning system using routine surveillance data. BMJ Open. 2025;15:e106182. https://doi.org/10.1136/bmjopen-2025-106182
18. Barrera R. New tools for *Aedes* control: mass trapping. Curr Opin Insect Sci. 2022;52:100942. https://doi.org/10.1016/j.cois.2022.100942
19. Camprubí-Ferrer D, Thayer MB, Madewell ZJ, Mac McCullough J, Sánchez-González L, Rivera A, et al. Economic burden of dengue in Puerto Rico, 2010–2023. Infect Dis Poverty. 2026;15:15. https://doi.org/10.1186/s40249-026-01412-1
20. Barrera R, Amador M, Acevedo V, Hemme RR, Félix G. Sustained, area-wide control of *Aedes aegypti* using CDC autocidal gravid ovitraps. Am J Trop Med Hyg. 2014;91:1269–76. https://doi.org/10.4269/ajtmh.14-0426
21. Hemme RR, Smith EA, Felix G, White BJ, Diaz-Garcia MI, Rodriguez D, et al. Multi-year mass-trapping with autocidal gravid ovitraps has limited influence on insecticide susceptibility in *Aedes aegypti* (Diptera: Culicidae) from Puerto Rico. J Med Entomol. 2022;59:314–9. https://doi.org/10.1093/jme/tjab162
22. Barrera R, Felix G, Acevedo V, Amador M, Rodriguez D, Rivera L, et al. Impacts of hurricanes Irma and Maria on *Aedes aegypti* populations, aquatic habitats, and mosquito infections with dengue, chikungunya, and Zika viruses in Puerto Rico. Am J Trop Med Hyg. 2019;100:1413–20. https://doi.org/10.4269/ajtmh.19-0015
23. Adams LE, Sánchez-González L, Rodriguez DM, Ryff K, Major C, Lorenzi O, et al. Risk factors for infection with chikungunya and Zika viruses in southern Puerto Rico: a community-based cross-sectional seroprevalence survey. PLoS Negl Trop Dis. 2022;16:e0010416. https://doi.org/10.1371/journal.pntd.0010416
24. Adams LE, Hitchings MDT, Medina FA, Rodriguez DM, Sánchez-González L, Moore H, et al. Previous dengue infection among children in Puerto Rico and implications for dengue vaccine implementation. Am J Trop Med Hyg. 2023;109:413–9. https://doi.org/10.4269/ajtmh.23-0091
25. Lorenzi OD, Major C, Acevedo V, Perez-Padilla J, Rivera A, Biggerstaff BJ, et al. Reduced incidence of chikungunya virus infection in communities with ongoing *Aedes aegypti* mosquito trap intervention studiezs—Salinas and Guayama, Puerto Rico, November 2015–February 2016. MMWR Morb Mortal Wkly Rep. 2016;65:479–80. https://doi.org/10.15585/mmwr.mm6518e3
26. Madewell ZJ, Hemme RR, Adams L, Barrera R, Waterman SH, Johansson MA. Comparing vector and human surveillance strategies to detect arbovirus transmission: a simulation study for Zika virus detection in Puerto Rico. PLoS Negl Trop Dis. 2019;13:e0007988. https://doi.org/10.1371/journal.pntd.0007988
27. Medina FA, Vila F, Premkumar L, Lorenzi O, Paz-Bailey G, Alvarado LI, et al. Capacity of a multiplex IgM antibody capture ELISA to differentiate Zika and dengue virus infections in areas of concurrent endemic transmission. Am J Trop Med Hyg. 2022;106:585–92. https://doi.org/10.4269/ajtmh.20-1651
28. Machado Portilho M, de Moraes L, Kikuti M, Jacob Nascimento LC, Galvão Reis M, Sampaio Boaventura V, et al. Accuracy of the Zika IgM antibody capture enzyme-linked immunosorbent assay from the Centers for Disease Control and Prevention (CDC Zika MAC-ELISA) for diagnosis of Zika virus infection. Diagnostics (Basel). 2020;10:835. https://doi.org/10.3390/diagnostics10100835
29. Gaspar-Castillo C, Rodríguez MH, Ortiz-Navarrete V, Alpuche-Aranda CM, Martinez-Barnetche J. Structural and immunological basis of cross-reactivity between dengue and Zika infections: implications in serosurveillance in endemic regions. Front Microbiol. 2023;14:1107496. https://doi.org/10.3389/fmicb.2023.1107496
30. Barrera R, Acevedo-Soto V, Ruiz-Valcarcel J, Medina J, Rivera R, Otero L, et al. Defining *Aedes aegypti* density thresholds for preventing human arboviral infections. Acta Trop. 2025;267:107688. https://doi.org/10.1016/j.actatropica.2025.107688
31. Aguilar-Durán JA, Hamer GL, Reyes-Villanueva F, Fernández-Santos NA, Uriegas-Camargo S, Rodríguez-Martínez LM, et al. Effectiveness of mass trapping interventions using autocidal gravid ovitraps (AGO) for the control of the dengue vector, *Aedes* (*Stegomyia*) *aegypti*, in Northern Mexico. Parasit Vectors. 2024;17:344. https://doi.org/10.1186/s13071-024-06361-y
32. Figurskey AC, Hollingsworth B, Doyle MS, Reiskind MH. Effectiveness of autocidal gravid trapping and chemical control in altering abundance and age structure of *Aedes albopictus*. Pest Manag Sci. 2022;78:2931–9. https://doi.org/10.1002/ps.6917
33. Krow-Lucal ER, Biggerstaff BJ, Staples JE. Estimated incubation period for Zika virus disease. Emerg Infect Dis. 2017;23:841–5. https://doi.org/10.3201/eid2305.161715
34. Facchinelli L, Badolo A, McCall PJ. Biology and behaviour of *Aedes aegypti* in the human environment: opportunities for vector control of arbovirus transmission. Viruses. 2023;15:636. https://doi.org/10.3390/v15030636
35. Madewell ZJ, Sosa S, Brouwer KC, Juárez JG, Romero C, Lenhart A, et al. Associations between household environmental factors and immature mosquito abundance in Quetzaltenango, Guatemala. BMC Public Health. 2019;19:1729. https://doi.org/10.1186/s12889-019-8102-5
36. Achee NL, Grieco JP, Vatandoost H, Seixas G, Pinto J, Ching-Ng L, et al. Alternative strategies for mosquito-borne arbovirus control. PLoS Negl Trop Dis. 2019;13:e0006822. https://doi.org/10.1371/journal.pntd.0006822
37. Wilson AL, Courtenay O, Kelly-Hope LA, Scott TW, Takken W, Torr SJ, et al. The importance of vector control for the control and elimination of vector-borne diseases. PLoS Negl Trop Dis. 2020;14:e0007831. https://doi.org/10.1371/journal.pntd.0007831

38. Stoddard ST, Forshey BM, Morrison AC, Paz-Soldan VA, Vazquez-Prokopec GM, Astete H, et al. House-to-house human movement drives dengue virus transmission. Proc Natl Acad Sci U S A. 2013;110:994–9. https://doi.org/10.1073/pnas.1213349110
39. Wesolowski A, Qureshi T, Boni MF, Sundsøy PR, Johansson MA, Rasheed SB, et al. Impact of human mobility on the emergence of dengue epidemics in Pakistan. Proc Natl Acad Sci U S A. 2015;112:11887–92. https://doi.org/10.1073/pnas.1504964112
40. Phillips MT, Sánchez-González L, Shragai T, Rodriguez DM, Major CG, Johansson MA, et al. Quantifying the relationship between arboviral infection prevalence and human mobility patterns among participants of the Communities Organized to Prevent Arboviruses cohort (COPA) in southern Puerto Rico. PLoS Negl Trop Dis. 2023;17:e0011840. https://doi.org/10.1371/journal.pntd.0011840
41. Griffin I, Martin SW, Fischer M, Chambers TV, Kosoy O, Falise A, et al. Zika virus IgM detection and neutralizing antibody profiles 12–19 months after illness onset. Emerg Infect Dis. 2019;25:299–303. https://doi.org/10.3201/eid2502.181286
42. Gordon A, Gresh L, Ojeda S, Katzelnick LC, Sanchez N, Mercado JC, et al. Prior dengue virus infection and risk of Zika: a pediatric cohort in Nicaragua. PLoS Med. 2019;16:e1002726. https://doi.org/10.1371/journal.pmed.1002726

Address for correspondence: Zachary J. Madewell, Dengue Branch, Centers for Disease Control and Prevention, 1324 Cañada St, San Juan, PR 00920-3860, USA; email: ock0@cdc.gov

October 2025

Microbial World

- Retrospective Analysis of Historical *Listeria monocytogenes* Clinical Isolates, New York, USA, 2000–2021
- Organ Donor Transmission of *Rickettsia typhi* to Kidney Transplant Recipients, Texas, USA, 2024
- Recent Systemic Antifungal Exposure and Nonsusceptible *Candida* in Hospitalized Patients, South Africa, 2012–2017
- Reptile Exposure in Human Salmonellosis Cases and *Salmonella* Serotypes Isolated from Reptiles, Ontario, Canada, 2015–2022
- Comparative Epidemiology of *Salmonella enterica* Serovars Paratyphi A and Typhi Causing Enteric Fever, Bangladesh, 2018–2020
- Prolonged Monkeypox Virus Infections, California, USA, May 2022–August 2024
- Differences in COVID-19 Fatality Rates among Ethnic Groups, Hawaii, USA, 2020–2022
- Effect of Seasonal Influenza Vaccines on Avian Influenza A(H5N1) Clade 2.3.4.4b Virus Infection in Ferrets
- Spotted Fever Group Rickettsioses among Hospitalized Patients and Circulation of Rickettsia in Ticks, Kazakhstan, 2019
- Detection of Monkeypox Virus Clade Ib DNA in Wastewater Solids at Wastewater Treatment Plants, United States

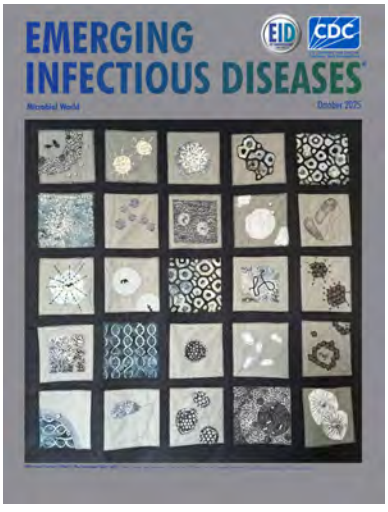

- Multidrug-Resistant pESI-Harboring *Salmonella enterica* Serovar Muenchen Sequence Type 82 in Poultry and Humans, Israel, 2020–2023
- Bat-Associated Hemotropic Mycoplasmas in Immunosuppressed Children, Spain, 2024
- Seoul Virus Infection Acquired at Private Pet Rat Breeding Facility, Germany, 2024
- Antimicrobial-Resistant Clonal Complex 11 *Neisseria meningitidis*–Associated Urethritis Cluster, Thailand
- Zoonotic Soil-Transmitted Helminth Infections among Humans, Gabon
- Detection of Monkeypox Virus Clade Ib DNA in Wastewater Solids at Wastewater Treatment Plants, United States
- Emergence and Polyclonal Dissemination of bla_{NDM-7}–Carrying InX3 Plasmid in *Enterobacter cloacae* Complex, France, 2021–2023
- Genomic Investigation of Disseminated Gonococcal Infections, Minnesota, USA, 2024
- Fatal Pneumocephalus Caused by Hypervirulent *Klebsiella pneumoniae*, Germany
- Zoonotic *Baylisascaris procyonis* Infection in Raccoons, Mississippi, USA, 2023–2024
- Genetic Cluster of Extended-Spectrum β-lactamase–Producing *Klebsiella pneumoniae* in Humans and Food, Switzerland, 2018–2019
- Emergence of *Bordetella holmesii*–Associated Pertussis-Like Illness, Northern India, 2019–2023
- Investigation of Possible Intraoperative Transmission of Brucella melitensis, Slovenia
- Emerging Sexual Transmission of *Trichophyton mentagrophytes* Genotype VII Infections, United States
- Cutaneous Coccidioidomycosis Mimicking Rosacea in Immunosuppressed Patient, Arizona, USA, 2024

EMERGING INFECTIOUS DISEASES

To revisit the October 2025 issue, go to:
https://wwwnc.cdc.gov/eid/articles/issue/31/10/table-of-contents

Geographically Distinct Circulation of Genotype II and III St. Louis Encephalitis Virus, Texas, USA, 2009–2024

Alexander R. Kneubehl, Daniel P. Rehm, Michael W. Curtis, Bianca M. Wimmer, Bethany Bolling, Angie Broussard, Jeremy Vela, Jennifer Rocha, Lindsey Templeton, Maximea Vigilant, Courtney Standlee, Steven M. Presley, Job E. Lopez, Shannon E. Ronca

We conducted a retrospective genomic surveillance study of St. Louis encephalitis virus (SLEV) in Texas, USA, to determine the genotypes circulating in the region. By using a custom tiled-amplicon assay with Oxford Nanopore sequencing, we generated 63 genomes from SLEV-positive mosquito pools and viral isolates collected during 2009–2024. Phylogenomic analysis revealed temporal overlap of genotype II and III circulation, but with distinct geographic segregation. Genotype II was confined to Gulf Coast counties with sustained local transmission, whereas genotype III was only in north and west Texas, but with persistent circulation and repeated introductions. We identified the earliest known US genotype III sequences, although their phylogenetic placement leaves the entry point of genotype III into the United States unresolved. Our findings emphasize the need for clinical vigilance in West Texas, where SLEV and West Nile virus co-circulate, and suggest the Gulf Coast may be buffered against foreign genotype introduction.

St. Louis encephalitis virus (SLEV) is a recently reemerged mosquitoborne orthoflavivirus found in the Americas (*1*). SLEV is maintained in an enzootic cycle between mosquitoes (primarily *Culex* spp.) and avian reservoirs; mammals are dead-end hosts (*2*–*5*). Since the virus's first identification in 1933 in St. Louis, Missouri, USA (*6*), focal SLEV outbreaks have been reported throughout the United States; disease manifestations range from nonspecific influenza-like symptoms to severe, potentially fatal, neurologic complications (*7*–*9*). After West Nile virus (WNV) was introduced to the United States in 1999 (*10*), a marked decrease in SLEV-positive mosquito pools and human cases occurred in areas where WNV was present (*11*,*12*). Both viruses, members of the Japanese encephalitis virus serocomplex, confer cross-reactive immunity in avian hosts (*13*–*15*), and the decrease in SLEV occurrence potentially is driven by ecologic competition between WNV and SLEV in reservoir populations because of cross-protective immune responses (*11*,*14*). SLEV reemerged in the United States after the introduction of a new genotype to the southwestern United States.

Eight genotypes of SLEV exist. Genotypes I, II, IV, and V are historically found in North America, and genotypes III, V, VI, VII, and VIII are found in South America (*16*,*17*). SLEV human cases and outbreaks have occurred in North America, and none had been reported in South America (*1*,*7*) until 2005, when an outbreak caused human fatalities in Argentina (*18*). Subsequent 2010 and 2011 outbreaks in Argentina were identified as genotype III, which previously had not been associated with human cases (*1*). In 2015, the first concurrent outbreak of WNV and SLEV occurred in Arizona, USA, prompting SLEV surveillance efforts (*19*,*20*). That same year, genotype III SLEV was detected in California, USA, after nearly a decade without reported activity despite ongoing monitoring. Retrospective analyses identified

Author affiliations: Baylor College of Medicine, Houston, Texas, USA (A.R. Kneubehl, D.P. Rehm, M.W. Curtis, J.E. Lopez, S.E. Ronca); Texas Children's Hospital William T. Schearer Center for Human Immunobiology, Houston (A.R. Kneubehl, D.P. Rehm, S.E. Ronca); Texas Tech University Institute of Environmental and Human Health, Lubbock, Texas, USA (B.M. Wimmer, S.M. Presley); Texas Department of State Health Services, Austin, Texas, USA (B. Bolling); Harris County Public Health Division of Mosquito and Vector Control, Houston (A. Broussard, J. Vela, J. Rocha, L. Templeton, M. Vigilant, C. Standlee)

DOI: https://doi.org/10.3201/eid3204.250934

the viruses in both states as genotype III and revealed a 2014 mosquito pool from Arizona that was positive for SLEV and WNV (*20*). Genotype III outbreaks in California and Arizona had a case-fatality rate of ≈8% (*8*,*19*–*22*). Further genomic surveillance indicated that SLEV genotype III replaced all other SLEV genotypes in the western United States (*21*,*22*) but analyzed samples from as far east as El Paso, Texas, USA.

SLEV was a prevalent mosquitoborne virus in Texas, particularly along the Gulf Coast, before the introduction of WNV in 2002; SLEV cases and mosquito activity declined in the region after WNV was established (*1*,*23*–*26*). During the past 20 years, sporadic reports of SLEV human cases and SLEV-positive mosquito pools occurred throughout Texas (Figure 1, panels A–D). However, only 2 full-length Texas SLEV genomes (GenBank accession nos. EF158052.1 and MN233324.1) have been detected, and no information is available regarding which genotypes are currently circulating. To address those deficiencies and determine whether genotype III is widespread throughout Texas, we performed a retrospective genomic surveillance study analyzing SLEV genomes from SLEV-positive mosquito pools during 2009–2024.

Materials and Methods

We have described in detail the methods used in this study (Appendix, https://wwwnc.cdc.gov/EID/article/32/4/25-0934-App1.pdf). In addition, a GitHub repository for this work (https://github.com/kneubehl/Texas-SLEV-Genome-Surveillance) (*27*) contains other ancillary items (e.g., scripts).

Mosquito Pools

Mosquito pools were provided by the Texas Department of Safety and Health Services, Harris County Public Health Mosquito and Vector Control Division, or Texas Tech University's Biologic Threat Research Laboratory, each having their own respective collection and testing strategies (Appendix). We summarized mosquito pool metadata (Appendix Table 1) (*27*). Because virus screening modalities varied on the basis of a mosquito pool's origin, we screened all pools by using a real-time reverse transcription PCR (rRT-PCR) to confirm positivity.

Virus Isolation

We performed virus isolation by incubating mosquito pool homogenate with Vero CCL81 cells in T75 flasks. When cytopathic effects were apparent or after 7 days, whichever came first, we clarified cell culture supernatants by using centrifugation. We stored an aliquot of supernatant in 2x DNA/RNA Shield (Zymo, https://www.zymoresearch.com) for RNA extraction. We obtained 4 SLEV isolates through BEI Resources at the National Institutes of Health National Institute of Allergy and Infectious Diseases (V07457, V08449, V08458, and TXAR 9-6038). We summarized virus isolate metadata (Appendix Table 2) (*27*).

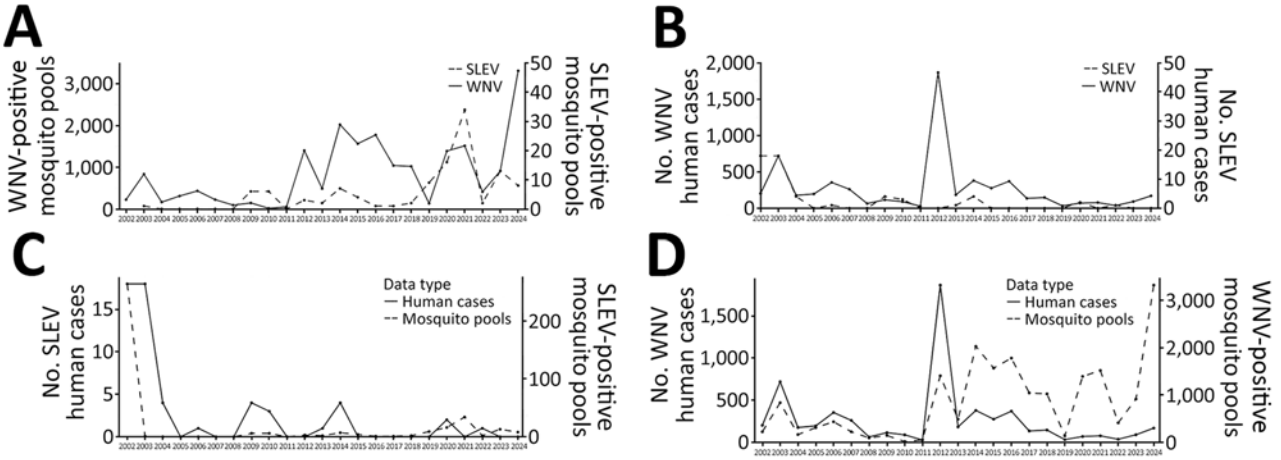

Figure 1. Annual SLEV and WNV mosquito and human case activity from study of circulation of genotype II and III SLEV, Texas, USA, 2002–2024. A) Annual number of reported SLEV-positive and WNV-positive mosquito pools. B) Annual number of reported human SLEV and WNV infection cases. C) Annual number of reported human SLEV infection cases and number of SLEV-positive mosquito pools. D) Annual number of reported human WNV infection cases and number of WNV-positive mosquito pools. Scales for the y-axes differ substantially to underscore patterns but do not permit direct comparisons. Data from Texas DSHS Arbovirus Activity Reports (https://www.dshs.texas.gov/mosquito-borne-diseases/dshs-arbovirus-weekly-activity-reports) and Texas DSHS Arbovirus Field Surveillance Report 1985–2012 (https://www.dshs.texas.gov/laboratory-services/programs-laboratories/microbiology-unit/arbovirus-surveillance-program/arbovirus-field-surveillance-report). SLEV, St. Louis encephalitis virus; WNV, West Nile virus.

RNA Isolation and SLEV rRT-PCR Testing

We isolated total RNA and DNA from samples by using a modified Zymo Quick-DNA/RNA Pathogen Miniprep protocol (Appendix). We tested all samples for the presence of SLEV RNA by using a modified rRT-PCR protocol (*28*) (Appendix).

Tiled-Amplicon Sequencing Primer Development

We designed a tiled-amplicon primer scheme to amplify the entire coding sequence of the SLEV genome (97.4% of the entire genome sequence) by using the Olivar tool with SLEV genomes sourced from GenBank. We used DQ525916.1 as the reference genome (*27*,*29*) (Appendix Table 3).

Virus Genome Amplification, Sequencing, and Assembly

We generated SLEV tiled amplicons by using reverse transcription-PCR (Appendix). We prepared sequencing libraries by using the SQK-RBK114.96 kit (Oxford Nanopore Technologies, https://www.nanoporetech.com) and sequenced them with an R10.4.1 flow cell (Oxford Nanopore), per manufacturer's instructions, on a MinION Mk1B (Oxford Nanopore) or PromethION P2 solo (Oxford Nanopore). We generated consensus genome assemblies by sample with the ViralRecon nextflow pipeline with the ARTIC minion pipeline (https://zenodo.org/records/7764938) option with modifications (Appendix). Sequencing data and genomes generated in this study are available through BioProject PRJNA1273178.

Maximum-Likelihood Analyses of All SLEV Genotypes and SLEV Genotype II Envelope

To determine the phylogenetic placement of our SLEV assemblies, we inferred a maximum-likelihood tree of all SLEV genotypes with available genomes on GenBank. We obtained SLEV genomes from GenBank, and we analyzed only genomes with ≥70% completeness. We aligned the nucleotide sequences by using MAFFT (*30*). We inferred a maximum-likelihood tree by using IQ-TREE2 (*31*,*32*). We used the same process for SLEV genotype II envelope sequences. We visualized and annotated the phylogenies in R (The R Project for Statistical Computing, https://www.r-project.org) and Inkscape (Inkscape, https://inkscape.org). Newick tree files for each phylogeny are available (*27*).

Bayesian Phylogenetic Analysis of SLEV Genotype III

We assessed the maximum-likelihood tree of all SLEV genotype III genomes with root-to-tip genetic divergence and time of sampling regression by using TempEst (*33*). That analysis determined a temporal signal that warranted generating a timetree (correlation coefficient 0.8284). We used BEAST for Bayesian phylogenetic analysis (*34*). We used an uncorrelated relaxed clock model, a general time reversible plus empirical base frequencies plus gamma-distributed rate heterogeneity with 4 categories substitution model, and a Bayesian skyline with a 2-groups tree prior and a Markov chain Monte Carlo chain length of 100 million with sampling every 10,000 trees to infer the timetree. We ran 2 independent MCMC chains, and we confirmed convergence with Tracer before combining with LogCombiner (*34*), using a 10% burn-in for each log and tree file. We generated the maximum clade credibility tree with TreeAnnotator (*34*). The XML generated by BEAUti for running BEAST and the nexus file generated by TreeAnnotator have been described previously (*27*). We visualized and annotated the phylogenies by using R and Inkscape.

Results

Genotyping SLEV-Positive *Cx. quinquefasciatus* and *Cx. tarsalis* Mosquito Pools

Our sample set included 75 SLEV-positive mosquito pools from 11 counties in Texas and 4 previously generated Texas SLEV isolates (Figure 2). Each pool consisted of *Cx. tarsalis* (36 pools) or *Cx. quinquefasciatus* (39 pools) collected during 2009–2024. *Cx. tarsalis* pools came from northwestern Texas, whereas *Cx. quinquefasciatus* pools were collected throughout the state (Figure 2). Our sample set included 5 mosquito pools positive for SLEV and WNV from El Paso County (4 pools) and Lubbock County (1 pool).

We used a tiled-amplicon sequencing approach for genome sequencing of SLEV. We also attempted virus isolation on all 64 mosquito pools not in a preservative to amplify the virus in case sequencing attempts from the mosquito pool RNA failed. Of the 123 samples tested (75 mosquito pools, 44 successful virus isolations, and 4 preexisting virus isolates), 63 unique SLEV genomes had ≥70% genome completeness. We assembled 37 genomes directly from mosquito pools, 22 from virus isolates that yielded more complete genomes than their corresponding mosquito pools, and 4 from previously available isolates. Six other mosquito pools had genome assemblies with <70% completeness; we genotyped those but did not use them for phylogenetic analysis. We plotted virus genome completeness with each sample's cycle threshold (Ct) value determined by rRT-PCR for all 123 sequencing

attempts (Appendix Figure 1) (*27*). The median Ct for samples that were successful (≥70% genome completeness) was 22.7 (range 16.2–29.5). We summarized read depth across the genome from representative samples spanning different Ct values and genome recovery (Appendix Figure 2). We also summarized genome completeness for each sample (Appendix Tables 1, 2) (*27*).

Phylogenetic Analysis of SLEV Genomes

Maximum-likelihood phylogenetic analyses defined the genotypes of our samples and their genetic relatedness to 276 previously published SLEV genomes (63 of our assemblies and 213 GenBank assemblies). We genotyped the 6 samples with a genome completeness <70% but >5% by using BLASTn (https://blast.ncbi.nlm.nih.gov) (Appendix Table 4) (*27*). Our analyses indicated that genotypes II (n = 26) and III (n = 43) were present in Texas concurrently (Figure 3). Genotype II was detected in 2009, 2010, 2013, 2014, 2016, 2020, 2021, and 2023; genotype III was present in 2014, 2015, and 2017–2024 (Figure 4, panel A). Although temporal overlap of genotypes occurred, we noted spatial segregation: genotype II in coastal counties (Cameron, Harris, Galveston, Jefferson, Kleberg, and Nueces) and genotype III in northern and western counties (El Paso, Hunt, Lubbock, Randall, and Wichita) (Figure 4, panel B).

Phylogenetic Analysis of Genotype II Envelope Gene

Because only a limited number of whole-genome sequences of genotype II SLEV were publicly available (n = 28), we used the envelope gene for phylogenetic analysis to increase the sample size spanning a broader timeframe (n = 61 publicly available sequences) (Figure 5). That analysis indicated that these samples fell within 2 clusters in genotype IIB. Our samples all share a basal node from a 1991 Harris County sample, but another more derived sample from 1983 indicates persistence in the region since at least the 1980s. Harris and Nueces County samples from 2013 (n = 5) clustered together in a position basal to the other samples from our dataset. Other samples from Galveston, Harris, Jefferson, Kleberg, and Nueces Counties (n = 20) span from 2009 to 2023 and clustered into a polytomy with other previously sequenced samples from Harris and Jefferson Counties, including a sample from Louisiana. This clade has a basal node of 2 samples from

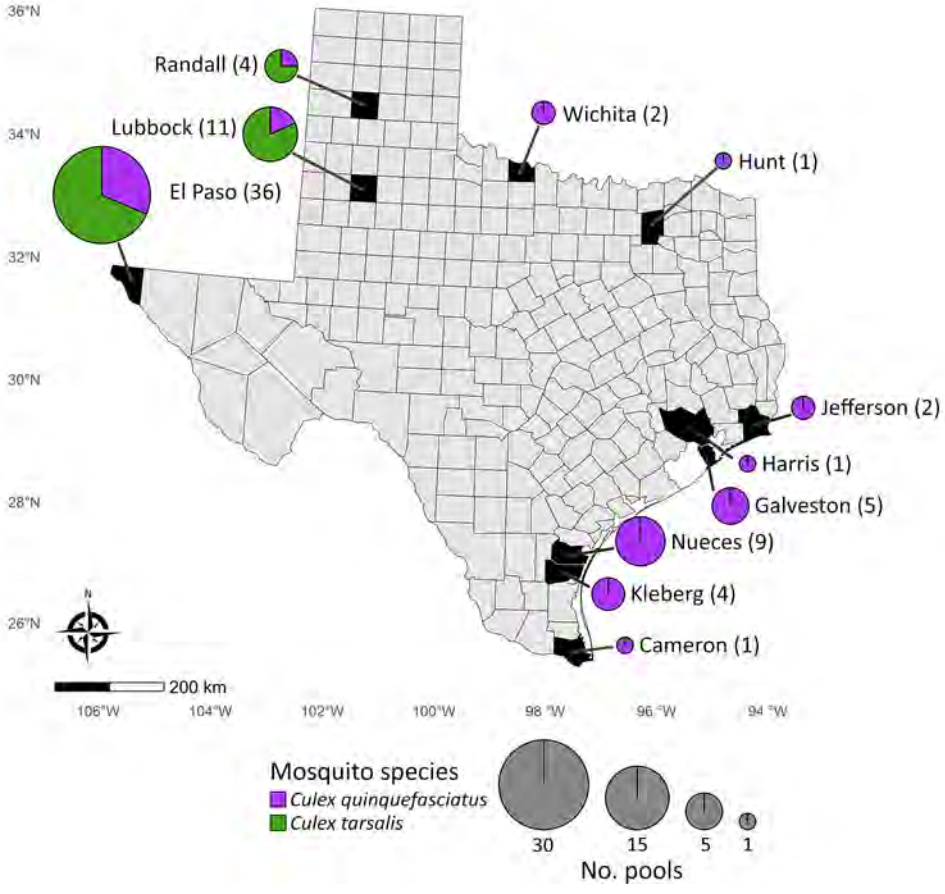

Figure 2. St. Louis encephalitis virus–positive mosquito pool samples from study of circulation of genotype II and III St. Louis encephalitis virus, by county of origin, Texas, USA, 2002–2024. Each county of origin is indicated in black. Pie charts indicate number of pools and proportion of *Culex* spp. mosquitoes contributing to those samples. Number of pools from each county is indicated in parentheses by the county name.

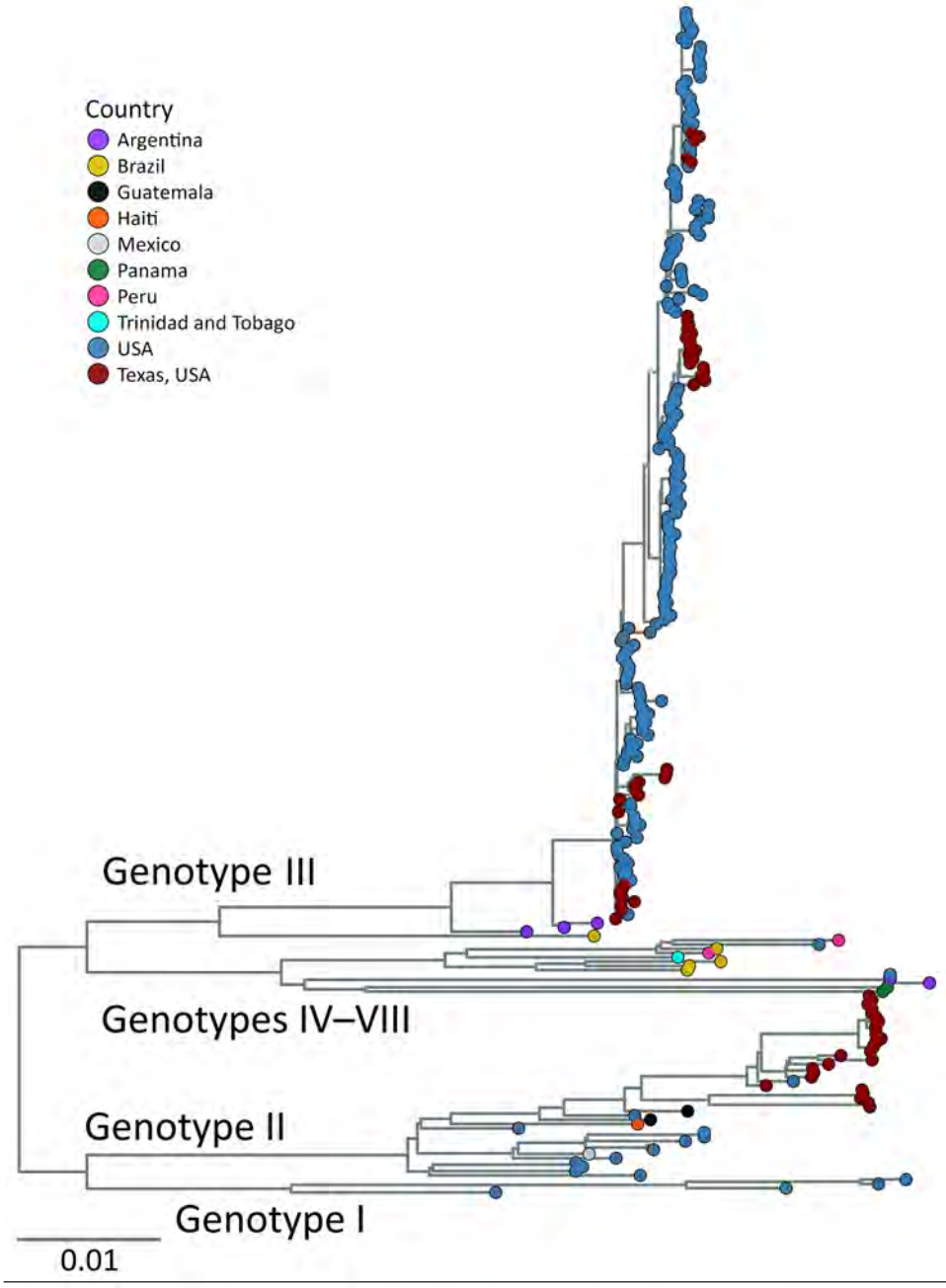

Figure 3. Maximum-likelihood phylogenic analysis of all St. Louis encephalitis virus genomes from study of circulation of genotype II and III St. Louis encephalitis virus, Texas, USA, 2009–2024. Maximum-likelihood inferred tree shows 276 genomes currently available that have <30% of the genome missing. Tip color represents sample's country of origin; samples from Texas are labeled with a separate color (red) to distinguish Texas samples from rest of United States. Genotypes annotated on the tree indicate which clade contains which genotype or genotypes. Tree was midpoint rooted. Scale bar indicates number of nucleotide substitutions per site.

Harris County collected in 2003. Samples from Kleberg, Nueces, and Galveston Counties (n = 14) from 2020 and 2021 all clustered together, to the exclusion of the 6 remaining samples from Harris, Jefferson, and Nueces Counties that had collection dates spanning from 2009 to 2023. We compared the pairwise percentage identity of each genotype II sequence and determined that, across both genotype IIA and IIB, they differed in sequence identity by at most 4.5% (Appendix Figure 2) (*27*). Within genotypes IIA and IIB, we found a 2.7% difference in sequence identity in the envelope gene.

Bayesian Phylogenetic Analysis of Genotype III Genomes

Given the epidemic potential of genotype III and to better understand introduction events and divergence times, we performed a more rigorous phylogenetic analysis by using Bayesian methods. TempEST (*33*) identified sufficient temporal signal (correlation coefficient 0.8284) in our genotype III dataset by using the root-to-tip distance compared with the date of collection from a maximum-likelihood tree inferred from the 216 genotype III genomes available (38 of our assemblies and 178 GenBank assemblies). The

Bayesian time tree recapitulated a similar topology to a previous analysis (*21*), which showed US samples forming 2 clades (clades 1 and 2) (Figure 6); the node of the time to most recent common ancestor (tMRCA) of genotype III in the United States was March 2013 (95% highest posterior density [HPD] interval December 2011–October 2014).

Clade 1 primarily contained US samples collected during 2014–2024 and included the country's earliest known genotype III sample, a SLEV- and WNV-positive *Cx. tarsalis* pool collected in July 2014 from Lubbock County. Clade 1 also contained 3 additional SLEV- and WNV-positive mosquito pools from El Paso County. Furthermore, this clade contained Lubbock County samples from 2024 with a well-supported basal node from a 2017 El Paso sample, suggesting sustained circulation of genotype III virus in West Texas. Other El Paso County samples from 2019 and 2021 did not form well-supported subclades, indicating possible introduction events from other regions. The newly sequenced 2014 Texas samples were not basal to the other US genotype III sequences, leaving the origin of genotype III introduction into the US unresolved.

Clade 2 consisted of samples from 2017 onward. The Bayesian time tree recapitulated subclades 2A, which were largely California samples (tMRCA June 2016 [95% HPD interval November 2015–March 2017]), and 2B (tMRCA December 2014 [95% HPD interval July 2014–March 2015]), which generally were Arizona samples. The Texas samples were within subclade 2B, clustering with the Arizona samples and subsequently forming 2 moderately supported subclades we called 2B1 (posterior probability 0.7898) and 2B2 (posterior probability 0.7933). Subclade 2B1 (tMRCA June 2016 [95% HPD interval August 2015–

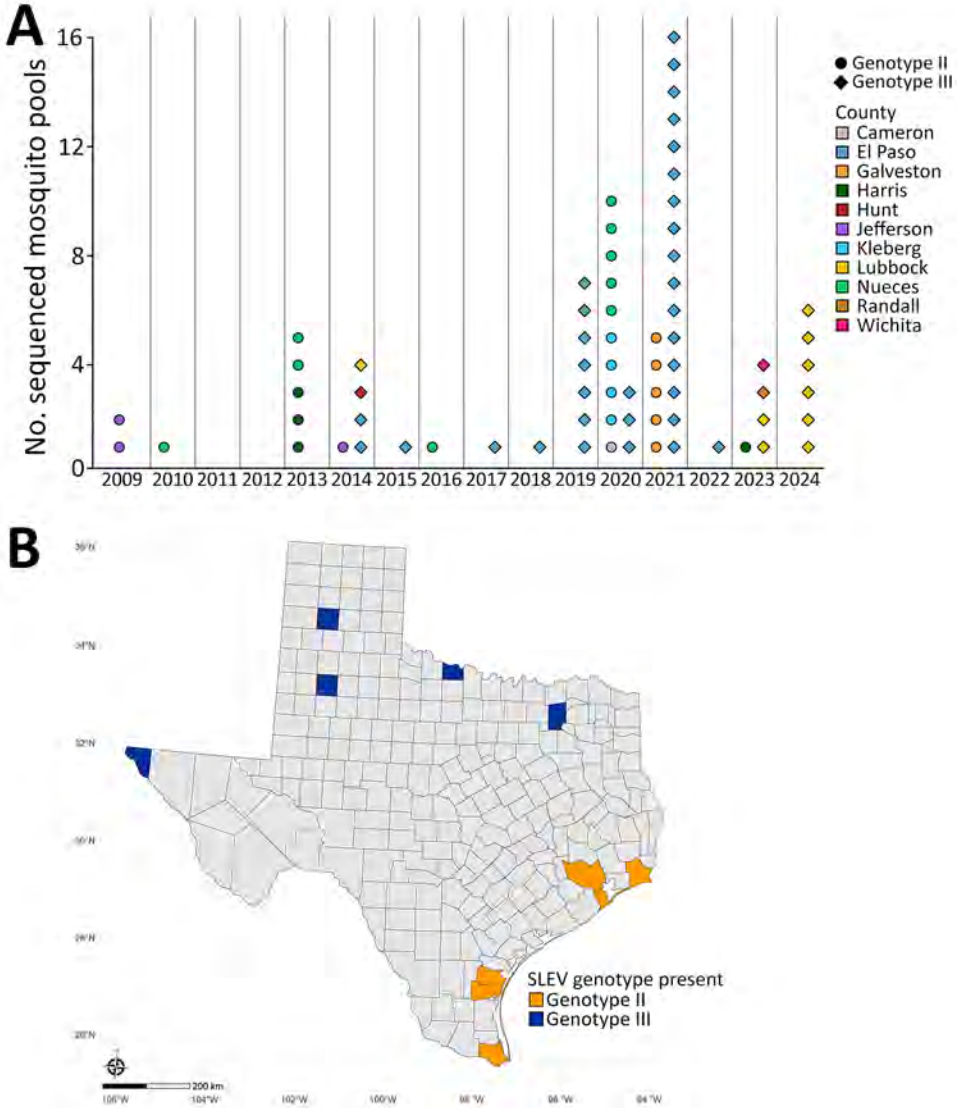

Figure 4. SLEV genotype distribution from study of circulation of genotype II and III SLEV, by year and county, Texas, USA, 2009–2024. A) Dot plot of number of sequenced SLEV-positive mosquito pools for each year, by genotype and county. Each shape represents an individual mosquito pool. B) Map of Texas indicating presence of SLEV genotype II or III. Each genotype exclusively found in its respective counties; no counties had presence of both genotypes. SLEV, St. Louis encephalitis virus.

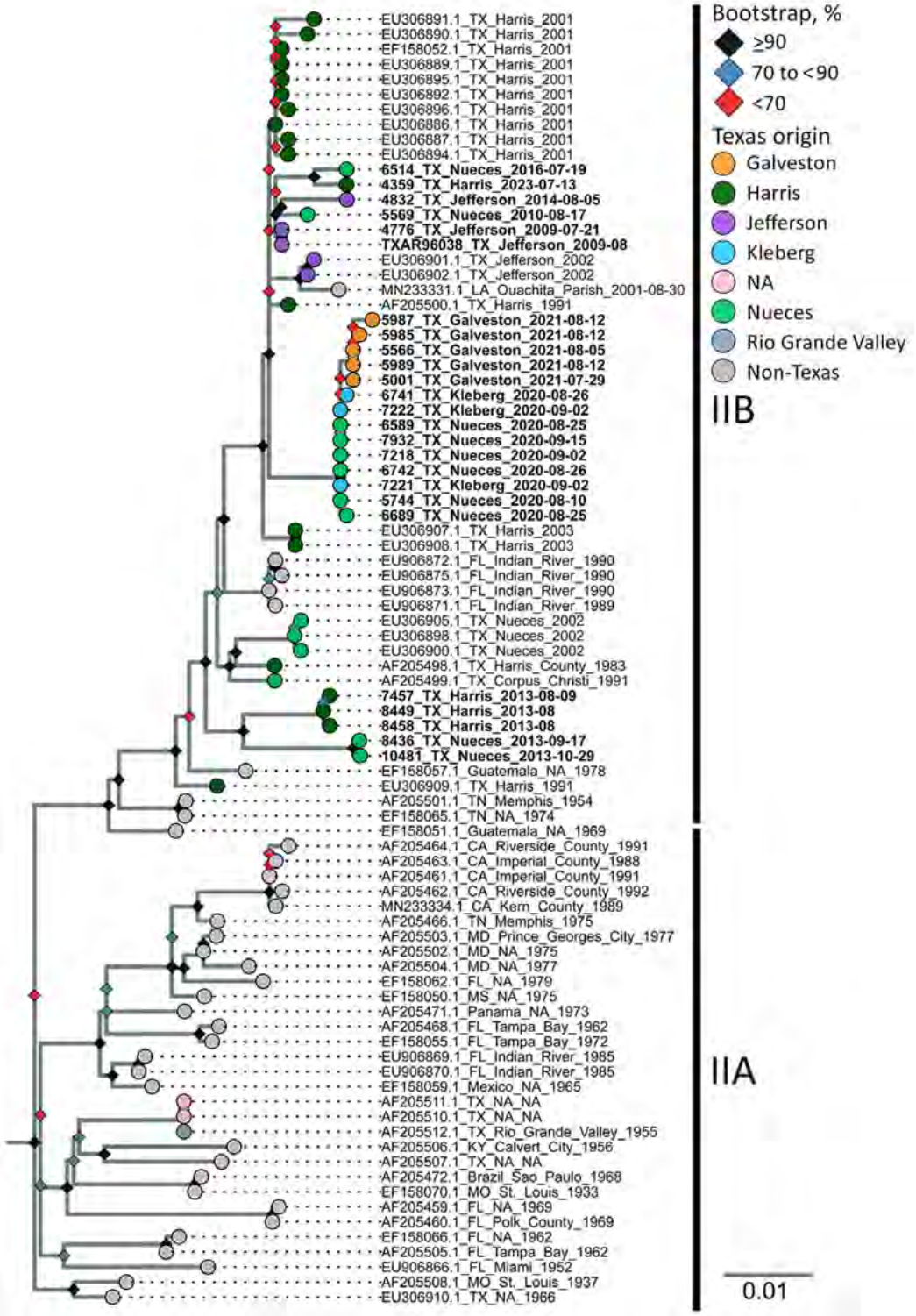

Figure 5. Maximum-likelihood phylogenic analysis of St. Louis encephalitis virus genotype IIA and IIB envelope gene sequences from study of circulation of genotype II and III St. Louis encephalitis virus, Texas, USA. Maximum-likelihood inferred tree of 86 SLEV genotype II envelope gene nucleotide sequences. Two genotype III outgroup sequences (not shown) were used to root tree (GenBank accession nos. FJ753287.2 and FJ753286.2). Tip labels indicate the GenBank accession number, sample origin, and collection date. Bold tip labels indicate samples generated by this study. Tip colors highlight different sample origins from within Texas, by county (or area, in the case of the Rio Grande Valley sample). Bootstrap support is shown at nodes; different colors indicate level of bootstrap support from 10,000 ultrafast bootstrap replicates. Scale bar indicates number of nucleotide substitutions per site. NA, not available (missing or unknown).

March 2017]) had limited sampling over multiple years from El Paso, Wichita, and Lubbock Counties, so determining persistence from year to year is limited. The Texas samples in this subclade were related to samples collected from Arizona, indicating an introduction from that region. The Texas samples bifurcated into sister clades; El Paso County samples clustered to the exclusion of Wichita and Lubbock Counties, although both clades shared a basal node from a 2021 El Paso County sample. In both groups, samples from ≥2 years are present (2021 and 2022 from El Paso County and 2023 and 2024 from Lubbock County), suggesting persistence of those viruses. Subclade 2B2 (tMRCA February 2015 [95% HPD interval November 2014–May 2015]) is a radiation with poorly supported virus population structure. This subclade is dominated by samples from Arizona; only 5 Texas samples (El Paso County 2019 and 2020) clustered into this group. These samples probably indicate introduction events into El Paso County from outside Texas that failed to persist or have remained undetected in subsequent years. El Paso County (2019 and 2021) and Lubbock County (2024) had clade 1 and clade 2 viruses, indicating SLEV genetic diversity within the same county. Collectively, the Bayesian phylogenetic analysis indicated repeated

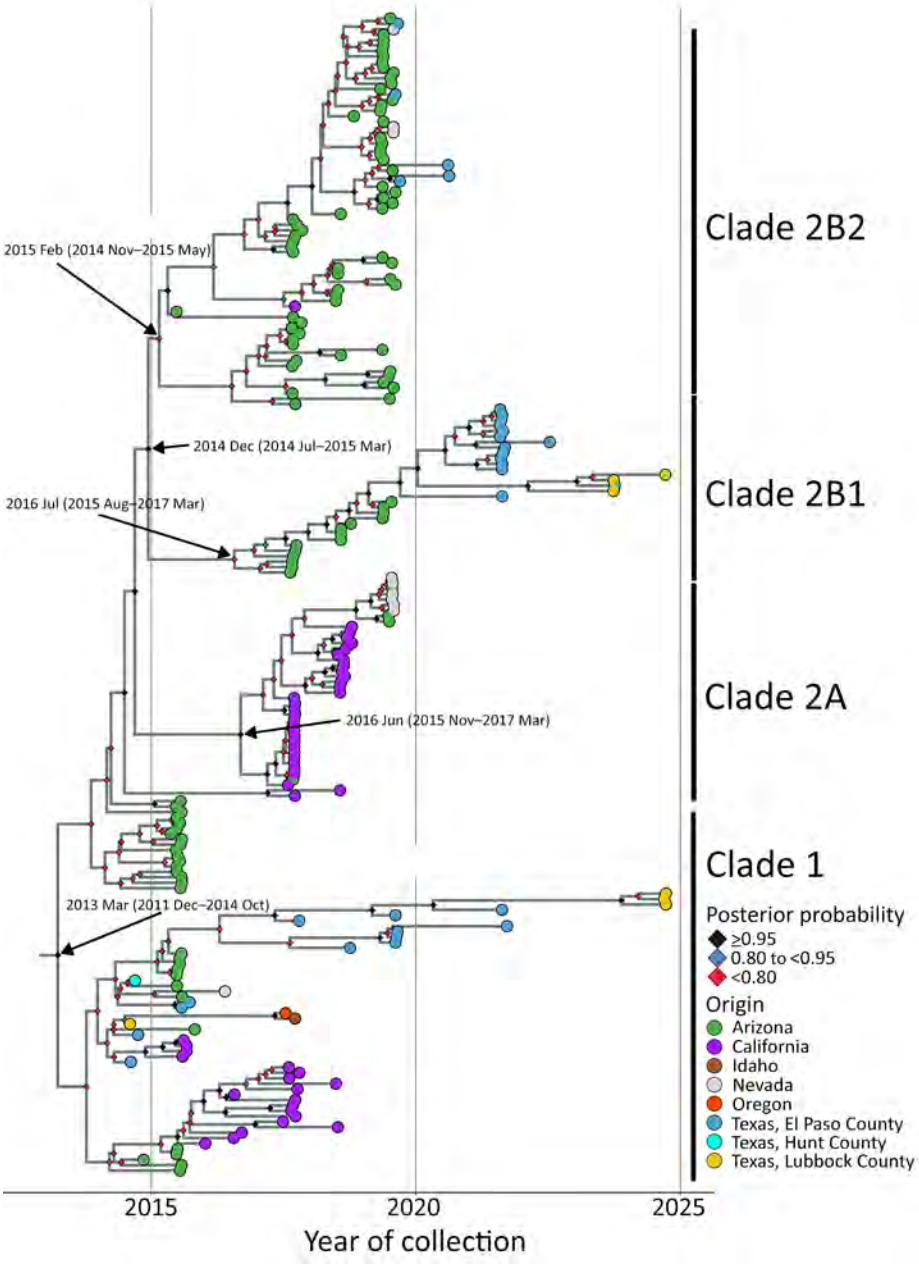

Figure 6. Bayesian phylogenetic analysis of SLEV genotype III from Texas and other states from study of circulation of genotype II and III St. Louis encephalitis virus, Texas, USA. Maximum clade credibility time tree of 216 whole genomes inferred by using BEAST (*34*). Tip colors reflect sample's place of origin. Texas samples are further subdivided by county. Clade annotations are indicated to right of tips. Posterior probability for each node is indicated at node with a colored diamond. The *y*-axis scales in years are based on date of sample collection. Arrow labels indicate time to most recent common ancestor and 95% highest posterior density for each clade.

introduction events of genotype III into Texas and persistence of phylogenetically distinct viruses falling into clades 1 and 2.

Discussion

This study highlights the importance of banking and sharing mosquito pool samples and collaborative surveillance efforts. Our retrospective study identified circulation of SLEV genotypes II and III in Texas during 2009–2024 and showed geographic segregation of each genotype, addressing a major gap in knowledge of genotype distribution in the state. Texas has 254 counties each with different mosquito sampling and pathogen testing algorithms, including some with no sampling or screening. Our sample size and scope were limited to those areas that tested and reported SLEV-positive mosquitoes. Of the 173 SLEV-positive mosquito pools reported since 2002 by Texas Department of Safety and Health Services, 43.3% (n = 75) were available, and 74 of those pools were collected after 2012. Because of availability of banked samples, our analysis did not include pools from the northern and western Texas counties before the introduction of genotype III, and it remains unknown which genotype or genotypes circulated immediately before the introduction. Further surveillance is needed to enhance the temporal resolution and improve classifications of introduction events from established virus lineages for SLEV and other arboviruses.

Genotypes I, II, and V SLEV historically are reported in Texas, and genotype II has dominated the Gulf Coast region since the 1980s (*16*,*35*). In line with previous findings, our results indicate that genotype IIB is still circulating ≥40 years after becoming dominant in the region. We detected different genotype IIB variants circulating in Nueces and Harris Counties at different times. The 2013 samples from Nueces and Harris Counties shared a recent common ancestor with samples from the same counties from 1991, 1983, and 2002, suggesting that the 2013 samples stem from an older lineage of genotype II that had not been sampled for at least a decade. No genotype III–positive samples were detected in the Gulf Coast region (Cameron, Galveston, Harris, Jefferson, Kleberg, and Nueces Counties) during 2009–2024 but were present during 2014–2024 in northern and western Texas counties (El Paso, Hunt, Lubbock, and Randall). These genotype III samples included the earliest known examples of genotype III virus in the United States. Our new data indicate that the genotype III introduction timeframe was December 2011–October 2014, differing slightly from previous reports of September 2011–May 2014 (*21*) and August 2012–October 2013 (*22*), suggesting that genotype III was circulating in the United States well before it was first detected in 2014. Our 2014 Texas samples were not basal to the other genotype III samples, indicating that the introduction site to the United States is still unknown. The earliest genotype III sample from Lubbock County was related to samples collected in Oregon and Idaho in 2017, indicating that Texas may have been an early area of genotype III introduction and that genotype III may have been exported to parts of the West Coast. We detected phylogenetically related viruses across years in clade 1 (early introduction) and clade 2 (later introduction), indicating establishment in Texas and greater viral diversity compared with Arizona and California, where clade 1 circulation is no longer reported (*21*,*22*). We detected introduction events with no direct ancestors from Texas in all clades, suggesting that West Texas is a site of continuous introduction events of SLEV genotype III.

The importation and circulation of new SLEV genotypes in West Texas, particularly in El Paso County, is not a new phenomenon. In the early 2000s, genotype VA circulated in El Paso County, whereas genotype IIB circulated in the Gulf Coast region (*35*). The El Paso isolates were genetically similar to genotype VA from South America that was contemporaneously circulating in California (*16*,*35*). Others hypothesized that cooler regions, such as El Paso County, require annual reintroduction of SLEV because overwintering does not appear to be effective for virus maintenance; however, in the subtropical Texas Gulf Coast region, SLEV can overwinter by unknown means (*35*). In contrast, our data supports year-to-year persistence of related genotype III viruses in El Paso County and potential SLEV overwintering in the county. Given the dispersal of SLEV occurs South-to-North from Central and South America to North America (*36*), and given the importance of the Texas Gulf Coast region in the Central Flyway for migratory birds from Central and South America (*37*), we would expect the Gulf Coast region rather than West Texas to be a major site for SLEV introductions. Further work is necessary to determine which migratory birds in West Texas are facilitating SLEV introduction events and how genotype III is overwintering in West Texas.

The observation that western and northern Texas counties harbor a different circulating genotype than Gulf Coast counties was previously reported and probably is likely driven by differences in rural–urban transmission cycles shaped by *Culex* mosquito distribution (*16*,*35*). *Cx. tarsalis* mosquitoes, typically involved in the rural transmission cycle of SLEV and

associated with sporadic human infections (*38*,*39*), are better adapted to habitats in western Texas (*40*). *Cx. quinquefasciatus* mosquitoes, the primary vector in the urban transmission cycle and a driver of SLEV epidemics (*25*,*26*,*41*,*42*), are better adapted to habitats along the Gulf Coast region (*40*). Our samples generally align with this geographic dichotomy: all West Texas pools contained *Cx. tarsalis* mosquitoes, and 56% of Gulf Coast pools contained *Cx. quinquefasciatus* mosquitoes. SLEV genotypes and variants circulating in West Texas' rural cycle can invade and establish urban cycles in more populated parts of Texas, resulting in SLEV outbreaks. Spillover from the SLEV rural cycle in West Texas to the Dallas metropolitan area in the 1960s probably resulted in outbreaks (*41*). Although we detected a SLEV genotype III–positive *Cx. quinquefasciatus* mosquito pool from 2014 in Hunt County, bordering the Dallas metropolitan area, this virus probably was an introduction from outside of Texas. Continued surveillance is necessary to determine whether genotype III spillover from West Texas into metropolitan areas is occurring, potentially initiating urban transmission cycles that could drive SLEV outbreaks.

Our data indicate that SLEV genotype III is established in Texas and importation events continue in the western counties. Despite genotype III circulation in Texas for nearly a decade, human cases have not increased. Since 2002, SLEV is a reportable disease in the state, where case counts are collected by the state contingent on diagnoses. The lack of cases in the northern and western counties could be attributable to several factors, such as the lack of clinical awareness to distinguish SLEV from WNV, the lack of incentive to test for arboviruses, potential misdiagnosis as WNV because of assay cross-reactivity, or the inability of SLEV genotype III from the rural transmission cycle to infect a large enough human population that it would be detected (*43*,*44*). Although genotype IIB remains the dominant strain in the Gulf Coast region >40 years after its introduction, whether genotype III possibly was introduced but failed to establish is unclear, given the limitations of sampling and testing in our retrospective study. Ongoing surveillance is critical to ensure that genotype III–associated outbreaks do not go undetected in affected counties and to monitor whether this genotype spreads to the Gulf Coast where an urban cycle with *Cx. quinquefasciatus* mosquitoes could cause epidemics. Genotype III became the dominant genotype in the western United States in <5 years, raising important questions about why a similar shift did not occur throughout Texas after nearly a decade. Whether any possible geographic and ecologic factors may be preventing the establishment of other genotypes in the Gulf Coast region is unknown. Incorporating accurate clinical data with robust mosquito surveillance data would provide a clearer measure of surveillance coverage across the state, which is currently unknown. Collectively, this study demonstrates the establishment and persistence of SLEV genotype III in Texas, which co-circulates with WNV and can cause concurrent outbreaks, underscoring the need for heightened clinical vigilance and ongoing surveillance.

Acknowledgments

The authors express sincere gratitude to the City of Lubbock Health Department and the Zoonoses Control Veterinarian, Public Health Region 1, Texas Department of State Health Services, for their assistance in mosquito collection and processing.

SLEV isolates were obtained through BEI Resources at the National Institutes of Health National Institute of Allergy and Infectious Diseases, as part of the World Reference Center for Emerging Viruses and Arboviruses program: SLEV V07457, NR-49781; SLEV V08449, NR-49782; SLEV V08458, NR-49783; and SLEV, TXAR 9-6038, NR-50061.

This work was funded by intramural startup funds provided to S.E.R. from Texas Children's Hospital and Baylor College of Medicine Department of Pediatrics. This work also was supported by the Texas Children's Hospital William T. Schearer Center for Human Immunobiology.

About the Author

Dr. Kneubehl is an assistant professor in the Division of Tropical Medicine, Department of Pediatrics, Baylor College of Medicine, Houston, Texas. His research focuses on vector biology and vectorborne diseases with broad interests in genomics, epidemiology, and molecular pathogenesis.

References

1. Diaz A, Coffey LL, Burkett-Cadena N, Day JF. Reemergence of St. Louis Encephalitis virus in the Americas. Emerg Infect Dis. 2018;24:2150–7. https://doi.org/10.3201/eid2412.180372
2. Reisen WK, Fang Y, Martinez VM. Avian host and mosquito (Diptera: Culicidae) vector competence determine the efficiency of West Nile and St. Louis encephalitis virus transmission. J Med Entomol. 2005;42:367–75. https://doi.org/10.1603/0022-2585(2005)042[0367:AHAMDC]2.0.CO;2
3. Reisen WK, Chiles RE, Martinez VM, Fang Y, Green EN. Experimental infection of California birds with western equine encephalomyelitis and St. Louis encephalitis viruses. J Med Entomol. 2003;40:968–82. https://doi.org/10.1603/0022-2585-40.6.968

4. Gruwell JA, Fogarty CL, Bennett SG, Challet GL, Vanderpool KS, Jozan M, et al. Role of peridomestic birds in the transmission of St. Louis encephalitis virus in southern California. J Wildl Dis. 2000;36:13–34. https://doi.org/10.7589/0090-3558-36.1.13
5. McLean RG, Mullenix J, Kerschner J, Hamm J. The house sparrow (*Passer domesticus*) as a sentinel for St. Louis encephalitis virus. Am J Trop Med Hyg. 1983;32:1120–9. https://doi.org/10.4269/ajtmh.1983.32.1120
6. Leake J, Musson E, Chope H. Epidemiology of epidemic encephalitis, St. Louis type. JAMA. 1934;103:728–31. https://doi.org/10.1001/jama.1934.02750360004003
7. Curren EJ, Lindsey NP, Fischer M, Hills SLS. St. Louis encephalitis virus disease in the United States, 2003–2017. Am J Trop Med Hyg. 2018;99:1074–9. https://doi.org/10.4269/ajtmh.18-0420
8. Danforth ME, Snyder RE, Feiszli T, Bullick T, Messenger S, Hanson C, et al. Epidemiologic and environmental characterization of the re-emergence of St. Louis encephalitis virus in California, 2015–2020. PLoS Negl Trop Dis. 2022;16:e0010664. https://doi.org/10.1371/journal.pntd.0010664
9. Venkat H, Krow-Lucal E, Kretschmer M, Sylvester T, Levy C, Adams L, et al. Comparison of characteristics of patients with West Nile Virus or St. Louis encephalitis virus neuroinvasive disease during concurrent outbreaks, Maricopa County, Arizona, 2015. Vector Borne Zoonotic Dis. 2020;20:624–9. https://doi.org/10.1089/vbz.2019.2572
10. Centers for Disease Control and Prevention. Outbreak of West Nile–like viral encephalitis—New York, 1999. MMWR Morb Mortal Wkly Rep. 1999;48:845–9.
11. Reisen WK, Lothrop HD, Wheeler SS, Kennsington M, Gutierrez A, Fang Y, et al. Persistent West Nile virus transmission and the apparent displacement St. Louis encephalitis virus in southeastern California, 2003-2006. J Med Entomol. 2008;45:494–508.
12. Reimann CA, Hayes EB, DiGuiseppi C, Hoffman R, Lehman JA, Lindsey NP, et al. Epidemiology of neuroinvasive arboviral disease in the United States, 1999–2007. Am J Trop Med Hyg. 2008;79:974–9. https://doi.org/10.4269/ajtmh.2008.79.974
13. Mackenzie JS, Barrett AD, Deubel V. The Japanese encephalitis serological group of flaviviruses: a brief introduction to the group. Curr Top Microbiol Immunol. 2002;267:1–10. https://doi.org/10.1007/978-3-642-59403-8_1
14. Fang Y, Reisen WK. Previous infection with West Nile or St. Louis encephalitis viruses provides cross protection during reinfection in house finches. Am J Trop Med Hyg. 2006;75:480–5. https://doi.org/10.4269/ajtmh.2006.75.480
15. Bosco-Lauth AM, Kooi K, Hawks SA, Duggal NK. Cross-protection between West Nile virus and emerging flaviviruses in wild birds. Am J Trop Med Hyg. 2024;112:657–62. https://doi.org/10.4269/ajtmh.24-0363
16. Kramer LD, Chandler LJ. Phylogenetic analysis of the envelope gene of St. Louis encephalitis virus. Arch Virol. 2001;146:2341–55. https://doi.org/10.1007/s007050170007
17. Rodrigues SG, Nunes MR, Casseb SM, Prazeres AS, Rodrigues DS, Silva MO, et al. Molecular epidemiology of Saint Louis encephalitis virus in the Brazilian Amazon: genetic divergence and dispersal. J Gen Virol. 2010;91:2420–7. https://doi.org/10.1099/vir.0.019117-0
18. Diaz LA, Ré V, Almirón WR, Farías A, Vázquez A, Sanchez-Seco MP, et al. Genotype III Saint Louis encephalitis virus outbreak, Argentina, 2005. Emerg Infect Dis. 2006;12:1752–4. https://doi.org/10.3201/eid1211.060486
19. Venkat H, Krow-Lucal E, Hennessey M, Jones J, Adams L, Fischer M, et al. Concurrent outbreaks of St. Louis encephalitis virus and West Nile Virus disease—Arizona, 2015. MMWR Morb Mortal Wkly Rep. 2015;64:1349–50.
20. White GS, Symmes K, Sun P, Fang Y, Garcia S, Steiner C, et al. Reemergence of St. Louis encephalitis Virus, California, 2015. Emerg Infect Dis. 2016;22:2185–8. https://doi.org/10.3201/eid2212.160805
21. Ridenour CL, Cocking J, Poidmore S, Erickson D, Brock B, Valentine M, et al. St. Louis encephalitis virus in the southwestern United States: a phylogeographic case for a multi-variant introduction event. Front Genet. 2021;12:667895. https://doi.org/10.3389/fgene.2021.667895
22. Swetnam DM, Stuart JB, Young K, Maharaj PD, Fang Y, Garcia S, et al. Movement of St. Louis encephalitis virus in the Western United States, 2014–2018. PLoS Negl Trop Dis. 2020;14:e0008343. https://doi.org/10.1371/journal.pntd.0008343
23. Chandler LJ, Parsons R, Randle Y. Multiple genotypes of St. Louis encephalitis virus (Flaviviridae: *Flavivirus*) circulate in Harris County, Texas. Am J Trop Med Hyg. 2001;64:12–9. https://doi.org/10.4269/ajtmh.2001.64.1.11425155
24. Lillibridge KM, Parsons R, Randle Y, Travassos da Rosa AP, Guzman H, Siirin M, et al. The 2002 introduction of West Nile virus into Harris County, Texas, an area historically endemic for St. Louis encephalitis. Am J Trop Med Hyg. 2004;70:676–81. https://doi.org/10.4269/ajtmh.2004.70.676
25. Williams KH, Hollinger FB, Metzger WR, Hopkins CC, Chamberlain RW. The epidemiology of St. Louis encephalitis in Corpus Christi, Texas, 1966. Am J Epidemiol. 1975;102:16–24. https://doi.org/10.1093/oxfordjournals.aje.a112129
26. Luby JP, Miller G, Gardner P, Pigford CA, Henderson BE, Eddins D. The epidemiology of St. Louis encephalitis in Houston, Texas, 1964. Am J Epidemiol. 1967;86:584–97. https://doi.org/10.1093/oxfordjournals.aje.a120768
27. Kneubehl AR. Texas-SLEV-genome-surveillance. 2025 [cited 2025 Jan 1]. https://github.com/kneubehl/Texas-SLEV-Genome-Surveillance
28. Lanciotti RS, Kerst AJ. Nucleic acid sequence-based amplification assays for rapid detection of West Nile and St. Louis encephalitis viruses. J Clin Microbiol. 2001;39:4506–13. https://doi.org/10.1128/JCM.39.12.4506-4513.2001
29. Wang MX, Lou EG, Sapoval N, Kim E, Kalvapalle P, Kille B, et al. Olivar: towards automated variant aware primer design for multiplex tiled amplicon sequencing of pathogens. Nat Commun. 2024;15:6306. https://doi.org/10.1038/s41467-024-49957-9
30. Katoh K, Standley DM. MAFFT multiple sequence alignment software version 7: improvements in performance and usability. Mol Biol Evol. 2013;30:772–80. https://doi.org/10.1093/molbev/mst010
31. Hoang DT, Chernomor O, von Haeseler A, Minh BQ, Vinh LS. UFBoot2: Improving the ultrafast bootstrap approximation. Mol Biol Evol. 2018;35:518–22. https://doi.org/10.1093/molbev/msx281
32. Minh BQ, Schmidt HA, Chernomor O, Schrempf D, Woodhams MD, von Haeseler A, et al. IQ-TREE 2: new models and efficient methods for phylogenetic inference in the genomic era. Mol Biol Evol. 2020;37:1530–4. https://doi.org/10.1093/molbev/msaa015
33. Rambaut A, Lam TT, Max Carvalho L, Pybus OG. Exploring the temporal structure of heterochronous sequences using TempEst (formerly Path-O-Gen). Virus Evol. 2016;2:vew007. https://doi.org/10.1093/ve/vew007

34. Drummond AJ, Rambaut A. BEAST: Bayesian evolutionary analysis by sampling trees. BMC Evol Biol. 2007;7:214. https://doi.org/10.1186/1471-2148-7-214
35. May FJ, Li L, Zhang S, Guzman H, Beasley DWC, Tesh RB, et al. Genetic variation of St. Louis encephalitis virus. J Gen Virol. 2008;89:1901–10. https://doi.org/10.1099/vir.0.2008/000190-0
36. Auguste AJ, Pybus OG, Carrington CV. Evolution and dispersal of St. Louis encephalitis virus in the Americas. Infect Genet Evol. 2009;9:709–15. https://doi.org/10.1016/j.meegid.2008.07.006
37. Lincoln FC. The waterfowl flyways of North America. Washington: US Department of Agriculture; 1935. p. 7–8.
38. Tasi TF, Smith GC, Ndukwu M, Jakob WL, Happ CM, Kirk LJ, et al. Entomologic studies after a St. Louis encephalitis epidemic in Grand Junction, Colorado. Am J Epidemiol. 1988;128:285–97. https://doi.org/10.1093/oxfordjournals.aje.a114969
39. Hayes RO, LaMotte LC, Holden P. Ecology of arboviruses in Hale County, Texas, during 1965. Am J Trop Med Hyg. 1967;16:675–87.
40. Gorris ME, Bartlow AW, Temple SD, Romero-Alvarez D, Shutt DP, Fair JM, et al. Updated distribution maps of predominant *Culex* mosquitoes across the Americas. Parasit Vectors. 2021;14:547. https://doi.org/10.1186/s13071-021-05051-3
41. Luby JP, Haley RW. Recurrent St. Louis encephalitis infection in residents of a flood plain of the Trinity River, Roosevelt Heights (Dallas, Texas). Am J Epidemiol. 1972;96:107–13. https://doi.org/10.1093/oxfordjournals.aje.a121436
42. Wiseman J, Grimes J, Eads RS. Louis encephalitis outbreak in Cameron County, Texas. Mosquito News. 1959;19(1). https://doi.org/10.5281/zenodo.16196516
43. Erickson TA, Ronca SE, Gunter SM, Brown EL, Hasbun R, Murray KO. Zoonotic disease testing practices in pediatric patients with meningitis and encephalitis in a subtropical region. Pathogens. 2022;11:501. https://doi.org/10.3390/pathogens11050501
44. Vanichanan J, Salazar L, Wootton SH, Aguilera E, Garcia MN, Murray KO, et al. Use of testing for West Nile virus and other arboviruses. Emerg Infect Dis. 2016;22:1587–93. https://doi.org/10.3201/eid2209.152050

Address for correspondence: Shannon E. Ronca, Baylor College of Medicine, Houston, 1102 Bates Ave, Ste 340, Houston, TX 77030, USA; email: ronca@bcm.edu

etymologia revisited

Plague
[plāg]

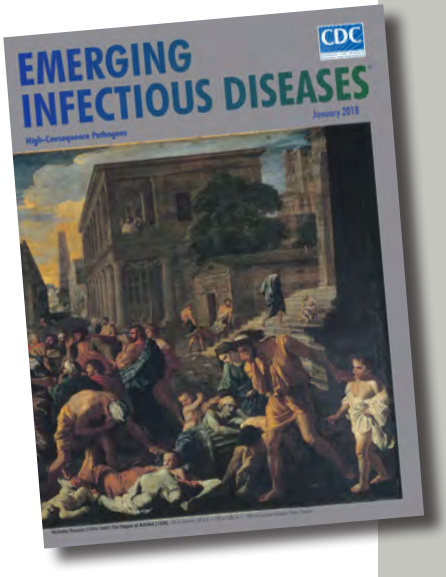

Originally published in January 2018

Plague (from the Latin plaga, "stroke" or "wound") infections are believed to have been common since at least 3000 BCE. Plague is caused by the ancestor of current Yersinia (named for Swiss bacteriologist Alexandre Yersin, who first isolated the bacterium) pestis strains. However, this ancestral Y. pestis lacked the critical Yersinia murine toxin (ymt) gene that enables vectorborne transmission. After acquiring this gene (sometime during 1600–950 BCE), which encodes a phospholipase D that protects the bacterium inside the flea gut, Y. pestis evolved the ability to cause pandemics of bubonic plague. The first recorded of these, the Justinian Plague, began in 541 CE and eventually killed more than 25 million persons.

References:

1. Alexandre Yersin BW. Etymologia: yersinia. Emerg Infect Dis. 2010;16:496.
2. Centers for Disease Control and Prevention. History of plague [cited 2017 Oct 19]. https://www.cdc.gov/plague/history/index.html.
3. Rasmussen S, Allentoft ME, Nielsen K, Orlando L, Sikora M, Sjögren K-G, et al. Early divergent strains of Yersinia pestis in Eurasia 5,000 years ago. Cell. 2015;163:571–82.

https://wwwnc.cdc.gov/eid/article/24/1/et-2401_article

Confirming ERVEBO Vaccination to Support Ebola Virus Surveillance

Elif Karaaslan, Amy Whitesell, Jason Malenfant, William C. Carson, Michael Townsend, Kasongo Kayembe Jolie, Enogo Koivogui, Siba Michel Grovogui, Boubacar Diallo, Nouonan Gbamou, Salomon Corvil, Sanaba Boumbaly, Lise Martel, Julie R. Sinclair, Alimou Camara, Trevor Shoemaker, Mary J. Choi, Joel M. Montgomery, Christina F. Spiropoulou, Éric Bergeron

Accurate confirmation of Ebola vaccination (ERVEBO) is essential for interpreting serologic data and assessing vaccine coverage during Ebola virus (EBOV) outbreaks. Current GP1,2-based assays cannot reliably distinguish vaccine-induced immunity from responses generated by natural infection. We developed a multiplex Luminex assay incorporating EBOV GP1,2, secreted glycoprotein (sGP), and a modified vesicular stomatitis virus nucleoprotein (VSV-P-N), a vector antigen encoded by ERVEBO but absent from wild-type EBOV. By using samples from US vaccinees and controls and a small comparison set from the Democratic Republic of the Congo, we found sGP and VSV-P-N demonstrated 100% sensitivity and ≥97.6% specificity for identifying vaccinees. In samples collected after a ring vaccination campaign in Guinea, combined sGP and VSV-P-N positivity confirmed vaccination in 94.8% of persons with written and 90.8% of persons with verbal confirmation of vaccination history. Our findings show that sGP and VSV-P-N provide a reliable signature of ERVEBO vaccination and support improved Ebola surveillance.

Ebolaviruses, from the Filoviridae family, include 6 known species in the *Orthoebolavirus* genus, 4 of which cause disease in humans: Ebola virus (EBOV), Sudan virus (SUDV), Bundibugyo virus, and Taï Forest virus. Ebola virus disease (EVD) is a rare but severe illness that begins with a nonspecific febrile phase and progresses to gastrointestinal symptoms and multiorgan failure; case-fatality rates are 25%–90% (*1*–*3*). Since 1976, when EBOV was first identified in the northern Democratic Republic of Congo (DRC), ebolaviruses have caused >40 outbreaks, >35,000 cases, and >15,000 deaths (*4*,*5*).

Efforts to control and prevent outbreaks of EVD has led to the development of 2 vaccines, each incorporating the EBOV envelope glycoprotein (GP1,2) as the primary antigen. The recombinant vesicular stomatitis virus (rVSV) vector-based vaccine for EBOV, ERVEBO (Merck, https://www.merck.com), contains the GP1,2 of the EBOV Kikwit strain (*6*). The use of ERVEBO was approved by the US Food and Drug Administration in 2019. The single-dose ERVEBO vaccine demonstrated efficacy by reducing the risk of EVD and death (*7*,*8*). ERVEBO provides protection beginning 10 days postvaccination, with glycoprotein (GP) antibody becoming detectable within 7–10 days (*7*,*9*). The second available vaccine is administered as a heterologous, 2-dose regimen: an adenovirus type 26 vectored vaccine with the GP of EBOV Mayinga variant as the first dose and a modified vaccinia Ankara virus vaccine containing GP of EBOV Mayinga, SUDV Gulu, and Marburg virus Musoke variants and nucleoprotein of Taï Forest virus as the second dose (*10*). Both vaccines induce strong humoral immune responses; the highest titers were detected on day 1 and at the 3-month post booster doses, and by month 12, titers decreased to prebooster levels. Both vaccines induce long-term memory cellular responses and antibody responses that remain detectable for up to 5 years (*11*,*12*).

Several factors lead to an increased risk for EVD outbreaks, including zoonotic spillovers, the expansion of at-risk areas, deficiencies in healthcare

Author affiliations: Centers for Disease Control and Prevention, Atlanta, Georgia, USA (E. Karaaslan, A. Whitesell, J. Malenfant, W.C. Carson, M. Townsend, L. Martel, J.R. Sinclair, T. Shoemaker, M.J. Choi, J.M. Montgomery, C.T. Spiropoulou, É. Bergeron); African Field Epidemiology Network, Conakry, Guinea (K.K. Jolie, S. Corvil); Ministry of Health, Conakry (E. Koivogui, S.M. Grovogui); US Centers for Disease Control and Prevention, Conakry (B. Diallo); Agence Nationale de Sécurité Sanitaire, Conakry (N. Gbamou); International Center for Research of Tropical Infections in Guinea, N'Zerekore, Guinea (S. Boumbaly); Ministry of Higher Education, Scientific Research, and Innovation, Conakry (A. Camara); University of Georgia, Athens, Georgia, USA (É. Bergeron).

DOI: https://doi.org/10.3201/eid3204.251906

systems, and socioeconomic challenges. Among those factors, persistent infections in survivors represents a major concern and has been implicated as the origin of one quarter of outbreaks (*13*–*15*). Although vaccine successes might address many of those challenges, robust and high-sensitivity assays remain essential for accurately determining vaccination status for surveillance and to monitor waning vaccine immunity (*16*). Ebola GP1,2 is the favored antigen, albeit with caveats, for detecting immune responses after vaccination and infection; however, there remains a need to distinguish vaccinees from survivors. Incorporating viral antigens that are not present in the vaccines can better identify survivors, yet identifying vaccinees and monitoring vaccine immunity can benefit from assays targeting vector immunity. Assays that successfully identify vector immunity after rVSV vaccination will be a valuable tool, especially because other rVSV-based vaccines, such as those for SUDV, Nipah virus, and Lassa virus, are currently in various phases of preclinical assessments and clinical trials (*17*–*19*). We describe a multiplex Luminex assay (Diasorin, https://us.diasorin.com) that incorporates Ebola GP1,2, Ebola secreted glycoprotein (sGP), and VSV-P-N antigen detection to confirm Ebola vaccination.

Materials and Methods

Ethics Approval

All research activities were performed in compliance with the regulations and policies to protect human participants, including written consent. For the samples from the Centers for Disease Control and Prevention (CDC), written informed consent was obtained, and the study was approved for use in this research by CDC Institutional Review Board (IRB) (approval no. 7302). The DRC specimens were originally collected under separate study protocol approvals from the CDC IRB and the Kinshasa School of Public Health IRB. Specimens were deidentified (CDC IRB protocol no. 7294) with no reidentification key retained, and this activity was determined to be exempt human subjects research under CDC authority (45 C.F.R. §46.104). In Guinea, the study was approved by the Comité National d'Ethique pour la Recherche en Santé. Negative control human serum from the United States used in this study were obtained from BioIVT (New York, USA), a commercial biorepository. Written informed consent was obtained from all donors before sample collection, and IRB approval was secured by BioIVT for the procurement and use of the specimens in research. Because the samples were fully anonymized, no additional ethics review was required for their use. All samples were stored at −80°C and heat-inactivated at 56°C for 30 minutes before use.

Recombinant Protein Production

We designed the construct for the ectodomain of EBOV GP1,2 (variant Kikwit9; GenBank accession no. P87666) with trimer stabilizing mutations and C-terminal His and Avi-Tags as previously described (Figure 1, panel A) (*20*). We also designed the construct of EBOV soluble GP (variant Ituri2018; GenBank accession no. AYN74068.1) to have C-terminal His and Avi-Tags. We codon-optimized the cDNA sequences for mammalian expression, synthesized, and cloned them into a pEEV-Puro (*21*) episomal expression vector (Twist Bioscience, https://www.twistbioscience.com). To express EBOV GP1,2 and sGP, we grew Expi293F cells (Thermo Fisher Scientific, https://www.thermofisher.com) in Expi293 expression medium (Thermo Fisher Scientific) and transiently transfected them by using the ExpiFectamine 293 Transfection Kit (Thermo Fisher Scientific) following the manufacturer's recommendations. Four to 6 days after transfection, we collected the culture supernatants, cleared them of cell debris by centrifugation at 10,000 rpm for 20 minutes, and processed them for protein purification.

To increase the solubility, stability, and yield of the nucleoprotein of VSV, we designed a construct with phosphoprotein (P protein) fused to the N-terminus of the nucleoprotein (*22*,*23*). The construct also included an N terminal His-Tag and glutathione S-transferase separated by human rhinovirus 3C cleavage site and a C-terminal Avi-Tag. We codon-optimized the sequence for bacterial expression and cloned into a pET28a bacterial expression vector (Twist Bioscience). The recombinant protein was expressed as described previously (*24*).

We loaded the cleared mammalian cell supernatants and bacterial cell lysates onto HisTrap Excel columns (Cytiva, https://www.cytivalifesciences.com). We biotinylated purified proteins with Avi-Tags by using BirA biotin-protein ligase according to the manufacturer's instructions (Avidity Biosciences, https://www.aviditybiosciences.com). We removed excess biotin and further purified proteins by using size exclusion chromatography (Superdex 200 pg [Cytiva]). We pooled, aliquoted, and stored protein-containing fractions at −80°C. We produced the cross-neutralizing monoclonal antibody 114 (*25*) in-house by transfecting plasmids encoding the heavy and light chains into Expi293 cells (Thermo Fisher Scientific), and we expressed and purified the monoclonal antibody as described previously (*26*).

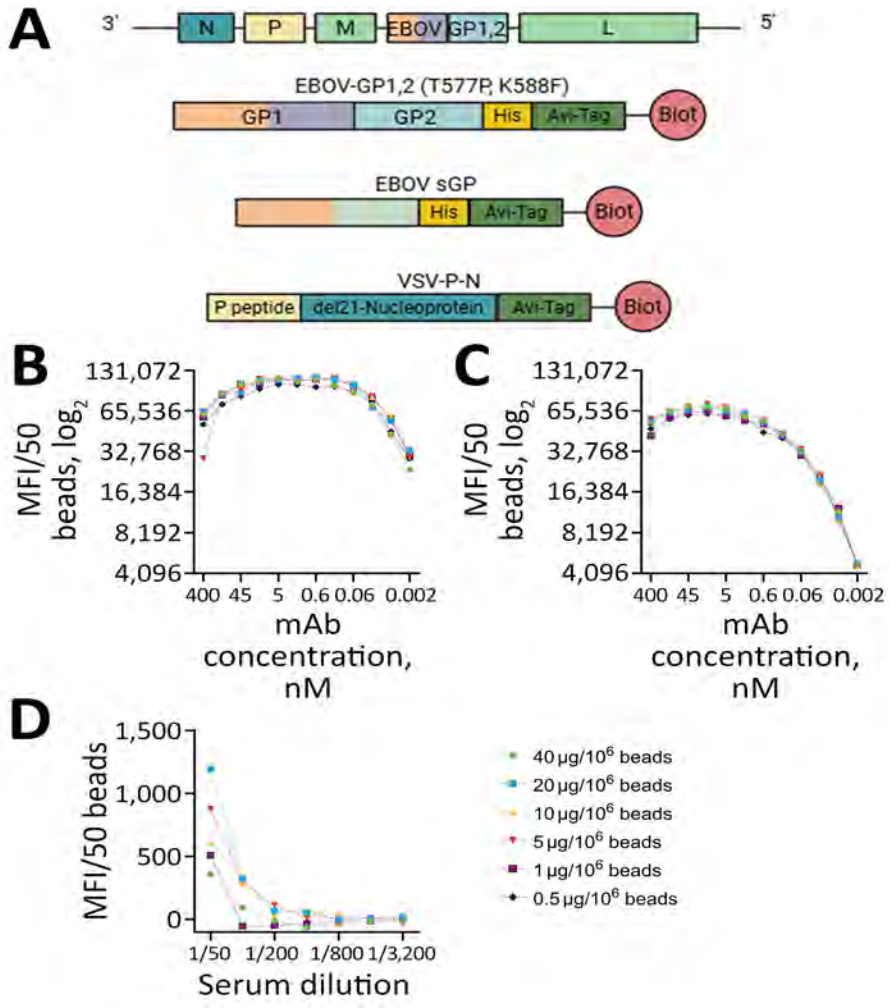

Figure 1. Antigen selection and assay optimization for study of development of multiplex assay to confirm Ebola vaccination. A) Schematic illustration of the rVSVΔG-ZEBOV-GP genome and proteins used in the assay design. Orange indicates the shared portion in GP1 and sGP. del21-nucleoprotein denotes the deletion of the N terminal 21 amino acids of VSV nucleoprotein. B–D) The effect of coupling protein concentration on detection was measured as MFI/50 beads by using mAb114 for EBOV GP1,2 (B) and EBOV sGP (C) and a serum sample from an ERVEBO vaccinee for VSV-P-N (D). Figure created using BioRender (https://www.biorender.com). Avi-tag, Avidin tag; Biot, protein biotinylation; EBOV, Ebola virus; GP, glycoprotein; His-tag, histidine tag; L, large RNA polymerase; M, matrix; mAb, monoclonal antibody; MFI, mean fluorescence intensity; N, nucleocapsid; P, phosphoprotein; P peptide, the first 60 amino acids of the VSV phosphoprotein; rVSVΔG-ZEBOV-GP, recombinant vesicular stomatitis virus where VSV glycoprotein G gene is deleted and replaced with the Ebola virus glycoprotein gene; sGP, secreted glycoprotein; VSV, vesicular stomatitis virus; VSV-P-N, vesicular stomatitis virus nucleoprotein N-terminally fused with P peptide.

Development of Multiplex Luminex Assay

We used Luminex xMAP (Diasorin) technology to develop the multiplex assay. We bound the biotinylated Avi-tagged EBOV GP1,2, EBOV sGP, and VSV-P-N to avidin-coupled magnetic microspheres (Diasorin), following manufacturer instructions. We removed the storage buffer by magnetic separation and then resuspended the beads in assay buffer (phosphate-buffered saline [PBS; ThermoFisher Scientific] with 1% bovine serum albumin [BSA; Millipore Sigma, https://www.sigmaaldrich.com]). We diluted biotinylated proteins in assay buffer and added them to the microsphere suspension. We incubated the bead-protein mixture for 2 hours at room temperature with rotation. After incubation, we washed the beads 3 times with wash buffer (PBS with 1% BSA and 0.02% Tween-20 [Millipore Sigma]). We counted protein-coupled beads by using the Moxi Z Mini cell counter (ORFLO, https://biofrontiertechnology.com) and stored them in assay buffer at 4°C in the dark. Detailed protocols for assay optimization, validation procedures, and comparison with Filovirus animal nonclinical group (FANG) ELISA standards are provided (Appendix, http://wwwnc.cdc.gov/EID/article/32/4/25-1906-App1.pdf).

Statistical Analysis

We conducted receiver operating characteristic (ROC) analyses by testing samples from unvaccinated US donors and US vaccinees to determine assay cutoffs, the area under the curve, and the sensitivity and specificity of the assays. We calculated the correlation between assays by using Spearman correlation. We calculated the 95% CIs of the assays percent positivity by using the R package binom (The R Project for Statistical Computing, https://www.r-project.org). We tested the statistical difference in the normalized mean fluorescence intensity (MFI) values in US vaccinees grouped on the basis of time postvaccination by using the Kruskal-Wallis test with the 2-stage step-up method of Benjamini,

Krieger, and Yekutieli to correct for multiple comparisons. We determined the statistical significance of the change in the sensitivity of the assays by using Fisher exact test. We performed all analyses by using GraphPad version 10.1.2 (www.graphpad.com) and RStudio (The R Project for Statistical Computing). We created the figures by using BioRender (https://www.biorender.com).

Results

Assay Optimization and Internal Reference Standard

Site-specific transcriptional editing of the GP gene of EBOV results in 2 main products: the cleaved structural GP1,2 and the sGP. sGP shares the same N terminal sequence as the GP1 subunit of GP1,2, encompassing the glycan cap and receptor-binding region (*28*). GP1,2 is the trimeric surface protein that enables virus entry and fusion, whereas sGP is produced in large quantities in the plasma of infected patients (Appendix Figure 1). Along with EBOV GP1,2, we investigated EBOV sGP's performance in serologic assays (Figure 1, panel A). During optimization, we observed a consistent difference between the 2 proteins. Although increasing the coupled protein concentration did not enhance signal intensity for either protein, sGP consistently produced higher signals than GP1,2 at the same monoclonal antibody 114 concentration (Figure 1, panels B, C). Similarly, the use of sGP resulted in higher signals with FANG ELISA reference samples and a serum sample from an ERVEBO vaccinee (Appendix Figure 2, panels A, B). Although the signal with the negative sample (BMI529) was similar (Appendix Figure 2, panels A, B), sGP yielded a 2- to 3.7-fold higher signal with those samples. The higher signal confirmed the observed difference was not limited to monoclonal antibodies but was also possible in polyclonal antibodies. Although that difference might be explained by the larger size of GP1,2, the orientation of the protein during biotin-mediated bead coupling, and epitope accessibility, it also suggests improved separation between negative and positive samples with sGP compared with GP1,2.

As a reference and comparator, we defined the concentration of internal control by using reference and quality control samples in the FANG ELISA to measure Ebola GP1,2 antibodies in vaccine efficacy studies. Our internal reference standard was assigned as 1,024 EU/mL (Appendix Figure 2, panel A).

To express VSV nucleoprotein (VSV-N), we incorporated 2 previously reported modifications into the construct (*22*,*23*). We fused the first 60 amino acids of the P protein to the N-terminus of the VSV-N to prevent N from binding to cellular RNA and self-oligomerization. Next, we expressed VSV-N without the first 21 amino acids, a truncation known to stabilize RNA-bound N oligomers. The design resulted in an RNA-free form of VSV-N, termed VSV-P-N, with the desired solubility and stability (Figure 1, panel A). On the basis of the optimizations, we selected the concentration at which the highest signal was obtained for further assays (Figure 1, panel D). The signal obtained with EBOV-infected nonhuman primate samples was below that of the negative control, whereas FANG ELISA references and ERVEBO vaccinee samples yielded signals 4- to 25-fold higher than the negative control (Appendix Figure 2, panel C).

Enhanced Detection of ERVEBO Vaccination Status

To assess the performance of sGP and VSV-P-N antigens in confirming ERVEBO vaccination status, we determined assay cutoffs by using samples collected from healthy US donors as negatives (n = 84) and from US ERVEBO vaccinees (n = 48). The cutoffs were determined to be 668.7 MFI for EBOV GP1, 2 (Figure 2, panels A–D), 400 MFI for EBOV SGP (Figure 2, panels B–E), and 1,350 MFI for VSV-P-N (Figure 2, panels C–F). With those cutoffs, EBOV GP1,2 could detect antibodies in 46 of 48 vaccinees (sensitivity 95.8% [95% CI 86.02%–99.26%], specificity 98.8% [95% CI 92.83%–99.93%]) (Figure 2, panel D; Appendix Figure 3). In comparison, EBOV sGP detected all vaccinees (sensitivity 100% [95% CI 92.59%–100%], specificity 97.6% [95% CI 91.73%–99.58%]) (Figure 2, panel E). Similar to EBOV sGP, VSV-P-N detected all vaccinees, indicating that vector-induced immunity after rVSV vaccination is sufficient as a marker of vaccination status (sensitivity 100% [95% CI 92.59%–100%], specificity 100% [95% CI 93.56%–99.94%]) (Figure 2, panel F). Analysis of correlation between assays revealed a strong correlation between EBOV GP1,2 and EBOV sGP (r = 0.8668; 95% CI 0.7696–0.9248). The correlation between VSV-P-N and EBOV sGP was 0.6080 (95% CI 0.3842–0.7643), whereas the correlation between VSV-P-N and EBOV GP1,2 was 0.5916 (95% CI 0.3621–0.7535) (Appendix Figure 4, panels A–C). Overall, our results reveal the higher sensitivity of EBOV sGP compared with EBOV GP1,2 and underscore the value of including VSV-P-N to identify ERVEBO vaccinees.

Although we used US samples as a negative control group for assay development and cutoff determination, we also evaluated background reactivity by using samples from DRC, an EVD-endemic country that has experienced multiple outbreaks. We included

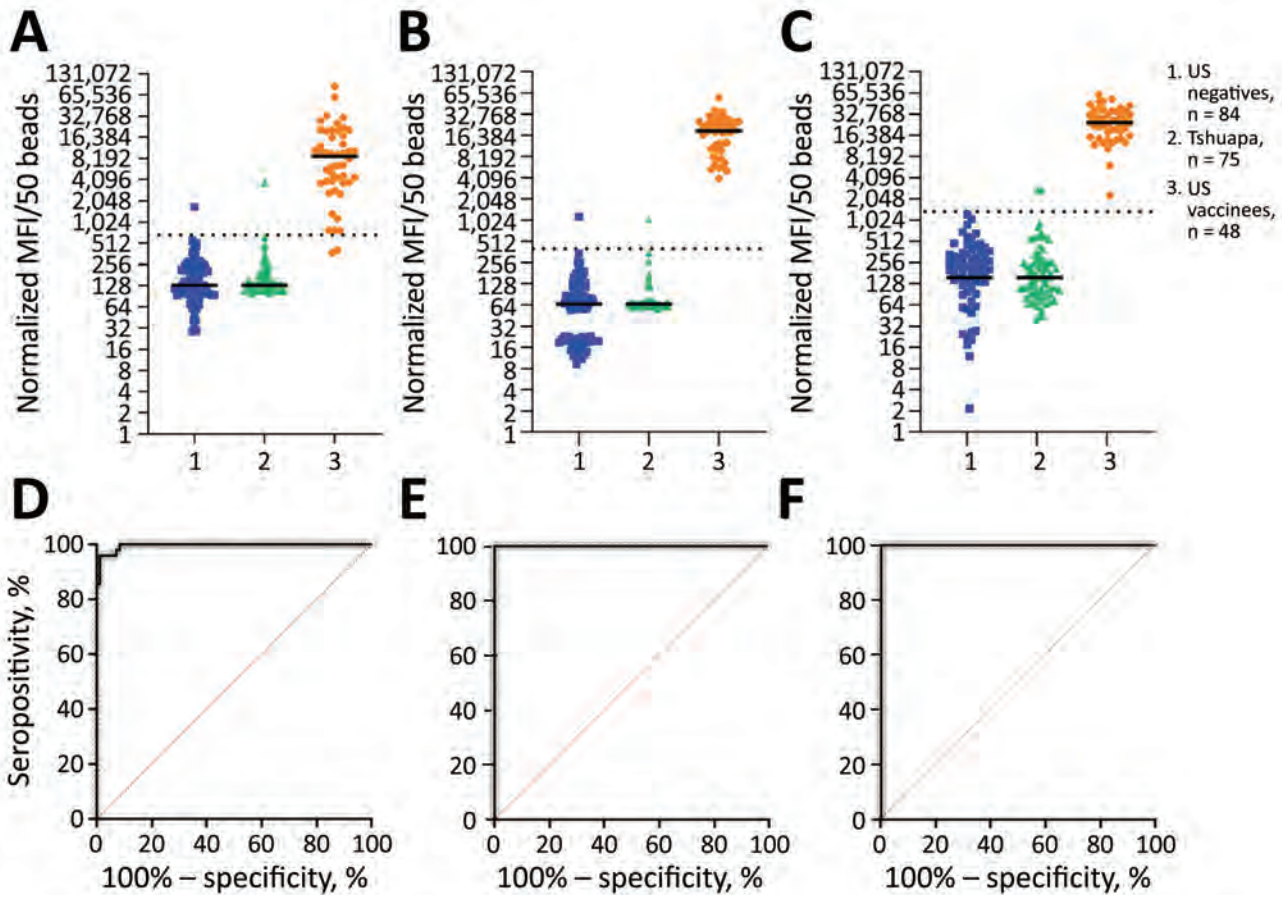

Figure 2. Detection of ERVEBO vaccinees enhanced with EBOV sGP and VSV-P-N for study of development of multiplex assay to confirm Ebola vaccination. A–C) The $\log_2$-normalized MFI values for EBOV GP1,2 (A), EBOV sGP (B), and VSV-P-N (C) assays for US negative controls (n = 84), Tshuapa samples (n = 75), and US vaccinees (n = 48) are shown in scatter plots. Horizontal solid lines indicate medians; horizontal dotted lines indicate the assay-specific cutoff values. D–F) Receiver operating characteristic (ROC) curves (black lines) and sensitivity and specificity were measured at the defined cutoffs for EBOV GP1,2 (D), EBOV sGP (E), and VSV-P-N (F). ROC area values: D, 0.9950 (95% CI 0.9870–1.000); E, F, 1.000. Sensitivity: D, 95.8% (95% CI 86.02%–99.26%); E, 100% (95% CI 92.59%–100%); F, 100% (95% CI 92.59%–100%). Specificity: D, 98.6% (95% CI 92.83%–99.93%); E, 97.6% (95% CI 91.73%–99.58%); F, 98.8% (95% CI 93.56%–99.94%). EBOV, Ebola virus; GP, glycoprotein; MFI, mean fluorescence intensity; sGP, secreted glycoprotein; VSV-P-N, vesicular stomatitis virus nucleoprotein N-terminally fused with P peptide.

75 samples collected from healthcare workers in 2017 from the Bokungu and Mondombe territories in Tshuapa Province, DRC. The Tshuapa territories are located outside the Boende health zone, where an EVD outbreak occurred in 2014. This population is considered high risk for natural infection and did not receive an Ebola vaccine before sample collection. Only 1 person from the Tshuapa cohort yielded a signal above the cutoff for both EBOV GP1,2 and sGP, and 2 samples were above the cutoff for VSV-P-N (Figure 2, panels A–C), revealing a 1.3% reactivity for EBOV GP1,2 and sGP and 2.7% reactivity for VSV-P-N in Tshuapa samples.

By using those markers to determine vaccination status, we have raised the question of antibody waning and the long-term durability of the immune response. To evaluate this aspect, we grouped samples from the US vaccinees who received 1 dose of the vaccine into time intervals of ≤6 months, 6–12 months, and >12 months postvaccination and evaluated the changes in median MFI signal over time (Figure 3, panels A–C). Although our sample sizes were limited, we did not detect any major differences in the median MFI signals. However, EBOV GP1,2 did not detect all vaccinees: 3 vaccinees had no positive EBOV GP1,2 at the tested dilution, and 1 additional vaccinee showed discordant results across longitudinal draws (6-month sample detectable by EBOV GP1,2, >12 month sample not detected).

VSV-P-N and EBOV sGP Identification of ERVEBO Vaccinees After Ring Vaccination Campaign

In 2021, an EVD outbreak was reported with 7 cases in Gouéké, Nzérékoré region, Guinea. A ring vaccination campaign with ERVEBO was initiated for contacts of the EVD cases. Approximately 14 months after vaccination, samples were collected from persons who verbally confirmed EBOV vaccination (n = 411) or presented a vaccination card as written proof (n = 115). Among persons with vaccination cards, 94.8% were positive for both VSV-P-N and EBOV sGP, compared with 71.3% who were positive for both VSV-P-N and EBOV GP1,2 (Figure 4, panel A), a statistically significant difference (p<0.0001). Sensitivity for EBOV GP1,2 was 72.1%, for EBOV sGP was 99.1%, and for VSV-P-N was 96.5% (Appendix Figure 5, panels A–C). The correlation between assays was 0.5687 (95% CI 0.4259–0.6838) for VSV-P-N and EBOV sGP and 0.4266 (95% CI 0.2590–0.5692) for EBOV GP1,2 (Figure 4, panels B, C). Similarly, in the group with only verbal confirmation of vaccination, double-positivity for VSV-P-N and EBOV sGP identified 90.8% of persons as vaccinees, compared with 63.3% with EBOV GP1,2, a statistically significant difference (p<0.0001) (Figure 4, panel D). The correlation between assays was 0.6852 (95% CI 0.6285–0.7346) for VSV-P-N and EBOV sGP, and 0.59 (95% CI 0.5210–0.6513) for EBOV GP1,2 (Figure 4 panels E and F). Consistent with the results from persons who presented a vaccination card, VSV-P-N and EBOV sGP showed strong agreement with a Cohen's κ coefficient of 0.85 (95% CI 0.79–0.90) compared with VSV-P-N and EBOV GP1,2 (Cohen's κ coefficient 0.46 [95% CI 0.39–0.53]).

Discussion

We developed and validated a multiplex Luminex (Diasorin) assay that can simultaneously detect antibodies binding to 3 antigens: EBOV sGP, EBOV GP1,2, and VSV-P-N. Our findings demonstrate robust performance of the assay across different cohorts, including US vaccinees, samples from the Tshuapa province in the DRC, and samples from Guinea with high sensitivity and specificity.

Previous studies in EVD survivors reported 80%–90% seroconversion to GP and sGP, and responses to nucleoprotein (NP) were the next most frequent (*29*,*30*). GP1,2 has been the primary antigen used in serologic assay platforms because it is incorporated into current vaccines and survivors typically exhibit robust seroconversion (*27*,*29*–*34*). However, the use of different cutoff values and reliance on baseline samples to adjust thresholds, weak correlation among GP1,2-based assays, and the need to include multiple antigen targets to improve specificity highlight the limitations and the need for alternatives to currently available assays (*30*–*32*). Despite sharing a common N terminal region with GP1,2 and the demonstrated cross-reactivity of antibodies, sGP's potential for identifying vaccine-induced immunity remains largely unexplored. In this study, we tested samples from 48 ERVEBO vaccinees from the United States. All

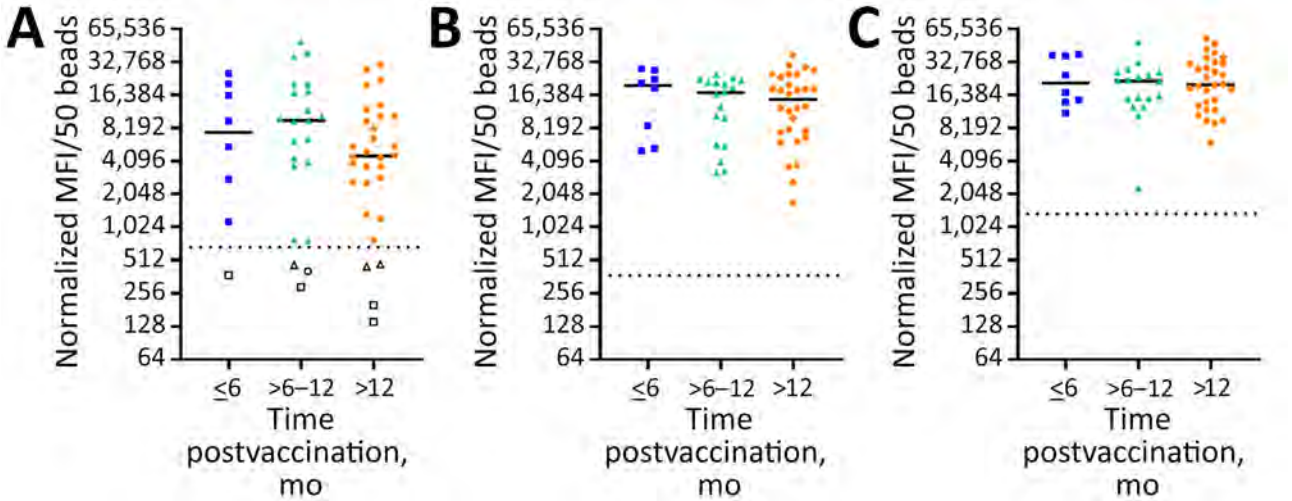

Figure 3. Kinetics of antibody responses in ERVEBO vaccinees for study of development of multiplex assay to confirm Ebola vaccination. US vaccinees who received 1 dose of ERVEBO vaccine were grouped into time intervals of ≤6 months, >6–12 months, and >12 months postvaccination, and changes in median MFI signal over time were evaluated. A) Ebola virus (EBOV) glycoprotein (GP) 1,2; B) EBOV secreted GP; C) vesicular stomatitis virus nucleoprotein N-terminally fused with P peptide. The scatter plots represent readings from each sample; horizontal solid lines represent group medians, and horizontal dotted lines represent the cutoff for the given protein. The empty squares, triangles, and circle represent samples from 3 vaccinees that were not detected with EBOV GP1,2. MFI, mean fluorescence intensity.

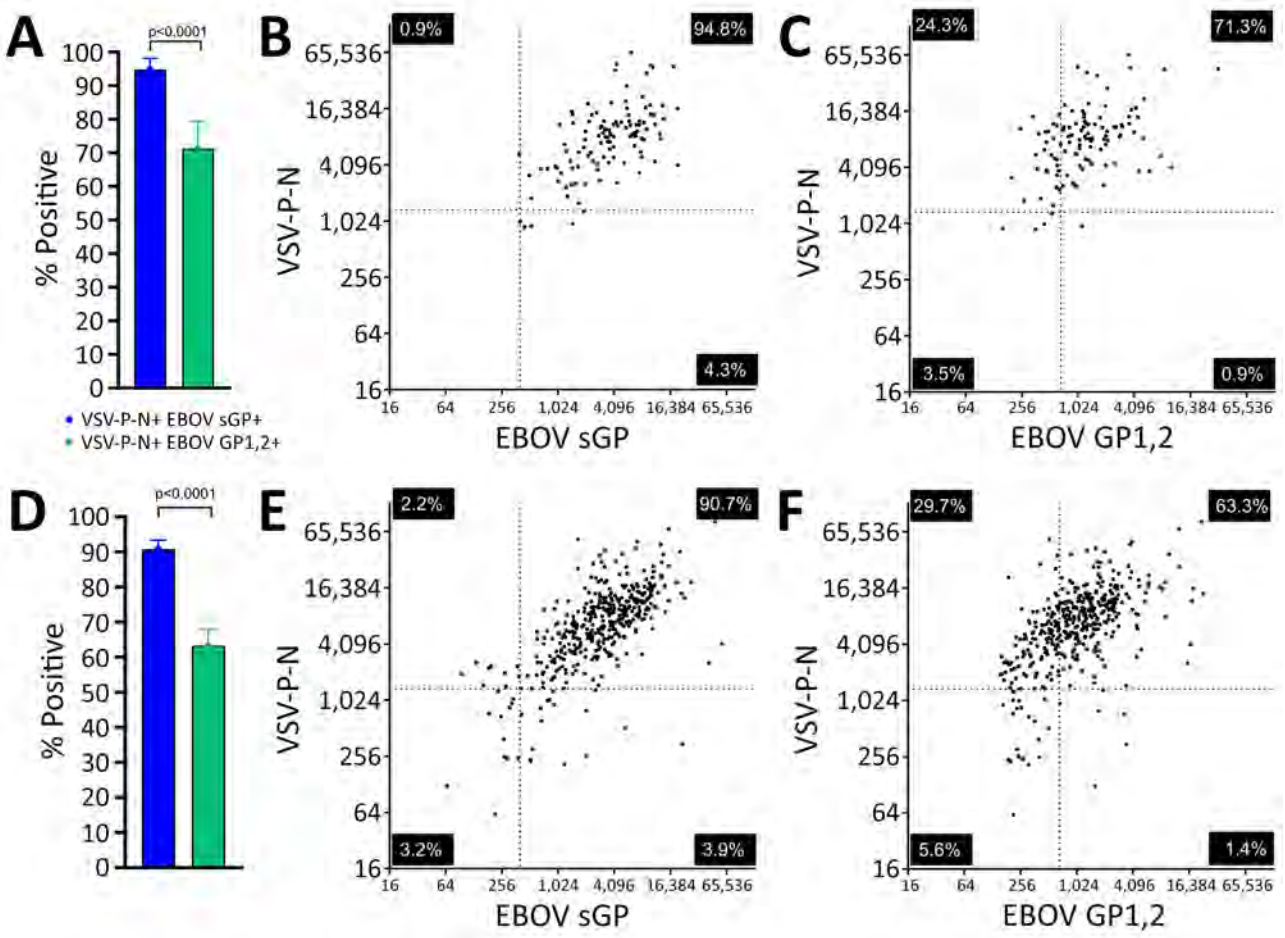

Figure 4. Superiority of EBOV sGP and VSV-P-N in identifying ERVEBO vaccinees for study of development of multiplex assay to confirm Ebola vaccination. A) Percentages of persons with vaccination cards (n = 115) whose vaccination status was confirmed by either positive VSV-P-N and EBOV sGP or positive VSV-P-N and EBOV GP1,2. B, C) Correlation of VSV-P-N and EBOV sGP (B) and VSV-P-N and EBOV GP1,2 (C). D) Percentages of persons with verbally confirmed vaccination status (n = 411) that were confirmed as vaccinees on the basis of positivity for either VSV-P-N and EBOV sGP, or VSV-P-N and EBOV GP1,2. E, F) Correlation of VSV-P-N and EBOV sGP (E) and VSV-P-N and EBOV GP1,2 (F). Error bars indicate 95% CIs. Correlations between results were tested by Spearman correlation r values with 95% CIs. Horizontal and vertical lines in the scatter plots indicate the established cutoff values for the antigens shown on the corresponding axes. Each quadrant of the correlation graphs is labeled with the percentage of the samples that tested negative, single positive, and double positive by assays given on the *x*- and *y*-axes. Figure created using BioRender (https://www.biorender.com). EBOV, Ebola virus; GP, glycoprotein; sGP, secreted glycoprotein; VSV-P-N, vesicular stomatitis virus nucleoprotein N-terminally fused with P peptide.

vaccinee samples tested positive with EBOV sGP (100% sensitivity, 97.6% specificity), demonstrating that sGP effectively detects antibody responses to EBOV GP1,2. In contrast, EBOV GP1,2 testing detected antibodies in 46 vaccinees (95.8% sensitivity, 98.8% specificity), indicating that sGP not only detects antibodies to EBOV GP1,2 but outperformed GP1,2.

Reliable identification of vaccine-induced immunity is essential for monitoring immune durability, assessing vaccine efficacy, and detecting breakthrough infections. To differentiate vaccine-induced immunity, one strategy is to target viral antigens absent from current vaccine formulations; another is to detect immune responses against the vaccine vector itself. A previous study addressing the strategy to target viral antigens developed an assay by using peptides from viral protein (VP) 40, VP35, and NP, viral antigens not included in the current EBOV vaccines (*35*). Two studies investigating vector immunity reported suboptimal responses, with only 28% seroconversion to VSV-M at 56 days postvaccination, no response to VSV-M, and only 1 vaccinee with VSV-N antibodies in another study (*36*,*37*). In this study, we show that VSV-P-N antibodies are detected in all vaccinees. Of note, similar to sGP, VSV-P-N detected vaccinees that were missed by GP1,2, highlighting its

added sensitivity. Although the samples were limited to US vaccinees, we did not observe a decline in either assay sensitivity or median signal intensity. That observation contrasts with a previous study that reported waning VSV-N responses over time, with a corresponding decrease in assay sensitivity from 90% to 65% 1 year after vaccination (*38*). Further studies with larger longitudinal cohorts are needed to confirm those findings. Overall, our results support the utility of this assay for long-term monitoring of immune responses to both the target antigen and the vaccine vector.

A study conducted during the 10th EVD epidemic in DRC (*8*) described the protective efficacy of ERVEBO vaccination against death in patients with confirmed EVD. The study reported a 25% case-fatality rate among vaccinated patients, contrasting with the 100% vaccine efficacy previously reported (*7*). Although an inadequate immune response because of host-related factors, logistical issues, and administration errors could explain the discrepancy between the 2 studies, potential misclassification of vaccination status might have contributed to the differences observed. Without reliable assays, such insights depend solely on self-reported vaccination status. Our results from the Guinea cohort with samples from persons who had a vaccination card revealed that VSV-P-N and EBOV sGP double positivity confirmed the ERVEBO vaccination status of 94.8% of persons. In contrast, the percentage of double positivity by using EBOV GP1,2 was much lower at 71.3%. Similarly, a greater number of persons who had verbally confirmed their vaccination status were identified by double positivity for VSV-P-N and EBOV sGP (VSV-P-N and EBOV sGP 90.8%, VSV-P-N and EBOV GP1,2 63.3%). Those results underscore the value of this assay in verifying vaccination status and support the use of VSV-P-N with EBOV sGP as a superior alternative to EBOV GP1,2 for detecting vaccine-induced antibody responses.

A 2023 study assessed the seroreactivity of 698 samples from healthcare providers and frontline workers to EBOV GP1,2 by using both FANG ELISA and a Luminex assay targeting additional antigens (*39*). The study reported that 1.4% of samples were reactive to >1 EBOV antigen with the Luminex (Diasorin) assay. Of note, only 0.8% of the samples were positive by both FANG ELISA and Luminex GP1,2, despite individual positivity rates of 7% for FANG ELISA and 9.4% for Luminex GP1,2, highlighting poor agreement between the 2 assays. The study was conducted at Boende General Hospital in Tshuapa Province, whereas samples used in our study were collected from healthcare workers in Tshuapa territories outside the Boende health zone. Consistent with the 2023 study, we found only 1 sample reactive to both EBOV sGP and GP1,2, corresponding to a seroreactivity rate of 1.3%.

The first limitation of our study is the absence of samples from unvaccinated EVD survivors, which would have provided further insights into the assay's ability to differentiate between vaccine-induced and infection-acquired immunity. Because survivors typically exhibit higher GP antibody levels than vaccinated persons, we anticipate that the assay would demonstrate high sensitivity for detecting survivor antibodies. However, comprehensive differentiation between vaccination and natural infection would require incorporation of additional viral antigens such as NP and VP40, because antibody responses to those antigens are typically observed only after natural infection. An additional limitation of this study is that the assay is specific to identifying ERVEBO vaccination status. Future studies incorporating survivor samples and expanded antigen panels will be essential for complete assay validation and epidemiologic applications.

In conclusion, our study introduces a novel multiplex serologic assay that includes EBOV sGP and VSV-P-N antigens to improve detection of postvaccination antibodies. The assay demonstrates high sensitivity and specificity and requires minimal sample volume. With the assay's increased sensitivity, this platform could strengthen the evaluation of vaccine-induced immunity by helping identify correlates of protection, assess the durability of immune responses, and support adverse event reporting by differentiating vaccine-related reactions from symptoms of concurrent infection. By using samples from US ERVEBO vaccinees and post–ring vaccination samples from Guinea, we found that sGP offers superior sensitivity compared with GP1,2, and that the combined use of sGP and VSV-P-N reliably identifies vaccinated persons.

Deidentified datasets generated and analyzed during this study are available from the corresponding author upon reasonable request.

This work was supported by the Centers for Disease Control and Prevention, Emerging Infectious Diseases Program. Support for E.K. was provided through an Oak Ridge Institute for Science and Education fellowship.

Artificial intelligence (AI) tools were used to assist with language editing and organization. No AI tool contributed to the scientific content, analysis, interpretation of data, or conceptual development of the manuscript. All authors

reviewed and verified the accuracy and originality of all text. No confidential or nonpublic data were entered into any AI tool.

About the Author

Dr. Karaaslan is a scientist in the Viral Special Pathogens Branch, Division of High-Consequence Pathogens and Pathology, National Center for Emerging and Zoonotic Infectious Diseases, CDC, whose research centers on immunology and the development of multiplex and high-throughput diagnostic platforms for high-consequence viral pathogens. Her interests include developing these tools to advance the understanding of vaccine-induced immunity and enhance laboratory capacity in outbreak and endemic settings.

References

1. Jacob ST, Crozier I, Fischer WA II, Hewlett A, Kraft CS, Vega M-AL, et al. Ebola virus disease. Nat Rev Dis Primers. 2020;6:13. https://doi.org/10.1038/s41572-020-0147-3
2. World Health Organization. Ebola virus disease [cited 2025 Mar 21]. https://www.who.int/news-room/fact-sheets/detail/ebola-virus-disease
3. Judson SD, Munster VJ. The multiple origins of Ebola disease outbreaks. J Infect Dis. 2023;228(Suppl 7):S465–73. https://doi.org/10.1093/infdis/jiad352
4. Izudi J, Bajunirwe F. Case fatality rate for Ebola disease, 1976–2022: a meta-analysis of global data. J Infect Public Health. 2024;17:25–34. https://doi.org/10.1016/j.jiph.2023.10.020
5. Rugarabamu S, Mboera L, Rweyemamu M, Mwanyika G, Lutwama J, Paweska J, et al. Forty-two years of responding to Ebola virus outbreaks in Sub-Saharan Africa: a review. BMJ Glob Health. 2020;5:e001955. https://doi.org/10.1136/bmjgh-2019-001955
6. Huttner A, Agnandji ST, Combescure C, Fernandes JF, Bache EB, Kabwende L, et al.; VEBCON; VSV-EBOVAC; VSV-EBOPLUS Consortia. Determinants of antibody persistence across doses and continents after single-dose rVSV-ZEBOV vaccination for Ebola virus disease: an observational cohort study. Lancet Infect Dis. 2018;18:738–48. https://doi.org/10.1016/S1473-3099(18)30165-8
7. Henao-Restrepo AM, Camacho A, Longini IM, Watson CH, Edmunds WJ, Egger M, et al. Efficacy and effectiveness of an rVSV-vectored vaccine in preventing Ebola virus disease: final results from the Guinea ring vaccination, open-label, cluster-randomised trial (Ebola Ça Suffit!). Lancet. 2017;389:505–18. https://doi.org/10.1016/S0140-6736(16)32621-6
8. Coulborn RM, Bastard M, Peyraud N, Gignoux E, Luquero F, Guai B, et al. Case fatality risk among individuals vaccinated with rVSVΔG-ZEBOV-GP: a retrospective cohort analysis of patients with confirmed Ebola virus disease in the Democratic Republic of the Congo. Lancet Infect Dis. 2024;24:602–10. https://doi.org/10.1016/S1473-3099(23)00819-8
9. Kucharski AJ, Eggo RM, Watson CH, Camacho A, Funk S, Edmunds WJ. Effectiveness of ring vaccination as control strategy for Ebola virus disease. Emerg Infect Dis. 2016;22:105–8. https://doi.org/10.3201/eid2201.151410
10. Ishola D, Manno D, Afolabi MO, Keshinro B, Bockstal V, Rogers B, et al.; EBL3001 study group. Safety and long-term immunogenicity of the two-dose heterologous Ad26.ZEBOV and MVA-BN-Filo Ebola vaccine regimen in adults in Sierra Leone: a combined open-label, non-randomised stage 1, and a randomised, double-blind, controlled stage 2 trial. Lancet Infect Dis. 2022;22:97–109. https://doi.org/10.1016/S1473-3099(21)00125-0
11. Farooq F, Beck K, Paolino KM, Phillips R, Waters NC, Regules JA, et al. Circulating follicular T helper cells and cytokine profile in humans following vaccination with the rVSV-ZEBOV Ebola vaccine. Sci Rep. 2016;6:27944. https://doi.org/10.1038/srep27944
12. Wiedemann A, Lhomme E, Huchon M, Foucat E, Bérerd-Camara M, Guillaumat L, et al.; Prevac study team. Long-term cellular immunity of vaccines for Zaire Ebola virus diseases. Nat Commun. 2024;15:7666. https://doi.org/10.1038/s41467-024-51453-z
13. World Health Organization. Ebola, West Africa, 2014–2016 [cited 2024 Nov 6]. https://www.who.int/emergencies/situations/ebola-outbreak-2014-2016-West-Africa
14. Liu J, Trefry JC, Babka AM, Schellhase CW, Coffin KM, Williams JA, et al. Ebola virus persistence and disease recrudescence in the brains of antibody-treated nonhuman primate survivors. Sci Transl Med. 2022;14:eabi5229. https://doi.org/10.1126/scitranslmed.abi5229
15. MacIntyre CR, Chughtai AA. Recurrence and reinfection—a new paradigm for the management of Ebola virus disease. Int J Infect Dis. 2016;43:58–61. https://doi.org/10.1016/j.ijid.2015.12.011
16. Valayer S, Alexandre M, Prague M, Beavogui AH, Doumbia S, Kieh M, et al. Evaluation of waning of IgG antibody responses after rVSVΔG-ZEBOV-GP and Ad26.ZEBOV, MVA-BN-Filo Ebola virus disease vaccines: a modelling study from the PREVAC randomized trial. Emerg Microbes Infect. 2025;14(1):0.
17. Adepoju P. Uganda launches vaccine trial for Sudan virus disease. Lancet Microbe. 2025;6:101110. https://doi.org/10.1016/j.lanmic.2025.101110
18. Malkin E, Zaric M, Kieh M, Baden LR, Fitz-Patrick D, Marini A, et al.; rVSVΔG-LASV-GPC Study Group. Safety and immunogenicity of an rVSV Lassa Fever vaccine candidate. N Engl J Med. 2025;393:1807–18. https://doi.org/10.1056/NEJMoa2501073
19. Pigeaud DD, Borisevich V, Agans KN, Harrison MB, O'Toole R, Martinez J, et al. A single-cycle recombinant VSV vaccine displaying the Hendra virus glycoprotein uniformly protects against Hendra and Nipah virus challenge. NPJ Vaccines. 2026;11:21. https://doi.org/10.1038/s41541-025-01343-2
20. Kainulainen MH, Harmon JR, Whitesell AN, Bergeron É, Karaaslan E, Cossaboom CM, et al. Recombinant Sudan virus and evaluation of humoral cross-reactivity between Ebola and Sudan virus glycoproteins after infection or rVSV-ΔG-ZEBOV-GP vaccination. Emerg Microbes Infect. 2023;12:2265660. https://doi.org/10.1080/22221751.2023.2265660
21. Kainulainen MH, Bergeron E, Chatterjee P, Chapman AP, Lee J, Chida A, et al. High-throughput quantitation of SARS-CoV-2 antibodies in a single-dilution homogeneous assay. Sci Rep. 2021;11:12330. https://doi.org/10.1038/s41598-021-91300-5
22. Leyrat C, Yabukarski F, Tarbouriech N, Ribeiro EA Jr, Jensen MR, Blackledge M, et al. Structure of the vesicular stomatitis virus N^0-P complex. PLoS Pathog. 2011;7:e1002248. https://doi.org/10.1371/journal.ppat.1002248
23. Leyrat C, Jensen MR, Ribeiro EA Jr, Gérard FCA, Ruigrok RWH, Blackledge M, et al. The N^0-binding region of

the vesicular stomatitis virus phosphoprotein is globally disordered but contains transient α-helices. Protein Sci. 2011;20:542–56. https://doi.org/10.1002/pro.587
24. Karaaslan E, Sorvillo TE, Scholte FEM, O'Neal TJ, Welch SR, Davies KA, et al. Crimean Congo hemorrhagic fever virus nucleoprotein and GP38 subunit vaccine combination prevents morbidity in mice. NPJ Vaccines. 2024;9:148. https://doi.org/10.1038/s41541-024-00931-y
25. Corti D, Misasi J, Mulangu S, Stanley DA, Kanekiyo M, Wollen S, et al. Protective monotherapy against lethal Ebola virus infection by a potently neutralizing antibody. Science. 2016;351:1339–42. https://doi.org/10.1126/science.aad5224
26. Durie IA, Tehrani ZR, Karaaslan E, Sorvillo TE, McGuire J, Golden JW, et al. Structural characterization of protective non-neutralizing antibodies targeting Crimean-Congo hemorrhagic fever virus. Nat Commun. 2022;13:7298. https://doi.org/10.1038/s41467-022-34923-0
27. Rudge TL Jr, Sankovich KA, Niemuth NA, Anderson MS, Badorrek CS, Skomrock ND, et al. Development, qualification, and validation of the filovirus animal nonclinical group anti-Ebola virus glycoprotein immunoglobulin G enzyme-linked immunosorbent assay for human serum samples. PLoS One. 2019;14:e0215457. https://doi.org/10.1371/journal.pone.0215457
28. Pallesen J, Murin CD, de Val N, Cottrell CA, Hastie KM, Turner HL, et al. Structures of Ebola virus GP and sGP in complex with therapeutic antibodies. Nat Microbiol. 2016;1:16128. https://doi.org/10.1038/nmicrobiol.2016.128
29. Bond NG, Shore KR, Engel EJ, Coonan EE, Al-Hasan F, Gbakie MA, et al. Ebola virus–specific neutralizing antibody persists at high levels in survivors 2 years after resolution of disease in a Sierra Leonean cohort. J Infect Dis. 2024; 230:e929–37. https://doi.org/10.1093/infdis/jiae155
30. Gunn BM, Roy V, Karim MM, Hartnett JN, Suscovich TJ, Goba A, et al. Survivors of Ebola virus disease develop polyfunctional antibody responses. J Infect Dis. 2020;221:156–61. https://doi.org/10.1093/infdis/jiz364
31. Ayouba A, Touré A, Butel C, Keita AK, Binetruy F, Sow MS, et al. Development of a sensitive and specific serological assay based on Luminex technology for detection of antibodies to zaire Ebola virus. J Clin Microbiol. 2016;55:165–76. https://doi.org/10.1128/JCM.01979-16
32. Logue J, Tuznik K, Follmann D, Grandits G, Marchand J, Reilly C, et al. Use of the filovirus animal non-clinical group (FANG) Ebola virus immuno-assay requires fewer study participants to power a study than the alpha diagnostic international assay. J Virol Methods. 2018;255:84–90. https://doi.org/10.1016/j.jviromet.2018.02.018
33. Simon JK, Kennedy SB, Mahon BE, Dubey SA, Grant-Klein RJ, Liu K, et al. Immunogenicity of rVSVΔG-ZEBOV-GP Ebola vaccine (ERVEBO) in African clinical trial participants by age, sex, and baseline GP-ELISA titer: a post hoc analysis of three Phase 2/3 trials. Vaccine. 2022;40:6599–606. https://doi.org/10.1016/j.vaccine.2022.09.037
34. Kennedy SB, Bolay F, Kieh M, Grandits G, Badio M, Ballou R, et al.; PREVAIL I Study Group. Phase 2 placebo-controlled trial of two vaccines to prevent Ebola in Liberia. N Engl J Med. 2017;377:1438–47. https://doi.org/10.1056/NEJMoa1614067
35. Ravichandran S, Khurana S. Ebola-Detect: a differential serodiagnostic assay for Ebola virus infections and surveillance in the presence of vaccine-induced antibodies. EBioMedicine. 2022;82:104186. https://doi.org/10.1016/j.ebiom.2022.104186
36. Poetsch JH, Dahlke C, Zinser ME, Kasonta R, Lunemann S, Rechtien A, et al.; VSV-Ebola Consortium (VEBCON). Detectable vesicular stomatitis virus (VSV)–specific humoral and cellular immune responses following VSV–Ebola virus vaccination in humans. J Infect Dis. 2019;219:556–61. https://doi.org/10.1093/infdis/jiy565
37. Raabe V, Lai L, Morales J, Xu Y, Rouphael N, Davey RT, et al. Cellular and humoral immunity to Ebola Zaire glycoprotein and viral vector proteins following immunization with recombinant vesicular stomatitis virus-based Ebola vaccine (rVSVΔG-ZEBOV-GP). Vaccine. 2023; 41:1513–23. https://doi.org/10.1016/j.vaccine.2023.01.059
38. Chandrasekaran P, Berry IM, Callier V, Anthony SM, Hensley K, Kuhn JH, et al. Vector induced humoral responses after rVSVΔG-ZEBOV-GP immunization identify vaccinated individuals and correlate with Ebola virus glycoprotein antibodies. J Infect Dis. 2025;232:1004–14. https://doi.org/10.1093/infdis/jiae632
39. Zola Matuvanga T, Mariën J, Larivière Y, Osang'ir BI, Milolo S, Meta R, et al. Low seroprevalence of Ebola virus in health care providers in an endemic region (Tshuapa province) of the Democratic Republic of the Congo. PLoS One. 2023;18:e0286479. https://doi.org/10.1371/journal.pone.0286479

Address for correspondence: Éric Bergeron, Centers for Disease Control and Prevention, 1600 Clifton Rd NE, Mailstop G14, Atlanta, GA 30329-4018, USA; email: ebergeron@cdc.gov

Seroprevalence of Crimean-Congo Hemorrhagic Fever Virus Infection in Humans and Domestic Ruminants, Democratic Republic of the Congo

Boniface Pongombo Lombe,[1] Yannick Munyeku-Bazitama,[1] Gracia Kashitu-Mujinga, Patrick Kakoni Mukadi, Honoré Mampasi, Curé Georges Mbuyi Tshilenge, Marguerite Pemba Manwana, Noël Mwayakala, Niclette Bibi Zenga, Patient Okitale-Talunda, Elisabeth Pukuta-Simbu, Suguru Taga, Gaston Sefu Amzati, Masahiro Kajihara, Pierre Nsele Mutantu, Jean-Jacques Muyembe-Tamfum, Steve Ahuka-Mundeke, Justin Masumu, Sheila Makiala-Mandanda, Ayato Takada

Crimean-Congo hemorrhagic fever virus (CCHFV) was first isolated in the Democratic Republic of the Congo (DRC) in 1956. To date, only 3 sporadic human cases have been reported in the DRC, and data on CCHFV infection in livestock, which are key players in transmission, are scant. We conducted a cross-sectional seroepidemiological study on archived human and animal serum samples collected from 25 provinces across the DRC. Samples were tested using an ELISA detecting CCHFV nucleoprotein-specific antibodies. The seroprevalence of CCHFV infection in humans was 4.4% (55/1,239) and in domestic ruminants was 28.9% (322/1,114). High seroprevalences tended to correlate with increased age, specific climate conditions (e.g., tropical monsoon) and vegetation (e.g., mountain savanna) types, and higher elevation (>600 m). Our findings suggest that CCHFV actively circulates in animals and sporadically transmits to humans in the DRC, highlighting the need for continued surveillance of CCHFV infection.

Crimean-Congo hemorrhagic fever (CCHF) is a severe and potentially fatal human illness caused by CCHF virus (CCHFV), an orthonairovirus belonging to the family Nairoviridae (*1*). CCHFV is mainly transmitted by infected ticks (through bites or crushing) or through direct contact with infected biologic materials (*2*,*3*). Nosocomial and sexual transmission has also been reported (*2*,*3*). CCHFV, formerly known as Congo virus, was first isolated in the blood of a febrile teenage patient and a doctor who had taken care of him in 1956 in Kisangani, Democratic Republic of the Congo (DRC) (*4*–*6*). Soon after, the virus was found to be serologically and morphologically similar to a pathogen causing a disease clinically characterized by fever and hemorrhage occurring among peasants, agricultural workers, and soldiers in the Crimean Peninsula in 1944–1945. Hence the combined name, CCHFV, was proposed and has been used thus far (*7*).

CCHFV infection has been continuously reported in humans, livestock, wildlife, and ticks, becoming

Author affiliations: Central Veterinary Laboratory of Kinshasa, Kinshasa, Democratic Republic of the Congo (B.P. Lombe, C.G.M. Tshilenge, J. Masumu); National Pedagogical University, Kinshasa (B.P. Lombe, N. Mwayakala, G.S. Amzati, J. Masumu); University of Kikwit, Kikwit, Democratic Republic of the Congo (Y. Munyeku-Bazitama); University of Kinshasa, Kinshasa (Y. Munyeku-Bazitama, G. Kashitu-Mujinga, P.K. Mukadi, C.G.M. Tshilenge, P. Okitale-Talunda, P.N. Mutantu, J.J. Muyembe-Tamfum, S. Ahuka-Mundeke, S. Makiala-Mandanda); Institut National de Recherche Biomédicale, Kinshasa (Y. Munyeku-Bazitama, G. Kashitu-Mujinga, P.K. Mukadi, M.P. Manwana, N.B. Zenga, P. Okitale-Talunda, E. Pukuta-Simbu, P.N. Mutantu, J.J. Muyembe-Tamfum, S. Ahuka-Mundeke, J.M. Masumu, S. Makiala-Mandanda); Hokkaido University, Sapporo, Japan (Y. Munyeku-Bazitama, P. Okitale-Talunda, S. Taga, M. Kajihara, A. Takada); Institute of Tropical Medicine, Nagasaki University, Nagasaki, Japan (P.K. Mukadi), Compagnie des grands élevages de Katongola, Lubumbashi, Democratic Republic of the Congo (H. Mampasi); University of Zambia School of Veterinary Medicine, Lusaka, Zambia (M. Kajihara, A. Takada)

DOI: https://doi.org/10.3201/eid3204.250969

[1]These first authors contributed equally to this article.

the most widely distributed tickborne virus (*6*). It is endemic to Africa, Asia, the Middle East, and the Balkans, and its geographic distribution has been recently expanded to areas believed to be nonendemic in Europe (Italy, France, Portugal, and Spain), where the virus has been detected in humans and ticks (*2*,*8*–*11*). However, although its isolation and the initial human cases were described nearly 70 years ago, reports from the DRC are limited or outdated. Besides the initial human cases, CCHFV has been detected in a 26-year-old man in Biruwe (2008), a city neighboring Kisangani (*12*). Furthermore, only 1 survey conducted in Kamina and Lubumbashi, 2 cities in the southeastern DRC, has documented CCHFV circulation in domestic ruminants (*13*). Little is known about the prevalence of CCHFV infection in domestic animals, risk factors, preferential tick vectors, amplifying hosts, and circulating virus strains (*12*–*15*). Because the DRC often faces hemorrhagic fever outbreaks, including some with unknown causative agents, continuously monitoring pathogens causing hemorrhagic syndromes, such as CCHFV, is essential to enhance preparedness (*16*,*17*).

In this study, we investigated seroprevalence of CCHFV infection in the DRC, focusing on both humans and domestic ruminants. Domestic animals such as cattle, goats, and sheep are often infected with CCHFV without exhibiting major clinical signs (*18*). They harbor the virus and can mount specific antibody responses (*18*). Thus, serosurveys of CCHFV infection in animals are useful for the risk assessment of human infection (*14*,*19*). In this study, we aimed to determine the prevalence of CCHFV-specific antibodies and associated factors in humans and domestic ruminants in the DRC.

Methods

Study Design

We conducted a retrospective cross-sectional study using archived human and animal serum samples collected during 2017–2019 in 25 provinces of the DRC (Figure 1). The surveyed provinces represented 3 major DRC climates (tropical savanna, tropical rainforest, and tropical monsoon), 4 main vegetation types

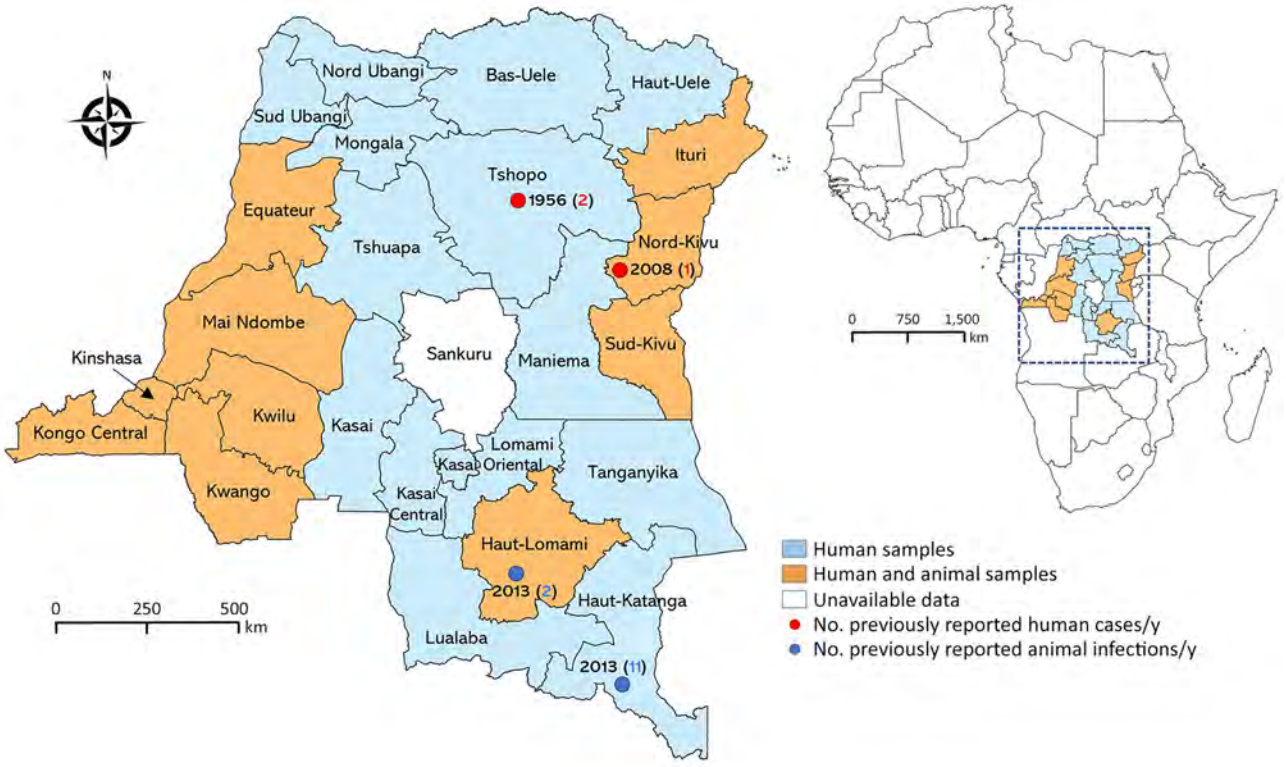

Figure 1. Provinces of sample collection and locations of previously reported human and animal infections in study of seroprevalence of Crimean-Congo hemorrhagic fever virus infection in humans and domestic ruminants, Democratic Republic of the Congo. Light blue shading indicates sites where only human samples were collected; orange shading indicates those where both human and animal samples were collected. Red dots represent locations where human cases have been reported, including number of cases and year of report. Blue dots represent locations with serologic evidence of Crimean-Congo hemorrhagic fever virus in animals, including number of seropositive animals and year of report. Inset shows location of the Democratic Republic of the Congo within Africa. QGIS software version 3.14 (https://qgis.com) was used to generate maps.

(savanna woodland, grassy savanna, dense moist forest, and mountain savanna), and different elevations above sea level (Figure 2) (*20*–*22*).

Procedures

Sample Collection and Processing

Human serum samples were collected in 2017 and 2018 in 25 of the 26 DRC provinces as part of the national yellow fever surveillance system. Of the 1,562 yellow fever–suspected serum samples analyzed at the National Institute for Biomedical Research, 1,492 tested negative using an ELISA for yellow fever virus–specific IgM. Of the samples from that study, we used 1,239 deidentified samples with valid sociodemographic data and sufficient volume for this study. We estimated the minimum required sample size on the basis of an expected seroprevalence of 50% (previous DRC human data were unavailable when the study was conducted and available data on animals were sparse), a precision of 1%, a design effect of 1, and a nonresponse rate of 30%. At least 949 samples had to be included.

Animal serum samples were collected in 2018 and 2019 from markets and different flocks in commercial and small-holder breeder farms located in 10 provinces. Those samples were primarily collected for seroepidemiological studies targeting common diseases including CCHF, African animal trypanosomiasis, Rift Valley fever, and foot-and-mouth disease. In the sampled provinces, animal samples were collected from multiple farms and flocks. Within a given flock, investigators determined the number of animals to be sampled to ensure the herd's representativeness and that of the area visited. Except for very young animals (<1 month of age) and females in advanced gestation, any animal could be captured and included in the study. We sorted those animal samples to represent different geographic and ecologic patterns related to DRC climate or vegetation, then randomly selected cattle, goat, and sheep samples for this study. The study was approved by the Kinshasa School of Public Health Ethics Committee (ESP/CE/148/2021).

Variables

The study's primary outcome was CCHFV serologic status, which could be positive or negative. We used 8 independent variables (sex, age, type of residence, season, climate, vegetation, elevation, and year of sample collection) for the analyses.

Antibody Detection

We aliquoted serum samples used in this study after collection and stored them in deep freezers for subsequent analyses. We heat-inactivated all serum samples at 56°C for 30 minutes before use (*23*) to inactivate complement in serum while preserving antibody binding activity and for biosafety reasons. We used an in-house CCHFV nucleoprotein (N)–based ELISA to detect CCHFV-specific antibodies (mainly IgG) as described previously (*24*,*25*). In brief, we coated Nunc MaxiSorp 96-well ELISA plates (Electron Microscopy Sciences, https://www.emsdiasum.com) with purified N antigen overnight at 4°C then blocked with 3% skim milk in phosphate-buffered saline (PBS) for 1 hour at room temperature. After washing the plates 3 times with PBS containing 0.05% Tween-20 (PBST), we added serum samples diluted (1:100) in PBST containing 1% skim milk and incubated them for 1 hour at room temperature. We then washed the plates ≥5 times with PBST and detected bound antibodies by using horseradish peroxidase-conjugated protein

Figure 2. Distribution of provinces by climate, vegetation, and elevation in study of seroprevalence of Crimean-Congo hemorrhagic fever virus infection in humans and domestic ruminants, Democratic Republic of the Congo. A) Climate types based on Köppen-Geiger climate classification (1991–2020 dataset). B) Vegetation type by province. C) Provinces by elevation. QGIS software version 3.14 (https://qgis.com) was used to generate maps.

A/G (Thermo Fisher Scientific, https://www.thermofisher.com) diluted 10,000-fold in 1% skim milk PBST and a 3,3′,5,5′-tetramethylbenzidine substrate. We added 1 normality phosphoric acid to stop the reaction and measured the optical density. We included previously generated mouse N monoclonal antibodies and CCHFV IgG-positive and naive human serum samples as positive and negative controls for assay validation (*24*,*25*). To investigate cross-reactivity with Nairobi sheep disease virus (NSDV), we tested CCHFV N IgG-positive animal samples for NSDV N IgG as described previously using the purified NSDV N antigen in the same ELISA conditions described previously (*24*). We read absorbance at 450 nm using an 800TS Microplate Absorbance Reader (Agilent BioTek, https://www.agilent.com). We carried out assays in duplicate and used the average optical density (OD) value for statistical analyses.

Statistical Analyses

We analyzed data using Stata version 15.1 (https://www.stata.com) and summarized categorical data using proportions with 95% CIs. We used median and interquartile range (IQR) to summarize continuous variables. Regarding serologic data analysis, we determined the positivity cutoff value using the Smirnov-Grubbs rejection test as described elsewhere; we set the significance threshold at p<0.01 (*26*,*27*). The cutoff OD values were 0.8 for animal samples and 0.95 for human samples. We applied logistic regression to investigate the association between primary outcome and independent variables (sex, age, type of living area, season, climate, vegetation, elevation, and year of sample collection). This preliminary analysis generated estimates of univariable odds ratios (ORs). Next, we performed multivariable logistic regression including all risk factors with the statistical significance threshold set at p<0.05. We used QGIS version 3.16.8 (https://qgis.org) to generate maps.

Results

Human Participants, Detection of CCHFV N-Specific Antibodies, and Factors Associated with Seropositivity

Overall, we analyzed 1,239 samples from patients with symptoms suggestive of yellow fever (Table 1; Appendix Table 1, https://wwwnc.cdc.gov/EID/article/32/4/25-0969-App1.pdf). Of those patients, 729 (58.8%) were male and 510 (41.2%) female. The median patient age was 16 (IQR 5–31) years. Most (842 [68.0%]) patients lived in rural areas. Most (906 [73.1%]) samples were collected during the rainy season. Sampling locations differed in climate (tropical savanna, rainforest, and monsoon), vegetation (savanna woodland, grassy savanna, dense moist forest, and mountain savanna), and elevation above sea level (<600, 600–799, and ≥800 m). Among those categories, the tropical savanna climate (862 [69.6%]), savanna woodland vegetation (596 [48.1%]), and elevations <600 m (860 [69.4%]) were the most represented.

The overall CCHFV seroprevalence was 4.4% (95% CI 3.4%–5.7%). We found an association between seropositivity and age and noted a trend (p = 0.0384 by Cochran-Armitage test for trend) toward increased seropositivity odds with age, especially for persons 20–29 years of age (adjusted odds ratio [aOR] 3.1 [95% CI 1.4–6.8]; p = 0.005) and those >50 years of age (aOR 2.9 [95% CI 1.1–7.6]; p = 0.027). Although results were not statistically significant, samples collected in urban areas or during the rainy season were slightly less likely to test positive. Similarly, samples originating from locations with a predominant tropical rainforest climate were less likely to test positive. Of note, samples from locations with a tropical monsoon climate were 40% more likely to test positive than samples from a tropical savanna climate; however, that association was not statistically significant (aOR 1.4 [95% CI 0.4–5.0]; p = 0.613). Samples from grassy savanna and mountain savanna areas were ≥5 times more likely to test positive than those from savanna woodland areas, although that difference was not statistically significant (for grassy savanna, aOR 5.7 [95% CI 0.7–45.2], p = 0.101; for mountain savanna, aOR 6.2 [95% CI 0.5–69.4]; p = 0.136). Conversely, samples from areas with an elevation 600–799 meters above sea level were 3 times more likely to test positive (aOR 3.0 [95% CI 1.2–7.8]; p = 0.023).

Domestic Animals, Detection of CCHFV N-Specific Antibodies, and Factors Associated with Seropositivity

We analyzed a total of 1,114 serum samples from domestic animals, including cattle (706 [63.4%]), goats (357 [32.0%]), and sheep (51 [4.6%]) (Table 2; Appendix Tables 2, 3). Most animals were female (788 [70.7%] vs. 326 [29.3%] male) and <6 years of age (885 [79.4%]). The median age was 4 (IQR 2–5) years. As with human samples, sampling locations differed in terms of climate, vegetation, and elevation above sea level. Study animals originated mainly from areas with a tropical savanna climate (870 [78.1%]) or an elevation of ≥800 m above sea level (702 [63.0%]).

The overall seroprevalence among animals was 28.9% (95% CI 26.3–31.6). That seroprevalence varied among species. The lowest and highest seroprevalence levels were recorded in sheep (2.0% [95% CI 0.3%–12.8%]) (Appendix Table 3) and cattle (42.8%

[95% CI 39.2%–46.5] %). Cattle were nearly 9 times more likely to test positive than other species (aOR 8.7 [95% CI 2.3–32.9]; p = 0.001) (Table 2). We noted a trend toward increased seropositivity with age (p<0.0001 by Cochran-Armitage test for trend); animals 6–9 years of age had the highest seroprevalence (40.6% [95% CI 32.8%–48.8%]). However, in multivariable analyses, the association between age and seropositivity decreased both in magnitude and statistical significance. Regarding climate, we recorded the highest seropositivity rate (76.1% [95% CI 61.6%–86.2%]) (Table 2) among animals originating from areas with a tropical monsoon climate. Animals from tropical monsoon climates were 30% more likely to test positive than animals from areas with a tropical savanna climate, although that association was not statistically significant (aOR 1.3 [95% CI 0.6–2.7]; p = 0.578). Of note, animals from areas with mountain savanna vegetation (54.4% [95% CI 49.8%–58.9%]) and those from areas located ≥800 m above sea level (42.7% [95% CI 39.1%–46.4%]) had high seropositivity rates (Table 2). Odds of seropositivity in animals originating from areas located ≥600 meters above sea level were ≥2 times higher.

Because cross-reactivity of orthonairovirus antibodies remains a key issue for serologic analyses using the N antigen of some nairoviruses (*28*,*29*), we sought to distinguish CCHFV-specific antibodies from NSDV, a virus serologically close to CCHFV (*25*,*30*). We retested samples that reacted to the CCHFV N antigen for cross-reactivity to the NSDV N antigen (Appendix Figure). Although some of the CCHFV N IgG-positive serum samples showed appreciable reactivity to NSDV N, OD values were lower than they were to CCHFV N, with 1 exception, indicating that detected antibodies were mostly specific to CCHFV N and cross-reactivity with NSDV was limited.

Discussion

Investigating CCHFV at the human–animal interface is crucial to learn more about and effectively control CCHF. Animals, particularly domestic ruminants, play an essential role in maintaining and transmitting CCHFV (*14*). In this study, we used domestic

Table 1. Sociodemographic characteristics and seroprevalence of Crimean-Congo hemorrhagic fever virus infection in humans in study of seroprevalence in humans and domestic ruminants, Democratic Republic of the Congo*

Variable	No. (%) participants	Seropositivity		OR (95% CI)	p value	aOR (95% CI)	p value
		No.	% (95% CI)				
All participants	1,239	55	4.4 (3.4–5.7)				
Sex							
F	510 (41.2)	21	4.1 (2.7–6.2)	Referent		Referent	
M	729 (58.8)	34	4.7 (3.3–6.4)	1.1 (0.7–1.9)	0.646	1.1 (0.6–1.9)	0.780
Median age, y (IQR)	16 (5–31)						
Age range, y							
0–9	484 (39.1)	13	2.7 (1.6–4.6)	Referent		Referent	
10–19	222 (17.9)	10	4.5 (2.4–8.2)	1.7 (0.7–3.9)	0.211	1.8 (0.8–4.3)	0.165
20–29	214 (17.3)	16	7.5 (4.6–11.8)	2.9 (1.4–6.2)	0.005	3.1 (1.4–6.8)	0.005
30–39	127 (10.2)	4	3.1 (1.2–8.1)	1.2 (0.4–3.7)	0.778	1.2 (0.4–3.9)	0.709
40–49	88 (7.1)	5	5.7 (2.4–13.0)	2.2 (0.7–6.3)	0.148	2.2 (0.8–6.6)	0.139
≥50	104 (8.4)	7	6.7 (3.2–13.5)	2.6 (1.0–6.7)	0.046	2.9 (1.1–7.6)	0.027
Type of living area							
Rural	842 (68.0)	41	4.9 (3.6–6.5)	Referent		Referent	
Urban	397 (32.0)	14	3.5 (2.1–5.9)	0.7 (0.4–1.3)	0.286	0.8 (0.3–2.1)	0.662
Season of collection							
Dry season	333 (26.9)	18	5.4 (3.4–8.4)	Referent		Referent	
Rainy season	906 (73.1)	37	4.1 (2.9–5.6)	0.7 (0.4–1.3)	0.318	0.8 (0.4–1.4)	0.453
Climate							
Tropical savanna	862 (69.6)	37	4.3 (3.1–5.9)	Referent		Referent	
Tropical rainforest	283 (22.8)	12	4.2 (2.4–7.3)	0.9 (0.5–1.9)	0.970	0.9 (0.3–2.7)	0.848
Tropical monsoon	94 (7.6)	6	6.4 (2.9–13.5)	1.5 (0.6–3.7)	0.357	1.4 (0.4–5.0)	0.613
Vegetation							
Savanna woodland	596 (48.1)	23	3.9 (2.6–5.7)	Referent		Referent	
Grassy savanna	160 (12.9)	10	6.3 (3.4–11.2)	1.6 (0.8–3.6)	0.193	5.7 (0.7–45.2)	0.101
Dense moist forest	438 (35.4)	19	4.3 (2.8–6.7)	1.1 (0.6–2.1)	0.700	1.2 (0.3–4.1)	0.765
Mountain savanna	45 (3.6)	3	6.7 (2.1–18.7)	1.8 (0.5–6.2)	0.364	6.2 (0.5–69.4)	0.136
Elevation, m							
<600	860 (69.4)	32	3.7 (2.6–5.2)	Referent		Referent	
600–799	90 (7.3)	9	10.0 (5.2–18.1)	2.9 (1.3–6.2)	0.008	3.0 (1.2–7.8)	0.023
≥800	289 (23.3)	14	4.8 (2.9–8.0)	1.3 (0.7–2.5)	0.401	0.4 (0.0–2.8)	0.332
Year of collection							
2017	757 (61.1)	33	4.4 (3.1–6.1)	Referent		Referent	
2018	482 (38.9)	22	4.6) (3.0–6.8)	1.0 (0.6–1.8)	0.864	0.9 (0.5–1.6)	0.680

*aOR, adjusted odds ratio; IQR, interquartile range; OR, odds ratio.

Table 2. Sociodemographic characteristics and seroprevalence of Crimean-Congo hemorrhagic fever virus infection in animals in study of seroprevalence in humans and domestic ruminants, Democratic Republic of the Congo*

Variable	No. (%) animals	Seropositivity		OR (95% CI)	p value	aOR (95% CI)	p value
		No.	% (95% CI)				
All animals	1,114	322	28.9 (26.3–31.6)				
Species							
Other	408 (36.6)	20	4.9 (3.2–7.5)	Referent		Referent	
Cattle	706 (63.4)	302	42.8 (39.2–46.5)	14.5 (9.0–23.3)	<0.001	8.7 (2.3–32.9)	0.001
Sex							
F	788 (70.7)	244	30.9 (27.8–34.3)	Referent		Referent	
M	326 (29.3)	78	23.9 (19.6–28.9)	0.7 (0.5–0.9)	0.019	1.2 (0.8–1.7)	0.333
Median age, y (IQR)	4 (2–5)						
Age range, y							
0–2	291 (26.1)	43	14.8 (11.1–19.3)	Referent		Referent	
3–5	594 (53.3)	189	31.8 (28.2–35.7)	2.7 (1.9–3.9)	<0.001	1.3 (0.8–2.0)	0.226
6–8	143 (12.8)	58	40.6 (32.8–48.8)	3.9 (2.5–6.3)	<0.001	1.6 (0.9–2.8)	0.135
9–12	86 (7.7)	32	37.2 (27.6–47.9)	3.4 (2.0–5.9)	<0.001	1.9 (0.9–3.6)	0.071
Climate							
Tropical savanna	870 (78.1)	201	23.1 (20.4–26.0)	Referent		Referent	
Tropical rainforest	198 (17.8)	86	43.4 (36.7–50.4)	2.6 (1.9–3.5)	<0.001	0.4 (0.2–0.6)	<0.001
Tropical monsoon	46 (4.1)	35	76.1 (61.6–86.2)	10.6 (5.3–21.2)	<0.001	1.3 (0.6–2.7)	0.578
Vegetation							
Savanna woodland	412 (37.0)	23	5.6 (3.7–8.3)	Referent		Referent	
Grassy savanna	240 (21.5)	51	21.3 (16.5–26.9)	4.6 (2.7–7.7)	<0.001	0.2 (0.0–1.0)	0.052
Dense moist forest	10 (0.9)	2	20.0 (5.0–54.1)	4.2 (0.8–21.1)	0.079	1.2 (0.2–9.4)	0.806
Mountain savanna	452 (40.6)	246	54.4 (49.8–58.9)	20.2 (12.8–31.9)	<0.001	0.7 (0.1–3.5)	0.666
Elevation, m							
<600	237 (21.3)	9	3.8 (1.9–7.1)	Referent		Referent	
600–799	175 (15.7)	13	7.4 (4.3–12.4)	2.0 (0.8–4.9)	0.112	2.6 (1.0–6.8)	0.047
≥800	702 (63.0)	300	42.7 (39.1–46.4)	18.9 (9.6–37.4)	<0.001	4.2 (1.3–13.9)	0.019
Year of collection							
2018	301 (27.0)	184	61.1 (55.5–66.5)	Referent		Referent	
2019	813 (73.0)	138	17.0 (14.5–19.7)	0.1 (0.1–0.2)	<0.001	0.3 (0.2–0.5)	<0.001

*aOR, adjusted odds ratio; IQR, interquartile range; OR, odds ratio.

ruminants as indicators for the presence of CCHFV infection in the environment and used humans living in the same areas as evidence of ongoing transmission and circulation of the virus. Information is limited on CCHFV circulation among both humans and domestic ruminants across multiple provinces of the DRC, and this study contributes to filling that gap.

In our study, we found an overall seroprevalence of 4.4% (95% CI 3.4%–5.7%) among humans. Similar seroprevalences (4.4%) have been reported among pygmies in Cameroon (*31*) and among farm and wildlife workers (3.9%) in South Africa (*32*). Lower estimates have been reported in Pakistan (2.7%), among blood donors in Mali (1.75%), and among persons living with HIV in the Republic of the Congo (0.6%) (*33*). In contrast, much higher seroprevalence has been reported in Mauritania (11.8%), Tanzania (15.1%), and Uganda (27.0%) (*34*–*36*). Disparities in seroprevalence across surveys might be attributed to the heterogeneity in study populations, sampling strategies, and environmental factors such as climate, vegetation, and elevation. Studies conducted in the general population, including in blood donors, tend to report lower estimates than those targeting populations at high risk that have direct occupational exposure to ticks or studies conducted in locations where environmental factors are favorable for tick development. In fact, our analysis revealed higher seroprevalences in locations characterized by a tropical monsoon climate, a grassy/mountain savanna vegetation, or elevations of ≥600 meters above sea level, all of which are favorable for tick development (*37*–*41*). Of note, participants living in locations at 600–799 meters above sea level were 3 times more likely to test positive. Conversely, participants from areas located ≥800 meters above sea level were less likely to test positive. Although those areas are considered to be at high risk for transmission, participants living there might have had lower environmental and occupational exposure to tick bites. Seropositivity significantly increased with age, especially among participants 20–29 years of age and those >50 years of age, who were nearly 3 times more likely to test positive. A similar trend has been reported in other studies (*32*,*34*,*36*,*42*). That finding might reflect cumulative exposure to tick bites, because older participants are more likely to have experienced prolonged or repeated exposure than are younger persons.

CCHFV N-specific antibodies were detected in 28.9% (95% CI 26.3%–31.6%) of animals. That finding is consistent with studies on domestic ruminants

in Senegal (32.5%) and Mauritania (33.1%) (*34*,*43*). In contrast, higher seroprevalence estimates have been reported in Cameroon (61.7%) and in Uganda (74.4%), a country neighboring the DRC (*36*,*44*). Surprisingly, a much lower seroprevalence (1.6%) was previously reported in 2 cities in southeastern DRC (*13*). Of note, samples collected in those cities, especially samples from cattle, originated from a single farm; goat and sheep samples were collected from different commercial and private farms within the same city (*13*). Our nearly nationwide study involved multiple sites with diverse ecology, climate, and elevation and used a highly specific assay, which likely resulted in higher seroprevalence estimates. Besides the species composition of the tested animals, differences in the living area or livestock management system, including tick control strategies on farms, might explain the observed variation in seroprevalence. Among tested animals, cattle had a higher seroprevalence (42.8%) than goats (5.3%) and sheep (2.0%). Cattle were nearly 9 times more likely to be seropositive than were other species. A similar trend was also noted in a study from Tanzania (*35*). In most studies conducted in livestock, cattle tend to have the highest seropositivity (*32*,*34*–*36*,*42*,*44*). Higher seroprevalences in larger ruminants such as cattle may be explained by host feeding preferences of ticks. Cattle have been described as suitable hosts for a large number of tick species, including *Hyalomma* spp. (*34*,*45*). In addition, the longevity of larger ruminants could lead to repeated exposure to ticks, increasing the likelihood of persistent infection and sustained antibody responses (*34*).

Male animals were 30% less likely to test positive than female animals in the univariable analysis, corroborating previous studies that have reported sex-related differences in CCHFV infection (*36*,*46*). That finding could be explained by the fact that female animals are kept longer for breeding purposes and milk production on reproductive farms and thereby experience prolonged exposure to tick bites (*34*). Seroprevalence significantly increased with age in the univariable analysis, consistent with earlier reports (*32*,*34*,*36*,*42*). However, the association decreased in magnitude and statistical significance in multivariable analysis. In line with our findings in humans and in previous reports, animal seropositivity was associated with particular climate zones (tropical rainforest and tropical monsoon), vegetation types (grassy savanna and mountain savanna), and elevation above sea level (≥800 m) in the univariable analysis. Of note, the association with climate persisted in the multivariable analysis (*37*–*41*).

CCHFV-suitable habitats have previously been shown to be associated with climate and vegetation (grass and shrub cover) that are favorable for tick proliferation (*47*,*48*). Our analysis suggests that the ecologic niche for CCHFV in the DRC might be located in mountainous areas. Indeed, those areas provide grazing lands and climatic conditions suitable for livestock breeding or pasture. Those conditions account for high densities of livestock, especially cattle, which are known to play a critical role in CCHFV transmission (*14*). The mountain climate zone includes the provinces of Ituri, Nord, and Sud Kivu, all of which exhibited high prevalences of CCHFV infection in animals or humans in this study (Appendix Tables 1, 2). Furthermore, because eastern DRC is part of the African Great Lakes region, that area of high CCHFV prevalence is particularly relevant for cattle movement related to breeding and trade (*49*). Cross-border cattle movement might contribute to the spread of tickborne pathogens, particularly through *Hyalomma* ticks, which are capable of surviving under various temperature and humidity conditions (*45*,*49*,*50*). The potential of *Hyalomma* ticks to spread across borders and eventually trigger CCHFV transmission underscores the urgent need for coordinated transboundary disease control strategies. Those strategies should also consider climate change and urbanization as a result of population growth. Both of those factors might act as drivers for CCHFV spread, especially in Africa. Rising temperatures and changing precipitation patterns will contribute to altering the vector ecology, thus establishing *Hyalomma* ticks in new areas.

Because the geographic distributions of CCHFV and some CCHFV-related zoonotic orthonairoviruses, such as NSDV and Dugbe virus (DUGV), might overlap in the DRC, cross-reactivity of N antibodies is a key issue for the serologic diagnosis and surveillance of CCHF. Indeed, our previous study revealed the presence of shared epitopes among the N proteins of CCHFV, NSDV, and DUGV (*24*,*25*). However, those cross-reactive epitopes were not considered to be dominant, because polyclonal antiserum against NSDV and DUGV showed little reactivity with CCHFV N antigens (*24*,*25*). Therefore, those viruses appear to be antigenically distinguishable from each other. Nevertheless, the potential effects of cross-reactivity should not be overlooked in binding assays based on a single antigen. For example, 1 sample exhibited a higher OD value against the NSDV antigen than against the CCHFV antigen (Appendix Figure); thus, NSDV infection cannot be ruled out.

The first limitation of this study is that tick collection for viral genome detection was not performed.

A more comprehensive investigation, including CCHFV genome detection from ticks, would provide further insights into the transmission dynamics and phylogeny of strains circulating in the DRC. In addition, the use of samples from febrile patients, although geographically representative, might have introduced selection bias because those patients might have exposure patterns that differ from those of the general population. Future studies should focus on the identified high-risk areas and conduct in-depth analyses of interactions among humans, livestock, and ticks.

In conclusion, we performed a comprehensive investigation of CCHFV infection in the DRC using geographically diverse and representative human and animal samples collected across multiple provinces. Although province-level analyses could not be performed in depth because of small sample sizes, particularly for human samples, the data generated are crucial because they pinpoint regions of interest where CCHFV transmission could be actively occurring and where targeted public health interventions should be initiated. Our study also highlights the potential of leveraging the yellow fever surveillance system as a dual-purpose platform to obtain epidemiologic and clinical data on CCHF, which might not necessarily be associated with a deadly viral hemorrhagic fever. Strengthening this system could enhance preparedness against CCHF outbreaks in the DRC and support transboundary disease control efforts.

This article was preprinted at https://papers.ssrn.com/sol3/papers.cfm?abstract_id=5316031.

Acknowledgments

We thank Kim Barrymore for editing the manuscript.

This work was supported by the Japan Agency for Medical Research and Development (AMED) and the Japan International Cooperation Agency under the framework of the Science and Technology Research Partnership for Sustainable Development (grant no. JP22jm0110019) and the Japan Program for Infectious Diseases Research and Infrastructure (grant no. JP-20wm0125008) and the Research Program on Emerging and Re-emerging Infectious Diseases (grant nos. JP24fk0108906 and JP25wm0225051) from AMED. P.M.K. was supported by AMED under grant number JP223fa627004. The funders of the study had no role in study design, data collection, data analysis, data interpretation or writing of the report.

Deidentified data can be made available for research from the corresponding author upon reasonable request and approval by the Kinshasa School of Public Health Ethics Committee.

B.P.L., A.T., Y.M.-B., S.M.-M., M.K., and J.M. conceived the study. B.P.L., Y.M.-B., P.K.M., P.N.M., H.M., and C.G.M.T. collected samples. E.P.-S., S.M.-M., J.M., J.-J.M.-T., S.T., and S.A.-M. supervised data collection. B.P.L., A.T., and Y.M.-B. conceptualized laboratory analyses. B.P.L., Y.M.-B., G.K.-M., M.P.M., N.B.Z., P.O.-T., and N.M. performed laboratory analyses. B.P.L., Y.M.-B., G.S.A., and A.T. performed statistical analyses and interpreted the results. B.P.L. and Y.M.-B. wrote the first version of the manuscript, which was critically revised by A.T. and edited by all the authors. All authors had full access to all the data in the study and had final responsibility for the decision to submit for publication. A.T., B.P.L., Y.M.-B., G.S.A., and P.K.M. directly accessed and verified the underlying data reported in the manuscript.

About the Author

Dr. Lombe is a researcher and head of the epidemiological research unit at the central veterinary laboratory in Kinshasa, Democratic Republic of the Congo. His research interests include the epidemiology of emerging viral zoonoses. Dr. Munyeku-Bazitama is a researcher at the virology department of the National Institute of Biomedical Research in Kinshasa, and a postdoctoral fellow at the Hokkaido University International Institute for Zoonosis Control. His research interests include emerging and reeemerging viral zoonoses causing hemorrhagic fevers, as well as differential diagnosis of fevers of unknown origin.

References

1. ICTV. Genus: *Orthonairovirus* [cited 2025 Jun 14]. https://ictv.global/report/chapter/nairoviridae/nairoviridae/orthonairovirus
2. Hawman DW, Feldmann H. Crimean-Congo haemorrhagic fever virus. Nat Rev Microbiol. 2023;21:463–77. https://doi.org/10.1038/s41579-023-00871-9
3. Pshenichnaya NY, Sydenko IS, Klinovaya EP, Romanova EB, Zhuravlev AS. Possible sexual transmission of Crimean-Congo hemorrhagic fever. Int J Infect Dis. 2016;45:109–11. https://doi.org/10.1016/j.ijid.2016.02.1008
4. Hoogstraal H. The epidemiology of tick-borne Crimean-Congo hemorrhagic fever in Asia, Europe, and Africa. J Med Entomol. 1979;15:307–417. https://doi.org/10.1093/jmedent/15.4.307
5. Simpson DI, Knight EM, Courtois G, Williams MC, Weinbren MP, Kibukamusoke JW. Congo virus: a hitherto undescribed virus occurring in Africa. I. Human isolations—clinical notes. East Afr Med J. 1967;44:86–92.
6. Balinandi S, Patel K, Ojwang J, Kyondo J, Mulei S, Tumusiime A, et al. Investigation of an isolated case of human Crimean-Congo hemorrhagic fever in Central Uganda, 2015. Int J Infect Dis. 2018;68:88–93. https://doi.org/10.1016/j.ijid.2018.01.013
7. Casals J. Antigenic similarity between the virus causing Crimean hemorrhagic fever and Congo virus. Proc Soc Exp Biol Med. 1969;131:233–6. https://doi.org/10.3181/00379727-131-33847

8. Temur AI, Kuhn JH, Pecor DB, Apanaskevich DA, Keshtkar-Jahromi M. Epidemiology of Crimean-Congo hemorrhagic fever (CCHF) in Africa—underestimated for decades. Am J Trop Med Hyg. 2021;104:1978–90. https://doi.org/10.4269/ajtmh.20-1413
9. Mora-Rillo M, Díaz-Menéndez M, Crespillo-Andujar C, Arribas JR. Autochthonous Crimean-Congo haemorrhagic fever in Spain: so much to learn. Enferm Infecc Microbiol Clin (Engl Ed). 2018;36:202. https://doi.org/10.1016/j.eimce.2017.05.003
10. Moraga-Fernández A, Ruiz-Fons F, Habela MA, Royo-Hernández L, Calero-Bernal R, Gortazar C, et al. Detection of new Crimean-Congo haemorrhagic fever virus genotypes in ticks feeding on deer and wild boar, Spain. Transbound Emerg Dis. 2021;68:993–1000. https://doi.org/10.1111/tbed.13756
11. Zé-Zé L, Nunes C, Sousa M, de Sousa R, Gomes C, Santos AS, et al. Fatal case of Crimean-Congo hemorrhagic fever, Portugal, 2024. Emerg Infect Dis. 2025;31:139–43. https://doi.org/10.3201/eid3101.241264
12. Grard G, Drexler JF, Fair J, Muyembe JJJ, Wolfe ND, Drosten C, et al. Re-emergence of Crimean-Congo hemorrhagic fever virus in Central Africa. PLoS Negl Trop Dis. 2011;5:e1350. https://doi.org/10.1371/journal.pntd.0001350
13. Sas MA, Mertens M, Kadiat JG, Schuster I, Pongombo CPS, Maloba AGK, et al. Serosurvey for Crimean-Congo hemorrhagic fever virus infections in ruminants in Katanga province, Democratic Republic of the Congo. Ticks Tick Borne Dis. 2017;8:858–61. https://doi.org/10.1016/j.ttbdis.2017.07.001
14. Spengler JR, Bergeron É, Rollin PE. Seroepidemiological studies of Crimean-Congo hemorrhagic fever virus in domestic and wild animals. PLoS Negl Trop Dis. 2016;10:e0004210. https://doi.org/10.1371/journal.pntd.0004210
15. Kajihara M, Simuunza M, Saasa N, Dautu G, Mori-Kajihara A, Qiu Y, et al. Serologic and molecular evidence for circulation of Crimean-Congo hemorrhagic fever virus in ticks and cattle in Zambia. PLoS Negl Trop Dis. 2021;15:e0009452. https://doi.org/10.1371/journal.pntd.0009452
16. Kavulikirwa OK, Sikakulya FK. Recurrent Ebola outbreaks in the eastern Democratic Republic of the Congo: a wake-up call to scale up the integrated disease surveillance and response strategy. One Health. 2022;14:100379. https://doi.org/10.1016/j.onehlt.2022.100379
17. Sopbué Kamguem I, Kirschvink N, Wade A, Linard C. Determinants of viral haemorrhagic fever risk in Africa's tropical moist forests: a scoping review of spatial, socio-economic, and environmental factors. PLoS Negl Trop Dis. 2025;19:e0012817. https://doi.org/10.1371/journal.pntd.0012817
18. Celina SS, Italiya J, Tekkara AO, Černý J. Crimean-Congo haemorrhagic fever virus in ticks, domestic, and wild animals. Front Vet Sci. 2025;11:1513123. https://doi.org/10.3389/fvets.2024.1513123
19. Bernard C, Holzmuller P, Bah MT, Bastien M, Combes B, Jori F, et al. Systematic review on Crimean-Congo hemorrhagic fever enzootic cycle and factors favoring virus transmission: special focus on France, an apparently free-disease area in Europe. Front Vet Sci. 2022;9:932304. https://doi.org/10.3389/fvets.2022.932304
20. Beck HE, McVicar TR, Vergopolan N, Berg A, Lutsko NJ, Dufour A, et al. High-resolution (1 km) Köppen-Geiger maps for 1901–2099 based on constrained CMIP6 projections. Sci Data. 2023;10:724. https://doi.org/10.1038/s41597-023-02549-6
21. Verhegghen A, Mayaux P, De Wasseige C, Defourny P. Mapping Congo Basin vegetation types from 300 m and 1 km multi-sensor time series for carbon stocks and forest areas estimation. Biogeosciences. 2012;9:5061–79. https://doi.org/10.5194/bg-9-5061-2012
22. Mushi CA, Ndomba PM, Trigg MA, Tshimanga RM, Mtalo F. Assessment of basin-scale soil erosion within the Congo River Basin: a review. Catena. 2019;178:64–76. https://doi.org/10.1016/j.catena.2019.02.030
23. Raabe VN. Diagnostic testing for Crimean-Congo hemorrhagic fever. J Clin Microbiol. 2020;58:e01580–19. https://doi.org/10.1128/JCM.01580-19
24. Lombe BP, Miyamoto H, Saito T, Yoshida R, Manzoor R, Kajihara M, et al. Purification of Crimean-Congo hemorrhagic fever virus nucleoprotein and its utility for serological diagnosis. Sci Rep. 2021;11:2324. https://doi.org/10.1038/s41598-021-81752-0
25. Lombe BP, Saito T, Miyamoto H, Mori-Kajihara A, Kajihara M, Saijo M, et al. Mapping of antibody epitopes on the Crimean-Congo hemorrhagic fever virus nucleoprotein. Viruses. 2022;14:544. https://doi.org/10.3390/v14030544
26. Ogawa H, Miyamoto H, Nakayama E, Yoshida R, Nakamura I, Sawa H, et al. Seroepidemiological prevalence of multiple species of filoviruses in fruit bats (*Eidolon helvum*) migrating in Africa. J Infect Dis. 2015;212(Suppl 2):S101–8. https://doi.org/10.1093/infdis/jiv063
27. Changula K, Kajihara M, Mori-Kajihara A, Eto Y, Miyamoto H, Yoshida R, et al. Seroprevalence of filovirus infection of *Rousettus aegyptiacus* bats in Zambia. J Infect Dis. 2018;218(suppl_5):S312–7. https://doi.org/10.1093/infdis/jiy266
28. Davies FG, Casals J, Jesset DM, Ochieng P. The serological relationships of Nairobi sheep disease virus. J Comp Pathol. 1978;88:519–23. https://doi.org/10.1016/0021-9975(78)90005-1
29. Hartlaub J, Gutjahr B, Fast C, Mirazimi A, Keller M, Groschup MH. Diagnosis and pathogenesis of Nairobi sheep disease Orthonairovirus infections in sheep and cattle. Viruses. 2021;13:1250. https://doi.org/10.3390/v13071250
30. Hartlaub J, Keller M, Groschup MH. Deciphering antibody responses to orthonairoviruses in ruminants. Microorganisms. 2021;9:1493. https://doi.org/10.3390/microorganisms9071493
31. Sadeuh-Mba SA, Yonga Wansi GM, Demanou M, Gessain A, Njouom R. Serological evidence of rift valley fever Phlebovirus and Crimean-Congo hemorrhagic fever orthonairovirus infections among pygmies in the east region of Cameroon. Virol J. 2018;15:63. https://doi.org/10.1186/s12985-018-0977-8
32. Msimang V, Weyer J, le Roux C, Kemp A, Burt FJ, Tempia S, et al. Risk factors associated with exposure to Crimean-Congo haemorrhagic fever virus in animal workers and cattle, and molecular detection in ticks, South Africa. PLoS Negl Trop Dis. 2021;15:e0009384. https://doi.org/10.1371/journal.pntd.0009384
33. Malonga GA, Maiga AI, Moudiongui Mboungou Malanda D, Saliou M, Malanda-Kiminou JP, Dolo O, et al. Seroprevalence of Crimean-Congo hemorrhagic fever virus among people living with HIV in Brazzaville, Congo and among blood donors in Bamako, Mali. Ticks Tick Borne Dis. 2024;15:102276. https://doi.org/10.1016/j.ttbdis.2023.102276
34. El Ghassem A, Apolloni A, Vial L, Bouvier R, Bernard C, Khayar MS, et al. Risk factors associated with Crimean-Congo hemorrhagic fever virus circulation among human, livestock and ticks in Mauritania through a one health

retrospective study. BMC Infect Dis. 2023;23:764. https://doi.org/10.1186/s12879-023-08779-8
35. Hughes EC, de Glanville W, Kibona T, Mmbaga BT, Rostal MK, Swai ES, et al. Crimean-Congo hemorrhagic fever virus seroprevalence in human and livestock populations, northern Tanzania. Emerg Infect Dis. 2024;30:836–8. https://doi.org/10.3201/eid3004.231204
36. Atim SA, Ashraf S, Belij-Rammerstorfer S, Ademun AR, Vudriko P, Nakayiki T, et al. Risk factors for Crimean-Congo Haemorrhagic Fever (CCHF) virus exposure in farming communities in Uganda. J Infect. 2022;85:693–701. https://doi.org/10.1016/j.jinf.2022.09.007
37. Mukhaye E, Akoko JM, Nyamota R, Mwatondo A, Muturi M, Nthiwa D, et al. Exposure patterns and the risk factors of Crimean Congo hemorrhagic fever virus amongst humans, livestock and selected wild animals at the human/livestock/wildlife interface in Isiolo County, upper eastern Kenya. PLoS Negl Trop Dis. 2024;18:e0012083. https://doi.org/10.1371/journal.pntd.0012083
38. Papa A, Sidira P, Tsatsaris A. Spatial cluster analysis of Crimean-Congo hemorrhagic fever virus seroprevalence in humans, Greece. Parasite Epidemiol Control. 2016;1:211–8. https://doi.org/10.1016/j.parepi.2016.08.002
39. Cikman A, Aydin M, Gulhan B, Karakecili F, Kesik OA, Ozcicek A, et al. Seroprevalence of Crimean-Congo hemorrhagic fever virus in Erzincan Province, Turkey, relationship with geographic features and risk factors. Vector Borne Zoonotic Dis. 2016;16:199–204. https://doi.org/10.1089/vbz.2015.1879
40. Ilboudo AK, Oloo SO, Sircely J, Nijhof AM, Bett B. Spatial analysis and risk mapping of Crimean-Congo hemorrhagic fever (CCHF) in sub-Saharan Africa. Sci Rep. 2025;15:2292. https://doi.org/10.1038/s41598-025-85873-8
41. Vescio FM, Busani L, Mughini-Gras L, Khoury C, Avellis L, Taseva E, et al. Environmental correlates of Crimean-Congo haemorrhagic fever incidence in Bulgaria. BMC Public Health. 2012;12:1116. https://doi.org/10.1186/1471-2458-12-1116
42. Zohaib A, Saqib M, Athar MA, Hussain MH, Sial AU, Tayyab MH, et al. Crimean-Congo hemorrhagic fever virus in humans and livestock, Pakistan, 2015–2017. Emerg Infect Dis. 2020;26:773–7. https://doi.org/10.3201/eid2604.191154
43. Mangombi JB, Roqueplo C, Sambou M, Dahmani M, Mediannikov O, Comtet L, et al. Seroprevalence of Crimean-Congo hemorrhagic fever in domesticated animals in northwestern Senegal. Vector Borne Zoonotic Dis. 2020;20:797–9. https://doi.org/10.1089/vbz.2019.2592
44. Simo Tchetgna H, Yousseu FS, Cosset FL, de Freitas NB, Kamgang B, McCall PJ, et al. Molecular and serological evidence of Crimean-Congo hemorrhagic fever orthonairovirus prevalence in livestock and ticks in Cameroon. Front Cell Infect Microbiol. 2023;13:1132495. https://doi.org/10.3389/fcimb.2023.1132495
45. Hyalomma marginatum [cited 2025 Jun 13]. https://www.sciencedirect.com/topics/immunology-and-microbiology/hyalomma-marginatum
46. David-West TS, Cooke AR, David-West AS. Seroepidemiology of Congo virus (related to the virus of Crimean haemorrhagic fever) in Nigeria. Bull World Health Organ. 1974;51:543–6.
47. Estrada-Peña A, Zatansever Z, Gargili A, Aktas M, Uzun R, Ergonul O, et al. Modeling the spatial distribution of Crimean-Congo Hemorrhagic Fever outbreaks in Turkey. Vector Borne Zoonotic Dis. 2007;7:667–78. https://doi.org/10.1089/vbz.2007.0134
48. Shayan S, Bokaean M, Shahrivar MR, Chinikar S. Crimean-Congo hemorrhagic fever. Lab Med. 2015;46:180–9. https://doi.org/10.1309/LMN1P2FRZ7BKZSCO
49. Amzati GS, Pelle R, Muhigwa JBB, Kanduma EG, Djikeng A, Madder M, et al. Mitochondrial phylogeography and population structure of the cattle tick *Rhipicephalus appendiculatus* in the African Great Lakes region. Parasit Vectors. 2018;11:329. https://doi.org/10.1186/s13071-018-2904-7
50. Tonk-Rügen M, Kratou M, Cabezas-Cruz A. A warming world, a growing threat: the spread of ticks and emerging tick-borne diseases. Pathogens. 2025;14:213. https://doi.org/10.3390/pathogens14030213

Address for correspondence: Ayato Takada, Division of Global Epidemiology, International Institute for Zoonosis Control, Hokkaido University, Sapporo 001-0020, Japan; email: atakada@czc.hokudai.ac.jp

Border Region Surveillance of Malaria Drug Resistance, Northern Burundi, 2023–2024

Denis Niyomwungere, Pierre Sinarinzi, Emmanuelle Caspar, Lucas Thiebaut, Pierre-Emeric Strubel, Yssimini Nadège Guillène Tibiri, Laurence Ma, Jérôme Rurihafi, Pierre Ndizeyimana, Pierre Hakizimana, Nestor Niyizompa, Adélin Witonze, Vénant Ndayiragije, Floride Ndayisenga, Malachie Ndikumukiza, Olive Niyonkuru, Jean Claude Niyonsaba, Césaire Bangirinama, Jolis Lazare Bigirimana, Nicaise Ntahondi, Landrine Mugisha, Marcelline Nibakire, Néhémie Nzoyikorera, Denis Sinzinkayo, Didier Menard, Joseph Nyandwi

To evaluated artemisinin partial resistance (ART-R) in malaria in Burundi, during December 2023–June 2024, we studied 423 children <5 years of age with uncomplicated *Plasmodium falciparum* malaria in 8 health facilities in the northern part of the country. After artemether/lumefantrine treatment with only the first dose directly observed, 4.5% remained parasitemic on day 3. No *pfkelch13* mutations, validated or candidate markers of ART-R, were detected. However, markers of antifolate and 4-aminoquinoline resistance were widespread: the *dhfr* triple mutant N51I/C59R/S108N was nearly fixed (92%), *dhps* double and triple mutants were common (41% and 47%), and *pfcrt* CVIET, associated with chloroquine and amodiaquine resistance, predominated (84%). Geographic differences occurred in day-3 positivity and haplotype frequencies. Although ART-R markers were absent, delayed parasite clearance and near fixation of multidrug-resistant haplotypes serve as a warning. Strengthened efficacy monitoring and regional molecular surveillance are urgently needed to prevent drug-resistant *P. falciparum* from becoming established in Burundi.

Malaria remains a leading cause of illness and death in low- and middle-income countries, and sub-Saharan Africa bears the greatest burden. In 2024, an estimated 280 million malaria cases and 610,000 deaths occurred globally, of which 94% of cases and 95% of deaths were in sub-Saharan Africa. Children <5 years of age and pregnant women are the most affected groups (*1*,*2*).

To accelerate control, the World Health Organization (WHO) launched the Global Technical Strategy for Malaria 2016–2030, targeting a 90% reduction in incidence and mortality and elimination in 35 countries by 2030 (*3*). Burundi has scaled up core interventions, including artemisinin-based combination therapies (ACTs) since 2003, long-lasting insecticidal nets, indoor residual spraying, and intermittent preventive treatment in pregnancy (IPTp) (*4*–*7*). First-line treatment shifted from artesunate/amodiaquine to artemether/lumefantrine in 2019 (*4*). More recently, perennial malaria chemoprevention (PMC) was introduced in 5 districts, and RTS,S/AS01 vaccine (GSK, https://www.glaxosmithkline.com) was integrated into routine

Author affiliations: Institut National de Santé Publique, Bujumbura, Burundi (D. Niyomwungere, P. Ndizeyimana, P. Hakizimana, J. Nyandwi); Programme National Intégré de Lutte contre le Paludisme, Bujumbura (P. Sinarinzi, J. Rurihafi, N. Niyizompa, A. Witonze, F. Ndayisenga, L. Mugisha, M. Nibakire, N. Nzoyikorera); Malaria Genetics and Resistance Team, Pathogens Host Arthropods Vectors Interactions Unit, University of Strasbourg, Strasbourg, France (E. Caspar, L. Thiebaut, P.-E. Strubel, Y.N.G. Tibiri, D. Menard); Institut de Recherche en Sciences de la Santé, Clinical Research Unit of Nanoro, Nanoro, Burkina Faso (Y.N.G. Tibiri); Biomics Platform, Institut Pasteur, Université Paris Cite, Paris, France (L. Ma); Centre Hospitalo-universitaire de Kamenge, Bujumbura (V. Ndayiragije, M. Ndikumukiza, O. Niyonkuru, C. Bangirinama, J.L. Bigirimana, N. Ntahondi); Université du Burundi, Bujumbura (M. Ndikumukiza, D. Sinzinkayo, J. Nyandwi); Tanganyika Care Hospital, Bujumbura (J.C. Niyonsaba); Malaria Parasite Biology and Vaccines, INSERM Unit 1347, ParasitInnov, Institut Pasteur, Université Paris Cité, Paris (D. Menard); Laboratory of Parasitology and Medical Mycology, CHU Strasbourg, Strasbourg (D. Menard); Institut universitaire de France, Paris (D. Menard)

DOI: https://doi.org/10.3201/eid3204.251711

immunization in March 2025, with initial deployment in 25 of the country's 47 health districts (*5*,*6*). Despite those efforts, malaria transmission remains intense; 4.9 million cases and 809 deaths were reported by the national surveillance system in 2023–2024, including 2.2 million cases among children <5 years of age (*5*,*6*).

The emergence and spread of drug resistance is a looming threat. Artemisinin partial resistance (ART-R), defined by day 3 parasitemia and validated *pfkelch13* mutations, has been confirmed in Rwanda and Tanzania (*8*–*14*). Given porous borders and high population mobility, Burundi faces increased risk for resistant *Plasmodium falciparum* introduction. We conducted a prospective study in northern Burundi using a simplified day 3 follow-up design after artemether/lumefantrine treatment to assess delayed parasite clearance and the key molecular resistance markers, *pfkelch13*, *pfcrt*, *pfmdr1*, *dhfr*, and *dhps*.

Methods

Study Design and Population

Study Design and Setting

We conducted the study during December 2023–June 2024 in 8 health facilities across 5 districts of northern Burundi, a high *P. falciparum* transmission zone bordering Rwanda (Figure). Sites were located in Kirundo Province (2 facilities in Kirundo, 1 in Vumbi) and Ngozi Province (3 facilities in Buye, 1 in Ngozi, and 1 in Kiremba). This region experiences intense perennial transmission with seasonal peaks during March–June and October–December. According to national surveillance data, parasitemia prevalence in children <5 years of age reaches 79% in Kirundo and 54% in Ngozi (*15*), and clinical incidence approaches 400 cases/1,000 population annually (*5*,*6*,*15*).

Study Population and Eligibility Criteria

We screened children <5 years of age who had fever (≥37.5°C axillary or history of fever within the previous 24 h). Inclusion required microscopically confirmed *P. falciparum* monoinfection. We applied no minimum parasite density or hemoglobin thresholds for enrollment. Exclusion criteria were signs of severe malaria, mixed infections, or known hypersensitivity to artemisinin derivatives.

Treatment, Follow-up Procedures, and Outcomes

Participants received a standard 3-day course of artemether/lumefantrine (Lumartem DT, https://www.cipla.com; WHO-prequalified dispersible tablets, 20 mg artemether/120 mg lumefantrine) according to Burundi national guidelines (*4*). Dosing followed WHO weight-based recommendations: children 5 to <15 kg received 1 dispersible tablet per dose, and children 15 to <25 kg received 2 tablets per dose. Each treatment course consisted of 6 doses administered at 0, 8, 24, 36, 48, and 60 hours. The first dose was directly observed and was administered with fatty food to enhance lumefantrine absorption. Caregivers were instructed to administer subsequent doses with food at home with reinforced instructions. On day 0 and day 3, we collected capillary blood samples for Giemsa-stained smears and dried blood spots for molecular analysis. On day 3, all children underwent clinical assessment including temperature measurement and symptom evaluation. We referred children with persistent fever or clinical deterioration for management, according to national guidelines. We did not re-treat those with persistent parasitemia but no danger signs because the study assessed day 3 positivity for surveillance purposes rather than to guide individual treatment.

Microscopy

We prepared thick and thin smears and stained with 10% Giemsa (pH 7.2) for 15 minutes. We used thick smears for parasite detection and density quantification and thin smears for species identification on the basis of parasite morphology when mixed infections were suspected or when species confirmation was required. Two certified microscopists independently read slides at 1,000× magnification; discrepancies >25% in parasite density were resolved by a third reader, and we calculated the final parasite density as the mean of the 2 closest readings. We calculated parasite density per 200 leukocytes (8,000/μL) and recorded gametocyte presence.

Molecular Analysis

We collected dried blood spots on Whatman 903 filter paper, air-dried, stored with desiccant, and shipped to the University of Strasbourg (Strasbourg, France) for analysis. We extracted DNA from dried blood spots by using the QIAamp DNA Blood Mini Kit (QIAGEN, https://www.qiagen.com). We confirmed *Plasmodium* species by real-time PCR targeting *cytb* and by nested species-specific PCR (*16*).

We analyzed drug-resistance markers by targeted amplicon sequencing of *pfkelch13* (codons 430–720), *pfcrt* (codons 72–76, 93, 97, 145, 218, 343, 350, 353, and 356), *pfmdr1* (codons 86, 184, 1034, 1042, and 1246), *dhfr* (codons 16, 50, 51, 59, 108, and 164), and *dhps* (codons 431, 436, 437, 540, 581, and 613) (*17*). We multiplexed and barcoded amplicons, then pooled, purified, and

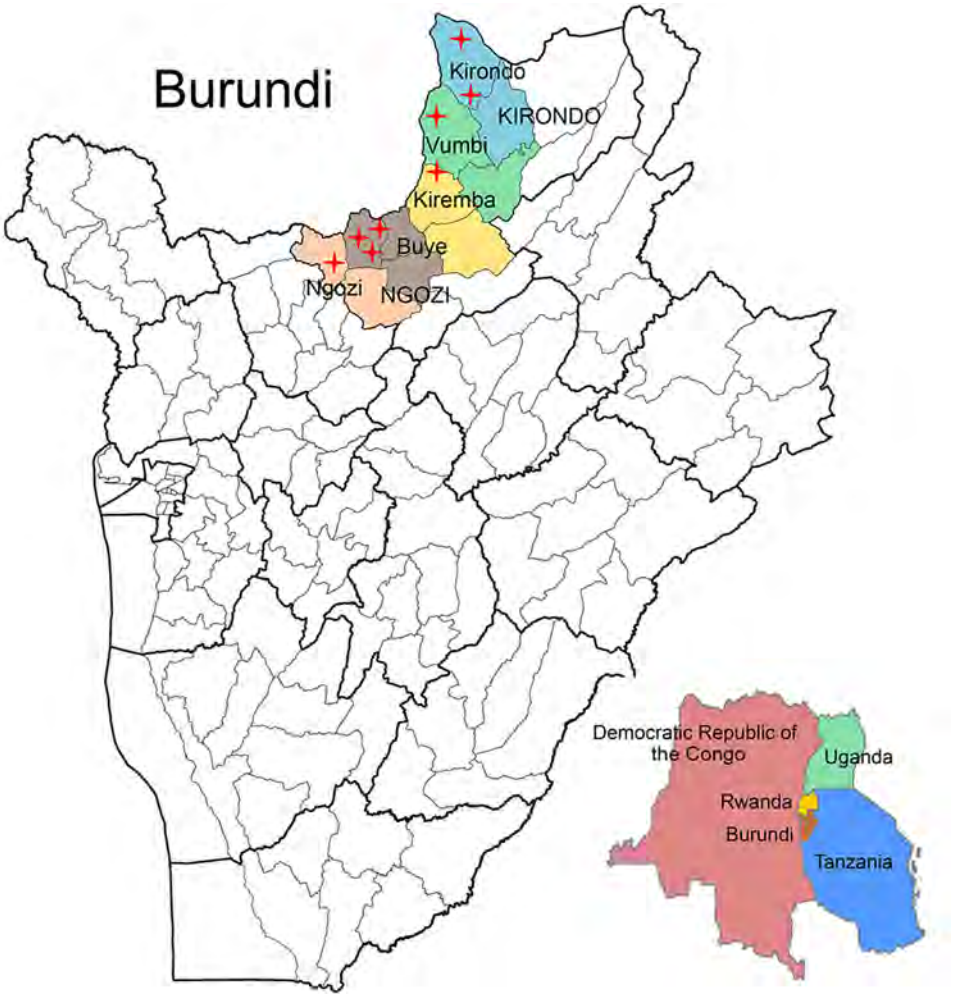

Figure. Locations of 8 sentinel health facilities used for study of border region surveillance of malaria drug resistance, northern Burundi, 2023–2024. Red crosses show locations of participating health facilities across the provinces of Ngozi and Kirundo, where clinical and molecular surveillance of artemisinin partial resistance was conducted during December 2023–June 2024. District health facilities included were in Ngozi, Kiremba, and Buye in Ngozi Province and Kirundo and Vumbi in Kirondo Province. Inset shows bordering countries in Africa.

sequenced on an Illumina MiSeq platform (300-cycle v2 kit; Illumina, https://www.illumina.com). We quality-trimmed reads (Phred score ≥30; https://www.phrap.com/phred) and aligned reads to the *P. falciparum* 3D7 reference genome (v45) by using CLC Genomics Workbench version 22 (QIAGEN). We called variants that were supported by ≥20 reads and allele frequency ≥5%. Reference strains Dd2, 7G8, HB3, and 3D7 served as positive controls (*17*).

Sample Size Considerations

This surveillance was designed to detect circulating *pfkelch13* mutant parasites, particularly the R561H allele, validated in neighboring Rwanda and Tanzania. We targeted ≈50 children per site (400 total) to ensure broad geographic coverage of the border region while maintaining logistical feasibility. This sample size provides 95% confidence to detect mutant alleles circulating at ≥0.75% prevalence if none are observed (rule of three: 3/n). The study was not powered for formal interdistrict comparisons; district-level differences in baseline characteristics and molecular markers are reported as exploratory observations to generate hypotheses for future targeted investigations.

Study Outcomes

The primary outcome was the percentage of children with persistent parasitemia on day 3 (day 3 positivity), defined as microscopically detectable asexual *P. falciparum* parasites on day 3 after treatment initiation. That indicator serves as a clinical proxy for delayed parasite clearance associated with ART-R. Secondary outcomes included the prevalence of molecular markers associated with malaria drug resistance: *pfkelch13* mutations (ART-R), *pfcrt* and *pfmdr1* haplotypes (chloroquine, amodiaquine, and piperaquine resistance), and *dhfr/dhps* mutations (sulfadoxine/pyrimethamine resistance).

Statistical Analysis

We summarized demographic and clinical variables by using descriptive statistics and compared continuous

variables by using the Kruskal-Wallis test and categorical variables by using χ^2 or Fisher exact tests. We considered $p<0.05$ significant.

We assessed day 3 positivity after treatment with only the first dose directly observed, estimated prevalence with exact binomial 95% CIs and compared across provinces (Kirundo and Ngozi) to assess geographic heterogeneity. We calculated allele frequencies for *pfkelch13*, *pfcrt*, *pfmdr1*, *dhfr*, and *dhps* and stratified by district. We classified mixed infections as mutant for allele-frequency estimates. We reconstructed inferred *dhfr-dhps* haplotypes from unphased single-nucleotide polymorphism data and compared them between districts; we interpreted results as inferred patterns rather than observed genotypes. We performed analyses with MedCalc version 20.218 (MedCalc Software Ltd, https://www.medcalc.org).

Ethical Considerations

The study followed the Declaration of Helsinki and WHO guidelines for human research. Approval was obtained from the Burundi National Ethics Committee for the Protection of Human Subjects (approval no. CNE/25/2023). Written informed consent was obtained from parents or legal guardians. Participant confidentiality and data security were strictly maintained.

Results

We screened 873 febrile children <5 years of age across the 8 health facilities. Of those, 423 met the inclusion criteria and completed clinical follow-up through day 3, corresponding to 1 day after completion of artemether/lumefantrine treatment. Of the 423 samples collected, 365 (86.3%) day 0 samples were successfully confirmed as *P. falciparum* infections and subsequently analyzed by molecular sequencing to address the secondary objective: detection of *pfkelch13* mutations, notably R561H, a validated marker of ART-R. Sequencing success varied by district: 100% in Kiremba and Ngozi, 91% in Kirundo, 75% in Buye, and 76% in Vumbi. We excluded the other 58 samples (13.7%) because of insufficient DNA quality.

The median age of enrolled children was 30 (IQR 17–45) months, and the sex ratio was balanced (1.0). Baseline characteristics showed variation across districts (Table). Median axillary temperatures ranged from 37.8°C (Buye) to 39.0°C (Kirundo). Pretreatment asexual *P. falciparum* parasite density varied widely; median values ranged from 10,543/μL (Vumbi) to 42,400/μL (Kirundo). Gametocyte carriage was detected in 5.4% of children overall, with district-specific prevalence ranging from 1.2% (Kirundo) to 22.0% (Ngozi). Mixed-species infections were uncommon (1.2% *P. malariae* in Ngozi Province), confirming *P. falciparum* as the predominant species.

Among the 423 children enrolled, 19 (4.5%; 95% CI 2.7%–6.9%) remained parasitemic on day 3 after artemether/lumefantrine treatment. That overall prevalence was below the WHO 10% threshold, but we observed marked heterogeneity across districts. Vumbi (13.6%) exceeded the WHO 10% threshold and neighboring districts, identifying a localized hotspot of delayed clearance. Those differences were statistically significant within Kirundo Province districts ($p = 0.0002$), but we observed no significant variation between provinces ($p = 0.06$).

The median asexual parasite density on day 3 was 260 parasites/μL (IQR 141–1,659 parasites/μL), with no significant variation across districts ($p = 0.96$). Nevertheless, district-specific values showed marked variation, from very low medians in Buye and Kiremba (≈100 parasites/μL) to >1,800 parasites/μL in Ngozi district. Gametocytes were detected microscopically in 11 (2.6%) children on day 3. Their prevalence varied geographically: uncommon in Kirundo Province (1.2%) but more frequent in Ngozi Province (4.8%) and peaked at 10.0% in Kiremba district (Table).

For day 0 isolates, of the 423 children enrolled, 365 (86.3%) samples yielded high-quality sequences and were included in the molecular analysis (Appendix Tables 1, 2, https://wwwnc.cdc.gov/EID/article/32/4/25-1711-App1.pdf). Most (97.5%, 356/365), isolates were wild-type at *pfkelch13*. We detected no validated or candidate WHO-associated mutations linked to ART-R. We did observe nonsynonymous variants in 9 (2.5%) isolates. The most frequent variant was A578S (4 cases, 1.1%), whereas R513S, A626S, H644R, and N672H were each detected in 1 or 2 isolates. None of those polymorphisms are currently associated with delayed parasite clearance, but their detection might indicate ongoing low-level diversification of the *pfkelch13* locus in this setting.

Mutant *pfcrt* haplotypes were nearly fixed. The CVIET triple mutant, defined by mutations at *pfcrt* codons 72–76 (C72/V73/I74/E75/T76), predominated (84.4%, 308/365), whereas the CVIET+356T haplotype was detected in 9.3% (34/365) of isolates. The CVMNK wild-type was uncommon (4.9%, 18/365). Minor variants included SVMNT (72S/76T, 1.1%) and 356T alone (0.3%). We observed no significant difference in overall *pfcrt* haplotype distribution between provinces ($p = 0.25$). However, intraprovincial heterogeneity was evident, particularly for codon 356 in Ngozi Province ($p = 0.01$), suggesting

Table. Baseline characteristics and day 3 parasitologic outcomes for patients with *Plasmodium falciparum* malaria, northern Burundi, December 2023–June 2024*

Baseline characteristics	Kirundo Province			Ngozi Province				Total	p value
	Kirundo	Vumbi	Total	Buye	Kiremba	Ngozi	Total		
No. patients	170	82	252	97	30	44	171	423	–
Gender ratio, M/F	0.9	1.5	1.1	0.8	2.0	1.0	1.0	1.0	0.77
Age, mo									
Median	32	30	31	28	29	32	30	30	0.5
95% CI	27–36	22.2–33	27–34.3	23–35.5	17–36.65	28.5–36	25.9–34	28–32	–
IQR	19–47	13.75–38.25	18–46	14–42	15–42	20.75–45	16–42	17–45	–
Weight, kg									
Median	11	10	11	10	11.5	10	10	10	0.5
95% CI	10–12	9–11.2	10–11	10–11	9.2–13.8	10–12.2	10–11	10–11	–
IQR	9–13.5	8.1–12.9	9–13	8–13	10–13	10–14	9–13	9–13	–
Temperature, °C									
Median	39.0	38.3	38.6	37.8	38.1	38.7	38.4	38.5	**0.01**
95% CI	38.6–39.0	38.0–38.5	38.4–38.9	37.8–38.4	37.8–39.0	38.5–38.9	38.0–38.5	38.4–38.6	–
IQR	38.0–39.6	38.0–38.9	38.0–39.2	37.4–38.9	37.7–39.0	38.3–39.0	37.7–39.0	37.8–39.0	–
Pretreatment asexual *P. falciparum* density, parasites/µL									
Median	42,400	10,543	36,734	10,745	12,743	27,661	19,374	27,313	**0.01**
95% CI	33,663–54,525	7,499–39,836	25,325–46,160	3,846–26,436	8,028–38,878	15,887–41,680	10,733–26,650	22,511–35,539	–
IQR	7,566–108,166	2,759–72,886	4,615–102,933	1,625–48,692	5,128–44,000	9,746–59,628	2,400–51,912	3,521–79,513	–
Pretreatment sexual *P. falciparum* density, parasites/µL, %	1.2	3.7	2	7.4	3.3	22.0	10.2	5.3	**0.0003**
Mixed infections with other species, %									
P. vivax	0	0	0	0	0	0	0	0	0.08
P. malariae	0	0	0	1.1	0	2.4	1.2	0.5	
P. ovale	0	0	0	0	0	0	0	0	
Day 3 positivity rate, %†	1.8	13.6	5.7	2.1	0	7.3	3.0	4.5	0.06
Day 3 asexual *P. falciparum* density, parasites/µL									
Median	1,480	240	260	100	–	1,832	103	260	0.96
95% CI	–	177–281	200–1,522	–	–	–	–	175–1,290	–
IQR	5,475–23,172	192–275	202–1,140	98–103	–	494–13,381	85–5681	141–1,659	–
Day 3 sexual *P. falciparum* density, parasites/µL, %	1.2	1.2	1.2	4.2	10.0	2.4	4.8	2.6	**0.02**

*Demographic, clinical, and parasitologic parameters recorded at enrollment and on day 3 after initiation of artemether/lumefantrine treatment. The study covered 5 districts: Kirundo and Vumbi in Kirundo Province; and Buye, Kiremba, and Ngozi in Ngozi Province. Data are disaggregated by site and province. Continuous variables are reported as medians with IQRs and 95% CIs; categorical variables are expressed as percentages. p values reflect statistical comparisons between the 2 provinces (Kirundo vs. Ngozi); bold indicates significant p values. IQR, interquartile range; –, not applicable.
†Day 3 positivity indicates the presence of microscopically detectable asexual *P. falciparum* parasitemia on day 3 after treatment initiation.

microgeographic clustering of resistant variants. The predominance of CVIET confirms that chloroquine resistance remains highly fixed in northern Burundi, with additional mutations such as 356T emerging at low frequency. Of note, we detected no *pfcrt* mutations associated with piperaquine resistance. All isolates were wild-type at positions H97, F145, I218, M343, C350, and G353. Although the 356T variant occurred in 9.6% (35/365) of isolates, that mutation alone does not confer piperaquine resistance.

Mutant haplotypes were common at the *pfmdr1* locus. We identified the wild-type NYSND haplotype, defined by *pfmdr1* codons 86-184-1034-1042-1246 (N86/Y184/S1034/N1042/D1246), in 31.2% (114/365) of isolates. The most frequent mutant was the single 184F allele, detected in 57.3% (209/365) of isolates, followed by 86Y (7.9%). Additional combinations involving 86Y, 1034C, 1042D, or 1246Y remained uncommon (≤1.6% each). We noted significant differences in haplotype distribution between provinces ($p = 0.03$), suggesting that selective pressures on *pfmdr1* might vary geographically, potentially reflecting differences in drug use or drug pressure intensity.

At the *dhfr* locus, resistance alleles were nearly fixed. The triple mutant 51I/59R/108N predominated (92.1%, 336/365), confirming widespread pyrimethamine resistance. Other haplotypes were uncommon, including the double mutant 51I/108N (1.1%) and

the single 108N variant (0.5%), and we detected the quadruple mutant 51I/59R/108N/164L in 12 (3.3%) isolates. Although infrequent, the quadruple mutant genotype is clinically relevant because the addition of 164L confers high-grade pyrimethamine resistance and has been associated with sulfadoxine/pyrimethamine treatment failure in East Africa. We detected the wild-type haplotype in only 12 (3.3%) isolates. Variation between provinces was not statistically significant (p = 0.2).

Mutations at the *dhps* locus were also widespread. Only 21/365 (5.8%) isolates were wild-type. The double mutant 437G/540E was detected in 148/365 (40.5%) isolates, whereas the triple mutant 437G/540E/581G was even more frequent (172/365 isolates, 47.1%). Minor haplotypes included 436A (3.8%) and 613S (0.3%). Although we observed no significant difference in overall haplotype proportions between provinces (p = 0.6), district-level variation within Kirundo Province was significant for codons 436A (p = 0.0001), 437G (p = 0.001), and 540E (p = 0.02).

Analysis of combined genotypes enabled inference of multilocus *dhfr*/*dhps* haplotypes, highlighting the extensive accumulation of antifolate resistance alleles. The fully wild-type *dhfr*/*dhps* combination was nearly absent (1/365 isolates, 0.3%). The most prevalent inferred haplotype was the sextuple mutant (*dhfr* triple 51I/59R/108N + *dhps* triple 437G/540E/581G), detected in 161/365 (44.1%) isolates. That genotype has been associated with markedly reduced efficacy of IPTp in East Africa. The classic quintuple mutant (*dhfr* triple 51I/59R/108N + *dhps* double 437G/540E) was also common, found in 134/365 (36.7%) isolates. Together, those 2 high-resistance genotypes accounted for >80% of infections. Less frequent combinations included quadruple or septuple haplotypes, each detected in ≤3% of isolates. Although overall haplotype distribution did not differ significantly between provinces (p = 0.2), variation occurred at the district level.

We performed molecular analysis on isolates from the 19 children who remained parasitemic on day 3. All isolates were wild-type at *pfkelch13*, confirming the absence of validated or candidate ART-R mutations. At *pfcrt*, the CVIET haplotype predominated (84.2%), and additional variants included CVIET+356T (10.5%) and SVMNT (5.3%). At *pfmdr1*, the 184F allele occurred in 57.9% of isolates, consistent with findings from day 0. Mutations at the *dhfr* locus were nearly fixed, the triple mutant 51I/59R/108N was present in 94.7% of isolates. At *dhps*, the double (437G/540E) and triple (437G/540E/581G) mutants together accounted for >85% of samples. Inferred *dhfr*/*dhps* haplotypes showed a high prevalence of quintuple and sextuple genotypes, mirroring the overall population.

Paired analysis of baseline (day 0) and follow-up (day 3) samples revealed that most isolates retained identical molecular profiles across time points. Nonetheless, we observed a few discordances, particularly in *pfmdr1* (184F/Y) and *dhps* alleles (e.g., detection of 581G or 164L in some day 3 samples). Those differences likely reflect within-host selection of minority clones under drug pressure rather than de novo mutations.

Discussion

ART-R is a growing threat to malaria control in sub-Saharan Africa, and validated *pfkelch13* mutations are already established in Rwanda, Uganda, and Tanzania (*8*,*9*,*13*,*17*–*20*). Of particular concern is the detection of the *pfkelch13* R561H mutation, a validated marker of delayed parasite clearance, in the Huye district of Rwanda and the Kagera region of Tanzania (*8*–*10*,*12*–*14*,*21*,*22*). Those findings raise the alarm over possible spread into neighboring countries, including Burundi, underscoring the urgent need for localized therapeutic and molecular surveillance.

We adopted a simplified surveillance design to detect ART-R, combining day 3 parasitemia assessment with *pfkelch13* molecular screening. That approach provides complementary clinical and genetic indicators without replacing traditional therapeutic efficacy studies, which remain essential for evaluating ACT efficacy and informing treatment policy. The limited follow-up period and dried blood spot collection enable rapid geographic mapping of ART-R risk across multiple sites in resource-constrained contexts (*23*).

In 5 districts across northern Burundi, 4.5% of children treated with artemether/lumefantrine remained parasitemic on day 3, below the 10% WHO threshold for confirmed ART-R (*24*), but the Vumbi district exceeded the WHO threshold. However, the sample size was calculated for surveillance purposes and was not powered to detect statistically significant differences between districts. Consequently, the geographic comparisons we describe should be interpreted as exploratory findings, rather than definitive evidence of spatial heterogeneity.

None of the day 3 positivity cases harbored validated or candidate *pfkelch13* mutations. That discordance suggests either false-positive results driven by imperfect adherence to the 6-dose artemether/lumefantrine regimen (*25*,*26*), variability in lumefantrine exposure (food intake, vomiting, drug–drug interactions), age-dependent immunity in young children

(*27*), or genuine delayed clearance mediated by polygenic architecture of artemisinin response (e.g., *coronin*, *ap2μ*, or *ubp-1*) (*28*,*29*). Pharmacokinetics/adherence verification and broader genomic profiling are needed to resolve those alternatives.

The overall clinical response to artemether/lumefantrine treatment appeared satisfactory despite 4.5% day 3 positivity, likely because lumefantrine, the partner drug with a longer half-life, remains fully effective at eliminating residual parasites. The *pfmdr1* mutations observed (low N86, high 184F) indicate drug pressure but are not validated markers of lumefantrine failure. Those findings suggest lumefantrine efficacy is currently maintaining artemether/lumefantrine effectiveness in Burundi, underscoring the importance of monitoring both artemisinin and partner drug susceptibility.

The absence of *pfkelch13* mutants in Burundi, despite their presence in neighboring countries, might reflect intense transmission (*5*,*7*), where parasite diversity and immunity limit resistant lineage expansion. However, *pfkelch13* mutations have been documented in high-transmission areas of Uganda (*20*), demonstrating that transmission intensity alone does not prevent resistance selection or spread. The absence of validated mutations should not be interpreted as protection. Importation risk remains high, given porous borders and regional connectivity, underscoring the urgency of cross-border surveillance (*24*).

Beyond ART-R, this study revealed a concerning accumulation of antifolate resistance. The *dhfr* triple mutant was nearly fixed, and >80% of infections carried highly resistant multilocus haplotypes. At the *dhps* locus, mutations were also highly prevalent. The 437G/540E/581G triple mutant was present in 47.1% of isolates, whereas only 5.8% of parasites remained wild-type. That pattern indicates widespread sulfadoxine resistance, with direct implications for malaria prevention in Burundi. Sulfadoxine/pyrimethamine is used for IPTp and more recently in PMC. The high prevalence (44%) of the sextuple haplotype raises serious concerns because that genotype is associated with reduced IPTp effectiveness and adverse birth outcomes and likely compromises PMC efficacy. Those findings warrant urgent reassessment of sulfadoxine/pyrimethamine-based prevention strategies in Burundi (*30*–*32*).

ACT partner-drug resistance markers were entrenched. The *pfcrt* CVIET haplotype (74I/75E/76T) predominated (84.4%), with an additional subset carrying 356T (9.3%). Wild-type CVMNK was infrequent (4.9%). Those results confirm that chloroquine resistance remains essentially fixed in the parasite population, consistent with observations across East Africa, despite chloroquine withdrawal (*33*,*34*). That pattern contrasts with observations from several other countries in Africa, where chloroquine-sensitive parasites have reexpanded after drug withdrawal (*35*). The persistence of CVIET in Burundi likely reflects the use of artesunate/amodiaquine as first-line treatment until 2019, which maintained selective pressure favoring *pfcrt* mutant parasites. Similar persistence of CVIET has been reported in other countries that used artesunate/amodiaquine, such as South Sudan. A decline in CVIET prevalence might require several more years to become apparent (*36*–*39*).

We detected no *pfcrt* mutations associated with piperaquine resistance (e.g., F145I, H97Y, M343L, G353V) in this study (*40*–*42*). Those mutations have been identified as key drivers of dihydroartemisinin/piperaquine treatment failures in Southeast Asia, but they appear absent in East Africa parasite populations.

At the *pfmdr1* locus, the Y184F mutation was the dominant variant (57.3%), whereas the wild-type NYSND was found in 31.2%. Other variants involving 86Y, 1034C, 1042D, or 1246Y were uncommon (≤1.6%). The predominance of 184F is consistent with reports from Zanzibar (Tanzania) and Senegal (*43*,*44*). The Y184F mutation is frequently selected by artemether/lumefantrine treatment and can modulate parasite responses in vitro, but it should be regarded as a marker of drug pressure rather than a validated clinical marker of lumefantrine resistance (*45*).

The limitations of this study include partially supervised drug treatment, unmeasured drug concentrations, day 3 follow-up only, and no assessment of copy number variation in *pfmdr1* and *plasmepsin 2/3*, the established markers associated with reduced lumefantrine (*46*–*48*) and piperaquine (*40*,*49*,*50*) susceptibility. Study strengths include multiple sentinel sites in a high-risk border region, combined clinical and molecular surveillance, and an integrated baseline dataset informing national and regional strategies.

WHO recommends deploying multiple first-line ACTs to delay malaria drug resistance emergence. In Burundi, where artemether/lumefantrine is the sole first-line treatment, introducing an alternative such as dihydroartemisinin/piperaquine could reduce selective pressure. The absence of *pfcrt* mutations associated with piperaquine resistance suggests dihydroartemisinin/piperaquine could retain full efficacy and serve as a second first-line option.

In conclusion, our findings highlight a critical juncture for Burundi. We detected no *pfkelch13* mutants, but excess localized day 3 positivity and entrenched sulfadoxine/pyrimethamine resistance

represent clear warning signals. High-transmission dynamics may currently protect Burundi against *pfkelch13*-mediated ART-R, but that protection is fragile. Strengthened therapeutic efficacy monitoring, expanded molecular surveillance, including genomic approaches, and cross-border collaboration are urgently required to prevent resistant *P. falciparum* establishment and spread in the Great Lakes region of Burundi.

Acknowledgments

We sincerely thank all the children and their caregivers who participated in this study. We are also grateful to the clinical and laboratory teams across the 8 participating health facilities for their dedication and professionalism. We acknowledge the support of the Burundian Ministry of Health, the National Malaria Control Program, and local health authorities for facilitating field implementation. We also thank the staff of the National Reference Laboratory of Institut National de Santé Publique in Burundi and community health workers for their valuable contributions.

The datasets used and analyzed during this study are available from the corresponding author upon reasonable request. The nucleotide sequences generated in this study have been deposited in GenBank (accession nos. PZ122655–9; BankIt submission no. 3061318).

This study was conducted as part of the IMPRIMA project and received support from the Global Health EDCTP3 Joint Undertaking (GH EDCTP3 JU; grant agreement no. 101103213). Additional funding was provided by the Fondation pour la Recherche Médicale (FRM) through the 'Équipes FRM 2024' program (grant no. EQU202403018026), by the Université de Strasbourg (grant no. R42PHAV), and by the Institut Universitaire de France under the Senior Chair program (2024–2029). The funders had no role in the study design, data collection and analysis, interpretation of results, or writing of the manuscript.

Author contributions: conceptualization: D.N., P.S., D.M., J.N.; methodology: E.C., P.-E.S., L.T., Y.N.G.T., D.N., D.M.; investigation: P.S., D.N., J.N., L. Mugisha, N.N., D.S., M.N., V.N., O.N., J.-C.N., A.W., C.B., J.-L.B., N.N., M.N., F.N., N.N., P.H., P.N., L. Ma, J.R.; data curation: D.N., P.S., D.M.; formal analysis: D.N., P.S., D.M.; data access and verification: D.N., P.S., D.M.; writing, original draft: D.N., D.M.; writing, review and editing: D.N., D.M.; supervision: D.M., J.N.; project administration: D.N., J.N.; funding acquisition: D.M., J.N. All authors read and approved the final version of the manuscript. D.M. and D.N. are joint guarantors of the study.

About the Author

Dr. Niyomwungere is a physician and public health specialist at the Institut National de Santé Publique in Bujumbura, Burundi. His work focuses on malaria control and surveillance of malaria drug resistance to support national elimination efforts.

References

1. World Health Organization. World malaria report 2025: addressing the threat of antimalarial drug resistance. Geneva: The Organization; 2025.
2. van Eijk AM, Hill J, Noor AM, Snow RW, ter Kuile FO. Prevalence of malaria infection in pregnant women compared with children for tracking malaria transmission in sub-Saharan Africa: a systematic review and meta-analysis. Lancet Glob Health. 2015;3:e617–28. https://doi.org/10.1016/S2214-109X(15)00049-2
3. World Health Organization. Global technical strategy for malaria 2016–2030. 2021 update. Geneva: The Organization; 2021.
4. Programme National Intégré de Lutte contre le Paludisme. Guidelines for malaria case management in Burundi [in French]. Bujumbura (Burundi): Ministère de la Santé Publique; 2019.
5. US President's Malaria Initiative. Burundi malaria profile. Washington: The Initiative; 2023.
6. Programme National Intégré de Lutte contre le Paludisme. National strategic plan for the fight against malaria (2021–2027) [in French]. Bujumbura (Burundi): Ministère de la Santé Publique; 2021.
7. Sinzinkayo D, Baza D, Gnanguenon V, Koepfli C. The l ead-up to epidemic transmission: malaria trends and control interventions in Burundi 2000 to 2019. Malar J. 2021;20:298. https://doi.org/10.1186/s12936-021-03830-y
8. Uwimana A, Legrand E, Stokes BH, Ndikumana JM, Warsame M, Umulisa N, et al. Emergence and clonal expansion of in vitro artemisinin-resistant *Plasmodium falciparum kelch13* R561H mutant parasites in Rwanda. Nat Med. 2020;26:1602–8. https://doi.org/10.1038/s41591-020-1005-2
9. Uwimana A, Umulisa N, Venkatesan M, Svigel SS, Zhou Z, Munyaneza T, et al. Association of *Plasmodium falciparum kelch13* R561H genotypes with delayed parasite clearance in Rwanda: an open-label, single-arm, multicentre, therapeutic efficacy study. Lancet Infect Dis. 2021;21:1120–8. https://doi.org/10.1016/S1473-3099(21)00142-0
10. Bergmann C, van Loon W, Habarugira F, Tacoli C, Jäger JC, Savelsberg D, et al. Increase in *Kelch 13* polymorphisms in *Plasmodium falciparum*, southern Rwanda. Emerg Infect Dis. 2021;27:294–6. https://doi.org/10.3201/eid2701.203527
11. Kirby R, Giesbrecht D, Karema C, Watson O, Lewis S, Munyaneza T, et al. Examining the early distribution of the artemisinin-resistant *Plasmodium falciparum kelch13* R561H mutation in areas of higher transmission in Rwanda. Open Forum Infect Dis. 2023;10:ofad149. https://doi.org/10.1093/ofid/ofad149
12. Assey A, Scialabba S, Zinga MM, Koliopoulos P, van Loon W, Minja CA, et al. Artemisinin and partner drug resistance markers in *Plasmodium falciparum* from Tanzanian paediatric malaria patients, 2016–2022. Malar J. 2025;24:209. https://doi.org/10.1186/s12936-025-05447-x
13. Ishengoma DS, Mandara CI, Bakari C, Fola AA, Madebe RA, Seth MD, et al. Evidence of artemisinin partial resistance in

northwestern Tanzania: clinical and molecular markers of resistance. Lancet Infect Dis. 2024;24:1225–33. https://doi.org/10.1016/S1473-3099(24)00362-1
14. Juliano JJ, Giesbrecht DJ, Simkin A, Fola AA, Lyimo BM, Pereus D, et al. Prevalence of mutations associated with artemisinin partial resistance and sulfadoxine-pyrimethamine resistance in 13 regions in Tanzania in 2021: a cross-sectional survey. Lancet Microbe. 2024;5:100920. https://doi.org/10.1016/S2666-5247(24)00160-5
15. Institut de Statistiques et d'Études Économiques du Burundi, The DHS Program. Third demographic and health survey in Burundi (EDSB-III), 2016–2017 [in French]. Bujumbura (Burundi): The Institute; 2017.
16. Canier L, Khim N, Kim S, Sluydts V, Heng S, Dourng D, et al. An innovative tool for moving malaria PCR detection of parasite reservoir into the field. Malar J. 2013;12:405. https://doi.org/10.1186/1475-2875-12-405
17. Mihreteab S, Platon L, Berhane A, Stokes BH, Warsame M, Campagne P, et al. Increasing prevalence of artemisinin-resistant HRP2-negative malaria in Eritrea. N Engl J Med. 2023;389:1191–202. https://doi.org/10.1056/NEJMoa2210956
18. Balikagala B, Fukuda N, Ikeda M, Katuro OT, Tachibana SI, Yamauchi M, et al. Evidence of artemisinin-resistant malaria in Africa. N Engl J Med. 2021;385:1163–71. https://doi.org/10.1056/NEJMoa2101746
19. Fukuda N, Tachibana SI, Ikeda M, Sakurai-Yatsushiro M, Balikagala B, Katuro OT, et al. Ex vivo susceptibility of *Plasmodium falciparum* to antimalarial drugs in Northern Uganda. Parasitol Int. 2021;81:102277. https://doi.org/10.1016/j.parint.2020.102277
20. Rosenthal PJ, Asua V, Conrad MD. Emergence, transmission dynamics and mechanisms of artemisinin partial resistance in malaria parasites in Africa. Nat Rev Microbiol. 2024;22:373–84. https://doi.org/10.1038/s41579-024-01008-2
21. Kayiba NK, Yobi DM, Tshibangu-Kabamba E, Tuan VP, Yamaoka Y, Devleesschauwer B, et al. Spatial and molecular mapping of *pfkelch13* gene polymorphism in Africa in the era of emerging *Plasmodium falciparum* resistance to artemisinin: a systematic review. Lancet Infect Dis. 2021;21:e82–92. https://doi.org/10.1016/S1473-3099(20)30493-X
22. Straimer J, Gandhi P, Renner KC, Schmitt EK. High prevalence of *Plasmodium falciparum* K13 mutations in Rwanda is associated with slow parasite clearance after treatment with artemether-lumefantrine. J Infect Dis. 2022;225:1411–4. https://doi.org/10.1093/infdis/jiab352
23. World Health Organization. Report on antimalarial drug efficacy, resistance and response: 10 years of surveillance (2010–2019). Geneva: The Organization; 2020.
24. World Health Organization. Strategy to respond to antimalarial drug resistance in Africa. Geneva: The Organization; 2022.
25. Banek K, Lalani M, Staedke SG, Chandramohan D. Adherence to artemisinin-based combination therapy for the treatment of malaria: a systematic review of the evidence. Malar J. 2014;13:7. https://doi.org/10.1186/1475-2875-13-7
26. Challenger JD, Bruxvoort K, Ghani AC, Okell LC. Assessing the impact of imperfect adherence to artemether-lumefantrine on malaria treatment outcomes using within-host modelling. Nat Commun. 2017;8:1373. https://doi.org/10.1038/s41467-017-01352-3
27. Khoury DS, Cromer D, Akter J, Sebina I, Elliott T, Thomas BS, et al. Host-mediated impairment of parasite maturation during blood-stage *Plasmodium* infection. Proc Natl Acad Sci U S A. 2017;114:7701–6. https://doi.org/10.1073/pnas.1618939114
28. Mukherjee A, Bopp S, Magistrado P, Wong W, Daniels R, Demas A, et al. Artemisinin resistance without *pfkelch13* mutations in *Plasmodium falciparum* isolates from Cambodia. Malar J. 2017;16:195. https://doi.org/10.1186/s12936-017-1845-5
29. Demas AR, Sharma AI, Wong W, Early AM, Redmond S, Bopp S, et al. Mutations in *Plasmodium falciparum* actin-binding protein coronin confer reduced artemisinin susceptibility. Proc Natl Acad Sci U S A. 2018;115:12799–804. https://doi.org/10.1073/pnas.1812317115
30. Hansson H, Minja DTR, Moeller SL, Lusingu JPA, Bygbjerg IC, Yde AM, et al. Reduced birth weight caused by sextuple drug-resistant *Plasmodium falciparum* infection in early second trimester. J Infect Dis. 2021;224:1605–13. https://doi.org/10.1093/infdis/jiab117
31. Naidoo I, Roper C. Mapping 'partially resistant', 'fully resistant', and 'super resistant' malaria. Trends Parasitol. 2013;29:505–15. https://doi.org/10.1016/j.pt.2013.08.002
32. Plowe CV. Malaria chemoprevention and drug resistance: a review of the literature and policy implications. Malar J. 2022;21:104. https://doi.org/10.1186/s12936-022-04115-8
33. Hassen J, Alemayehu GS, Dinka H, Golassa L. High prevalence of *pfcrt* 76T and *pfmdr1* N86 genotypes in malaria infected patients attending health facilities in East Shewa zone, Oromia Regional State, Ethiopia. Malar J. 2022;21:286. https://doi.org/10.1186/s12936-022-04304-5
34. Mongella S, Enweji N, Mnong'one N, Minde M, Kamugisha E, Swedberg G. High prevalence of *Plasmodium falciparum pfcrt* K76T mutation in children with sickle cell disease at a tertiary hospital in north-western Tanzania. Tanzan J Health Res. 2014;16:256–60. https://doi.org/10.4314/thrb.v16i4.1
35. Laufer MK, Thesing PC, Eddington ND, Masonga R, Dzinjalamala FK, Takala SL, et al. Return of chloroquine antimalarial efficacy in Malawi. N Engl J Med. 2006;355:1959–66. https://doi.org/10.1056/NEJMoa062032
36. Dagnogo O, Ako AB, Ouattara L, Dago ND, Coulibaly DN, Touré AO, et al. Towards a re-emergence of chloroquine sensitivity in Côte d'Ivoire? Malar J. 2018;17:413. https://doi.org/10.1186/s12936-018-2551-7
37. Laufer MK, Takala-Harrison S, Dzinjalamala FK, Stine OC, Taylor TE, Plowe CV. Return of chloroquine-susceptible falciparum malaria in Malawi was a reexpansion of diverse susceptible parasites. J Infect Dis. 2010;202:801–8. https://doi.org/10.1086/655659
38. Mwanza S, Joshi S, Nambozi M, Chileshe J, Malunga P, Kabuya JB, et al. The return of chloroquine-susceptible *Plasmodium falciparum* malaria in Zambia. Malar J. 2016;15:584. https://doi.org/10.1186/s12936-016-1637-3
39. Ndam NT, Basco LK, Ngane VF, Ayouba A, Ngolle EM, Deloron P, et al. Reemergence of chloroquine-sensitive *pfcrt* K76 *Plasmodium falciparum* genotype in southeastern Cameroon. Malar J. 2017;16:130. https://doi.org/10.1186/s12936-017-1783-2
40. Amato R, Lim P, Miotto O, Amaratunga C, Dek D, Pearson RD, et al. Genetic markers associated with dihydroartemisinin-piperaquine failure in *Plasmodium falciparum* malaria in Cambodia: a genotype-phenotype association study. Lancet Infect Dis. 2017;17:164–73. https://doi.org/10.1016/S1473-3099(16)30409-1
41. Dhingra SK, Small-Saunders JL, Ménard D, Fidock DA. *Plasmodium falciparum* resistance to piperaquine driven by PfCRT. Lancet Infect Dis. 2019;19:1168–9. https://doi.org/10.1016/S1473-3099(19)30543-2
42. Ross LS, Dhingra SK, Mok S, Yeo T, Wicht KJ, Kümpornsin K, et al. Emerging Southeast Asian PfCRT mutations confer

Plasmodium falciparum resistance to the first-line antimalarial piperaquine. Nat Commun. 2018;9:3314. https://doi.org/10.1038/s41467-018-05652-0
43. Connelly SV, Brazeau NF, Msellem M, Ngasala BE, Aydemir O, Goel V, et al. Strong isolation by distance and evidence of population microstructure reflect ongoing *Plasmodium falciparum* transmission in Zanzibar. eLife. 2024;12:RP90173. https://doi.org/10.7554/eLife.90173
44. Ahouidi A, Oliveira R, Lobo L, Diedhiou C, Mboup S, Nogueira F. Prevalence of *pfk13* and *pfmdr1* polymorphisms in Bounkiling, southern Senegal. PLoS One. 2021; 16:e0249357. https://doi.org/10.1371/journal.pone.0249357
45. Veiga MI, Dhingra SK, Henrich PP, Straimer J, Gnädig N, Uhlemann AC, et al. Globally prevalent PfMDR1 mutations modulate *Plasmodium falciparum* susceptibility to artemisinin-based combination therapies. Nat Commun. 2016;7:11553. https://doi.org/10.1038/ncomms11553
46. Fançony C, Fortes-Gabriel E, Zage F, Alexiou E, Broumou I, Pernaute-Lau L, et al. Artemether-lumefantrine treatment selects *Plasmodium falciparum* multidrug resistance 1 (*pfmdr1*) increased copy number among African malaria infections. J Infect Dis. 2025;231:e1119–28. https://doi.org/10.1093/infdis/jiaf155
47. Sidhu AB, Uhlemann AC, Valderramos SG, Valderramos JC, Krishna S, Fidock DA. Decreasing *pfmdr1* copy number in *Plasmodium falciparum* malaria heightens susceptibility to mefloquine, lumefantrine, halofantrine, quinine, and artemisinin. J Infect Dis. 2006;194:528–35. https://doi.org/10.1086/507115
48. Tumwebaze PK, Conrad MD, Okitwi M, Orena S, Byaruhanga O, Katairo T, et al. Decreased susceptibility of *Plasmodium falciparum* to both dihydroartemisinin and lumefantrine in northern Uganda. Nat Commun. 2022;13:6353. https://doi.org/10.1038/s41467-022-33873-x
49. Bopp S, Magistrado P, Wong W, Schaffner SF, Mukherjee A, Lim P, et al. Plasmepsin II-III copy number accounts for bimodal piperaquine resistance among Cambodian *Plasmodium falciparum*. Nat Commun. 2018;9:1769. https://doi.org/10.1038/s41467-018-04104-z
50. Witkowski B, Duru V, Khim N, Ross LS, Saintpierre B, Beghain J, et al. A surrogate marker of piperaquine-resistant *Plasmodium falciparum* malaria: a phenotype-genotype association study. Lancet Infect Dis. 2017;17:174–83. https://doi.org/10.1016/S1473-3099(16)30415-7

Address for correspondence: Denis Niyomwungere, Institut National de Santé Publique, Avenue de l'Hôpital, BP 6807, Bujumbura, Burundi; email: dniyomwungere84@gmail.com; or Didier Menard, University of Strasbourg, Pathogens Host Arthropods Vectors Interactions Unit (UR 3073), 3 rue Koeberlé, 67000 Strasbourg, Grand Est, France; email: dmenard@unistra.fr

etymologia

Anopheles stephensi [ə-nah′ -fuhl-ēz ste′ -fen-zī]

Gaurav Kumar, Jaspreet Kaur

In 1901, George Michael James Giles, a lieutenant colonel and physician in the Indian Medical Service, described the *Anopheles stephensi* mosquito. He collected the mosquitoes from Ellichpur (currently Amravati district), India, and named the species in honor of John William Watson Stephens, a prominent British parasitologist who first described *Plasmodium ovale*, one of the human malaria parasites. Morphologically, *An. stephensi* mosquitoes can be identified by distinctive palpal ornamentation of equal apical and subapical pale bands and speckled appearance, pale and dark scales arranged along the veins of the wings, and dark and speckled pale bands on the hind tarsi.

An. stephensi (family Culicidae, subgenus *Cellia*) is an urban malaria vector responsible for ≈12% of malaria cases in India annually. After its detection in Africa in 2012, *An. stephensi* mosquitoes, if not controlled, are projected to put more than 126 million persons at risk for malaria.

Figure. Female *Anopheles stephensi* mosquito. Photograph by Jim Gathany, from the Centers for Disease Control and Prevention Public Health Image Library.

Acknowledgments
We are grateful to Anup Anvikar, director of ICMR-National Institute of Malaria Research, Delhi, for providing institutional support.

Sources
1. Liston WG. A year's experience of the habits of *Anopheles* in Ellichpur. The description of the species of *Anopheles* found in Ellichpur during the year. Indian Med Gaz. 1901;36:441–3.
2. Sharma VP. Current scenario of malaria in India. Parassitologia. 1999;41:349–53.
3. Sinka ME, Pironon S, Massey NC, Longbottom J, Hemingway J, Moyes CL, et al. A new malaria vector in Africa: predicting the expansion range of *Anopheles stephensi* and identifying the urban populations at risk. Proc Natl Acad Sci U S A. 2020;117:24900–8. https://doi.org/10.1073/pnas.2003976117
4. Subbarao SK, Vasantha K, Adak T, Sharma VP, Curtis CF. Egg-float ridge number in *Anopheles stephensi*: ecological variation and genetic analysis. Med Vet Entomol. 1987;1:265–71. https://doi.org/10.1111/j.1365-2915.1987.tb00353.x
5. Sweet WC, Rao BA. Races of *A. stephensi* Liston, 1901. Ind Med Gaz. 1937;72:665–74.

Authors affiliation: Indian Council of Medical Research National Institute of Malaria Research, Delhi, India
DOI: https://doi.org/10.3201/eid3204.241933
Address for correspondence: Jaspreet Kaur, ICMR-National Institute of Malaria Research, Sector-8, Dwarka, Delhi 110077, India; email: kaur.jaspreet0708@gmail.com

Accelerated Increase in *Candida auris* Bloodstream Infections during COVID-19 Pandemic, South Africa

Husna Ismail, Olga Perovic, Ruth Mpembe, Warren Lowman, Chetna Govind, Pieter Ekermans, Waasila Jassat, Richard Welch, Nelesh P. Govender

The COVID-19 pandemic coincided with rising secondary bloodstream infections (BSIs) from multidrug-resistant organisms, including *Candida auris*. To assess candidemia trends, we conducted a retrospective analysis of blood culture isolates from public and private laboratories in South Africa taken during January 2019–June 2022. We evaluated weekly aggregated *Candida* BSI counts and COVID-19 cases using segmented regression within an interrupted time-series framework. In total, 15,393 candidemia cases were identified, 70% from the private sector. *C. parapsilosis* accounted for 39% of cases, whereas *C. auris* represented 26%. The proportion of *C. auris* increased significantly from 17% in 2019 to 31% in 2021 ($p<0.01$). After the pandemic onset, *Candida* BSIs rose by 11 cases per week ($p = 0.03$), largely driven by *C. auris* (+5 cases/week; $p<0.01$); peaks coincided with COVID-19 waves. Those results highlight an accelerated shift toward *C. auris* in *Candida* BSIs and the urgent need for enhanced surveillance, diagnostics, and infection prevention.

The COVID-19 pandemic, caused by the novel respiratory virus SARS-CoV-2, created strains on the global healthcare system that were experienced mainly in the delivery of acute hospital services (*1*,*2*). Those challenges led to secondary healthcare-associated bloodstream infections (BSIs) caused by multidrug-resistant bacteria and fungi, partially related to increased background use of antimicrobial agents, steroids, and immunomodulatory agents (*3*–*5*). In addition, viral-induced immune-mediated damage by SARS-CoV-2 might have encouraged bacterial and fungal colonization (*6*).

Candida BSI is a growing concern worldwide. More than 90% of *Candida* BSIs are caused by 1 of 6 species: *C. albicans*, *Nakaseomyces glabratus* (previously *C. glabrata*), *C. tropicalis*, *C. parapsilosis*, *Pichia kudriavzevii* (previously *C. krusei*), and, increasingly, *C. auris (7)*. Those 6 species are also included in the World Health Organization Fungal Priority Pathogen List (*8*). In the EUROBACT-2 international cohort study, fungal pathogens accounted for ≈8% (230/2,927) of all healthcare-associated BSIs from 2,600 enrolled patients in 333 intensive care units in 52 countries during June 2019–January 2020 (*8*). *Candida* species were the most common fungi; 58% (133/230) were identified as non–*C. albicans Candida* species (*9*). *Candida* spp. was the third most common healthcare-associated BSI pathogen (≈12% [333/2,828]) in a prepandemic multicenter study from India (*10*).

The emergence of *C. auris* in South Africa was first recognized retrospectively from a BSI isolate collected in 2009, which was initially misidentified as *C. haemulonii* because of limitations in standard diagnostic methods (*11*). National surveillance during October 2012–November 2016 identified a total of 1,692 cases of confirmed or probable *C. auris* infections across South Africa; cases were concentrated in Gauteng Province, where 92% of cases were reported from private-sector hospitals (*11*). Nationally, the number of cases rose exponentially from 18 in the

Author affiliations: National Institute for Communicable Diseases, a Division of the National Health Laboratory Service, Johannesburg, South Africa (H. Ismail, O. Perovic, R. Mpembe, W. Jassat, R. Welch, N.P. Govender); University of the Witwatersrand, Johannesburg South Africa (R. Mpembe, W. Lowman, N.P. Govender); Vermaak and Partners/Pathcare Pathologists, Pretoria, South Africa (W. Lowman); Wits Donald Gordon Medical Centre, Johannesburg (W. Lowman); Lancet Laboratories, Durban, South Africa (C. Govind); Ampath Microbiology National Reference Laboratory, Centurion, South Africa (P. Ekermans)

DOI: https://doi.org/10.3201/eid3204.251407

baseline period (October 2012–November 2013) to 861 in the corresponding final period (October 2015–November 2016) (*11*). By 2016–2017, *C. auris* was the third most common cause of BSI nationally, surpassing most other non–*C. albicans* species (*12*). Molecular epidemiology revealed that isolates in South Africa predominantly belonged to the African clade III, which is genetically distinct and almost universally resistant to fluconazole; ≈6% had reduced susceptibility to amphotericin B (MIC ≥2 μg/mL) (13). Of note, 5% of isolates were resistant to both fluconazole and amphotericin B (*13*).

The COVID-19 pandemic coincided with a marked increase in *C. auris* outbreaks worldwide, particularly in intensive care settings (*14*). Several contributing factors were identified, including prolonged mechanical ventilation, widespread antimicrobial use, increased indwelling device exposure, and compromised infection prevention protocols (*14*). A systematic review (*14*) documented *C. auris* outbreaks in >10 countries, including India, Brazil, Mexico, Pakistan, the United States, and multiple countries in Europe; reported crude mortality rates among COVID-19 co-infected patients ranged from 30% to 72%. Evidence from Orange County, California, USA, further illustrated this trend (*15*); in long-term acute-care hospitals, the probability of new *C. auris* colonization during the first COVID-19 wave reached 22.5% (95% CI 18.5–26.6) within 30 days of admission. That increase coincided with widespread disruptions in infection prevention practices and shortages of protective equipment, and although incidence declined in later phases of the pandemic, the overall prevalence of colonization remained high (*15*). Schaefer et al. (*16*) reported that *C. auris* incidence at a major academic hospital in New York increased nearly 3-fold, from 2.6 cases/10,000 admissions in 2019 to 7.8 cases/10,000 admissions in 2022 (*16*). Similarly, national surveillance data from China revealed 1,846 laboratory-confirmed *C. auris* cases across 22 provinces; ≈80% of isolates were resistant to fluconazole and ≈7% were resistant to amphotericin B (*17*).

In this study, we aimed to evaluate the distribution of *Candida* species isolated from blood cultures from both private and public health sectors in South Africa and to describe changes during the COVID-19 pandemic. Permission to conduct this study was obtained from the South African Society of Clinical Microbiology and NHLS, and ethics approval was obtained from the Human Research Ethics Committee (Medical) of the University of the Witwatersrand (clearance no. M210752).

Materials and Methods

Study Design, Population, and Setting

We conducted a secondary analysis of blood culture data archived in pathology laboratory information systems from January 1, 2019, through June 30, 2022, in South Africa. The study population consisted of all patients who had a blood culture submitted either to the National Health Laboratory Service (NHLS) or to 1 of 3 large amalgamated private pathology practices (Ampath [https://www.ampath.co.za], Lancet Laboratories [https://www.lancet.co.za], or PathCare/Vermaak and Partners [https://www.vpath.co.za]). The NHLS provides routine diagnostic pathology services to the public health sector, serving ≈83% of the population of South Africa, and has 60 laboratories that offer microbiology testing, including automated blood culture systems and culture identification (*11*). The 3 large private pathology groups provide a full range of microbiology testing for almost all inpatients in South Africa with private health insurance (*11*). The NHLS used several platforms to identify *Candida* to species level at the time of this study: Vitek 2 YST, API 20C Aux, or API ID 32C (bioMérieux, https://www.biomerieux.com); Auxacolor (Bio-Rad Laboratories, https://www.bio-rad.com); and Microscan (Beckman Coulter, https://www.beckmancoulter.com) (*11*). The private pathology groups identified *Candida* primarily using matrix-assisted laser desorption/ionization time-of-flight mass spectrometry methods (Bruker, https://www.bruker.com; or bioMérieux). The total number of blood culture specimens collected during the study period was not available as a denominator. The private health sector represents a small proportion of the general population, and laboratory data from this sector might not be directly comparable with the public sector owing to factors such as specimen-taking practices (*18*). We included patients with blood cultures positive with any of the 6 most common *Candida* species (*C. albicans*, *C. auris*, *N. glabratus*, *P. kudriavzevii*, *C. parapsilosis*, and *C. tropicalis*) in this analysis. Blood culture data from NHLS were obtained from the surveillance data warehouse at the National Institute for Communicable Diseases (NICD) (*19*). Blood culture data from the private sector were obtained through the South African Society of Clinical Microbiology, which has formed a public–private partnership with the NICD (*19*).

Definitions

We defined a case of *Candida* BSI was defined as illness in a person seen at a healthcare facility in South Africa who had a blood culture from which *C. albicans*, *C. auris*, *N. glabratus*, *P. kudriavzevii*, *C. parapsilosis*,

or *C. tropicalis* was isolated. We regarded positive blood cultures with the same organism that had been collected within 30 days of a first positive blood culture as duplicates and excluded them.

DATCOV and SARS-CoV-2

We extracted COVID-19 hospital admission data from March 5, 2020, through June 30, 2022, from the inpatient national surveillance system, DATCOV. Established in April 2020 by the NICD, DATCOV served as an active surveillance program for COVID-19 hospital admissions for both public and private hospitals in South Africa (*1*). We extracted routine surveillance data for SARS-CoV-2 infections from the reengineered Notifiable Medical Conditions Surveillance System for the period March 1, 2020, through June 30, 2022. In July 2020, the NICD established the Notifiable Medical Conditions Surveillance System, which contains data for all SARS-CoV-2 tests (PCR or antigen detection) conducted in South Africa (*20*). January 2019–February 2020 was considered the prepandemic baseline, and March 2020–June 2022 was the COVID-19 pandemic period.

Data Management and Analysis

We reported categorical variables for blood culture data in tables as frequencies and percentages or presented them as bar charts and tables. We used the Pearson χ^2 test or Fisher exact test to compare *Candida* species distribution among years, sectors, and provinces. We performed all analyses using Stata version 15 (StataCorp LLC, https://www.stata.com) or R Studio version 4.5.1 (https://rstudio.com/products/rstudio). We prepared and tabulated blood culture, DATCOV, and SARS-CoV-2 datasets in Microsoft Excel (https://www.microsoft.com). We used those tabulated datasets to plot graphs and apply 30-day moving averages for cases of *C. auris* and *C. parapsilosis* BSI. We conducted interrupted time series analysis to assess the effects of the COVID-19 pandemic on the incidence of *Candida* BSI, with a specific focus on *C. auris*. We defined the intervention point as the onset of the COVID-19 pandemic in South Africa (i.e., March 2020). We aggregated *Candida* BSI and COVID-19 case counts by week and scaled COVID-19 count data to enable visual comparison. We then plotted weekly counts to examine trends before and after the interruption. We used segmented regression to estimate changes in the level and slope of *Candida* BSI incidence associated with the pandemic. We annotated national lockdown levels 1–5 in increasing order of restrictiveness. We used interrupted time series models to evaluate both immediate and gradual changes in weekly *Candida* BSI rates.

Results

Distribution of Cases of *Candida* BSI

Over the 42-month period, 15,393 cases of *Candida* BSI were reported: 3,415 cases in 2019, 4,229 cases in 2020, 5,315 cases in 2021 and 2,434 cases during January–June 2022. The private sector accounted for 70% (10,826/15,393) of all cases. Cases of *Candida* BSI increased across the country, from 4,048 during the 14-month baseline period (January 2019–February 2020) to 5,413 in the first 14 months of the pandemic (March 2020–April 2021), a 34% rise; cases then increased to 5,932 in the following 14-month period (May 2021–June 2022), a further 10% increase (Figure 1). Cases in Gauteng Province accounted for 50% (7,706/15,393) of all *Candida* BSI cases, followed by KwaZulu-Natal Province (14% [2,163/15,393]) and the Western Cape Province (12% [1,809/15,393]). Similar distribution patterns were observed for

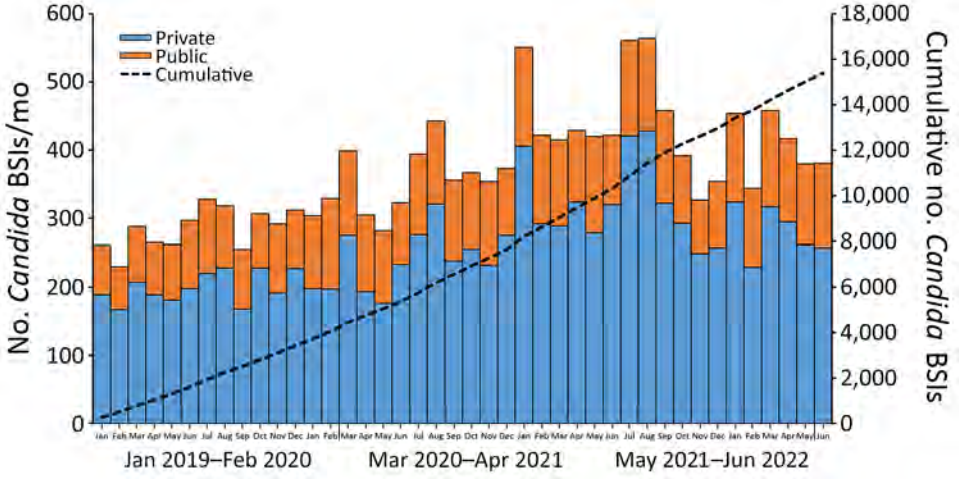

Figure 1. Total number of cases of *Candida* BSI by health sector in study of accelerated increase in *C. auris* BSIs during COVID-19 pandemic, by month and cumulative, South Africa, January 2019–June 2022. Blue bars represent cases in the private sector (n = 10,826), orange bars represent cases in the public sector (n = 4,567), and black dashed line represents the cumulative number of *Candida* BSI cases in South Africa. Scales for the y-axes differ substantially to underscore patterns but do not permit direct comparisons. BSI, bloodstream infection.

Table. Distribution of 6 *Candida* species isolated from bloodstream infection by health sector in study of accelerated increase in *Candida auris* bloodstream infections during COVID-19 pandemic, South Africa, January 2019–June 2022

Category	*Candida* species	No. (%)					p value
		2019	2020	2021	2022	Total	
National	*Candida albicans*	793 (23)	959 (23)	1,200 (23)	597 (25)	3,549 (23)	0.26
	Candida auris	597 (17)	1,012 (24)	1,626 (31)	693 (28)	3,928 (26)	<0.01
	*Nakaseomyces glabratus**	332 (10)	339 (8)	359 (7)	209 (9)	1,239 (8)	<0.01
	Pichia kudriavzevii†	63 (2)	93 (2)	73 (1)	31 (1)	260 (2)	0.01
	Candida parapsilosis	1,555 (46)	1,734 (41)	1,955 (37)	836 (34)	6,080 (39)	<0.01
	Candida tropicalis	75 (2)	92 (2)	102 (2)	68 (3)	337 (2)	0.11
	Total	3,415 (100)	4,229 (100)	5,315 (100)	2,434 (100)	15,393 (100)	
Private	*C. albicans*	364 (15)	431 (15)	605 (16)	266 (16)	1,666 (15)	0.88
	C. auris	580 (24)	863 (30)	1,439 (37)	625 (37)	3,507 (32)	<0.01
	N. glabratus	172 (7)	163 (6)	190 (5)	127 (8)	652 (6)	0.01
	P. kudriavzevii	22 (1)	51 (2)	39 (1)	6 (0.4)	118 (1)	0.01
	C. parapsilosis	1,217 (51)	1,329 (46)	1,567 (40)	629 (37)	4,742 (44)	<0.01
	C. tropicalis	38 (2)	32 (1)	40 (1)	31 (2)	141 (1)	0.04
	Total	2,393 (100)	2,869 (100)	3,880 (100)	1,684 (100)	10,826 (100)	
Public	*C. albicans*	429 (42)	528 (39)	595 (41)	331 (44)	1,883 (41)	0.11
	C. auris	17 (2)	149 (11)	187 (13)	68 (9)	421 (9)	<0.01
	N. glabratus	160 (16)	176 (13)	169 (12)	82 (11)	587 (13)	0.01
	P. kudriavzevii	41 (4)	42 (3)	34 (2)	25 (3)	142 (3)	0.14
	C. parapsilosis	338 (33)	405 (30)	388 (27)	207 (28)	1,338 (29)	0.01
	C. tropicalis	37 (4)	60 (4)	62 (4)	37 (5)	196 (4)	0.59
	Total	1,022 (100)	1,360 (100)	1,435 (100)	750 (100)	4,567 (100)	

*Previously *Candida glabrata*.
†Previously *Candida krusei*.

those provinces in both private and public sectors (Appendix Table).

C. parapsilosis accounted for 39% (6,080/15,393) of all *Candida* BSI cases in South Africa, followed by *C. auris* (26% [3,928/15,393]). Nationally, there were notable differences in the distribution of *Candida* species. The relative frequencies of cases of *C. auris* BSI increased from 17% (597/3,415) in 2019 to 31% (1,626/5,315) in 2021 (p<0.01); a corresponding decrease was noted in the percentage of *C. parapsilosis*, from 46% (1,555/3,415) in 2019 to 37% (1,955/5,315) in 2021 (p<0.01), as well as a percentage decrease for *N. glabratus* from 10% (332/3,415) in 2019 to 7% (359/5,315) in 2021 (p<0.01). The relative frequencies of *C. albicans, P. kudriavzevii*, and *C. tropicalis* were relatively unchanged (Table). *C. parapsilosis* was the most common species in 8 of the 9 provinces in South Africa. *C. auris* was the dominant species in the North West Province and accounted for 42% (312/749) of cases (Appendix Figure). In the private sector, *C. parapsilosis* was the dominant species, accounting for 44% (4,742/10,826) of cases, followed by *C. auris,* which accounted for 32% (3,507/10,826) of cases. We observed a more marked increase in the percentage of cases of *C. auris* BSI in the private sector, from 24% (580/2,393) in 2019 to 37% (1,439/3,880) in 2021 (p<0.01); we observed a corresponding decrease in the percentage of *C. parapsilosis*, from 51% (1,217/2,393) in 2019 to 40% (1,567/3,880) in 2021, with a further decrease to 37% (629/1,684) in 2022 (p<0.01). In the public sector, *C. albicans* was the dominant species, accounting for 41% (1,883/4,567) of cases, followed by *C. parapsilosis*, which accounted for 29% (1,338/4,567) of cases. Similar to the private sector, the percentage of cases of *C. auris* BSI in the public sector increased substantially, from 2% (17/1,022) in 2019 to 13% (187/1,435) in 2021 (p<0.01); we noted a corresponding decrease in the percentage of *C. parapsilosis*, from 33% (338/1,022) in 2019 to 27% (388/1,435) in 2021 (p<0.01), as well as a decrease in *N. glabratus* BSIs, from 16% (160/1,022) in 2019 to 12% (169/1,435) in 2021 (p = 0.01) (Table).

Of the 15,393 total cases, 54% (8,333) of patients were male and 46% (7,060) female. The highest number of cases of *Candida* BSI were seen in persons <1 year of age (17% [2,561]), 51–60 years of age (16% [2,480]) and 61–70 years of age (15% [2,348]). When stratified by health sector, 38% (1,745/4,567) of cases in the public sector were in persons <1 year of age, whereas 40% (4,316/10,826) of cases from the private sector were in persons 51–70 years of age (Figure 2, panels A, B). With the exception of 2 age categories (21–30 years of age and 51–60 years of age) in the private sector, we observed distinct differences among the other age categories across all 4 years. We observed that 74% (201/273) of persons <1 year of age with a *C. auris* BSI were from the public sector. In contrast, almost all *C. auris* BSI cases in persons 51–60 years of age (98% [821/834]) and in persons 61–70 years of age (99% [769/775]) were reported from the private sector (Figure 2, panels C, D).

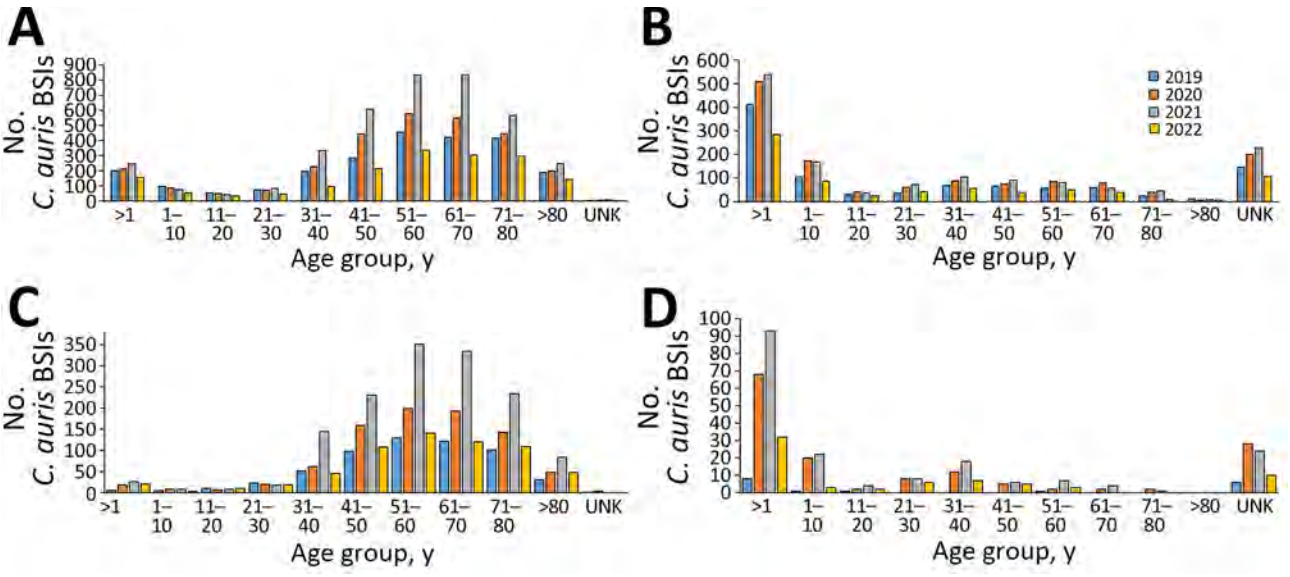

Figure 2. Cases of BSI by type in study of accelerated increase in *Candida auris* BSIs during COVID-19 pandemic, by year and age group, South Africa, January 2019–June 2022. A, B) Total number of cases of *Candida* BSI in private sector (A; n = 10,826) and public sector (B; n = 4,567) (N = 15,393). C, D) Total number of cases of *C. auris* BSI in private sector (C; n = 3,507) and public sector (D; n = 421). BSI, bloodstream infection; UNK, unknown.

Distribution of Cases of *Candida* BSI before and during the COVID-19 Pandemic

The first laboratory-confirmed case of SARS-CoV-2 infection was documented in South Africa on March 5, 2020. During the study period, 3,995,881 cases of COVID-19 were reported; 486,789 of those resulted in hospital admission. More than half of COVID-19 hospital admissions (52% [254,975/486,789]) occurred in the public sector.

During the pandemic period (March 2020–June 2022), the number of COVID-19 cases and admissions increased together; the admission peak lagged behind the case peak for each major COVID-19 wave. We observed a temporally related increase in the 30-day moving average of *Candida* BSI cases after each of the 4 waves caused by the ancestral SARS-CoV-2 and 3 variants, Beta, Delta, and Omicron BA.1, in South Africa during the study period. The monthly average number of *Candida* BSI cases was 419 in August 2020, 487 in February 2021, 563 in August 2021, and 438 in April 2022. We also observed fluctuations of the 30-day moving average in *Candida* BSI in the prepandemic period. In the public sector, an increase in the *Candida* BSI 30-day moving average was only noted after the second COVID-19 wave, caused by the Beta variant; a monthly average of 138 cases was reported in February 2021 (Figure 3).

Using *C. parapsilosis* (the most common species in the private sector and second most common species in the public sector) as a comparator, we found that, as the COVID-19 pandemic progressed from March 2020 to June 2022, the average number of cases of *C. auris* BSI increased to the point where *C. parapsilosis* and *C. auris* had similar 30-day moving averages. That phenomenon occurred in both the private and public health sectors, although in the private sector, by the end of the study period, *C. auris* increased from an average of 2 cases/day in February 2019 to 3 cases/day in June 2022 (Figure 4).

Interrupted Time Series Analysis

Before the COVID-19 pandemic (January 2019–February 2020), the weekly trend in *Candida* BSI was gradually increasing, and the slope before the pandemic was significantly positive (cases increasing by 0.038/week before March 2020; p = 0.02). The onset of the pandemic in March 2020 was associated with a significant increase in *Candida* BSI cases (immediate jump of 11 cases/week; p = 0.03). However, the postintervention slope for *Candida* BSIs did not differ significantly from the prepandemic slope (cases decreasing by 0.023/week; p = 0.20). Peaks in *Candida* BSI were temporally aligned with each of the 4 major COVID-19 waves in South Africa (Figure 5). *C. auris* alone showed a different pattern. Before the COVID-19 pandemic, cases of *C. auris* were increasing, but not significantly (cases increasing by 0.010/week before March 2020; p = 0.37). After the pandemic began, *C. auris* exhibited a sharp immediate increase (*C. auris* cases jumped by 5/week; p<0.01) and continued to increase after March 2020 (cases increasing by 0.032/week; p<0.01) (Figure 6).

Discussion

After the pandemic, *C. auris* cases of candidemia immediately increased sharply and continued to increase. One quarter of all cases of BSI in South Africa were caused by *C. auris*; more cases of *C. auris* infection in infants were diagnosed in the public sector, and more cases in older age groups were diagnosed in the private sector.

We observed a substantial increase in cases of *Candida* BSI after the peak of COVID-19 hospital admissions. Overall, this trend was similar across all 4 COVID-19 waves and most pronounced for the Delta wave in the Southern Hemisphere in winter of 2021. Fungal infections are a substantial concern in managing patients infected with SARS-CoV-2 (*21*). Our study showed that the number of cases of *C. auris* increased and were similar in monthly averages to cases of *C. parapsilosis*, particularly in the private sector. *C. parapsilosis* and *C. auris* are both species known to cause invasive infections because of their ability to contaminate the hospital environment, form biofilms on medical devices, colonize the hands of healthcare

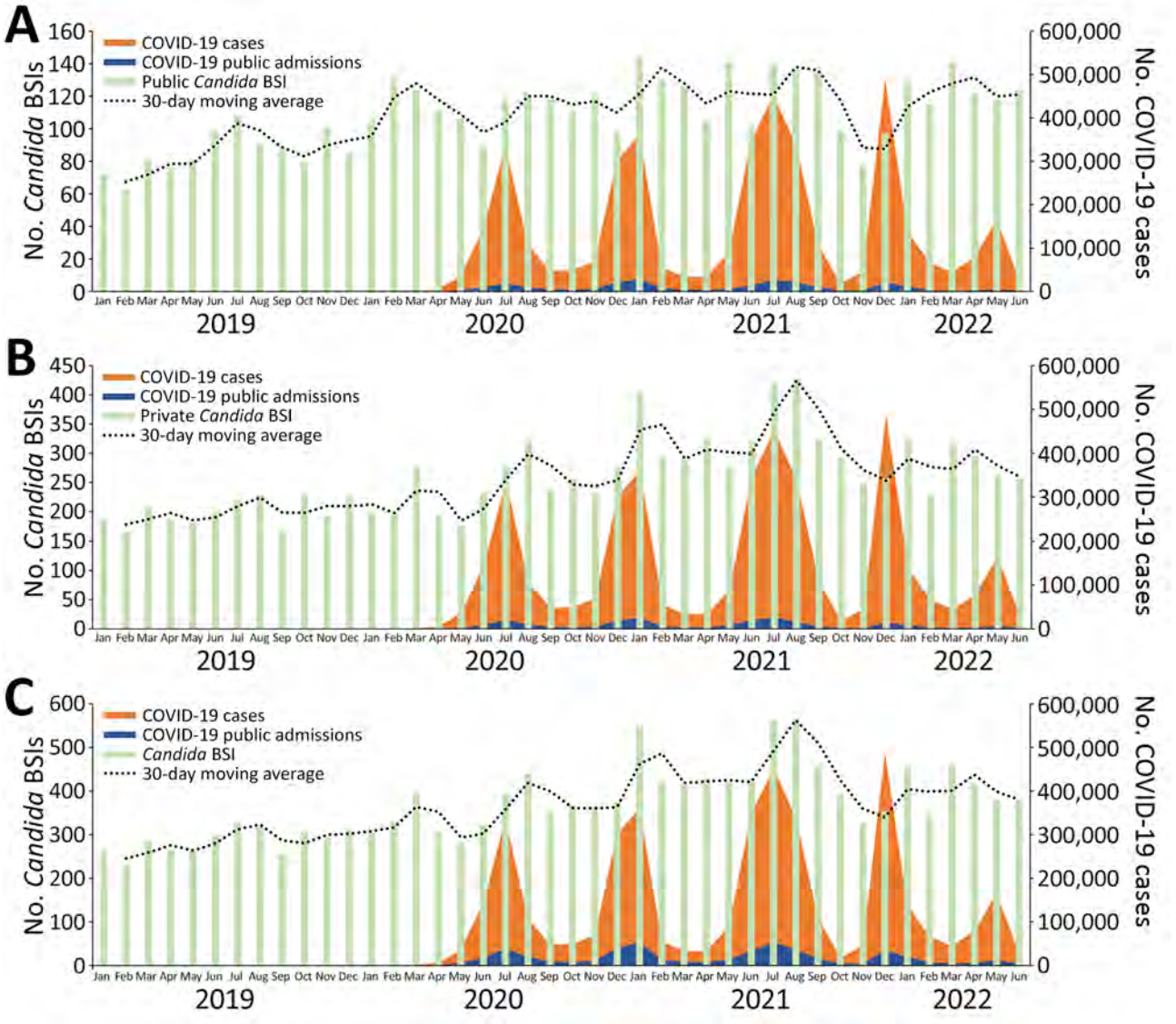

Figure 3. Total number of cases of *Candida* BSIs (n = 15,393), COVID-19 cases (n = 3,995,881), and COVID-19 hospital admissions (n = 486,789), by month and 30-day moving average, in study of accelerated increase in *C. auris* BSIs during COVID-19 pandemic, South Africa, January 2019–June 2022. Numbers are shown for public health sector (A), private health sector (B), and total national (C). Light green bars represent cases of *Candida* BSI (private, n = 10,826; public, n = 4,567), orange bars represent COVID-19 cases, blue bars represent COVID-19 hospital admissions (private, n = 231,814; public, n = 254,975), and black dotted line represents the 30-day moving average number cases. Scales for the y-axes differ substantially to underscore patterns but do not permit direct comparisons. BSI, bloodstream infection.

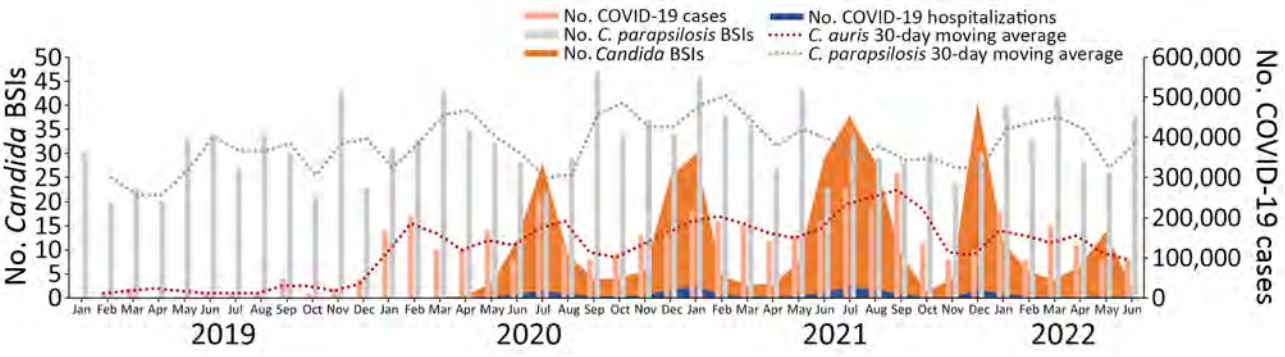

Figure 4. Numbers of *Candida auris* and *C. parapsilosis* BSIs, COVID-19 cases, and COVID-19 hospital admissions, by month, in study of accelerated increase in *C. auris* BSIs during COVID-19 pandemic, South Africa, January 2019–June 2022. Light red bars represent cases of *C. auris* BSI (private n = 3,507; public n = 421), light gray bars represent cases of *C. parapsilosis* BSI (private n = 4,742; public n = 1,338), orange shading represents total number of COVID-19 cases (N = 3,995,881), blue shading represents number of COVID-19 hospital admissions (private n = 231,814; public n = 254,975), dark red dotted line represents 30-day moving average for *C. auris*, and dark gray dotted line represents 30-day moving average for *C. parapsilosis*. BSI, bloodstream infection.

workers, and contribute to healthcare-associated outbreaks (*14*,*21*). Outbreaks are more likely to occur when hospital services are strained, as occurred during the height of the pandemic.

Although *C. albicans* is a common colonizer of the skin and mucous membrane, a virulent species, and causes a high proportion of invasive infections, non–*C. albicans Candida* species have greater antifungal drug resistance (*22*,*23*). In South Africa, the species causing infection might be used as a proxy for azole resistance, particularly for *C. auris*, *N. glabratus*, *P. kudriavzevii*, and *C. parapsilosis*. For instance, *C. albicans* isolated from patients with BSI have the lowest incidence of azole resistance, whereas *N. glabratus* has decreased susceptibility across the azole class (*24*). On the basis of national laboratory-based *Candida* BSI surveillance data in South Africa from 2009–2010, almost 25% of isolates were resistant to fluconazole and 10% were resistant to voriconazole (*25*). At a tertiary care hospital in Johannesburg during 2016–2020, a total of 47% (201/426) of non–*C. albicans Candida* isolates were azole-resistant and 0.9% (4/491) were resistant to amphotericin B (*26*).

Overall, we demonstrated a change in the distribution of BSI *Candida* species isolated during 2019–2022; *C. auris* was the second most common species. An earlier national survey conducted during 2016–2017 found that *C. parapsilosis* was the most

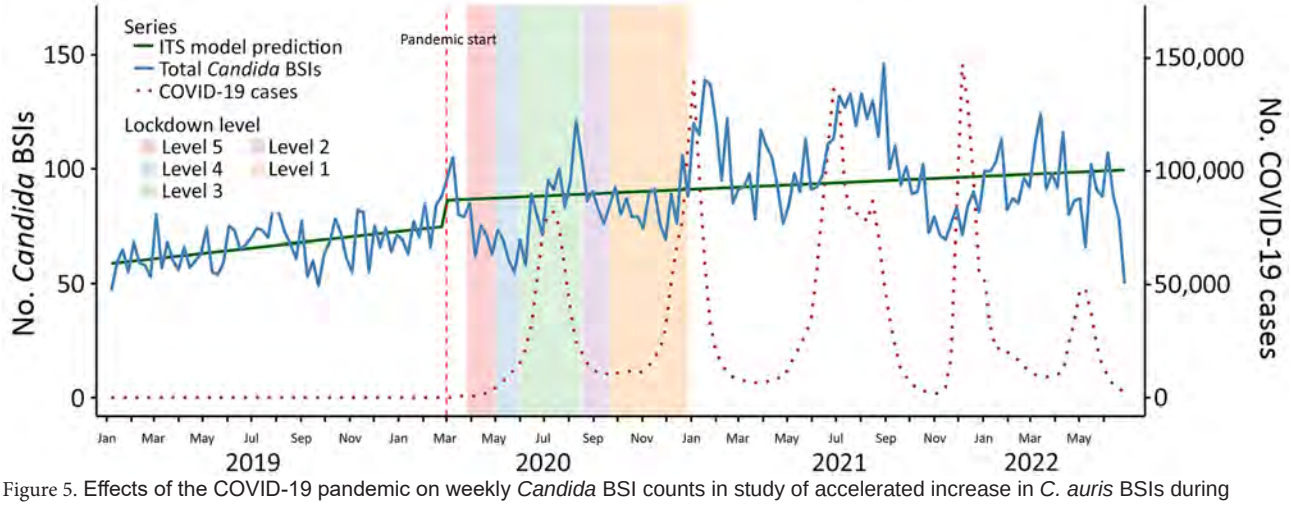

Figure 5. Effects of the COVID-19 pandemic on weekly *Candida* BSI counts in study of accelerated increase in *C. auris* BSIs during COVID-19 pandemic, South Africa, January 2019–June 2022. Vertical dashed red line marks the onset of the COVID-19 pandemic in South Africa (March 5, 2020). Solid green line represents the ITS model prediction for *Candida* BSIs; solid blue line indicates the actual number of *Candida* BSIs. Weekly COVID-19 case counts are scaled (dotted red line) and overlaid for comparison. Background shading indicates timing and duration of national lockdown alert levels: level 5, March 27–April 30, 2020; level 4, May 1–May 31, 2020; level 3, June 1–August 17, 2020; level 2, August 18–September 20, 2020; level 1, September 21–December 28, 2020. BSI, bloodstream infection; ITS, interrupted time series.

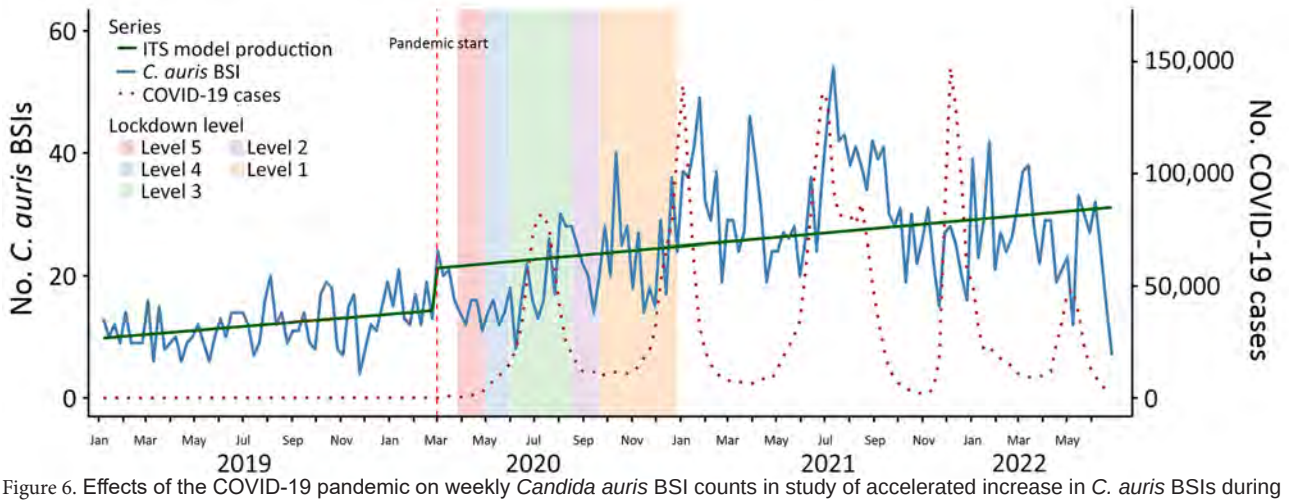

Figure 6. Effects of the COVID-19 pandemic on weekly *Candida auris* BSI counts in study of accelerated increase in *C. auris* BSIs during COVID-19 pandemic, South Africa, January 2019–June 2022. Vertical dashed red line marks the onset of the COVID-19 pandemic in South Africa (March 5, 2020). Solid green line represents ITS model prediction for *C. auris* BSIs; solid blue line indicates the actual number of *C. auris* BSIs. Weekly COVID-19 case counts are scaled (dotted red line) and overlaid for comparison. Background shading indicates timing and duration of national lockdown alert levels: level 5, March 27–April 30, 2020; level 4, May 1–May 31, 2020; level 3, June 1–August 17, 2020; level 2, August 18–September 20, 2020; level 1, September 21–December 28, 2020. BSI, bloodstream infection; ITS, interrupted time series.

common species causing BSI and accounted for 44% (2,600/5,876) of cases, followed by *C. albicans* (23% [1,353/5,876]) and *C. auris* (14% [794/5,876]) (*27*).

Fifty percent of *Candida* BSI cases reported in our study were from the Gauteng Province, the most densely populated region of South Africa and the region with the most healthcare facilities and hospital beds (*25*,*28*). That province accounted for almost one third of *C. auris* cases. We found that *C. auris* caused more than one third of *Candida* BSI cases from the North West province. The Eastern Cape, KwaZulu-Natal, Limpopo, and Mpumalanga Provinces each accounted for >20% of *C. auris* cases in South Africa.

The observed changes in *C. auris* case numbers during the study period might have been caused by the patterns of COVID-19 through the pandemic waves (*29*). Alternatively, *C. auris* has spread out of Gauteng Province to cause outbreaks in multiple new facilities. Of concern, the incidence of *C. auris* in Northern Cape Province might be underestimated in the public sector. That finding might reflect differences in the extent of laboratory investigation of BSI between the public and private sectors in the Northern Cape Province.

The first limitation of our study is that overall, more than two thirds of all cases of *Candida* BSI were reported from the private sector in South Africa and half were reported from the Gauteng Province. Fewer cases of *Candida* BSI were reported from the public sector. Because we excluded *Candida* species other than the 6 most common species, we might have undercounted cases in the public sector because some laboratories either did not identify *Candida* to species level or misclassified the common *Candida* species as rarer species (*22*). Not all the data from the private laboratories were included in this study, and therefore these data do not necessarily represent the overall epidemiology of *Candida* BSI in the private sector. The prevalence and incidence of *Candida* BSI in South Africa could not be determined because denominator data were not available. Furthermore, we could not determine whether any cases were co-infections with *Candida* and SARS-CoV-2.

In conclusion, we identified changes in the distribution of *Candida* species in both the private and public heath sectors and in different provinces in South Africa during 2019–2021, particularly for *C. auris*. From 2017 to 2019, *C. auris* increased from 14% to 17%. However, large percentage increases occurred during the COVID-19 pandemic in 2020 (24%), 2021 (31%), and 2022 (28%). Taken together with temporal increases after each wave, our findings suggest that the COVID-19 pandemic might have driven the major increase in *C. auris* and thus accelerated the epidemiologic shift of *C. auris* in South Africa.

Acknowledgments

We thank the team from the Surveillance Information Management Unit at the National Institute for Communicable Diseases for making National Health Laboratory Service data available and the South African Society of Clinical Microbiology editorial committee for comments and suggestions. In addition, we thank

Andronica Moipone Shonhiwa, Genevie Ntshoe, Joy Ebonwu, Lactatia Motsuku, Liliwe Shuping, Mazvita Muchengeti, Jackie Kleynhans, Gillian Hunt, Victor Odhiambo Olago, Husna Ismail, Nevashan Govender, Ann Mathews, Vivien Essel, Veerle Msimang, Tendesayi Kufa-Chakezha, Nkengafac Villyen Motaze, Natalie Mayet, Tebogo Mmaborwa Matjokotja, Mzimasi Neti, Tracy Arendse, Teresa Lamola, Itumeleng Matiea, Darren Muganhiri, Babongile Ndlovu, Khuliso Ravhuhali, Emelda Ramutshila, Salaminah Mhlanga, Akhona Mzoneli, Nimesh Naran, Trisha Whitbread, Mpho Moeti, Chidozie Iwu, Eva Mathatha, Fhatuwani Gavhi, Masingita Makamu, Matimba Makhubele, Simbulele Mdleleni, Bracha Chiger, Jackie Kleynhans, and the information technology team, Tsumbedzo Mukange, Trevor Bell, Lincoln Darwin, Fazil McKenna, Ndivhuwo Munava, Muzammil Raza Bano, Themba Ngobeni, Vusumzi Tshetu, and Gloseijie Bazolana, for making the COVID-19 data available. We also thank Lucille Blumberg, Maureen Masha, Caroline Vika, Caroline Mudara, Tracy Arendse, Lovelyn Ozougwu, and Rebone Kai for making the DATCOV data available.

This study was supported by the National Institute for Communicable Diseases. N.P.G. was supported by the National Institute for Health and Care Research (NIHR) (grant nos. NIHR134342 and NIHR303140) with UK international development funding from the UK government to support global health research. The views expressed in this article are those of the authors and not necessarily those of the NIHR or the UK government.

All authors contributed significantly to this paper. H.I. contributed to conceptualization, methodology, data cleaning, data analysis, writing, review, and editing. O.P. and R.M. contributed writing, review, and editing. W.L., C.G., P.E., W.J., and R.W. performed data curation, writing, review, and editing. N.P.G. contributed to conceptualization, methodology, data cleaning, data analysis, writing, review, editing, and supervision of the study.

About the Author

Dr. Ismail is a PhD medical scientist and trained field epidemiologist at the National Institute for Communicable Diseases. Her primary research interests are public health research and disease surveillance.

References

1. Jassat W, Cohen C, Tempia S, Masha M, Goldstein S, Kufa T, et al.; DATCOV author group. Risk factors for COVID-19-related in-hospital mortality in a high HIV and tuberculosis prevalence setting in South Africa: a cohort study. Lancet HIV. 2021;8:e554–67. https://doi.org/10.1016/S2352-3018(21)00151-X
2. Edoka I, Fraser H, Jamieson L, Meyer-Rath G, Mdewa W. Inpatient care costs of COVID-19 in South Africa's public healthcare system. Int J Health Policy Manag. 2022;11:1354–61. https://doi.org/10.34172/ijhpm.2021.24
3. Gomez-Simmonds A, Annavajhala MK, McConville TH, Dietz DE, Shoucri SM, Laracy JC, et al. Carbapenemase-producing Enterobacterales causing secondary infections during the COVID-19 crisis at a New York City hospital. J Antimicrob Chemother. 2021;76:380–4. https://doi.org/10.1093/jac/dkaa466
4. Nori P, Cowman K, Chen V, Bartash R, Szymczak W, Madaline T, et al. Bacterial and fungal coinfections in COVID-19 patients hospitalized during the New York City pandemic surge. Infect Control Hosp Epidemiol. 2021;42:84–8. https://doi.org/10.1017/ice.2020.368
5. Machado M, Estévez A, Sánchez-Carrillo C, Guinea J, Escribano P, Alonso R, et al. Incidence of candidemia Is higher in COVID-19 versus non-COVID-19 patients, but not driven by intrahospital transmission. J Fungi (Basel). 2022;8:305. https://doi.org/10.3390/jof8030305
6. Shafran N, Shafran I, Ben-Zvi H, Sofer S, Sheena L, Krause I, et al. Secondary bacterial infection in COVID-19 patients is a stronger predictor for death compared to influenza patients. Sci Rep. 2021;11:12703. https://doi.org/10.1038/s41598-021-92220-0
7. Reda NM, Hassan RM, Salem ST, Yousef RHA. Prevalence and species distribution of *Candida* bloodstream infection in children and adults in two teaching university hospitals in Egypt: first report of *Candida kefyr*. Infection. 2023;51:389–95. https://doi.org/10.1007/s15010-022-01888-7
8. World Health Organization. WHO fungal priority pathogens list to guide research, development and public health action [cited 2025 Dec 8]. https://www.who.int/publications/i/item/9789240060241
9. Tabah A, Buetti N, Staiquly Q, Ruckly S, Akova M, Aslan AT, et al.; EUROBACT-2 Study Group, ESICM, ESCMID ESGCIP and the OUTCOMEREA Network. Epidemiology and outcomes of hospital-acquired bloodstream infections in intensive care unit patients: the EUROBACT-2 international cohort study. Intensive Care Med. 2023;49:178–90. https://doi.org/10.1007/s00134-022-06944-2
10. Mathur P, Malpiedi P, Walia K, Srikantiah P, Gupta S, Lohiya A, et al.; Indian Healthcare Associated Infection Surveillance Network collaborators. Health-care-associated bloodstream and urinary tract infections in a network of hospitals in India: a multicentre, hospital-based, prospective surveillance study. Lancet Glob Health. 2022;10:e1317–25. https://doi.org/10.1016/S2214-109X(22)00274-1
11. Govender NP, Magobo RE, Mpembe R, Mhlanga M, Matlapeng P, Corcoran C, et al. *Candida auris* in South Africa, 2012–2016. Emerg Infect Dis. 2018;24:2036–40. https://doi.org/10.3201/eid2411.180368
12. Naicker SD, Maphanga TG, Chow NA, Allam M, Kwenda S, Ismail A, et al. Clade distribution of *Candida auris* in South Africa using whole genome sequencing of clinical and environmental isolates. Emerg Microbes Infect. 2021;10:1300–8. https://doi.org/10.1080/22221751.2021.1944323
13. Maphanga TG, Mpembe RS, Naicker SD, Govender NP; for GERMS-SA. In vitro antifungal activity of manogepix and other antifungal agents against South African *Candida auris* isolates from bloodstream infections. Microbiol Spectr. 2022;10:e0171721. https://doi.org/10.1128/spectrum.01717-21
14. Najeeb H, Siddiqui SA, Anas Z, Ali SH, Usmani SUR, Jawed F, et al. The menace of *Candida auris* epidemic amidst

the COVID-19 pandemic: a systematic review. Diseases. 2022;10:58. https://doi.org/10.3390/diseases10030058
15. Dratch AH, Le M, Zahn M. Increased incidence of *Candida auris* colonization in early COVID-19 pandemic, Orange County, California, USA. Emerg Infect Dis. 2025;31:1747–54. https://doi.org/10.3201/eid3109.241342
16. Schaefer S, Walits E, Thaler K, Patel G. Impact of the COVID-19 pandemic on *Candida auris* infections: a retrospective analysis in an academic medical center in New York City. Open Forum Infect Dis. 2024;11:ofae148. https://doi.org/10.1093/ofid/ofae148
17. Bing J, Huang Y, Du H, Guo P, Cao J, Kang M, et al. Rapid spread of *Candida auris* in China after COVID-19. J Infect. 2025;90:106476. https://doi.org/10.1016/j.jinf.2025.106476
18. Ismail H, Lowman W, Bch MB, Path FC, Microbiol SA, Microbiol M, et al. Surveillance and comparison of antimicrobial susceptibility patterns of ESKAPE organisms isolated from patients with bacteraemia in South Africa, 2016–2017. S Afr Med J. 2019;109:934–40.
19. National Department of Health. Surveillance for antimicrobial resistance and consumption of antimicrobials in South Africa, 2021 [cited 2025 Sep 8]. https://knowledgehub.health.gov.za/system/files/elibdownloads/2023-04/AMR%2520and%2520AMC%2520report%2520for%25202021%2520in%2520South%2520African_June2022.pdf
20. Pulliam JRC, van Schalkwyk C, Govender N, von Gottberg A, Cohen C, Groome MJ, et al. Increased risk of SARS-CoV-2 reinfection associated with emergence of Omicron in South Africa. Science. 2022;376:eabn4947. https://doi.org/10.1126/science.abn4947
21. Ramos-Martínez A, Pintos-Pascual I, Guinea J, Gutiérrez-Villanueva A, Gutiérrez-Abreu E, Díaz-García J, et al. Impact of the COVID-19 pandemic on the clinical profile of candidemia and the incidence of fungemia due to fluconazole-resistant *Candida parapsilosis*. J Fungi (Basel). 2022;8:1–12. https://doi.org/10.3390/jof8050451
22. Lockhart SR, Jackson BR, Vallabhaneni S, Ostrosky-Zeichner L, Pappas PG, Chiller T. Thinking beyond the common *Candida* species: need for species-level identification of *Candida* due to the emergence of multidrug-resistant *Candida auris*. J Clin Microbiol. 2017;55:3324–7. https://doi.org/10.1128/JCM.01355-17
23. Mroczyńska M, Brillowska-Dąbrowska A. Virulence of clinical *Candida* isolates. Pathogens. 2021;10:466. https://doi.org/10.3390/pathogens10040466
24. Whaley SG, Berkow EL, Rybak JM, Nishimoto AT, Barker KS, Rogers PD. Azole antifungal resistance in *Candida albicans* and emerging non-*albicans Candida* species. Front Microbiol. 2017;7:2173. https://doi.org/10.3389/fmicb.2016.02173
25. Govender NP, Patel J, Magobo RE, Naicker S, Wadula J, Whitelaw A, et al.; TRAC-South Africa group. Emergence of azole-resistant *Candida parapsilosis* causing bloodstream infection: results from laboratory-based sentinel surveillance in South Africa. J Antimicrob Chemother. 2016;71:1994–2004. https://doi.org/10.1093/jac/dkw091
26. Chibabhai V. Incidence of candidemia and prevalence of azole-resistant candidemia at a tertiary South African hospital—a retrospective laboratory analysis 2016–2020. S Afr J Infect Dis. 2022;37:326. https://doi.org/10.4102/sajid.v37i1.326
27. van Schalkwyk E, Mpembe RS, Thomas J, Shuping L, Ismail H, Lowman W, et al.; GERMS-SA. Epidemiologic shift in candidemia driven by *Candida auris*, South Africa, 2016–2017. Emerg Infect Dis. 2019;25:1698–707. https://doi.org/10.3201/eid2509.190040
28. Alavinejad M, Mellado B, Asgary A, Mbada M, Mathaha T, Lieberman B, et al. Management of hospital beds and ventilators in the Gauteng province, South Africa, during the COVID-19 pandemic. PLOS Glob Public Health. 2022;2:e0001113. https://doi.org/10.1371/journal.pgph.0001113
29. Yang W, Shaman JL. COVID-19 pandemic dynamics in South Africa and epidemiological characteristics of three variants of concern (Beta, Delta, and Omicron). eLife. 2022;11:1–50. https://doi.org/10.7554/eLife.78933

Address for correspondence: Nelesh P. Govender, Wits Mycology Division, 1 Modderfontein Rd, Sandringham 2131, South Africa; email: nelesh.govender@wits.ac.za

Dengue Incidence, Seroprevalence, and Expansion Factors from Active Surveillance, Brazil, 2016–2021

Eliana Nogueira Castro de Barros, Manuela de Almeida Roediger, Maïna L'Azou Jackson, Morgan A. Marks, Elizabeth M. Anderson, Alejandra Esteves-Jaramillo, Germán Áñez, José A. Sousa Moreira, Fernanda Castro Boulos

Dengue is hyperendemic in Brazil and is underestimated by passive surveillance. To better understand dengue incidence, we conducted epidemiologic analyses among participants, 2–59 years of age, from the placebo arm of a phase 3 dengue vaccine trial. During 2016–2021, a total of 5,947 participants contributed to 22,028 person-years of follow-up. We identified and virologically confirmed dengue (VCD), Zika, and chikungunya infections. We observed VCD and chikungunya incidence heterogeneity by age, geographic location, and study year. Children 2–6 years of age experienced the highest VCD (2.33/100 person-years) and chikungunya (1.02/100 person-years) incidence. VCD peaked in 2019 (n = 148) whereas chikungunya peaked in 2017 (n = 51). VCD incidence rates from active surveillance were generally higher than those reported to the national passive surveillance system; expansion factor range was <1–9.5 by municipality. Active surveillance is critical to better understand and characterize dengue epidemiology.

Dengue, caused by infection with one of 4 dengue virus (DENV) serotypes, is endemic in over 100 countries (*1*–*4*). Clinical manifestations of dengue range from asymptomatic to severe illness that can be fatal. Dengue is the most rapidly spreading mosquitoborne viral disease, increasing faster than any other communicable disease (*5*). Dengue mainly circulates in tropical and subtropical climates; most cases occur in Southeast Asia and Latin America (*2*,*4*). However, cases outside endemic areas are becoming more frequent because of increases in urbanization, travel to endemic regions, and the expansion of the primary vector (*6*,*7*).

Author affiliations: Instituto Butantan, São Paulo, Brazil (E.N.C. Barros, M.A. Roediger, J.A.S. Moreira, F.C. Boulos); MSD (UK) Limited, London, UK (M. L'Azou Jackson); Merck & Co., Inc., Rahway, New Jersey, USA (M.A. Marks, E.M. Anderson, A. Esteves-Jaramillo, G. Áñez)

DOI: https://doi.org/10.3201/eid3204.250942

More than 50% of the dengue cases in Latin America are reported in Brazil (*8*,*9*). In a 2024 outbreak, >10 million cases and >6,000 deaths were reported across Brazil (*10*,*11*). All 4 DENV serotypes have been reported in Brazil since 2010; typically, 2 serotypes cocirculate with variations in the dominant serotype over time (*10*). In addition to DENV, chikungunya virus (CHIKV) and Zika virus (ZIKV), which are transmitted by the same *Aedes* spp. mosquito vector, circulate in Brazil (*12*). CHIKV was first identified in Brazil in 2014 and causes annual epidemics (*13*,*14*). In 2015, a major outbreak of Zika led the Brazil Ministry of Health to declare a national health emergency (*15*,*16*).

The epidemiology of dengue in Brazil has previously been described using data collected through passive surveillance (*17*). Dengue, chikungunya, and Zika are notifiable diseases in Brazil; healthcare institutions report suspected, probable, and laboratory-confirmed cases, along with basic demographic information, to the national passive surveillance system, Sistema de Informação de Agravos de Notificação (SINAN) (*17*). However, because of the subclinical manifestation of dengue, many patients do not seek medical care. In addition, the nonspecific clinical presentation that overlaps with other arboviral diseases, including chikungunya and Zika, can cause misclassification. Those factors, along with reporting biases, can result in an underestimation of dengue burden by passive surveillance systems (*18*). Instead, active surveillance of prospective longitudinal cohorts can better estimate the burden of dengue with generally higher incidence rates than those reported by the national surveillance system (*19*,*20*).

[1]Preliminary results from this study were presented at the American Society for Tropical Medicine and Hygiene annual meeting; November 13–17, 2024; New Orleans, Louisiana, USA.

To better understand dengue in Brazil, we conducted epidemiologic analyses among participants enrolled in a large phase 3 efficacy trial of a live attenuated tetravalent dengue vaccine, Butantan-DV (*21,22*). We described dengue serostatus by demographic characteristics before receipt of vaccine or placebo. We used the active surveillance of participants in the placebo arm of the trial to estimate incidence rates of dengue during 2016–2021 and determine the degree of underreporting compared with the national passive surveillance system.

Materials and Methods

Dengue Vaccine Efficacy Trial Design and Participants

DEN-03-IB (clinical trials identifier NCT02406729) is a double-blind, randomized, placebo-controlled, phase 3 trial to assess the safety and efficacy of a single dose of Butantan-dengue vaccine (Butantan-DV) for the prevention of symptomatic virologically confirmed dengue (VCD) (*21,22*). Participants included healthy persons 2–59 years of age who were enrolled and randomized 2:1 (Butantan-DV:placebo), stratified by age group (2–6, 7–17, and 18–59 years), at 16 sites in 15 municipalities across the 5 geographic regions of Brazil; 3 sites in the North, 4 sites in the Northeast, 3 sites in the Center-West, 5 sites in the Southeast, and 1 site in the South region. National Commission for Research Ethics (approval no. CAAE 44462915.8.1001.0068) and local ethics committees approved the study; it was conducted in accordance with the principles of good clinical practice.

Seropositivity Measurements

We determined baseline dengue serostatus retrospectively using blood samples collected on day 0 from enrolled participants, before receipt of vaccine or placebo. Samples were tested in a validated virus reduction neutralization test (VRNT), as previously described (*21–24*). In brief, serially diluted serum samples were mixed with wild-type DENV representing each of the 4 serotypes (DENV-1–4) before incubation with Vero cells. Cells were then fixed, stained with custom DENV-specific primary antibodies (GenScript, https://genscript.com) followed by Alexa Fluor 448-conjugated secondary antibodies (Invitrogen, https://invitrogen.com), and counted. The results were reported as a 60% VRNT ($VRNT_{60}$) titer, the reciprocal of the serum dilution that reduced the number of infected cells by 60% compared with the virus control. We defined prior exposure to any DENV serotype (i.e., dengue seropositive at baseline) as having a $VRNT_{60}$ titer against any of the 4 DENV serotypes above the lower limit of quantification (i.e., a $VRNT_{60}$ titer of DENV-1 $\geq$18 or DENV-2 $\geq$15 or DENV-3 $\geq$12 or DENV-4 $\geq$13) at baseline (*21–24*).

Active Surveillance of Participants in the DEN-03-IB Placebo Arm

We conducted active surveillance of the 5,947 participants who received placebo and were in the per-protocol population of DEN-03-IB over 64 months from start through the data cutoff for the primary analysis, February 22, 2016–July 13, 2021. We defined the data cutoff as the date at which all enrolled participants in either treatment group had completed $\geq$2 years of follow-up (22). We analyzed deidentified data to assess the epidemiology and natural history of dengue in Brazil.

Site staff contacted participants by email, text message, or telephone at least monthly in the first 2 years and every 3 months afterwards to identify post-vaccination adverse events and potential dengue cases. The sites could increase the frequency of follow-up contacts during times of localized outbreaks. In addition, we instructed participants in both treatment arms to seek out the trial team if they experienced a febrile illness or illness suspected to be dengue on the basis of clinical symptoms. We evaluated the presence and intensity of clinical symptoms during each unscheduled visit to assess suspected cases.

In cases of suspected dengue, a blood sample was collected, preferably within 9 days of symptom onset, for virologic confirmation. We extracted total RNA using QIAamp Viral RNA Mini Kit (QIAGEN, https://qiagen.com) before conducting reverse transcription PCR (RT-PCR) assays in a central laboratory. We made virologic confirmation of wild-type DENV and serotype determinations using a validated fourplex RT-PCR assay as previously described (*25*). In brief, we reversed transcribed and amplified total isolated RNA using DENV serotype–specific primer/probe sets targeting each of the 4 DENV serotypes (DENV-1–4). In addition, we tested samples separately for the presence of CHIKV and ZIKV viral RNA using previously described singleplex RT-PCRs with primer/probe sets targeting CHIKV or ZIKV (*26*, *27*).

National Data

SINAN is a passive surveillance system that collects information from healthcare providers and institutions throughout Brazil on nationally notifiable diseases (*17*). Dengue cases in SINAN were defined by 2009 WHO diagnostic criteria (*28*) and confirmed through laboratory testing. In addition, healthcare providers reported basic demographic data (sex,

age, race/ethnicity, and geographic location) from each dengue case (suspected, probable or confirmed) to SINAN. We pulled laboratory-confirmed dengue cases (confirmed by RT-PCR or IgM) from SINAN for the municipalities and time that DEN-03-IB took place. We disaggregated census data from the Instituto Brasileiro de Geografia e Estatística for the 15 municipalities that contained ≥1 of the 16 study sites.

Expansion Factors

We determined expansion factors (EF) as the ratio of VCD incidence from active surveillance of the placebo arm of DEN-03-IB per 100,000 person-years divided by laboratory-confirmed dengue incidence from the national passive surveillance system, SINAN, per 100,000 population, as described previously (*19*). We defined VCD incidence from active surveillance as the number of virologically confirmed cases over person-years of follow-up, determined weekly as the cumulative time that each participant contributed during active surveillance over the duration of the study, and in 2019 during an epidemic year. Given the large age groups (2–59 years of age) included in DEN-03-IB, we calculated EF for the entire population of the 15 municipalities for interpretation feasibility. We calculated laboratory-confirmed dengue incidence from passive surveillance by dividing laboratory-confirmed dengue cases using RT-PCR or IgM by the municipality population based on census data (*19*). An EF >1 indicates potential underreporting by SINAN; an EF <1 indicates potential underreporting by active follow-up.

Statistical Analyses

We summarized baseline demographics of all participants enrolled in the phase 3 trial (n=16,235) (Table 1). Covariates included age group at enrollment (2–6, 7–17, and 18–59 years of age), biologic sex (M/F), race (Pardo [multiracial Brazilian], White, Black, Asian, and Indigenous or Other), geographic region in Brazil (North, Northeast, Central-West, South, Southeast), prior exposure to any DENV serotype (yes/no) and a self-reported history of yellow fever vaccination before study enrollment (yes/no).

We calculated estimates of incidence of virologically confirmed dengue, chikungunya, or Zika only among placebo recipients in the per-protocol population (n = 5,947) using a person-time approach. We defined incidence rate as cases per 100 person-years. We counted participants who experienced recurrent infections by >1 DENV serotype once in the total incidence and separately by serotype for the serotype-specific incidence. We determined incidence by age group according to participant age at the time of the event. We summarized incidence rates by demographic subgroup, baseline dengue serostatus for those with a known serostatus, and by study year. We calculated 95% CI for incidence rates using Poisson exact (*29*).

Table 1. Baseline demographics for participants enrolled in large phase 3 efficacy trial of a dengue vaccine, Brazil, 2016–2021*

Characteristic	Vaccine recipients	Placebo recipients
Total participants	10,259	5,976
Sex		
F	5,555 (54.1)	3,216 (53.8)
M	4,704 (45.9)	2,760 (46.2)
Age group, y		
2–6	3,337 (32.5)	1,679 (28.1)
7–17	3,376 (32.9)	1,771 (29.6)
18–59	3,546 (34.6)	2,526 (42.3)
Median age, y (range)	11 (2–59)	14 (2–59)
Race		
Pardo†	7,017 (68.4)	4,036 (67.5)
White	2,410 (23.5)	1,402 (23.5)
Black	655 (6.4)	408 (6.8)
Asian	149 (1.5)	114 (1.9)
Indigenous or other	28 (0.3)	16 (0.3)
Prior exposure to DENV, any serotype‡		
Y	5,009 (48.8)	3,041 (50.9)
N	4,855 (47.3)	2,700 (45.2)
Unknown or missing§	395 (3.9)	235 (3.9)
History of yellow fever vaccination		
Y	10,259 (100)	5,976 (100)
N	0	0

*Values are no. (%) except as indicated. Participants were from the DEN-03-IB trial of a live attenuated tetravalent dengue vaccine, Butantan-DV. DENV, dengue virus.
†Multiracial Brazilian.
‡Prior exposure to DENV is defined as baseline 60% virus reduction neutralization test titer to any of the 4 DENV serotypes above the assay limit of detection.
§Unknown result indicates missing test result, not consented sample, or participants who were not tested for DENV-3. Missing result indicates nonconsented participants for serology testing or participants who were not tested for other reasons.

Table 2. Dengue serostatus at baseline for participants enrolled in large phase 3 efficacy trial of a dengue vaccine trial, Brazil, 2016–2021*

Characteristic	Seropositive, no. (%)	Seronegative, no. (%)
Participants with a known baseline dengue serostatus	8,050 (49.6)	7,555 (46.5)
Sex		
F	4,493 (51.2)	3,910 (44.6)
M	3,557 (47.7)	3,645 (48.8)
Age at enrollment, y		
2–6	870 (17.3)	4,061 (81.0)
7–17	3,120 (60.6)	1,860 (36.1)
18–59	4,060 (66.9)	1,634 (26.9)
Race		
Pardo†	5,685 (51.4)	4,942 (44.7)
White	1,693 (44.4)	1,991 (52.2)
Black	514 (48.4)	492 (46.3)
Asian	133 (50.6)	115 (43.7)
Indigenous or other	25 (56.8)	15 (34.1)
Geographic region		
North	2,531 (51.1)	2,154 (43.5)
Northeast	2,591 (57.1)	1,766 (38.9)
Center-West	1,489 (52.9)	1,243 (44.2)
South	28 (5.7)	449 (91.8)
Southeast	1,411 (41.0)	1,943 (56.5)

*Participants were from the DEN-03-IB trial of a live attenuated tetravalent dengue vaccine, Butantan-DV. Prior exposure (i.e., dengue seropositive) is defined as having a baseline 60% virus reduction neutralization test titer to any of the 4 dengue virus serotypes above the assay limit of detection.
†Multiracial Brazilian.

We estimated EFs for each municipality to understand the degree of underreporting of dengue illness in the national passive surveillance system (*30*). We calculated 95% CI for EFs using Clopper-Pearson exact method (*31*). We calculated EFs and 95% CI during the entire follow-up study period (2016–2021) and during an outbreak year (2019).

We summarized the frequency and distribution of clinical signs and symptoms associated with virologically confirmed dengue-associated or chikungunya-associated illness among placebo recipients and calculated 95% CIs using Clopper-Pearson exact method (*31*). We performed statistical analyses using SAS software version 9.4 (SAS Institute, Inc., https://www.sas.com).

Results

Participant Demographics and Baseline Serostatus

A total of 16,235 participants underwent randomization and received Butantan-DV (n = 10,259) or placebo (n = 5,976) during February 2016–July 2019. The baseline characteristics were comparable between the 2 arms; all participants had a history of previous yellow fever vaccination and approximately half of participants did not have evidence of prior dengue exposure before vaccination (Table 1). Of the 16,235 participants, 15,605 (96.1%) had a known dengue serostatus at baseline; 9,864 in the Butantan-DV arm and 5,741 in the placebo arm (Table 2). At baseline, most children ages 2–6 years of age (81.0%) and participants in the South region (91.8%) were DENV-naive. Although DENV seropositivity increased with age, 26.9% of adults (18–59 years old) were seronegative at baseline (Table 2).

Incidence of VCD

Participants had completed ≥2 years of follow-up by the data cutoff (July 13, 2021). In total, 5,947 participants in the placebo arm had contributed to 22,028 person-years of follow-up. During follow-up, 228 cases of VCD from any DENV serotype were reported after Day 28 (incidence rate = 1.04/100 person-years), accounting for 1.71% of fever episodes (Appendix Table 1). Children 2–6 years of age had the highest rate of VCD (2.33/100 person-years) compared with older age groups (1.38/100 person-years for the 7–17 group and 0.68/100 person-years for the 18–59 group) (Figure 1). The Center-West region had the highest incidence (1.64/100 person-years); VCD was not observed in the South (Figure 2). VCD incidence peaked in 2019 (148 cases; 2.56/100 person-years).

We observed VCD cases resulting from DENV-1 (n = 111; 0.50/100 person-years) and DENV-2 (n = 119; 0.54/100 person-years) among participants in the placebo arm (Appendix Table 2); we did not observe cases of VCD resulting from DENV-3 or DENV-4 in the trial by the cutoff date. Two participants had dual infections of DENV-1 and DENV-2; in 1 participant they were concurrent and in the other, sequential. The Center-West and Southeast regions had a higher rate of DENV-2 (1.3/100 person-years in Center-West and 0.80/100 person-years in Southeast) compared with

the North and Northeast, which were dominated by DENV-1 (0.58/100 person-years in the North region and 0.77/100 person-years in Northeast). We also observed differences in DENV serotype-specific incidence by age groups; DENV-1 incidence was higher in the 2–6 age group, DENV-2 was higher in the 18–59 age group, and both DENV serotypes had comparable incidence rates in the 7–17 age group.

Estimating the Degree of Passive Surveillance System Underreporting for Dengue

Underreporting in the national passive surveillance system, SINAN, varied by municipality and over time (Figure 3). By municipality, considering the entire study period (2016–2021), EF range was <1 to 9.5 (Table 3). When considering only 2019, the year in which a major dengue outbreak occurred in Brazil (*10*, *32*, *33*), the EF range by municipality was 0–492.9 (Table 4).

Incidence of Other Laboratory-Confirmed Arboviral-Associated Illness

During the study period, 3 laboratory-confirmed Zika episodes (incidence rate 0.01/100 person-years) and 106 laboratory-confirmed chikungunya cases (incidence rate 0.48/100 person-years) were captured. We observed the highest incidence of laboratory-confirmed chikungunya in the 2–6 age group (1.02/100 person-years) spread out across the geographic locations; the Northeast region had the highest rates (0.70/100 person-years). Furthermore, we observed most laboratory-confirmed chikungunya cases (n = 54) in 2016 (0.99/100 person-years) and 2017 (1.68/100 person-years), the 2 years with the lowest rates of VCD during the study (Figure 2).

The clinical manifestations of VCD and chikungunya cases during the follow-up were generally comparable; arthralgia, pyrexia, and headache were the most commonly reported symptoms among either VCD or chikungunya cases (Figure 4). Arthritis was more commonly reported among chikungunya cases (11%) than VCD cases (1%).

Discussion

We used active surveillance from a phase 3 dengue vaccine efficacy trial (DEN-03-IB) to better understand dengue incidence in Brazil during 2016–2021. Dengue incidence was generally higher in our study than estimates reported in the national passive surveillance system but varied by municipality and study year. Nonspecific clinical manifestations overlapping with other circulating arboviruses, as we observed with laboratory-confirmed chikungunya in this study, may further contribute to underreporting of dengue.

We used data from ≈6,000 participants 2–59 years of age who were enrolled in the placebo arm of the study to assess the incidence of dengue. Nearly a third of the participants in DEN-03-IB were adults (18–59 years of age); a large proportion of whom (26.9%) were dengue seronegative at baseline. Furthermore,

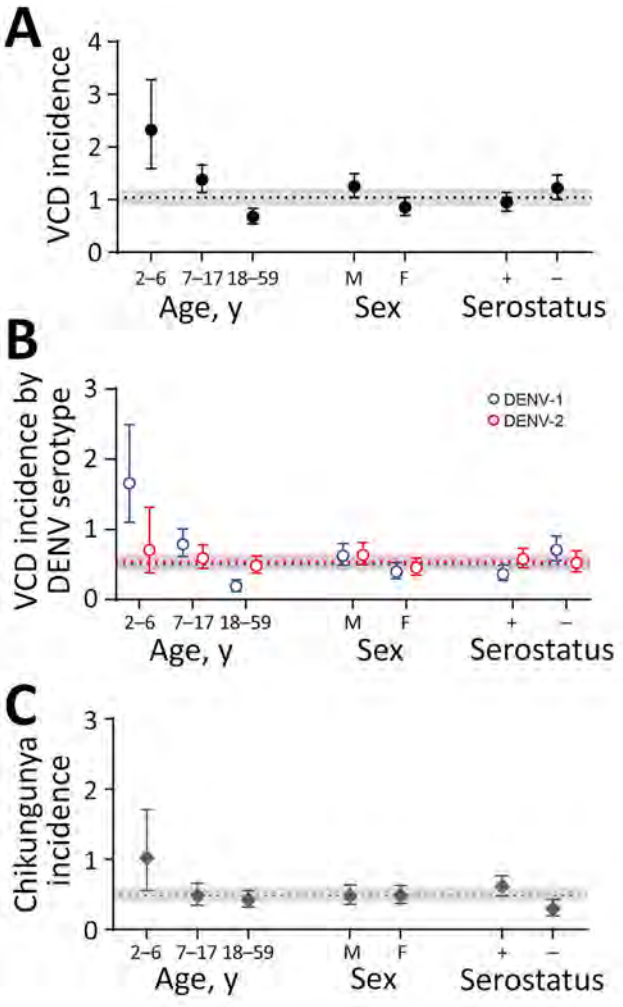

Figure 1. VCD and laboratory-confirmed chikungunya incidence by demographic characteristics, Brazil, 2016–2021. Incidence per 100 person-years of VCD is shown regardless of serotype (A), VCD by DENV serotypes DENV-1 and DENV-2 (B), and laboratory-confirmed chikungunya (C) among participants in the placebo arm of the DEN-03-IB trial of a live attenuated tetravalent dengue vaccine, Butantan-DV, by demographic characteristic (age at event, sex, and baseline dengue serostatus). Points represent incidence estimates and error bars represent 95% CIs. Dashed lines represent the overall incidence per 100 person-years and shaded areas around the dashed lines represent 95% CIs for the overall incidence estimates. Prior exposure (i.e., dengue seropositive) is defined as having a baseline 60% virus reduction neutralization test titer to any of the 4 DENV serotypes above the assay limit of detection. +, positive; –, negative; DENV, dengue virus; VCD, virologically confirmed dengue.

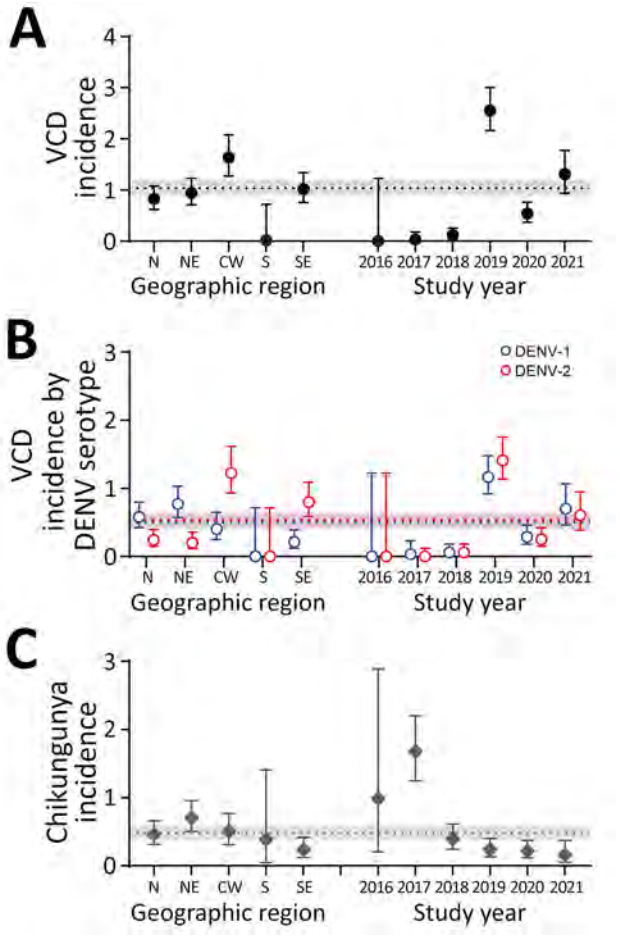

Figure 2. VCD and laboratory confirmed chikungunya incidence by temporospatial characteristics, Brazil, 2016–2021. Incidence per 100 person-years of VCD is shown regardless of serotype (A), VCD by DENV serotypes DENV-1 and DENV-2 (B), and laboratory-confirmed chikungunya (C) among participants in the placebo arm of the DEN-03-IB trial of a live attenuated tetravalent dengue vaccine, Butantan-DV, by temporospatial characteristic (geographic region and study year). Points represent incidence estimates and error bars represent 95% CIs. Dashed lines represent the overall incidence per 100 person-years and shaded areas around the dashed lines represent 95% CIs for the overall incidence estimates. CW, Center-West; DENV, dengue virus; N, North; NE, Northeast; S, South; SE, Southeast; VCD, virologically confirmed dengue.

active surveillance ensured that even mild cases of dengue were detected and distinguished from other arboviruses (ZIKV and CHIKV). Although the follow-up spanned multiple seasons (2016–2021), we detected only DENV-1 and DENV-2 in the study; we did not observe cases of VCD caused by DENV-3 or DENV-4. The absence of DENV-3 and DENV-4 reflects the reported circulation of DENV in Brazil during the period in which the trial was conducted (*10*). We observed regional and age differences in serotype-specific incidence for DENV-1 and DENV-2, suggesting previous population exposure histories may affect DENV serotype circulation. Consistent with previous reports that used passive surveillance (*34*, *41*), we found that the highest burden of dengue occurred in the Central-West region. Furthermore, in our study, children 2–6 years of age had the highest incidence of laboratory-confirmed dengue and chikungunya compared with the older age subgroups.

Placebo cohorts from phase 3 efficacy trials are a valuable data source to characterize dengue epidemiology within a country. Our findings add to previous results from other dengue vaccine phase 3 trials conducted in Brazil and provide a report of active surveillance among adults (≥18 years of age). Although those datasets are complementary, between-study comparisons are challenging because of differences

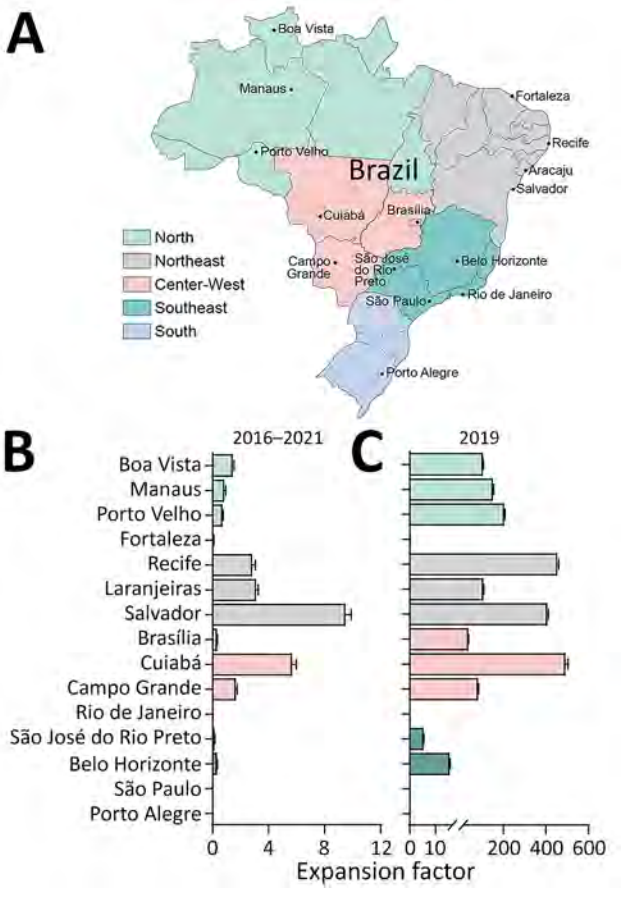

Figure 3. Locations of DEN-03-IB clinical study sites and expansion factors by municipality, Brazil, 2016–2021. A) Locations of clinical sites that enrolled participants in the DEN-03-IB phase 3 study of a live attenuated tetravalent dengue vaccine, Butantan-DV, in the 5 geographic regions (North, Northeast, Center-West, Southeast, South). B, C) Expansion factors and 95% CIs by municipality for the entire study period 2016–2021 (B) and during an outbreak year, 2019 (C). Note that 2 clinical sites were located in São Paulo and that Laranjeiras was the municipality closest to the clinical site in Aracaju.

Table 3. Incidence rates of virologically confirmed dengue and expansion factors, by municipality and state, Brazil, 2016–2021*

Municipality	DEN-03-IB incidence rate (95% CI)	SINAN incidence rate (95% CI)	Expansion factor (95% CI)†
São Paulo, SP‡	0 (0–414.4)	978.0 (972.5–983.5)	0 (0.0–0.004)
São José do Rio Preto, SP	2,069.1 (1,385.7–2,971.6)	14,134.9 (14,027.5–14,242.9)	0.15 (0.14–0.15)
Belo Horizonte, MG	1,249.2 (763.1–1,929.3)	3,951.4 (3,927.0–3,976.0)	0.32 (0.30–0.33)
Rio de Janeiro, RJ	0 (0–625.4)	283.6 (279.6–287.6)	0 (0–0.013)
Laranjeiras, SE§	1,576.2 (1,078.1–2,225.1)	507.8 (430.8–594.6)	3.1 (3.0–3.3)
Recife, PE	673.4 (336.1–1,204.8)	237.9 (230.6–245.5)	2.8 (2.6–3.1)
Fortaleza, CE	53.4 (1.4–297.5)	834.5 (823.6–845.4)	0.06 (0.05–0.08)
Salvador, BA	2,170.0 (1,083.3–3,882.8)	228.6 (223.1–234.1)	9.5 (9.1–9.9)
Manaus, AM	444.1 (213.0–816.8)	527.0 (517.6–536. 6)	0.84 (0.77–0.93)
Boa Vista, RR	1,214.5 (800.4–1,767.0)	846.8 (819.7–874.5)	1.4 (1.4–1.5)
Porto Velho, RO	786.5 (458.2–1,259.2)	1,110.1 (1,082.4–1,138.3)	0.71 (0.66–0.76)
Brasília, DF	1,480.9 (948.8–2,203.4)	4,661.7 (4,637.7–4,685.8)	0.32 (0.30–0.33)
Cuiabá, MT	1,494.4 (984.8–2,174.3)	263.0 (250.4–276.0)	5.7 (5.4–6.0)
Campo Grande, MS	2,030.7 (1,183.0–3,251.4)	1,219.4 (1,197.0–1,242.3)	1.7 (1.6–1.7)
Porto Alegre, RS	0 (0–705.7)	504.1 (492.8–515.6)	0 (0–0.007)

*Incidence rates of virologically confirmed dengue in the placebo arm of the DEN-03-IB trial of a live attenuated tetravalent dengue vaccine, Butantan-DV (cases/100,000 person-years), or dengue confirmed cases in SINAN (cases/100,000 population). AM, Amazonas; BA, Bahia; CE, Ceará; DF, Distrito Federal; MG, Minas Gerais; MS, Mato Grosso do Sul; MT, Mato Grosso; PE, Pernambuco; RJ, Rio de Janeiro; RO, Rondônia; RR, Roraima; RS, Rio Grande do Sul; SE, Sergipe; SINAN, Sistema de Informação de Agravos de Notificação; SP, São Paulo.
†Expansion factor is the ratio of virologically confirmed dengue cases from active surveillance of the placebo arm of DEN-03-IB per 100,000 person-years over dengue confirmed cases from the national passive surveillance system, SINAN, per 100,000 population. A value >1 would indicate potential underreporting by SINAN, whereas a value <1 is indicative of potential underreporting by active follow-up.
‡Two DEN-03-IB clinical sites were located in São Paulo.
§Used for the municipality closest to the Aracaju, SE, clinical site.

in participant demographics, study site locations, and the period of follow-up. CYD15 was a phase 3 trial of the tetravalent dengue vaccine CYD-TDV (Dengvaxia; Sanofi, https://www.sanofi.com) conducted in 5 countries across 22 sites, including 5 sites in Brazil, during June 2011–April 2014 (*42*). In CYD15, overall VCD incidence was 3.5/100 person-years among 1,177 placebo recipients 9–16 years of age in Brazil (*43*), higher than what we observed in the DEN-03-IB trial from 2016–2021 (1.04/100 person-years). TIDES was a phase 3 trial of the tetravalent dengue vaccine TAK-003 (Qdenga; Takeda, https://www.takeda.com) conducted at 26 sites in 8 countries, including 4 sites in Brazil during September 2016–December 2021 (*44*, *45*, *46*). In this similar timeframe, VCD incidence among 560 participants 4–16 years of age in Brazil (0.9/100 person-years) was generally comparable to rates observed in DEN-03-IB; incidence peaked in 2016 (caused by DENV-1) and 2019 (caused by DENV-2), consistent with DEN-03-IB. Still, the differences between incidence rates across trials could be attributed to differences by age or underlying serostatus of the study population and emphasize the variability and unpredictability of dengue epidemiology.

Table 4. Incidence rates of virologically confirmed dengue and expansion factors, by municipality and state, during the 2019 outbreak, Brazil*

Municipality	DEN-03-IB incidence rate (95% CI)	SINAN incidence rate (95% CI)	Expansion factor (95% CI)†
São Paulo, SP‡	0 (0.0–50,500.9)	235.9 (233.2–238.7)	0 (0.0–0.016)
São José do Rio Preto, SP	20,875.7 (11,412.9–35,025.9)	3,886.7 (3,830.2–3,944.1)	5.4 (5.3–5.4)
Belo Horizonte, MG	23,789.9 (14,323.1–37,150.9)	1,537.0 (1,521.7–1,552.4)	15.5 (15.3–15.7)
Rio de Janeiro, RJ	0 (0–83,895.6)	88.2 (86.0–90.5)	0 (0.0–0.042)
Laranjeiras, SE§	20,562.3 (14,064.6–29,027.8)	194.5 (147.7–251.4)	105.7 (104.3–107.2)
Recife, PE	25,657.6 (11,732.3–48,706.1)	56.5 (52.9–60.3)	454.0 (448.5–459.6)
Fortaleza, CE	0 (0–6,348.0)	57.7 (54.9–60.7)	0 (0.0–0.064)
Salvador, BA	33,913.6 (14,641.5–66,823.4)	83.3 (80.0–86.7)	407.1 (402.7–411.4)
Manaus, AM	7,180.1 (1,480.7–20,983.2)	47.6 (44.8–50.6)	150.8 (147.4–154.4)
Boa Vista, RR	20,652.3 (13,091.8–30,988.6)	197.9 (184.3–212.2)	104.4 (102.9–105.8)
Porto Velho, RO	14,922.4 (5,476.2–32,479.7)	73.1 (66.0–80.7)	204.2 (200.9–207.5)
Brasília, DF	22,474.3 (12,846.0–36,496.9)	625.6 (616.7–634.5)	35.9 (35.5–36.4)
Cuiabá, MT	7,557.4 (191.3–42,107.2)	15.3 (12.4–18.8)	492.9 (481.9–504.2)
Campo Grande, MS	21,297.4 (12,173.3–34,585.6)	259.9 (249.5–270.7)	81.9 (80.8–83.0)
Porto Alegre, RS	0 (0–26,450.0)	77.4 (73.0–82.0)	0 (0–0.048)

*Incidence rates of virologically confirmed dengue in the placebo arm of the DEN-03-IB trial of a live attenuated tetravalent dengue vaccine, Butantan-DV (cases/100,000 person-years), or dengue confirmed cases in SINAN (cases/100,000 population); AM, Amazonas; BA, Bahia; CE, Ceará; DF, Distrito Federal; MG, Minas Gerais; MS, Mato Grosso do Sul; MT, Mato Grosso; PE, Pernambuco; RJ, Rio de Janeiro; RO, Rondônia; RR, Roraima; RS, Rio Grande do Sul; SE, Sergipe; SINAN, Sistema de Informação de Agravos de Notificação; SP, São Paulo.
†Expansion factor is the ratio of virologically confirmed dengue cases from active surveillance of the placebo arm of DEN-03-IB per 100,000 person-years over dengue confirmed cases from the national passive surveillance system, SINAN, per 100,000 population. A value >1 would indicate potential underreporting by SINAN, whereas a value <1 is indicative of potential underreporting by active follow-up.
‡Two DEN-03-IB clinical sites were located in São Paulo.
§Used for the municipality closest to the Aracaju, SE, clinical site.

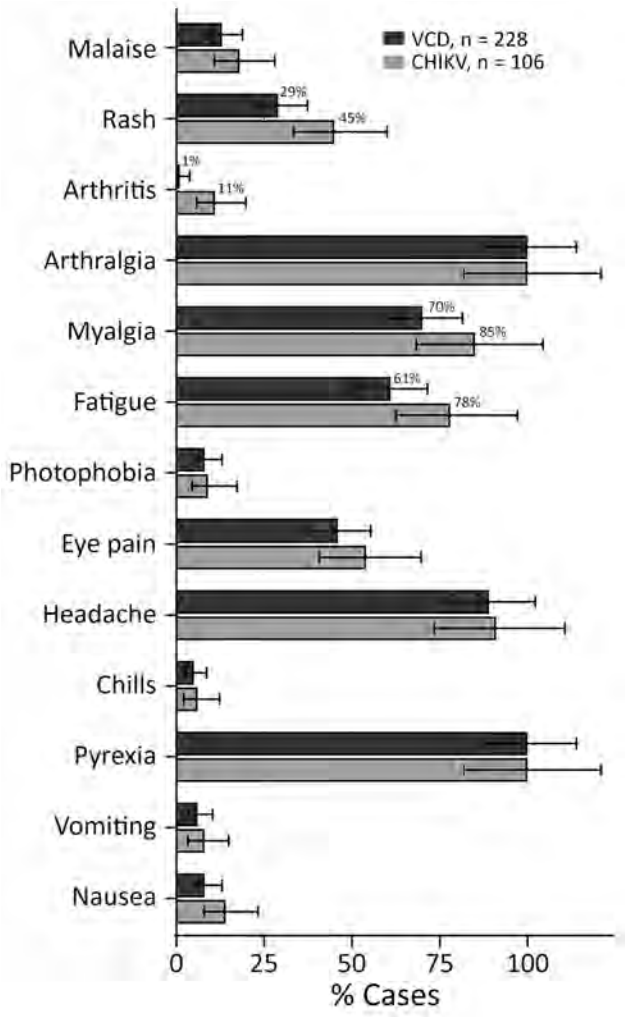

Figure 4. Clinical manifestations of VCD and CHIKV among participants in the placebo arm of the DEN-03-IB trial of a live attenuated tetravalent dengue vaccine, Butantan-DV, Brazil, 2016–2021. Bars represent percentages of participants with each symptom; error bars represent 95% CIs. Numeric percentages are indicated for symptoms with ≥10% difference between VCD and CHIKV cases. VCD, virologically confirmed dengue; CHIKV, laboratory-confirmed chikungunya.

Previous studies of dengue epidemiology in Brazil have relied on data from SINAN, the national passive surveillance system. However, incidence rates from passive surveillance are likely underestimating the true burden of dengue because of the subclinical nature of dengue, particularly with the first infection, and because the clinical manifestation of dengue is similar to that of other arboviral diseases, including chikungunya and Zika. In addition, laboratory confirmation practices vary across healthcare institutions. We observed a large degree of underreporting in the national passive surveillance system (ratio of DEN-03-IB/SINAN>1), particularly during the dengue outbreak in 2019 (*10*,*32*,*33*). The increased underreporting in 2019 was likely caused by differences in surveillance practices during an outbreak, when the volume of cases overwhelmed testing and reporting systems; it is more challenging to conduct laboratory confirmation on suspected cases in those conditions (*47*). We also observed underreporting in the active surveillance (ratio of DEN-03-IB/SINAN<1) in some sites, particularly across the full study period of 2016–2021. A possible cause of the underreporting in active surveillance could be our limited ability to calculate EF from only a subset of the population, because clinical sites do not necessarily represent the entire municipality. EFs estimated from CYD15 using similar methods indicated that dengue was underreported in Brazil during 2011–2014 at a national (EF = 26.7), state (EF = 16.9), and local level (EF = 19.4) (*19*). Although it is difficult to compare EF estimates that are highly dependent on data availability, including age stratification, case definitions, and temporospatial factors, those data support the finding that underreporting of dengue in passive surveillance systems remains an important issue (*19*).

Two other arboviruses, ZIKV and CHIKV, cocirculate with DENV in Brazil (*12*). ZIKV was first identified in Brazil in 2015, before the initiation of the DEN-03-IB vaccine trial (*16*); ZIKV caused a major outbreak that peaked in February 2016, just as trial enrollment began, and subsequently circulated at low levels. In our study, 3 episodes of ZIKV were confirmed in participants under active surveillance. A possible explanation for the rarity of Zika cases in DEN-03-IB is the limited number of participants under active surveillance during the Zika outbreak; the last study participant enrolled in 2019 (*22*). An outbreak of chikungunya peaked in 2017; we captured many cases in our study. The overall low specificity of symptoms between chikungunya and dengue among participants in this study represents a misclassification risk that could contribute to underreporting to SINAN. The detection of both CHIKV and ZIKV infections, albeit at lower rates than VCD, illustrates the co-circulation of arboviruses in Brazil and the potential for misclassification in syndromic surveillance systems. Those observations confirm the need to reinforce laboratory confirmation practices.

DEN-03-IB enrolled participants 2–59 years of age in predefined urban centers; generalizability to older adults, rural populations, or other geographic regions may be limited. Few participants were enrolled in the single clinical site located in the South region of Brazil, limiting the interpretation of dengue circulation in that region. Several factors can affect

incidence estimations including follow-up, withdrawal, or differential healthcare seeking across time and sites, although we minimized those factors in the randomized controlled trial. Nevertheless, the rigorous and standardized surveillance we conducted across all sites strengthens the internal validity and comparability of our findings.

EF calculations have inherent limitations, such as the comparison of active surveillance in healthy participants with passive surveillance data from the municipalities' general population. Furthermore, given the limited number of observations at the geographic level in this study, we did not stratify EFs by age. Although EF methodology is not perfect, EF estimates can provide a sense of the magnitude of dengue underreporting.

In sum, dengue epidemiology is unpredictable and varies over time by geography, serotype and age, even within a country. A better understanding of its epidemiology would inform public health interventions aimed at the prevention and control of dengue worldwide. Clinical manifestations are nonspecific, and surveillance remains an important tool to monitor arbovirus epidemiology. Furthermore, the differences in national surveillance systems, their reporting and laboratory-confirmation practices, and variable clinical definitions limit the extrapolation of surveillance data between countries. Our findings have direct implications for public health decision making, including the implementation of vaccination strategies and the interpretation of surveillance systems data. Longitudinal active surveillance embedded within vaccine trials represents a valuable approach to refining estimates of disease burden and informing control strategies in endemic settings.

Acknowledgments

We thank the participants (and their parents) who enrolled in the study, Monica Cintra (Instituto Butantan, São Paulo, Brazil) for her leadership and contributions to the study; Bo Zheng and Fansen Kong (Merck Sharp & Dohme LLC, a subsidiary of Merck & Co., Inc., Rahway, NJ, USA [MSD]) and Amit Bhaniani (MSD [UK] Limited, London, UK) for programming support. Editorial assistance was provided by Karyn Davis (MSD).

Data sharing: Data and code will be made to qualified scientific researchers with a specific purpose outlined in a proposal approved by Instituto Butantan. Requests will be evaluated for scientific validity within 6 months. Underlying code and complete deidentified patient data set will be shared after the researcher enters into standard data sharing agreement and the proposal is approved. Researchers must commit to transparency in publication. Requests for data must be sent to ensaiosclinicos@fundacaobutantan.org.

Instituto Butantan, São Paulo, Brazil sponsored the phase 3 trial with statistical analyses, data management, and assay support from MSD.

M.M., E.M.A, A.E-J., and G.A. are employees of MSD, and M.L.J. is an employee of MSD (UK) Limited, London, UK, all of whom may own stock or hold stock options in Merck & Co., Inc., Rahway, NJ, USA. E.N.C.B., M.A.R., J.A.M., and F.C.B. are employees of Instituto Butantan, a nonprofit public health institution of the State of São Paulo, Brazil. F.C.B. reports owning stock from Novartis.

About the Author

Ms. Barros is an epidemiologist manager leading epidemiologic and post-marketing studies on immunopreventable diseases and vaccines at Instituto Butantan, São Paulo, Brazil. Her area of interest includes developing epidemiologic studies on immunopreventable diseases and vaccine outcomes in the public health context.

References

1. Bhatt S, Gething PW, Brady OJ, Messina JP, Farlow AW, Moyes CL, et al. The global distribution and burden of dengue. Nature. 2013;496:504–7. https://doi.org/10.1038/nature12060
2. Stanaway JD, Shepard DS, Undurraga EA, Halasa YA, Coffeng LE, Brady OJ, et al. The global burden of dengue: an analysis from the Global Burden of Disease Study 2013. Lancet Infect Dis. 2016;16:712–23. https://doi.org/10.1016/S1473-3099(16)00026-8
3. Yang X, Quam MBM, Zhang T, Sang S. Global burden for dengue and the evolving pattern in the past 30 years. J Travel Med. 2021;28:taab146. https://doi.org/10.1093/jtm/taab146
4. Deng J, Zhang H, Wang Y, Liu Q, Du M, Yan W, et al. Global, regional, and national burden of dengue infection in children and adolescents: an analysis of the Global Burden of Disease Study 2021. EClinicalMedicine. 2024;78:102943. https://doi.org/10.1016/j.eclinm.2024.102943
5. Pan American Health Organization (PAHO). Dengue [cited 2025 Mar 28]. https://www3.paho.org/data/index.php/en/mnu-topics/indicadores-dengue-en.html
6. Paz-Bailey G, Adams LE, Deen J, Anderson KB, Katzelnick LC. Dengue. Lancet. 2024;403:667–82. https://doi.org/10.1016/S0140-6736(23)02576-X
7. Xu Z, Bambrick H, Frentiu FD, Devine G, Yakob L, Williams G, et al. Projecting the future of dengue under climate change scenarios: progress, uncertainties and research needs. PLoS Negl Trop Dis. 2020;14:e0008118. https://doi.org/10.1371/journal.pntd.0008118
8. Sansone NMS, Boschiero MN, Marson FAL. Dengue outbreaks in Brazil and Latin America: the new and continuing challenges. Int J Infect Dis. 2024;147:107192. https://doi.org/10.1016/j.ijid.2024.107192

9. Tapia-Conyer R, Betancourt-Cravioto M, Mendez-Galvan J. Dengue: an escalating public health problem in Latin America. Paediatr Int Child Health. 2012;32 Suppl 1:14–7. https://doi.org.10.1179/2046904712Z.00000000046
10. Brasil, Ministério da Saúde, Secretaria de Vigilância em Saúde. Monitoring of arboviruses and closing report of the Emergency Operations Committee (COE) Dengue and other Arboviruses 2024 [in Portuguese]. Bol Epidemiol (Porto Alegre). 2024;55 [cited 2026 Mar 12]. https://www.gov.br/saude/pt-br/centrais-de-conteudo/publicacoes/boletins/epidemiologicos/edicoes/2024/boletim-epidemiologico-volume-55-no-11.pdf
11. Pan American Health Organization. Dengue: analysis by country. 2024 [cited 2026 Mar 12]. https://www.paho.org/en/arbo-portal/dengue-data-and-analysis/dengue-analysis-country
12. Cardoso CW, Paploski IA, Kikuti M, Rodrigues MS, Silva MM, Campos GS, et al. Outbreak of exanthematous illness associated with Zika, chikungunya, and dengue viruses, Salvador, Brazil. Emerg Infect Dis. 2015;21:2274–6. https://doi.org/10.3201/eid2112.151167
13. Nunes MR, Faria NR, de Vasconcelos JM, Golding N, Kraemer MU, de Oliveira LF, et al. Emergence and potential for spread of chikungunya virus in Brazil. BMC Med. 2015;13:102. https://doi.org/10.1186/s12916-015-0348-x
14. de Souza WM, Ribeiro GS, de Lima STS, de Jesus R, Moreira FRR, Whittaker C, et al. Chikungunya: a decade of burden in the Americas. Lancet Reg Health Am. 2024;30:100673. https://doi.org/10.1016/j.lana.2023.100673
15. Faria NR, Azevedo RDSDS, Kraemer MUG, Souza R, Cunha MS, Hill SC, et al. Zika virus in the Americas: early epidemiological and genetic findings. Science. 2016;352:345–9. https://doi.org/10.1126/science.aaf5036
16. Campos GS, Bandeira AC, Sardi SI. Zika virus outbreak, Bahia, Brazil. Emerg Infect Dis. 2015;21:1885–6. https://doi.org/10.3201/eid2110.150847
17. Ministry of Health (Brazil). Brazil information system for notifiable diseases [cited 2026 Mar 12]. https://portalsinan.saude.gov.br
18. Silva MM, Rodrigues MS, Paploski IA, Kikuti M, Kasper AM, Cruz JS, et al. Accuracy of dengue reporting by national surveillance system, Brazil. Emerg Infect Dis. 2016;22:336–9. https://doi.org/10.3201/eid2202.150495
19. Sarti E, L'Azou M, Mercado M, Kuri P, Siqueira JB Jr, Solis E, et al. A comparative study on active and passive epidemiological surveillance for dengue in five countries of Latin America. Int J Infect Dis. 2016;44:44–9. https://doi.org/10.1016/j.ijid.2016.01.015
20. Gurgel-Gonçalves R, Oliveira WK, Croda J. The greatest dengue epidemic in Brazil: surveillance, prevention, and control. Rev Soc Bras Med Trop. 2024;57:e002032024. https://doi.org/10.1590/0037-8682-0113-2024
21. Kallás EG, Cintra MAT, Moreira JA, Patiño EG, Braga PE, Tenório JCV, et al. Live, attenuated, tetravalent Butantan-Dengue vaccine in children and adults. N Engl J Med. 2024;390:397–408. https://doi.org/10.1056/NEJMoa2301790
22. Nogueira ML, Cintra MAT, Moreira JA, Patiño EG, Braga PE, Tenório JCV, et al.; Phase 3 Butantan-DV Working Group. Efficacy and safety of Butantan-DV in participants aged 2–59 years through an extended follow-up: results from a double-blind, randomised, placebo-controlled, phase 3, multicentre trial in Brazil. Lancet Infect Dis. 2024;24:1234–44. https://doi.org/10.1016/S1473-3099(24)00376-1
23. Russell KL, Rupp RE, Morales-Ramirez JO, Diaz-Perez C, Andrews CP, Lee AW, et al. A phase I randomized, double-blind, placebo-controlled study to evaluate the safety, tolerability, and immunogenicity of a live-attenuated quadrivalent dengue vaccine in flavivirus-naïve and flavivirus-experienced healthy adults. Hum Vaccin Immunother. 2022;18:2046960. https://doi.org/10.1080/21645515.2022.2046960
24. Whiteman MC, Bogardus L, Giacone DG, Rubinstein LJ, Antonello JM, Sun D, et al. Virus reduction neutralization test: a single-cell imaging high-throughput virus neutralization assay for dengue. Am J Trop Med Hyg. 2018;99:1430–9. https://doi.org/10.4269/ajtmh.17-0948
25. Johnson BW, Russell BJ, Lanciotti RS. Serotype-specific detection of dengue viruses in a fourplex real-time reverse transcriptase PCR assay. J Clin Microbiol. 2005;43:4977–83. https://doi.org/10.1128/JCM.43.10.4977-4983.2005
26. Lanciotti RS, Kosoy OL, Laven JJ, Panella AJ, Velez JO, Lambert AJ, et al. Chikungunya virus in US travelers returning from India, 2006. Emerg Infect Dis. 2007;13:764–7. https://doi.org/10.3201/eid1305.070015
27. Lanciotti RS, Kosoy OL, Laven JJ, Velez JO, Lambert AJ, Johnson AJ, et al. Genetic and serologic properties of Zika virus associated with an epidemic, Yap State, Micronesia, 2007. Emerg Infect Dis. 2008;14:1232–9. https://doi.org/10.3201/eid1408.080287
28. Brasil. Ministério da Saúde. Secretaria de Vigilância em Saúde. Diretoria Técnica de Gestão. Dengue: diagnosis and clinical management: adult and child [in Portuguese]. Ministério da Saúde, Secretaria de Vigilância em Saúde, Diretoria Técnica de Gestão. 4th ed. Brasília (Brazil): Ministério da Saúde; 2013.
29. Ulm K. A simple method to calculate the confidence interval of a standardized mortality ratio (SMR). Am J Epidemiol. 1990;131:373–5. https://doi.org/10.1093/oxfordjournals.aje.a115507
30. Toan NT, Rossi S, Prisco G, Nante N, Viviani S. Dengue epidemiology in selected endemic countries: factors influencing expansion factors as estimates of underreporting. Trop Med Int Health. 2015;20:840–63. https://doi.org/10.1111/tmi.12498
31. Newcombe RG. Two-sided confidence intervals for the single proportion: comparison of seven methods. Stat Med. 1998;17:857–72. https://doi.org/10.1002/(SICI)1097-0258(19980430)17:8<857::AID-SIM777>3.0.CO;2-E
32. Brasil, Ministério da Saúde, Secretaria de Vigilância em Saúde. Death due to arboviruses in Brazil, 2008 to 2019 [in Portuguese]. Bol Epidemiol (Porto Alegre). 2020;51:1–28.
33. Brasil, Ministério da Saúde, Secretaria de Vigilância em Saúde. Monitoring of urban arbovirus cases transmitted by *Aedes* (dengue, chikungunya, and Zika), epidemiological weeks 01 to 50 [in Portuguese]. Bol Epidemiol (Porto Alegre). 2020;51:1-33.
34. Junior JBS, Massad E, Lobao-Neto A, Kastner R, Oliver L, Gallagher E. Epidemiology and costs of dengue in Brazil: a systematic literature review. Int J Infect Dis. 2022;122:521–8. https://doi.org/10.1016/j.ijid.2022.06.050
35. Hökerberg YHM, Kohn F, Souza TS, Passos SRL. Clinical profile of dengue in the elderly using surveillance data from two epidemics. Rev Soc Bras Med Trop. 2022;55:e0290. https://doi.org/10.1590/0037-8682-0290-2021
36. Macias AE, Werneck GL, Castro R, Mascareñas C, Coudeville L, Morley D, et al. Mortality among hospitalized dengue patients with comorbidities in Mexico, Brazil, and Colombia. Am J Trop Med Hyg. 2021;105:102–9. https://doi.org/10.4269/ajtmh.20-1163
37. Santana LMR, Baquero OS, Maeda AY, Nogueira JS, Chiaravalloti Neto F. Spatio-temporal dynamics of

dengue-related deaths and associated factors. Rev Inst Med Trop São Paulo. 2022;64:e30. https://doi.org/10.1590/s1678-9946202264030
38. Sousa SC, Silva TAMD, Soares AN, Carneiro M, Barbosa DS, Bezerra JMT. Factors associated with deaths from dengue in a city in a metropolitan region in southeastern Brazil: a case-control study. Rev Soc Bras Med Trop. 2022;55:e0043-2022. https://doi.org/10.1590/0037-8682-0043-2022
39. Werneck GL, Macias AE, Mascarenas C, Coudeville L, Morley D, Recamier V, et al. Comorbidities increase in-hospital mortality in dengue patients in Brazil. Mem Inst Oswaldo Cruz. 2018;113:e180082. https://doi.org/10.1590/0074-02760180082
40. Queiroga AS, Barbosa DAM, Campos TL, Schwarzbold AV, Siqueira AM, Salvato RS, et al. Severe dengue-related deaths in the elderly population soared in Southern Brazil in 2024. IJID Reg. 2025;14:100577. https://doi.org/10.1016/j.ijregi.2025.100577
41. Burattini MN, Lopez LF, Coutinho FA, Siqueira JB Jr, Homsani S, Sarti E, et al. Age and regional differences in clinical presentation and risk of hospitalization for dengue in Brazil, 2000–2014. Clinics (Sao Paulo). 2016;71:455–63. https://doi.org/10.6061/clinics/2016(08)08
42. Villar L, Dayan GH, Arredondo-García JL, Rivera DM, Cunha R, Deseda C, et al.; CYD15 Study Group. Efficacy of a tetravalent dengue vaccine in children in Latin America. N Engl J Med. 2015;372:113–23. https://doi.org/10.1056/NEJMoa1411037
43. L'Azou M, Moureau A, Sarti E, Nealon J, Zambrano B, Wartel TA, et al.; CYD14 Primary Study Group; CYD15 Primary Study Group. Symptomatic dengue in children in 10 Asian and Latin American countries. N Engl J Med. 2016;374:1155–66. https://doi.org/10.1056/NEJMoa1503877
44. Biswal S, Reynales H, Saez-Llorens X, Lopez P, Borja-Tabora C, Kosalaraksa P, et al.; TIDES Study Group. Efficacy of a tetravalent dengue vaccine in healthy children and adolescents. N Engl J Med. 2019;381:2009–19. https://doi.org/10.1056/NEJMoa1903869
45. Kastner R, López-Medina E, Sirivichayakul C, Biswal S, Escudero I, Folschweiller N, et al. The burden of dengue in Latin America and Asia: Epidemiological data over 57 months of follow-up in a phase 3 trial. Poster presented at: The American Society of Tropical Medicine and Hygiene Annual Meeting; November 13–17, 2024; New Orleans, Louisiana, USA.
46. Tricou V, Yu D, Reynales H, Biswal S, Saez-Llorens X, Sirivichayakul C, et al. Long-term efficacy and safety of a tetravalent dengue vaccine (TAK-003): 4.5-year results from a phase 3, randomised, double-blind, placebo-controlled trial. Lancet Glob Health. 2024;12:e257–70. https://doi.org/10.1016/S2214-109X(23)00522-3
47. Brasil. Ministério da Saúde. Health surveillance guide. 4th edition. Brasília: Ministério da Saúde; 2019.

Address for correspondence: Maïna L'Azou Jackson, Epidemiology, MSD (UK) Ltd, 120 Moorgate, London EC2M 6UR, UK; email: maina.lazou.jackson@msd.com

etymologia revisited

Originally published in November 2021

Prototheca

[pro"to-the'kə]

From the Greek *proto-* (first) + *thēkē* (sheath), *Prototheca* is a genus of variably shaped spherical cells of achloric algae in the family *Chlorellaceae*. Wilhelm Krüger, a German expert in plant physiology and sugar production, reported *Prototheca* microorganisms in 1894, shortly after spending 7 years in Java studying sugarcane. He isolated *Prototheca* species from the sap of 3 tree species. Krüger named these organisms as *P. moriformis* and *P. zopfii*, the second name as a tribute to Friedrich Wilhelm Zopf, a renowned botanist, mycologist, and lichenologist.

References:

1. Davies RR, Spencer H, Wakelin PO. A case of human protothecosis. Trans R Soc Trop Med Hyg. 1964;58:448–51. https://doi.org/10.1016/0035-9203(64)90094-X
2. Dorland's illustrated medical dictionary. 32nd ed. Philadelphia: Elsevier Saunders; 2012.
3. Kano R. Emergence of fungal-like organisms: Prototheca. Mycopathologia. 2020;185:747–54. https://doi.org/10.1007/s11046-019-00365-4
4. Krüger W. Brief characteristics of some lower organisms in the sap flow of deciduous trees [in German]. Hedwigia. 1894;33:241–66.
5. Todd JR, Matsumoto T, Ueno R, Murugaiyan J, Britten A, King JW, et al. Medical phycology 2017. Med Mycol. 2018;56(suppl 1):S188–204. https://doi.org/10.1093/mmy/myx162

https://wwwnc.cdc.gov/eid/article/27/11/21-1554_article

Transmissibility and Disease Progression of *Asymptomatic Mycobacterium* tuberculosis Infection, Lima, Peru

Ruitong Wang, Chuan-Chin Huang, Mercedes C. Becerra, Roger I. Calderon, Carmen C. Contreras, Jerome T. Galea, Judith Jimenez, Leonid Lecca, Rosa M. Yataco, Zibiao Zhang, Megan B. Murray

Estimating the transmissibility of asymptomatic *Mycobacterium tuberculosis* infection can clarify its contribution to tuberculosis (TB) spread. We conducted a prospective cohort study in Lima, Peru, enrolling index TB patients and their household contacts (HHCs) and classifying patients by the presence of symptoms including cough, night sweats, weight loss, or fever. We followed HHCs with serial tuberculin skin testing and clinical evaluations. Among 4,296 child HHCs, adjusted estimates for baseline infection (prevalence ratio 0.62 [95% CI 0.37–1.03]), incident infection at 6 months (hazard ratio (aHR) 0.63 [95% CI 0.27–1.49]), and TB disease during 1 year of follow-up (aHR 0.74 [95% CI 0.35–1.56]) were all consistent with lower risk for infection and disease progression among HHCs of asymptomatic compared with symptomatic index patients. Although asymptomatic infections may be less transmissible than symptomatic infections, the high prevalence of asymptomatic patients in national surveys suggest that they may contribute substantially to transmission.

Tuberculosis (TB) remains a global health concern, with an estimated 10.8 million persons falling ill in 2024 (*1*). National TB prevalence surveys show that a large proportion of persons with bacteriologically confirmed *Mycobacterium tuberculosis* infection do not report symptoms during screening (*2*). This group is considered to have subclinical TB, which the World Health Organization (WHO) terms asymptomatic TB (*3*). Traditional TB control strategies focus on symptomatic persons seeking care at healthcare facilities or on screening algorithms that initiate testing among those who report symptoms (*4*). Asymptomatic patients and those with mild or nonspecific symptoms that are not recognized during symptom-based screening (i.e., minimally symptomatic TB) (*5*) are often missed and may contribute to transmission.

Estimating the transmissibility of asymptomatic TB may clarify its contribution to TB transmission. Although studies suggest that asymptomatic TB can be transmitted (*6*,*7*), it remains unclear how its infectiousness and potential for disease progression compares with symptomatic TB. Most evidence comes from national prevalence surveys that compared infection prevalence among household contacts (HHCs) of symptomatic and asymptomatic index patients but did not assess incident infection or incident disease (*8*,*9*).

Using data from a longitudinal cohort of TB index patients and their HHCs in Lima, Peru, we assessed the relative transmissibility of TB and risk for disease progression after exposure to TB patients who did not report symptoms when they tested positive for *M. tuberculosis*. We compared infection prevalence at enrollment among HHCs exposed to asymptomatic versus symptomatic index patients as a proxy for baseline transmission and evaluated incident infection at 6 and 12 months to assess ongoing transmission risk. We then compared 12-month disease incidence to estimate progression potential and examined

Author affiliations: Harvard T.H. Chan School of Public Health, Boston, Massachusetts, USA (R. Wang, M.B. Murray); Harvard Medical School, Boston (C.-C. Huang, M.C. Becerra, L. Lecca, M.B. Murray); Brigham and Women's Hospital, Boston (C.-C. Huang, Z. Zhang, M.B. Murray); Advanced Research and Health, Lima, Peru (R.I. Calderon); Universidad de San Martin de Porres, Lima (R.I. Calderon); Partners In Health—Socios En Salud Sucursal Peru, Lima (C.C. Contreras, J. Jimenez, L. Lecca, R.M. Yataco); University of South Florida, Tampa, Florida, USA (J.T. Galea)

DOI: https://doi.org/10.3201/eid3104.251947

transmission risk factors among asymptomatic index patients. Together, those analyses provide empirical estimates of the transmissibility and disease progression potential of asymptomatic TB and clarify its contribution to overall TB transmission.

Materials and Methods

Study Design and Participants

We conducted a prospective cohort study among HHCs of index TB patients in Lima, Peru, during September 2009–September 2012. We recruited patients >15 years of age with newly diagnosed pulmonary TB from 106 district health centers in Lima. TB diagnosis required either microbiological evidence (positive sputum smear or culture) or a clinician's judgment based on chest radiograph, clinical manifestation, or both. We collected demographic and clinical data for index patients, including age, sex, employment status, symptom status, HIV status, smoking, alcohol use, diabetes, socioeconomic status, and sputum smear results.

Within 2 weeks of index patient enrollment, we identified and enrolled HHCs and collected data on age, sex, HIV status, smoking, alcohol use, diabetes, bacille Calmette–Guérin (BCG) vaccination status, and body mass index (BMI). We assessed baseline *M. tuberculosis* infection using the tuberculin skin test (TST) among HHCs without a prior positive TST or TB disease. We considered a TST positive at ≥10 mm induration in HIV-uninfected persons and ≥5 mm in those with HIV. We retested HHCs with a prior negative TST at 6 and 12 months. We followed up with HHCs at 2, 6, and 12 months to assess TB symptoms and document interval diagnoses; we referred symptomatic participants for clinical evaluation and reviewed medical records to identify TB diagnoses during follow-up. Additional study design details have been published elsewhere (*10*).

Ethics committees at Harvard University and at the National Institute of Health in Peru approved the study. All study participants or their guardians provided written informed consent, and children <18 years old provided assent.

Exposure and Outcomes

We stratified index patients by the presence of baseline symptoms included in the WHO 4-symptom screen (W4SS) (*11,12*): cough, night sweats, weight loss, and fever. We evaluated 4 outcomes: baseline TB infection among HHCs; incident infection over 6 months among those uninfected at baseline; incident infection over 12 months among those uninfected at baseline; and incident TB disease over 12 months among HHCs without coprevalent TB at baseline.

We classified HHCs as infected at baseline if they had TB disease or a positive TST at enrollment. To reduce misclassification of community-acquired infection as household transmission, we excluded HHCs with a prior history of TB disease or a positive TST from the analysis. We considered HHCs to have incident TB infection if they were uninfected at baseline and subsequently had a positive TST or experienced secondary TB disease. We considered HHCs to have incident TB disease if they received a diagnosis of TB disease at any time from 2 weeks after enrollment to the end of follow-up.

Statistical Analysis

We included only index patients with microbiologically confirmed TB. To assess the association between index patient symptom status and baseline HHC infection, we used generalized estimating equations with modified Poisson regression, specifying an exchangeable correlation structure to account for clustering within households. We estimated prevalence ratios (PR) and 95% CIs. We evaluated associations with incident TB infection at 6 and 12 months and incident TB disease at 12 months using Cox frailty models and reported hazard ratio (HRs) and 95% CIs.

We first fitted univariable models, then multivariable models, adjusting for prespecified confounders and predictors of TB infection or disease. Covariates included index patient age group, HIV status, smoking, alcohol use, diabetes, and household socioeconomic status. Additional predictors of HHC infection included index patient sex and employment status and HHC sex, age group, HIV status, diabetes status, BCG vaccination status, smoking and alcohol use, and BMI category (Appendix Table 1, https://wwwnc.cdc.gov/EID/article/32/4/25-1947-App1.pdf). A second multivariable model retained confounders and variables with $p<0.10$ in the initial multivariable analysis. Because sputum smear status might lie on the causal pathway between disease severity and transmission, we did not include it in regression models.

For analyses of TB infection, we restricted the primary sample to child HHCs ≤15 years of age because infection in that group is more consistent with recent household transmission. Sensitivity analysis included HHCs of all ages. Analyses of incident TB disease included HHCs of all ages, given the relative rarity of disease compared with infection. We conducted complete-case analyses, excluding 13% of observations (Appendix Table 2), and assessed robustness using

multiple imputation. Finally, we examined specific symptom patterns by classifying index patients into 4 groups: asymptomatic; cough only; no cough but ≥1 of night sweats, weight loss, or fever; and cough plus ≥1 of those symptoms. We evaluated associations between symptom patterns and baseline infection and 6-month incident infection among child HHCs.

We next explored factors associated with transmission or disease progression from asymptomatic index patients. For that exploratory analysis, we restricted the sample to HHCs of asymptomatic index cases. We estimated PRs for baseline TB infection and odds ratios (ORs) for incident TB infection at 6 months and incident TB disease at 12 months, to identify potential associated factors. Given the limited sample size in the subgroup, we limited analyses to univariable models examining associations between characteristics of asymptomatic index patients and each outcome among their HHCs.

Results

We identified 3,109 microbiologically confirmed *M. tuberculosis*–infected index patients with known baseline symptom status (Appendix Table 3), including 113 asymptomatic and 2,996 symptomatic patients. Asymptomatic patients were significantly more likely to be smear-negative (OR 3.15 [95% CI 2.14–4.65]; p<0.001).

We enrolled 12,230 HHCs (Appendix Table 4), of whom 4,296 (35.1%) were ≤15 years of age (Table 1). Most (80.9%) had a BCG scar; 62.4% were ≤30 years of age, 57.8% had normal BMI, 6.0% were current smokers, and 25.7% were current drinkers.

Baseline Infection

Among child HHCs, 23.0% exposed to symptomatic index patients and 15.0% exposed to asymptomatic index patients were TST-positive at baseline (Table 2). Exposure to asymptomatic index patients was associated with lower baseline infection (crude PR 0.60 [95% CI 0.36–1.01]). Adjusted PR was 0.62 (95% CI 0.37–1.03) for model A, in which we adjusted for age, sex, HIV status, alcohol consumption status, BCG vaccination, and BMI category, and 0.61 (95% CI 0.36–1.03) in model B, in which we excluded sex and alcohol consumption from the adjusted variables. When all HHCs were included, the association was attenuated (adjusted PR 0.94 [95% CI 0.79–1.11]) (Appendix Table 5). Multiple imputation yielded similar estimates, with lower prevalence among child HHCs (adjusted PR 0.58 [95% CI 0.35–0.95]) and comparable results among all HHCs (adjusted PR 0.88 [95% CI 0.74–1.04]) (Appendix Table 6).

Table 1. Characteristics of household contacts ≤15 years of age by symptom status of tuberculosis index patients in study of transmissibility of asymptomatic *Mycobacterium tuberculosis* infection, Lima, Peru*

Variable	No. (%) contacts		
	Total	Symptomatic index patient	Asymptomatic index patient
Age group, y, n = 4,296			
0–4	1,558 (36.3)	1,502 (36.1)	56 (42.4)
5–9	1,312 (30.5)	1,272 (30.5)	40 (30.3)
10–15	1,426 (33.2)	1,390 (33.4)	36 (27.3)
Sex, n = 4,296			
M	2,158 (50.2)	2,091 (50.2)	67 (50.8)
F	2,138 (49.8)	2,073 (49.8)	65 (49.2)
HIV status, n = 4,247			
Negative	4,243 (99.9)	4,115 (99.9)	128 (100)
Positive	4 (0.1)	4 (0.1)	0
BCG scar, n = 4,296			
No	820 (19.1)	801 (19.2)	19 (14.4)
Yes	3,476 (80.9)	3,363 (80.8)	113 (85.6)
Diabetes, n = 4,283			
No	4,281 (99.9)	4,149 (99.9)	132 (100)
Yes	2 (0.1)	2 (0.1)	0
Smoking, n = 4,294			
Nonsmoker	4,288 (99.9)	4,156 (99.9)	132 (100)
Smoker	6 (0.1)	6 (0.1)	0
Alcohol consumption, n = 4,293			
Nondrinker	4,257 (99.2)	4,126 (99.2)	131 (99.2)
Drinker	36 (0.8)	35 (0.8)	1 (0.8)
BMI category, n = 4,253†			
Normal	3,420 (80.4)	3,316 (80.4)	104 (79.4)
Underweight	116 (2.7)	109 (2.6)	7 (5.3)
Overweight	717 (16.9)	697 (16.9)	20 (15.3)

*BCG, bacille Calmette–Guérin; BMI, body mass index.
†For participants >19 years of age, we defined underweight as BMI <18.5 kg/m^2, normal as 18.5–24.9 kg/m^2, and overweight as BMI ≥25 kg/m^2. For participants ≤19 y, we defined status using World Health Organization BMI-for-age z-scores: underweight z-score <–2, normal z-score –2 to 2, and overweight z-score >2.

Table 2. Risk for *Mycobacterium tuberculosis* infection at baseline among household contacts of tuberculosis index patients in study of transmissibility of asymptomatic *M. tuberculosis* infection, Lima, Peru*

			Univariate model		Multivariate model A†		Multivariate model B‡	
Symptom status	No. contacts	No. (%) baseline infection	Crude PR (95% CI)	p value	Adjusted PR (95% CI)	p value	Adjusted PR (95% CI)	p value
Symptomatic	3,586	824 (22.98)	Referent		Referent		Referent	
Asymptomatic	113	17 (15.04)	0.60 (0.36–1.01)	0.06	0.62 (0.37– 1.03)	0.07	0.61 (0.36–1.03)	0.06

*Household contacts are children <15 years of age. PR, prevalence ratio.
†Multivariate model A was adjusted for the following characteristics of index patients: age, sex, HIV status, smoking status, alcohol consumption status, socioeconomic status, employment status, and diabetes; and the following characteristics of household contacts: age, sex, smoking status, alcohol consumption status, bacille Calmette–Guérin vaccination, and body mass index category. Diabetes and HIV status of household contacts were excluded due to sparse data in some of its categories, which led to unstable estimates and nonestimable coefficients in the model.
‡Multivariate model B did not adjust for employment status and sex of index patients.

Incident Infection

At 6 months, 14.5% of child HHCs exposed to symptomatic index patients and 10.3% exposed to asymptomatic index patients tested positive by TST (Table 3). Exposure to asymptomatic index patients was associated with lower hazard of infection (crude HR 0.63 [95% CI 0.27–1.49], adjusted HR 0.62 [95% CI 0.26–1.51] in both multivariable models). Estimates were similar when all HHCs were included (adjusted HR 0.78 [95% CI 0.50–1.20]) (Appendix Table 7).

At 12 months, infection occurred in 21.1% of child HHCs exposed to symptomatic index patients and 16.2% of those exposed to asymptomatic index patients, (Appendix Table 8). Hazard ratios remained lower for asymptomatic exposure among child HHCs (adjusted HR 0.73 [95% CI 0.35–1.50]) and all HHCs (adjusted HR 0.80 [95% CI 0.55–1.17]) (Appendix Table 9). Multiple imputation analyses were directionally consistent (Appendix Table 10).

Incident Disease

Within 12 months, 3.0% of HHCs exposed to symptomatic index patients and 2.4% exposed to asymptomatic index patients experienced TB disease (Table 4). HRs again favored lower risk with asymptomatic exposure (crude HR 0.74 [95% CI 0.35–1.56]; adjusted HR 0.80 [95% CI 0.38–1.67] for model A, 0.81 [95% CI 0.39–1.69] for model B), with similar findings under multiple imputation (Appendix Table 10).

Symptom Patterns and Infection Risk among Child HHCs

Baseline TST positivity among child HHCs was 15.0% for asymptomatic exposure, 12.4% for noncough symptoms only, 23.0% for cough only, and 24.0% for cough plus other symptoms (Table 5). Infection risk among children exposed to asymptomatic index patients was similar to risk among those exposed to index patients without cough but with other symptoms (adjusted PR 0.94–0.95 across models). At 6 months, infection risk was higher among children exposed to index patients with noncough symptoms only (adjusted HR 1.27–1.31), and larger still for cough only (adjusted HR 1.84) and cough plus other symptoms (adjusted HR 1.59–1.66) (Appendix Table 11).

Cough Duration and Infection Risk

Among child HHCs, longer cough duration in symptomatic index patients was associated with progressively higher baseline infection compared with asymptomatic exposure. Adjusted PRs increased as cough duration increased (Appendix Table 13). PR was 1.28 (95% CI 0.74–2.19) for 0–13 days up to PR 1.76 (95% CI 1.04–2.98) for ≥56 days, consistent with a dose-response pattern. Adjusted hazard ratios for incident infection and disease similarly increased with longer cough duration.

Transmission Potential among Asymptomatic Index Patients

Among asymptomatic index patients, HIV infection was associated with lower baseline infection among HHCs (PR 0.54 [95% CI 0.32–0.92]) (Appendix Table

Table 3. Hazard ratios of *Mycobacterium tuberculosis* infection at 6-month follow-up among initially uninfected household contacts of tuberculosis patients in study of transmissibility of asymptomatic *M. tuberculosis* infection, Lima, Peru*

			Univariate model		Multivariate model A†		Multivariate model B‡	
Symptom status	No. contacts	No. (%) incident infection	Crude HR (95% CI)	p value	Adjusted HR (95% CI)	p value	Adjusted HR (95% CI)	p value
Symptomatic	2,204	320 (14.52)	Referent		Referent		Referent	
Asymptomatic	68	7 (10.29)	0.63 (0.27–1.49)	0.29	0.62 (0.26–1.51)	0.29	0.62 (0.26–1.51)	0.30

*Household contacts are children <15 years of age. HR, hazard ratio.
†Multivariate model A was adjusted for the following characteristics of index patients: age, sex, HIV status, smoking status, alcohol consumption status, socioeconomic status, employment status, and diabetes; and the following characteristics of household contacts: age, sex, HIV status, alcohol consumption status, bacille Calmette–Guérin vaccination, and body mass index category. Diabetes and smoking status of household contacts excluded due to sparse data in some of its categories, which led to unstable hazard ratio estimates and nonestimable coefficients in the Cox model.
‡Multivariate model B did not adjust for sex and alcohol consumption of household contact.

Table 4. Hazard ratios of incident tuberculosis disease among all household contacts of index patients by symptom status in study of transmissibility of asymptomatic *M. tuberculosis* infection, Lima, Peru*

		No. (%)	Univariate model		Multivariate model A†		Multivariate model B	
Symptom status	No. contacts	incident disease	Crude HR (95% CI)	p value	Adjusted HR (95% CI)	p value	Adjusted HR (95% CI)	p value
Symptomatic	10,375	313 (3.02)	Referent		Referent		Referent	
Asymptomatic	410	10 (2.44)	0.74 (0.35–1.56)	0.43	0.80 (0.38–1.67)	0.55	0.81 (0.39–1.69)	0.57

* Household contacts are children <15 years of age. HR, hazard ratio.
†Multivariate model A was adjusted for the following characteristics of index patients: age, sex, HIV status, smoking status, alcohol consumption status socioeconomic status, employment status, and diabetes; and the following characteristics of household contacts: age, sex, HIV status, smoking status, alcohol consumption status, diabetes, bacille Calmette–Guérin vaccination, and body mass index category.
‡Multivariate model B did not adjust for employment status of index patients and sex, smoking status, and alcohol consumption of household contact.

12). At 6-month follow-up, we observed higher odds of infection among HHCs exposed to asymptomatic patients 46–60 years of age (OR 3.00 [95% CI 1.41–6.37]) and with high socioeconomic status (OR 4.30 [95% CI 1.49–12.40]). We observed lower odds among HHCs of asymptomatic patients with HIV (OR 0.37 [95% CI 0.19–0.74]) and those ≥61 years of age (OR 0.40 [95% CI 0.19–0.89]) (Table 6). We observed no significant associations for incident disease (Appendix Table 14).

Discussion

In this study, baseline and incident infection among HHCs were lower after exposure to asymptomatic versus symptomatic index patients. Incident disease estimates were also lower, although 95% CIs were wide and included the null (no effect). Because we recruited index patients from local clinics, most were experiencing symptoms when they sought care, limiting the number of asymptomatic cases. Given the high prevalence of asymptomatic TB reported in national surveys, our findings are consistent with the possibility that asymptomatic TB contributes meaningfully to transmission, although the magnitude remains uncertain.

Our infection estimates are broadly consistent with those from previous studies. A 2007 survey in Vietnam found that child HHCs exposed to symptomatic index patients had more than twice the risk for TST positivity compared with those exposed to asymptomatic patients (*9*). In Brazil, a prospective cohort reported 1.5-fold higher odds of TST conversion among contacts of patients with prolonged cough (>4 weeks) (*13*). Those effects were somewhat stronger than ours, possibly reflecting differences in infection definitions (e.g., TST cutoffs) and symptom classification. A pooled analysis from Vietnam, Bangladesh, and the Philippines reported an OR of 1.2 for infection (*8*), closely aligning with our converted estimate. Those studies were conducted in settings dominated by lineages 1 and 2, whereas lineage 4 predominates in Peru (*14*). Because *M. tuberculosis* lineages differ in host immune response, disease severity, and transmissibility (*15*), lineage distribution might influence relative transmission from asymptomatic versus symptomatic patients. Molecular epidemiologic data also support transmission from asymptomatic patients; whole-genome sequencing and phylogenetic modeling suggested that 514 patients transmitted TB before symptom onset (*16*).

Several mechanisms may explain transmission from asymptomatic patients. First, aerosolization of *M. tuberculosis* bacilli is not limited to coughing. Exhaled *M. tuberculosis* has been detected in the absence

Table 5. Risk for *Mycobacterium tuberculosis* infection at baseline among household contacts of tuberculosis index patients by symptom pattern in study of transmissibility of asymptomatic *M. tuberculosis* infection, Lima, Peru*

		No. (%)	Univariate model		Multivariate model A‡		Multivariate model B§	
Symptom status†	No. contacts	baseline infection	Crude PR (95% CI)	p value	Adjusted PR (95% CI)	p value	Adjusted PR (95% CI)	p value
Asymptomatic	113	17 (15.04)	Referent		Referent		Referent	
Cough only	296	68 (22.97)	1.64 (0.92–2.90)	0.09	1.59 (0.90–2.80)	0.11	1.61 (0.92–2.82)	0.10
Noncough symptoms only	266	33 (12.41)	0.94 (0.51–1.73)	0.83	0.94 (0.51–1.72)	0.83	0.95 (0.52–1.75)	0.87
Cough and any noncough symptoms	2,964	712 (24.02)	1.73 (1.03–2.90)	0.04	1.67 (1.00–2.78)	0.05	1.68 (1.01–2.79)	0.05

*Household contacts are children <15 years of age. PR, prevalence ratio.
†Noncough symptoms include fever, weight loss and night sweats.
‡Multivariate model A was adjusted for the following characteristics of index patients: age, sex, HIV status, smoking status, alcohol consumption status, socioeconomic status, employment status, and diabetes; and the following characteristics of household contacts: age, sex, smoking status, alcohol consumption status, bacille Calmette–Guérin vaccination, and body mass index category. Diabetes and HIV status of household contacts excluded due to sparse data in some of its categories, which led to unstable estimates and nonestimable coefficients in the model.
§Multivariate model B did not adjust for employment status of index patients and sex, bacille Calmette–Guérin scar, alcohol consumption, and body mass index category of household contacts.

Table 6. Association between characteristics of asymptomatic index patients and risk for *Mycobacterium tuberculosis* infection at 6-month follow-up of all household contacts in study of transmissibility of asymptomatic *M. tuberculosis*, Lima, Peru*

Characteristic	No. (%) uninfected contacts	No. (%) infected contacts	Odds ratio (95%CI)	p value
Age group, y, n = 230				
16–30	92 (50.5)	26 (54.2)	Referent	Referent
31–45	20 (11.0)	6 (12.5)	1.08 (0.44–2.68)	0.87
46–60	12 (6.59)	10 (20.8)	3.00 (1.41–6.37)	0.004
≥61	58 (31.9)	6 (12.5)	0.40 (0.19–0.89)	0.02
Sex, n = 230				
M	143 (78.6)	42 (87.5)	Referent	Referent
F	39 (21.4)	6 (12.5)	0.48 (0.17–1.37)	0.17
HIV status, n = 230				
Negative	131 (72.0)	42 (87.5)	Referent	Referent
Positive	51 (28.0)	6 (12.5)	0.37 (0.19–0.74)	0.005
Smoking status, n = 230				
Nonsmoker	171 (94.5)	45 (93.8)	Referent	Referent
Smoker	10 (5.52)	3 (6.25)	1.02 (0.40–2.60)	0.85
SES, n = 222†				
Low	58 (32.6)	10 (22.7)	Referent	Referent
Medium	105 (59.0)	23 (52.3)	1.36 (0.61–3.03)	0.46
High	15 (8.43)	11 (25.0)	4.30 (1.49–12.4)	0.007
Employment status, n = 228				
Stay at home	121 (67.2)	37 (77.1)	Referent	Referent
Work outside	59 (32.8)	11 (22.9)	0.54 (0.26–1.14)	0.11
Alcohol consumption, n = 208				
Drinker	41 (24.8)	17 (39.5)	Referent	Referent
Nondrinker	124 (75.2)	26 (60.5)	0.53 (0.27–1.03)	0.06
Diabetes, n = 230				
No	179 (98.4)	47 (97.9)	Referent	Referent
Yes	3 (1.65)	1 (2.08)	1.21 (0.12–11.9)	0.87

*Results of univariate analysis. SES, socioeconomic status.
†We created a continuous variable to capture summarize household-level socioeconomic status by including variables on housing quality, water supply and sanitation in a principal component analysis. The continuous SES score was categorized into tertiles corresponding to relative low, middle, and upper SES.

of cough (*6*,*17*); 1 study estimated that tidal breathing accounted for 93% of daily aerosolized *M. tuberculosis* (*7*), although participants were symptomatic. Second, some patients classified as asymptomatic may experience nonspecific symptoms they consider normal and therefore do not report. In Lima, chronic cough related to air pollution may reduce reporting of symptom changes; in 2011–2014, average concentration of particulate matter with a diameter <2.5 μm ($PM_{2.5}$) levels were approximately twice the then-current WHO annual guideline of 10 μg/m^3 (*18*). Such misattribution could result in underreporting and misclassification of symptomatic patients as asymptomatic, inflating observed transmission risk. Similar misclassification could arise from smoking-related cough or seasonal respiratory symptoms (*19*,*20*).

We classified TB patients on the basis of self-reported symptoms at the time patients sought care, a process shaped by individual interpretation, stigma, timing of assessment, and interview practices (*21*). Although widely used in clinical settings, dichotomizing symptom status is increasingly recognized as imprecise and lacking clear biologic validity as a marker of disease severity (*21*,*22*).

Although they are not designed to estimate population-level contribution of asymptomatic TB, national prevalence surveys and meta-analyses consistently report that 50%–60% of bacteriologically confirmed cases are asymptomatic; some analyses suggested even higher proportions after accounting for diagnostic misclassification (*2*,*23*–*25*). If a conservative estimate of 60% asymptomatic disease is considered alongside our adjusted hazard ratio of 0.6 for incident infection among child HHCs, and if that hazard ratio reflects proportional differences in per-unit-time infectiousness, then asymptomatic patients could account for a substantial share of transmission, potentially approaching one half. That interpretation assumes comparable exposure duration and minimal unmeasured confounding and should be viewed as an illustrative extrapolation rather than a formal transmission model.

Our estimates align with modeling studies attributing a large fraction of TB transmission to asymptomatic or subclinical disease. One analysis of 14 high-burden countries estimated that 68% of transmission arose from asymptomatic cases (*6*), and another projected that subclinical patients accounted for 50%–62% of transmission over 5 years across multiple countries in Asia (*26*). Those findings consistently suggest the limits of symptom-based screening. Passive case finding, or algorithms that trigger

testing only after symptoms appear, inevitably miss large numbers of infectious persons. By quantifying the transmissibility of asymptomatic patients, our study adds to evidence that symptom-independent approaches are needed to improve early detection, reduce transmission, and strengthen TB control.

A limitation of our study is that the small number of asymptomatic TB patients in our sample limits our analysis power and constrains the strength of inference. Second, we cannot rule out the possibility of symptom status misclassification from underreporting. Third, within the high-transmission setting in Lima, some HHCs may have acquired TB infection in the community rather than the household. Such misclassification of the source of infection is likely nondifferential to the symptom status of index patients, which would bias the relative transmissibility of asymptomatic index patients toward the null result of no effect. To address that possibility, we focused on child HHCs, for whom recent household transmission data are more consistent. We excluded participants with a history of positive TST or TB disease; baseline TST positivity could be influenced by cumulative exposure and is therefore an imperfect proxy for transmissibility from index patients. We were not able to directly measure the duration of exposure between HHCs and index patients. If asymptomatic TB patients received diagnosis earlier in the course of disease (*27*), their HHCs may have experienced a shorter period of exposure before diagnosis. Our finding that longer reported coughing duration was associated with higher risks of infection and disease among HHCs underscores the importance of cumulative exposure over time. Those results support the interpretation that part of the lower risk observed among contacts of asymptomatic patients reflects reduced cumulative infectious exposure rather than differences in intrinsic infectiousness per unit time. At the same time, because symptom duration is a proxy for total exposure and we were not able to directly incorporate exposure time into our primary models, we cannot exclude the possibility that asymptomatic TB may also be less infectious per unit time than symptomatic disease. Our findings, therefore, reflect differences in cumulative transmission risk; uncertainty remains about the contribution of biologic infectiousness per unit time. Furthermore, prior BCG vaccination might contribute to the false-positive TST reactions, particularly in young children (*28*). In Peru, BCG vaccination is administered at birth; evidence suggests that vaccination in infancy has limited effect on TST interpretation (*29*). We used a cutoff of 10 mm, even for children <5 years of age; we adjusted for BCG vaccination status in all models to reduce potential confounding. Last, because our study was a large prospective cohort in Peru, the ability to generalize our results is limited, particularly to settings with low TB incidence and different dominant lineages.

In conclusion, our findings are consistent with lower infectiousness and lower risk for disease progression among HHCs exposed to asymptomatic TB patients than for those exposed to symptomatic patients. Given the high prevalence of asymptomatic TB reported in national surveys, our results highlight the limitations of symptom-triggered testing within current TB screening algorithms and are consistent with the potential value of symptom-independent approaches to improve early detection and reduce transmission.

Acknowledgments

We thank the patients and their families, and the healthcare personnel at the 106 participating health centers in Lima, Peru.

About the Author

Miss Wang is a second-year master's student in the Department of Global Health and Population at the Harvard T.H. Chan School of Public Health. Her primary research interests include tuberculosis epidemiology, infectious disease modeling, and the social determinants of health.

References

1. World Health Organization. Global tuberculosis report 2024 [cited 2025 Oct 15]. https://iris.who.int/handle/10665/379339
2. Frascella B, Richards AS, Sossen B, Emery JC, Odone A, Law I, et al. Subclinical tuberculosis disease—a review and analysis of prevalence surveys to inform definitions, burden, associations, and screening methodology. Clin Infect Dis. 2021;73:e830–41. https://doi.org/10.1093/cid/ciaa1402
3. World Health Organization. Report of the WHO consultation on asymptomatic tuberculosis. Geneva: The Organization; 2025.
4. World Health Organization. Report of the WHO consultation on systematic screening for tuberculosis, Geneva, Switzerland, 16–18 October 2024 [cited 2025 Oct 15]. https://iris.who.int/items/4aab6cc2-8367-4b71-92a1-e734b787dc18
5. Coussens AK, Zaidi SMA, Allwood BW, Dewan PK, Gray G, Kohli M, et al.; International Consensus for Early TB (ICE-TB) group. Classification of early tuberculosis states to guide research for improved care and prevention: an international Delphi consensus exercise. Lancet Respir Med. 2024; 12:484–98. https://doi.org/10.1016/S2213-2600(24)00028-6
6. Dinkele R, Gessner S, McKerry A, Leonard B, Seldon R, Koch AS, et al. Capture and visualization of live *Mycobacterium tuberculosis* bacilli from tuberculosis patient bioaerosols. PLoS Pathog. 2021;17:e1009262. https://doi.org/10.1371/journal.ppat.1009262

7. Dinkele R, Gessner S, McKerry A, Leonard B, Leukes J, Seldon R, et al. Aerosolization of *Mycobacterium tuberculosis* by tidal breathing. Am J Respir Crit Care Med. 2022;206:206–16. https://doi.org/10.1164/rccm.202110-2378OC
8. Emery JC, Dodd PJ, Banu S, Frascella B, Garden FL, Horton KC, et al. Estimating the contribution of subclinical tuberculosis disease to transmission: An individual patient data analysis from prevalence surveys. eLife. 2023;12:e82469. https://doi.org/10.7554/eLife.82469
9. Nguyen HV, Tiemersma E, Nguyen NV, Nguyen HB, Cobelens F. Disease transmission by patients with subclinical tuberculosis. Clin Infect Dis. 2023;76:2000–6. https://doi.org/10.1093/cid/ciad027
10. Becerra MC, Huang CC, Lecca L, Bayona J, Contreras C, Calderon R, et al. Transmissibility and potential for disease progression of drug resistant *Mycobacterium tuberculosis*: prospective cohort study. BMJ. 2019;367:l5894. https://doi.org/10.1136/bmj.l5894
11. World Health Organization. WHO consolidated guidelines on tuberculosis. Module 1: prevention: tuberculosis preventive treatment. 2nd ed. Geneva: The Organization; 2024.
12. Getahun H, Kittikraisak W, Heilig CM, Corbett EL, Ayles H, Cain KP, et al. Development of a standardized screening rule for tuberculosis in people living with HIV in resource-constrained settings: individual participant data meta-analysis of observational studies. PLoS Med. 2011;8:e1000391. https://doi.org/10.1371/journal.pmed.1000391
13. Cubillos-Angulo JM, Arriaga MB, Silva EC, Müller BLA, Ramalho DMP, Fukutani KF, et al. Polymorphisms in TLR4 and TNFA and risk of *Mycobacterium tuberculosis* infection and development of active disease in contacts of tuberculosis cases in Brazil: a prospective cohort study. Clin Infect Dis. 2019;69:1027–35. https://doi.org/10.1093/cid/ciy1001
14. Gagneux S. Ecology and evolution of *Mycobacterium tuberculosis*. Nat Rev Microbiol. 2018;16:202–13. https://doi.org/10.1038/nrmicro.2018.8
15. Coscolla M, Gagneux S. Consequences of genomic diversity in *Mycobacterium tuberculosis*. Semin Immunol. 2014;26:431–44. https://doi.org/10.1016/j.smim.2014.09.012
16. Xu Y, Cancino-Muñoz I, Torres-Puente M, Villamayor LM, Borrás R, Borrás-Máñez M, et al. High-resolution mapping of tuberculosis transmission: whole genome sequencing and phylogenetic modelling of a cohort from Valencia Region, Spain. PLoS Med. 2019;16:e1002961. https://doi.org/10.1371/journal.pmed.1002961
17. Williams CM, Abdulwhhab M, Birring SS, De Kock E, Garton NJ, Townsend E, et al. Exhaled *Mycobacterium tuberculosis* output and detection of subclinical disease by face-mask sampling: prospective observational studies. Lancet Infect Dis. 2020;20:607–17. https://doi.org/10.1016/S1473-3099(19)30707-8
18. Hansel NN, Romero KM, Pollard SL, Bose S, Psoter KJJ, J Underhill L, et al.; GASP Study Investigators. Ambient air pollution and variation in multiple domains of asthma morbidity among Peruvian children. Ann Am Thorac Soc. 2019;16:348–55. https://doi.org/10.1513/AnnalsATS.201807-448OC
19. Kuznetsov VN, Grjibovski AM, Mariandyshev AO, Johansson E, Bjune GA. Two vicious circles contributing to a diagnostic delay for tuberculosis patients in Arkhangelsk. Emerg Health Threats J. 2014;7:24909. https://doi.org/10.3402/ehtj.v7.24909
20. Ahmad Z, Zubair I, Ahmad S, Zuber N, Salar W. Reasons and extent of delay in the diagnosis of pulmonary tuberculosis after the appearance of symptoms. J Family Med Prim Care. 2024;13:1683–7. https://doi.org/10.4103/jfmpc.jfmpc_1246_23
21. McCreesh N, MacPherson P, Bampi JVB, Engel N, Kranzer K, Khan PY. Reported tuberculosis symptoms: an inadequate classifier of disease state. Clin Infect Dis. 2025;ciaf611. https://doi.org/10.1093/cid/ciaf611
22. Dale KD. Why we should move away—not towards—symptom-based terminology and policy in tuberculosis. Clin Infect Dis. 2025;ciaf667. https://doi.org/10.1093/cid/ciaf667
23. Teo AKJ, MacLean ELH, Fox GJ. Subclinical tuberculosis: a meta-analysis of prevalence and scoping review of definitions, prevalence and clinical characteristics. Eur Respir Rev. 2024;33:230208. https://doi.org/10.1183/16000617.0208-2023
24. Mahmoudi S, Hamidi M, Drain PK. Present outlooks on the prevalence of minimal and subclinical tuberculosis and current diagnostic tests: a systematic review and meta-analysis. J Infect Public Health. 2024;17:102517. https://doi.org/10.1016/j.jiph.2024.102517
25. Stuck L, Klinkenberg E, Abdelgadir Ali N, Basheir Abukaraig EA, Adusi-Poku Y, Alebachew Wagaw Z, et al.; scTB Meta Investigator Group. Prevalence of subclinical pulmonary tuberculosis in adults in community settings: an individual participant data meta-analysis. Lancet Infect Dis. 2024;24:726–36. https://doi.org/10.1016/S1473-3099(24)00011-2
26. Ryckman TS, Dowdy DW, Kendall EA. Infectious and clinical tuberculosis trajectories: Bayesian modeling with case finding implications. Proc Natl Acad Sci U S A. 2022;119:e2211045119. https://doi.org/10.1073/pnas.2211045119
27. Drain PK, Bajema KL, Dowdy D, Dheda K, Naidoo K, Schumacher SG, et al. Incipient and subclinical tuberculosis: a clinical review of early stages and progression of infection. Clin Microbiol Rev. 2018;31:e00021–18. https://doi.org/10.1128/CMR.00021-18
28. Pelzer PT, Stuck L, Martinez L, Richards AS, Acuña-Villaorduña C, Aronson NE, et al. Effectiveness of the primary bacillus Calmette-Guérin vaccine against the risk of *Mycobacterium tuberculosis* infection and tuberculosis disease: a meta-analysis of individual participant data. Lancet Microbe. 2025;6:100961. https://doi.org/10.1016/j.lanmic.2024.100961
29. Menzies D. What does tuberculin reactivity after bacille Calmette-Guérin vaccination tell us? Clin Infect Dis. 2000;31(Suppl 3):S71–4. https://doi.org/10.1086/314075

Address for correspondence: Megan B. Murray, Department of Global Health and Social Medicine, Harvard Medical School, 641 Huntington Ave, 4th Fl, Rm 4A07, Boston, MA 02115, USA; email: megan_murray@hms.harvard.edu

Hemolytic Uremic Syndrome Outbreak in Adults and Shiga Toxin–Producing *Escherichia coli* Negative for Locus of Enterocyte Effacement, France, 2025

Justine de Larminat, Kevin La, Philippe Bidet, André Birgy, Sandrine Liguori, Pierre Phlipaux, Celine Courroux, Florence Crombé, Jorge Blanco, Paul Coppo, Antoine Dossier, Laurence Armand-Lefevre, François Xavier Weill, Carolina Silva Nodari, Gabrielle Jones, Aurelie Cointe, Stéphane Bonacorsi

In January 2025, the *Escherichia coli* National Reference Center of France detected an outbreak of hemolytic uremic syndrome (HUS) in adults, caused by Shiga toxin–producing *E. coli* negative for locus of enterocyte effacement (LEE). The outbreak included 18 confirmed cases of *E. coli* infection, 5 probable or possible cases detected by in-house specific PCR, and 2 additional cases from Scotland and Belgium. Whole-genome sequencing identified the outbreak strain as O77 g:K92:H18, belonging to phylogroup D; the strain harbored the Shiga toxin 2 gene variant *stx2d*-073-C165-02 and a 134-kb plasmid with enterotoxin genes (*estb-STb2* and *eltAB*). Epidemiologic investigation implicated raw-milk cheese as the contamination source. The strain represents a singular hybrid pathotype of Shiga toxin–producing and enterotoxigenic *E. coli*, expressing a K92 capsule with known cross-immunogenicity to *Neisseria meningitidis* group C, which could explain the absence of pediatric cases. Related strains have been identified in international databases since 2005, suggesting global emergence.

Hemolytic uremic syndrome (HUS) is the most severe and potentially lethal complication of infections caused by Shiga toxin–producing *E. coli* (STEC), characterized by 3 features: thrombocytopenia, mechanical hemolytic anemia with schistocytosis, and renal injury (*1*). HUS primarily affects children; incidence in children in France is 1 case/100,000 person-years, 10 times higher than in adults (*2*,*3*). In France, most HUS cases are sporadic, but several outbreaks are reported each year. Those outbreaks are identified through the national pediatric nephrologists' surveillance network, which declares HUS cases to Santé Publique France, and through sequencing of all STEC isolates from HUS cases referred to the associated National Reference Center (NRC) for *E. coli.*

In France, STEC strains causing HUS mainly belong to serogroups O26, O80, and O157 and, to a lesser extent, to O121, O145, O55, and O103 (*4*). Most of those strains harbor genes encoding Shiga toxin type 2 and notably the 2a or 2d subtypes, which are carried on a prophage. They also contain a chromosomal pathogenicity island, the locus enterocyte effacement (LEE), which mediates intimate adhesion to epithelial cells and is characterized by the presence of the *eae* gene, encoding the intimin protein. Some strains may lack the gene *eae* and are therefore classified as LEE-negative STEC. In addition, the

Author affiliations: *Escherichia coli* National Reference Center, Robert-Debré University Hospital, Assistance Publique–Hôpitaux de Paris, Paris, France (J. de Larminat, K. La, P. Bidet, A. Birgy, S. Liguori, P. Phlipaux, C. Courroux, A. Cointe, S. Bonacorsi); Infection, Antimicrobien, Modélisation, Évolution, INSERM, Université Paris Cité, Paris (J. de Larminat, K. La, P. Bidet, A. Birgy, L. Armand-Lefevre, A. Cointe, S. Bonacorsi); Universitair Ziekenhuis Brussel, Brussels, Belgium (F. Crombé); Vrije Universiteit Brussel–Campus Jette, Brussels (F. Crombé); University of Santiago de Compostela, Lugo, Spain (J. Blanco); Hôpital Saint-Antoine, Paris (P. Coppo); Sorbonne Université, Paris (P. Coppo); Hôpital Bichat–Claude-Bernard, APHP, Paris (A. Dossier, L. Armand-Lefevre); Université Paris Diderot UFR de Médecine Site Xavier-Bichat, Paris (L. Armand-Lefevre); Institut Pasteur, Université Paris Cité, Paris (F.X. Weill, C. Silva Nodari); Santé Publique France, Saint-Maurice, France (G. Jones)

DOI: https://doi.org/10.3201/eid3204.251417

gene encoding enterohemolysin (*ehxA*) is frequently present among STEC (*1*).

In January 2025, the NRC for *E. coli* identified several samples positive for a LEE-negative STEC isolate of an unusual serogroup that harbored *stx*2 alone, mostly from elderly patients hospitalized with HUS in mainland France. Surprisingly, no pediatric HUS cases were reported with that strain. Whole-genome sequencing confirmed the clonality of all isolates, indicating an outbreak of HUS caused by the STEC strain.

The aim of our study was to describe the outbreak and the LEE-negative STEC strain responsible for severe HUS cases in elderly patients in France with 2 additional cases in Europe. We intended to understand the particular virulence of the strain and the reasons there were no pediatric cases.

Materials and Methods

Diagnosis of STEC Infections

The NRC for *E. coli* receives fecal samples collected across France, from patients suspected of HUS or experiencing hemorrhagic diarrhea at any age, as well as from at-risk populations with diarrhea. STEC diagnosis at the NRC is performed by DNA extraction using the Elite Ingenius instrument (Elitech, https://www.elitechgroup.com), followed by PCR with the RIDA GENE *E. coli* Stool Panel (R Biopharm, https://clinical.r-biopharm.com), which enables detection of *stx1, stx2*, and *eae* genes.

We inoculated positive samples onto selective culture media, including CHROMagar STEC (CHROMagar, https://www.chromagar.com), MacConkey CT (bioMérieux, https://www.biomerieux.com), and chromogenic medium chromID CPSO (bioMérieux). Chromogenic medium enables direct identification of *E. coli* when selective media are negative. We identified and confirmed colonies of STEC using the eazyplex EHEC complete kit (Amplex Diagnostics, https://www.eazyplex.com), which detects *stx1, stx2, eae,* and *ehxA* genes. We tested for 10 major STEC serogroups by in-house multiplex PCR as previously described (*5*). Finally, we conducted antimicrobial susceptibility testing on STEC strains by disk diffusion method, before storing them at –80°C.

Sequencing

We sequenced all strains at Institut Pasteur (Paris, France) using Illumina technology, as previously described (*6*). For 3 isolates, we performed hybrid assemblies with Unicycler (https://github.com/rrwick/Unicycler) to obtain circularized chromosomes and plasmids, using long-read sequencing with the Native Barcoding Kit 96 V14 (SQK-NBD114.96) on a GridION Flow Cell R10 with MinION (Oxford Nanopore, https://nanoporetech.com), combined with Illumina short-read data generated on a MiniSeq (https://illumina.com). We performed quality control short reads and long reads by fastQC (https://github.com/s-andrews/FastQC) combined with multiQC (https://github.com/MultiQC/MultiQC) for short reads and fastQC combined with nanoQC (https://github.com/wdecoster/nanoQC) for long reads.

Bioinformatics Analysis

We determined the isolate's phylogroup using Clermontyping (http://clermontyping.iame-research.center). We obtained sequence type (ST) and hierarchical clustering (HC), notably HC5, from Enterobase (https://enterobase.warwick.ac.uk). We performed chromosome and plasmid annotations, including the search for potential virulence genes, with Prokka version 1.14.6 (https://github.com/tseemann/prokka) using a LA database (https://github.com/Kevi84LA/LA-database/blob/main/LA_database.faa). The LA database was built by compiling an updated set of reviewed bacterial entries from UniProt (https://www.uniprot.org), gene sets from the Center for Genomic Epidemiology (https://www.genomicepidemiology.org), the virulence factor database (https://www.mgc.ac.cn/VFs), and in-house sources as previously described (*7*), translated into amino acid format. To avoid redundancy across the multiple databases, we used CD-HIT version 4.8.1 (https://github.com/weizhongli/cdhit) to cluster identical genes into a single representative sequence with 100% identity and 100% coverage.

We performed resistance gene search using Abricate tool on Resfinder database (*8*,*9*). We used PlasmidFinder (https://cge.food.dtu.dk/services/PlasmidFinder) and pMLST (https://cge.food.dtu.dk/services/pMLST) (*10*) for plasmid characterization and performed plasmid alignment using BRIG version 1.0.0 (https://github.com/happykhan/BRIG).

We performed phylogenic analysis with IQ-Tree version 2.4.0 (https://iqtree.github.io); we based the analysis on core-genome alignment of isolates produced by Panaroo version 1.5.2 (https://github.com/gtonkinhill/panaroo). We identified single-nucleotide polymorphisms (SNPs) on the basis of core-genome alignment using pairsnp (https://github.com/gtonkinhill/pairsnp).

Serotyping

Because the O serogroup deduced from the *wzx* and *wzy* sequences by Enterobase could not distinguish

between O17/O44/O73/O77/O106, defining the O77-group (O77 g) as previously described (*11*), we further investigated the O serogroup and H serogroup by phenotypic method at the NRC for *E. coli* in Spain. We determined O and H antigens using the method previously described (*12*); all available O (O1 to O181) antiserums were produced in the Laboratorio de Referencia de *E. coli*—University of Santiago de Compostela (Lugo, Spain). Finally, we used the K1/*Neisseria meningitidis* B antiserum (Bio-Rad Laboratories, https://www.bio-rad.com) to characterize the capsular serogroup.

Specific PCR

To identify patients potentially infected with the outbreak strain (i.e., patients with fecal PCR positive for *stx2* and negative for *eae* during the outbreak period but without a cultured STEC isolate), we developed an in-house quadruplex PCR targeting specific regions. We designed 2 primer pairs to target the large virulence plasmid characteristic of the outbreak strain: the first pair amplifies a 285-bp fragment located between 2 open-reading frames encoding phytase/esterase activity and a putative thiol peroxidase (*tpx* gene), and the second pair amplifies a 163-bp fragment of an open-reading frame encoding a putative thermolabile enterotoxin (*elt* chain A). We designed 2 additional primer pairs to target chromosomal genes, the *wzy* gene encoding the O77-group and the *neuS* K92 capsule gene (Appendix, https://wwwnc.cdc.gov/EID/article/32/4/25-1417-App1.pdf).

Case Definitions

We classified patients with HUS, diarrhea, or both in whom the outbreak strain was isolated from stool sample as confirmed cases. We classified those patients without the outbreak strain but with a positive quadruplex PCR in stool sample as probable cases. We classified those patients without isolation of the outbreak strain and showing only the chromosomal (plasmid markers negative) on quadruplex PCR in their sample as possible cases.

Results

Outbreak Cases

At the end of December, the NRC for *E. coli* identified 4 adult HUS cases, caused by a LEE-negative STEC that did not belong to the 10 usual major serogroups determined by routine PCR and harbored that *stx2* but not *eae* or *ehxA* genes. Of note, isolates failed to grow on selective STEC media and were recovered only on CPSO plates. Illumina sequencing confirmed that the outbreak was caused by a unique strain, O77 g:H18, belonging to ST69 of phylogroup D, harboring the *stx2d* subtype and lacking *eae* and *ehxA*. The strain belonged to the novel cluster at the HC5 level 326896, consistent with the core genome multilocus sequence typing–based hierarchical clustering scheme proposed by EnteroBase; outbreak-related isolates presented allelic distances ≤5. We further confirmed isolate similarity by a core-genome SNP phylogenetic analysis with a SNP median of 4 (range 1–29) (Figures 1–3; Appendix Figure 1).

In total, we identified 18 confirmed cases of STEC infection with the outbreak strain. The cases occurred during December 15, 2024–April 11, 2025 (2024 epidemiologic week 50 through 2025 epidemiologic week 15) (Figure 4); most cases were reported during December 15, 2024–February 3, 2025 (2024 epidemiologic week 50 through 2025 epidemiologic week 6). Cases were distributed nationwide with no clusters (Appendix Figure 2).

To explore the potential extent of the outbreak in patients without STEC isolation, we implemented an in-house specific multiplex PCR. During the outbreak period, extended to 1 month before and 1 month after, we found 38 patients (3 experiencing HUS symptoms and 35 with diarrhea) from whom no STEC was isolated from their fecal cultures to be positive for *stx2* and negative for *eae*. We validated our in-house quadruplex PCR, targeting 2 chromosomal genes and 2 genes present in the 134-kb plasmid, for specificity (Appendix Figure 3) and then applied directly to fecal DNA extracts to identify additional cases. We classified 4 additional patients who tested positive for all 4 target genes as probable cases; 1 patient, whose sample was positive for 2 chromosomal targets, was classified as a possible case (Figures 4, 5).

All patients were adults; median age was 72.1 (interquartile range 66.7–81.8; range 34.3–89.4) years, and female/male ratio was 0.56. Among the 18 confirmed cases and 5 probable and possible cases, 17 (94%) confirmed and 4 (80%) probable and possible, had HUS. Among the 23 case-patients, 13 experienced diarrhea; 4 of those had bloody diarrhea. Three (13%) patients died. We expect to publish clinical details of patients and their outcomes in the future.

Investigations and Control Measures

Epidemiologic and traceback investigations, including food questionnaires and supermarket loyalty card records, indicated that by the end of January 2025 a total of 15/17 (88%) confirmed and 2/4 probable case-patients had consumed the same brand of raw cow's-milk

cheese. We excluded 2 probable and 1 possible cases, as well as 1 case confirmed late in our investigation on April 11. We identified the outbreak strain in a cheese sample collected from a patient's refrigerator. As of January 24, 2025, authorities initiated recall and withdrawal of the suspected cheese produced starting November 12, 2024. In February 2025, we identified 2 additional cases through Enterobase; both had STEC isolates belonging to the same HC5 cluster (Figure 1). One case-patient in Belgium experienced HUS; the patient had not consumed the implicated cheese. The other case was in Scotland; the patient's clinical condition and exposure data were unknown.

Molecular Characterization of Outbreak Strain

We submitted the 18 isolates from France to short-read whole-genome sequencing; they belonged to ST69 (phylogroup D) and HC5 326896. The *rfb*

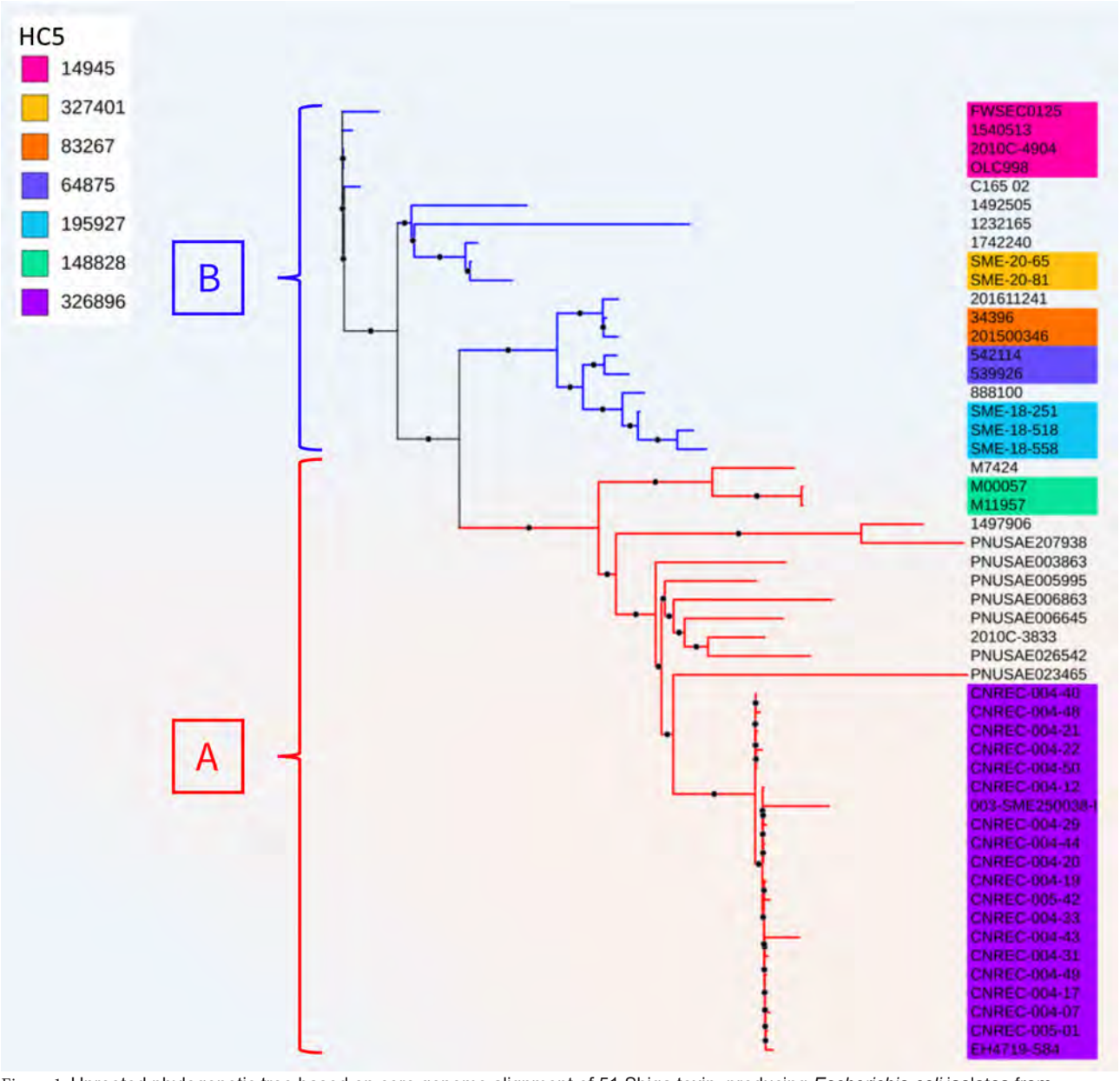

Figure 1. Unrooted phylogenetic tree based on core genome alignment of 51 Shiga toxin–producing *Escherichia coli* isolates from study of hemolytic uremic syndrome outbreak in adults and Shiga toxin–producing *Escherichia coli* negative for locus of enterocyte effacement, France, 2025. Shown are the France 2025 outbreak strain (HC5 326896, in purple) and other strains with the same core-genome multilocus sequence typing HC200 2073 group identified in EnteroBase and GenBank (Appendix Table 1, https://wwwnc.cdc.gov/EID/article/32/4/25-1417-App1.pdf). Isolates are divided into 2 main groups, A and B, in accordance with their phylogenetic distribution. Only HC5 comprising ≥2 genomes are colored. Figures 1–3 are combined in Appendix Figure 1.

	Country	Year	Source	Disease	O group	H group
FWSEC0125	CAN	2019	Human	-	O77g	H18
1540513	UK	2021	-	-	-	H18
2010C-4904	USA	2010	-	-	O77g	H18
OLC998	CAN	2010	Food	-	O77g	H18
C165 02	USA	2005	Human	Diarrhea	O77g	H18
1492505	UK	2021	Human	-	O77g	H18
1232165	UK	2023	Human	-	O77g	H18
1742240	UK	2025	Human	-	O77g	H18
SME-20-65	SCT	2025	-	-	O77g	H18
SME-20-81	SCT	2020	-	-	O77g	H18
201611241	FRA	2016	Human	HUS	-	H18
34396	FRA	2012	Human	HUS	O77g	H18
201500346	FRA	2014	Human	HUS	-	H18
542114	UK	2018	Human	-	-	H18
539926	UK	2018	Human	-	O77g	H18
888100	UK	2020	Human	-	O77g	H18
SME-18-251	SCT	2012	Human	Diarrhea	O77g	H18
SME-18-518	SCT	2012	Human	Diarrhea	O77g	H18
SME-18-558	SCT	2012	Human	Diarrhea	O77g	H18
M7424	AUS	2014	Human	HUS	O77g	H18
M00057	AUS	2020	Human	HUS	O77g	H18
M11957	AUS	2019	Human	HUS	O77g	H18
1497906	UK	2021	Human	-	O77g	H18
PNUSAE207938	USA	2025	-	-	O77g	H18
PNUSAE003863	USA	2016	-	-	O77g	H18
PNUSAE005995	USA	2017	-	-	O77g	H18
PNUSAE006863	USA	2017	-	-	O77g	H18
PNUSAE006645	USA	2017	-	-	O77g	H18
2010C-3833	USA	2010	Human	-	O77g	H18
PNUSAE026542	USA	2019	Human	-	O77g	H18
PNUSAE023465	USA	2019	Human	-	O77g	H18
CNREC-004-40	FRA	2025	Human	Diarrhea	O77g	H18
CNREC-004-48	FRA	2025	Human	HUS	O77g	H18
CNREC-004-21	FRA	2025	Human	HUS	O77g	H18
CNREC-004-22	FRA	2025	Human	HUS	O77g	H18
CNREC-004-50	FRA	2025	Human	HUS	O77g	H18
CNREC-004-12	FRA	2024	Human	HUS	O77g	H18
003-SME250038-I	SCT	2025	Human	-	O77g	H18
CNREC-004-29	FRA	2025	Human	HUS	O77g	H18
CNREC-004-44	FRA	2025	Human	HUS	O77g	H18
CNREC-004-20	FRA	2024	Human	HUS	O77g	H18
CNREC-004-19	FRA	2024	Human	HUS	O77g	H18
CNREC-005-42	FRA	2025	Human	Diarrhea	O77g	H18
CNREC-004-33	FRA	2025	Human	HUS	O77g	H18
CNREC-004-43	FRA	2025	Human	HUS	O77g	H18
CNREC-004-31	FRA	2025	Human	HUS	O77g	H18
CNREC-004-49	FRA	2025	Human	HUS	O77g	H18
CNREC-004-17	FRA	2024	Human	HUS	O77g	H18
CNREC-004-07	FRA	2024	Human	HUS	O77g	H18
CNREC-005-01	FRA	2025	Human	HUS	O77g	H18
EH4719-S84	BEL	2025	Human	HUS	O77g	H18

Figure 2. Origins and serotypes of 51 Shiga toxin–producing *Escherichia coli* isolates from study of HUS in adults and Shiga toxin–producing *Escherichia coli* negative for locus of enterocyte effacement, France, 2025. Shown are the outbreak strain (HC5 326896, in purple) and other strains with the same core-genome multilocus sequence typing HC200 2073 group identified in EnteroBase and GenBank (Appendix Table 1, https://wwwnc.cdc.gov/EID/article/32/4/25-1417-App1.pdf). Only HC5 comprising ≥2 genomes are colored. Country of origin, year of isolation, source, disease, and O and H serotypes are indicated; O77 g denotes serogroup from the O77 group. Dash indicates the serotype is not available. AUS, Australia; BEL, Belgium; CAN, Canada; FRA, France; HUS, hemolytic uremic syndrome; SCT, Scotland; UK, United Kingdom; USA, United States. Figures 1–3 are combined in Appendix Figure 1.

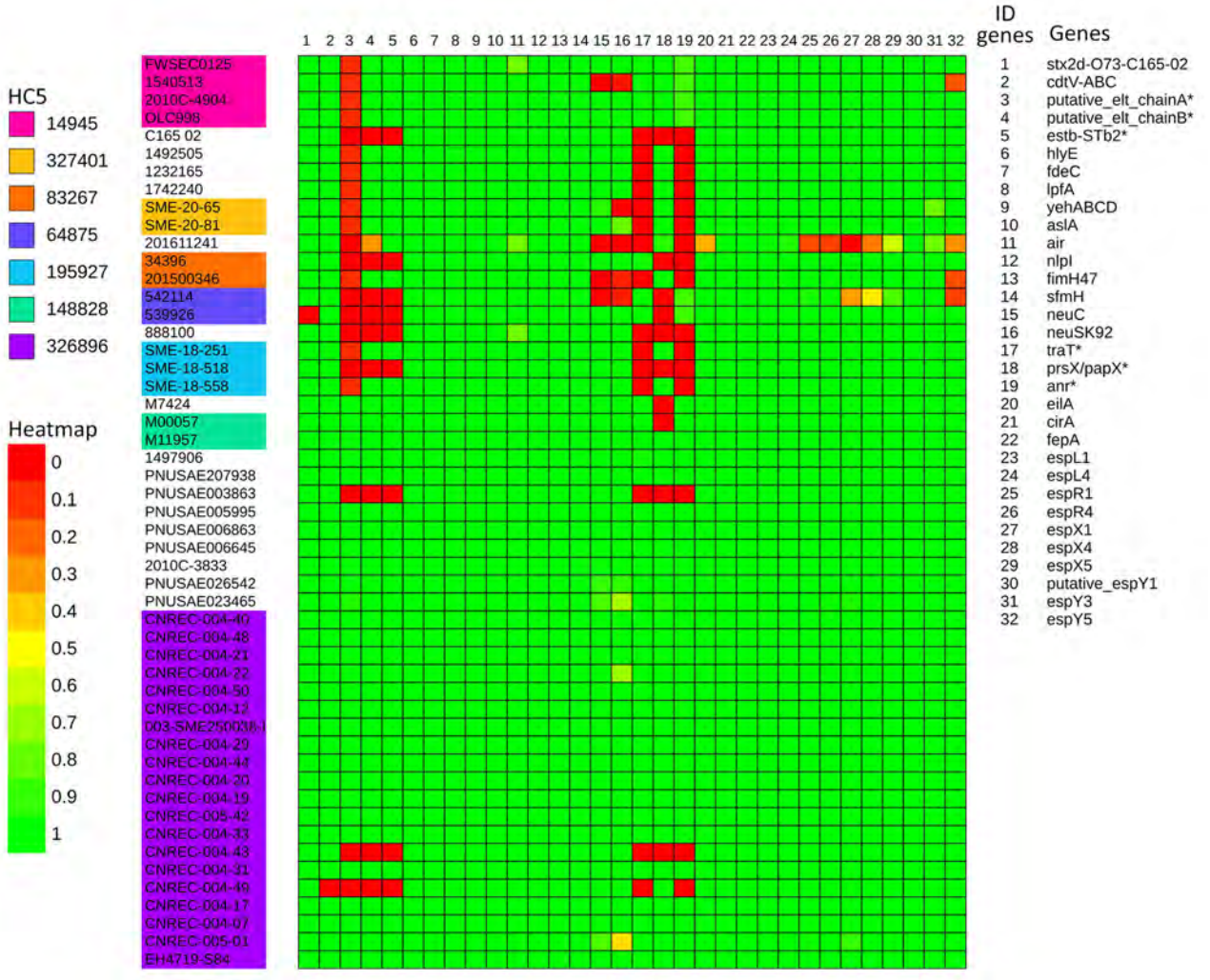

Figure 3. Distribution of genes encoding major virulence factors of 51 Shiga toxin–producing *Escherichia coli* isolates from study of hemolytic uremic syndrome outbreak in adults and Shiga toxin–producing *Escherichia coli* negative for locus of enterocyte effacement, France, 2025. Shown are the France 2025 outbreak strain (HC5 326896, in purple) and other strains with the same core-genome multilocus sequence typing HC200 2073 group identified in EnteroBase and GenBank (Appendix Table 1, https://wwwnc.cdc.gov/EID/article/32/4/25-1417-App1.pdf). Heatmap assembled from phylogenic tree using ITOL tool (https://itol.embl.de), based on gene sequences of reference isolate CNREC_004-7. The score represents the combination of percentage coverage and percentage nucleotide identity. Asterisk indicates genes located on the large plasmid (134 kb). Figures 1–3 are combined in Appendix Figure 1.

gene cluster sequence did not allow discrimination between O17/44/73/77/106 antigens, defining the O77-group (O77 g) described previously (*11*), whereas the *fliC* gene corresponded to H18. Agglutination with O antiserum specific to those 5 antigens was negative; therefore, the outbreak strain was designated O77 g:H18. All isolates harbored the *stx2d*-O73-C165-02 variant and were negative for *eae* and *ehxA*, as expected. We long-read sequenced 3 isolates (CNREC-004-07, CNREC-004-31, CNREC-004-43), revealing a chromosome of ≈4,934 kb, a plasmid of ≈96 kb, and, in the first 2 isolates, an additional plasmid of ≈134 kb (Appendix Table 2). The 134-kb plasmid was an IncF plasmid with a complete *tra* operon. The pMLST tool could not precisely identify the F replicon ST (F-:A17*:B24–79*, in which the asterisks indicate new alleles closely related to A17 and B24/B79). The 96-kb plasmid was an IncY plasmid, lacking a *tra* operon (Appendix Table 2).

Putative Virulence Factors

We identified several putative virulence factors (Figure 3), some of which were located on the 134-kb plasmid (Figure 6), whereas we detected no known virulence factors on the 96-kb plasmid (data not shown). In addition to the main virulence factor *stx2d*-O73-C165-02, we identified several toxin-encoding genes, including *cdt*-VABC (cytolethal distending toxin

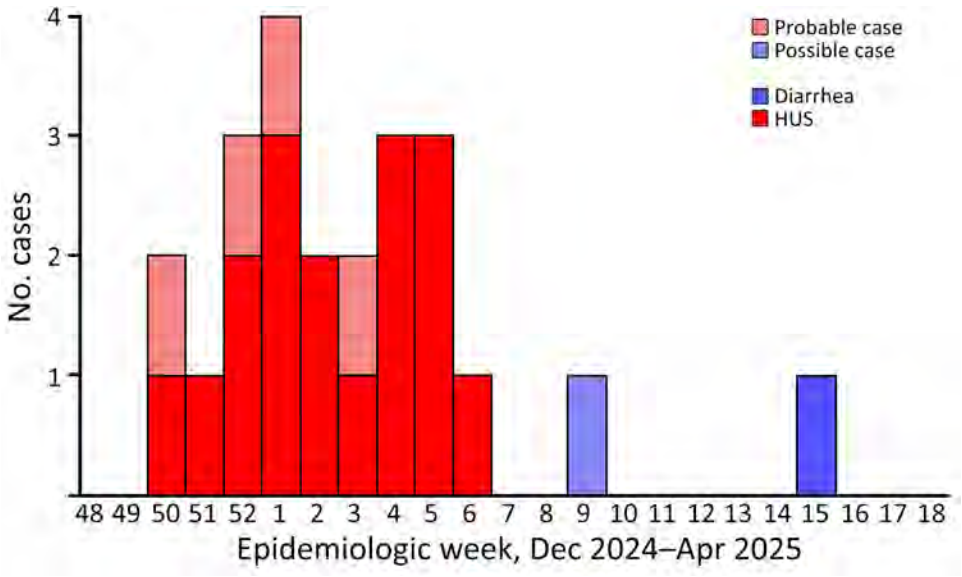

Figure 4. Epidemic curve of confirmed, probable, and possible cases of Shiga toxin–producing *Escherichia coli* infection caused by the outbreak strain (HC5 326896) from study of HUS outbreak in adults and Shiga toxin–producing *Escherichia coli* negative for locus of enterocyte effacement, France, 2025. HUS, hemolytic uremic syndrome.

subtype V), a putative *elt*AB (heat-labile enterotoxin II), *estb*-STb2 (heat stable enteroxin), and *hlyE* (avian hemolysin). We also detected genes encoding adhesion or invasion factors, particularly *fdeC*, *lpfA*, *yehABCD*, *aslA*, *air*, *fimH*47, and *nlpI*. Furthermore, protectin-encoding genes such as *traT* and *neuABCDES* were present. Other virulence genes with diverse putative functions included the transcriptional regulators *prsX/papX* and *anr*, as well as *eilA*, a transcriptional regulator of the enteropathogenic *E. coli* type III secretion system 2, characteristic of ST69 strains (*13*), and several type III secretion system effectors. None of the 18 outbreak isolates we sequenced carry the *iha* and *aggR* genes, which have been described in LEE-negative STEC (*14*).

The detection of the *neuC* gene suggested the presence of a K1 capsule. However, agglutination with K1-specific antiserum was negative for all isolates except CNREC-004-43. Sequence analysis of the entire *neu* gene cluster showed high homology across all genes (>98%), except for *neuS* (87%). BLAST analysis of the *neuS* sequence revealed 99.92% identity with the K92 *neuS* gene (Appendix Figure 4). Therefore, we considered the outbreak strain serotype O77 g:K92:H18. In isolate CNREC-004-43, which tested K1-positive, we identified a C154A substitution in *neuS* that led to an H52N amino acid change (Appendix Figure 4). That mutation is known to be sufficient to convert a K92 capsule into K1 capsule, explaining the phenotype observed in this isolate (*15*). The outbreak strain carried no antimicrobial resistance genes, confirmed by phenotypic tests. Only a rarely reported parC.S57T mutation was identified, with no effect on quinolone susceptibility.

Similar Strains Worldwide

To determine whether other isolates closely related to our outbreak strain exist worldwide, we searched Enterobase for isolates with the same HC200 2073. We identified 30 such isolates (Figure 1), spanning 3 continents. Moreover, we found in GenBank the strain C165-02, linked to *stx2d*-O73-C165-02, which is the oldest strain we reported here, isolated in 2005 in Maryland from a patient with bloody diarrhea (*16*). Almost all isolates were of human origin, but clinical information, including patient age, was missing for most. Several cases were associated with HUS, consistent with the virulence of the outbreak strain. All those isolates are ST69 and have common features, including the *stx2d*-O73-C165-02 variant (except 1), *cdtV* (except 1 outbreak isolate), *hlyE*, and multiple adhesion and miscellaneous genes. We divided the population into 2 main groups, A and B, on the basis of phylogenetic analysis and gene distribution (Figure 1).

Group A (n = 32), which includes our outbreak isolates and, of note, 3 circularized strains from Australia, carried nearly all of the putative virulence factors described, with the exception of 3 isolates. The 3 exceptions were characterized by partial or complete loss of 134 kb plasmid-borne genes (putative *eltAB*, *STb*, *traT*, *prsX/papX*, and *anr*) (Figure 1–3). To further investigate the plasmid content of all HC200 2073 strains, we performed multi-alignments using BRIG. As previously indicated, CNREC-004-43, one of our long-read sequenced isolates, had completely lost the 134-kb plasmid, whereas CNREC-004-49 and PNUSAE003863 had deletions encompassing large portions of the plasmid (Appendix Figure 5, panels A, B).

Of interest, our in-house quadruplex PCR detected plasmid target signals in stool samples containing CNREC-004-49, suggesting in vitro plasmid loss. Altogether, those findings indicate that the 134-kb plasmid is relatively unstable and can be lost either partially or entirely, even in the context of an outbreak and over a short time. In contrast, in group A, only 3 isolates outside the outbreak carried the 96-kb plasmid (Appendix Figure 6, panels A, B).

Group B isolates (n = 19) were all characterized by the loss of ≥1 plasmidborne gene (putative *eltAB*, *STb*, *traT*, *prsX/papX*, and *anr*) (Figure 1–3). Of note, although isolates were from different countries in Europe or North America, none carried the putative *elt* chain A gene. Only 4 group B isolates harbored an almost complete 134-kb plasmid, and all shared the same HC5 14945 (Figure 1; Appendix Figure 5, panel C). Nine isolates retained a large portion of the 134-kb plasmid but lacked the *tra* operon (Appendix Figure 5, panel C). Ten isolates carried the 96-kb plasmid, including the oldest strain, C165-02 (Appendix Figure 6, panel C). Six group B isolates might not produce a K92 capsule (Figure 1), because *neuC* and *neuS* K92 were absent. Sequence alignment of those 6 isolates with the capsular operon of CNREC-004-31 revealed the presence of a complete *kps* operon but high fragmentation of *neu* genes (Appendix Figure 7).

Discussion

In this study, we describe a LEE-negative STEC/enterotoxigenic (ETEC) *E. coli* strain with several unique features that was linked to a HUS outbreak occurring exclusively in adults. The outbreak strain belonged to ST69, a major ST of phylogroup D. In contrast, most STEC-causing HUS belong to phylogroups B1 or E (*17*). ST69 strains are usually associated with extraintestinal infections (*17*); however, none of our patients experienced systemic infection. Thus, the genetic background of this intestinal pathogenic *E. coli* is highly unusual.

Clinical manifestations associated with infection by the outbreak strain were highly severe; HUS rate was 91%, one of the highest ever reported among STEC outbreaks internationally whether in children

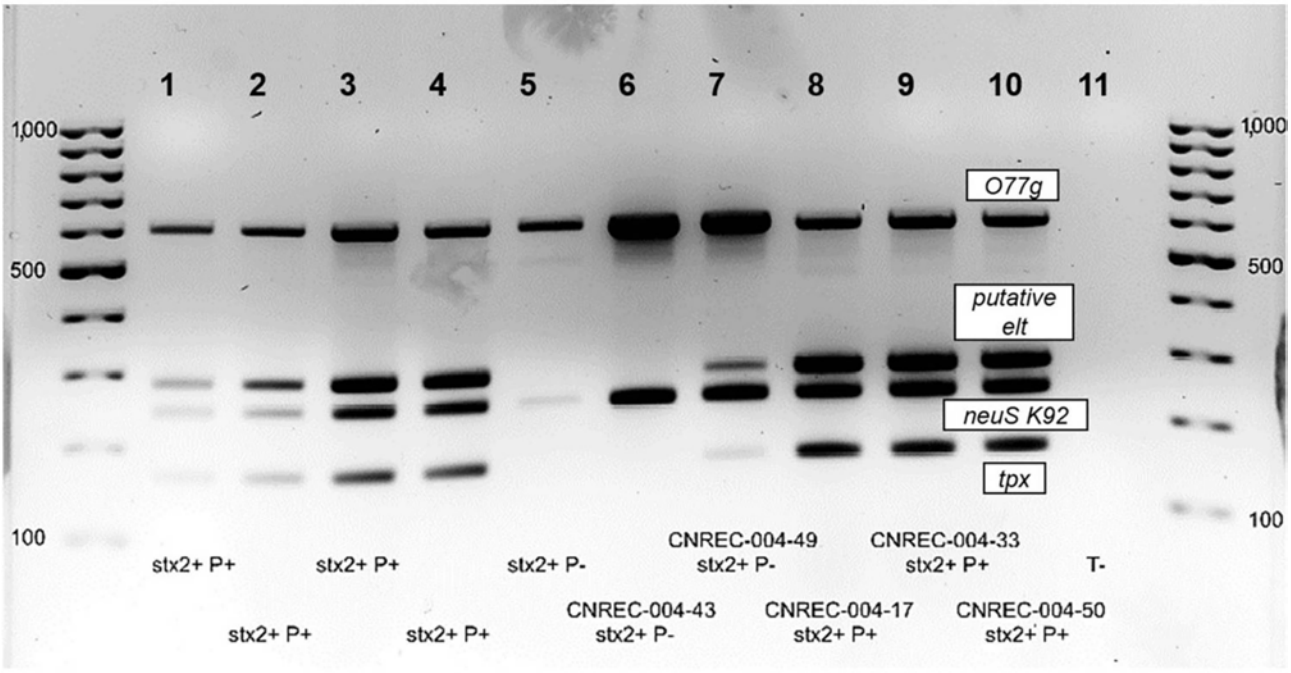

Figure 5. Quadruplex PCR results from study of hemolytic uremic syndrome outbreak in adults and Shiga toxin–producing *Escherichia coli* negative for locus of enterocyte effacement, France, 2025. We performed quadruplex PCR on fecal extracts targeting 2 chromosomic genes: *O77 g* (*wzy*) (609-bp) and *neuS* K92 (247-bp), and 2 loci on the 134 kb plasmid: *elt* (163-bp) and the phytase-*tpx* region (285-bp). Wells 1 to 4, fecal samples (*stx2*+ but culture negative) positive for both chromosomal and plasmid targets (P+) defining probable cases. Well 5, fecal samples positive only for chromosomal targets defining possible case. Well 6, fecal specimen from patient with isolate CNREC-004–43, which had lost its 134kb plasmid probably in vivo. Well 7, specimen from patient with isolate CNREC-004-49, showing plasmid target signals absent in the corresponding isolate DNA, suggesting partial plasmid loss in vitro (Figure 3). Wells 8–10, fecal extracts from patients with outbreak isolates harboring the complete 134kb plasmid (CNREC-004-17, -33 and -50). Well 11, negative control.

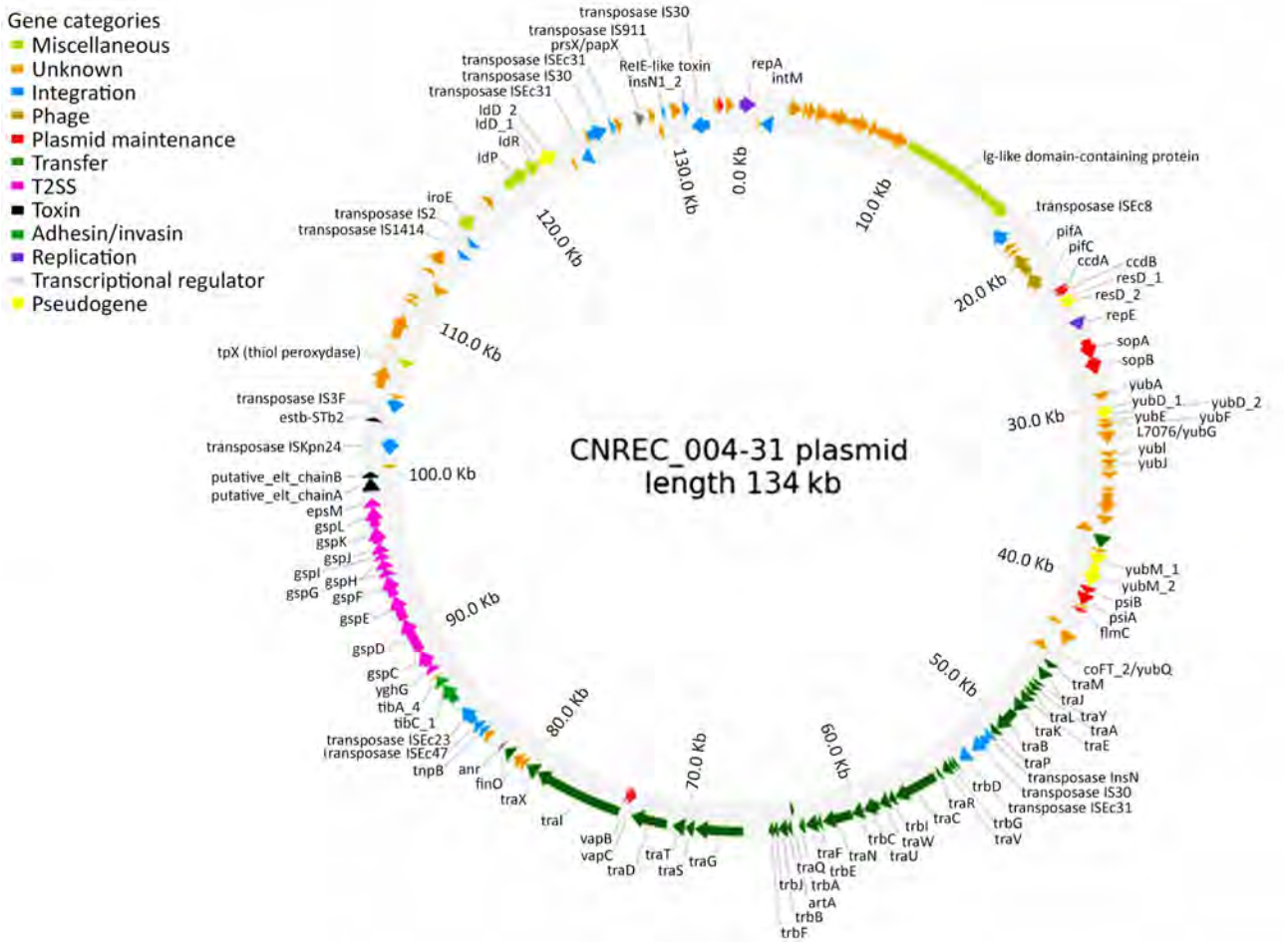

Figure 6. Representation of the 134-kb plasmid from isolate CNREC-004-31 in study of hemolytic uremic syndrome outbreak in adults and Shiga toxin–producing *Escherichia coli* negative for locus of enterocyte effacement, France, 2025. Annotated genes were categorized by function.

(1%–56% of HUS) or adults (3%–24%) (*2*). The predominance of elderly patients, higher than previously reported for adult HUS sporadic cases in France (*18*), partly explains the severity, although only 1 patient, a 72-year-old kidney transplant recipient, was immunocompromised and at higher risk for HUS (*19*).

Several other features of the outbreak strain may have contributed to its severity. First, the toxin Stx2d is strongly associated with HUS in France, both in children and adults (*20*). The specific variant identified in this study, *stx2d*-O73-C165-02, is rare (*21*), was described in 2007 (*22*), and may display higher virulence compared with other *stx2d* variants (*23*). Second, the outbreak strain harbors additional toxin genes that could have exacerbated disease. Those genes include the putative heat labile enterotoxin II (*eltAB*) and the heat-stable enterotoxin type b (*STb*), suggesting a hybrid STEC/ETEC pathotype. Emerging STEC/ETEC hybrids have been increasingly reported worldwide, isolated from animals, food, and humans in the context of diarrhea or HUS (*24*–*26*). Finally, the strain encodes the toxin CDT-V, previously identified in other *eae*–non-O157 STEC, such as O91 (*14*), which might also have contributed to its pathogenicity. Indeed, CDT-V is a genotoxin and cyclomodulin that causes DNA damage, cell cycle arrest, and ultimately the death of human microvascular endothelial cells.

Our outbreak was also characterized by infections occurring exclusively in adults. STEC infections, particularly HUS, are ≈10 times less frequent in adults than in children (*2*,*3*). However, few outbreaks exclusively affecting adults have been reported internationally, all caused by O157:H7 STEC, and most of them occurred in nursing homes, which explains the population affected (*2*,*27*–*29*).

Several hypotheses may explain the unusual epidemiology. First, in France, several widely publicized HUS outbreaks in children during 2014–2024,

many linked to raw milk cheese, have likely increased awareness of the illness and at-risk foods. National recommendations on STEC prevention explicitly include advising against the consumption of raw milk cheese in children <5 years of age. Second, and perhaps more intriguingly in this outbreak, protection in children could be linked to the expression of the rare K92 capsule by the outbreak strain. The K92 capsule, structurally related to the K1 capsule, is composed of a homopolymer of N-acetyl-neuraminic acid with alternating, α2–8 and α2–9 linkages. Of note, the meningococcal C capsule (α2–9 linkages) and meningococcal B capsule (α2–8 linkages) share structural similarities. There is therefore a homology between those capsules; experimental cross-immunogenicity between *E. coli* K92 and meningococcus C has already been demonstrated (*15*,*30*). Thus, mandatory meningococcal C vaccination of infants in France since 2018, with a high pediatric population coverage of 88.6% in 2024 (*31*), might have conferred cross-protection against K92 *E. coli* infections in children. However, we note that we did not demonstrate the expression of the K92 capsule because K92 antiserum was unavailable. Finally, our in-house quadruplex PCR showed that we missed few cases by culture, and the assay could serve to detect the reemergence of this strain. It could also help ecologic niche investigations of the unusual STEC/ETEC strain.

Interrogation of international databases identified 31 additional stains, all belonging to HC200 2073, that were closely related to our outbreak strain and were distributed across 3 continents. The earliest reported isolate, C165-02, was recorded in 2005 in Maryland, USA, from a patient with bloody diarrhea; its name is used for the *stxd2*-O73-C165-02 variants. Almost all the HC200 2073 strains have been isolated from humans. Of note, some shared the same HC5 and were potentially involved in small outbreaks (Figures 1, 2). Those findings highlight that the *E. coli* hybrid pathotype ST69, carrying the *stx2d*-O73-C165-02 variant, has been spreading worldwide and warrants close monitoring, given its outbreak potential and severity.

In conclusion, we characterized a singular emerging hybrid STEC/ETEC pathotype responsible for a severe HUS outbreak exclusively in elderly patients. The identification of genetically related isolates worldwide since 2005 suggests recent global emergence and underscores the need for strengthened epidemiologic surveillance to track its spread. Just before the outbreak, HUS surveillance in France for adults was formally implemented to better capture the characteristics of STEC infections in this population. While such outbreaks remain rare, occurrence of this outbreak highlights the severe health impact and outbreak potential of STEC in adults and the risk presented by atypical emerging strains. Our in-house PCR can help detect outbreaks, investigate their sources, and identify reservoirs. Finally, the possible protective effect of meningococcal C vaccination could represent an unexpected defense against this clone.

Acknowledgments

We thank Fanny Chereau and Edith Laurent for their contribution to epidemiologic investigations and Sophie Belichon for coordinating traceback investigations.

About the Author

Dr. de Larminat is a medical resident in pediatric infectious disease, completing her formation with a research year at the *Escherichia coli* National Reference Center, in Robert Debré Hospital, Université Paris Cité, Paris, France. Her primary research interests are pediatric infectious diseases, notably antibacterial stewardship and gastrointestinal infections, emerging infectious disease, and visceral leishmaniasis.

References

1. Joseph A, Cointe A, Mariani Kurkdjian P, Rafat C, Hertig A. Shiga toxin–associated hemolytic uremic syndrome: a narrative review. Toxins (Basel). 2020;12:67. https://doi.org/10.3390/toxins12020067
2. Travert B, Rafat C, Mariani P, Cointe A, Dossier A, Coppo P, et al. Shiga toxin–associated hemolytic uremic syndrome: specificities of adult patients and implications for critical care management. Toxins (Basel). 2021;13:306. https://doi.org/10.3390/toxins13050306
3. Majowicz SE, Scallan E, Jones-Bitton A, Sargeant JM, Stapleton J, Angulo FJ, et al. Global incidence of human Shiga toxin–producing *Escherichia coli* infections and deaths: a systematic review and knowledge synthesis. Foodborne Pathog Dis. 2014;11:447–55. https://doi.org/10.1089/fpd.2013.1704
4. Bruyand M, Mariani-Kurkdjian P, Le Hello S, King LA, Van Cauteren D, Lefevre S, et al.; Réseau français hospitalier de surveillance du SHU pédiatrique. Paediatric haemolytic uraemic syndrome related to Shiga toxin–producing *Escherichia coli*, an overview of 10 years of surveillance in France, 2007 to 2016. Euro Surveill. 2019;24:1800068. https://doi.org/10.2807/1560-7917.ES.2019.24.8.1800068
5. Soysal N, Mariani-Kurkdjian P, Smail Y, Liguori S, Gouali M, Loukiadis E, et al. Enterohemorrhagic *Escherichia coli* hybrid pathotype O80:H2 as a new therapeutic challenge. Emerg Infect Dis. 2016;22:1604–12. https://doi.org/10.3201/eid2209.160304
6. Jones G, Pardos de la Gandara M, Herrera-Leon L, Herrera-Leon S, Varela Martinez C, Hureaux-Roy R, et al. Outbreak of *Salmonella enterica* serotype Poona in infants linked to persistent *Salmonella* contamination in an infant formula manufacturing facility, France, August 2018 to February 2019. Euro Surveill. 2019;24:1900161. https://doi.org/10.2807/1560-7917.ES.2019.24.13.1900161

7. Bidet P, Birgy A, Ouldali N, Béchet S, Levy C, Madhi F, et al. Comparative genomic analysis of ESBL-producing *Escherichia coli* from faecal carriage and febrile urinary tract infection in children: a prospective multicentre study. JAC Antimicrob Resist. 2022;4:dlac056. https://doi.org/10.1093/jacamr/dlac056
8. Bortolaia V, Kaas RS, Ruppe E, Roberts MC, Schwarz S, Cattoir V, et al. ResFinder 4.0 for predictions of phenotypes from genotypes. J Antimicrob Chemother. 2020;75:3491–500. https://doi.org/10.1093/jac/dkaa345
9. Camacho C, Coulouris G, Avagyan V, Ma N, Papadopoulos J, Bealer K, et al. BLAST+: architecture and applications. BMC Bioinformatics. 2009;10:421. https://doi.org/10.1186/1471-2105-10-421
10. Carattoli A, Zankari E, García-Fernández A, Voldby Larsen M, Lund O, Villa L, et al. In silico detection and typing of plasmids using PlasmidFinder and plasmid multilocus sequence typing. Antimicrob Agents Chemother. 2014;58:3895–903. https://doi.org/10.1128/AAC.02412-14
11. Wang W, Perepelov AV, Feng L, Shevelev SD, Wang Q, Senchenkova SN, et al. A group of *Escherichia coli* and *Salmonella enterica* O antigens sharing a common backbone structure. Microbiology (Reading). 2007;153:2159–67. https://doi.org/10.1099/mic.0.2007/004192-0
12. Guinée PAM, Jansen WH, Wadström T, Sellwood R. *Escherichia coli* associated with neonatal diarrhoea in piglets and calves. In: de Leeuw PW, Guinée PAM, eds. Laboratory diagnosis in neonatal calf and pig diarrhoea. Current Topics in Veterinary Medicine and Animal Science, vol. 13. Dordrecht (Netherlands): Springer; 1981. p. 13126–162. https://doi.org/10.1007/978-94-009-8328-1_18
13. Fox S, Goswami C, Holden M, Connolly JPR, Mordue J, O'Boyle N, et al. A highly conserved complete accessory *Escherichia coli* type III secretion system 2 is widespread in bloodstream isolates of the ST69 lineage. Sci Rep. 2020;10:4135. https://doi.org/10.1038/s41598-020-61026-x
14. Bielaszewska M, Fell M, Greune L, Prager R, Fruth A, Tschäpe H, et al. Characterization of cytolethal distending toxin genes and expression in Shiga toxin–producing *Escherichia coli* strains of non-O157 serogroups. Infect Immun. 2004;72:1812–6. https://doi.org/10.1128/IAI.72.3.1812-1816.2004
15. Keys TG, Fuchs HLS, Galuska SP, Gerardy-Schahn R, Freiberger F. A single amino acid toggles *Escherichia coli* polysialyltransferases between mono- and bifunctionality. Glycobiology. 2013;23:613–8. https://doi.org/10.1093/glycob/cwt003
16. Steyert SR, Sahl JW, Fraser CM, Teel LD, Scheutz F, Rasko DA. Comparative genomics and *stx* phage characterization of LEE-negative Shiga toxin–producing *Escherichia coli*. Front Cell Infect Microbiol. 2012;2:133. https://doi.org/10.3389/fcimb.2012.00133
17. Denamur E, Clermont O, Bonacorsi S, Gordon D. The population genetics of pathogenic *Escherichia coli*. Nat Rev Microbiol. 2021;19:37–54. https://doi.org/10.1038/s41579-020-0416-x
18. Travert B, Dossier A, Jamme M, Cointe A, Delmas Y, Malot S, et al.; Centre de Référence des Microangiopathies Thrombotiques2. Shiga toxin–associated hemolytic uremic syndrome in adults, France, 2009–2017. Emerg Infect Dis. 2021;27:1876–85. https://doi.org/10.3201/eid2707.204638
19. Mazloum M, Trémolières P, Baili N, Rafat C, Kaminski H, Kamar N, et al. Shiga toxin–producing *Escherichia coli*–associated hemolytic uremic syndrome in adult kidney transplant recipients. Kidney Int Rep. 2025;10:3843–54. https://doi.org/10.1016/j.ekir.2025.08.004
20. French Agency for Food, Environmental and Occupational Health & Safety. Shiga toxin–producing *Escherichia coli* (STEC)/enterohemorrhagic *Escherichia coli* (EHEC) [in French]. 2024 [cited 2025 Aug 7]. https://www.anses.fr/sites/default/files/Fiche-EHEC-2024-MPEX-0031.pdf
21. Scheutz F, Teel LD, Beutin L, Piérard D, Buvens G, Karch H, et al. Multicenter evaluation of a sequence-based protocol for subtyping Shiga toxins and standardizing Stx nomenclature. J Clin Microbiol. 2012;50:2951–63. https://doi.org/10.1128/JCM.00860-12
22. Persson S, Olsen KEP, Ethelberg S, Scheutz F. Subtyping method for *Escherichia coli* Shiga toxin (verocytotoxin) 2 variants and correlations to clinical manifestations. J Clin Microbiol. 2007;45:2020–4. https://doi.org/10.1128/JCM.02591-06
23. Pedersen MG, Hansen C, Riise E, Persson S, Olsen KEP. Subtype-specific suppression of Shiga toxin 2 released from *Escherichia coli* upon exposure to protein synthesis inhibitors. J Clin Microbiol. 2008;46:2987–91. https://doi.org/10.1128/JCM.00871-08
24. Nyholm O, Heinikainen S, Pelkonen S, Hallanvuo S, Haukka K, Siitonen A. Hybrids of shigatoxigenic and enterotoxigenic *Escherichia coli* (STEC/ETEC) among human and animal isolates in Finland. Zoonoses Public Health. 2015;62:518–24. https://doi.org/10.1111/zph.12177
25. Johura FT, Parveen R, Islam A, Sadique A, Rahim MN, Monira S, et al. Occurrence of hybrid *Escherichia coli* strains carrying Shiga toxin and heat-stable toxin in livestock of Bangladesh. Front Public Health. 2017;4:287. https://doi.org/10.3389/fpubh.2016.00287
26. Rodwell EV, Greig DR, Gokool S, Olonade I, Swift C, Chan YW, et al. Hybrid strains of enterotoxigenic/Shiga toxin–producing *Escherichia coli*, United Kingdom, 2014–2023. J Med Microbiol. 2025;74:001946. https://doi.org/10.1099/jmm.0.001946
27. Tabuchi A, Wakui T, Yahata Y, Yano K, Azuma K, Yamagishi T, et al. A large outbreak of enterohaemorrhagic *Escherichia coli* O157, caused by low-salt pickled Napa cabbage in nursing homes, Japan, 2012. Western Pac Surveill Response J. 2015;6:7–11. https://doi.org/10.5365/wpsar.2014.5.1.012
28. Reiss G, Kunz P, Koin D, Keeffe EB. *Escherichia coli* O157:H7 infection in nursing homes: review of literature and report of recent outbreak. J Am Geriatr Soc. 2006;54:680–4. https://doi.org/10.1111/j.1532-5415.2006.00682.x
29. Riley LW, Remis RS, Helgerson SD, McGee HB, Wells JG, Davis BR, et al. Hemorrhagic colitis associated with a rare *Escherichia coli* serotype. N Engl J Med. 1983;308:681–5. https://doi.org/10.1056/NEJM198303243081203
30. Glode MP, Robbins JB, Liu TY, Gotschlich EC, Orskov I, Orskov F. Cross-antigenicity and immunogenicity between capsular polysaccharides of group C *Neisseria meningitidis* and of *Escherichia coli* K92. J Infect Dis. 1977;135:94–102. https://doi.org/10.1093/infdis/135.1.94
31. Santé Publique France. Vaccination. 2025 [cited 2026 Mar 26]. https://www.santepubliquefrance.fr/determinants-de-sante/vaccination

Address for correspondence: Stéphane Bonacorsi, Service de Microbiologie, Hôpital Universitaire Robert-Debré, AP-HP, 48 Boulevard Sérurier, 75935 Paris CEDEX 19, France; email: stephane.bonacorsi@aphp.fr

Respirable Aerosol Production and Reduction of Avian Influenza Transmission Risk during Chicken Processing, Bangladesh

Nadia Ali Rimi, Md. Khaled Saifullah, Md. Habibullah Fahad, Kamal Hossain, Rebeca Sultana, Ireen Sultana Shanta, David E. Swayne, Syed Mohammad Golam Mortaza, Md. Giasuddin, Md. Zakir Hassan, Christopher LeBoa, Debashish Biswas, Mahbubur Rahman, Joshua A. Mott, Erin D. Kennedy, William G. Lindsley[1]

In Bangladesh, influenza A(H5N1) viruses are endemic in poultry. Processing infected chickens can aerosolize viruses, increasing the risk for human infections. We evaluated particulate matter ($PM_{2.5}$) mass concentration during slaughtering and defeathering methods used in live bird markets in Bangladesh to identify solutions to reduce aerosol exposure. We slaughtered 675 chickens using cones and barrels with 3 lid types and defeathered 45 chickens using a defeathering machine with 5 lid types. We interviewed 3 slaughterers to understand method preference. For slaughtering, barrels with a solid or star-cut lid reduced $PM_{2.5}$ mass concentrations by 65%–73% compared with uncovered barrels. For defeathering, machines fully covered by a solid lid or lid with a hole and pivot door reduced $PM_{2.5}$ mass concentrations by 50% compared with machines with no lid. Slaughterers preferred barrels covered with solid lids and defeathering machines covered with solid or hinged lids. Those methods might reduce aerosol exposure during poultry processing.

The possible human-to-human transmission of respiratory pathogens such as novel influenza viruses and coronaviruses poses an ongoing pandemic risk (*1*,*2*). Highly pathogenic avian influenza (HPAI) A(H5N1) viruses pose a major concern because of the potential for animal-to-human transmission and severe outcomes in humans (*3*). In addition, influenza A viruses, including H5N1, have pandemic potential because of their ability to reassort and mutate, possibly leading to novel strains that can spread efficiently among humans (*4*). As of November 2025, a total of 992 human cases of influenza A(H5N1), including 476 deaths (48% case-fatality rate), had been reported across 25 countries (*5*).

Live bird markets (LBMs) are globally recognized as high-risk environments for the transmission and possible reassortment of avian influenza viruses (AIV) (*6*–*8*), including in Bangladesh, where HPAI H5N1 is endemic in poultry (*9*). Transmission of AIV through aerosols is of concern because of the potential for respirable aerosols containing particulate matter <4 μm to penetrate deeply into the lungs during inhalation (*10*). Human exposure to the slaughtering and processing of sick or healthy-appearing poultry in LBMs has frequently been identified as a cause of AIV infections (*7*,*11*–*14*), and the detection of AIV RNA in environmental samples and workers underscores the persistent risk for transmission (*15*–*17*).

The slaughtering practices in LBMs are often conducted without adequate safety measures (*18*) and can contribute to generating and disseminating aerosolized

Author affiliations: University of Glasgow, Glasgow, Scotland, UK (N.A. Rimi); icddr,b, Dhaka, Bangladesh (N.A. Rimi, M.K. Saifullah, M.H. Fahad, K. Hossain, R. Sultana, I.S. Shanta, S.M.G. Mortaza, D. Biswas); University of Georgia, Athens, Georgia, USA (D.E. Swayne); Agricultural Research Service, US Department of Agriculture, Athens (D.E. Swayne); Bangladesh Livestock Research Institute, Dhaka (M. Giasuddin, M.Z. Hassan); University of California, Berkeley, California, USA (C. LeBoa); The University of Western Australia, Crawley, Western Australia, Australia (D. Biswas); Institute of Epidemiology, Disease Control and Research, Directorate General of Health Services, Dhaka (M. Rahman); Centers for Disease Control and Prevention, Atlanta, Georgia, USA (J.A. Mott, E.D. Kennedy); Centers for Disease Control and Prevention, Morgantown, West Virginia, USA (W.G. Lindsley)

DOI: https://doi.org/10.3201/eid3204.251878

[1]Current affiliation: Virginia Polytechnic Institute and State University, Blacksburg, Virginia, USA.

particles into the human breathing zone, particularly during exsanguination and mechanical defeathering of slaughtered poultry (*19*). Recognizing the need for context-specific interventions, recent efforts have focused on evaluating methods to reduce aerosol production during poultry slaughtering and defeathering (*19*–*21*). In this study, we measured particulate matter mass concentration, a commonly used measure of indoor air pollution consisting of the total mass concentration of all airborne particles <2.5 microns in diameter. We used particulate matter 2.5 ($PM_{2.5}$), indicating particulates that are <2.5 μm in diameter, as a proxy for aerosolized virus to identify methods that mitigate aerosol production during exsanguination and mechanical defeathering of slaughtered chickens.

Materials and Methods

Study Site

During January–March 2020, we replicated the slaughtering and defeathering steps commonly performed in LBMs and employed commonly used tools within a constructed booth in the National Reference Laboratory for Avian Influenza, Bangladesh Livestock Research Institute (BLRI), Savar, Dhaka (Appendix Table) (*19*). To conduct the experiments, the team followed similar procedures to those described in the pilot experiment (*19*).

Animal Selection

We used broiler chickens (*Gallus gallus domesticus*), a commonly sold species in Bangladesh LBMs (*22*). All chickens were normal market weight (≈1.7 kg) (*19*) and appeared healthy. A total of 750 chickens were used in the study: 30 chickens were used to test and standardize each experimental condition (1–2 chickens per condition), 675 were used for slaughtering experiments, and 45 were used for defeathering experiments.

Placement of Aerosol Particle Monitors

We used Particle and Temperature Sensor Plus (PATS+) particle monitors (Berkeley Air Monitoring Group, https://berkeleyair.com) to assess aerosolized $PM_{2.5}$ mass concentration (μg/m^3) during slaughtering and defeathering (*23*) (Appendix Table). To optimize measurement of $PM_{2.5}$ mass concentrations without interfering with slaughtering (Figure 1) and defeathering (Figure 2) processes, we placed the monitors 17 cm from the barrel or defeathering machine and positioned at human breathing level (148 cm) (*19*) in 3 directions: left (90°), opposite (180°), and right side (270°) relative to the entrance (Figures 1, 2).

Experiment Setup and Procedures

We hired 3 workers from the nearest local LBM on the basis of their experience in slaughtering and defeathering with commonly used equipment and their willingness to work with PPE inside the booth at BLRI. We trained each worker in the study procedure and rotated roles during the experiment to ensure consistency and minimize variability in results. We recorded baseline measurements of aerosol particles inside the booth for 5 minutes before initiating each experiment, when no slaughtering or defeathering activity was ongoing. The researchers recorded the timing of each slaughtering and defeathering and the temperature and humidity during each experiment.

Slaughtering Experiments

We used plastic barrels or slaughtering cones to contain chickens during exsanguination (Appendix Table). We used 2 types of lids to cover the plastic barrel: a solid lid and a star-cut lid (Appendix Figure 1) (*19*). We conducted 2 types of slaughtering experiments: single chicken slaughter (1 chicken per experiment) and multiple chicken slaughter (4 chickens per experiment). We performed each slaughter across 5 intervention types: open barrel without a lid, barrel covered with a solid lid, barrel covered with a star-cut lid, small cone, and large cone (Appendix Figure 1). Inside the booth, 2 workers slaughtered a chicken with a knife over the bucket and immediately put it inside the barrel or cone for its exsanguination. Open barrel experiments used no lid. For covered barrel experiments, barrels were covered with solid or star-cut lids. During multiple-slaughter experiments, chickens were quickly put inside the barrel one after another after slaughtering by sliding the solid lid or by inserting them through the star cut on the lid. We recorded aerosol $PM_{2.5}$ mass concentration measurements from the point the worker entered the booth until 5 minutes afterwards. A worker then removed the chicken from the barrel or cone and the booth. We recorded the death struggle time of each slaughtered chicken during the experiments, defined as the time between placement of the chicken into the barrel or cone after slaughtering and the cessation of visible body movements or sound or movement of flapping of the chicken from inside the barrel. In the case of multiple-chicken slaughtering, we considered the death struggle time as the time between placement of the first slaughtered chicken into the barrel or cone and cessation of movement or sound of the last chicken. We refreshed the room and booth air between each

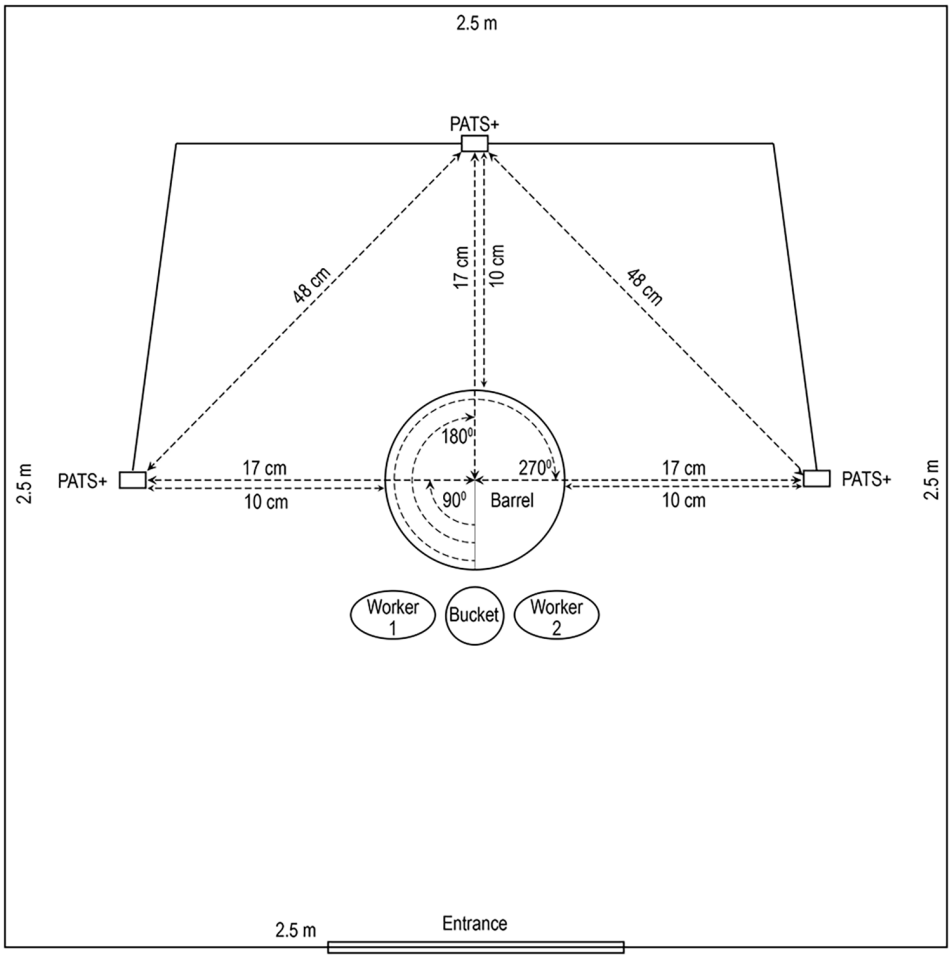

Figure 1. Diagram of placement of equipment and particle monitors inside booth for chicken slaughtering experiments at Bangladesh Livestock Research Institute, Savar, Dhaka, 2020, in study of respirable aerosol production and reduction of avian influenza transmission risk during chicken processing. The PATS+ monitors (Berkeley Air Monitoring Group, https://berkeleyair.com) were positioned at human breathing level (148 cm) in 3 angular positions: left (90°), opposite (180°), and right (270°) relative to the entrance. PATS+, Particle and Temperature Sensor Plus.

slaughtering event by removing the booth curtains and turning on air purifiers and stand fans for 5 minutes. We then recorded a baseline measurement for 5 minutes. The door and windows of the room were closed throughout the experiment. A previous study showed that aerosol $PM_{2.5}$ mass concentrations peaked and then fell within a 5-minute interval during poultry slaughtering events as recorded with the PATS+; concentrations returned close to the baseline after 5 minutes of refreshing time (*19*). We repeated the procedure 27 times for each intervention type (Figure 3).

Defeathering Experiments

The defeathering experiments consisted of 5 defeathering machine lid modifications: open machine without a lid, machine half-covered by a hinged lid (to allow for pouring water) that could be closed fully if needed, machine partially covered by a lid with a hole smaller than the defeathering machine's mouth (*19*,*21*), machine fully covered by a lid with a hole and pivot door (to cover the hole once the chicken was placed inside), and machine fully covered by a solid lid (Appendix Figure 2). Inside the booth, we placed a defeathering machine and a bucket of room-temperature water on the ground in the middle of the booth. Outside the booth, we set up a bucket, a barrel, and a container with hot water (60°C) 80 cm away from the booth. Two workers slaughtered a chicken outside the booth with a knife over the bucket, then placed the chicken inside the barrel and covered the barrel for exsanguinations for 160 seconds. The slaughterer dipped the carcass in hot water for 17 seconds, carried the chicken inside the booth using a bucket, placed it inside the defeathering machine, and ran the machine for 20 seconds. While the machine was running, the worker poured 2.5 L of room-temperature water into the machine by moving the solid lid, pouring through the hole or uncovered half of the hinged lid, or moving the pivot door of the lids. No lid was used for open defeather experiments. For covered defeather experiments, the machine was fully covered with solid lid or partially covered with the hinged or customized lids. We

recorded aerosol $PM_{2.5}$ mass concentration measurements for 5 minutes from the point the worker entered the booth. We repeated the experiment 9 times for each lid modification. We performed the same procedure of taking a baseline measurement and refreshing the air in the booth before each defeathering experiment, as was performed for the slaughtering experiments (Figure 3).

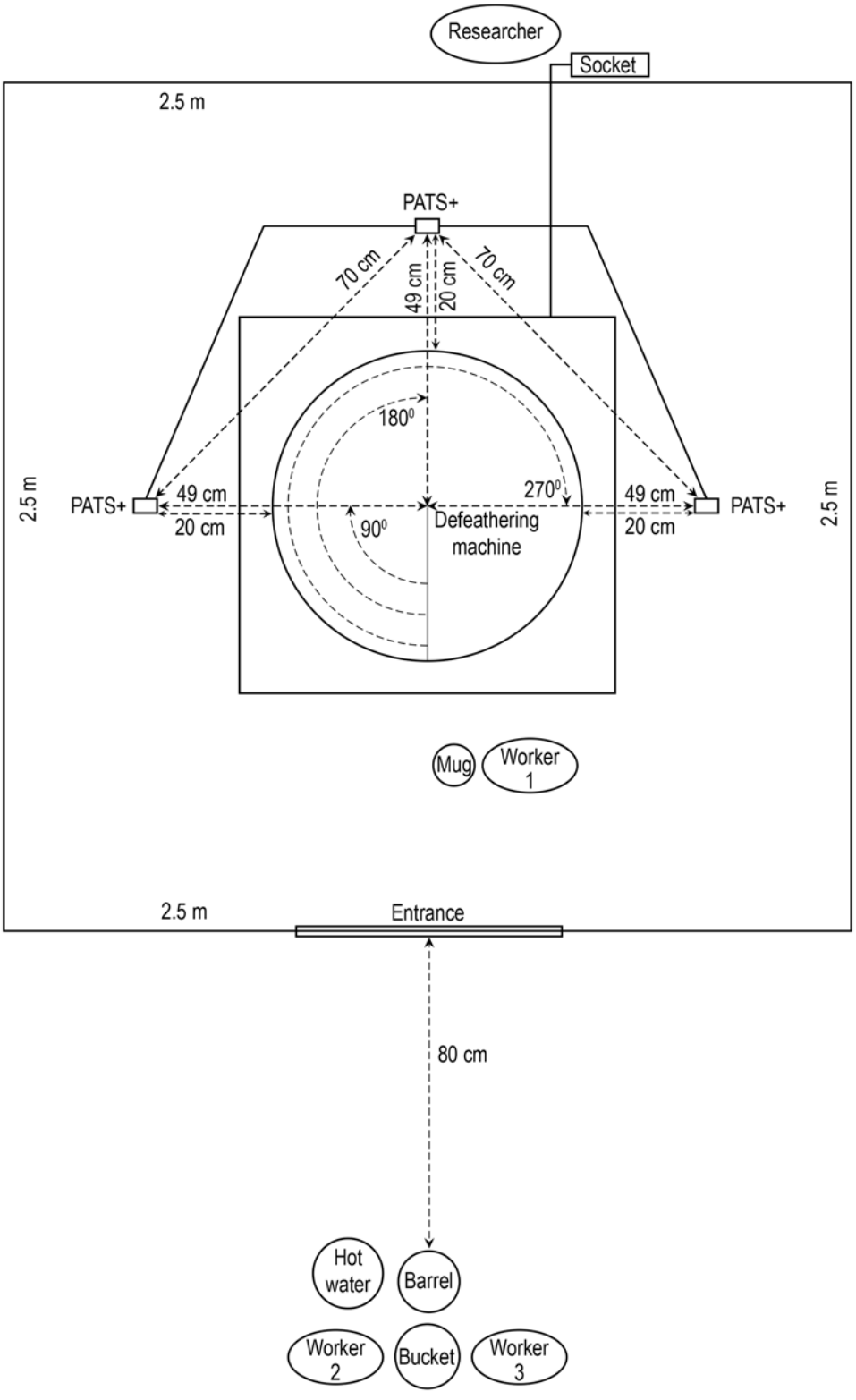

Figure 2. Diagram of placement of equipment and particle monitors inside and outside booth for chicken defeathering experiments at Bangladesh Livestock Research Institute, Savar, Dhaka, 2020, in study of respirable aerosol production and reduction of avian influenza transmission risk during chicken processing. The PATS+ monitors (Berkeley Air Monitoring Group, https://berkeleyair.com) were positioned at human breathing level (148 cm) in 3 angular positions: left (90°), opposite (180°), and right (270°) relative to the entrance. PATS+, Particle and Temperature Sensor Plus.

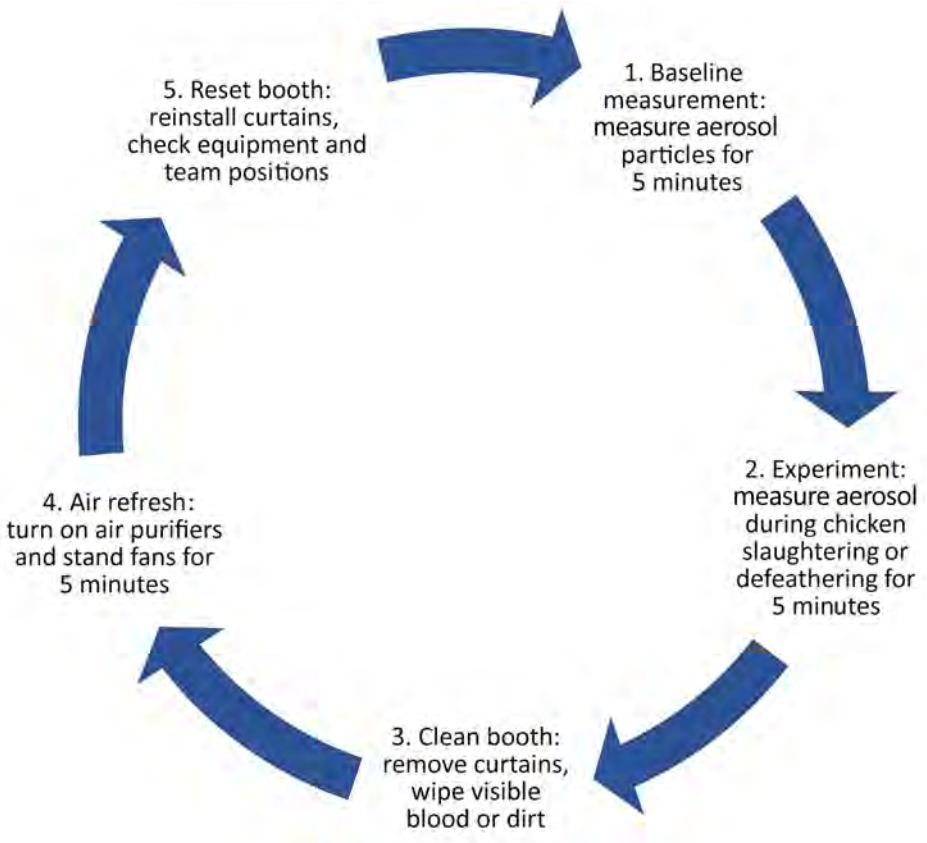

Figure 3. Chronology of each experimental event in study of respirable aerosol production and reduction of avian influenza transmission risk during chicken processing, Bangladesh Livestock Research Institute, Savar, Dhaka, 2020. Events were repeated consistently to ensure uniformity throughout the experiments. Baseline measurement of particulate matter <2.5 μm in diameter mass concentrations were measured for 5 minutes before each experiment. Aerosol measurements during processing included single chicken slaughtering (1 chicken at a time), multiple chicken slaughtering (4 chickens at a time), and single chicken defeathering (1 chicken at a time).

Sample Size Calculation

A previous pilot study reported an average $PM_{2.5}$ mass concentration of 75.8 μg/m^3 (SD 55.5 μg/m^3) during chicken slaughtering in an open barrel with the PATS+ (*24*). On the basis of that finding, we assumed a minimum difference in the mean of 50% (37.9 μg/m^3) compared with the open barrel mean of 75.8 μg/m^3; we assumed a common SD of 55.5 μg/m^3. Using a 1-sided t-test with a 5% significance level and 80% power, the estimated sample size was 135 poultry for single slaughter and 540 poultry for multiple slaughter experiments (27 per arm). Similarly, the previous experiment also found an average $PM_{2.5}$ mass concentration of 19.9 μg/m^3 (SD 8.2 μg/m^3) during defeathering using a defeathering machine without a lid (*24*). Assuming a minimum difference in the mean of 50% (9.9 μg/m^3) from the open defeathering mean of 19.9 μg/m^3 and using a 1-sided t-test with a 5% significance level and 80% power, the estimated sample size was determined to be 45 poultry (9 per arm).

Qualitative Data Collection

We conducted an in-depth interview with each of the 3 workers who had been employed to conduct the experiment to understand the advantages, disadvantages, feasibility, durability, and likelihood of adoption of each method (Appendix). Because of COVID-19 lockdown restrictions imposed by the government of Bangladesh, those interviews were conducted over mobile phone within 1 month of completing the experiments to minimize recall bias.

Data Analysis

We summarized the $PM_{2.5}$ mass concentrations using the mean and SD for each slaughtering and defeathering method, on the basis of the recorded concentrations from all experiments conducted under each condition combined and across different placements of the particle monitor. The open barrel and defeathering machine without a lid were used as reference for comparison among the different methods, because these practices were common (*19*) and were assumed to produce the highest mass concentrations. A 2-sample t-test was used to compare mean mass concentrations, and we reported the percentage difference of mean $PM_{2.5}$ mass concentration with 95% CI for each slaughtering and defeathering method, using Poisson regression with robust variance. Because we used the baseline data for each type of experiment (single and multiple slaughtering and defeathering) to test 4 different hypotheses, we considered 1.25% as level

of significance instead of 5% according to Bonferroni correction to account for multiple comparisons. We conducted data management and analysis using Stata software version 15 (StataCorp, LLC, https://www.stata.com) and performed data visualization using R version 4.3.2 (The R Project for Statistical Computing, https://www.r-project.org).

We transcribed interviews verbatim and analyzed them manually using inductive coding to identify emerging themes. Two authors independently read through the transcripts and collaboratively developed initial codes. Those codes were refined through discussion, leading to identifying themes that captured key insights. We then summarized coded data according to the study objectives and relevant themes.

Ethics

This study was reviewed and approved by the Institutional Review Boards of icddr,b (protocol number PR-19053) and US Centers for Disease Control and Prevention (see 45 C.F.R. part 46 and 21 C.F.R. part 56 and Protocol number 7237) and Institutional Animal Care and Use Committee (protocol number 3054KILCHIX). All participants provided written consent.

Results

The average $PM_{2.5}$ mass concentrations during baseline for all experiments were relatively consistent, ranging from 10.0 to 12.6 μg/m^3 (Table; Figures 4, 5), which is near the limit of detection (LOD) of the particle monitors used (LOD = 10 μg/m^3) (Appendix Table). Higher variations in baseline $PM_{2.5}$ mass concentrations (range 10.01–36 μg/m^3) were observed in 109 of 810 total readings from 3 monitors during 270 slaughter experiments.

$PM_{2.5}$ mass concentrations varied across different slaughtering methods compared with the open barrel experiments, where the mass concentration was 49.6 μg/m^3 for single slaughtering and 130.1 μg/m^3 for multiple slaughtering (Table; Figure 4). In both single and multiple slaughtering experiments, covering the barrel with a solid lid significantly reduced $PM_{2.5}$ mass concentrations. For single slaughtering, the reduction was 71.6% (95% CI 63.9%–77.7%), whereas for multiple slaughtering, the reduction was 65% (95% CI 59.7%–69.2%). We observed a similar reduction trend for barrels covered with a star-cut lid: 73.1% (95% CI 65.8%–78.9%) for single slaughtering and 65.5% (95% CI 57.7%–71.9%) for multiple slaughtering. The use of slaughtering cones did not significantly reduce aerosol levels for any slaughtering experiments (Table; Figure 4). During defeathering experiments, fully covering the machine with a solid lid or a lid with a hole and pivot door reduced $PM_{2.5}$ mass concentrations to minimum detectable levels of 10 μg/m^3. The reduction in both cases was 50% (95% CI 59.3%–38.3%) (Table; Figure 5).

The relative humidity fluctuated slightly but remained generally stable (mean 53%, SD 5.1%), and

Table. $PM_{2.5}$ mass concentration across combined sensor positions during experiments of chicken slaughtering and defeathering methods in study of respirable aerosol production and reduction of avian influenza transmission risk during chicken processing, Bangladesh Livestock Research Institute, Savar, Dhaka, 2020*

Method	Mean $PM_{2.5}$ mass concentration during baseline, μg/m^3 (min–max)†	Mean $PM_{2.5}$, μg/m^3 (SD)	$PM_{2.5}$ mass concentration difference from referent, μg/m^3	Percentage of reduced $PM_{2.5}$ mass concentration (95% CI)	p value‡
Single chicken slaughtering, n = 27					
Open barrel without lid	11.1 (10–18)	49.6 (25.4)	Referent	–	–
Barrel covered with solid lid	10.1 (10–12)	14.1 (5.5)	–35.5	–71.6 (–77.7 to –63.9)	<0.001
Barrel covered with star-cut lid	10 (10–10)	13.3 (5.2)	–36.2	–73.1 (–78.9 to –65.8)	<0.001
Small cone	10.3 (10–16)	57.4 (47.7)	7.8	15.7 (–19.6 to 66.6)	0.458
Large cone	11.4 (10–24)	44.4 (31.6)	–5.2	–10.5 (–35.5 to 24.2)	0.509
Multiple chicken slaughtering, n = 27§					
Open barrel without lid	10.4 (10–14)	130.1 (27.5)	Referent	–	–
Barrel covered with solid lid	10 (10–10)	36 (13.6)	–84.5	–64.8 (–69.2 to –59.7)	<0.001
Barrel covered with star-cut lid	10.7 (10–20)	34.3 (21.2)	–85.5	–65.5 (–71.9 to –57.7)	<0.001
Small cone	10.2 (10–12)	112 (52.3)	–8.3	–6.3 (–21.6 to 11.9)	0.470
Large cone	12.6 (10–36)	131 (60.1)	13.1	10 (–8.2 to 31.8)	0.327
Single chicken defeathering, n = 9					
Open machine without lid	10 (10–10)	20 (6.5)	Referent	–	–
Machine half covered by hinged lid	10 (10–10)	17.5 (6.7)	–2.5	–12.5 (–36.4 to 20.5)	0.438
Machine partially covered by lid with hole	10 (10–10)	13.3 (3.4)	–6.7	–33.5 (–49.0 to –13.3)	0.019
Machine fully covered by lid with hole and pivot door	10 (10–10)	10.0 (0.0)	–10	–50 (–59.4 to –38.5)	0.002
Machine fully covered by solid lid	10 (10–10)	10.0 (0.1)	–10	–49.9 (–59.3 to –38.3)	0.002

*$PM_{2.5}$, particulate matter <2.5 μm in diameter.
†$PM_{2.5}$ mass concentrations were measured for 5 minutes before each experiment.
‡Calculated using 2-sample t-test. 1.25% was considered as level of significance instead of 5% according to Bonferroni correction.

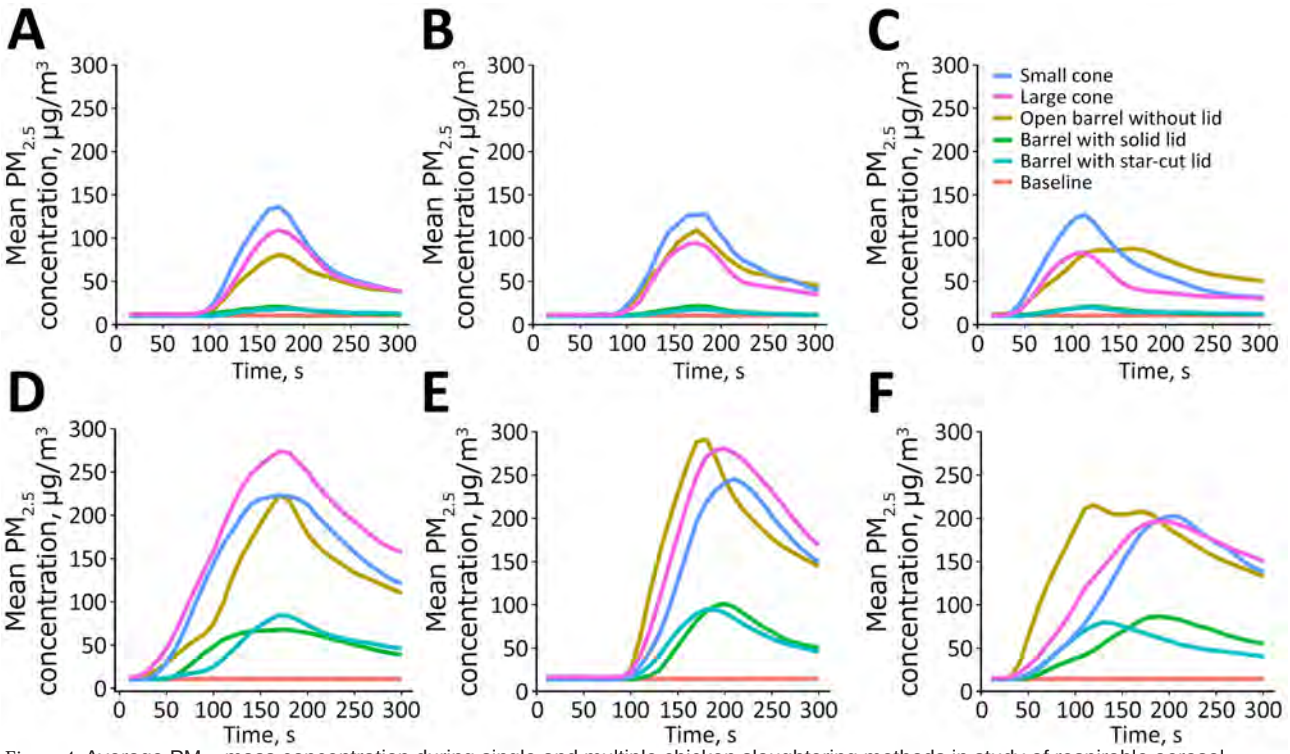

Figure 4. Average $PM_{2.5}$ mass concentration during single and multiple chicken slaughtering methods in study of respirable aerosol production and reduction of avian influenza transmission risk during chicken processing, Bangladesh Livestock Research Institute, Savar, Dhaka, 2020. Results reported by Particle and Temperature Sensor Plus monitors (Berkeley Air Monitoring Group, https://berkeleyair.com) are shown for each angle position of sensor. A) Single chicken slaughtering; angle 90°. B) Single chicken slaughtering; angle 180°. C) Single chicken slaughtering; angle 270°. D) Multiple chicken slaughtering; angle 90°. E) Multiple chickens slaughtering; angle 180°. F) Multiple chicken slaughtering; angle 270°. $PM_{2.5}$, particulate matter <2.5 μm in diameter.

temperature was also maintained without substantial variation throughout the experiment period (mean 25°C, SD 1.4°C) (Figure 6). The average duration of the death struggle was 97 (range 94–101) seconds for single slaughtering experiments and 122 (range 112–134) seconds for multiple slaughtering experiments.

The average age of the 3 hired workers was 20 (range 19–21) years; the average amount of experience work in the LBMs was 7.5 years, and all had completed primary education. Workers preferred the barrel covered with a solid lid method for poultry slaughtering, followed by the barrel covered with a star-cut lid, citing those tools' usefulness in preventing blood splattering and their ease of operation (Appendix). However, methods involving cones were met with less enthusiasm because of their unsuitability for containing >4–6 poultry at a time during busy hours and their higher associated costs (Appendix). For defeathering, workers expressed a strong preference for full cover with a solid lid, citing their familiarity with its operation and ease of use (Appendix). The half-covered hinged lid, which enabled water pouring during the process, also garnered favor among workers for its practicality. Workers were less inclined toward the lid with a hole and pivot door method, because it was less familiar and was perceived as more challenging to use (Appendix).

Discussion

Our findings show that $PM_{2.5}$ mass concentrations increased during chicken slaughtering and defeathering events across all experimental conditions; each method influenced aerosolized mass concentration levels in varying ways. Covering slaughtering containers with solid or star-cut lids and fully covering defeathering machines consistently resulted in substantial reductions in aerosolized $PM_{2.5}$ mass concentrations. Those methods were also preferred by the workers.

The open barrel method, identified as the most commonly used slaughtering practices in Dhaka City (*19*), increased airborne $PM_{2.5}$ by 38.5 μg/m^3 for a single chicken slaughter and 120.1 μg/m^3 for multiple chicken slaughter over the baseline $PM_{2.5}$ mass concentrations measured before any slaughtering took place. During both single and multiple slaughtering experiments, barrels covered with either a solid lid or a star-cut lid showed the greatest

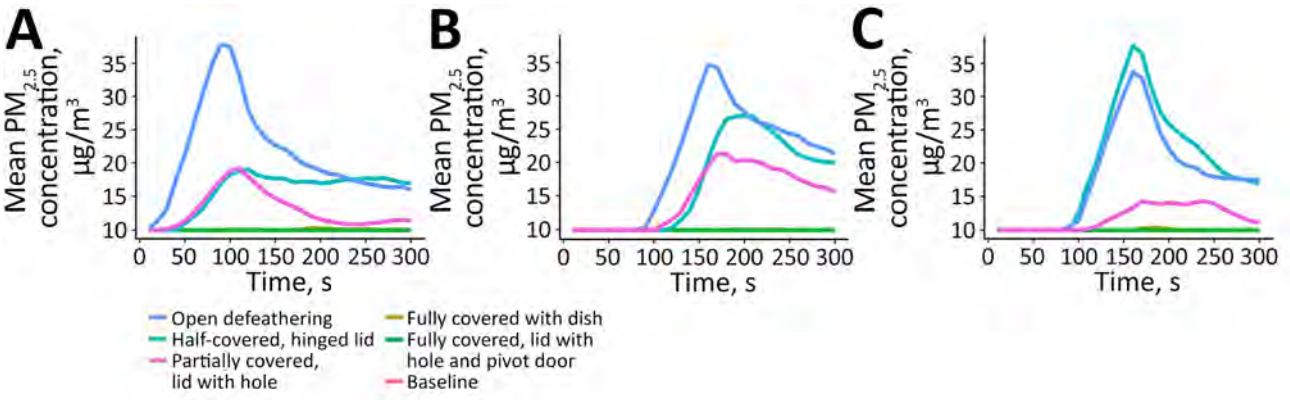

Figure 5. Average $PM_{2.5}$ mass concentration during single chicken defeathering in study of respirable aerosol production and reduction of avian influenza transmission risk during chicken processing, Bangladesh Livestock Research Institute, Savar, Dhaka, 2020. Results reported by Particle and Temperature Sensor Plus monitors (Berkeley Air Monitoring Group, https://berkeleyair.com) are shown for angle position of sensor and time of measurement in seconds: A) 90° angle; B) 180° angle; C) 270° angle. $PM_{2.5}$, particulate matter <2.5 μm in diameter.

reductions in $PM_{2.5}$ mass concentrations compared with open barrels. Multiple slaughtering produced a higher mass concentration of $PM_{2.5}$, likely because of the cumulative aerosol production from multiple chickens. Cone-based slaughtering methods increased aerosolization more than the open barrel. That outcome could be because of the distance between the slaughtered chicken and the monitor was relatively short in cones, where the chickens were positioned ≈50 cm above ground instead of at ground level (Appendix Table). Those findings suggest that improved slaughtering methods, such as the use of covered barrels, could reduce infectious disease exposure and the circulation of airborne pathogens in LBMs, thereby mitigating the risk for zoonotic transmission.

The fully covered defeathering machines (e.g., those with a solid lid or a lid with a hole and pivot door) reduced $PM_{2.5}$ mass concentrations to the minimum detectable levels of 10 μg/m^3, demonstrating their ability to prevent aerosol escape. Defeathering machines that were partially covered (e.g., with hinged lids or lids with holes) generated detectable levels of aerosol $PM_{2.5}$ mass concentration, although those levels were lower than those observed with completely open defeathering machines. That finding suggests that even partial coverings can reduce aerosol concentrations but that

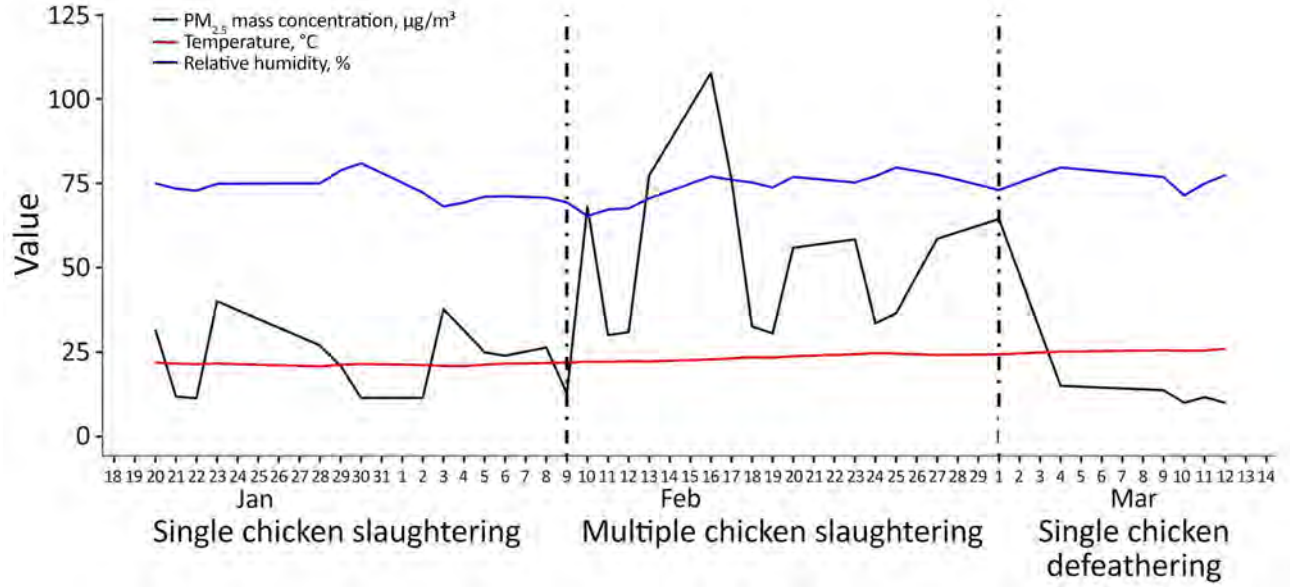

Figure 6. Trend and variability of average particulate matter mass concentration, temperature, and relative humidity in study of respirable aerosol production and reduction of avian influenza transmission risk during chicken processing, Bangladesh Livestock Research Institute, Savar, Dhaka, 2020. Results are shown for single (1 chicken at a time) and multiple (4 chickens at a time) chicken slaughtering events and defeathering events (1 chicken at a time). $PM_{2.5}$, particulate matter <2.5 μm in diameter.

they are less effective than fully closed methods. A survey conducted in LBMs of Dhaka City in 2018 found that 33% of shops used mechanical defeathering (*19*), which substantially increased the total number of generated aerosol $PM_{2.5}$ mass concentrations over manual defeathering (*20*). The use of such motor-driven devices produces strong air circulation, which is favorable for generating and dispersing aerosolized particles and is discouraged (*20*). However, such devices are increasingly popular, particularly for defeathering broiler chickens in cities (*19*). Fully covering the defeathering machine with lids might play a role in preventing aerosolized particles from escaping, potentially reducing the risk for airborne transmission of pathogens such as HPAI H5N1.

Some countries have banned LBMs to reduce risk for AIV spread (*25*,*26*). In a Muslim-majority country such as Bangladesh, adherence to halal dietary laws while slaughtering poultry requires using a well-sharpened knife to make a swift, deep incision that cuts the front of the esophagus, trachea, the jugular veins, and the carotid arteries; lining up the head of the animal to be slaughtered in the direction of the Mecca; and pronouncing Islamic invocation (*27*,*28*). A common cultural preference of consumers in Muslim-majority countries is to observe the slaughter to ensure halal requirements are met and also to verify the health and quality of the poultry (*29*). For that reason, poultry is mostly traded at LBMs (*30*), where slaughtering of live birds is commonly practiced, and efforts to ban or control markets are less likely to succeed. Therefore, improving the environment to limit the spread of viruses in LBMs is crucial. Using covered barrels and fully closed defeathering machines could be simple yet effective methods to reduce aerosol production in LBMs, where implementing more advanced biosecurity measures might be challenging because of infrastructural or economic constraints. Interventions that can involve personal discomfort, such as use of masks, are often resisted by market workers, as was observed in a behavior change intervention that identified discomfort as a reason for not following recommendations to cover the nose and mouth during poultry slaughtering (*31*). Using covered barrels and defeathering machines requires minimal behavioral change and can be integrated seamlessly into existing workflows, increasing the likelihood of adoption and sustained use. The practices of LBMs in Bangladesh, such as exsanguination into barrels or cones and mechanical defeathering, are not unique to Bangladesh; they are also used in countries such as Pakistan (*32*), Burkina Faso (*33*), and China (*34*). Our findings might be relevant for countries with LBMs and similar slaughtering practices, particularly in resource-limited Muslim communities and other settings where on-site poultry processing remains common.

The first limitation of our study is that it focused on measuring aerosol concentrations as a proxy for potential viral transmission risk and did not directly assess the presence or infectivity of AIV in the aerosols produced. We assume that aerosolized $PM_{2.5}$ mass concentration is proxy for AIV in this setting because AIVs are prevalent in the air of LBMs (*35*). However, the use of $PM_{2.5}$ as a proxy for AIV or other bioaerosols is not well understood and does not reliably estimate infectious dose or AIV particles generated in the environment. The exclusive focus on $PM_{2.5}$ in this study might restrict a comprehensive understanding of aerosol size distribution relevant to bioaerosol transmission. Future studies could include other size fractions, such as PM_1 and PM_{10}, to provide a more complete characterization of aerosolized particles involved in AIV transmission. Second, the experiments were conducted in a controlled environment with a specific poultry species, which might not fully replicate the conditions of LBMs, where factors such as airflow, crowd density, variety in poultry species (including duck), and variability in worker practices could influence aerosol dynamics and AIV infection risk. Despite those limitations, this study provides a critical roadmap for future experiments by establishing baseline data for aerosol generation during slaughtering and defeathering methods.

In conclusion, this study provides evidence that specific containment methods during exsanguination and mechanical defeathering of slaughtered chickens can substantially reduce aerosolized $PM_{2.5}$ mass concentration, potentially mitigating the risk for AIV transmission in LBMs to poultry workers and customers. Implementing those measures could be an effective, feasible, and acceptable strategy to enhance biosecurity in settings where AIV poses a persistent threat to both poultry and human health. Future studies could incorporate virological assessments to better understand the relationship between aerosol concentrations and actual viral transmission risk. Integrating lid-based interventions with other biosecurity measures, such as improved ventilation, regular disinfection, and worker health monitoring, might provide a more robust defense against zoonotic transmission of the virus.

Acknowledgments

We thank the governments of Bangladesh and Canada for providing unrestricted support. We highly appreciate the contribution of Andrew Clark for his original idea for this approach to disease control and methodology, as well as William Davis for his invaluable guidance on data analysis. We are grateful to Asadulghani and Suman Kumer Paul for their technical guidance. We also extend our thanks to Md. Nazir Ahmed and Mohammad Sabbir Hossain for their assistance in conducting the experiments. We thank Mahbub-ul-Alam and Md. Fahim Fardin for their assistance in preparing the diagrams and figures. icddr,b acknowledges with gratitude the commitment of the US Centers for Disease Control and Prevention (CDC) to its research efforts.

This study was supported by the CDC through a cooperative agreement (cooperative agreement no. 5U01GH001207) with icddr,b. The funding agency contributed to the design of the study, data analysis and interpretation, and reviewed the final manuscript. However, the funder had no role in the conduct of the study or data collection and management.

The authors have not been paid to write this article by any pharmaceutical company or other agency. Mention of any company or product does not constitute endorsement by CDC.

The corresponding author affirms that all authors had full access to the data in the study and accept responsibility for the decision to submit the manuscript for publication. Data are available on request from the authors.

N.A.R., R.S., I.S.S., D.E.S., J.A.M., E.D.K., and W.G.L. contributed to the conceptualization of the study. N.A.R. secured funding for the study. N.A.R. and R.S. were responsible for the investigation, and the methodology was developed by N.A.R., R.S., M.H.F., K.M., and W.G.L. Project administration was done by N.A.R., R.S., I.S.S., M.K.S., M.H.F., and S.M.G.M. Resources were provided by M.G., M.R., and M.Z.H. N.A.R. supervised the project, while data curation and validation was performed by M.K.S., M.H.F., S.M.G.M., and K.M. Formal analysis was conducted by M.K.S., M.H.F., K.M., C.L., N.A.R., and W.G.L. The original draft was written by N.A.R., M.K.S., and W.G.L. All authors contributed to the review and editing of the manuscript. They had full access to all the data and verify the accuracy and integrity of the data reported in the manuscript.

About the Author

Ms. Rimi works as a program coordinator and associate scientist at icddr,b, Bangladesh. Her research work centers on zoonotic diseases and One Health, exploring risk perception and behaviors for disease transmission at high-risk locations including live bird markets and designing, implementing, and evaluating context-specific biosecurity and hygiene interventions.

References

1. Richard M, Fouchier RA. Influenza A virus transmission via respiratory aerosols or droplets as it relates to pandemic potential. FEMS Microbiol Rev. 2016;40:68–85. https://doi.org/10.1093/femsre/fuv039
2. Rabaan AA, Al-Ahmed SH, Al-Malkey M, Alsubki R, Ezzikouri S, Al-Hababi FH, et al. Airborne transmission of SARS-CoV-2 is the dominant route of transmission: droplets and aerosols. Infez Med. 2021;29:10–9.
3. Charostad J, Rezaei Zadeh Rukerd M, Mahmoudvand S, Bashash D, Hashemi SMA, Nakhaie M, et al. A comprehensive review of highly pathogenic avian influenza (HPAI) H5N1: an imminent threat at doorstep. Travel Med Infect Dis. 2023;55:102638. https://doi.org/10.1016/j.tmaid.2023.102638
4. Jackson S, Van Hoeven N, Chen LM, Maines TR, Cox NJ, Katz JM, et al. Reassortment between avian H5N1 and human H3N2 influenza viruses in ferrets: a public health risk assessment. J Virol. 2009;83:8131–40. https://doi.org/10.1128/JVI.00534-09
5. World Health Organization. Cumulative number of confirmed human cases for avian influenza A(H5N1) [cited 2025 Nov 23]. https://cdn.who.int/media/docs/default-source/influenza/h5n1-human-case-cumulative-table/cumulative-number-of-confirmed-human-cases-for-avian-influenza-a(h5n1)-reported-to-who--2003-2025ac90dee8-f1c4-4ff6-b891-f92e0df414cb.pdf
6. Zhou J, Wu J, Zeng X, Huang G, Zou L, Song Y, et al. Isolation of H5N6, H7N9 and H9N2 avian influenza A viruses from air sampled at live poultry markets in China, 2014 and 2015. Euro Surveill. 2016;21:30331. https://doi.org/10.2807/1560-7917.ES.2016.21.35.30331
7. Lai S, Qin Y, Cowling BJ, Ren X, Wardrop NA, Gilbert M, et al. Global epidemiology of avian influenza A H5N1 virus infection in humans, 1997–2015: a systematic review of individual case data. Lancet Infect Dis. 2016;16:e108–18. https://doi.org/10.1016/S1473-3099(16)00153-5
8. Wei J, Zhou J, Cheng K, Wu J, Zhong Z, Song Y, et al. Assessing the risk of downwind spread of avian influenza virus via airborne particles from an urban wholesale poultry market. Build Environ. 2018;127:120–6. https://doi.org/10.1016/j.buildenv.2017.10.037
9. Loth L, Gilbert M, Osmani MG, Kalam AM, Xiao X. Risk factors and clusters of highly pathogenic avian influenza H5N1 outbreaks in Bangladesh. Prev Vet Med. 2010;96:104–13. https://doi.org/10.1016/j.prevetmed.2010.05.013
10. Bertran K, Balzli C, Kwon Y-K, Tumpey TM, Clark A, Swayne DE. Airborne transmission of highly pathogenic influenza virus during processing of infected poultry. Emerg Infect Dis. 2017;23:1806–14. https://doi.org/10.3201/eid2311.170672
11. Van Kerkhove MD, Mumford E, Mounts AW, Bresee J, Ly S, Bridges CB, et al. Highly pathogenic avian influenza (H5N1): pathways of exposure at the animal-human interface, a systematic review. PLoS One. 2011;6:e14582. https://doi.org/10.1371/journal.pone.0014582
12. Institute of Epidemiology Disease Control and Research. Fifth and sixth H5N1 human case in Bangladesh [cited 2015 March 15]. http://www.iedcr.org/pdf/files/influenza/Fifth_and_Sixth_H5N1.pdf

13. Chakraborty A, Rahman M, Hossain MJ, Khan SU, Haider MS, Sultana R, et al. Mild respiratory illness among young children caused by highly pathogenic avian influenza A (H5N1) virus infection in Dhaka, Bangladesh, 2011. J Infect Dis. 2017;216(suppl_4):S520–8. https://doi.org/10.1093/infdis/jix019
14. Dong Z, Ma J, Qiu J, Ren Q, Shan Q, Duan X, et al. Airborne fine particles drive H1N1 viruses deep into the lower respiratory tract and distant organs. Sci Adv. 2023;9:eadf2165. https://doi.org/10.1126/sciadv.adf2165
15. Nasreen S, Khan SU, Luby SP, Gurley ES, Abedin J, Zaman RU, et al. Highly pathogenic avian influenza A(H5N1) virus infection among workers at live bird markets, Bangladesh, 2009–2010. Emerg Infect Dis. 2015;21:629–37. https://doi.org/10.3201/eid2104.141281
16. Hassan MZ, Sturm-Ramirez K, Islam MS, Afreen S, Rahman MZ, Kafi MAH, et al. Interpretation of molecular detection of avian influenza A virus in respiratory specimens collected from live bird market workers in Dhaka, Bangladesh: infection or contamination? Int J Infect Dis. 2023;136:22–8. https://doi.org/10.1016/j.ijid.2023.08.020
17. Chen X, Wang W, Wang Y, Lai S, Yang J, Cowling BJ, et al. Serological evidence of human infections with highly pathogenic avian influenza A(H5N1) virus: a systematic review and meta-analysis. BMC Med. 2020;18:377. https://doi.org/10.1186/s12916-020-01836-y
18. UNICEF. Evaluation of avian influenza communication for development initiative—improving biosecurity in live bird markets: lessons learned report. Dhaka (Bangladesh): Center for Communicable Diseases; 2013.
19. Rimi NA, Fahad MH, Clark A, Sultana R, Hossain K, Saifullah MK, et al. Developing a method to estimate aerosol generation during poultry slaughtering and defeathering in Bangladesh: an experimental study. Build Environ. 2025; 271:112621. https://doi.org/10.1016/j.buildenv.2025.112621
20. Bertran K, Clark A, Swayne DE. Mitigation strategies to reduce the generation and transmission of airborne highly pathogenic avian influenza virus particles during processing of infected poultry. Int J Hyg Environ Health. 2018;221:893–900. https://doi.org/10.1016/j.ijheh.2018.05.013
21. Wei J, Zhou J, Liu Y, Wu J, Jin T, Li Y, et al. A novel partial lid for mechanical defeatherers reduced aerosol dispersion during processing of avian influenza virus infected poultry. PLoS One. 2019;14:e0216478. https://doi.org/10.1371/journal.pone.0216478
22. Moyen N, Hoque MA, Mahmud R, Hasan M, Sarkar S, Biswas PK, et al. Avian influenza transmission risk along live poultry trading networks in Bangladesh. Sci Rep. 2021;11:19962. https://doi.org/10.1038/s41598-021-98989-4
23. Group BAM. Integrated cookstove assessment software (PICA) and the Particle and Temperature Sensor (PATS+) for air pollution measurements [cited 2025 Mar 28]. https://berkeleyair.com/wp-content/publications/Berkeley%20Air%20PICA%20and%20PATS+%20Flyer.pdf
24. Rimi N, Lindsley W, Clark A, Swayne D, Kile J, Fahad MH, et al. Pilot experiments to estimate respirable aerosols produced during poultry slaughtering and defeathering. Presented at: 10th Edition of Options for the Control of Influenza (Options X); August 28–September 1, 2019; Suntec City, Singapore.
25. Food and Agriculture Organization of the United Nations. All poultry must be slaughtered at the poultry slaughter-house to minimize the risk of avian influenza spread [cited 2024 Sep 17]. https://openknowledge.fao.org/server/api/core/bitstreams/2a64b049-a751-4416-bc65-52f827276c1c/content
26. Chen Y, Cheng J, Xu Z, Hu W, Lu J. Live poultry market closure and avian influenza A (H7N9) infection in cities of China, 2013–2017: an ecological study. BMC Infect Dis. 2020;20:369. https://doi.org/10.1186/s12879-020-05091-7
27. Aghwan ZA, Regenstein JM. Slaughter practices of different faiths in different countries. J Anim Sci Technol. 2019;61:111–21. https://doi.org/10.5187/jast.2019.61.3.111
28. Rimi NA, Sultana R, Ishtiak-Ahmed K, Khan SU, Sharker MA, Uz Zaman R, et al. Poultry slaughtering practices in rural communities of Bangladesh and risk of avian influenza transmission: a qualitative study. EcoHealth. 2014;11:83–93. https://doi.org/10.1007/s10393-013-0885-8
29. Sinclair M, Hötzel MJ, Lee NY, De Luna MCT, Sharma A, Idris M, et al. Animal welfare at slaughter: perceptions and knowledge across cultures. Front Anim Sci. 2023;4:1141789. https://doi.org/10.3389/fanim.2023.1141789
30. Dolberg F. Poultry sector country review—Bangladesh [cited 2025 Mar 28]. http://www.fao.org/3/a-ai319e.pdf
31. Rimi NA, Sultana R, Ishtiak-Ahmed K, Rahman MZ, Hasin M, Islam MS, et al. Understanding the failure of a behavior change intervention to reduce risk behaviors for avian influenza transmission among backyard poultry raisers in rural Bangladesh: a focused ethnography. BMC Public Health. 2016;16:858. https://doi.org/10.1186/s12889-016-3543-6
32. Hasnain K. City diary: new paradigm for chicken slaughter [cited 2025 Mar 28]. https://www.dawn.com/news/1238285/city-diary-new-paradigm-for-chicken-slaughter
33. Assefa A, Dione M, Ilboudo G, Lallogo V, Gemeda BA, Grace D, et al. Quantitative analysis of knowledge, attitude and practice of workers in chicken slaughter slabs toward food safety and hygiene in Ouagadougou, Burkina Faso. Front Sustain Food Syst. 2022;6:1091209.
34. Cheng KL, Wu J, Shen WL, Wong AYL, Guo Q, Yu J, et al. Avian influenza virus detection rates in poultry and environment at live poultry markets, Guangdong, China. Emerg Infect Dis. 2020;26:591–5. https://doi.org/10.3201/eid2603.190888
35. Wang K, Shen D, Dai P, Li C. Particulate matter in poultry house on poultry respiratory disease: a systematic review. Poult Sci. 2023;102:102556. https://doi.org/10.1016/j.psj.2023.102556

Address for correspondence: Nadia Ali Rimi, Infectious Diseases Division, icddr,b, 68, Shaheed Tajuddin Ahmed Sarani, Mohakhali, Dhaka-1212, Bangladesh; email: nadiarimi@icddrb.org

Chronic Wasting Disease in Farmed Cervids, South Korea, 2001–2024

Young Pyo Choi, Yu-Ran Lee, Hoo Chang Park, Yoon Hee Lee, Gordon Mitchell, In-Soon Roh, Hyun-Joo Sohn

Chronic wasting disease (CWD) was identified in imported elk in South Korea in 2001 and has spread among cervids nationwide. The country's surveillance and control policy culls cervids from any CWD-positive farms, and prevalence during 2020–2024 was <0.5%. Maintaining low prevalence in cervids will limit livestock, wildlife, and human CWD exposure.

Chronic wasting disease (CWD) is a highly contagious prion disease in free-ranging and farmed cervids, affecting species such as sika deer (*Cervus nippon*), red deer (*C. elaphus*), and elk (*C. canadensis*). Since it was first recognized in Colorado, USA, in the 1960s (*1*), CWD has spread widely across North America, where cases have been identified in 36 US states and 5 provinces of Canada (*2*,*3*). CWD has also been detected in parts of the Scandinavian Peninsula (*4*,*5*). In South Korea, CWD was first detected in 2001 in elk imported from Canada, and cervid cases occurred annually during 2016–2024 (*6*–*9*). To study of the epidemiology of CWD in cervids and understand the exposure risk other species, we assessed CWD occurrence among farmed cervids in South Korea during 2001–2024.

The Study

South Korea conducts CWD surveillance in accordance with the Korean Act on the Prevention of Contagious Animal Diseases, under which CWD is designated as a Type 2 infectious disease (Appendix, https://wwwnc.cdc.gov/EID/article/32/4/25-1046-App1.pdf). The World Organisation for Animal Health Reference Laboratory at the Animal and Plant Quarantine Agency in South Korea performs CWD diagnosis for surveillance. The Korea Animal Health Integrated System maintains detailed CWD occurrence records (https://home.kahis.go.kr). We obtained annual farmed cervid population data from Ministry of Agriculture, Food and Rural Affairs of Korea reports.

CWD surveillance in farmed cervids in South Korea comprises 2 primary categories: high-risk and routine slaughter. High-risk animals include cervids found dead or exhibiting clinical signs suggestive of CWD, animals culled from CWD-positive farms, and animals culled from farms epidemiologically linked to CWD-positive farms. When CWD is confirmed in a high-risk animal, all remaining animals on the affected and epidemiologically linked farms are culled, as detailed elsewhere (*10*). For routine slaughter surveillance, brain and lymph node samples from cervids slaughtered for human consumption are routinely collected and sent for testing.

Since 2001, a total of 429 farmed cervids in South Korea have tested positive for CWD (Table 1; Appendix Table 1). During 2001–2005, all CWD-positive animals were elk imported from Canada. After a 5-year period with no cases, CWD reemerged in 2010, affecting elk, red deer, and sika deer. The 19 cases reported in 2010, comprising 6 elk, 6 red deer, and 7 sika deer, were the first direct evidence of domestic CWD transmission. After a second 5-year interval (2011–2015), CWD reemerged in 2016, with 44 infected animals across the 3 cervid species at 8 farms. Since 2016, CWD has been detected nearly annually at a rate of 13–104 cases per year across multiple farms, indicating its endemic status in South Korea's farmed cervids. Of note, cases in red and sika deer have sharply declined, and fewer annual cases were reported during 2020–2024.

Of the 429 CWD cases in farmed cervids during 2001–2024, most (97.9%) were detected through high-risk surveillance, and only 9 (2.1%) were identified through routine slaughter surveillance. The percentage of CWD cases detected through high-risk surveillance varied by occurrence stage: 78.3% of cases were

Author affiliations: Korea Brain Research Institute, Daegu, South Korea (Y.P. Choi); World Organisation for Animal Health Reference Laboratory for Chronic Wasting Disease, Gimcheon, South Korea (Y.-R. Lee, H.C. Park, Y.H. Lee, I.-S. Roh, H.-J. Sohn); National and World Organisation for Animal Health Reference Laboratory for Scrapie and Chronic Wasting Disease, Canadian Food Inspection Agency, Ottawa, Ontario, Canada (G. Mitchell)

DOI: https://doi.org/10.3201/eid3204.251046

Table 1. Occurrence stage and animals affected by CWD in farmed cervids, South Korea, 2001–2024*

Occurrence stage	No. farms	CWD testing, no. positive/no. tested			
		Total	Red deer (*Cervus elephus*)	Elk (*C. canadensis*)	Sika deer (*C. nippon*)
Imported elk stage, 2001–2005					
2001	4	9/177	–	9/177	–
2004	5	12/75	–	12/75	–
2005	1	2/130	–	2/130	–
Initial domestic transmission stage, 2010	3	19/185	6/80	6/82	7/23
Endemic stage, 2016–2024					
2016	8	44/299	22/62	6/151	16/86
2018	6†	13/359	7/91	5/218	1/50
2019	4‡	62/391	52/162	10/224	0/5
2020	4	104/672	9/65	70/471	25/136
2021	3†	21/290	4/46	14/171	3/73
2022	7†	60/463	1/12	53/367	6/84
2023	5	34/573	–	34/481	0/92
2024	3§	49/439	0/5	46/429	3/5
Total	53	429/4,053	101/523	267/2,976	61/554

*CWD, chronic wasting disease; –, no species testing.
†Includes 1 recurrence farm in Gyeongnam province where CWD recurred after remediation and subsequent reintroduction of cervids.
‡Includes 1 recurrence farm in Chungnam province where CWD recurred after remediation and subsequent reintroduction of cervids.
§Includes 1 recurrence farm in Jeonnam province where CWD recurred after remediation and subsequent reintroduction of cervids.

detected among high-risk animals during the imported elk stage (2001–2005), 89.5% during the initial domestic transmission stage (2010), and 99.5% during the endemic stage (2016–2024). Although most (71.7%, 276/385) cases during the endemic stage were from animals culled on CWD-confirmed farms within the high-risk category, cases during the imported elk stage were more evenly distributed across the 3 high-risk groups. Among the high-risk groups, animals found dead or exhibiting clinical signs had the highest CWD positivity rates during the endemic (36.7%) and imported elk (9.5%) stages, whereas animals culled from CWD-confirmed farms showed the highest positivity rate (23.5%) during the initial domestic transmission stage.

Since 2014, more than 2,800 wild cervids have been tested for CWD. Surveillance mainly targeted Korean water deer (*Hydropotes inermis argyropus*; 85.4% of tested animals) on the mainland and Siberian roe deer (*Capreolus pygargus*) on Jeju Island, but no positive cases had been detected by 2024 (Table 2).

Herd size on the 53 CWD-affected farms varied widely, ranging from 2 to 275 cervids (Figure 1). More than 70% of the farms raised <100 animals; only 3 farms had >200 animals. The number of CWD-positive animals also varied widely across farms; 38 farms had <10 CWD-positive animals, and 11 of those reported only 1 case (Figure 1, panel A). The highest number of CWD-positive animals on a single farm was 54 of 275 animals, corresponding to a positivity rate of 19.6%. Among the farms, 39 (73.9%) had CWD positivity rates <20%, of which 26 (49% of the 53 farms) had rates <10%. In contrast, 4 farms exhibited positivity rates of ≥50%, 2 of which had only 2 cervids. Analysis by species showed that 42.3% of the farms raising red deer, 52.4% of the farms raising sika

Table 2. Surveillance results for CWD in farmed cervids, South Korea, 2001–2024*

Stage†	Farmed cervids								
	High-risk cervids				Slaughtered cervids				
	Found dead or showing clinical signs	Culled from CWD-confirmed farms	Culled from CWD-linked farms	Total	Routine surveillance	Culled from CWD-linked farms	Total	Total	Wild cervids‡
Imported elk	6/63 (9.5)	5/279 (1.8)	7/278 (2.5)	18/620 (2.9)	4/167 (2.4)	1/31 (3.2)	5/198 (2.5)	23/818 (2.8)	NA
Initial domestic transmission§	1/22 (4.5)	8/34 (23.5)	8/208 (3.8)	17/264 (6.4)	1/65 (1.5)	1/102 (1.0)	2/167 (1.2)	19/431 (4.4)	NA
Endemic	47/128 (36.7)	276/2,894 (9.5)	62/988 (6.3)	385/4,010 (9.6)	2/126 (1.6)	NA	2/126 (1.6)	387/4,136 (9.4)	0/2,867
Total	54/213 (25.4)	289/3,207 (9.0)	77/1,474 (5.2)	420/4,894 (8.6)	7/358 (2.0)	2/133 (1.5)	9/491 (2.0)	429/5,385 (8.0)	0/2,867

*Values are no. CWD-positive/no. tested (%). CWD, chronic wasting disease; NA, not applicable.
†Imported elk stage was 2001–2005; initial domestic transmission was 2010; endemic stage was 2016–2024.
‡CWD surveillance of wild cervids in South Korea began in 2014. The data indicate the number of wild cervids tested during the period 2014−2024. Most (85.4%) tested wild cervids are Korean water deer (*Hydropotes inermis argyropus*), which is the dominant wild cervid species on the mainland of South Korea. On Jeju Island, testing focused on Siberian roe deer (*Capreolus pygargus*), the region's resident species.
§In 2010, 493 cervids culled from 14 farms as part of tuberculosis control measures were also tested for CWD; all were CWD-negative.

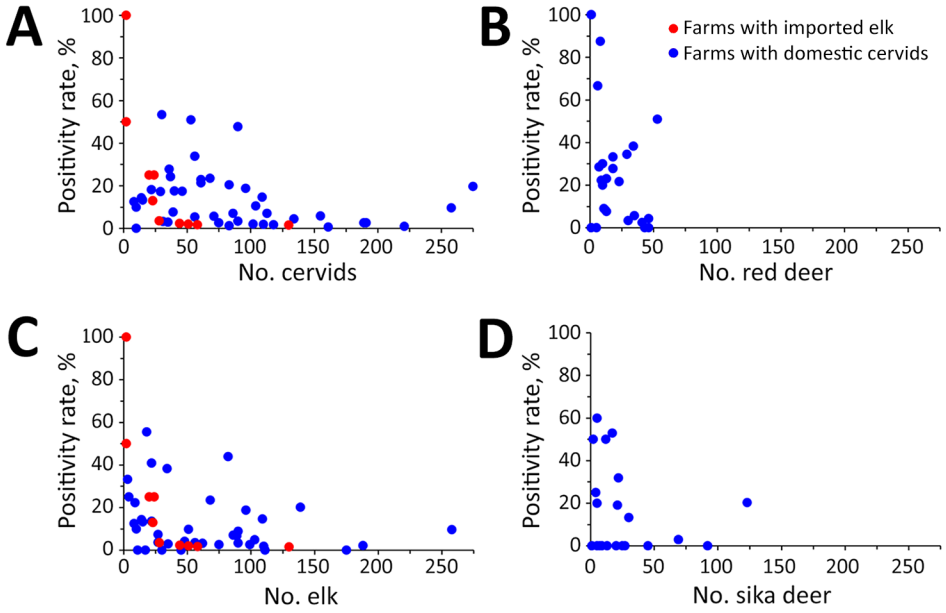

Figure 1. Chronic wasting disease positivity rates in farmed cervids, South Korea, 2001–2024. A) All farmed cervids; B) red deer; C) elk; D) sika deer. Each dot represents a single farm. Positivity rates were calculated as no. animals testing positive/no. animals tested on each farm. Dots reflect the farm's cervid population because all farmed cervids were culled and tested on farms with positive cases. For species-specific analyses, each cervid species on each farm was assessed separately.

deer, and 58.0% of farms raising elk had CWD positivity rates <10% (Figure 1, panels B–D). Positivity rates of ≥50% were more commonly observed in red and sika deer (19.0%–19.2%) than in elk (6.0%).

We investigated the annual nationwide CWD prevalence from its first detection in 2001 through 2024. We calculated prevalence by dividing the number of CWD cases by the total farmed cervid population in the country for each corresponding year. The imported elk stage (2001–2005) and the initial domestic transmission stage (2010) both showed low (<0.3%) CWD prevalence, whereas the endemic stage (2016–2024) exhibited markedly higher and more variable prevalence rates (Figure 2). The highest (4.22%) prevalence occurred in red deer in 2019 (Figure 2, panel B). Although prevalence in elk remained relatively stable during 2022–2024 (Figure 2, panel C), prevalence

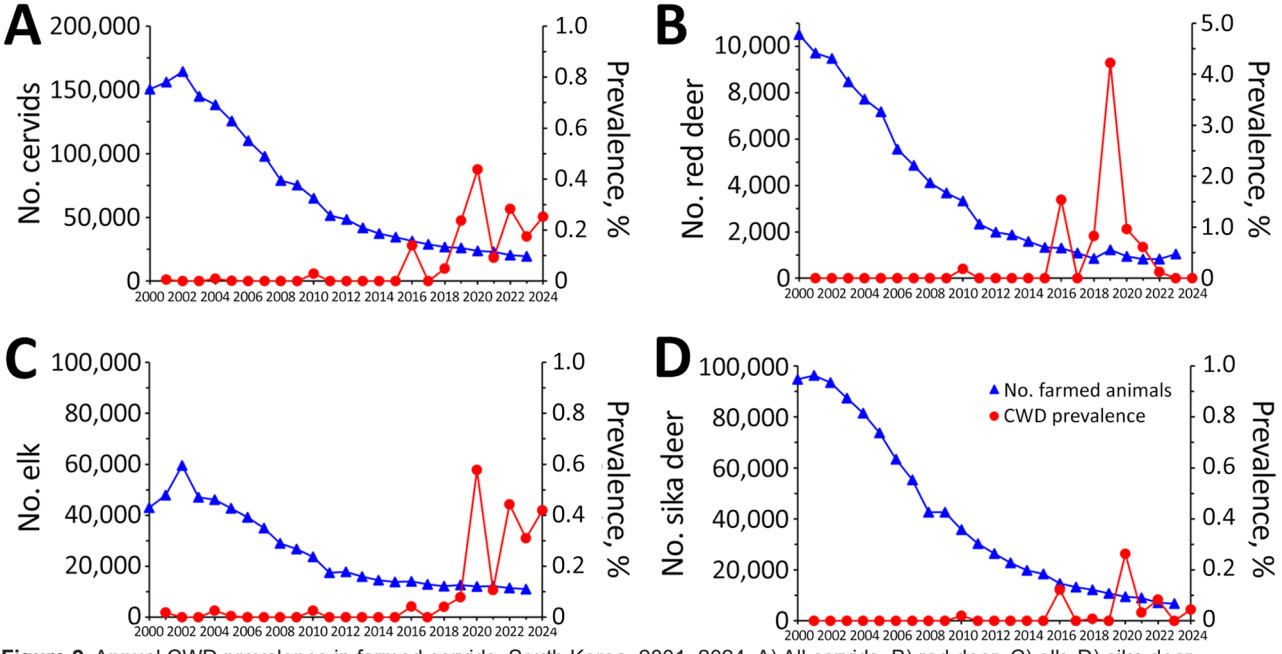

Figure 2. Annual CWD prevalence in farmed cervids, South Korea, 2001–2024. A) All cervids; B) red deer; C) elk; D) sika deer. Prevalence (%) was calculated as no. CWD-positive cervids/nationwide farmed cervid population for each species per year. Population data for 2024 was not available, so 2023 population data was used to calculate prevalence for 2024. CWD, chronic wasting disease.

declined to near zero in red and sika deer (Figure 2, panels B, D). Of note, the farmed cervid population declined markedly over the 2 decades we studied, particularly in red and sika deer. Red deer numbers fell from 9,712 in 2001 to 1,040 in 2023, and sika deer numbers fell from 96,282 to 6,673 over the same period.

During 2001–2024, South Korea confirmed a total of 429 CWD cases across 3 cervid species on 53 farms, most of which occurred during the endemic stage (2016–2024). CWD has progressed from an initial localized cluster to nationwide endemic distribution (Appendix Figure). That geographic expansion could be associated with 2 major factors. One is the residual stock of high-risk imported cervids from Canada that could not be fully traced during the initial control measures of the imported elk stage (*7*). The other is unrestricted movement of cervids between farms, which is difficult to manage because no animal tracking system is available for farmed cervids in South Korea (*10*). In addition, infectious prions can remain in the farm environment, even after intensive decontamination measures, and farms could serve as long-term reservoirs for recurrent CWD (*11*–*14*).

Conclusions

Although CWD prevalence in farmed red and sika deer has declined in South Korea, approaching zero in recent years, it remains endemic at low levels in elk, and overall prevalence is ≈0.4%. The sharp contrast between North America's increasing CWD rates (*12*) and South Korea's decline in CWD prevalence could be associated with contextual and policy differences. South Korea implemented an aggressive national policy to eliminate CWD, which is a feasible strategy in that country because CWD remains confined to farmed cervids (*10*,*15*). Adherence to the current disease control policy is projected to manage the disease at its current low prevalence of <0.5%. Although the risk for CWD transmission to humans is believed to be low (*12*), South Korea's continued efforts to reduce CWD prevalence among farmed cervids will limit human exposure and help mitigate such risks.

The data supporting the findings of this study are available from the corresponding authors, I.-S.R. and H.-J.S., upon reasonable request.

This research was supported by the Animal and Plant Quarantine Agency, Ministry for Agriculture, Food and Rural Affairs, Korea (approval no. B-1543085-25-27-01).

Author contributions: Y.P.C. and H.-J.S. conceived and designed the experiment; Y.-R.L., H.C.P., Y.-H.L., and I.-S.R. performed the experiments; Y.P.C., Y.-H.L., G.M., I.-S.R., and H.-J.S. analyzed the data; H.-J.S. and Y.P.C. wrote the manuscript. All authors read and approved the final manuscript.

About the Author

Dr. Choi is a principal researcher at the Korea Brain Research Institute, Daegu, South Korea. His research interests include prion diseases, zoonotic infectious diseases, and neurodegenerative diseases involving protein misfolding.

References

1. Williams ES, Young S. Chronic wasting disease of captive mule deer: a spongiform encephalopathy. J Wildl Dis. 1980;16:89–98. https://doi.org/10.7589/0090-3558-16.1.89
2. Bartz JC, Benavente R, Caughey B, Christensen S, Herbst A, Hoover EA, et al.; The Nc North American Interdisciplinary Chronic Wasting Disease Research Consortium Members. Chronic wasting disease: state of the science. Pathogens. 2024;13:138. https://doi.org/10.3390/pathogens13020138
3. US Geological Survey. Distribution of chronic wasting disease in North America (updated) [cited 2025 Jul 7]. https://www.usgs.gov/centers/nwhc/science/expanding-distribution-chronic-wasting-disease
4. Tranulis MA, Gavier-Widén D, Våge J, Nöremark M, Korpenfelt SL, Hautaniemi M, et al. Chronic wasting disease in Europe: new strains on the horizon. Acta Vet Scand. 2021;63:48. https://doi.org/10.1186/s13028-021-00606-x
5. Benestad SL, Mitchell G, Simmons M, Ytrehus B, Vikøren T. First case of chronic wasting disease in Europe in a Norwegian free-ranging reindeer. Vet Res. 2016;47:88. https://doi.org/10.1186/s13567-016-0375-4
6. Sohn HJ, Kim JH, Choi KS, Nah JJ, Joo YS, Jean YH, et al. A case of chronic wasting disease in an elk imported to Korea from Canada. J Vet Med Sci. 2002;64:855–8. https://doi.org/10.1292/jvms.64.855
7. Kim TY, Shon HJ, Joo YS, Mun UK, Kang KS, Lee YS. Additional cases of chronic wasting disease in imported deer in Korea. J Vet Med Sci. 2005;67:753–9. https://doi.org/10.1292/jvms.67.753
8. Roh IS, Kim YC, Kim HJ, Won SY, Jeong MJ, Hwang JY, et al. Polymorphisms of the prion-related protein gene are strongly associated with cervids' susceptibility to chronic wasting disease. Vet Rec. 2022;190:e940. https://doi.org/10.1002/vetr.940
9. Park KJ, Park H-C, Lee Y-R, Mitchell G, Choi YP, Sohn H-J. Detection of chronic wasting disease prions in the farm soil of the Republic of Korea. MSphere. 2025;10:e0086624. https://doi.org/10.1128/msphere.00866-24
10. Park KJ, Park HC, Lee YR, Roh IS, Mitchell G, Choi YP, et al. Addressing chronic wasting disease in Korean farms: topsoil removal and 2N NaOH treatment before cervid restocking. Prion. 2025;19:20–7. https://doi.org/10.1080/19336896.2025.2527588
11. Miller MW, Williams ES, Hobbs NT, Wolfe LL. Environmental sources of prion transmission in mule deer.

Emerg Infect Dis. 2004;10:1003–6. https://doi.org/10.3201/eid1006.040010
12. Saunders SE, Bartelt-Hunt SL, Bartz JC. Occurrence, transmission, and zoonotic potential of chronic wasting disease. Emerg Infect Dis. 2012;18:369–76. https://doi.org/10.3201/eid1803.110685
13. Konold T, Spiropoulos J, Bellerby P, Simmons HA. Failure to prevent classical scrapie after repeated decontamination of a barn. BMC Res Notes. 2025;18:126. https://doi.org/10.1186/s13104-025-07188-1
14. Denkers ND, McNulty EE, Kraft CN, Nalls AV, Westrich JA, Hoover EA, et al. Temporal characterization of prion shedding in secreta of white-tailed deer in longitudinal study of chronic wasting disease, United States. Emerg Infect Dis. 2024;30:2118–27. https://doi.org/10.3201/eid3010.240159
15. Rivera NA, Brandt AL, Novakofski JE, Mateus-Pinilla NE. Chronic wasting disease in cervids: prevalence, impact and management strategies. Vet Med (Auckl). 2019;10:123–39. https://doi.org/10.2147/VMRR.S197404

Address for correspondence: In-Soon Roh or Hyun-Joo Sohn, WOAH Reference Laboratory for CWD, Foreign Animal Disease Division, Animal and Plant Quarantine Agency, 177 Hyeoksin 8 ro, Gimcheon 39660, South Korea; email: rohis@korea.kr or shonhj@korea.kr

November 2025

Vectorborne Diseases

- *Haematospirillum jordaniae* Infections after Recreational Exposure to River Water, Pennsylvania, USA, 2020
- Tickborne *Neoehrlichia mikurensis* in the Blood of Blood Donors, Norway, 2023
- Two Independent Acquisitions of Multidrug Resistance Gene *lsaC* in *Streptococcus pneumoniae* Serotype 20 Multilocus Sequence Type 1257
- Community-Driven, Text Message–Based COVID-19 Surveillance System, Los Angeles County, California, USA, 2020–2024
- Isolation and Characterization of *Rickettsia finnyi*, Novel Pathogenic Spotted Fever Group Rickettsia in Dogs, United States
- Monkeypox Virus Partial-Genome Amplicon Sequencing for Improvement of Genomic Surveillance during Mpox Outbreaks
- *Bjerkandera* spp. Pulmonary Infection in Immunocompromised Hosts, Germany
- Novel Dolphin Tupavirus from Stranded Atlantic White-Sided Dolphin with Severe Encephalitis, Canada, 2024

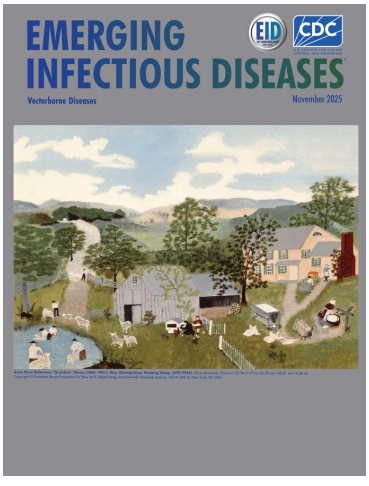

- *Neoehrlichia mikurensis* in Ticks and Tick-Bitten Persons, Sweden and Finland, 2008–2009
- Shifting Dynamics of Dengue Virus Serotype 2 and Emergence of Cosmopolitan Genotype, Costa Rica, 2024
- *Spiroplasma ixodetis* in Ticks Removed from Humans, Sweden and Åland Islands, Finland
- Two Autochthonous Cases of Anaplasmosis, Washington, USA, 2022–2023
- Emergence of Dengue Virus Serotype 3, Lineage III_B.3.2, Angola
- *Borrelia afzelii* Hepatitis in Patient Treated with Venetoclax and Obinutuzumab, Switzerland
- Two Cases of Autochthonous West Nile Virus Encephalitis, Paris, France, 2025
- Detection of *Aedes* (*Fredwardsius*) *vittatus* Mosquitoes, Yucatán Peninsula, Mexico, 2025
- Fatal Tick-Borne Encephalitis in Unvaccinated Traveler from the United States to Switzerland, 2022
- Crimean-Congo Hemorrhagic Fever Virus in Cattle and Ticks, Israel
- Extensively Drug-Resistant Tuberculosis with Conflicting Resistance Testing Results, Lesotho
- *Orientia tsutsugamushi* Antibodies in Patients with Eschars and Suspected Tickborne Disease
- Mortality Event in Rainbow Snakes Linked to Snake Fungal Disease, United States
- Yellow Fever Virus in *Aedes albopictus* Mosquitoes from Urban Green Area, São Paulo State, Brazil
- Molecular Evidence of Dengue Virus Serotype 2 in Travelers Returning to Israel from the Sinai Peninsula

EMERGING INFECTIOUS DISEASES

To revisit the November 2025 issue, go to: https://wwwnc.cdc.gov/eid/articles/issue/31/11/table-of-contents

Outbreak of Dengue Virus Serotype 3, Republic of the Marshall Islands, 2019–2021

Tomás M. León, Jill McCready, Erlynda Chutaro, Janet McAllister, Bobson Solomon, Limb K. Hapairai

During 2019–2021, the Republic of the Marshall Islands experienced a dengue outbreak involving 1,908 cases. Environmental sanitation helped stop transmission on Ebeye island, but transmission continued for >1 year on Majuro atoll. The Pacific region urgently needs to develop vector control capacity to address future dengue outbreaks.

Dengue, caused by dengue virus (DENV), is a vectorborne disease transmitted by *Aedes* spp. mosquitoes. DENV has 4 major serotypes (1–4); infection with one serotype protects against future infection with that serotype but leads to antibody-dependent enhancement and potentially more severe disease upon infection with a heterologous serotype (*1*).

The primary global dengue vector is the *Ae. aegypti* mosquito, which has a widespread and ever-expanding range (*2*). In the Western Pacific, *Ae. albopictus*, *Ae. polynesiensis*, and *Ae. hensili* dengue vectors coexist with *Ae. aegypti* (*3*). Some Pacific Island countries and territories are dengue-endemic, but many others have periodic outbreaks in which DENV presumably is introduced by travelers returning from endemic areas (*4*). Introduction via infected mosquitoes brought by plane or boat also is possible and difficult to definitively rule out (*4*). In the Pacific, most DENV introductions are thought to be from returning residents rather than visiting tourists.

Before 2019, the last major dengue outbreak in the Republic of the Marshall Islands (RMI) was during 2011–2012 and involved DENV-4 (*5*). The attack rate (AR) during that outbreak was 1.6% among laboratory-confirmed cases, and suspected AR was 3% (*5*). In that outbreak, 95% of tested samples (50% in children 0–4 years of age, 80% in children 5–9 years of age, >90% in persons ≥10 years of age) had evidence of secondary infection, showing a history of substantial DENV circulation in RMI (*5*).

On May 15, 2019, a dengue case was identified in a patient on Ebeye island in the Kwajalein atoll of RMI. The case-patient had no travel history outside RMI. Another suspected case occurred on Ebeye on June 4, 2019. Subsequently, case counts rapidly increased and were detected across much of RMI, mainly on Kwajalein and Majuro atolls (Figure). Serotyping showed the outbreak was caused by DENV-3, which had not been recorded in RMI for 30 years, although DENV-3 possibly circulated in RMI during the mid-1990s or early 2000s (*6*). To investigate effectiveness of vector control strategies, we compared dengue ARs between the island of Ebeye, where systematic, islandwide vector control began soon after case detection, and the Majuro atoll, where human disease and vector surveillance is not routinely conducted.

The Study

In response to dengue case detections, the Ministry of Health and Human Services (MOHHS) and the RMI Environmental Protection Authority (RMIEPA) initiated vector control activities across Ebeye on July 16, 2019. Ebeye government officials also began islandwide cleanup campaigns when dengue cases began increasing. RMIEPA used BG-Sentinel Mosquito Traps (Biogents, https://eu.biogents.com) for surveillance of adult mosquitoes and larvae or pupae to check for vectors before applying pesticides, when possible. *Ae. aegypti* mosquitoes were the only dengue vector found on Ebeye.

On Ebeye, RMIEPA applied indoor and outdoor residual adulticide bifenthrin or deltamethrin spray, and pyriproxyfen or *Bacillus thuringiensis* larvicide, on the basis of the larval survey, following the

Author affiliations: Pacific Island Health Officers' Association, Honolulu, Hawaii, USA (T.M. León, L.K. Hapairai); Republic of the Marshall Islands Ministry of Health and Human Services, Majuro, Marshall Islands (J. McCready, E. Chutaro, B. Solomon); Centers for Disease Control and Prevention, Atlanta, Georgia, USA (J. McAllister); City of New Orleans Mosquito Termite & Rodent Control Board, New Orleans, Louisiana, USA (J. McAllister)

DOI: https://doi.org/10.3201/eid3204.251135

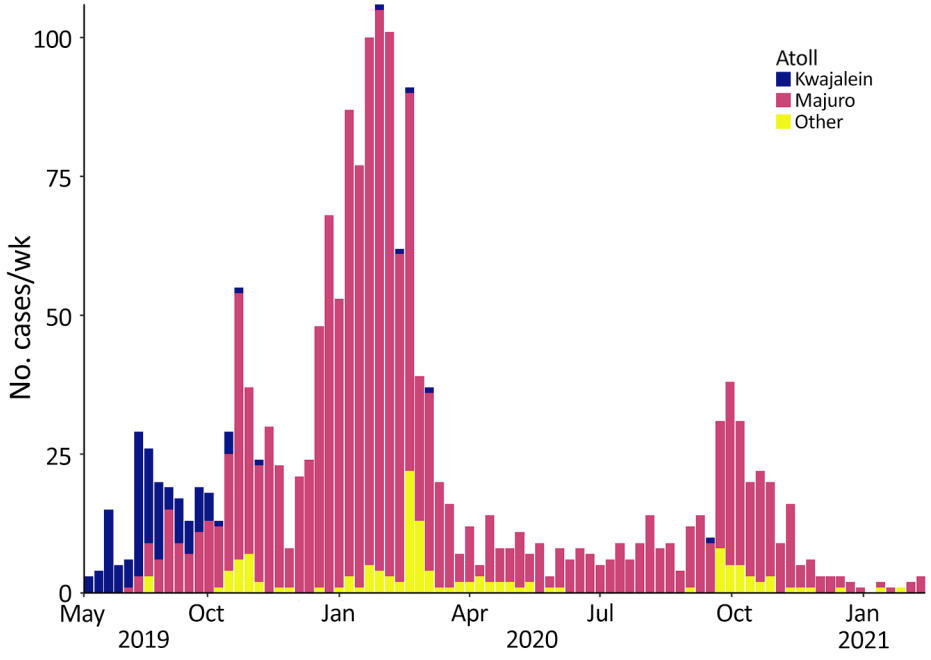

Figure. Number of confirmed cases per atoll in an outbreak of dengue virus serotype 3, Republic of the Marshall Islands, 2019–2021. Bars show weekly case counts. Although the first case was detected on Ebeye island in the Kwajalein atoll in May 2019, effective environmental sanitation and other vector control measures kept case counts low there, while cases spiked in Majuro atoll and persisted for >1 year.

manufacturer's labels. The vector assessment found *Ae. aegypti* mosquitoes in containers in about half of homes inspected (Table 1); the most productive larval mosquito containers were drums for storing water, mainly used for washing, not drinking.

On August 6, 2019, the RMI government declared a state of emergency for the entire territory. MOHHS provided vector management efforts against *Aedes* spp. mosquito breeding sites through community engagement campaigns, including informational radio spots, social media posts, press reporting, and advocacy by traditional and ecclesial leaders. MOHHS and RMIEPA provided vector control to households with suspected and confirmed dengue cases.

Table 1. Summary of immature mosquito vector assessment conducted on Ebeye island during outbreak of dengue virus serotype 3, Republic of the Marshall Islands, August 2019

Assessment	Value
Total no. households assessed	1,135
No. sampled for immature mosquitoes	105
House index*	50
No. containers inspected	476
Container index†	17
Breteau index‡	
Water cisterns	21
Drums	61
Buckets	6
Coolers	4
Abandoned appliances, boats, or vehicles	3
Bowls or pans	1
Overall	76

*Percentage of properties with ≥1 container positive for immature mosquitoes.
†Percentage of containers positive for immature mosquitoes/100 properties.
‡Number of containers positive for immature mosquitoes/100 properties.

PCR testing for RMI is only available in Hawaii, USA, as is common for many Pacific islands, so most (82%) confirmatory test results were ELISA of the nonstructural protein 1 antigen, 18% were DENV IgM, and <1% were PCR. Of note, most (59%) confirmed cases were among children 5–17 years of age (Table 2); however, only 44% of patients experiencing dengue-like illness during the outbreak were 5–17 years of age (Table 3).

Ebeye, where earliest dengue activity for this outbreak occurred, comprises ≈23% of the RMI population (*7*). By October 2019, case counts on Ebeye declined, and most dengue activity occurred on Majuro atoll, where ≈55% of the RMI population resides (*7*). Other atolls with documented cases were Ailinglaplap, Arno, Aur, Enewetak, Jaluit, Kili, Maloelap, Mili, Namu, Utrik, and Wotje. The overall dengue AR on Ebeye island was 1.3%, compared with the 7.1% AR on Majuro atoll, where vector control was only initiated in response to confirmed case identifications. After a spike in detected DENV transmission during December 2019–March 2020, dengue persisted on Majuro atoll with decreased case activity during March–September 2020 before cases increased in again in late 2020, preceding the eventual end of the outbreak in February 2021 (Figure).

RMIEPA conducted mosquito surveys on Majuro and other atolls, including Ailinglaplap, Arno, Aur, Enewetak, Jaluit, Kili, Kwajalein, Maloelap, Mili, and Wotje atolls, which confirmed *Ae. aegypti*, *Ae. albopictus*, and *Ae. marshallensis* mosquito vectors. Of note, those atolls had dengue ARs similar

Table 2. Characteristics of patients with confirmed dengue in an outbreak of DENV serotype 3, Republic of the Marshall Islands, 2019–21

Characteristics	No. (%) of cases, n = 1,908	Attack rate, %	No. (%) hospitalized
Sex			
F	882 (46)	4.3	313 (35)
M	1,018 (53)	4.7	401 (39)
Age group, y			
0–4	121 (6)	2.6	34 (28)
5–17	1,119 (59)	8.7	432 (39)
18–49	521 (27)	2.8	196 (38)
≥50	104 (5)	1.7	28 (27)
Atoll			
Majuro	1,642 (86)	7.1	576 (35)
Kwajalein	132 (7)	1.3	88 (67)
Other	134 (7)	1.4	52 (39)
Disease severity			
Death	2 (0.1)	NA	NA
Hospitalized	716 (38)	NA	NA
Not hospitalized, recovered	1,190 (62)	NA	NA
Laboratory test results			
ELISA NS1 antigen–positive	1,565 (82)	NA	NA
ELISA IgM–positive	334 (18)	NA	NA
PCR-positive	9 (0.4)	NA	NA

*DENV, dengue virus; NA, not applicable; NS1, nonstructural protein 1.

to Majuro. Although RMIEPA did not conduct mosquito surveys on Namu and Utrik atolls, the agency suspects those atolls likely had ≥1 of the *Aedes* spp. mosquito vectors.

The final confirmed case associated with this outbreak was recorded on February 20, 2021, resulting in a total of 1,908 laboratory-confirmed cases, among which 716 case-patients were hospitalized and 2 died. Officially, the dengue outbreak lasted 21 months, overlapping with the beginning of the COVID-19 global pandemic and associated travel restrictions that halted most international and intraisland travel beginning in March 2020. Of note, most dengue cases on Ebeye occurred in the first 2 months of the outbreak, suggesting successful vector control kept the overall AR low at 1.3%, compared with the 7.1% AR on Majuro atoll. Vector control was only initiated on Majuro in response to positive case identification, and DENV transmission persisted on the atoll. Recommendations by the US Centers for Disease Control and Prevention and the Pacific Island Health Officers Association for future dengue prevention and control efforts on the basis of the vector assessment included continued capacity building, environmental sanitation through improved waste management, chemical vector control, and improved domestic water collection and storage.

Conclusions

RMI experienced an extended dengue outbreak during 2019–2021, overlapping with COVID-19 restrictions, suggesting that local transmission was sustained throughout the period unaided by additional case introductions. Initial cases were concentrated on Ebeye island in Kwajalein atoll, where vector control and environmental health activities helped mitigate local mosquito populations and curtail DENV transmission. Transmission persisted in Majuro atoll for an additional 18 months. Of note, Majuro is 4 times more densely populated than Kwajalein atoll (*7*), likely another contributing factor to the sustained transmission on Majuro compared with Kwajalein during

Table 3. Characteristics of patients with dengue-like illness during outbreak of dengue virus serotype 3, Republic of the Marshall Islands, 2019–2021

Characteristics	No. (%) persons, n = 3,859	Attack rate, %	No. (%) hospitalized
Sex			
F	1,907 (49)	9.2	684 (36)
M	1,934 (50)	8.9	456 (24)
Age group, y			
0–4	412 (11)	8.7	50 (12)
5–17	1,685 (44)	13.1	454 (27)
18–49	1,381 (36)	7.3	290 (21)
≥50	381 (10)	6.4	42 (11)
Atoll			
Majuro	3,403 (88)	14.7	636 (19)
Kwajalein	277 (7)	2.8	143 (52)
Other	179 (5)	1.9	57 (32)

this outbreak. The 2011–2012 dengue outbreak in RMI showed a similar AR between Kwajalein and Majuro (*5*). Compared with the 2011–2012 outbreak, confirmed dengue cases in the 2019–2021 outbreak had a younger age distribution and a higher concentration of cases in children 5–17 years of age. The relative lack of burden in the adult population suggests possible DENV-3 transmission in RMI in the 1990s, when that population might have experienced infection and therefore acquired immunity.

In summary, distribution of dengue cases across multiple atolls, several with high ARs, highlights the challenges for outbreak control in the Pacific and other regions where human disease and vector surveillance is not conducted regularly and systematically. Vector control and environmental health efforts on Ebeye successfully averted further DENV-3 transmission. Those findings support the need for building vector control capacity in the Pacific, where dengue outbreaks of this scale are likely to continue.

Acknowledgments

We thank Dominic Rose for completing the Ebeye larval surveys, Jackson Jacklick for the vector management, and the numerous partners who worked tirelessly during this response effort.

This work was conducted as part of surveillance and outbreak response activities of the Republic of the Marshall Islands Ministry of Health and Human Services (RIM-MOHHS). Per advisement by RMI-MOHHS institutional review board, these activities are not considered human subjects research; thus, institutional review board review and approval were not required.

T.M.L. and L.K.H. were partly funded by a grant to the Pacific Island Health Officers' Association from the US Department of State (cooperative agreement no. SLMAQM20CA2490). The opinions, findings, and conclusions stated herein are those of the authors and do not necessarily reflect those of the US Department of State.

About the Author

Dr. León conducted this research as an early warning system consultant for the Pacific Island Health Officers' Association. His primary research interests focus on applying modeling and advanced analytic methods to support dengue outbreak preparedness and response in the Pacific.

References

1. Paz-Bailey G, Adams LE, Deen J, Anderson KB, Katzelnick LC. Dengue. Lancet. 2024;403:667–82. https://doi.org/10.1016/S0140-6736(23)02576-X
2. Kraemer MUG, Reiner RC Jr, Brady OJ, Messina JP, Gilbert M, Pigott DM, et al. Past and future spread of the arbovirus vectors *Aedes aegypti* and *Aedes albopictus*. Nat Microbiol. 2019;4:854–63. https://doi.org/10.1038/s41564-019-0376-y
3. Russell TL, Burkot TR. A guide to mosquitoes in the Pacific. Cairns (Australia): Pacific Community; 2023.
4. Matthews RJ, Kaluthotage I, Russell TL, Knox TB, Horwood PF, Craig AT. Arboviral disease outbreaks in the Pacific Islands countries and areas, 2014 to 2020: a systematic literature and document review. Pathogens. 2022;11:74. PubMed https://doi.org/10.3390/pathogens11010074
5. Sharp TM, Mackay AJ, Santiago GA, Hunsperger E, Nilles EJ, Perez-Padilla J, et al. Characteristics of a dengue outbreak in a remote Pacific Island chain—Republic of the Marshall Islands, 2011–2012. PLoS One. 2014;9:e108445. https://doi.org/10.1371/journal.pone.0108445
6. Singh N, Kiedrzynski T, Lepers C, Benyon EK. Dengue in the Pacific—an update of the current situation. Pac Health Dialog. 2005;12:111–9.
7. Marshall Islands Economic Policy, Planning and Statistics Office. Republic of the Marshall Islands 2021 census report [cited 2025 Feb 18]. https://rmihealth.org/media/attachments/2025/08/08/marshall_islands_2021_census_vol1_table_report.pdf

Address for correspondence: Tomás M. León, Pacific Island Health Officers' Association, 733 Bishop Street, Suite 1820, Honolulu, HI 96813, USA; email: tomasl@pihoa.org

Treatment of Severe Ocular Mpox with Cidofovir and Tecovirimat

Xavier Brousse, Rayan Kreidie, Eugénie Mourgues, Luna Fraysse, Marin Lahouati, Vincent Servant, Sonia Burrel, Valentine Saunier, Charles Cazanave

Mpox, a reemerging zoonotic disease since 2022, primarily affects the skin; ocular involvement is rarely reported. We present a case of mpox-caused disciform keratitis treated with a combination of cidofovir and tecovirimat. The patient recovered without residual ocular sequelae, suggesting these drugs are an option to treat ocular mpox manifestations.

Mpox is a reemerging zoonotic disease, with >140,000 cases reported worldwide since 2022 (*1*). A major outbreak of mpox caused by clade IIb monkeypox virus (MPXV) occurred in Western Europe and the United States in 2022, although MPXV clade I has caused high mortality rates in Central Africa for decades (*2*). MPXV, a member of the Poxviridae family (*3*), is primarily transmitted through close physical contact between humans and typically causes disseminated cutaneomucosal lesions (*4*). Ocular involvement occurs in ≈1%–10% of cases, with a higher frequency in MPXV clade I infections (*5*). Although conjunctivitis is the most common ocular manifestation, more severe manifestations such as keratitis and corneal ulceration have been reported (*6*). At that time, data regarding the use of tecovirimat for mpox treatment were limited. Case reports have suggested tecovirimat could have a role in viral clearance, enabling the resolution of lesions (*7*). In severe infections, particularly those with disseminated disease or ocular complications, cidofovir has been used (*8*,*9*). We describe the use of a combination therapy involving tecovirimat and cidofovir for treating a case of mpox-associated disciform keratitis.

Author affiliations: Bordeaux University Hospital, Bordeaux, France (X. Brousse, R. Kreidie, E. Mourgues, L. Fraysse, M. Lahouati, V. Servant, S. Burrel, V. Saunier, C. Cazanave); Bordeaux University, Inserm, UMR1034, Pessac, France (M. Lahouati); CNRS UMR 5234, Bordeaux University, Bordeaux (S. Burrel, C. Cazanave)

DOI: https://doi.org/10.3201/eid3204.250882

The Case

A 31-year-old man with an unremarkable medical history was admitted to the ophthalmology clinic with sudden-onset visual acuity loss for the past 72 hours, ocular redness, and pain in the left eye. He was not taking any regular medications, except for on-demand preexposure prophylaxis for HIV. The patient had not received an mpox vaccination and reported recent sexual encounters with men involving unprotected oral sex.

The patient's recent medical history included a confirmed MPXV infection beginning a month earlier, characterized by disseminated cutaneous lesions and anal ulcerations, later progressing to an anal abscess requiring surgical intervention. MPXV infection was confirmed by PCR from an anal swab. Test results for other sexually transmitted infections, including HIV, were negative.

One week after the anal surgery, at the initial consultation (day 0 [D0]) a slit-lamp examination revealed disciform keratitis characterized by corneal edema, a pseudodendritic ulcer, and conjunctival hyperemia (Figure, panel A). Corrected distance visual acuity (CDAV) was 0.4 logMAR (base 10 logarithm of the minimum angle of resolution). We initiated empirical treatment with oral valaciclovir (1 g 2×/d), followed 48 hours later by topical dexamethasone (3 drops 4×/d, decreasing by 2 drops every 3 days) and neomycin (1 drop 4×/d), on the basis of a presumptive diagnosis of herpes simplex virus (HSV) or varicella-zoster virus (VZV) infection. However, conjunctival swab testing was negative for both HSV and VZV.

Despite initial antiviral drug therapy, follow-up examination on D4 revealed persistent keratitis (Figure, panel B) with no notable clinical improvement (CDAV was 0.7 logMAR). New corneal infiltrates had developed, along with signs of anterior chamber inflammation, including a positive Tyndall effect and central granulomatous retrodescemetic precipitates. Because of the suspicion of a mpox-related ocular

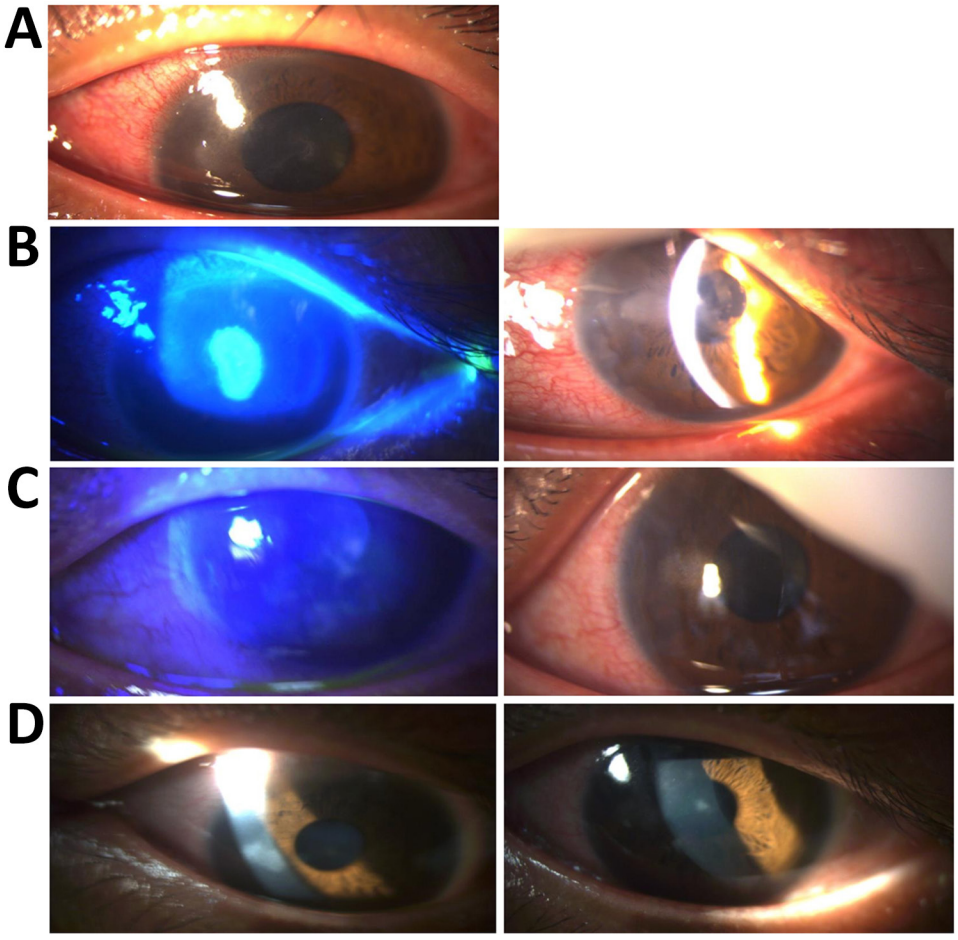

Figure. Ophthalmologic evaluation of patient with severe ocular mpox treated with cidofovir and tecovirimat. Images are of patient's left eye over course of diagnosis and treatment. A) Slit-lamp examination at day 0, showing corneal edema, a pseudodendritic ulcer, and conjunctival hyperemia characteristic of disciform keratitis. B) On day 5, before first-line treatment with valaciclovir, fluorescein staining (left) and slit-lamp examination (right) showing persistent keratitis and formation of new corneal infiltrates. C) On day 21, seven days after initiation of second-line antiviral drug treatment with cidofovir and tecovirimat, fluorescein staining (left) and slit-lamp examination (right) showing marked clinical improvement and reduction in infiltrates. D) On day 29, fourteen days after treatment with second-line antiviral drug treatment with cidofovir and tecovirimat, left and right images are of slit-lamp examination showing complete resolution of corneal edema, conjunctival hyperemia, and inflammatory signs.

complication, we performed an anterior chamber tap on D6. The sample tested negative for MPXV, HSV, and VZV.

We tested a corneal swab on D8 that was positive for MPXV with a cycle threshold (Ct) value of 29. We confirmed the MPXV infection and clade IIb identification by using real-time PCR (*10*,*11*). Retrospective analysis of the initial conjunctival swab from D0 also revealed MPXV positivity, with a Ct value of 29.4. Because of those findings, we discontinued valaciclovir and maintained topical treatment. Despite that approach, the condition progressed to ulcerative keratitis, with visual acuity deteriorating to complete visual blur (counting fingers without CDAV available).

Because of the severity of the ocular involvement and the shortage of other local treatments available at that time in France, and after a multidisciplinary discussion, we initiated second-line antiviral drug therapy consisting of a single intravenous infusion of cidofovir (5 mg/kg) and oral tecovirimat (600 mg 2×/d for 2 weeks). In accordance with clinical guidelines, intravenous cidofovir administration was accompanied by probenecid (1.5 g 3 hours before and 0.5 g 2 hours after cidofovir infusion). We initiated that combination therapy on D15 after the initial ophthalmologic evaluation. Baseline renal function was unremarkable. No proteinuria was detected before treatment. The patient tolerated the antiviral drug regimen well and maintained stable renal function. Topical corticosteroid therapy was continued.

At the follow-up visit on D21, one week after the cidofovir infusion, we observed marked regression of the ocular lesions (Figure, panel C). CDAV improved to 0.2 logMAR. MPXV PCR testing of the conjunctival swab sample was negative. By D29, two weeks post-infusion, we confirmed substantial clinical improvement (Figure, panel D), including complete resolution of corneal edema, conjunctival hyperemia, and inflammatory signs. Visual acuity was almost normal with a CDAV of 0.1 logMAR. Only minor epithelial opacities remained. By D56, the patient had fully recovered, with only faint epithelial opacities persisting, none staining with fluorescein.

Conclusions

We present the use of cidofovir and tecovirimat to treat a severe mpox infection. Although ocular complications of mpox are rare (*5*), they represent a critical subset of cases with the potential to impair visual outcomes. Those severe manifestations, along with extensively disseminated mucocutaneous lesions, constitute some of the most serious clinical manifestations of mpox. Clinicians should remain alert to the possibility of ocular involvement in patients with mpox, because early recognition and prompt treatment are crucial to preventing complications.

Current data suggest tecovirimat provides limited benefit for infections caused by MPXV clade Ib (*12*). In addition, results from the STOMP trial (*13*), which investigated tecovirimat in patients with MPXV clade IIb infections, revealed no major effect on viral clearance or lesion resolution. The therapeutic options for mpox remain limited, with cidofovir being the primary alternative. Cidofovir has been approved since 1996 for the treatment of cytomegalovirus retinitis in patients with AIDS (*14*). Once phosphorylated, cidofovir inhibits viral DNA synthesis by targeting DNA polymerase (*15*). In contrast, tecovirimat blocks extracellular virus release at a later stage of the viral life cycle, highlighting the potential benefit of combining those agents with distinct mechanisms of action (Appendix Reference 16, https://wwwnc.cdc.gov/EID/article/32/4/25-0882-App1.pdf). The availability of newer antiviral drugs with less nephrotoxicity, such as maribavir (Appendix Reference 17), has led to a limited prescription of cidofovir. However, mpox typically affects younger persons without major underlying conditions, which can reduce cidofovir's adverse effects.

The treatment of ocular manifestations of mpox remains entirely nonstandardized. The clinical course observed in our case is consistent with previous reports (*9*), supporting the hypothesis that cidofovir might be effectively combined with tecovirimat in this setting. Other promising topical treatments, such as trifluridine, have been proposed for treating this type of infection (Appendix Reference 18). Because of the severity of the ocular involvement, the shortage of this treatment at that time, and the poor visual prognosis, we preferred to use systemic treatment.

Other studies have documented favorable outcomes with tecovirimat monotherapy. Those improvements might reflect the natural course of the disease rather than the specific efficacy of the antiviral drug treatment. For instance, the median time to lesion resolution reported in the literature is ≈29 (interquartile range 25–39) days (Appendix Reference 18), whereas in our case, we observed major clinical improvement within 7 days of initiating treatment, with complete resolution within 14 days.

Although rare, clinicians should remain vigilant for ocular complications associated with mpox. Cidofovir might hold promise as a therapeutic option in this context, particularly considering its manageable toxicity profile. However, more robust prospective data are needed to confirm those observations. Ocular involvement in mpox warrants prompt therapeutic intervention because of the risk for major and potentially irreversible visual sequelae. Cidofovir, alone or in combination with tecovirimat, might be a therapeutic option to treat ocular manifestations of mpox.

The patient provided written informed consent. Cidofovir was administered under a compassionate use authorization granted by the French National Agency for Medicines and Health Products Safety.

About the Author

Dr. Brousse is a resident of infectious diseases at Bordeaux University Hospital, France. His interests include the management of complex bacterial infections, emerging infections, and immunocompromised patients.

References

1. World Health Organization. Multi-country outbreak of mpox, external situation report #50 – 11 April 2025 [cited 2025 Apr 12]. https://www.who.int/publications/m/item/multi-country-outbreak-of-mpox--external-situation-report--50---11-april-2025
2. Besombes C, Mbrenga F, Schaeffer L, Malaka C, Gonofio E, Landier J, et al. National monkeypox surveillance, Central African Republic, 2001–2021. Emerg Infect Dis. 2022;28:2435–45. https://doi.org/10.3201/eid2812.220897
3. Faye O, Pratt CB, Faye M, Fall G, Chitty JA, Diagne MM, et al. Genomic characterisation of human monkeypox virus in Nigeria. Lancet Infect Dis. 2018;18:246. https://doi.org/10.1016/S1473-3099(18)30043-4
4. Thornhill JP, Barkati S, Walmsley S, Rockstroh J, Antinori A, Harrison LB, et al.; SHARE-net Clinical Group. Monkeypox virus infection in humans across 16 countries—April–June 2022. N Engl J Med. 2022;387:679–91. https://doi.org/10.1056/NEJMoa2207323
5. Rohilla S, Gaidhane S, Balaraman AK, Padmapriya G, Kaur I, Lal M, et al. Ophthalmic manifestations of the mpox virus: a systematic review and meta-analysis. J Infect Dis. 2025;232:220–9. https://doi.org/10.1093/infdis/jiaf066
6. Mailhe M, Beaumont A-L, Thy M, Le Pluart D, Perrineau S, Houhou-Fidouh N, et al. Clinical characteristics of ambulatory and hospitalized patients with monkeypox virus infection: an observational cohort study. Clin Microbiol Infect. 2023;29:233–9. https://doi.org/10.1016/j.cmi.2022.08.012
7. Lucar J, Roberts A, Saardi KM, Yee R, Siegel MO, Palmore TN. Monkeypox virus-associated severe proctitis treated with oral tecovirimat: a report of two cases. Ann Intern Med. 2022;175:1626–7. https://doi.org/10.7326/L22-0300

8. Stafford A, Rimmer S, Gilchrist M, Sun K, Davies EP, Waddington CS, et al. Use of cidofovir in a patient with severe mpox and uncontrolled HIV infection. Lancet Infect Dis. 2023;23:e218–26. https://doi.org/10.1016/S1473-3099(23)00044-0
9. Raccagni AR, Clemente T, Ranzenigo M, Cicinelli MV, Castagna A, Nozza S. Persistent ocular mpox infection in an immunocompetent individual. Lancet Infect Dis. 2023;23:652–3. https://doi.org/10.1016/S1473-3099(23)00266-9
10. Schuele L, Masirika LM, Udahemuka JC, Siangoli FB, Mbiribindi JB, Ndishimye P, et al.; GREATLIFE MPOX group. Real-time PCR assay to detect the novel clade Ib monkeypox virus, September 2023 to May 2024. Euro Surveill. 2024;29:2400486. https://doi.org/10.2807/1560-7917.ES.2024.29.32.2400486
11. Li Y, Zhao H, Wilkins K, Hughes C, Damon IK. Real-time PCR assays for the specific detection of monkeypox virus West African and Congo Basin strain DNA. J Virol Methods. 2010;169:223–7. https://doi.org/10.1016/j.jviromet.2010.07.012
12. Ali R, Alonga J, Biampata JL, Kombozi Basika M, Maljkovic Berry I, Bisento N, et al.; PALM007 Writing Group. Tecovirimat for clade I MPXV infection in the Democratic Republic of Congo. N Engl J Med. 2025;392:1484–96. https://doi.org/10.1056/NEJMoa2412439
13. Zucker J, Fischer WA II, Zheng L, McCarthy C, Saha PT, Javan AC, et al.; STOMP/A5418 Investigators. Tecovirimat for the treatment of Mpox. N Engl J Med. 2026;394:884–95. https://doi.org/10.1056/NEJMoa2506495
14. Whitley RJ. Guidelines for the treatment of cytomegalovirus diseases in patients with AIDS in the era of potent antiretroviral therapy: recommendations of an international panel. Arch Intern Med. 1998;158:957. https://doi.org/10.1001/archinte.158.9.957
15. Siegrist EA, Sassine J. Antivirals with activity against mpox: a clinically oriented review. Clin Infect Dis. 2023;76:155–64. https://doi.org/10.1093/cid/ciac622

Address for correspondence: Xavier Brousse, CHU de Bordeaux, Place Amélie Raba Léon, 33000 Bordeaux, France; email: xavier.brousse@chu-bordeaux.fr

EID journal

Want to stay updated on the latest news in *Emerging Infectious Diseases*? Let us connect you to the world of global health. Discover groundbreaking research studies, pictures, podcasts, and more by following us on Instagram at @eidjournal

Disseminated *Acanthamoeba* Infection with Necrotic Skin Lesions and Granulomatous Vasculitis, United States

Maria Koshy, Carrie Flynn, Marat Kribis, Jennifer McNiff, Matthew Grant, Shana Elizabeth Gleeson

An elderly man, on dupilumab therapy for asthma and sinus polyposis, sought care for necrotic skin lesions. Biopsy revealed granulomatous vasculitis and he received immunosuppressive therapy but worsened. We diagnosed an *Acanthamoeba* infection that was treated with multidrug therapy including nitroxoline. Clinicians should be aware of this rare etiology for infectious vasculitis.

Acanthamoeba spp. are free-living amoeba (FLA) that can be pathogenic in humans. *Acanthamoeba* amebae are most known for causing contact lens-related keratitis. Nonkeratitis invasive disease is primarily an opportunistic infection, and often fatal (*1*,*2*).

The number of persons at risk for opportunistic infections is increasing and is compounded by a growing number of drugs with unique targets on the inflammatory cascade (*3*). Dupilumab is a fully human monoclonal antibody that inhibits interleukin-4 and interleukin-13 cytokines and the T2 inflammatory response (*4*). It was first approved in 2017 for the treatment of atopic dermatitis and has since been used to treat several allergic diseases (*4*).

We report an elderly man on dupilumab therapy who sought care for progressive necrotic skin lesions and granulomatous vasculitis. We describe the clinical manifestations, diagnostic approach, and management considerations in this patient who was ultimately diagnosed with disseminated *Acanthamoeba* infection.

The Case

A 78-year-old man was admitted to a tertiary-care academic hospital with a 6-month history of progressive skin lesions. The lesions developed after he returned from Florida, USA. The lesions began as reddish nodules that progressed to develop central darkening. Some lesions evolved into deep ulcers; others developed necrosis with eschar. The lesions began on the legs but progressed to involve all extremities, the trunk, head, and neck. The back was spared. He denied fever but reported a 16-pound weight loss.

His past medical history included asthma and sinus polyposis treated with dupilumab for the past 18 months. He performed nasal rinses with normal saline. He spent winters in Florida, and during his last trip he had exposure to red tide and knee-deep brackish water when engaged in cleaning efforts after a hurricane.

Prior to admission, the patient underwent multiple skin biopsies that revealed focal granulomatous medium-vessel vasculitis with neutrophilic infiltrates, and negative acid-fast bacillus, fungal, and periodic acid–Schiff stains. Clinicians were concerned that the vasculitis was immune-mediated, and he received immunosuppressive therapy including prednisone at doses up to 80 mg daily, mycophenolate mofetil, rituximab, and cyclophosphamide. However, the lesions progressed. He was transferred to our hospital for clinical deterioration requiring a higher level of care.

At physical examination, he was febrile (temperature 102°F), tachycardic (heart rate 122 beats per minute), and had unremarkable blood pressure (130/80 mm Hg). He was frail and ill-appearing. Skin examination revealed extensive lesions in varying stages, some were erythematous and nodular, but the more predominant appearance was that of necrotic lesions with black central eschars (Figure 1 panel A); some lesions had formed deep ulcers (Figure 1 panel B). Head and neck examination disclosed similar lesions (Figure 1 panel C), palatal fistula, and a lesion causing

Author affiliations: Yale School of Medicine, New Haven, Connecticut, USA (M. Koshy, M. Kribis, J. McNiff, M. Grant, S.E. Gleeson); Brigham and Women's Hospital, Boston, Massachusetts, USA (C. Flynn).

DOI: https://doi.org/10.3201/eid3204.251201

Figure 1. Images of skin lesions on a patient with disseminated *Acanthamoeba* infection with necrotic skin lesions and granulomatous vasculitis. A) Lesions on the patient's body. B) Deeply ulcerated lesions on the patient. C) Lesions that extended to the head and face.

Figure 2. Positron emission tomography/computed tomography showing innumerable widespread ^{18}F-fluorodeoxyglucose avid cutaneous and subcutaneous lesions that developed in a patient with disseminated *Acanthamoeba* infection.

partial loss of left upper eyelid with corneal exposure. Neurologic exam revealed confusion and drowsiness, with no neck stiffness. The remainder of the examination was unremarkable.

The patient's laboratory results revealed a leukocyte count of 26 × 10^3 cells/μL (reference range 4–11 × 10^3 cells/μL), hemoglobin of 8.8 g/dL (reference range 13.2–17.1 g/dL), albumin of 2.1 g/dL (reference range 3.6–5.1 g/dL), and high sensitivity C-reactive protein of 173 mg/L (reference range <1 mg/L). Testing for hepatitis B, C, and HIV was negative. No growth was reported from blood culture. Antinuclear antibodies and antineutrophilic cytoplasmic antibodies were not detected. Complement levels were unremarkable. A positron emission tomography computed tomography revealed innumerable widespread ^{18}F-fluorodeoxyglucose avid cutaneous and subcutaneous lesions (Figure 2).

Because of the disease progression despite treatment for immune-mediated vasculitis, the skin biopsy was repeated. The biopsy again showed medium-vessel vasculitis with cutaneous necrosis. On periodic acid–Schiff stain, a few large histiocytoid cells around the vessels stained positive, indicating possible amoebic trophozoites (Figures 3, 4). The cells were confirmed to be *Acanthamoeba* spp. on 18S rDNA amoeba PCR testing. Blood cell–free DNA (Karius, https://kariusdx.com) testing detected high levels of *Acanthamoeba lugdunensis* (400,000 DNA molecules/μL, analytical range of 10–316,000 DNA molecules/μL). Brain magnetic resonance imaging revealed a punctate focus within the right cerebellar hemisphere but no leptomeningeal enhancement. We sent cerebrospinal fluid for free-living amoeba PCR testing to the Centers for Disease Control and Prevention (Atlanta, Georgia, USA). The result was negative, with the comment that although cerebrospinal fluid was an ideal specimen for the detection of *Naegeleria fowleri*, it was not an ideal specimen for *Acanthamoeba* spp.

We started the patient on a multidrug regimen that included sulfadiazine, flucytosine, fluconazole, pentamidine, and miltefosine (*5*). We tapered and then discontinued steroids. The patient continued to deteriorate. On the basis of a separate clinical case of the successful use of nitroxoline in the treatment of *Balamuthia mandrillaris* encephalitis, and unpublished in vitro data from our institution, we obtained Food and Drug Administration approval to use nitroxoline through single-patient expanded-access of an investigational new drug. We initiated the use of nitroxoline 20 days after diagnosis (250 mg 3×/d). Chlorhexidine soaks, anidulafungin (100 mg 1×/d), and isuvaconazole (372 mg 1×/d) were added (*6*,*7*).

After those modifications in treatment, the patient showed initial signs of improvement: some lesions over the face and trunk improved and no new lesions appeared. His fevers briefly resolved. Unfortunately, his renal function worsened and we were concerned that nitroxoline was contributing to kidney injury. We stopped the drug after 7 days, along with pentamidine and sulfadiazine. Many of his wounds showed signs of secondary infection and multiorgan failure developed. The patient died 6 weeks after *Acanthamoeba* infection diagnosis.

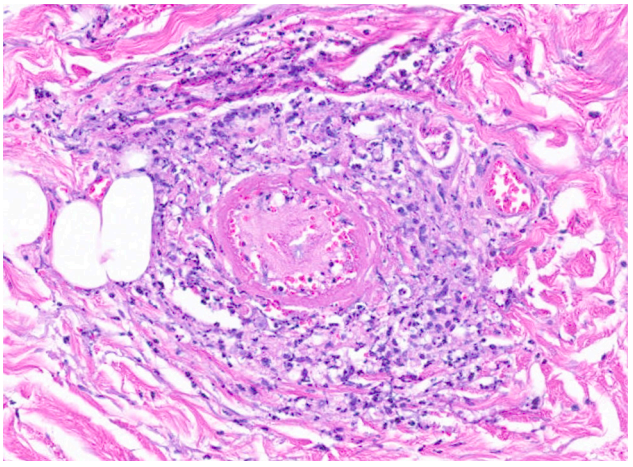

Figure 3. Hematoxylin and eosin stain of skin biopsy showing medium-vessel vasculitis; original magnification x200

Conclusions

Acanthamoeba are ubiquitous in soil and water, and one study from the United States noted their presence in 51% of household water samples (*1*,*2*,*8*). However, invasive disease in humans is rare, and manifestations include granulomatous amoebic encephalitis, cutaneous disease, rhinosinusitis, pulmonary disease, and osteomyelitis. Reports of invasive *Acanthamoeba* infection with HIV cases have increased (*2*). Other risk factors include malignancy and receipt of solid organ or hematopoietic stem-cell transplant (*9*). Tap water nasal irrigation is another well described risk factor and could have played a role in this patient's infection (*10*).

The treatment of *Acanthamoeba* infections is on the basis of survivor case reports and in vitro drug studies. The Centers for Disease Control and Prevention recommends a multidrug regimen including miltefosine, sulfadiazine, pentamidine, flucytosine, and a nonfluconazole triazole. A host of empiric therapies have been tried (*5*). Nitroxoline is a hydroxyquinolone used to treat urinary tract infections, and has good clinical efficacy and a good safety profile (*11*). Nitroxoline has successfully been used in treating

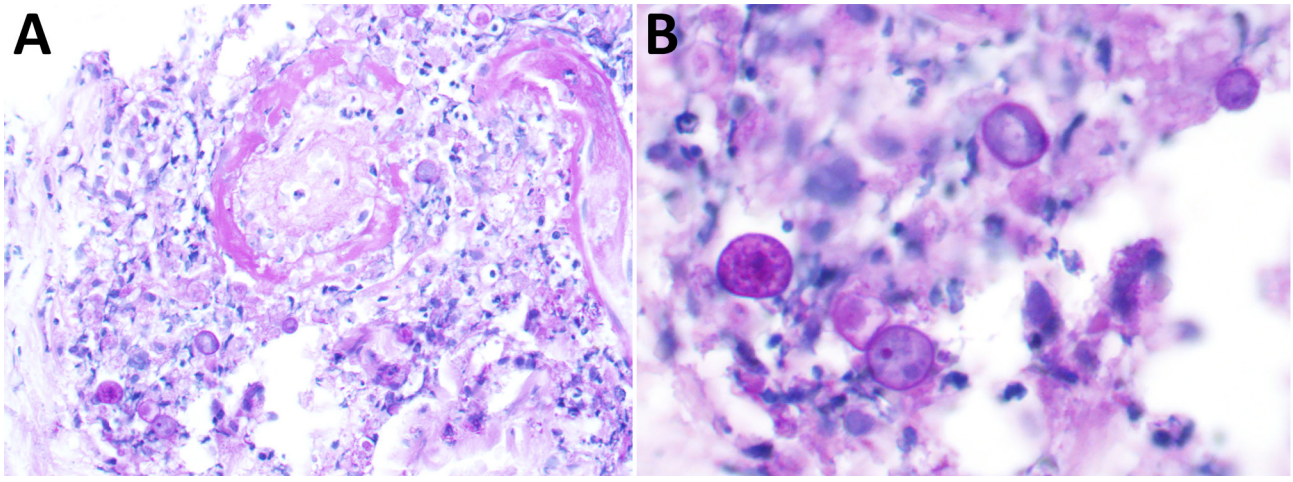

Figure 4. Periodic acid-Schiff positive large histiocytoid cells near the vessel, from a patient with disseminated Acanthamoeba infection with necrotic skin lesions and granulomatous vasculitis. Cells are potential amoebic trophozoites. A) Original magnification ×400; B) Original magnification ×600

Balamuthia encephalitis, and in vitro data from our institution also demonstrated its efficacy in killing *Acanthamoeba castellanii* trophozoites (*6*,*7*). Although this patient ultimately died from the infection, he showed initial signs of improvement, the first during his long illness, after starting nitroxoline.

Increased risk for parasitic infections have been reported with therapies targeting IgE and the T2 inflammatory response. A recent study suggested that although the numbers are low, the disproportionate safety signal warranted investigation (*12*). In the VOYAGE trial, which studied the use of dupilumab in children with asthma, 6 cases of helminthiasis were reported, including enterobiasis and ascariasis (*13*). Although dupilumab is not classically considered an immunosuppressive agent, it possibly increases the risk for parasitic infections.

In summary, we believe the disseminated *Acanthamoeba* infection in our patient occurred because of multiple factors that included his environmental exposure, his age-related immune decline, and dupilumab therapy. FLA are rarely included in reviews on etiology of granulomatous vasculitis. Physicians should be aware of this under-recognized etiology, and this case adds to the body of literature supporting the use of nitroxoline in FLA infections.

Acknowledgments

We thank the patient's family for giving us permission to publish this case. We thank Natasha Spottiswoode for helping us procure nitroxoline and make it available to our patient. We also thank Julia C. Haston for providing guidance in case management.

About the Author

Dr. Koshy is a clinical fellow in infectious diseases at the Yale School of Medicine. Her research interests include tropical diseases, HIV, infections in immunocompromised persons, and medical education.

References:

1. Schuster FL, Visvesvara GS. Free-living amoebae as opportunistic and non-opportunistic pathogens of humans and animals. Int J Parasitol. 2004;34:1001–27. https://doi.org/10.1016/j.ijpara.2004.06.004
2. Haston JC, O'Laughlin K, Matteson K, Roy S, Qvarnstrom Y, Ali IKM, et al. The epidemiology and clinical features of non-keratitis *Acanthamoeba* infections in the United States, 1956–2020. Open Forum Infect Dis. 2023;10:ofac682. https://doi.org/10.1093/ofid/ofac682
3. Monzo-Gallo P, Teijon-Lumbreras C, Aiello TF, Gallardo-Pizarro A, Martinez-Urrea A, Chumbita M, et al. Epidemiological shifts of invasive fungal infections in the current era of haematology. Med Mycol. 2025;63:myaf070. https://doi.org/10.1093/mmy/myaf070
4. Regeneron Pharmaceuticals, Inc. Full prescribing information. 2022 [cited 2025 Aug 1]. https://www.accessdata.fda.gov/drugsatfda_docs/label/2022/761055s046lbl.pdf
5. Spottiswoode N, Haston JC, Hanners NW, Gruenberg K, Kim A, DeRisi JL, et al. Challenges and advances in the medical treatment of granulomatous amebic encephalitis. Ther Adv Infect Dis. 2024;11:20499361241228340. https://doi.org/10.1177/20499361241228340
6. Spottiswoode N, Pet D, Kim A, Gruenberg K, Shah M, Ramachandran A, et al. Successful treatment of *Balamuthia mandrillaris* granulomatous amebic encephalitis with nitroxoline. Emerg Infect Dis. 2023;29:197–201. https://doi.org/10.3201/eid2901.221531
7. Flynn CA, Colón-Ríos RI, Harmez A, Flynn WF, Kazmierczak BI. New viability assays for *Acanthamoeba castellanii* trophozoites and cysts allow rapid assessment of drug activity. J Infect Dis. 2026;233:e766–76. https://doi.org/10.1093/infdis/jiaf599
8. Stockman LJ, Wright CJ, Visvesvara GS, Fields BS, Beach MJ. Prevalence of *Acanthamoeba* spp. and other free-living amoebae in household water, Ohio, USA—1990–1992. Parasitol Res. 2011;108:621–7. https://doi.org/10.1007/s00436-010-2120-7
9. Banerjee CT, Conlan S, Mostaghim A, Michelin A, Arduino M, Mattioli M, et al. *Acanthamoeba* infection in a hematopoietic cell transplant recipient: challenges in diagnosis, management, and source identification. Transpl Infect Dis. 2025;27:e14425. https://doi.org/10.1111/tid.14425
10. Haston JC, Serra C, Imada E, Martin E, Ali IKM, Cope JR. *Acanthamoeba* infection and nasal rinsing, United States, 1994–2022. Emerg Infect Dis. 2024;30:783–5. https://doi.org/10.3201/eid3004.231076
11. Naber KG, Niggemann H, Stein G, Stein G. Review of the literature and individual patients' data meta-analysis on efficacy and tolerance of nitroxoline in the treatment of uncomplicated urinary tract infections. BMC Infect Dis. 2014;14:628. https://doi.org/10.1186/s12879-014-0628-7
12. Pera V, Brusselle GG, Riemann S, Kors JA, Van Mulligen EM, Parry R, et al. Parasitic infections related to anti-type 2 immunity monoclonal antibodies: a disproportionality analysis in the food and drug administration's adverse event reporting system (FAERS). Front Pharmacol. 2023;14:1276340. https://doi.org/10.3389/fphar.2023.1276340
13. Bacharier LB, Maspero JF, Katelaris CH, Fiocchi AG, Gagnon R, de Mir I, et al.; Liberty Asthma VOYAGE Investigators. Dupilumab in children with uncontrolled moderate-to-severe asthma. N Engl J Med. 2021;385:2230–40. https://doi.org/10.1056/NEJMoa2106567

Address for correspondence: Maria Koshy, Yale School of Medicine, 333 Cedar St, New Haven, CT 06520, USA; email: maria.koshy@yale.edu

Cardiomyopathy Caused by Coxsackievirus Strain A9 in Previously Healthy Child, Northeastern France, 2024

Anne-Laure Lebreil,[1] Maxime Bisseux,[1] Audrey Mirand, Marie Glenet, Yohan N'Guyen, Norhan Taha, Pierre Mauran, Cecile Henquell, Laurent Andreoletti

We characterized a recombinant mosaic coxsackievirus A9 strain responsible for severe inflammatory cardiomyopathy in a previously healthy child in northeastern France in 2024 by using whole-genome sequencing. This case highlights that enterovirus species other than coxsackievirus strain B3 can cause cardiomyopathy in otherwise healthy pediatric patients.

Coxsackievirus strain A9 (CVA9) is a human pathogen classified within the species *Enterovirus betacoxsackievirus* (species B enterovirus [EV-B]). Infections linked to CVA9 show up in children, typically hand, foot, and mouth disease or episodes of aseptic meningitis (*1*). Epidemiologic tracking points to CVA9 as a frequent nonpolio enterovirus found in patient samples worldwide (*1*). During a 5-year survey in Europe from 2018–2023, this virus appeared among the 10 most documented enterovirus strains in clinical samples (*2*). Recent findings document CVA9 involvement in bronchiolitis, pneumonia, meningitis, and encephalitis; severe complications are rare but can be fatal (*1*,*3*,*4*). The severe neurologic or respiratory complications induced by CVA9 highlight its emerging clinical significance beyond its association with benign illnesses (*1*). Molecular epidemiology studies show frequent recombination in CVA9 coding and noncoding regions, potentially enhancing virulence and broadening the clinical spectrum of recombinant strains (*5*,*6*). We describe the clinical and virologic characterization of a recombinant mosaic CVA9 strain identified by whole-genome sequencing and involved in a severe inflammatory cardiomyopathy in a previously healthy child in France in 2024.

The study

A <24-month-old girl was admitted to the pediatric emergency unit of the Centre Hospitalier Universitaire de Reims in Reims, France, in mid-July 2024 with a 6-week history of cough, parentally reported fever (temperature of 38°C), and suspected cardiomegaly on a chest radiograph obtained the day before (Figure 1). Her general practitioner had prescribed treatment for bronchiolitis (without viral documentation) and amoxicillin, followed by azithromycin and a chest radiograph. The child was born at term and had unremarkable growth and development, no history of recurrent infections, and unremarkable baseline immune globulin levels. Clinical examination revealed tympanic temperature of 38.2°C, blood pressure 112/65 mm Hg, sinus tachycardia (150 beats/min), gallop rhythm, and liver edge 3 cm below the costal border. Transthoracic echocardiography revealed severe left ventricular dilation and markedly reduced left ventricular ejection fraction (≈27.5%); cardiac structures and coronary arteries appeared unremarkable. Cardiac troponin T was 57 ng/L (reference range <14 ng/L), and N-terminal prohormone of brain natriuretic peptide (NT-ProBNP) was 32,486 pg/mL (reference range <300 pg/mL). We conducted a nasopharyngeal swab specimen multiplex real-time PCR

Author affiliations: INSERM UMR-S 1320, University of Reims Champagne-Ardenne, Reims, France (A.-L. Lebreil, M. Glenet, Y. N'Guyen, L. Andreoletti); National Reference Center for Enteroviruses and Parechoviruses, CHU Clermont-Ferrand, Clermont-Ferrand, France (M. Bisseux, A. Mirand, C. Henquell); UMR CNRS 6023, Université Clermont Auvergne, Clermont-Ferrand (M. Bisseux, A. Mirand, C. Henquell); University Hospital Centre of Reims, Reims (Y. N'Guyen, L. Andreoletti); American Memorial Hospital, Reims University Hospital, Reims (N. Taha, P. Mauran).

DOI: https://doi.org/10.3201/eid3204.251574

[1]These authors contributed equally to this article.

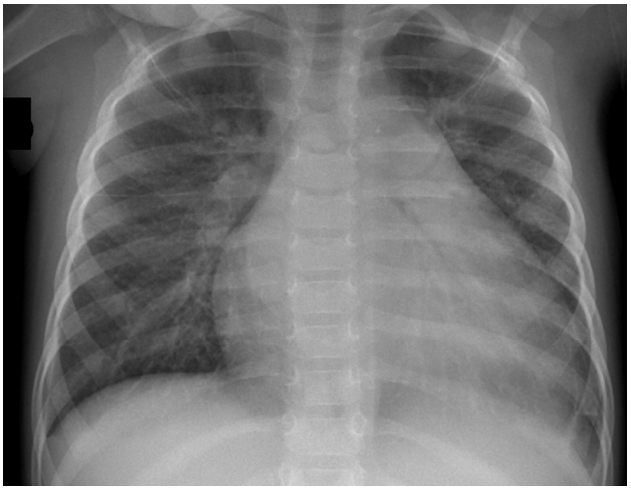

Figure 1. Chest radiograph of a pediatric patient with severe inflammatory cardiomyopathy caused by coxackievirus strain A9, northeastern France, 2024. Imaging was performed the day before admission to the pediatric ward and demonstrated unclear cardiomegaly.

on July 11 (R-GENE Respiratory PCR Kit; bioMérieux, https://www.biomerieux.com) that was negative for adenovirus, respiratory syncytial virus, metapneumovirus, influenza, and parainfluenza but detected enterovirus RNA. Results of blood real-time PCRs for human herpes virus 1–6, adenovirus, and parvovirus B19 were negative, whereas enterovirus viremia was detected and quantified in peripheral EDTA blood samples (1.32×10^4 copies/mL). Throat and blood cultures showed no pathogenic bacterial growth (*7*).

Besides congestive heart failure therapy, the patient received corticosteroids for 2 days and 1 course of intravenous immunoglobulin (IVIg) on day 2. Two supplemental courses of IVIg were prescribed on day 7 and 16 (Table). Cardiac magnetic resonance imaging done on day 19 revealed left ventricle dilation without enhancement after gadolinium injection. Outcome was ultimately favorable, with normalization of troponin T and NT-ProBNP levels within 3 months and of left ventricular ejection fraction within 6 months (Table). Results of genetic screening for inherited cardiomyopathies were negative (*8*). Although a cardiac biopsy was not performed because of an unfavorable benefit to risk ratio in this infant, stage C myocarditis was diagnosed according to recent American College of Cardiology guidelines (*9*). Written informed consent was obtained from a parent for research use of clinical and biologic data.

Published studies on cardiac tissue and whole blood from myocarditis patients identified EV-B populations with 5′-terminal RNA deletions. We assessed those forms in our patient's blood specimen by using validated rapid amplification of cDNA ends PCR (*7*,*10*). Our findings indicate that the major CVA9 genome exhibited a 50-nt 5′-terminal deletion, previously reported in a coxsackievirus B (CVB) 3 strain as a cardiotropic, replication-competent form (*11*) (Appendix Figure 1, http://wwwnc.cdc.gov/EID/article/32/4/25-1574-App1.pdf).

Reverse transcription PCR targeting the complete viral capsid protein viral protein (VP) 1 genomic region with Sanger sequencing or the complete genome with Illumina sequencing (Illumina, https://www.illumina.com) enabled genotypic identification of 2 original CVA9 clinical strains from our study patient (GenBank accession nos. PV939324 and PX441804) (*12*). Those strains exhibited 100% nucleotide and amino acid identity in VP1. Phylogenetic analysis of complete CVA9 VP1 genomic region sequences indicated strong homology with another CVA9 isolated in 2024 in Versailles, France (GenBank accession no. PQ612466), from the peripheral blood of a 28-day-old infant with acute respiratory tract infection. The strain from our patient also closely clustered with another CVA9 isolated in 2024 in Versailles, France, and other CVA9 strains isolated in China during 2012–2021 (Figure 2, panel A).

Whole-genome sequencing of CVA9 strains by using Illumina protocols (*12*) provided interpretable data only for our study respiratory sample. Phylogenetic analysis revealed elongated branches and close clustering of genetically distinct sequences within the first polyprotein precursor region region (e.g., E6/E3 and E11) (Figure 2, panel B), suggesting recombination hotspots in structural or nonstructural protein-coding regions, which likely drive CVA9 diversity and evolution (*5*).

To investigate CVA9 genomic recombination, we conducted SimPlot analyses (Figure 3). The 2 CVA9 isolates from 2024 (a cardiotropic reference and the Versailles strain) were colinear across the genome, indicating no evidence of recombination between them. Sequence comparison between our reference

Table. Laboratory tests performed on a child with recombinant mosaic coxsackievirus strain A9, associated with severe inflammatory cardiomyopathy, northeastern France, 2024*

Laboratory tests	Day 1	Day 19	Day 97	Day 179
LVTDD, mm	47.1 (TTE)	47.6 (MRI)		34.4 (TTE)
T troponin, ng/L	57	41.3	12	
NT ProBNP, pg/mL	32,843	2,897	251	

*Corticosteroids plus intravenous Ig were administered on day 2, day 7, and day 16 of hospitalization. LVTDD, left ventricular tele diastolic diameters; MRI, magnetic resonance imaging; NT Pro BNP, N-terminal prohormone of brain natriuretic peptide; TTE, transthoracic echocardiography.

cardiotropic strain, a CVA9 isolated in 2025 in France and the virus isolated in China in 2019 revealed high similarity (≈95%) within the first polyprotein precursor region and 5′ regions, but a distinct breakpoint within the 2A gene, suggesting recombination in our sequence. Of note, between positions 3,600 and 3,900, sequence similarity increased with the CVA9 2022 strain from Russia, consistent with recombination events involving viruses isolated in Russia and Kazakhstan. An additional recombination event likely involved a strain related to E3 France 2024. Furthermore, the E3 strain itself is recombinant, sharing a genomic segment with E6 from position 4,700 to the genome terminus (Appendix Figure 2). This terminal region, which encodes RNA polymerase (positions 5,960–7,645), appears to have been further acquired by recombination with an E11 strain associated with epidemics in Europe and severe neonatal infections (*12*). Phylogenetic analyses of partial protein 2A–2B and 3D polymerase (3Dpol) gene sequences confirmed the genetic homology between our CVA9 strain and the strain isolated in Versailles in 2024. Those analyses also clarified the geographic origins of the recombinant segments: the mid-part of P2A was derived from a CVA9 strain previously detected in Russia, whereas 3Dpol originated from E11 strains from Europe associated with severe neonatal infections (Appendix Figure 2) (*12*). P2A and 3Dpol genes are key determinants of enterovirus caused cardiac infection because they dampen innate

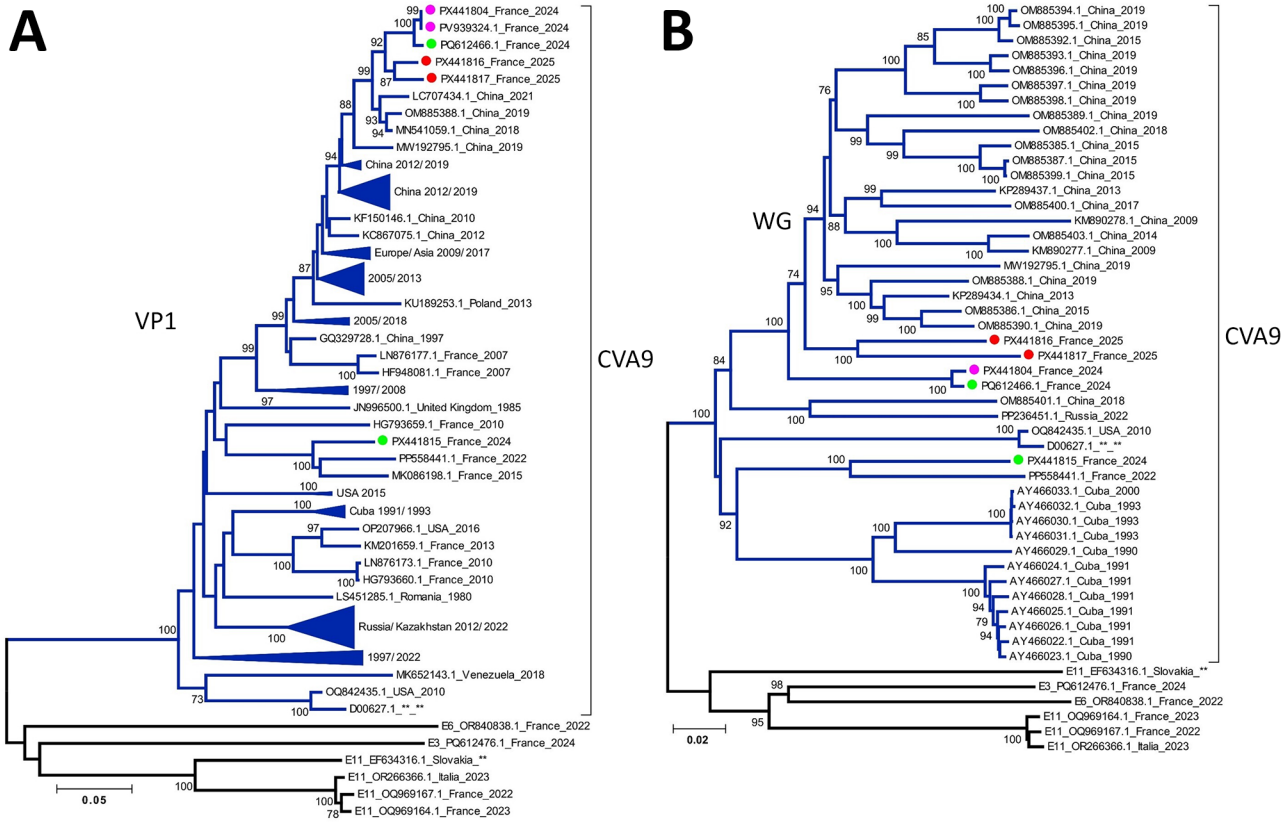

Figure 2. Phylogenetic analysis of CVA9 sequences from samples collected from a pediatric patient with severe inflammatory cardiomyopathy caused by CVA9, northeastern France, 2024, and reference sequences. A) All available CVA9 sequences from GenBank containing the complete VP1 (1D) gene (with a maximum of 25 missing bases at either end) aligned with CVA9 sequences obtained in this study and in France during 2024–2025. B) All available CVA9 sequences from GenBank containing the complete genome sequence (entire open reading frame with <60 bases missing from the 5′ UTR) aligned with CVA9 sequences obtained in this study and in France during 2024–2025, along with selected echovirus reference strains. We conducted sequence alignment by using BioEdit version 7.2.5 (https://thalljiscience.github.io/page2.html) and constructed phylogenetic trees by using the neighbor-joining method and the Tamura-Nei substitution model in MEGA 5 (http://www.megasoftware.net) We assessed the robustness of tree nodes with 1,000 bootstrap replicates; only bootstrap values ≥70% are shown. Pink circles indicate sequences generated in this study, red circles indicate CVA9 isolates from France in 2025, and green circles indicate CVA9 isolates from France in 2024. Sequences with close phylogenetic relationships were grouped into clusters, annotated with the country of origin and the range of isolation years. Clusters without specific geographic annotation contained sequences isolated from multiple continents. Branch numbers indicate bootstrap values. Scale bars represent substitutions per site. CVA9, coxsackievirus A9; VP, viral protein; WG, whole-genome.

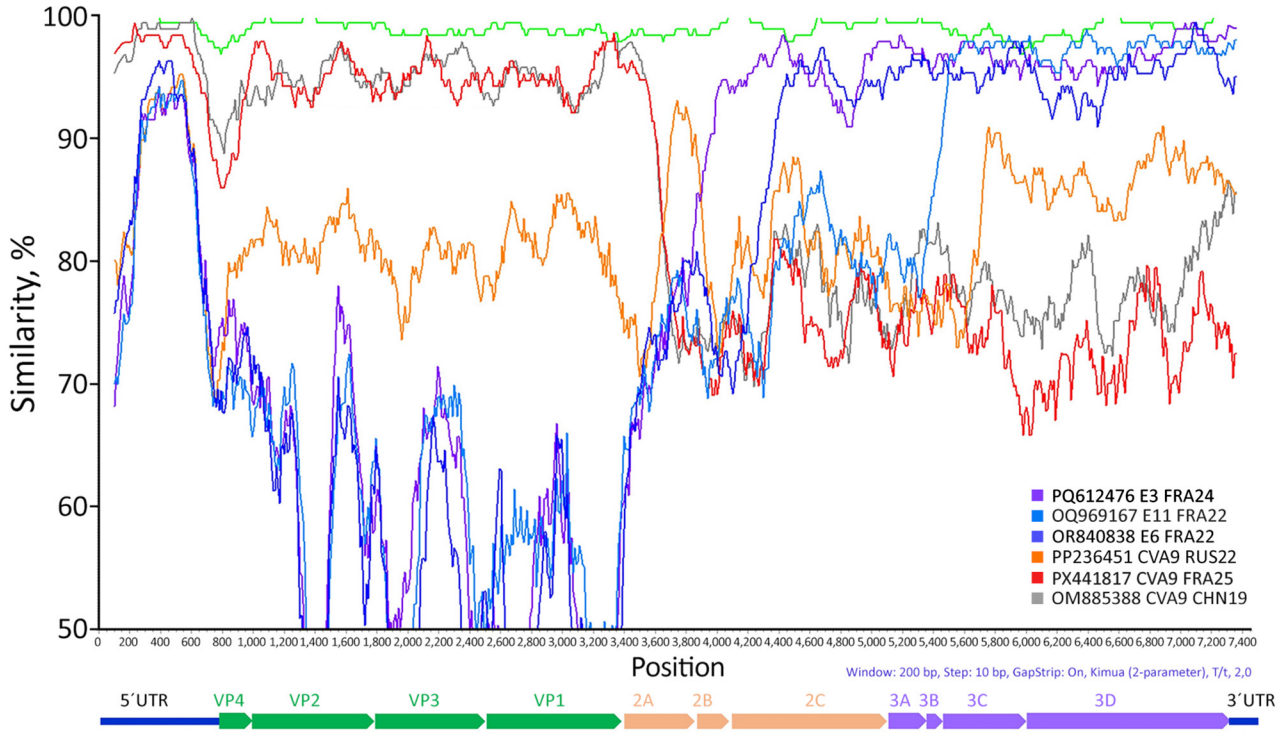

Figure 3. Similarity plot of complete CVA9 genome sequences from a pediatric patient with severe inflammatory cardiomyopathy caused by CVA9, northeastern France, 2024, and from GenBank. We generated the plot by using SimPlot version 3.5.1 (https://mybiosoftware.com/simplot-3-5-1-sequence-similarity-plotting.html). We calculated the pairwise nucleotide similarity between the sequence we obtained (GenBank accession no. PX441804) and all other available CVA9 genomes by using a 200-nt sliding window with a step size of 10-nt. We further analyzed regions showing marked decreases in similarity, suggestive of potential recombination events, by using BLAST (https://blast.ncbi.nlm.nih.gov), and the most closely related complete genome sequences for each region were included in the SimPlot analysis. Green indicates CVA9 isolates from France collected in 2024 and red those from 2025. A CVA9 isolate from China (2019) is shown in gray, and a 2022 Russian isolate is shown in orange. Echovirus reference sequences from France are also included: E3 (2024) in purple, E6 (2022) in dark blue, and E11 (2022) in light blue. CVA9, coxsackievirus A9; E, echovirus; VP, viral protein; UTR, untranslated region.

type I interferon responses and drive viral RNA replication, including production of 5′ terminally deleted RNA forms (*11*,*13*).

Conclusions

Unlike well-established cardiotropic species, B enterovirus strains such as CVB3 and CVB5, other species B enteroviruses such as CVA9, and some species A enteroviruses such as CVA6 have only sporadically been linked to myocarditis and cardiac histologic lesions, with rare fatal outcomes (*14*,*15*). Although the cardiotropic potential of those strains is not as well documented as for CVB viruses, recent molecular and clinical evidence supports the capacity of CVA9 to induce cardiac inflammation, particularly in neonates and children (*1*). Our study case not only confirms the myocardial tropism of CVA9 but also challenges its reputation as a predominantly benign childhood pathogen. This case highlights that other species B enteroviruses besides CVB3 can cause cardiomyopathy in otherwise healthy pediatric patients.

Acknowledgments

We sincerely thank all members of the pediatric ward at CHU de Reims, France.

About the Author

Ms. Lebreil is a molecular biology specialist developing genotyping technologies for RNA viruses. Her research interests include viral immune evasion mechanisms, host-pathogen interactions in cardiac tissue, and molecular determinants of enterovirus persistence in chronic diseases.

References

1. Machado RS, Tavares FN, Sousa IP Jr. Global landscape of coxsackieviruses in human health. Virus Res. 2024;344:199367. https://doi.org/10.1016/j.virusres.2024.199367
2. de Schrijver S, Vanhulle E, Ingenbleek A, Alexakis L, Johannesen CK, Broberg EK, et al.; ENPEN Study Collaborators. Epidemiological and clinical insights into enterovirus circulation in Europe, 2018–2023: a multicenter retrospective surveillance study. J Infect Dis. 2025;232:e104–15. https://doi.org/10.1093/infdis/jiaf179

3. Chen BS, Lee HC, Lee KM, Gong YN, Shih SR. Enterovirus and encephalitis. Front Microbiol. 2020 Feb 20 [cited 2025 Oct 3]. https://www.frontiersin.org/journals/microbiology/articles/10.3389/fmicb.2020.00261/full
4. Eisenhut M, Algawi B, Wreghitt T, Foweraker J, McKee T, Miles R, et al. Fatal coxsackie A9 virus infection during an outbreak in a neonatal unit. J Infect. 2000;40:297–8. https://doi.org/10.1053/jinf.2000.0650
5. Hietanen E, Susi P. Recombination events and conserved nature of receptor binding motifs in coxsackievirus A9 isolates. Viruses. 2020;12:68. https://doi.org/10.3390/v12010068
6. Zhao H, Wang J, Chen J, Huang R, Zhang Y, Xiao J, et al. Molecular epidemiology and evolution of coxsackievirus A9. Viruses. 2022;14:822. https://doi.org/10.3390/v14040822
7. Glenet M, N'Guyen Y, Mirand A, Henquell C, Lebreil AL, Berri F, et al.; French Enterovirus Myocarditis Study Group. Major 5′ terminally deleted enterovirus populations modulate type I IFN response in acute myocarditis patients and in human cultured cardiomyocytes. Sci Rep. 2020;10:11947. https://doi.org/10.1038/s41598-020-67648-5
8. Weizman O, Gandjbakhch E, Magnin-Poull I, Proukhnitzky J, Bordet C, Palmyre A, et al. Molecular genetic screening after non-ischaemic sudden cardiac arrest and no overt cardiomyopathy in real life: a major tool for the aetiological diagnostic work-up. Arch Cardiovasc Dis. 2024;117:382–91. https://doi.org/10.1016/j.acvd.2024.02.005
9. Drazner MH, Bozkurt B, Cooper LT, Aggarwal NR, Basso C, Bhave NM, et al.; Writing Committee. 2024 ACC expert consensus decision pathway on strategies and criteria for the diagnosis and management of myocarditis: a report of the American college of cardiology solution set oversight committee. J Am Coll Cardiol. 2025;85:391–431. https://doi.org/10.1016/j.jacc.2024.10.080
10. Mirabel M, Callon D, Bruneval P, Lebreil AL, Mousseaux E, Oudard S, et al. Late-onset giant cell myocarditis due to enterovirus during treatment with immune checkpoint inhibitors. JACC Cardiooncol. 2020;2:511–4. https://doi.org/10.1016/j.jaccao.2020.05.022
11. Callon D, Glenet M, Lebreil AL, Heng L, Bouland N, Fichel C, et al. Major group-B enterovirus populations deleted in the noncoding 5′ region of genomic RNA modulate activation of the type I interferon pathway in cardiomyocytes and induce myocarditis. PLoS Pathog. 2024; 20:e1012125. https://doi.org/10.1371/journal.ppat.1012125
12. Grapin M, Mirand A, Pinquier D, Basset A, Bendavid M, Bisseux M, et al. Severe and fatal neonatal infections linked to a new variant of echovirus 11, France, July 2022 to April 2023. Euro Surveill. 2023;28:2300253. https://doi.org/10.2807/1560-7917.ES.2023.28.22.2300253
13. Bouin A, Gretteau PA, Wehbe M, Renois F, N'Guyen Y, Lévêque N, et al. Enterovirus persistence in cardiac cells of patients with idiopathic dilated cardiomyopathy is linked to 5′ terminal genomic RNA-deleted viral populations with viral-encoded proteinase activities. Circulation. 2019;139:2326–38. https://doi.org/10.1161/CIRCULATIONAHA.118.035966
14. Callon D, N'Guyen Y, Fornes P, Andreoletti L. Fatal heart arrhythmia associated with enterovirus cardiac infection and SARS-CoV-2-induced cytokine storm. Pathology. 2024;56:434–7. https://doi.org/10.1016/j.pathol.2023.08.011
15. Andréoletti L, Lévêque N, Boulagnon C, Brasselet C, Fornes P. Viral causes of human myocarditis. Arch Cardiovasc Dis. 2009;102:559–68. https://doi.org/10.1016/j.acvd.2009.04.010

Address for correspondence: Laurent Andreoletti, Laboratoire de Virologie Médicale et Moléculaire, CHU & UMR-S INSERM 1320, Faculté de Médecine, 51 rue Cognacq-Jay, 51100 Reims CEDEX, France; email: landreoletti@chu-reims.fr

Whole-Genome Analysis of *Treponema pallidum* subspecies *endemicum* among Men Who Have Sex with Men, Japan, 2020–2023

Yuki Ohama, Kazuo Imai, Yuto Kotaka, Kenichi Lee, Ichiro Itoda, Shu-ichi Nakayama, Makoto Ohnishi, Yukihiro Akeda

Whole-genome sequencing of *Treponema pallidum* subsp. *endemicum* strains from men who have sex with men in Japan revealed a genetically distinct lineage from other geographic regions circulating via sexual transmission. Strengthening global molecular epidemiologic surveillance is essential for clarifying epidemiologic trends, clinical characteristics, and transmission pathways of this subspecies.

Treponema pallidum bacteria comprise 3 distinct subspecies: *T. pallidum* subsp. *pallidum* (TPA), *T. pallidum* subsp. *pertenue*, and *T. pallidum* subsp. *endemicum* (TEN) (*1*). TPA causes syphilis, a sexually transmitted infection prevalent worldwide. TEN causes bejel, which primarily affects children, and is transmitted through close contact (*1*). TEN is endemic to arid regions (e.g., Middle East and parts of Africa), particularly in populations with low socioeconomic status (*2*). Recent molecular studies revealed TEN in adults initially suspected of having syphilis (*3*-*7*). Evidence suggests that TEN can be transmitted sexually in nonendemic regions, including France, Cuba, and Japan (*3*-*5*). In Japan, researchers first identified a TEN infection in 2014, and 13 cases have since been reported among men who have sex with men (MSM) in urban centers, including Yamaguchi, Osaka, Kyoto, Hyogo, and Tokyo (*6*,*7*). Although typically considered nonvenereal, confirmed TEN have recently surfaced in MSM in nonendemic countries, raising questions about the bacterium's transmission dynamics and potential for sexual spread.

The National Institute of Infectious Diseases (Tokyo, Japan) serves as a reference laboratory and conducts surveillance of syphilis cases and molecular epidemiologic surveillance of TPA. That surveillance identified 5 new cases of TEN during 2020–2023. Initially, we performed multilocus sequence typing (MLST) to investigate circulating TPA sequence types and identify TEN in Japan. We followed that investigation by applying whole-genome sequencing (WGS) and single nucleotide polymorphism–based comparative analysis to assess phylogeny and possible sexual transmission of TEN in nonepidemic regions.

The Study

For our study, we obtained specimens through multicenter syphilis surveillance in Tokyo and Osaka during 2020–2023 (Appendix, https://wwwnc.cdc.gov/EID/article/32/4/25-1045-App1.pdf). Four clinics from 2 prefectures participated. The case definition included adult patients ≥18 years of age suspected of having primary or secondary syphilis. Submitted specimens were from 97 male patients, 98 female patients, and 2 persons of unknown sex. We performed PCR testing on collected specimens, targeting *TpN47* and *pol*A genes. We subjected residual samples to molecular epidemiologic analysis of TPA, using MLST and a microbial genome diversity database (PubMLST, https://pubmlst.org) in analyzing 3 genes: *TP0136*, *TP0548*, and *TP0705*.

We collected all 197 specimens from symptomatic sites, including swab samples from genital, anal, and oral lesions. Among the 97 male patients, we identified 28 (28.9%) as MSM. Using PubMLST, we

Author affiliations: National Institute of Infectious Diseases, Tokyo, Japan (Y. Ohama, Y. Kotaka, K. Lee, S. Nakayama, M. Ohnishi, Y. Akeda); Saitama Medical University, Saitama, Japan (K. Imai); Tokyo Metropolitan University, Tokyo (Y. Kotaka); Shirakaba Clinic, Tokyo (I. Itoda)

DOI: http://doi.org/10.3201/eid3204.251045

detected TEN in 5 male patients who visited sexually transmitted infection clinics in Tokyo and Osaka. We identified 4 of those patients as MSM, noting 1 man did not disclose his sexual orientation (Table). Clinic staff noted genital induration, ulcers, or erosions in all 5 patients, findings similar to those of syphilis. In addition, testing revealed positive results for both rapid plasma reagin and *T. pallidum* antibodies, and PCR targeting the *TpN47* and *pol*A genes also brought positive results. Based on the data, physicians determined a diagnosis of syphilis for all 5 patients. Further analysis included WGS (Appendix), which rendered high-quality TEN genomes from 3 strains isolated in Tokyo with >90% reference coverage and <5% estimated contamination (GenBank accession nos. DRX678426–8). We then conducted phylogenetic analysis using 8 available TEN genomes from GenBank (https://www.ncbi.nlm.nih.gov/genbank) (Table).

To accurately assess genetic relatedness, we analyzed aligned core genes and constructed a maximum-likelihood phylogenetic tree (Figure). That analysis showed that 7 TEN strains from Japan, isolated from 5 MSM and 2 male patients with unknown sexual orientation in Tokyo during 2019–2022 (*7*), belonged to the same clade, distinct from TEN strains from endemic regions, including Iraq B (1951) (*8*), Bosnia A (1950) (*9*), and Cuba (2 strains from MSM, 2014 and 2017) (*10*).

Conclusion

Phylogenetic analysis based on WGS of TEN isolates from 8 male patients (7 MSM and 1 of unknown sexual orientation) with syphilitic symptoms in 2019–2022 revealed that all Tokyo strains belonged to a single clade. That finding provides strong molecular evidence of sustained, local transmission of TEN among MSM in Tokyo.

Clustering of genetically near-identical TEN strains, isolated over several years from epidemiologically linked populations, supports an ongoing transmission network. Given that *T. pallidum* has a highly conserved genome with low single-nucleotide polymorphism accumulation rates, this distinct clade among these Japan isolates further substantiates their shared origin and recent divergence. Since 2019, reports of sporadic cases of TEN in Tokyo have continued to surface. In an MLST analysis, researchers identified TEN in 3 of 26 patients with HIV identifying as MSM who presented with syphilitic symptoms at Tokyo hospitals during 2019–2022 (*11*). Similar research revealed 1 case of TEN on the basis of both MLST and multilocus sequence analysis (MLSA) among 48 patients given a diagnosis of syphilis in Tokyo during 2023–2024 (*12*). These findings support the persistent circulation of TEN as a sexually transmitted infection among MSM in Tokyo.

In addition to the Tokyo cases, research uncovered 5 other cases of TEN infection during 2014–2018 among MSM in western Japan, including Yamaguchi, Osaka, Kyoto, and Hyogo prefectures (*6*). However, in those earlier investigations, clinicians analyzed isolates only by MLSA targeting *TP0548* and *TP0856* and we thus excluded that data from our study's phylogenetic analysis because of the lack of WGS data. In our study, testing resulted in TEN detection in 2 patients identifying as MSM; however, we did not achieve high-quality genome sequencing. Therefore, whether the strains from outside the core Tokyo and Kansai cohort belong to the same transmission cluster remains unclear. Nevertheless, our results underscore the potential undetected circulation of sexually transmitted TEN in nonendemic regions, highlighting the critical role of molecular surveillance in uncovering hidden transmission patterns. The MLSA results

Table. Summary of strains from a whole-genome analysis of *Treponema pallidum* subspecies *endemicum* among men who have sex with men, Japan, 2020–2023*

Strain name	Year detected	Patient sex	Sexual orientation	Source of transmission	Location	GenBank accession no.	Reference
NIIDTP373	2020	M	MSM	Sexual	Osaka, Japan	Not available	This study
NIIDTP389	2020	M	MSM	Sexual	Tokyo, Japan	Not available	This study
NIIDTP404	2021	M	MSM	Sexual	Tokyo, Japan	DRX678426	This study
NIIDTP415	2021	M	MSM	Sexual	Tokyo, Japan	DRX678427	This study
NIIDTP523	2022	M	Unknown	Sexual	Tokyo, Japan	DRX678428	This study
Japan320e	2019	M	MSM	Sexual	Tokyo, Japan	NZ_CP073523	(*7*)
Japan322e	2019	M	MSM	Sexual	Tokyo, Japan	NZ_CP073522	(*7*)
Japan326e	2019	M	MSM	Sexual	Tokyo, Japan	NZ_CP073518	(*7*)
Japan346e	2019	M	Unknown	Sexual	Tokyo, Japan	NZ_CP073506	(*7*)
Iraq B	1951	F	Unknown	Unknown	Iraq	NZ_CP032303	(*8*)
Bosnia A	1950	M	Unknown	Unknown	Bosnia	NZ_CP007548	(*9*)
C77	2014	M	MSM	Sexual	Cuba	NZ_CP081507	(*10*)
C279	2017	M	MSM	Sexual	Cuba	NZ_CP078090	(*10*)

*MSM, men who have sex with men.

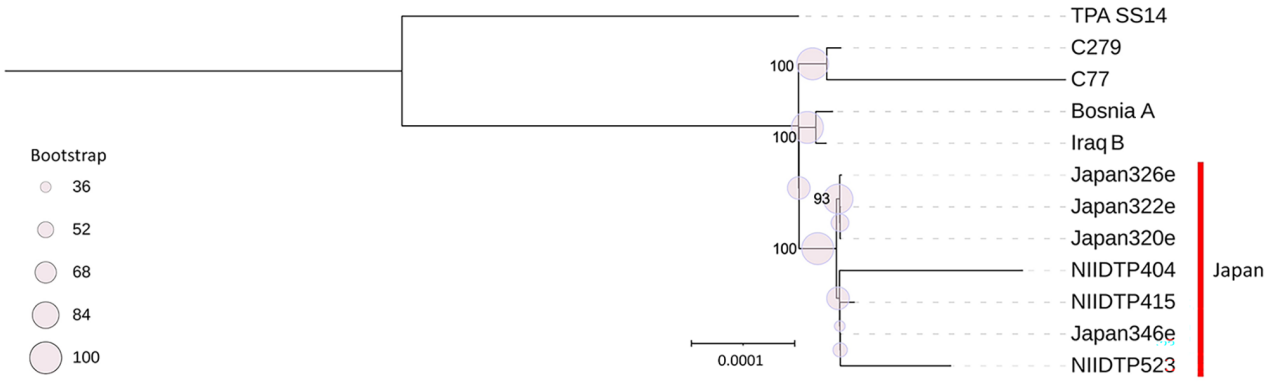

Figure. Phylogenetic analysis of isolates from a study of whole-genome analysis of *Treponema pallidum* subspecies *endemicum* among men who have sex with men, Japan, 2020–2023. Open reading frames annotated from de novo assembled contigs using Bakta version 1.7.0 (https://bakta.computational.bio), and corresponding GFF3 annotation files processed with Panaroo version 1.2.3 (https://zenodo.org/records/3945497) to define core genomes across isolates. Multiple alignments of core gene sequences generated by Panaroo were used for phylogenetic reconstruction. *T. pallidum* subsp. *pallidum* SS14 (GenBank accession no. NC_021508) was used as a reference strain. IQ-TREE version 2.2.0 (http://www.iqtree.org) was used to infer maximum-likelihood phylogenies, incorporating 1,000 ultrafast bootstrap replicates to assess nodal support. Phylogenetic tree was visualized by using Interactive Tree of Life (iTOL; https://itol.embl.de). The *T. pallidum* subsp. *endemicum* strains isolated in Japan formed a clade distinct from classic endemic strains, including Iraq B and strains from Cuba (C77 and C279). Scale bar indicates nucleotide substitutions per site.

indicated that these earlier strains also formed a distinct clade from Iraq B and Bosnia A, supporting the conclusion that TEN strains in Japan are genetically distinct. Furthermore, research has yet to isolate TEN from female patients.

Clinically, distinguishing between TPA and sexually transmitted TEN is challenging. Previous reports indicate that sexually transmitted TEN imparts symptoms indistinguishable from syphilis caused by TPA, and the medical literature offers no unique clinical markers for TEN infection. Serologic tests yield similar results for both subspecies. In addition, molecular targets like *TpN47* and *pol*A, commonly used in primary syphilis diagnostics, are present in both TPA and TEN. Therefore, only WGS, MLST, MLSA, or specific genetic assays can differentiate TPA from TEN (*13*,*14*). Accordingly, many TEN infections in Japan could be misclassified as syphilis caused by TPA. In our study, all 5 patients confirmed to have TEN received an initial diagnosis of typical syphilis.

Since 2012, reported syphilis cases in Japan have increased >10-fold, particularly among MSM in urban centers such as Tokyo, indicating expanding sexual transmission networks (Japan Institute for Health Security, https://id-info.jihs.go.jp/niid/en/iasr/9542-479te.html). Within that context, repeated detection of genetically related TEN strains suggests this typically nonvenereal pathogen could be established in these networks. Those findings suggest that TEN might be underdiagnosed and more widespread than currently recognized. In addition, TEN might have begun to spread beyond MSM populations through sexual transmission, raising the possibility of broader outbreaks.

In summary, although prior studies have suggested that TEN can be transmitted through close oral contact, such as kissing (*2*), the exact transmission route in the cases reported here remains unclear. To clarify epidemiologic trends, clinical characteristics, and transmission pathways of TEN, strengthening of molecular surveillance and continuing to accumulate clinical and genomic data are essential.

Acknowledgments

We sincerely acknowledge the contributions of Hiroshi Kameoka, Masayuki Sawamura, and Takashi Hamada for their invaluable support in patient enrollment and clinical coordination.

This study was approved by the ethics committee of NIID (approval no. 1605). Datasets analyzed during this study are available from the corresponding author on reasonable request.

This work was supported by the Japan Agency for Medical Research and Development (AMED) under the Research Program on Emerging and Re-emerging Infectious Diseases (grant no. 23fk0108676j0102).

About the Author

Dr. Ohama is a researcher at the National Institute of Infectious Diseases, specializing in clinical microbiology. Her research focuses on molecular biology, particularly on sexually transmitted infections such as syphilis and gonorrhea.

References

1. Mulligan CJ, Norris SJ, Lukehart SA. Molecular studies in *Treponema pallidum* evolution: toward clarity? PLoS Negl Trop Dis. 2008;2:e184. https://doi.org/10.1371/journal.pntd.0000184
2. Giacani L, Lukehart SA. The endemic treponematoses. Clin Microbiol Rev. 2014;27:89–115. https://doi.org/10.1128/CMR.00070-13
3. Noda AA, Grillová L, Lienhard R, Blanco O, Rodríguez I, Šmajs D. Bejel in Cuba: molecular identification of *Treponema pallidum* subsp. *endemicum* in patients diagnosed with venereal syphilis. Clin Microbiol Infect. 2018;24:1210.e1–5. https://doi.org/10.1016/j.cmi.2018.02.006
4. Grange PA, Mikalová L, Gaudin C, Strouhal M, Janier M, Benhaddou N, et al. *Treponema pallidum* 11qj subtype may correspond to a *Treponema pallidum* subsp. *endemicum* strain. Sex Transm Dis. 2016;43:517–8. https://doi.org/10.1097/OLQ.0000000000000474
5. Kawahata T, Kojima Y, Furubayashi K, Shinohara K, Shimizu T, Komano J, et al. Bejel, a nonvenereal treponematosis, among men who have sex with men, Japan. Emerg Infect Dis. 2019;25:1581–3. https://doi.org/10.3201/eid2508.181690
6. Shinohara K, Furubayashi K, Kojima Y, Mori H, Komano J, Kawahata T. Clinical perspectives of *Treponema pallidum* subsp. *endemicum* infection in adults, particularly men who have sex with men in the Kansai area, Japan: a case series. J Infect Chemother. 2022;28:444–50. https://doi.org/10.1016/j.jiac.2021.11.012
7. Lieberman NAP, Lin MJ, Xie H, Shrestha L, Nguyen T, Huang ML, et al. *Treponema pallidum* genome sequencing from six continents reveals variability in vaccine candidate genes and dominance of Nichols clade strains in Madagascar. PLoS Negl Trop Dis. 2021;15:e0010063. https://doi.org/10.1371/journal.pntd.0010063
8. Mikalová L, Janečková K, Nováková M, Strouhal M, Čejková D, Harper KN, et al. Whole genome sequence of the *Treponema pallidum* subsp. *endemicum* strain Iraq B: a subpopulation of bejel treponemes contains full-length *tprF* and *tprG* genes similar to those present in *T. p.* subsp. *pertenue* strains. PLoS One. 2020;15:e0230926. https://doi.org/10.1371/journal.pone.0230926
9. Staudová B, Strouhal M, Zobaníková M, Cejková D, Fulton LL, Chen L, et al. Whole genome sequence of the *Treponema pallidum* subsp. *endemicum* strain Bosnia A: the genome is related to yaws treponemes but contains few loci similar to syphilis treponemes. PLoS Negl Trop Dis. 2014;8:e3261. https://doi.org/10.1371/journal.pntd.0003261
10. Vrbová E, Noda AA, Grillová L, Rodríguez I, Forsyth A, Oppelt J, et al. Whole genome sequences of *Treponema pallidum* subsp. *endemicum* isolated from Cuban patients: the non-clonal character of isolates suggests a persistent human infection rather than a single outbreak. PLoS Negl Trop Dis. 2022;16:e0009900. https://doi.org/10.1371/journal.pntd.0009900
11. Sato W, Sedohara A, Koga M, Nakagama Y, Yotsuyanagi H, Kido Y, et al. Epidemic of multiple *Treponema pallidum* strains in men who have sex with men in Japan: efficient multi-locus sequence typing scheme and indicator biomarkers. AIDS Res Ther. 2024;21:71. https://doi.org/10.1186/s12981-024-00663-y
12. Imai K, Sato A, Tanaka M, Ohama Y, Nakayama S-I, Omachi R, et al. Prospective evaluation of non-invasive saliva specimens for the diagnosis of syphilis and molecular surveillance of *Treponema pallidum*. J Clin Microbiol. 2024;62:e0080924. https://doi.org/10.1128/jcm.00809-24
13. Chi KH, Danavall D, Taleo F, Pillay A, Ye T, Nachamkin E, et al. Molecular differentiation of *Treponema pallidum* subspecies in skin ulceration clinically suspected as yaws in Vanuatu using real-time multiplex PCR and serological methods. Am J Trop Med Hyg. 2015;92:134–8. https://doi.org/10.4269/ajtmh.14-0459
14. Centurion-Lara A, Molini BJ, Godornes C, Sun E, Hevner K, Van Voorhis WC, et al. Molecular differentiation of *Treponema pallidum* subspecies. J Clin Microbiol. 2006;44:3377–80. https://doi.org/10.1128/JCM.00784-06

Address for correspondence: Yuki Ohama, National Institute of Infectious Diseases, Japan Institute for Health Security, 1-23-1 Toyama, Shinjuku, Tokyo 162-8640, Japan; e-mail: ohama.y@jihs.go.jp

Panton-Valentine Leukocidin–Encoding Methicillin-Resistant *Staphylococcus aureus*, the Netherlands, 2023–2024[1]

Patrick van Schelven, Roel Nijhuis, Casper Jamin, Sophie Goemans, Putri Hintaran, Marischka van der Jagt-Zwetsloot, Annelies Smilde, Annelot ter Horst, Melanie de Graaf, Daan W. Notermans, Anne Russcher, Stijn Raven

We describe a community outbreak of Panton-Valentine leukocidin–positive methicillin-resistant *Staphylococcus aureus* (MRSA) during November 2023–June 2024 in the Netherlands. We identified a massage center as the source. Case-patients experienced skin infections and abscesses. This study highlights the importance of genomic surveillance of MRSA in distinguishing Panton-Valentine leukocidin–positive MRSA.

Methicillin-resistant *Staphylococcus aureus* (MRSA) of multilocus sequence type (MLST) clonal complex (CC) 398 is usually considered livestock-associated (LA) MRSA. Panton-Valentine leukocidin (PVL)–positive isolates of this type are increasingly detected in humans and not associated with livestock exposure (*1*–*5*). Those strains possess virulence genes that enhance human-to-human transmission (*6*). In November 2023, an outbreak of PVL-positive CC398 MRSA linked to a massage center occurred in the Netherlands. Here, we describe the course and characteristics of the outbreak and the management challenges specific to a community MRSA outbreak.

The Study

In November 2023, a microbiologic hospital laboratory notified the regional Public Health Service (PHS) of a potential outbreak of PVL-positive CC398 MRSA in the region. Within 3 weeks, 5 patients sought care at the hospital with MRSA-positive abscesses that required surgical drainage. All isolates were multilocus variable-number tandem-repeat analysis (MLVA) type MT2306, MLVA complex MC0398, a previously rarely encountered MLVA type. After notification, the PHS interviewed reported patients to identify potential infection sources and contacts at risk and collected clinical isolates for enhanced genomic surveillance using whole-genome sequencing (WGS) to further distinguish identical MLVA types.

From the first 5 interviews, we identified a specific massage center as a potential source location. PHS staff visited the massage center on 5 occasions during the outbreak (Figure 1). Employees of the center were screened for MRSA at multiple time points (Appendix Table 1, https://wwwnc.cdc.gov/EID/article/32/4/25-1646-App1.pdf). Initially, all employee samples tested negative; at the fourth visit, an employee previously unknown to the PHS was present and tested positive. The employee of the massage center who tested positive was advised to refrain from work and undergo MRSA eradication therapy. The employee resumed work after 3 consecutive negative tests. The employee reported no risk factors for MRSA acquisition (e.g., travel history). We conducted environmental sampling on 3 occasions; multiple samples tested positive (Appendix Table 1).

We identified a total of 31 cases during November 2023–June 2024 (Figure 1). Median age of all case-patients was 42 (range 3–69) years, and all but 1 were

Author affiliations: Public Health Service Region Utrecht, Zeist, the Netherlands (P. van Schelven, S. Goemans, P. Hintaran, M. van der Jagt-Zwetsloot, A. ter Horst, S. Raven); Meander Medical Centre, Amersfoort, the Netherlands (R. Nijhuis, A. Smilde, A. Russcher); National Institute for Public Health and the Environment, Bilthoven, the Netherlands (C. Jamin, D.W. Notermans); Unilabs-Saltro Diagnostic Centre, Utrecht, the Netherlands (M. de Graaf)

DOI: https://doi.org/10.3201/eid3204.251646

[1]Preliminary results from this study were presented at the European Scientific Conference on Applied Infectious Disease Epidemiology (ESCAIDE); Stockholm, Sweden; November 20–22, 2024.

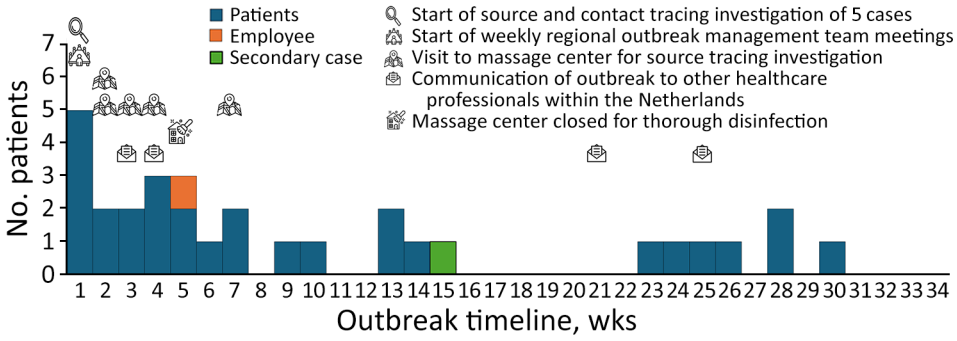

Figure 1. Epicurve and timeline of outbreak of Panton-Valentine leukocidin–encoding methicillin-resistant *Staphylococcus aureus*, the Netherlands, 2023–2024. Timeline of the outbreak in weeks was based on the date of notification to the Public Health Service, with the actions undertaken during the outbreak.

>18 years of age; 42% were female and 58% male. Of the 31 case-patients, 27 were symptomatic, 3 asymptomatic, and 1 of unknown status. Immune status of 3 case-patients was unknown, and none of the other case-patients were immunocompromised; 1 had type 2 diabetes mellitus. Most case-patients had mild skin infections from the MRSA infection. Ten cases required hospitalization; of those, 8 case-patients underwent surgery to relieve abscesses and 1 was admitted to the hospital with bacteremia.

In total, 22 of 31 case-patients reported visiting the massage center. Six case-patients did not report visiting the massage center; of those 6 cases, 1 was a secondary case because the patient was a household contact. The remaining 3 case-patients did not cooperate in source and contact investigation; nevertheless, we included them in the outbreak because of their geographic and microbiologic links. A year after the last notification, no new MRSA isolates of this specific MC0398-MT2306 strain had been reported in the PHS region, according to national MRSA surveillance.

We tested for the *mecA/mecC* gene in *S. aureus*–positive cultures using a laboratory-developed real-time PCR. We used an enrichment method to culture nose, throat, and rectal swab specimens (*7*). During the outbreak, we obtained environmental specimens in 2 ways: by wiping surfaces using gauze moistened with sterilized water and inserting the gauze in overnight enrichment broth, or by using PL agar contact plates (AnalytiChem, https://www.analytichem.com) and incubating them at 35°C for 24 hours. We took all colony-forming units (CFU) from the contact plates and inserted them in overnight enrichment broth, then tested the enrichment broths and CFU from the contact plates.

We determined that all MRSA isolates in the outbreak were MLVA type MT2306, complex MC0398, similar to CC398, as described previously (*8*). National surveillance data showed that this type was previously found in 4 isolates sampled during 2010–2021 in a different region of the country. All 4 previous isolates had tested PVL-negative. We performed WGS on MRSA isolates from the first 17 cases, the employee and all environmental isolates, as described previously (*9*). All MRSA isolates of the MC0398-MT2306 cluster belonged to MLST type ST1232 and Ridom core genome MLST complex type 35023 (Ridom GmbH, https://www.ridom.de). We analyzed genomic relatedness by whole-genome MLST analysis, using a cutoff of ≤15 alleles difference (*8*). The range of different alleles among all isolates related to the outbreak was 0–12 (mean 1) alleles. The 3 environmental isolates clustered with the human isolates with ≤1 allele difference. We compared the genomes from the 17 human isolates in our study with genomes of a PVL-negative MC0398-MT2306 strain isolated in 2019 that originated from a person who had close contact with pigs; that strain was ST398, complex type 7121, a PVL-negative MC0398-MT0398 from November 2023. We also compared those genomes with 4 international PVL-positive MRSA ST1232 isolates from the National Center for Biotechnology Information RefSeq database (https://www.ncbi.nlm.nih.gov/refseq; accession nos. GCF_019669165, GCF_019669245, GCF_019669345, GCF_019669385). The MC0398-MT2306 PVL-negative isolate from 2019 differed by 238 alleles from the nearest PVL-positive CC398 MRSA from the cluster in our outbreak, the MC0398-MT0398 PVL-negative differed by 226 alleles to isolates from our cluster, and the international PVL-positive MRSA ST1232 isolates differed by ≥48 alleles from our cluster (Figure 2). We also examined antimicrobial resistance in the study isolates (Appendix Tables 2, 3).

After notification of the first 5 cases, the region formed an outbreak management team composed of physicians and nurses of the PHS, medical microbiologists of the notifying laboratory, infection prevention experts of both the PHS and the hospital, and communication specialists. All general practitioners in the area were notified and advised to culture infected skin lesions not responding to first-line antimicrobial treatment. The outbreak was communicated via the national surveillance report 21 days after notification

to alert other PHS and clinical microbiologists. In addition, the National Institute for Public Health and the Environment issued an alert via EpiPulse, an online platform for sharing infectious disease among public health authorities in Europe.

We interviewed case-patients to identify potential at-risk contacts. We requested that symptomatic contacts, asymptomatic household contacts, and contacts working in healthcare or having a profession with intensive physical contact (i.e., masseuse, skin therapist) undergo testing for MRSA. It was not possible to screen all clients of the source location because of privacy issues. We advised all case-patients to undergo MRSA eradication therapy after full lesion healing, to prevent reintroduction in the source location. An infection prevention expert advised the staff at the source location about MRSA transmission and hygiene measures. In addition, the source location was thoroughly disinfected during the outbreak by a professional disinfection company in week 5 of the outbreak. The expert assisted by developing a disinfection plan, explaining its necessity and addressing questions of the source location's staff. The expert advised that objects that could not be sufficiently disinfected (e.g., fabric-covered tissue boxes, fabric decoration pieces) be permanently removed.

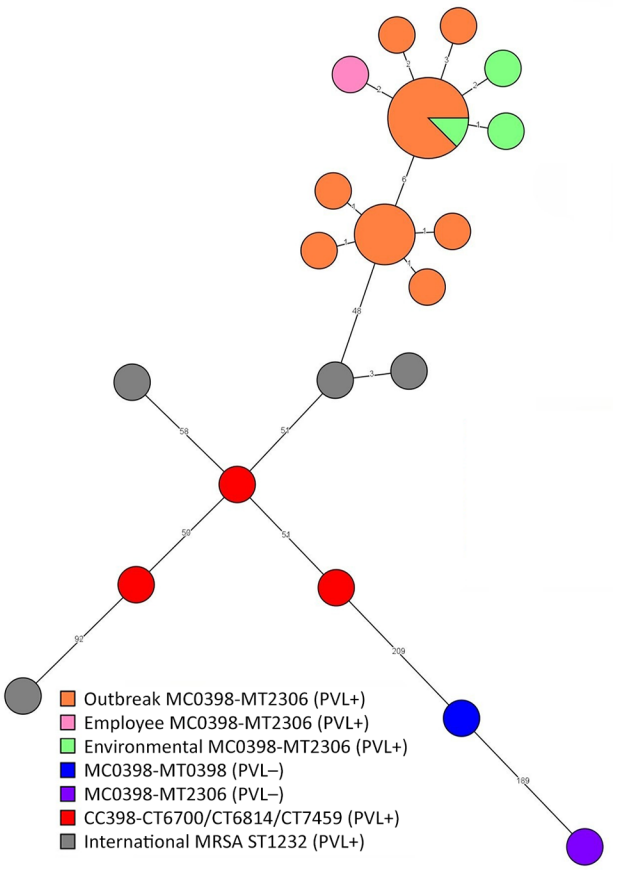

Figure 2. Whole-genome multilocus sequence typing minimum spanning tree in study of outbreak of PVL-encoding MRSA, the Netherlands, 2023–2024. We determined that all MRSA isolates were MLVA type MT2306, complex MC0398, similar to CC398. Tree shows the outbreak isolates of human cases (orange), employee case (pink), and environmental samples (green) clustering with a maximum difference of 12 alleles, confirming a microbiological link between the patients and the environmental samples. National PVL-positive, CC398 MRSA strains (red) and international PVL-positive MRSA ST1232 strains (gray) differ ≥48 alleles compared with the outbreak strain. The genome from a PVL-negative MC0398-MT2306 (purple) isolate from 2019 differs on 238 alleles from the outbreak isolates; the genome of the PVL-negative MC0398-MT0398 (blue) isolate differs 226 alleles from the outbreak isolates. CC, clonal complex; MLVA, multilocus variable number tandem repeat analysis; MRSA, methicillin-resistant *Staphylococcus aureus;* PVL, Panton-Valentine leucocidin; ST, sequence type.

Conclusions

We report a PVL-positive MRSA ST1232 strain similar to CC398 that caused a community outbreak with severe skin infections in the Netherlands. We confirmed human-to-human transmission in the community and detected viable MRSA on surfaces at the source location. This outbreak underscores the rise of PVL-positive CC398 MRSA strains in the community and its outbreak potential. The community setting of the source location posed several challenges in outbreak management, emphasizing the need for a tailored approach and rapid source tracing.

All WGS data has been deposited into the National Center for Biotechnology Information under BioProject PRJNA1254972.

About the Author

Dr. van Schelven is a physician specialized in infectious disease control at the Public Health Service region Utrecht in the Netherlands. His primary research interest is public health response to infectious disease outbreaks in the community.

References

1. Bosch T, van Luit M, Pluister GN, Frentz D, Haenen A, Landman F, et al. Changing characteristics of livestock-associated meticillin-resistant *Staphylococcus aureus* isolated from humans—emergence of a subclade transmitted without livestock exposure, the Netherlands, 2003 to 2014. Euro Surveill. 2016;21:21. https://doi.org/10.2807/1560-7917.ES.2016.21.21.30236
2. Konstantinovski MM, Schouls LM, Witteveen S, Claas ECJ, Kraakman ME, Kalpoe J, et al. Livestock-associated methicillin-resistant *Staphylococcus aureus* epidemiology, genetic diversity, and clinical characteristics in an urban region. Front Microbiol. 2022;13:875775. https://doi.org/10.3389/fmicb.2022.875775

3. Møller JK, Larsen AR, Østergaard C, Møller CH, Kristensen MA, Larsen J. International travel as source of a hospital outbreak with an unusual methicillin-resistant *Staphylococcus aureus* clonal complex 398, Denmark, 2016. Euro Surveill. 2019;24:1800680. https://doi.org/10.2807/1560-7917.ES.2019.24.42.1800680
4. Gooskens J, Konstantinovski MM, Kraakman MEM, Kalpoe JS, van Burgel ND, Claas ECJ, et al. Panton-Valentine leukocidin–positive CC398 MRSA in urban clinical settings, the Netherlands. Emerg Infect Dis. 2023;29:1055–7. https://doi.org/10.3201/eid2905.221717
5. Brodíková K, Destanque T, Haenni M, Karpíšková R. Clonal complex 398 methicillin-resistant *Staphylococcus aureus* producing Panton-Valentine leukocidin, Czech Republic, 2023. Emerg Infect Dis. 2025;31:174–7. https://doi.org/10.3201/eid3101.241323
6. Price LB, Stegger M, Hasman H, Aziz M, Larsen J, Andersen PS, et al. *Staphylococcus aureus* CC398: host adaptation and emergence of methicillin resistance in livestock. MBio. 2012;3:e00305-11. https://doi.org/10.1128/mBio.00305-11
7. Nijhuis RHT, van Maarseveen NM, van Hannen EJ, van Zwet AA, Mascini EM. A rapid and high-throughput screening approach for methicillin-resistant *Staphylococcus aureus* based on the combination of two different real-time PCR assays. J Clin Microbiol. 2014;52:2861–7. https://doi.org/10.1128/JCM.00808-14
8. Schouls LM, Witteveen S, van Santen-Verheuvel M, de Haan A, Landman F, van der Heide H, et al.; Dutch MRSA surveillance study group. Molecular characterization of MRSA collected during national surveillance between 2008 and 2019 in the Netherlands. Commun Med (Lond). 2023;3:123. https://doi.org/10.1038/s43856-023-00348-z
9. Landman F, Jamin C, de Haan A, Witteveen S, Bos J, van der Heide HGJ, et al.; Dutch CPE/MRSA surveillance study group. Genomic surveillance of multidrug-resistant organisms based on long-read sequencing. Genome Med. 2024;16:137. https://doi.org/10.1186/s13073-024-01412-6

Address for correspondence: Patrick van Schelven, Public Health Service Region Utrecht, Department of Infectious Disease Control, De Dreef 5, 3706 BR Zeist, the Netherlands; email: pvanschelven@ggdru.nl

etymologia revisited

Nipah Virus

[neˊ-pə vīˊ-rəs]

In 1994, a newly described virus, initially called equine morbillivirus, killed 13 horses and a trainer in Hendra, a suburb of Brisbane, Australia. The reservoir was subsequently identified as flying foxes, bats of the genus Pteropus (Greek pteron ["wing"] + pous ["foot"]). In 1999, scientists investigated reports of febrile encephalitis and respiratory illness among workers exposed to pigs in Malaysia and Singapore. (The pigs were believed to have consumed partially eaten fruit discarded by bats.)

The causative agent was determined to be closely related to Hendra virus and was later named for the Malaysian village of Kampung Sungai Nipah. The 2 viruses were combined into the genus Henipavirus, in the family Paramyxoviridae. Three additional species of Henipavirus—Cedar virus, Ghanaian bat virus, and Mojiang virus—have since been described, but none is known to cause human disease. Outbreaks of Nipah virus occur almost annually in India and Bangladesh, but Pteropus bats can be found throughout the tropics and subtropics, and henipaviruses have been isolated from them in Central and South America, Asia, Oceania, and East Africa.

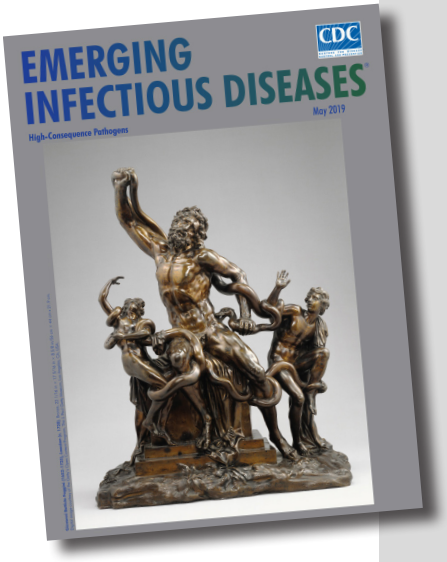

Originally published in May 2019

References

1. Centers for Disease Control and Prevention. Outbreak of Hendra-like virus—Malaysia and Singapore, 1998–1999. MMWR Morb Mortal Wkly Rep. 1999;48:265–9.
2. Selvey LA, Wells RM, McCormack JG, Ansford AJ, Murray K, Rogers RJ, et al. Infection of humans and horses by a newly described morbillivirus. Med J Aust. 1995;162:642–5.

https://wwwnc.cdc.gov/eid/article/25/5/et-2505_article

Guillain-Barré Syndrome and Visual Impairment Associated with Emerging Oropouche Virus Lineage, Brazil, 2024

Carlos Garcia Filho, Fernanda Martins Maia Carvalho, Antonio Silva Lima Neto, Ana Maria Cabral Maia, Matheus Andrighetti Rossi, Milena Sales Pitombeira, Paula Camila Alves de Assis Pereira Matos, Tania Mara Silva Coelho, Lauro Vieira Perdigão Neto, Lívia Mendes de Almeida, Felipe Gomes Naveca, Carla Santos de Oliveira, Fernanda de Bruycker-Nogueira, Ana Maria Bispo de Filippis, Kleber Giovanni Luz, André Ricardo Ribas Freitas, Luciano Pamplona de Góes Cavalcanti

We report a case of Guillain-Barré syndrome with visual impairment after confirmed Oropouche virus infection during the 2024 outbreak in Ceará, Brazil. Whole-genome sequencing revealed infection by a novel reassortant viral lineage (OROVBR_2025_2024), raising concern about the neurovirulence of this emerging orthobunyavirus strain.

Oropouche virus (OROV), an orthobunyavirus transmitted by mosquitoes and *Culicoides paraensis* midges, is emerging as a major arboviral pathogen in Latin America. Although typically associated with mild febrile illness, the current outbreak, which is linked to the novel reassortant lineage $OROV_{BR\text{-}2015\text{–}2024}$ (*1*), has been associated with severe cases, including fatalities, vertical transmission with fetal deaths (*2*–*4*), and Guillain-Barré syndrome (GBS) (*5*). We report a case of GBS with possible bilateral optic neuritis after OROV infection during the 2024 outbreak in Ceará state, Brazil.

The Study

On August 12, 2024, a previously healthy 48-year-old woman from Capistrano in Ceará state developed acute febrile illness, characterized by high fever (39°C), chills, severe headache, and myalgia. OROV cases had been previously documented in this locality (*2*,*6*). On August 14, OROV infection was confirmed through quantitative reverse transcription PCR (qRT-PCR) performed by the Ceará Central Public Health Laboratory. Dengue, Zika, chikungunya, and Mayaro virus infections were excluded through both molecular and serologic testing (Table) (*7*,*8*). Fever and systemic symptoms persisted for 2 weeks and were followed by the onset of neurologic manifestations, including paresthesia in her lower limbs, which progressively developed into ascending paresis affecting both upper and lower limbs. In addition, bilateral facial weakness and profound visual loss developed. Initial treatment with corticosteroids (prednisone 40 mg/day for 7 days) was prescribed on September 15 but improvement was minimal, and the patient was referred to a tertiary hospital.

Upon admission on September 17, 2024, the patient was experiencing flaccid tetraparesis, bilateral facial paresis, and areflexia. Blood tests results

Author affiliations: Secretaria da Saúde do Estado do Ceará, Fortaleza, Brazil (C. Garcia Filho, A.S. Lima Neto, A.M.C. Maia, T.M.S. Coelho, L.V.P. Neto); Universidade de Fortaleza, Fortaleza (C. Garcia Filho, F.M.M. Carvalho, A.S. Lima Neto); Hospital Geral de Fortaleza, Fortaleza (F.M.M. Carvalho, M.A. Rossi, M.S. Pitombeira, P.C.A. de Assis Pereira Matos); Programa de Pós-graduação em Saúde Pública da Universidade Federal do Ceará, Fortaleza (A.M.C. Maia); Universidade Federal do Ceará, Fortaleza (L.V.P. Neto); Faculdade de Medicina da Universidade de São Paulo, São Paulo, Brazil (L.V.P. Neto); Centro Universitário Christus, Fortaleza (L.M. de Almeida, L.P. de Góes Cavalcanti); Programa de Pós-graduação em Patologia da Universidade Federal do Ceará, Fortaleza (L.M. de Almeida, L.P. de Góes Cavalcanti); Instituto Oswaldo Cruz, Rio de Janeiro, Brazil (F.G. Naveca, C.S. de Oliveira, F. de Bruycker-Nogueira, A.M.B. de Filippis); Universidade Federal do Rio Grande do Norte, Natal, Brazil (K.G. Luz); São Leopoldo Mandic, Campinas, Brazil (A.R.R. Freitas); Escola de Saúde Pública do Ceará, Fortaleza (L.P. de Góes Cavalcanti)

DOI: https://doi.org/10.3201/eid3204.250617

Table. Results of laboratory screening in study of Guillain-Barré syndrome and visual impairment associated with emerging Oropouche virus lineage, Brazil, 2024*

Laboratory test	Result	Reference range or detection method
Hematology and biochemistry		
Hemoglobin	15.3 g/dL	11.5–15.0 g/dL
Leukocytes	8,500/µL	3,600–11,000 cells/µL
Platelets	346,000/µL	150,000–450,000/µL
C-reactive protein	5 mg/L	<5 mg/L
Erythrocyte sedimentation rate	27 mm/h	0–20 mm/h
Calcium	10.7 mg/dL	8.50–10.50 mg/dL
Creatinine	0.72 mg/dL	0.60–1.10 mg/dL
Alanine aminotransferase	63 U/L	<31 U/L
Aspartate aminotransferase	22 U/L	<32 U/L
C3	118 mg/dL	90–180 mg/dL
C4	43.8 mg/dL	10–40 mg/dL
Rheumatoid factor	20.7 IU/mL	0–15 IU/mL
Cerebrospinal fluid analysis		
Cell count	2 cells/µL	0–4 cells/µL
Protein	156 mg/dL	15–40 mg/dL
Glucose	135 mg/dL	40–70 mg/dL
Adenosine deaminase	0.72 U/L	0–9 U/L
Infectious disease markers		
HIV	Nonreactive	Chemiluminescent immunoassay
Hepatitis B surface antigen	Nonreactive	Chemiluminescent immunoassay
Hepatitis C	Nonreactive	Chemiluminescent immunoassay
Syphilis/neurosyphilis	Nonreactive	Flocculation (VDRL)
Mycobacterium tuberculosis DNA	Nonreactive	Xpert MTB/RIF (Cepheid, https://www.cepheid.com)
Zika virus†	Nonreactive	qRT-PCR, ELISA IgM (serum and CSF)
Chikungunya virus†	Nonreactive	qRT-PCR, ELISA IgM (serum and CSF)
Dengue virus†	Nonreactive	qRT-PCR, ELISA IgM (serum and CSF
Oropouche virus†	Positive	qRT-PCR (serum)
Autoimmune profile		
Antinuclear antibodies‡	Negative	Indirect immunofluorescence assay on Hep-2 cells
Aquaporin-4 antibodies‡	Negative	Cell-based assay
MOG antibodies‡	Negative	Cell-based assay

*MOG, myelin oligodendrocyte glycoprotein; qRT-PCR, quantitative reverse transcription PCR; VDRL, Venereal Disease Research Laboratory.
†Oropouche virus qRT-PCR and qRT-PCR for dengue, Zika, chikungunya, and Mayaro viruses, as well as serologic testing, were performed using serum collected on August 14, 2024.
‡Autoimmune screening tests, including antinuclear antibody (ANA), and aquaporin 4 and MOG antibodies, were collected during the home visit on February 5, 2025. All other tests were conducted during hospitalization, September 17–October 1, 2024.

were unremarkable. Analysis of cerebrospinal fluid revealed albuminocytologic dissociation, elevated protein levels, and unremarkable cell counts (Table), supporting a diagnosis of peripheral demyelinating neuropathy. Oligoclonal bands and IgG index testing of cerebrospinal fluid were unavailable.

Electroneuromyography showed absent sensory conduction in the left superficial fibular nerve, mildly prolonged motor latencies, and reduced motor potentials in fibular and tibial nerves. F-waves were delayed or absent, whereas the H-reflex was bilaterally absent. Electroneuromyography revealed reduced recruitment with high motor unit activity during voluntary movement, compatible with peripheral nervous system demyelination (Appendix Tables 1–5, https://wwwnc.cdc.gov/EID/article/32/4/25-0617-App1.pdf).

Magnetic resonance imaging (MRI) of the brain showed bilateral facial nerve swelling; cervical, thoracic, and lumbar spine MRI revealed edema of lumbar nerve roots (Figure 1). Orbital MRI results were unremarkable.

Bilateral vision loss developed, accompanied by painful eye movements, compromising functional capacity as reported by the patient and family. Although the neuroophthalmologic evaluation occurred only 3 weeks after onset and during steroid treatment, the examination revealed corrected visual acuity of 20/50 in both eyes, impaired pupillary light reflexes, red dyschromatopsia, nasal optic disc edema on fundoscopy, and peripapillary retinal nerve fiber layer edema on optical coherence tomography (Figure 1) without macular involvement. Visual field testing was not performed because of technical issues, and results of MRI performed at this stage were unremarkable. The evidence of subacute vision loss associated with orbital pain worsening with eye movement, reduced contrast and color vision, and pupillary deficit along with the mild optic disc swelling seen in optical coherence tomography favors the diagnosis of a possible optic neuritis (*9*). The temporal association of those findings with a preceding infectious episode (2–4 weeks) supports the possibility of bilateral postinfectious optic neuritis captured later in the disease evolution.

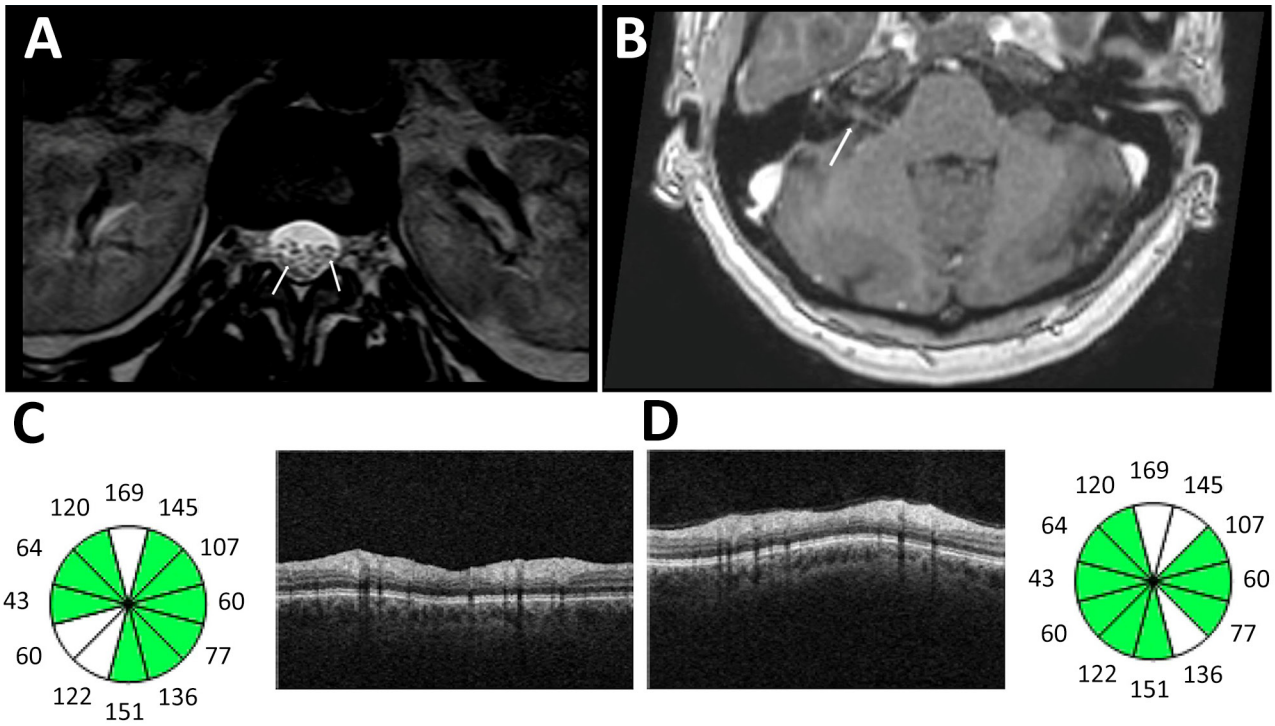

Figure 1. Imaging from study of Guillain-Barré syndrome and visual impairment associated with emerging Oropouche virus lineage, Brazil, 2024. A) T2-weighted magnetic resonance imaging of lumbar spinal cord. Arrows indicate nerve root edema. B) T1-weighted magnetic resonance imaging of brain with contrast. Arrow indicates enhancement of right facial nerve. C, D) Optical coherence tomography of right eye (C) and left eye (D) revealed bilateral loss of ganglionic cells in the papillomacular bundle, shown in white on the circle graphic.

Empiric antiviral drugs and antibiotics were initiated but discontinued after excluding infectious etiologies such as *Listeria* and herpes. Plasmapheresis was administered in 5 sessions and was generally well tolerated, although 1 session was followed by transient dysautonomia.

The patient showed gradual but partial neurologic improvement and was discharged on October 1 with moderate gains in motor function and visual acuity. At the 90-day follow-up, the patient was able to walk with assistance, and her visual acuity remained at 20/50 in both eyes. Mild proprioceptive and sensory deficits persisted, particularly in the left foot. Deep tendon reflexes were normal except for slightly diminished Achilles reflexes.

A home visit on February 5, 2025 (6 months after symptom onset), revealed that the patient continued to experience persistent visual impairment, distal hypoesthesia, and paresis in the right lower limb, as well as difficulty standing for >15 minutes. She remained unable to resume agricultural activities or manage household routines independently and required assistance from family members for daily living. Despite partial neurologic improvement, those ongoing limitations led to functional dependence and the need for social security support. During this home visit, additional autoimmune screening tests, including tests for antinuclear antibody and aquaporin 4 and myelin oligodendrocyte glycoprotein antibodies, were performed. Results of all tests were negative (Table).

We performed whole-genome sequencing on patient OROV samples using an amplicon-based protocol (*7*). We recovered and concatenated near-complete coding sequences of all 3 genome segments (large, medium, and small) for phylogenetic reconstruction using maximum-likelihood inference on IQ-TREE multicore version 2.1.1 (*10*), employing a nonredundant dataset containing previously published sequences (*1*,*2*). Sequence data are available on GISAID (https://www.gisaid.org; accession no. EPI_ISL_20332357).

The genome generated belongs to the new $OROV_{BR\text{-}2023\text{–}2024}$ lineage (*1*,*11*). Phylogenetic analysis (Figure 2) revealed a highly supported monophyletic clade (UltraFast Bootstrap 99.5, SH-aLRT 100) containing sequences from other severe cases, including a fatal vertical transmission case previously described in Ceará (*2*). This clade is part of a broader lineage linked to cases in Santa Catarina, Paraná, Amazonas, and Pernambuco states in Brazil, as well as to cases in Leticia, Colombia. Those sequences

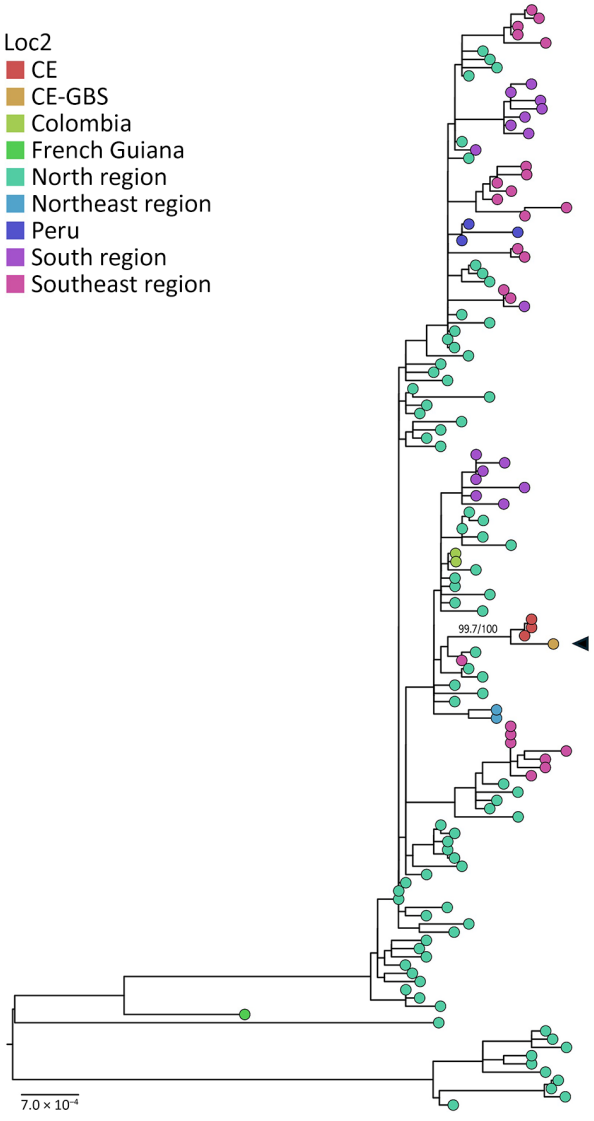

Figure 2. Maximum-likelihood tree of Oropouche virus concatenated segments from study of Guillain-Barré syndrome and visual impairment associated with emerging Oropouche virus lineage, Brazil, 2024. Black arrow indicates sequence from study patient. A reference dataset containing concatenated segments (large, medium, and small) of the recent Oropouche virus outbreak (2022–2024) representing different regions in Brazil and sequences obtained from Peru and Colombia were aligned using MAFFT version 7.490 (https://mafft.cbrc.jp/alignment/software/source.html) embedded in Geneious Prime 2025.0.3 (https://www.geneious.com). Subsequently, we used that alignment for phylogenomic reconstruction by maximum-likelihood using IQ-TREE multicore version 2.1.1 COVIDedition for Mac OS X 64-bit (http://www.iqtree.org). MODEL-FINDER (https://iqtree.github.io/ModelFinder) was used for evolutionary model choice, and 2,000 ultra-fast bootstraps and 2,000 SH-aLRT replicates were run to access the branches' support (support for the CE clade is shown). The maximum-likelihood tree was edited with FigTree version 1.4.4 (https://tree.bio.ed.ac.uk/software/figtree). Scale bar indicates nucleotide substitutions per site. CE, Ceará state; CE-GBS, Ceará–Guillain-Barré syndrome.

belong to the previously described AM-I sublineage of $OROV_{BR\text{-}2015\text{-}2024}$ (*1*,*2*,*11*).

Conclusions

We report a case of GBS with visual impairment possibly caused by optic neuritis associated with the novel $OROV_{BR\text{-}2015\text{-}2024}$ lineage, supported by clinical, laboratory, neuroimaging, electrophysiological, and genomic findings. Of note, the patient had been previously healthy and had no underlying conditions.

This case represents the second unusual severe event reported in this small region of Ceará, despite only a few hundred confirmed OROV cases, one of which involved a fetal death attributed to vertical transmission (*2*,*6*). This case highlights the neuropathogenic potential of OROV to trigger severe conditions. Although the patient received corticosteroids, intravenous immunoglobulin, and plasmapheresis, she continues to have severe neurologic impairment; whether that persistence is a result of delayed therapy or reflects a severe manifestation of OROV-associated GBS remains unclear. The phylogenetic relationship between this case and previously described cases of fetal and adult deaths (*2*,*4*), as well as GBS clusters reported in Cuba (*5*), reinforces the hypothesis that this viral lineage might possess increased pathogenicity (*12*).

This article was preprinted at https://preprints.scielo.org/index.php/scielo/preprint/view/10912/19832.

Acknowledgments

We thank the epidemiologic surveillance professionals of the state, the municipality of Capistrano, and the Decentralized Health Area, whose efforts were instrumental in the identification, investigation, and follow-up of the case. We also thank Laboratorio Emilio Ribas, Fortaleza, Ceará, for voluntarily performing laboratory tests not available in the public health system.

The patient involved in this study was fully informed about the nature and purpose of this report. She reviewed the content, provided her consent for publication, and signed an Informed Consent Form in accordance with ethical guidelines.

The study was approved by the Research Ethics Committee of Centro Universitário Christus accordance with the principles outlined in the Declaration of Helsinki. Ethical approval ensures that the investigation adhered to the highest standards of research ethics and the protection of patient rights.

This research received funding from the Brazilian Health Ministry Department of Science and Technology (file no.

421724/2017-0) and from the Brazilian Health Ministry Health Surveillance Secretariat (file no. 707272/19-002). L.P.d.G.C. receives a productivity grant from the Conselho Nacional de Desenvolvimento Científico e Tecnológico / Ministério da Ciência, Tecnologia e Inovações (CNPq/MCTI; file no. 310579/2022-8).

All authors contributed significantly to the conception, design, and writing of this manuscript and take full responsibility for its content. Each author has reviewed and approved the final version of the manuscript, ensuring its accuracy and compliance with scientific and ethical standards.

About the Author

Dr. Garcia Filho is a physician and epidemiologist at the Ceará State Health Department and a professor of medicine at the University of Fortaleza, Brazil. His primary research interests include epidemiologic surveillance and outbreak investigation.

References

1. Naveca FG, Almeida TAP, Souza V, Nascimento V, Silva D, Nascimento F, et al. Human outbreaks of a novel reassortant Oropouche virus in the Brazilian Amazon region. Nat Med. 2024;30:3509–21. https://doi.org/10.1038/s41591-024-03300-3
2. Garcia Filho C, Lima Neto AS, Maia AMPC, Da Silva LOR, Cavalcante RDC, Monteiro HDS, et al. A case of vertical transmission of Oropouche virus in Brazil. N Engl J Med. 2024;391:2055–7. https://doi.org/10.1056/NEJMc2412812
3. Ribas Freitas AR, Schwartz DA, Lima Neto AS, Rodrigues R, Cavalcanti LPG, Alarcón-Elbal PM. Oropouche virus (OROV): expanding threats, shifting patterns, and the urgent need for collaborative research in Latin America. Viruses. 2025;17:353. https://doi.org/10.3390/v17030353
4. Bandeira AC, Pereira FM, Leal A, Santos SPO, Barbosa AC, Souza MSPL, et al. Fatal Oropouche virus infections in nonendemic region, Brazil, 2024. Emerg Infect Dis. 2024;30:2370–4. https://doi.org/10.3201/eid3011.241132
5. de Armas Fernández JR, Peña García CE, Acosta Herrera B, Betancourt Plaza I, Gutiérrez de la Cruz Y, Resik Aguirre S, et al. Report of an unusual association of Oropouche fever with Guillain-Barré syndrome in Cuba, 2024. Eur J Clin Microbiol Infect Dis. 2024;43:2233–7. https://doi.org/10.1007/s10096-024-04941-5
6. de Lima STS, Hua X, Claro IM, Filho CG, Simões Mello LM, de Jesus R, et al. Molecular epidemiology of Oropouche virus, Ceará State, Brazil, 2024. Emerg Infect Dis. 2025;31:838–42. https://doi.org/10.3201/eid3104.241471
7. Naveca FG, Nascimento VAD, Souza VC, Nunes BTD, Rodrigues DSG, Vasconcelos PFDC. Multiplexed reverse transcription real-time polymerase chain reaction for simultaneous detection of Mayaro, Oropouche, and Oropouche-like viruses. Mem Inst Oswaldo Cruz. 2017;112:510–3. https://doi.org/10.1590/0074-02760160062
8. Mansuy JM, Lhomme S, Cazabat M, Pasquier C, Martin-Blondel G, Izopet J. Detection of Zika, dengue and chikungunya viruses using single-reaction multiplex real-time RT-PCR. Diagn Microbiol Infect Dis. 2018;92:284–7. https://doi.org/10.1016/j.diagmicrobio.2018.06.019
9. Petzold A, Fraser CL, Abegg M, Alroughani R, Alshowaeir D, Alvarenga R, et al. Diagnosis and classification of optic neuritis. Lancet Neurol. 2022;21:1120–34. https://doi.org/10.1016/S1474-4422(22)00200-9
10. Minh BQ, Schmidt HA, Chernomor O, Schrempf D, Woodhams MD, von Haeseler A, et al. IQ-TREE 2: new models and efficient methods for phylogenetic inference in the genomic era. Mol Biol Evol. 2020;37:1530–4. https://doi.org/10.1093/molbev/msaa015
11. Gräf T, Delatorre E, Do Nascimento Ferreira C, Rossi A, Santos HGG, Pizzato BR, et al. Expansion of Oropouche virus in non-endemic Brazilian regions: analysis of genomic characterisation and ecological drivers. Lancet Infect Dis. 2025;25:379–89. https://doi.org/10.1016/S1473-3099(24)00687-X
12. Scachetti GC, Forato J, Claro IM, Hua X, Salgado BB, Vieira A, et al. Re-emergence of Oropouche virus between 2023 and 2024 in Brazil: an observational epidemiological study. Lancet Infect Dis. 2025;25:166–75. https://doi.org/10.1016/S1473-3099(24)00619-4

Address for correspondence: Carlos Garcia Filho, Rua Oto de Alencar, nº 193, Segundo Andar (CEVEP), Centro, Fortaleza, Ceará, Brazil, CEP 60110-270; email: carlos.garcia@saude.ce.gov.br

Rapid Spread of Recombinant African Swine Fever Virus Genotypes I and II, Vietnam, 2023–2024

The Viet Hoang Nguyen,[1] Yeon-Hee Kim,[1] Viet Dung Nguyen,[1] Thi Chau Giang Tran,[1] Ngoc Duong Vu, Thi Thu Hang Vu, Van Tam Nguyen, Da-Young Kim, Ki-Hyun Cho, Seong-Keun Hong, Aruna Ambagala, Van Phan Le

Molecular analyses of African swine fever (ASF) outbreaks in northern and central Vietnam during 2023–2024 revealed a rapid expansion (14.1%–42.2%) of recombinant ASF virus genotypes I and II. Increased prevalence and resistance to commercial ASF vaccines underscore the urgent need for better ASF control and an updated vaccine in Vietnam.

African swine fever (ASF) is a highly contagious viral disease affecting domestic and wild pigs; mortality rates reach up to 100% (*1*). The causative agent, ASF virus (ASFV), is a large double-stranded DNA virus in the *Asfarviridae* family. ASFV strains have been classified into 24 genotypes, of which only genotypes I and II have spread beyond Africa (*2*).

In Asia, ASFV genotype II was first detected in China in 2018 (*3*) and in Vietnam in early 2019 (*4*). Since 2021, recombinant ASFV strains containing genetic elements from genotypes I and II (rASFV I/II) have emerged in China and subsequently in Vietnam in 2023, presenting new challenges for ASF control (*5*,*6*). Two live attenuated ASFV genotype II vaccines have been licensed in Vietnam; however, they provide protection only against homologous strains (*7*,*8*) and are ineffective against rASFV I/II (*9*). Studies conducted during 2019–2022 investigated the molecular epidemiology of ASFV in Vietnam (*10*,*11*), but little is known about circulating strains during 2023–2024. In our study, we aimed to characterize ASFV strains causing outbreaks in northern and central Vietnam during 2023–2024, focusing on the emergence and spread of rASFV I/II.

The Study

During January 2023–August 2024, we collected 182 clinical samples (spleen, lymph nodes, lung, and whole blood) from pigs suspected of having ASFV infection across 26 provinces in northern and central Vietnam (Appendix Figure 1, https://wwwnc.cdc.gov/EID/article/32/4/25-1688-App1.pdf). We extracted total nucleic acids and tested them by using real-time PCR, targeting the B646L (p72) gene (VDx ASFV qPCR version 2.1; Median Diagnostics, http://mediandiagnostics.com). All samples tested positive for ASFV DNA; cycle threshold values ranged from 14.96 to 32 (Appendix Table). We performed in-house genotyping assays (Phan G1 and G2 Realtime-PCR) to differentiate ASFV genotypes I and II, as previously described (*9*). Results showed that 133/182 samples (73.08%) contained genotype II p72 and 49/182 samples (26.92%) contained genotype I p72. To confirm those findings, we conducted conventional PCRs targeting partial B646L (p72), complete E183L (p54), complete EP402R (CD2v), intergenic region (IGR), and central variable region (CVR), as previously described (*11*). We performed Sanger sequencing on amplicons (1st BASE, https://base-asia.com) and analyzed them by using Geneious Prime 2024 (Geneious,

Author affiliations: Vietnam National University of Agriculture College of Veterinary Medicine, Hanoi, Vietnam (T.V.H Nguyen, V.D. Nguyen, T.C.G. Tran, N.D. Vu, V.P. Le); Animal and Plant Quarantine Agency Foreign Animal Disease Division, Gimcheon, South Korea (Y.-H. Kim, D.-Y. Kim, K.-H. Cho, S.-K. Hong); Vietnam Union of Science and Technology Associations Institute of Veterinary Science and Technology, Hanoi (T.T.H. Vu, V.T. Nguyen); Canadian Food Inspection Agency National Centre for Foreign Animal Disease, Winnipeg, Manitoba, Canada (A. Ambagala)

DOI: https://doi.org/10.3201/eid3204.251688

[1]These authors contributed equally to this article.

Table. Circulation rates of African swine fever virus p72 genotype II and recombinant p72 genotype I and II strains detected, Vietnam, January 2023–August 2024

Period	No. samples collected	Genotypes	No. positive	Positivity rate, %
Jan–Dec 2023	99	Genotype I and II	14	14.14
		Genotype II	85	85.86
Jan–Aug 2024	83	Genotype I and II	35	42.17
		Genotype II	48	57.83
Total	182			

https://www.geneious.com), GraphPad Prism 8.4.3 (GraphPad Software, https://www.graphpad.com), and MEGA 11 (MEGA Software, https://www.megasoftware.net). We visualized phylogenetic trees by using iTOL version 7.4 (Interactive Tree of Life, https://itol.embl.de). We submitted all sequences to GenBank (accession nos. PV975276–639 and PX205390–33).

Sequence analysis confirmed that Phan G2–positive samples contained the p72 gene of ASFV genotype II, whereas Phan G1–positive samples carried the p72 gene of genotype I. Of note, all genotype I p72–positive samples also possessed the p54 gene of genotype II and the CD2v gene of serogroup VIII (Figure 1; Appendix Figure 2), consistent with previously reported rASFV I/II strains (*5*,*6*). We detected rASFV I/II in 17 of 26 provinces, whereas genotype II was present nationwide. We identified rASFV I/II in Bac Giang Province in May 2023, four months earlier than previously reported (*5*). A recent study demonstrated high levels of recombination between closely related ASFV genotypes in vitro and in vivo (*12*). In our study, the co-circulation of rASFV I/II and genotype II across multiple provinces suggests an increased risk for further recombination arising from co-infection, particularly in high-density production systems characterized by repeated exposure and prolonged environmental virus persistence. We further characterized ASFV strains on the basis of tandem repeat sequences in the IGR and amino acid variations in the CVR of the B602L gene. To date, 4 IGR variants (IGR I–IV) have been described, and in Vietnam, all 4 IGR types have been reported (*10*). In our study, among the 133 genotype II viruses analyzed, we identified 3 IGR variants (IGR I–III) that showed no intravariant nucleotide differences. IGR II remained dominant, being detected in all 26 provinces, whereas IGR III appeared in only 2 samples (from Bac Giang and Ha Nam Provinces). We found IGR I in 18 samples from 8 provinces (Appendix Figure 3). Those findings suggest a shift in IGR variant distribution among genotype II strains in Vietnam. In contrast, all rASFV I/II strains carried only the IGR II variant, consistent with previous reports (*5*).

Analysis of the B602L CVR region revealed 2 variants (CVR14 and CVR15) among genotype II viruses and 13 variants among rASFV I/II strains (Appendix Figure 4). Genotype II viruses contained 7–10 tetrameric amino acid repeats, whereas rASFV I/II exhibited 42–70 repeats, reflecting greater genetic diversity.

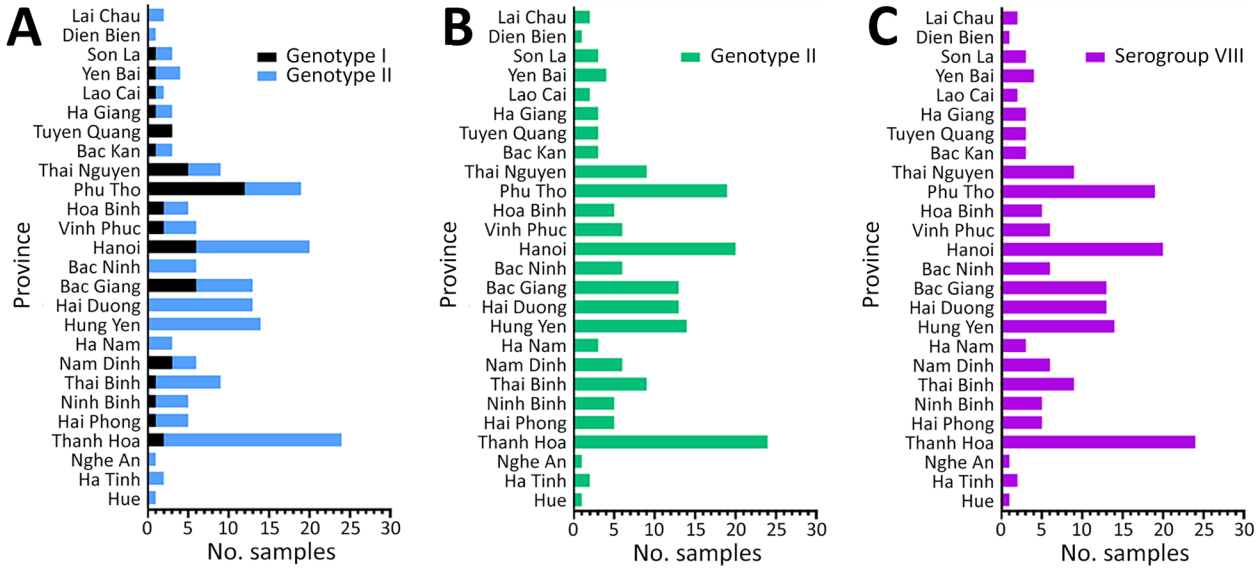

Figure 1. Prevalence and distribution of African swine fever virus genotypes I and II among strains detected, by province, Vietnam, January 2023–August 2024. Genotypes were based on the p72 gene (A) and p54 gene (B) and serogroup classification was based on the CD2v gene (C).

The CVR14 variant dominated genotype II strains (131/133), whereas CVR15 was rare. Among rASFV I/II, CVR4 and CVR11 were the most prevalent, being detected across several provinces. Provinces such as Tuyen Quang, Thai Nguyen, Phu Tho, Hanoi, Bac Giang, Nam Dinh, and Thanh Hoa harbored multiple CVR variants, indicating ongoing viral diversification. Some CVR variants showed homology with previously reported strains: CVR2 matched the rASFV strain pig/Henan/123014/2022 from China (*6*), CVR4 corresponded to the Vietnam strain VNUA/rASFV/HD1/23 (*5*), and CVR3 resembled genotype I ASFV OURT 88/3 (*13*). Detection of 13 CVR variants among rASFV I/II strains in 2024 indicates ongoing ASFV evolution and underscores the need to clarify the relationship between genetic diversity and virulence among ASFV strains currently circulating in Vietnam.

Spatial and temporal analyses showed a statistically significant increase (χ^2 17.7; p<0.001) in rASFV I/II among ASFV-positive samples submitted for laboratory diagnosis and confirmation (Figure 2). We detected rASFV I/II in 17 of 26 provinces and observed the proportion increasing from 14.14% (14/99 samples) in 2023 to 42.17% (35/83 samples) in 2024 (Table). That trend suggests rapid geographic expansion and a potential replacement of ASFV genotype II by rASFV I/II. However, those results should be interpreted with caution because they are based on laboratory submissions rather than systematic field surveillance. The mechanisms underlying the shift are unclear but could be attributable to resistance to the vaccines, higher virulence, increased viral shedding, or greater transmission efficiency of the rASFV I/II strains.

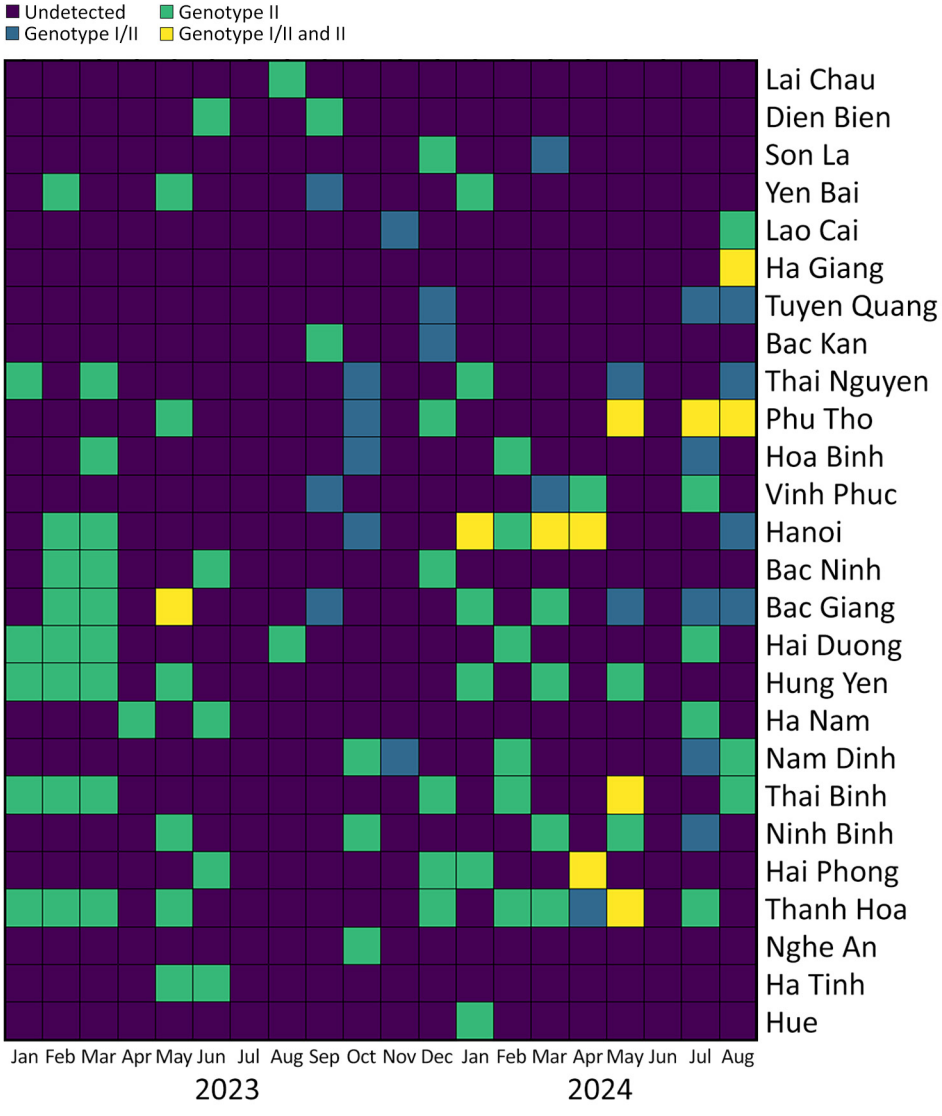

Figure 2. Spatial and temporal distribution of African swine fever virus genotype II and recombinant African swine fever virus strains detected, by province, Vietnam, January 2023–August 2024.

Conclusions

Our study provides strong evidence that highly pathogenic rASFV I/II strains are rapidly evolving and spreading in northern and central Vietnam, showing indications of partial displacement of classical genotype II viruses. Detection of rASFV I/II as early as May 2023 suggests these recombinant strains circulated months before official reporting, highlighting the need for continuous genetic surveillance for early detection. The widespread co-circulation of genotype II and rASFV I/II across multiple provinces underscores the importance of genotyping-based real-time PCR in routine monitoring. Limited cross-protection of existing vaccines emphasizes the urgency of updated immunization strategies and novel vaccine platforms targeting rASFV I/II. Moreover, marked genetic heterogeneity, particularly in CVR regions, indicates ongoing viral evolution with potential effects on virulence and transmission. The co-circulation of multiple ASFV strains raises concern over the emergence of new recombinant variants, complicating disease control. Enhanced genomic surveillance, improved diagnostic tools, and systematic vaccine evaluation are therefore essential for effective ASF prevention and control in Vietnam and the region.

This work was supported by the Vietnam National Project (project code DTDL.CN-53/19), South Korea's Animal and Plant Quarantine Agency, Ministry of Agriculture, Food and Rural Affairs (grant no. I-1543085-2025-26-01), and the Canadian Food Inspection Agency RPS Project (grant no. N-000534).

About the Author

Mr. Nguyen is a veterinarian and a master's student at Vietnam National University of Agriculture. His primary research interests include virology and animal pathology.

References

1. Penrith ML, Vosloo W. Review of African swine fever: transmission, spread and control. J S Afr Vet Assoc. 2009;80:58–62. https://doi.org/10.4102/jsava.v80i2.172
2. Bastos AD, Penrith ML, Crucière C, Edrich JL, Hutchings G, Roger F, et al. Genotyping field strains of African swine fever virus by partial p72 gene characterisation. Arch Virol. 2003;148:693–706. https://doi.org/10.1007/s00705-002-0946-8
3. Zhou X, Li N, Luo Y, Liu Y, Miao F, Chen T, et al. Emergence of African swine fever in China, 2018. Transbound Emerg Dis. 2018;65:1482–4. https://doi.org/10.1111/tbed.12989
4. Le VP, Jeong DG, Yoon SW, Kwon HM, Trinh TBN, Nguyen TL, et al. Outbreak of African swine fever, Vietnam, 2019. Emerg Infect Dis. 2019;25:1433–5. https://doi.org/10.3201/eid2507.190303
5. Le VP, Nguyen VT, Le TB, Mai NTA, Nguyen VD, Than TT, et al. Detection of recombinant African swine fever virus strains of p72 genotypes I and II in domestic pigs, Vietnam, 2023. Emerg Infect Dis. 2024;30:991–4. https://doi.org/10.3201/eid3005.231775
6. Zhao D, Sun E, Huang L, Ding L, Zhu Y, Zhang J, et al. Highly lethal genotype I and II recombinant African swine fever viruses detected in pigs. Nat Commun. 2023;14:3096. https://doi.org/10.1038/s41467-023-38868-w
7. Diep NV, Ngoc NT, Duc NV, Dang VX, Tiep TN, Quy CT, et al. Safety and efficacy profiles of the live attenuated vaccine AVAC ASF LIVE for preventing African swine fever in pigs. Transbound Emerg Dis. 2025;2025:8623876. https://doi.org/10.1155/tbed/8623876
8. Tran XH, Le TTP, Nguyen QH, Do TT, Nguyen VD, Gay CG, et al. African swine fever virus vaccine candidate ASFV-G-ΔI177L efficiently protects European and native pig breeds against circulating Vietnamese field strain. Transbound Emerg Dis. 2022;69:e497–504. https://doi.org/10.1111/tbed.14329
9. Diep NV, Duc NV, Ngoc NT, Dang VX, Tiep TN, Nguyen VD, et al. Genotype II live-attenuated ASFV vaccine strains unable to completely protect pigs against the emerging recombinant ASFV genotype I/II strain in Vietnam. Vaccines (Basel). 2024;12:1114. https://doi.org/10.3390/vaccines12101114
10. Mai NTA, Dam VP, Cho KH, Nguyen VT, Van Tuyen N, Nguyen TL, et al. Emergence of a novel intergenic region (IGR) IV variant of african swine fever virus genotype II in domestic pigs in Vietnam. Vet Res Commun. 2023;47:1773–6. https://doi.org/10.1007/s11259-022-10068-9
11. Mai NTA, Vu XD, Nguyen TTH, Nguyen VT, Trinh TBN, Kim YJ, et al. Molecular profile of African swine fever virus (ASFV) circulating in Vietnam during 2019–2020 outbreaks. Arch Virol. 2021;166:885–90. https://doi.org/10.1007/s00705-020-04936-5
12. Kitamura T, Masujin K, Ikezawa M, Ambagala A, Kokuho T. Generation of Chimeric African swine fever viruses through in vitro and in vivo intergenotypic gene complementation. Vaccines (Basel). 2025;13:462. https://doi.org/10.3390/vaccines13050462
13. Chapman DAG, Tcherepanov V, Upton C, Dixon LK. Comparison of the genome sequences of non-pathogenic and pathogenic African swine fever virus isolates. J Gen Virol. 2008;89:397–408. https://doi.org/10.1099/vir.0.83343-0

Address for correspondence: Van Phan Le, Department of Microbiology and Infectious Disease, College of Veterinary Medicine, Vietnam National University of Agriculture, Hanoi, Vietnam; email: letranphan@vnua.edu.vn

Who is this person and what did she accomplish?

This 19th-century physician organized women nurses during the US Civil War and promoted sanitary reforms when disease killed more soldiers than combat.

Who is she?

A) **Dorothea Dix**
B) **Lucy Stone**
C) **Clara Barton**
D) **Florence Nightingale**
E) **Elizabeth Blackwell**

Decide first, then see next page for the answer.

Elizabeth Blackwell, 19th Century Pioneer of Public Health

Nicolas Hoffmann

This is a photograph of Elizabeth Blackwell (1821–1910), an Anglo-American physician who helped open the medical profession to women in the United States. Born in Bristol, England, she emigrated with her family to New York, New York, USA, in 1832 and later settled in Cincinnati, Ohio, where financial hardship after her father's death led her and her sisters to support themselves through teaching. Raised in an abolitionist and reform-minded household, she resolved to pursue medicine despite widespread opposition.

Blackwell was rejected by numerous medical schools because she was a woman before Geneva Medical College admitted her in 1847, after the faculty submitted her application to the all-male student body for a vote. The students, reportedly believing the proposal to be a jest, voted unanimously to accept her. She graduated in 1849, becoming the first woman in the United States to earn a medical degree. She furthered her study in Paris and London, including work under James Paget, who first described Paget's disease. Blackwell treated an infant with neonatal conjunctivitis and accidentally contracted the infection in her left eye, leaving her partially blind and ending her hopes of becoming a surgeon but she became committed to sanitation. She returned to New York in 1851 to establish private practice.

Blackwell's early years in practice were difficult. Female medical practitioners of the time were often assumed to be abortionists, but Blackwell opposed both abortion and artificial contraception. She published *The Laws of Life with Special Reference to the Physical Education of Girls* in 1852, the first book on the subject written by a woman, and lectured widely on women's health and hygiene. In 1857, she founded the New York Infirmary for Indigent Women and Children, which became a model for female-led healthcare and medical education. The infirmary offered clinical training for women in medicine and later was among the first American women's medical colleges. Throughout that time, Blackwell wrote widely, submitting to journals but, more important, evangelizing the cause of women in medical care; she wrote *Medicine as a Profession for Women*, a textbook for the program she was starting.

However, when the Civil War began in 1861, the nation mobilized for the war effort. The onslaught of sick and wounded soldiers overwhelmed Union and Confederate military and civilian medical systems at the outset of the war. Both armies rapidly expanded their forces, but the infrastructure to support the wounded—especially medical supplies and trained personnel—lagged substantially. At the time, no nursing corps existed. The military and even most doctors did not consider nursing a profession. In hospitals, most nursing was done by strong men whose primary job was to move patients or to hold them down for surgery, which was performed without anesthetic. In the military, that job typically fell to enlisted men of low rank, who received a modest additional wage for their service.

The scale and severity of the conflict quickly exposed the inadequacy of that model. Disease, malnutrition, and grievous battlefield injuries demanded more competent and organized medical care. In the Union Armies alone, according to *The Medical and Surgical History of the War of the Rebellion (1861–65)*, published by the US Surgeon General's Office, 20,587,450 transmittable diseases and 879,717 nontransmittable conditions led to the deaths of 142,522 soldiers off the battlefields. Furthermore, there were >60,000 amputations. In response, a nationwide push began, especially in the North, to train and recruit professional nurses.

One of the most substantial of those efforts came from the Blackwell clinic, which became a central hub for nursing training. Hundreds of women received structured medical instruction there, and the school

Author affiliation: Marist School, Atlanta, Georgia, USA; Georgia Gwinnett College, Lawrenceville, Georgia, USA

DOI: https://doi.org/10.3201/eid3204.251083

produced nurses widely seen as more effective and capable than their untrained counterparts. Members of New York's congressional delegation urged Congress to appoint Blackwell to lead the Union nursing effort, citing her leadership and medical expertise. Despite Blackwell's qualifications and long-standing abolitionist commitments—shaped in part by her association with reformers such as William Lloyd Garrison—Congress instead selected Dorothea Dix. Lawmakers viewed Dix, whose national reputation stemmed from her asylum and prison reform campaigns, as the more politically acceptable choice.

Congress appointed Dix as Superintendent of Army Nurses, making her the first woman to head a federal bureau. Blackwell continued her work independently, expanding nursing training through the Women's Central Association of Relief, an outgrowth of the New York Infirmary for Women and Children.

Tensions emerged between the 2 reformers. Dix imposed strict age restrictions, 35–50 years, and appearance standards for nurses. She sought "matronly persons of experience… and serious disposition" and rejected applicants she deemed too young or insufficiently matronly. Blackwell, in contrast, emphasized medical training and professional competence. Dix's rigid administrative style drew criticism from military officials and reformers alike; General George McClellan reportedly nicknamed her "Dragon Dix," and Jane Grey Swisshelm called her a "self-sealing can of horror, tied up in red tape." Dix's style provoked criticism from fellow reformers, including Blackwell.

Although not a founder of the US Sanitary Commission (USSC), Blackwell supported its medically oriented and reform-driven approach to wartime care. The USSC emphasized sanitary inspection, improved hospital organization, and professional standards in nursing, principles aligned with Blackwell's advocacy for trained female medical workers. However, tensions soon emerged between Dix and other reformers over control of nurse appointments and qualifications. War Department General Order No. 351 in 1863 reduced Dix's unilateral authority, allowing surgeons and military officials greater discretion in staffing decisions and opening space for more formally trained women to serve. Throughout the war, Blackwell continued organizing women physicians and promoting professional medical education. The broader sanitary movement, including the efforts of the USSC, the US Christian Commission, and independent volunteers such as Clara Barton, helped shift American medicine toward greater institutional organization and professionalization in the postwar era.

Figure. Elizabeth Blackwell, seated in profile (ca. 1850–60). Source: Harvard University, Schlesinger Library on the History of Women in America, Radcliffe Institute.

Throughout her life, Elizabeth Blackwell championed abolition, public health reform, sanitation, and the professional training of women physicians. Although not an outspoken suffragist, she collaborated with leading advocates for women's rights and helped expand opportunities for women in medicine and science. Her enduring legacy lies not only in the institutions she founded but in the generations of women physicians she trained and inspired. Blackwell died on May 31, 1910, at her home in Hastings, England, remembered as a pioneer who overcame systemic exclusion to reshape both American and British medicine.

About the Author

Dr. Hoffmann is a historian specializing in 19th Century US history, particularly the history of medicine during the US Civil War. He teaches American studies at the Marist School in Atlanta, Georgia, and serves as a part-time lecturer at Georgia Gwinnett College in Lawrenceville, Georgia. His current research explores the intersections of trauma, public health, and memory in American history.

Suggested Reading

1. Blackwell E. The laws of life with special reference to the physical education of girls. New York: Putnam; 1852.
2. Blackwell E. Medicine as a profession for women. New York: Trustees of the New York Infirmary for Women; 1860.
3. Devine S. Learning from the wounded: the Civil War and the rise of American medical science. Chapel Hill (NC): The University of North Carolina Press; 2014.
4. Dix D. Circular, no. 8. Washington: US Government Printing Office; 1862.
5. Faust DG. This republic of suffering: death and the American Civil War [reprint]. New York: Vintage; 2009.
6. Maxwell WQ. Lincoln's fifth wheel: the political history of the U.S. Sanitary Commission. New York: Longmans, Green & Co.; 1956.
7. Nimura JP. The Doctors Blackwell: how two pioneering sisters brought medicine to women - and women to medicine. New York: W.W. Norton & Company; 2021.
8. American Battlefield Trust. Dorothea Lynde Dix [cited 2025 Jul 17]. https://www.battlefields.org/learn/biographies/dorothea-lynde-dix
9. US Government Publishing Office. The medical and surgical history of the War of Rebellion (1861–65). Washington: The Office; 1870.

Address for correspondence: Nicolas Hoffmann, Marist School, 3790 Ashford Dunwoody Rd, Atlanta, GA 30319, USA; email: nhoffmann@gmail.com, hoffmannn@marist.com

September 2025

Parasitic Infections

- Chagas Disease, an Endemic Disease in the United States
- Severe Group A *Streptococcus* Infection among Children, France, 2022–2024
- Rickettsioses as Underrecognized Cause of Hospitalization for Febrile Illness, Uganda
- Epidemiology of Chikungunya Hospitalizations, Brazil, 2014–2024
- Drivers of Crimean-Congo Hemorrhagic Fever in Natural Host and Effects of Control Measures, Bulgaria
- Increased Incidence of *Candida auris* Colonization in Early COVID-19 Pandemic, Orange County, California, USA
- Differences in Lyme Disease Diagnosis among Medicaid and Medicare Beneficiaries, United States, 2016–2021
- *Theileria luwenshuni* and Novel *Babesia* spp. Infections in Humans, Yunnan Province, China
- Detection of Multiple Nosocomial *Trichosporon asahii* Transmission Events via Microsatellite Typing Assay, South America
- *Sporothrix brasiliensis* Treatment Failure without Initial Elevated Itraconazole MICs in Felids at Border of Brazil
- Insights into Infant Strongyloidiasis, Papua New Guinea
- Detection of Rat Lungworms in Invasive Mollusks, Georgia, USA, 2024

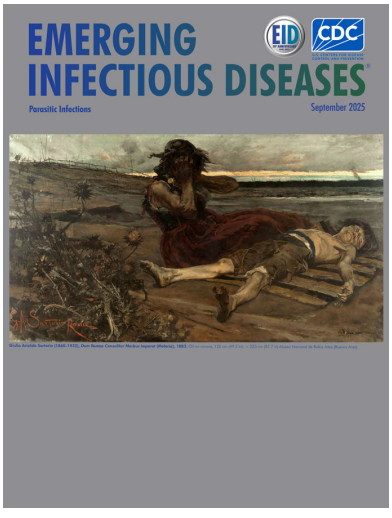

- Attachment Patterns of Avian Influenza H5 Clade 2.3.4.4b Virus in Respiratory Tracts of Marine Mammals, North Atlantic Ocean
- Related Melioidosis Cases with Unknown Exposure Source, Georgia, USA, 1983–2024
- CYP2D6 Genotype and Primaquine Treatment in Patients with Malaria, Venezuela
- Gastric Submucosal Tumor in Patient Infected with *Dioctophyme renale* Roundworm, South Korea, 2024
- Rapidly Progressing Melioidosis Outbreak in City Center Zoo, Hong Kong, 2024
- Genetic Characterization of *Orientia tsutsugamushi*, Bhutan, 2015
- Novel Henipavirus, Salt Gully Virus, Isolated from Pteropid Bats, Australia
- Modeling Case Burden and Duration of Sudan Ebola Virus Disease Outbreak in Uganda, 2022
- Detection of Rat Lungworm (*Angiostrongylus cantonensis*) in Rats and Gastropods, Italy
- Emergence of Autochthonous *Leishmania* (*Mundinia*) *martiniquensis* Infections in Horses, Czech Republic and Austria, 2019–2023
- Imported Malaria and Congenital Acquisition in Infant, Portugal, 2024
- Monkeypox Virus Clade IIa Infections, Liberia, 2023–2024
- Characterization of Emerging Human *Dirofilaria repens* Infections, Estonia, 2023
- Zoonotic Rat Lungworm *Angiostrongylus cantonensis* in Black Rats, Houston, Texas, 2024
- Human Babesiosis Caused by *Babesia venatorum*, Russia, 2024
- Linezolid and Meropenem for *Nocardia otitidiscaviarum* Actinomycetoma, India
- Subarachnoid Neurocysticercosis Caused by Larval-Stage *Taenia crassiceps* Tapeworm, Slovenia
- Detection of Rat Lungworms in Invasive Mollusks, Georgia, USA, 2024

EMERGING INFECTIOUS DISEASES

To revisit the September 2025 issue, go to: https://wwwnc.cdc.gov/eid/articles/issue/31/9/table-of-contents

The Weight of Waiting

Moussa Moise Diagne

In Ebola outbreaks, families wait to bury their dead until a PCR whispers yes or no. Amid outbreaks of hemorrhagic fever in Senegal, laboratories raced clocks they could not command as loved ones stood by. This essay explores the ethics and emotion of that fragile interval between sample and answer.

Between Sample and Answer

Outbreak science is often told as a story of discovery: the virus identified, genomes sequenced, clusters mapped. In the field, however, science is not measured in breakthroughs. Science is measured in waiting. Waiting for a test result. Waiting for permission. Waiting for certainty before grief can proceed, before care can begin.

In the laboratory, time feels technical, predictable. Thirty cycles of PCR. Forty minutes of centrifugation. Six hours on a sequencer. Time in the lab is a sequence of protocols. Some of that waiting is integral, not out of indifference but out of care. In outbreaks like Ebola, guidance from international agencies and national authorities determines what must happen before an answer can travel (*1*): how a sample is handled and moved, how results are checked and released, and when families can lay their dead to rest. Such protections save lives, even as they stretch the human space between a sample taken and certainty delivered. Outside the lab—in a hospital ward, in a village courtyard, at a laboratory gate—time fractures. Moments are felt in the rising panic of families who want to bury their dead, in the restrained hands of clinicians at a patient's bedside, in the quiet tension of how much longer waiting is possible.

This contradiction has followed my work as a virologist. My role has been to extract the truth from blood and tissue. In outbreak zones, I learned that the truth is not delivered in those controlled, sterile places in which it is revealed. Truth arrives against the backdrop of grief, fear, and trust stretched thin. Most often, it arrives too late for those seeking it.

Author affiliation: Arboviruses and Hemorrhagic Fever Viruses Unit, Institut Pasteur de Dakar, Dakar, Senegal

DOI: http://doi.org/10.3201/eid3204.251540

Scene 1—At the Laboratory Door (Beni, North Kivu, Democratic Republic of Congo, 2019)

The outbreak was already months old when I arrived in Beni, after an early stint in Mangina, where the first sparks had caught (*2*). In Mangina, confusion. In Beni, something heavier, grief hardened into suspicion.

One afternoon, a man died. His family was told to wait for the PCR result before burial. The epidemiologists and socio-anthropologists did the explaining. The family listened, at first. Then the hours stretched, elastic and cruel.

The delay was not owing to neglect. Samples poured in daily, from the living and the dead, and each tube demanded safe handling, logging, extraction, amplification. Couriers threaded insecure roads to bring samples in; machines ran almost constantly. Even so, the reality of field diagnostics often translates to abrupt nighttime pauses: patients arriving at night were typically sampled the next morning once the lab opened, and results were targeted within a day or two under difficult conditions (field laboratories tracked <48-hour turnaround for suspect samples during this outbreak) (*3*).

The family's patience broke. They came directly to the laboratory, voices raised, fists pounding on doors. For them, waiting had crossed into injustice. For us inside, the moment was suffocating, caught between stress and comprehension. We could not deny their grief, but we could not conjure truth faster than the cycles would allow.

I remember standing by the glass, seeing their anger, hearing their shouts, while technicians in suits kept their heads down, processing samples one by one. Between us lay racks of tubes, each a story held at 95°C, denatured and re-annealed, amplified toward a verdict. In that corridor, I realized that waiting was a shared burden, but not an equal one. The family waited to bury. We waited to be sure. Everyone paid the price of that interval.

As the outbreak unfolded across North Kivu and Ituri, the world's second-largest Ebola outbreak (*4*), field labs multiplied and testing volume surged. The World Health Organization's situational reports from 2019 described 10–11 operational field labs and

thousands of samples processed weekly despite conflict and access constraints (*2*,*5*). The technology promised speed; the terrain and insecurity rationed it. Families lingered overnight outside gates. Inside, we tallied cycles and prayed the power held. In the ledger of outbreak work, those hours accumulate like interest, emotional debt that someone, somewhere will have to pay.

The result eventually came. It always does. In Beni, though, as in so many places, the result arrived threaded with the memory of the wait, and with a thinner strand of trust.

Scene 2—Curves on a Screen, Silence in a Ward (Dakar and Podor, Senegal, 2022)

Years later, I lived another form of waiting, not at the bedside, but at the Institut Pasteur de Dakar bench. Calls came from Podor, in the Saint-Louis region. Fever, bleeding, collapse: suspected viral hemorrhagic fever. Tubes began to land on our benches, tagged with urgency and carefully packed miles away, where families and clinicians were bracing.

We moved as fast as protocols permitted. Extraction. Master mix. Plates set, sealed, and run. Confirmation assays. Each step deliberate, each minute felt. We knew the ward rhythm by proxy: the pacing in a corridor, the weight of a clinician's hesitation, the family watching the gate. In outbreaks, a lab result is never just data; a hinge turns on that result, and action swings.

That month, Podor learned Crimean-Congo hemorrhagic fever's terms. Three human cases were confirmed; 2 patients died. We documented virus circulation in local ticks and livestock. It was the first severe cluster of its kind there, and it cut fast (*6*). We delivered results quickly by laboratory standards. For some patients, the body ran ahead of the numbers. When the curves rose on our screen, they carried more than science. They carried the echo of the waiting we had all been doing.

Later analyses teased out the context. Podor had no sentinel site in the national syndromic surveillance network before the outbreak (*7*). In at least 1 fatal case, viral hemorrhagic fever was not among the diagnostic considerations at first, suggesting late recognition and confirmation. After the outbreak, sentinel coverage expanded to Podor (*6*). The science is clear, but the human lesson is clearer: surveillance and training shorten the wait, and sometimes that difference is a life.

We returned to our benches the next day. The machines hummed, the city stirred, and somewhere a family decided how to remember those last hours, the hours before the answer. An answer did come, of course, but not soon enough for everyone.

The Human Weight of Waiting

Ebola and Crimean-Congo hemorrhagic fever are different diseases, and the outbreak scenarios for each comprised different ecologies and fears. Still, between sample and answer lies the same fragile interval.

For families, waiting corrodes trust. Science can feel like the barrier between love and ritual, between mourning and the ground. For clinicians, waiting corrodes confidence. Hands hover over a patient because confirmation carries moral and occupational weight. For scientists, waiting corrodes certainty. Each required cycle takes place inside someone else's life.

On paper, the outbreak story celebrates speed, rapid sequencing, new assays, quick analyses. In practice, outbreak work is dominated by waiting together: with families at gates, with clinicians in wards, with technicians facing racks that do not end. Even in North Kivu, where field labs reported <48-hour targets for suspect samples, the night-to-morning gap and the realities of transport and insecurity meant that many woke up facing the same uncertainty that followed them to bed. That gap is real, measurable, and human.

Waiting is not absence; it is a charged presence. Medical anthropologists call this liminality (*8*): suspended between states, neither sick nor well, neither bereaved nor released. In that space, imagination does its worst and best, hope and dread balancing on the same fingertip. The ethical demand is simple to describe but difficult to meet: shorten the wait and empathize with those who are waiting. Achieving this initiative would mean investments in specimen transport and lab networks, decentralization when possible, transparent communication about where a sample is located and when a result is likely, and above all, acknowledging that every "pending" is a person.

Not Always in Time

The machine always finishes eventually. In Beni, the result authorized a burial, but it could not erase the anger shaped by hours outside a locked door. In Podor, confirmation guided the response and strengthened the system, but 2 families had already crossed into mourning.

This is the hardest truth I learned at the bench and at the door: the result always comes, but it does not always arrive in time. The philosophy of waiting in outbreak science is simply this: precision owes a debt to compassion. Between sample and answer, we either pay that debt together or we collect it in grief.

Acknowledgments

I thank my colleagues in North Kivu and at Institut Pasteur de Dakar for their courage and dedication. I am also grateful to the families and health workers whose resilience shaped these reflections.

About the Author

Dr. Moussa Moïse Diagne is a virologist at the Institut Pasteur de Dakar, where he works at the crossroads of pathogen discovery and One Health. His writing explores the human side of outbreak science, shaped by field experience across Africa.

References

1. Frieden TR, Damon IK. Ebola in West Africa—CDC's role in epidemic detection, control, and prevention. Emerg Infect Dis. 2015;21:1897–905. https://doi.org/10.3201/eid2111.150949
2. Aruna A, Mbala P, Minikulu L, Mukadi D, Bulemfu D, Edidi F, et al. CDC Ebola Response. Ebola virus disease outbreak—Democratic Republic of the Congo, August 2018–November 2019. MMWR Morb Mortal Wkly Rep. 2019; 68:1162–5. https://doi.org/10.15585/mmwr.mm6850a3
3. Mukadi-Bamuleka D, Mambu-Mbika F, De Weggheleire A, Edidi-Atani F, Bulabula-Penge J, Mfumu MMK, et al. Efficiency of field laboratories for Ebola virus disease outbreak during chronic insecurity, Eastern Democratic Republic of the Congo, 2018–2020. Emerg Infect Dis. 2023;29:1–9. https://doi.org/10.3201/eid2901.221025
4. World Health Organization. Ebola outbreak 2018–2020, North Kivu/Ituri. Geneva: The Organization; 2020 [cited 2025 Oct 4]. https://www.who.int/emergencies/situations/Ebola-2019-drc-
5. UNICEF/ReliefWeb. DRC Ebola situation report, North Kivu and Ituri—31 July. 2020 [cited 2025 Oct 4]. https://reliefweb.int/report/democratic-republic-congo/unicef-dr-congo-ebola-situation-report-north-kivu-and-ituri-31-july
6. Sene O, Sagne SN, Ngom D, Bocoum M, Diallo MK, Khoulé A, et al. Crimean-Congo hemorrhagic fever outbreak in Podor, Northern Senegal in 2022: two independent emergences and unprecedented mortality. Am J Trop Med Hyg. 2025;113:555–63. https://doi.org/10.4269/ajtmh.24-0445
7. Institut Pasteur de Dakar. Fever surveillance: Syndromic Sentinel Surveillance in Senegal 4S Network [cited 2025 Oct 4]. https://rh.pasteur.sn/en/research-and-public-health/epidemiology-clinical-research-and-data-science/fever-surveillance-syndromic-sentinel-surveillance-senegal-4s-network
8. Picione RL, Marsico G. The religious nature of the psyche, semiotic mediation, and the evanescence of identity in liminality. Integr Psychol Behav Sci. 2024;58:836–44. https://doi.org/10.1007/s12124-024-09850-y

Address for correspondence: Moussa Moise Diagne, Arboviruses and Hemorrhagic Fever Viruses Unit, Virology Department, Institut Pasteur de Dakar, 12500 Dakar, Senegal; email: MoussaMoise.DIAGNE@pasteur.sn

etymologia revisited

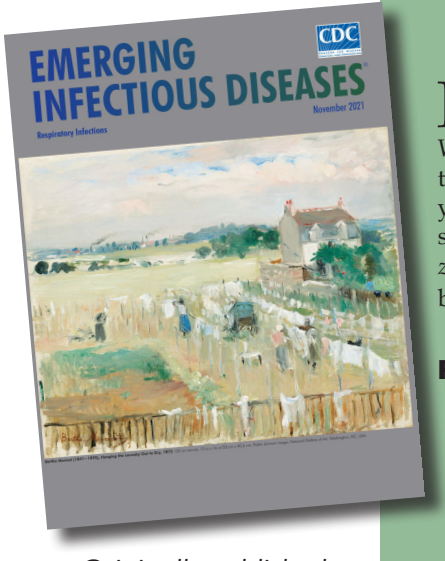

Originally published in November 2021

Prototheca

[pro"to-the'kə]

From the Greek *proto-* (first) + *thēkē* (sheath), *Prototheca* is a genus of variably shaped spherical cells of achloric algae in the family *Chlorellaceae*. Wilhelm Krüger, a German expert in plant physiology and sugar production, reported *Prototheca* microorganisms in 1894, shortly after spending 7 years in Java studying sugarcane. He isolated *Prototheca* species from the sap of 3 tree species. Krüger named these organisms as *P. moriformis* and *P. zopfii*, the second name as a tribute to Friedrich Wilhelm Zopf, a renowned botanist, mycologist, and lichenologist.

References:

1. Davies RR, Spencer H, Wakelin PO. A case of human protothecosis. Trans R Soc Trop Med Hyg. 1964;58:448–51. https://doi.org/10.1016/0035-9203(64)90094-X
2. Dorland's illustrated medical dictionary. 32nd ed. Philadelphia: Elsevier Saunders; 2012.
3. Kano R. Emergence of fungal-like organisms: Prototheca. Mycopathologia. 2020;185:747–54. https://doi.org/10.1007/s11046-019-00365-4
4. Krüger W. Brief characteristics of some lower organisms in the sap flow of deciduous trees [in German]. Hedwigia. 1894;33:241–66.
5. Todd JR, Matsumoto T, Ueno R, Murugaiyan J, Britten A, King JW, et al. Medical phycology 2017. Med Mycol. 2018;56(suppl 1):S188–204. https://doi.org/10.1093/mmy/myx162

https://wwwnc.cdc.gov/eid/article/27/11/21-1554_article

Acute Febrile Illness Surveillance for Estimating Population Immunity, Dominican Republic, 2021

Eric J. Nilles, Cecilia Then Paulino, Marietta Vasquez, William Duke, Petr Jarolim, Ronald Skewes Ramm, Adam Kucharski, Colleen L. Lau

Author affiliations: Harvard Humanitarian Initiative, Cambridge, Massachusetts, USA (E.J. Nilles); Brigham and Women's Hospital, Boston, Massachusetts, USA (E.J. Nilles, P. Jarolim); Ministry of Public Health and Social Assistance, Santo Domingo, Dominican Republic (C.T. Paulino, R.S. Ramm); Yale School of Medicine, New Haven, Connecticut, USA (M. Vazquez); National University Pedro Henríquez Ureña, Santo Domingo, (W. Duke); Harvard Medical School, Boston (P. Jarolim); London School of Hygiene & Tropical Medicine, London, UK (A. Kucharski); The University of Queensland, Brisbane, Queensland, Australia (C.L. Lau)

DOI: http://doi.org/10.3201/eid3204.251205

We assessed whether acute febrile illness surveillance could provide timely estimates of population immunity. In the Dominican Republic, antibody levels and inferred protection were similar between surveillance data and household survey serum samples, suggesting that surveillance platforms may offer a scalable approach to track population-level protection.

Cross-sectional population-representative serosurveys currently serve as the standard for estimating population immunity. However, the discrete timeframe, high cost, logistical complexity, and long timelines of that survey method often limit its utility during rapidly evolving outbreaks, when timely public health decision-making is essential. The COVID-19 pandemic evidenced this limitation, when the processing of serologic samples for a national household serosurvey in the Dominican Republic (*1*) in 2021—although methodologically rigorous—failed to keep up with a rapidly shifting postvaccine and postvariant immune landscape.

Researchers have referenced models based on reported case and death data to estimate cumulative infections (*2*), but those approaches rely on strong assumptions about testing access and outcome ascertainment and may be prone to error for pathogens with high proportions of asymptomatic infection. Moreover, such models estimate incidence rather than the level of immune protection in the population, which is the quantity most directly relevant for public health decision-making for pathogens that generate only partial or nonsterilizing immunity. There is a need, therefore, for alternative surveillance approaches, particularly those that can monitor changes over time and are rapid, scalable, low-cost, and feasible during periods of widespread social disruption (*3*).

We evaluated whether routinely collected serologic data from an acute febrile illness (AFI) clinical surveillance platform could serve as a proxy for estimating population immunity, using COVID-19 as proxy. We compared SARS-CoV-2 spike antibody data (Roche Diagnostics, https://www.roche.com) from 2 sources collected during July–October 2021 in the same Dominican Republic provinces: a longitudinal AFI surveillance system embedded in routine healthcare settings ("surveillance") (*4*), which included routine blood collection for serologic testing; and a multistage, population-representative household serologic survey ("survey") (*1*). We matched surveillance participants to survey participants by propensity score 1:5 using age and number of COVID-19 vaccine doses, reflecting a pragmatic approach based on covariates routinely available in surveillance systems. We looked at baseline characteristics before and after matching (Table). To evaluate the potential for type II error (failing to detect a meaningful difference when one exists), we estimated the detectable difference in the proportion above variant-specific protection thresholds given the matched sample sizes (surveillance, n = 115; survey, n = 575), which provided ≥80% power (2-sided $\alpha = 0.05$) to detect absolute differences of ≈6–8 percentage points. For each variant-specific protection threshold, we estimated the proportion of participants exceeding the threshold within each group using exact binomial methods. We evaluated differences between groups using 2-sample tests for equality of proportions with continuity correction. Those tests evaluate a 2-sided null hypothesis of equal proportions. We used the prespecified ±10-percentage-point margin as a benchmark of public health relevance and not as a formal statistical equivalence test (Appendix, https://wwwnc.cdc.gov/EID/article/32/4/25-1205-App1.pdf).

We included in the matched analysis all 115 surveillance participants and 575 matched survey counterparts (Table; Figure, panel A). We assessed seroprevalence, mean spike antibody levels, and the proportion of persons above thresholds corresponding to 75% protection against symptomatic SARS-CoV-2 infection (*5*). Unmatched mean antibody titers were similar: 2.4 $\log_{10}$ BAU/mL (95% CI 2.1–2.6) in

Table. Baseline characteristics of surveillance and survey participants before and after propensity score matching for study of acute febrile illness surveillance for estimating population immunity, Dominican Republic, 2021*

Variable	Surveillance, n = 115	Survey, unmatched, n = 962	Survey, matched,† n = 575
Age group, y			
0–14	10 (8.7)	91 (9.5)	55 (9.6)
15–34	52 (45.2)	316 (32.8)	239 (41.6)
35–54	29 (25.2)	280 (29.1)	156 (27.1)
≥55	24 (20.9)	275 (28.6)	125 (21.7)
Median age, y (IQR)	33 (25–52)	40 (24–57)	34 (22–53)
COVID-19 vaccines			
None	30 (26.1)	149 (15.5)	144 (25.0)
1	5 (4.3)	109 (11.3)	31 (5.4)
2	71 (61.7)	603 (62.7)	355 (61.7)
3	9 (7.8)	101 (10.5)	45 (7.8)
Mean (±SD)	1.5 (1.0)	1.7 (0.9)	1.5 (1.0)
Days since last vaccination, mean (±SD)	62.1 (54.3)	76.7 (44.7)	73.8 (40.4)
Sex			
F	78 (67.8)	658 (68.4)	408 (71.0)
M	37 (32.2)	304 (31.6)	167 (29.0)
Province			
Espaillat	60 (52.2)	309 (32.1)	203 (35.3)
San Pedro de Macorís	52 (45.2)	572 (59.5)	318 (55.3)
Santiago	3 (2.6)	81 (8.4)	54 (9.4)
Setting			
Rural	82 (71.3)	486 (50.5)	329 (57.2)
Urban	31 (27.0)	476 (49.5)	246 (42.8)
Seroprevalence, mean (±SD)	0.88 (0.33)	0.94 (0.25)	0.92 (0.27)
log_{10} spike antibody titer			
Mean (±SD)	2.4 (1.4)	2.6 (1.2)	2.5 (1.2)
Median (IQR)	2.6 (1.7–3.2)	2.7 (1.9–3.4)	2.6 (1.9–3.2)

*Values are no. (%) participants except as indicated. The study compared SARS-CoV-2 spike antibody data collected during July–October 2021 in the same Dominican Republic provinces from a longitudinal AFI surveillance system embedded in routine healthcare settings ("surveillance") (4), which included routine blood collection for serologic testing; and a multistage, population-representative household serologic survey ("survey") (1). Seroprevalence represents the percentage of participants with spike antibody titers above the manufacturer-specified cutoff (≥0.8 U/mL). IQR, interquartile range.
†The matched survey dataset was generated through 1:5 nearest-neighbor propensity score matching of survey participants to surveillance participants, using age and number of COVID-19 vaccine doses as matching variables. Because only those variables were included in the propensity model, differences in other characteristics (e.g., province, setting, days since last vaccination) reflect inherent differences between the underlying sampling frames rather than confounding in the matched analysis.
‡Two surveillance participants were missing data for setting.

the surveillance group versus 2.6 log_{10} BAU/mL (95% CI 2.5–2.7) in the survey group (p = 0.08 by 2-sample *t*-test). Results in the matched dataset were consistent (2.4 log_{10} BAU/mL in the surveillance group, 2.5 log_{10} BAU/mL in the survey group; p = 0.36). 3Matched seroprevalence was also comparable (surveillance: 88%; survey: 92%; p = 0.21 by 2-sample test for equality of proportions), and the percentage of persons with ≥75% protection differed by ≤6% (range 1.6%–5.4%) across all evaluated variants, with no statistically significant differences between groups (p = 0.18–0.97) (Figure, panels B, C; Appendix Table 1). Although the 95% CIs for the between-group differences in inferred protection slightly exceeded the prespecified ±10-percentage-point margin for some variants, the observed differences were small (≤5 percentage points) and centered near zero, and the study had ≥80% power to detect differences of ≈6–8 percentage points, making large discrepancies between sampling frames unlikely.

Given their low cost, integration within routine care, and ability to sample broad community segments, AFI surveillance platforms may complement or substitute for traditional serosurveys when rapid situational awareness or repeated assessments are needed. Unlike cross-sectional serosurveys, this approach could also support ongoing monitoring over time (*4*,*5*), enabling near real-time tracking of antibody levels and inferred immunity and informing decisions about school reopening, travel restrictions, and vaccine targeting. Pooling data from multiple sites could further improve representativeness and reduce spatial or demographic bias.

The primary limitation of this analysis is its cross-sectional design, which limits generalizability across timepoints. In addition, the study population had high exposure to SARS-CoV-2 vaccination and infection, which might not reflect settings with lower transmission and vaccination coverage (*6*). Nonetheless, our findings underscore the potential value of AFI and other clinical surveillance platforms as scalable, cost-effective tools for monitoring population immunity, particularly during pandemics, when speed, affordability, and feasibility are critical.

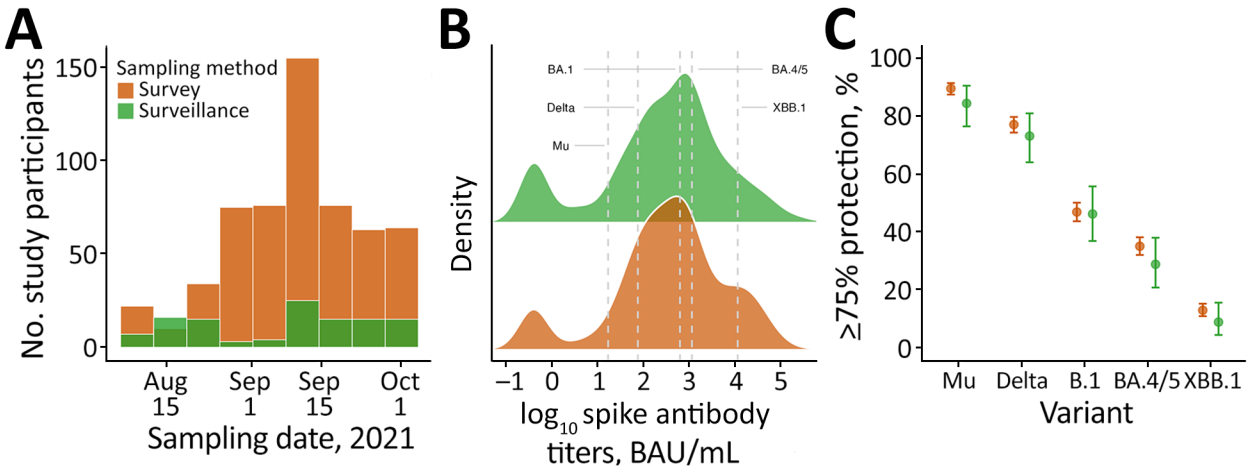

Figure. Spike antibody responses by surveillance and population survey sampling methods for study of acute febrile illness surveillance similar to household serosurvey for estimating population immunity, Dominican Republic. The study compared SARS-CoV-2 spike antibody data collected during July–October 2021 in the same provinces from a longitudinal AFI surveillance system embedded in routine healthcare settings ("surveillance") (*4*), which included routine blood collection for serologic testing; and a multistage, population-representative household serologic survey ("survey") (*1*). Participants were matched by age and number of COVID-19 vaccine doses at a 1:5 ratio (surveillance, n = 115; survey, n = 575). A) Histogram showing number of participants by sampling date. B) Density ridge plots illustrating titer distributions by sampling method. Dashed gray lines indicate previously reported spike antibody thresholds associated with ≥75% protection against symptomatic infection for Mu ($10^{1.23}$), Delta ($10^{1.88}$), BA.1 ($10^{2.80}$), and BA.4/5 ($10^{3.06}$). Threshold for XBB.1 was inferred based on ≈10-fold lower neutralizing response relative to BA.4/5. C) Dot-whisker plots showing estimated proportion of participants with antibody levels corresponding to ≥75% protection by variant or subvariant (underlying data in Appendix Table 1, https://wwwnc.cdc.gov/EID/article/32/4/25-1205-App1.pdf). Dots indicate point estimates; whiskers indicate 95% CIs. Protection thresholds taken from previously published variant-specific correlates of protection (*5*). Estimates show percentages of persons above those thresholds (uncertainty in thresholds [reported 95% CIs] not propagated into percentages).

Acknowledgments

We extend thanks to the many persons who volunteered to participate in this study. We also thank the study staff that collected the field data, the US Centers for Disease Control and Prevention Central America Regional Office, the Dominican Republic Ministry of Health and Social Assistance, and the Pedro Henriquez Ureña National University for their commitment and support for the study.

E.J.N. is the principal investigator on a US Centers for Disease Control and Prevention–funded award that funded the study (U01GH002238), and W.D., C.L.L., A.K., and M.V. have received salary support, consultancy fees, or travel paid through this award. C.T. and R.S.R. are employees of the Ministry of Health and Social Assistance, Dominican Republic, an office subcontracted with funds from the US Centers for Disease Control and Prevention award. A.K. is supported by the Welcome Trust, United Kingdom. We declare no other competing interests.

About the Author

Dr. Nilles is a clinician and infectious disease epidemiologist at the Brigham and Women's Hospital and Harvard Medical School in Boston, Massachusetts, USA, and the director of the Infectious Diseases and Epidemics Program at the Harvard Humanitarian Initiative, Cambridge, Massachusetts, USA. His primary research interests include epidemic transmission and control, surveillance of emerging diseases, and seroepidemiology.

References

1. Nilles EJ, Paulino CT, de St. Aubin M, Restrepo AC, Mayfield H, Dumas D, et al. SARS-CoV-2 seroprevalence, cumulative infections, and immunity to symptomatic infection—a multistage national household survey and modelling study, Dominican Republic, June–October 2021. Lancet Reg Health Am. 2022;16:100390. https://doi.org/10.1016/j.lana.2022.100390
2. Barber RM, Sorensen RJD, Pigott DM, Bisignano C, Carter A, Amlag JO, et al.; COVID-19 Cumulative Infection Collaborators. Estimating global, regional, and national daily and cumulative infections with SARS-CoV-2 through Nov 14, 2021: a statistical analysis. Lancet. 2022;399:2351–80. https://doi.org/10.1016/s0140-6736(22)00484-6
3. Hallal PC, Hartwig FP, Horta BL, Silveira MF, Struchiner CJ, Vidaletti LP, et al. SARS-CoV-2 antibody prevalence in Brazil: results from two successive nationwide serological household surveys. Lancet Glob Health. 2020;8:e1390–8. https://doi.org/10.1016/S2214-109X(20)30387-9
4. Nilles EJ, de St. Aubin M, Dumas D, Duke W, Etienne MC, Abdalla G, et al. Monitoring temporal changes in SARS-CoV-2 spike antibody levels and variant-specific risk for infection, Dominican Republic, March 2021–August 2022. Emerg Infect Dis. 2023;29:723–33. https://doi.org/10.3201/eid2904.221628
5. Nilles EJ, Paulino CT, de St. Aubin M, Duke W, Jarolim P, Sanchez IM, et al. Tracking immune correlates

of protection for emerging SARS-CoV-2 variants. Lancet Infect Dis. 2023;394:10–1. https://doi.org/10.1016/S1473-3099(23)00001-4
6. Nilles EJ, Roberts K, de St. Aubin M, Mayfield H, Restrepo AC, Garnier S, et al. Convergence of SARS-CoV-2 spike antibody levels to a population immune setpoint. EBioMedicine. 2024;108:105319. https://doi.org/10.1016/j.ebiom.2024.105319

Address for correspondence: Eric James Nilles, Brigham and Women's Hospital, 75 Francis St, Boston, MA 02115-6195, USA; email: enilles@bwh.harvard.edu

Seroepidemiologic Study of Oropouche Virus, Amazonas State, Brazil, 2015–2016

Julia Forato,[1] Gabriel C. Scachetti,[1] Bárbara B. Salgado, Carolina M.L. Singh, Nadielle C. Pereira, Renato dos Santos Reis, William M. de Souza, José Luiz Proenca-Modena,[2] Pritesh Lalwani[2]

Author affiliations: University of Campinas, Campinas, Brazil (J. Forato, G.C. Scachetti, J.L. Proenca-Modena); Fiocruz Amazônia, Manaus, Brazil (B.B. Salgado, C.M.L. Singh, N.C. Pereira, P. Lalwani); Universidade Federal do Amazonas, Manaus (B.B. Salgado, C.M.L. Singh, N.C. Pereira, R. dos S. Reis, P. Lalwani); University of Kentucky, Lexington, Kentucky, USA (W.M. de Souza)

DOI: https://doi.org/10.3201/eid3204.250917

We conducted a cross-sectional serosurvey for Oropouche virus (OROV) among residents of Amazonas State, Brazil, during 2015–2016. We detected OROV neutralizing antibodies in 85/814 (10.4%) participants; seroprevalence was higher in Manaus (49/440 [11.1%]) than in Coari (36/374 [9.6%]). Those findings suggest OROV circulation in Amazonas State before 2015.

Oropouche virus (OROV) is a neglected and re-emerging vectorborne orthobunyavirus endemic in Central and South America since the 1950s (*1*,*2*). OROV is mainly transmitted to humans by the bite of infected midges (*Culicoides paraensis*), which also spread OROV among sloths and other animals in the sylvatic cycle (*3*). OROV infection in humans causes Oropouche fever, characterized by self-limiting febrile illnesses but that can, in rare cases, lead to hemorrhagic, neurologic, and maternal–fetal complications, even death (*1*,*4*).

OROV has been endemic in the Amazon region and expanding in 2024 toward areas of high population density in all Brazil states, as well as to the Caribbean, including Cuba, Barbados, and Panama (*5*). In addition, traveler-imported cases were identified in the United States, Canada, and Europe. Reports of OROV infection have been identified predominantly by molecular assays; OROV serosurvey studies remain scarce, even in OROV-endemic areas. In this study, we conducted a retrospective cross-sectional serosurvey among residents from Coari and Manaus municipalities in Amazonas State, Brazil, during 2015–2016. The ethics committee of the Federal University of Amazonas approved all procedures for this study (approval nos. 5.876.612 and 6.629.451).

We collected blood samples by venipuncture from residents in Manaus and Coari municipalities (Figure 1). No participants reported any symptoms in the 30 days before blood sample collection. We tested serum samples by 90% plaque reduction neutralization test ($PRNT_{90}$) to assess the presence and titer of neutralizing antibodies against OROV (*5*). We determined $PRNT_{90}$ values from the mean of 2 technical replicates by fitting a 3-parameter log-logistic regression curve to plaque counts normalized to the positive control (Appendix, https://wwwnc.cdc.gov/EID/article/32/4/25-0917-App1.pdf).

We analyzed serum samples from 814 persons, 374 (45.9%) participants residing in Coari and 440 (54.1%) in Manaus. Median age was 36 (interquartile range [IQR] 26–48) years; 567 (69.7%) participants were female and 247 (30.3%) male. We detected OROV neutralizing antibodies in 85 (10.4%, 95% CI 8.5%–12.8%) participants (Figure 2, panel A). Seroprevalence, as indicated by presence of neutralizing antibodies, was higher in Manaus (49/440 [11.1%, 95% CI 8.4%–14.5%] positive) than in Coari (9.6%, 36/374, 95% CI 6.9%–13.2%) (Figure 2, panel A). The median $PRNT_{90}$ titer in Manaus was 80 (IQR 40–320), whereas in Coari the median $PRNT_{90}$ titer was 80 (IQR 20–160) (Figure 2, panel B). Participants testing seropositive for OROV had a median age of 47 (IQR 38–54) years; median age in Manaus was 48 (IQR 42–54) years and

[1]These authors contributed equally to this work.
[2]These senior authors contributed equally to this work..

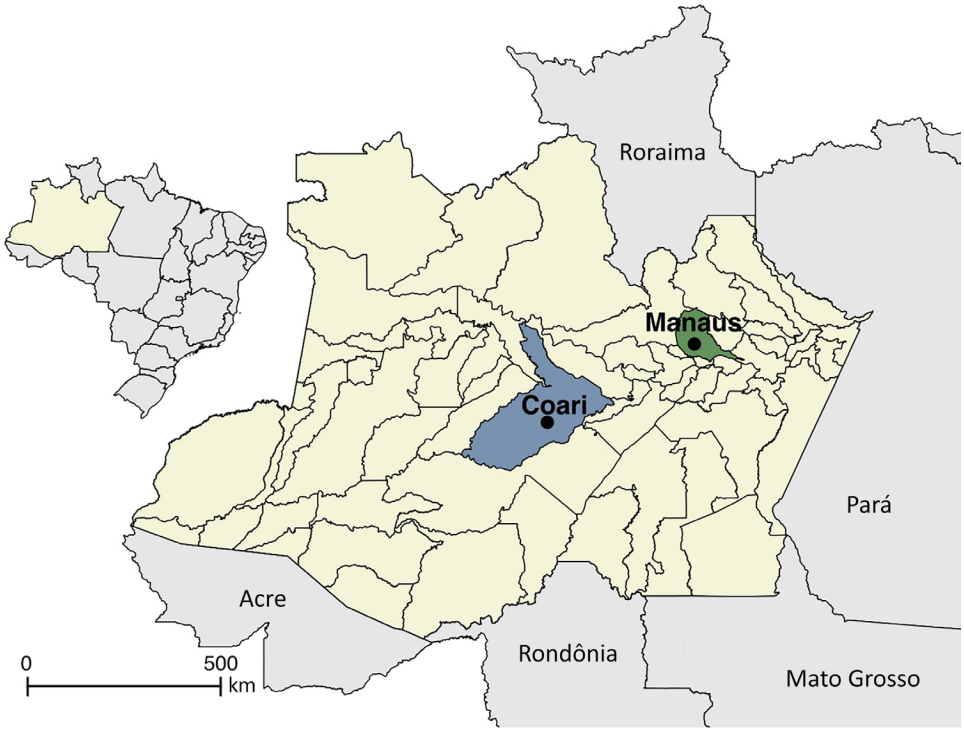

Figure 1. Coari and Manaus municipalities within Amazonas, Brazil, in seroepidemiologic study of Oropouche virus, 2015–2016. Inset shows location of Amazonas state in Brazil.

in Coari, 45 (IQR 33–53) years. OROV seropositivity rates were higher in female than male participants (65/85 [76.5%]) overall, 39/49 (79.6%) in Manaus and 26/36 (72.2%) in Coari. We observed no statistically significant difference in sex or age distribution in neutralizing antibody–positive participants between Coari and Manaus.

Our findings identified OROV neutralizing antibodies in residents of Coari and Manaus, suggesting prior OROV transmission in those locations during 2015–2016. The seropositivity rate found in our study was lower than that reported in previous studies from the Peruvian Amazon (18%–35%) (*6*,*7*). However, our results are similar to those of a 2014–2015 study in Amapá State, Brazil, which found a 10.2% seropositivity rate (*8*). We cannot ascertain the timing of OROV infection on the basis of neutralizing antibody data; however, some seropositive cases might be linked with OROV outbreak in Manaus during 1980–1981, where 83/496 (16.7%) of participants from 6 neighborhoods in Manaus tested positive for OROV-specific antibodies after a major OROV outbreak (*9*). Conversely, Oropouche fever was first reported to the Ministry of Health in Coari on December 18, 2023, suggesting a potential undetected OROV transmission not captured

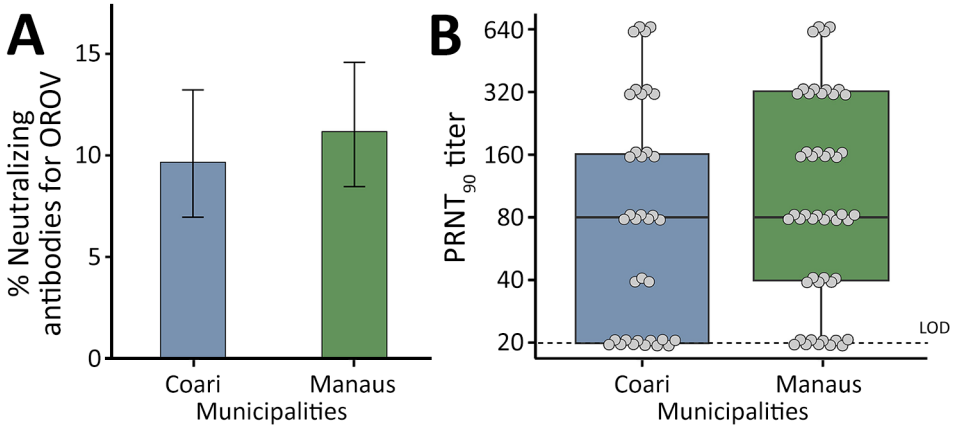

Figure 2. Serosurvey of Oropouche virus in Coari and Manaus municipalities, Amazonas state, Brazil, 2015–2016. A) Percentage of serum samples positive for neutralizing antibodies for OROV per municipality. Error bars indicate 95% CIs. B) Box plot showing the distribution of $PRNT_{90}$ titers of serum samples by municipality. Solid black horizontal line represents the median, box upper and lower limits represent the 75th and 25th percentiles, and whiskers represent minimum and maximum values. Dashed line represents LOD. Dots represent individual healthy volunteers. LOD, limit of detection; NAb, neutralizing antibodies; OROV, Oropouche virus; $PRNT_{90}$, 90% plaque reduction neutralization test.

by the local surveillance system. We hypothesize that underreporting of OROV infections in Coari could result from several factors, including variable healthcare-seeking behavior, potential higher levels of oligosymptomatic or asymptomatic cases during OROV infection, and misdiagnosis from similar clinical manifestations of other endemic arboviruses, such as dengue, chikungunya, Zika, and Mayaro viruses (*10*).

A limitation of our study is that we focused on previous OROV infections, using a serologic approach for previous infection; molecular studies and detection of IgM are needed to determine the percentage of participants actively infected, particularly during outbreaks. Second, we were unable to determine whether OROV infections occurred in urban or forest settings. Third, some positive samples could have resulted from the cross-reaction with other orthobunyaviruses that remain to be detected in this region. Finally, larger-scale longitudinal studies are needed to determine the effect of OROV, both before and after future OROV outbreaks.

In conclusion, our study demonstrated evidence of OROV circulation in Coari and Manaus before 2015–2016. Our findings highlight the critical need for continuous molecular and serologic laboratory surveillance for OROV to accurately assess its burden in the Amazon Region and beyond, particularly since its reemergence in 2023.

P.L. is supported by Fundação de Amparo à Pesquisa do Estado do Amazonas (Posgrad, CT&I Áreas Prioritárias, Iniciativa Amazônia +10, Chamada ERC 2022, and PEX-CT&I/FAPEAM); Coordenação de Aperfeiçoamento de Pessoal de Nível Superior, Funding 001). J.L.P.M. is supported by São Paulo Research Foundation (no. 2022/10442-0), and National Council for Scientific and Technological Development (CNPq, no. 309971/2023-3). W.M.dS. is supported by Burroughs Wellcome Fund – Climate Change and Human Health Seed Grants (no. 1022448), and Wellcome Trust–Digital Technology Development Award in Climate Sensitive Infectious Disease Modelling (no. 226075/Z/22/Z). J.F. is supported by the São Paulo Research Foundation (grant no. 25/18991-0). G.C.S. is supported by the São Paulo Research Foundation (grant no. 24/12668-0). B.B.S. is supported by Coordenação de Aperfeiçoamento de Pessoal de Nível Superior (grant no. 88887.967871/2024-00).

About the Author

Ms. Forato is a PhD student at the Department of Genetics, Evolution, Microbiology, and Immunology at the University of Campinas, São Paulo, Brazil. Her research interests include epidemiologic surveillance of emerging viruses, with a focus on arboviruses.

References

1. Travassos da Rosa JF, de Souza WM, Pinheiro FP, Figueiredo ML, Cardoso JF, Acrani GO, et al. Oropouche virus: clinical, epidemiological, and molecular aspects of a neglected orthobunyavirus. Am J Trop Med Hyg. 2017;96:1019–30. https://doi.org/10.4269/ajtmh.16-0672
2. de Souza WM, Calisher CH, Carrera JP, Hughes HR, Nunes MRT, Russell B, et al. ICTV virus taxonomy profile: *Peribunyaviridae* 2024. J Gen Virol. 2024;105:002034. https://doi.org/10.1099/jgv.0.002034
3. Pinheiro FP, Travassos da Rosa APA, Gomes MLC, LeDuc JW, Hoch AL. Transmission of Oropouche virus from man to hamster by the midge *Culicoides paraensis*. Science. 1982;215:1251–3.
4. das Neves Martins FE, Chiang JO, Nunes BTD, Ribeiro BFR, Martins LC, Casseb LMN, et al. Newborns with microcephaly in Brazil and potential vertical transmission of Oropouche virus: a case series. Lancet Infect Dis. 2024;25:155–65.
5. Scachetti GC, Forato J, Claro IM, Hua X, Salgado BB, Vieira A, et al. Re-emergence of Oropouche virus between 2023 and 2024 in Brazil: an observational epidemiological study. Lancet Infect Dis. 2025;25:166–75. https://doi.org/10.1016/S1473-3099(24)00619-4
6. Watts DM, Phillips I, Callahan JD, Griebenow W, Hyams KC, Hayes CG. Oropouche virus transmission in the Amazon River basin of Peru. Am J Trop Med Hyg. 1997;56:148–52. https://doi.org/10.4269/ajtmh.1997.56.148
7. Baisley KJ, Watts DM, Munstermann LE, Wilson ML. Epidemiology of endemic Oropouche virus transmission in upper Amazonian Peru. Am J Trop Med Hyg. 1998;59:710–6. https://doi.org/10.4269/ajtmh.1998.59.710
8. de Lima RC, Dias HG, de Souza TMA, Familiar-Macedo D, Ribeiro ED, Corrêa VCE, et al. Oropouche virus exposure in febrile patients during chikungunya virus introduction in the state of Amapá, Amazon Region, Brazil. Pathogens. 2024;13:469. https://doi.org/10.3390/pathogens13060469
9. Borborema CA, Pinheiro FP, Albuquerque BC, da Rosa AP, da Rosa JF, Dourado HV. 1st occurrence of outbreaks caused by Oropouche virus in the State of Amazonas [in Portuguese]. Rev Inst Med Trop Sao Paulo. 1982;24:132–9.
10. de Souza WM, Ribeiro GS, de Lima STS, de Jesus R, Moreira FRR, Whittaker C, et al. Chikungunya: a decade of burden in the Americas. Lancet Reg Health Am. 2024;30:100673. https://doi.org/10.1016/j.lana.2023.100673

Address for correspondence: Pritesh Lalwani, Instituto Leônidas e Maria Deane, Fiocruz Amazônia, Manaus, Brazil, Rua Terezina, 476–Adrianópolis, Manaus, Amazonas State, 69057-070, Brazil; email: pritesh.lalwani@fiocruz.br

Rickettsia lanei Rickettsiosis, Oregon, USA, 2025

Stephen G. Ladd-Wilson, Richard W. Fawcett, Sarah Y. Park, Shivkumar Venkatasubrahmanyam, Martin S. Lindner, Scott Davis, Alanna Spry, Joseph Singleton, Sandor E. Karpathy, Christopher D. Paddock

Author affiliations: Public Health Division, Oregon Health Authority, Portland, Oregon, USA (S.G. Ladd-Wilson); Columbia Sands Infectious Diseases, Redmond, Oregon, USA (R.W. Fawcett); Karius., Inc., Redwood City, California, USA (S.Y. Park, S. Venkatasubrahmanyam, M.S. Lindner); Home Town Animal Hospital, Prineville, Oregon, USA (S. Davis); Crook County Health Department, Prineville (A. Spry); Centers for Disease Control and Prevention, Atlanta, Georgia, USA (J. Singleton, S.E. Karpathy, C.D. Paddock)

DOI: https://doi.org/10.3201/eid3204.251962

Using metagenomic sequencing, we identified a patient infected with *Rickettsia lanei* who was initially diagnosed with Rocky Mountain spotted fever (RMSF), a clinically similar disease caused by infection with *R. rickettsii*. Our investigation highlights the importance of clinical, epidemiologic, and laboratory partnerships to leverage the discovery of novel pathogens.

Spotted fever group rickettsioses (SFGRs) comprise multiple febrile, rash-associated illnesses caused by various arthropodborne, intracellular *Rickettsia* bacteria. Rocky Mountain spotted fever (RMSF), the most severe SFGR, was first described in the western United States around the turn of the 20th Century (https://www.niaid.nih.gov/diseases-conditions/rocky-mountain-spotted-fever). For the next ≈100 years, RMSF was considered the only tickborne SFGR in the United States; however, since 2004, investigators have identified additional pathogens causing SFGRs of varying severity that share clinical features with RMSF (*1*–*3*). Cases of RMSF have been described in Oregon, USA, since 1903 (*4*,*5*). We describe an Oregon patient infected with the recently characterized pathogen *Rickettsia lanei* whose illness resembled RMSF.

In July 2025, a >50-year-old man sought care at an emergency department for 7 days of fever, headache, and myalgias that had progressed to altered mental status with acute delirium, intermittent tachypnea, and difficulty walking. He recalled a tick crawling on his body during outdoor activities in eastern Oregon within 2 weeks before disease onset. Physical examination revealed temperature of 39.3°C, respiratory rate 22 breaths/min, heart rate 112 bpm, and blood pressure 133/79 mm Hg. The man had difficulty following commands and with word-finding. A transitory macular rash was identified on his trunk on the evening following admission (Figure 1, panel A).

Laboratory abnormalities included low serum sodium (124 mEq/L, reference range 135–147 mEq/L), elevated aspartate transaminase (73 U/L, reference range 5–40 U/L), and elevated alanine transaminase (88 U/L, reference range 5–41 U/L). A lumbar puncture was performed; cerebrospinal fluid (CSF) revealed elevated leukocytes (36/μL, reference range 0–5/μL) with 60% lymphocytes and elevated protein (69.3 mg/dL, reference range 15–45 mg/dL). Routine cultures of blood and CSF yielded negative results. PCR and serologic tests for an extensive panel of viral, bacterial, and fungal pathogens also returned negative results, except for IgG (but no IgM) for *Francisella tularensis*.

The patient was treated empirically with intravenous ampicillin, ceftriaxone, and acyclovir. A petechial rash developed on his distal lower extremities (Figure 1, panels B, C). His mental status

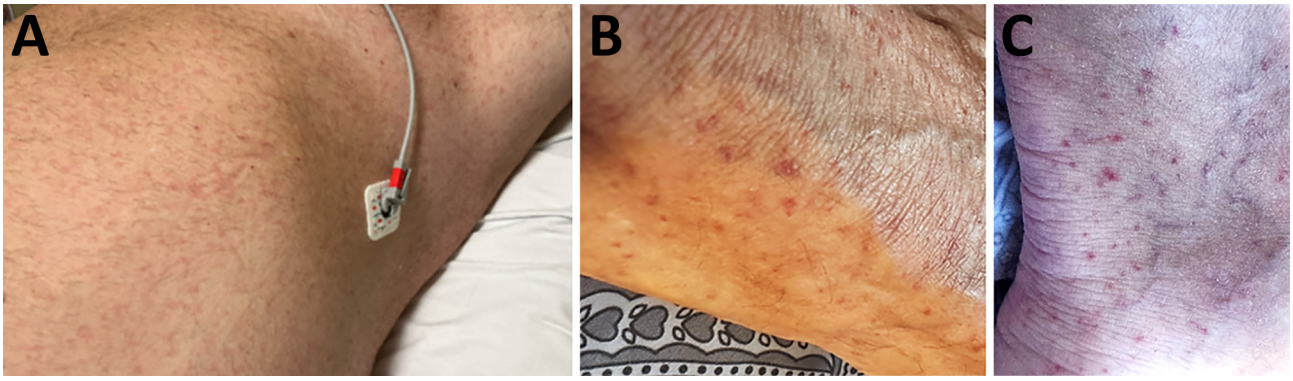

Figure 1. Rash lesions on a patient with *Rickettsia lanei* rickettsiosis, Oregon, USA. A) Pink blanching macules involving the trunk. B, C) Scattered petechiae on the lateral aspect of the foot (B) and posterior aspect of the ankle (C).

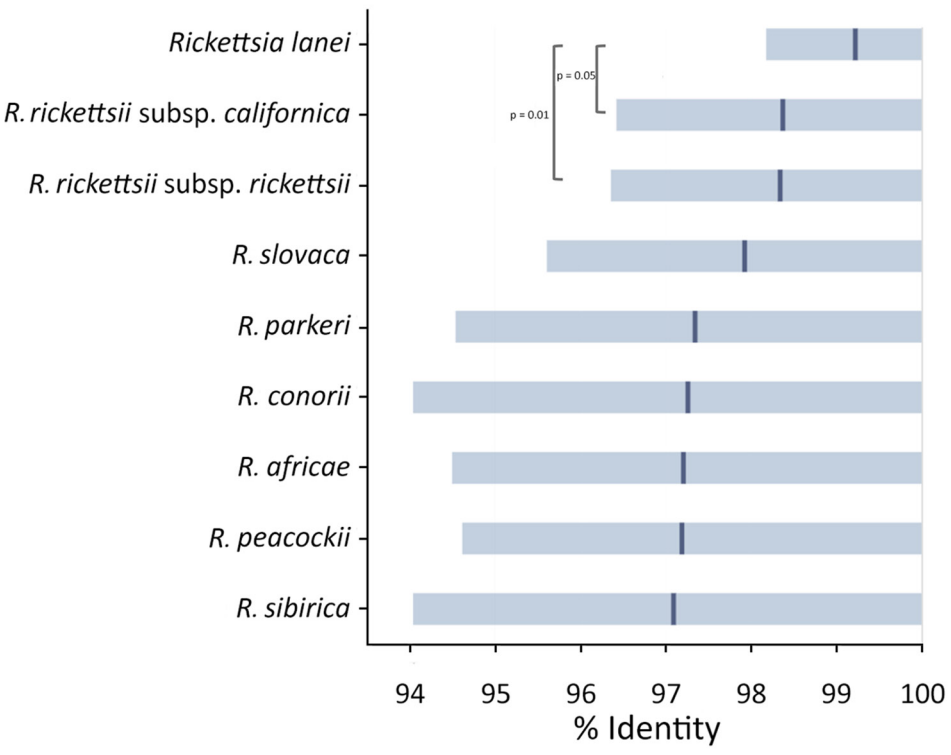

Figure 2. Sequence similarity of microbial cell-free DNA amplified and sequenced from a patient in Oregon, USA, to multiple *Rickettsia* spp. The sequences showed highest sequence similarity (99.2% mean identity) to the recently published *R. lanei* genome assembly (GenBank accession no. CP172233). Means (dark blue lines) and 10th–90th percentiles (light blue shading) of BLAST percentage identity of 967 sequencing reads were calculated for the most similar genome assemblies of related *Rickettsia* species in a custom microbial sequence database. p values indicated for significant differences between *R. lanei* and *R. rickettsii* subsp. *californica* and *R. rickettsii* subsp. *rickettsii*. p values of $\leq 10^{-6}$ were obtained by nonparametric (Wilcoxon signed-rank) and parametric (Student *t*) tests. For each pair, we compared the distribution of percentage identity values, penalized for partial alignment, and with lack of alignment filled in with a subthreshold value of 75%.

and transaminase elevations improved over several days, and he became afebrile. He was discharged after 4 days of hospitalization. Plasma was collected at discharge for microbial cell–free DNA (mcfDNA) metagenomic sequencing by using the Karius Spectrum test (Karius, Inc., https://kariusdx.com), which revealed mcfDNA of *R. rickettsii* at 219 molecules/100 nL.

After review by local and state public health officials, and because of the rarity of confirmed RMSF in Oregon, the Oregon Health Authority consulted with the Centers for Disease Control and Prevention, which determined clinical improvement within 11 days in the absence of doxycycline was unusual for classical RMSF. A discussion with medical and scientific staff at Karius, Inc., began and infection with *R. lanei* was considered; however, the recently assembled genome of *R. lanei* (*6*) was not yet publicly available, and the sequenced mcfDNA matched most closely (98%–98.5% average BLAST identity) by research-use only analysis with available genomes of *R. rickettsii* (Figure 2). Subsequent reanalysis using the since-released *R. lanei* genome (GenBank accession no. CP172233) showed 99.2% identity with *R. lanei* (Figure 2). The Centers for Disease Control and Prevention evaluated a convalescent serum specimen obtained 34 days after illness onset and the plasma specimen obtained at discharge by indirect immunofluorescence antibody assay to detect IgG for *R. rickettsii*. Results revealed reciprocal titers of <32 for the discharge specimen and 2,048 from the convalescent specimen.

Previous case reports of confirmed *R. lanei* rickettsiosis described several clinical characteristics shared with the patient we report, including fever, headache, myalgias, respiratory distress, altered mental status, hyponatremia, and transaminitis (*3*). However, other clinical and laboratory abnormalities identified in previous patients, including nausea, vomiting, respiratory failure, coma, and thrombocytopenia, were not identified in our patient. Rash was documented in our patient but for only 1 of the previously described patients. All 3 patients survived, despite delayed administration of doxycycline, which is uncharacteristic of RMSF (*7*). Those case descriptions suggest that *R. lanei* rickettsiosis can be clinically variable and shares many, but not all, features with classical RMSF.

Wide geographic variations in severity of RMSF have perplexed investigators since first reports of the disease emerged from the western United States >100 years ago. Milder manifestations of RMSF were described from several western states, including Oregon, characterized by lower fever and a

substantially lower case-fatality rate compared with classical RMSF (*4*,*5*,*8*–*10*). Other *Rickettsia* species could cause clinically similar diseases of varying severity and thereby account for historically recognized differences in severity described for RMSF in the western United States. Increasingly sensitive molecular detection methods, including mcfDNA sequencing, and access to expanding collections of whole genomes could aid in detection of otherwise unsuspected pathogens and contribute to a more nuanced understanding of SFGR epidemiology. Multidisciplinary partnerships among regional and federal health authorities, clinicians, and diagnostic laboratories led to recognition of *R. lanei* rickettsiosis in Oregon and could leverage identification of cases elsewhere. Clinicians should consider *R. lanei* when diagnosing patients with presumptive RMSF in the western United States, particularly in clinical scenarios that might appear unusual or atypical for classical RMSF.

This investigation was funded by the Centers for Disease Control and Prevention's Epidemiology and Laboratory Capacity Program.

About the Author

Mr. Ladd-Wilson is an Electronic Reporting, Infectious Waste, & Administrative Rules manager for the Acute and Communicable Disease Prevention section of the Oregon Public Health Division of the Oregon Health Authority. His research interests focus on surveillance of enteric, prion, and vectorborne diseases.

References

1. Paddock CD, Sumner JW, Comer JA, Zaki SR, Goldsmith CS, Goddard J, et al. *Rickettsia parkeri*: a newly recognized cause of spotted fever rickettsiosis in the United States. Clin Infect Dis. 2004;38:805–11. https://doi.org/10.1086/381894
2. Shapiro MR, Fritz CL, Tait K, Paddock CD, Nicholson WL, Abramowicz KF, et al. *Rickettsia* 364D: a newly recognized cause of eschar-associated illness in California. Clin Infect Dis. 2010;50:541–8. https://doi.org/10.1086/649926
3. Probert WS, Haw MP, Nichol AC, Glaser CA, Park SY, Campbell LE, et al. Newly recognized spotted fever group *Rickettsia* as cause of severe Rocky Mountain spotted fever–like illness, northern California, USA. Emerg Infect Dis. 2024;30:1344–51. https://doi.org/10.3201/eid3007.231771
4. Anonymous. Spotted fever in Oregon. Med Sentinel. 1903; 11:389–90.
5. Spencer WO. Mountain or spotted fever, as seen in Idaho and Eastern Oregon. Med Sentinel. 1907;15:532–7.
6. Paddock CD, Harris A, Clark TR, Bullock HA, Hecht JA, Ladner JT, et al. *Rickettsia lanei*, sp. nov. (Rickettsiales: Rickettsiaceae), a newly recognized pathogen of humans associated with the rabbit tick, *Haemaphysalis leporispalustris* (Acari: Ixodidae). Am J Trop Med Hyg. 2025;113:957–65. https://doi.org/10.4269/ajtmh.25-0134
7. Kirkland KB, Wilkinson WE, Sexton DJ. Therapeutic delay and mortality in cases of Rocky Mountain spotted fever. Clin Infect Dis 1995;20:1118-21.
8. Stricker FD. The prevalency and distribution of Rocky Mountain spotted fever in Oregon. Montana State Board of Hlth Spec Bull. 1923;26:18–20.
9. Wolbach SB. Studies on Rocky Mountain spotted fever. J Med Res. 1919;41:1–197, 41.
10. Philip CB. Rocky Mountain spotted fever. Bull Med Libr Assoc. 1940;29:86–92.

Address for correspondence: Stephen G. Ladd-Wilson, Oregon Health Authority Public Health Division, Acute and Communicable Disease Prevention, 800 NE Oregon St, Ste 370, Portland, OR 97232, USA; email: Stephen.G.Ladd-Wilson@oha.oregon.gov

Correction: Vol. 31, No. 4

Some of the summary data included in Appendix 2 was incorrect in Foodborne Illness Acquired in the United States—Major Pathogens, 2019 (Elaine J. Scallan Walter et al.). The article has been corrected online (https://wwwnc.cdc.gov/eid/article/31/4/24-0913_article).

Andrea Marrapodi, Gregorio Pampinella, and Daniele Tozzi, *Mural portrait of Giovanni Battista Grassi*, 2018. Aerosol paint and pigments on exterior concrete wall. From *Lessons from the Past, Challenges for the Future* (Hall of Fame of Science). National Institute for Infectious Diseases "Lazzaro Spallanzani," Rome, Italy. Reproduced with permission of the artists.

Giovanni Battista Grassi and Malaria

Stefano Pozzi, Michele A. Riva

This month's cover features a mural portrait of Giovanni Battista Grassi (1854–1925), created as part of the public art project *Lessons from the Past, Challenges for the Future* at the National Institute for Infectious Diseases "Lazzaro Spallanzani" in Rome, Italy. The installation, conceived as a "Hall of Fame of Science," extends along 270 meters of the institute's perimeter wall (≈810 m^2) and presents 13 scientists who shaped the history of biomedical and infectious disease research. The mural was executed by 3 Italian artists—Andrea Marrapodi (KIV TNT), Gregorio Pampinella (Greg Jager), and Daniele Tozzi—working collaboratively through a structured division of roles: chromatic backgrounds, portraits, and calligraphic elements. Created using aerosol paints and pigments applied directly onto the exterior concrete wall, the work integrates the wall's architectural seams into the composition. Grassi's likeness appears to derive from historical photographic sources, reinterpreted through a contemporary graphic-muralist style. Curated by Graffiti Zero, the project was commissioned to mark the institute's 80th anniversary and to symbolically link scientific heritage with present and future challenges.

Author affiliations: University of Milano–Bicocca School of Medicine and Surgery, Monza, Italy (S. Pozzi, M.A. Riva); Fondazione IRCCS San Gerardo dei Tintori, Monza (M.A. Riva)

DOI: https://doi.org/10.3201/eid3204.AC3204

By situating Grassi among pioneers of microbiology and infectious disease research, the mural underscores the continuity of scientific inquiry and the enduring relevance of his contributions to the understanding of malaria. The recent centenary of the death of this physician, zoologist, botanist, and entomologist provides an opportunity to revisit his scientific career, which was marked by original insights and a multidisciplinary approach to infectious diseases. He investigated parasites such as *Ancylostoma duodenale* and *Hymenolepis nana*, defined the role of fleas as vectors of *Taenia cucumerina*, studied flagellates aiding wood digestion in termites, identified houseflies as disease carriers, and researched eels and *Phylloxera vastatrix* insects to protect vineyards. He discovered the arachnid *Koenenia mirabilis* and examined diseases with strong social and environmental determinants, including phosphorus necrosis and endemic goiter.

Yet it was malaria that became his defining challenge. In 1890, working with clinician Raimondo Feletti, he identified *Plasmodium vivax* parasites. Building on Alphonse Laveran's hypothesis of mosquito involvement, Patrick Manson's studies on filariasis, and Ronald Ross's research on avian malaria, Grassi noted that malaria occurred only in certain mosquito-infested areas. This observation led him to propose that malaria was transmitted to humans by a specific group of mosquitoes. In 1898, through careful biogeographic study, he identified this group as belonging to the genus *Anopheles*.

That conclusion, reached with collaborators Giuseppe Bastianelli and Amico Bignami, was met with resistance. Robert Koch, visiting Rome that same year, rejected the *Anopheles* mosquito as a vector, citing its presence in malaria-free Grünewald near Berlin. Grassi persisted, and on November 1, 1898, he produced the first experimentally induced case of malaria in a healthy volunteer bitten by an *Anopheles claviger* mosquito, proving Koch wrong. Grassi emphasized the biologic complexity and specific ecology of *Anopheles* spp. mosquitoes, underlining Koch's limited entomological expertise. In 1899, he demonstrated that infection in mosquitoes occurs only after feeding on infected humans, formulating what became known as Grassi's Law: malaria = *Anopheles* + infected humans. Grassi urged the Italian Parliament to combine chemical protection with quinine and mechanical barriers—solid houses, metal screens—to prevent transmission, one of the earliest explicit proposals to use physical barriers against mosquitoborne infection. In direct relation to that last proposal, in 1899–1900, Grassi organized a large-scale experiment near Paestum, a malaria-endemic area. For several months, residents were monitored to assess whether metal nets installed on doors, windows, and chimneys could prevent malaria transmission. The results confirmed the accuracy of Grassi's research: with few exceptions, all protected residents remained disease-free, whereas unprotected participants became infected.

The story of the discovery of the *Anopheles* mosquito as the vector of human malaria was marked by intense rivalry. The 1902 Nobel Prize in Physiology or Medicine, awarded to Ross, reflected a dispute that went beyond personal pride. Ross accused Italian scientists of following his lead, claiming that his description of a "gray-spotted mosquito with wings" had guided Grassi. In truth, the two men embodied opposing scientific philosophies: Ross relied on analogy and intuition from avian malaria; Grassi demanded systematic, comparative experiments in human malaria, warning that analogies between diseases with different vectors, parasites, and hosts were scientifi-

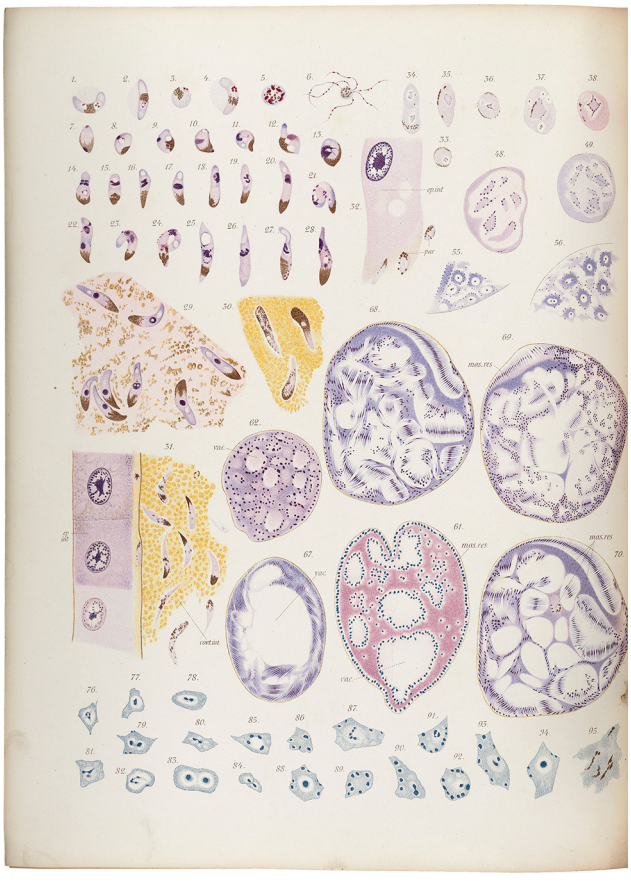

Figure. The life cycle of the malaria parasite, from Giovanni Battista Grassi's *Studies of a Zoologist on Malaria*. Drawn with a camera lucida directly at the microscope, the figures capture with extraordinary precision the life cycle of the malaria parasite. Source: Wellcome Collection, London, UK (https://wellcomecollection.org/works/baxa2uau).

cally unsound. The resolution of the controversy was further complicated by the involvement of English physician Edmonston Charles, who visited Grassi's laboratories in 1897–1898 and later reported his observations to Ross, and by the Swedish Royal Academy's ill-judged choice of Koch as a neutral referee. Given Koch's prior misjudgment on *An. claviger* mosquitos and his disagreements with Grassi, that decision only deepened tensions. Many historians now distinguish the achievements: Ross was the first to demonstrate transmission of avian malaria by mosquitoes, whereas Grassi was the first to identify and conclusively prove the vector of human malaria.

Grassi's work extended far beyond this rivalry. In 1896, the Royal Society of London awarded him the Darwin Medal for his studies on termites and eels. He was elected to the Royal Academy of Sciences and appointed Senator of the Kingdom of Italy in 1908 for scientific merit. He continued working until his final days, revising a manuscript on *An. superpictus* mosquitoes before his death.

Grassi's commitment to science is evident even in his meticulous drawings. At a time when photomicrography was not yet in widespread use, he recorded observations under the microscope by using a camera lucida, a device attached to the eyepiece that projected the image onto a surface for faithful reproduction. Plates such as those in *Studies of a Zoologist on Malaria* (Figure), produced more than a century ago, document the methods Grassi used to record microscopic observations. They illustrate an approach to scientific investigation based on careful observation, critical evaluation, and repeated verification.

Today, malaria continues to affect hundreds of millions of humans worldwide, despite decades of research, preventive programs, and pharmaceutical advances. The struggle against this ancient scourge illustrates the enduring relevance of Grassi's approach: understanding disease requires careful observation, attention to ecologic and biologic complexity, and collaboration across disciplines.

Bibliography

1. Bynum WF, Bynum E, editors. Dictionary of medical biography. Vol. 2 (C–G). Westport (CT) and London: Greenwood Press; 2007.
2. Capanna E. Grassi versus Ross: who solved the riddle of malaria? Int Microbiol. 2006;9:69–74.
3. Capanna E. Battista Grassi entomologist and the Roman School of Malariology. Parassitologia. 2008;50:201–11.
4. Chaudhury A. The forgotten malariologist: Giovanni Battista Grassi (1854–1925). Trop Parasitol. 2021;11:16–8. https://doi.org/10.4103/tp.tp_21_21
5. Dobson MJ. The malariology centenary. Parassitologia. 1999;41:21–32.
6. Grassi B. Studies of a zoologist about malaria [in Italian]. Rome: Regia Accademia dei Lincei; 1901 [cited 2025 Aug 15]. https://wellcomecollection.org/works/baxa2uau/items
7. Cappelletti MA. Grassi, Giovanni Battista [in Italian]. Dizionario biografico degli Italiani. Vol. 58. Rome: Istituto della Enciclopedia Italiana fondata da Giovanni Treccani; 2002 [cited 2025 Aug 15]. https://www.treccani.it/enciclopedia/giovanni-battista-grassi_(Dizionario-Biografico)
8. Majori G. Short history of malaria and its eradication in Italy with short notes on the fight against the infection in the mediterranean basin. Mediterr J Hematol Infect Dis. 2012;4:e2012016. https://doi.org/10.4084/mjhid.2012.016
9. Martini M, Orsini D. Giovanni Battista Grassi (1854–1925): a forgotten Italian scholar and his fundamental studies on malaria. J Prev Med Hyg. 2025;66:E194–201. https://doi.org/10.15167/2421-4248/jpmh2025.66.2.3642
10. Mazzarello P. Malaria. The Nobel Prize denied: the story of Battista Grassi [in Italian]. Vicenza: Neri Pozza; 2025.
11. Historical Archives of the Senate of the Republic. Senators of the Kingdom (1848–1943) [in Italian] [cited 2025 Aug 15]. https://patrimonio.archivio.senato.it/repertorio-senatori-regno
12. Palmarini MP, Corsi P, Mancassola G. Biographical dictionary of the history of medicine and natural sciences. Vol II (FK) [in Italian]. Porter R, editor. Fontanellato (Italy): Franco Maria Ricci; 1987.

Address for correspondence: Michele A. Riva, School of Medicine and Surgery, University of Milano-Bicocca, via Cadore 48, I-20900, Monza, Italy; email: michele.riva@unimib.it

EMERGING INFECTIOUS DISEASES®

Upcoming Issue • Zoonotic Infections

- Borna Disease virus 1 Infection Causing Fatal Meningoencephalomyelitis in Wild European Hedgehogs in Known Endemic Areas, Germany, 2022–2025
- Three Fatal Gestational Psittacosis Cases in Japan caused by *Chlamydia psittaci* Strains Belonging to Closely Related MLST Lineages (ST335 and ST269)
- Frequency, Duration, and Risk Factors for Diagnostic Delays Associated with Coccidioidomycosis
- Zoonotic and Anthroponotic *Plasmodium* spp. Circulation between Wild Primates and an Indigenous Community, Peruvian Amazon, 2007–2020.
- Investigation and Response to Autochthonous Dengue, Los Angeles County, August–November 2024
- Updated Genomic Epidemiologic Description of *Candida* (*Candidozyma*) *auris*, United States
- Detection of Human Rhinovirus B14 from Outbreak of Severe Respiratory Illness among Older Adults, France, 2024
- Retrospective Phylogenetic Analysis of Mayaro Virus, French Guiana, 1996–2024
- Development and Validation of Real-Time PCR for Detecting *Anaplasma bovis*–Like Agent in *Dermacentor* spp. Ticks
- Infection and Exposure to Human Tick-Borne Relapsing Fever Agent *Borrelia persica* in Horses, Israel, 2025
- A One Health Investigation into Fatal Encephalitis Caused by Pigeon Paramyxovirus Type 1 (PPMV-1) Infection in France
- Yezo Virus Diversity in Tick-Bitten Patients and Ticks, Russia
- Third Human Case of *Cryptosporidium* sp. *OTUi* in a Danish Tourist: Clinical, Molecular, and Zoonotic Perspectives
- Orthopoxvirus Antibodies Detection in Giant Pouched Rats, Shrews and Feral Cats in Communities with Confirmed Human Cases of Mpox, Nigeria
- Nipah Virus Shedding in Urine from Fruit Bats, Sri Lanka, 2018–2019
- High Pathogenicity Avian Influenza Virus H5N1 (Clade 2.3.4.4b) Drives Mass Mortality in Eurasian Crane (*Grus grus*) Populations, Germany, 2025
- Genomic Analysis of Sin Nombre Virus (*Orthohantavirus sinnombreense*) Genome Sequences, Northwestern United States, 2023
- Opportunity Drives Spillover: Serological Surveillance across Carnivores, Omnivores and Herbivores in an HPAIV H5 Hotspot in North-East Germany, 2023–2025
- Replication Efficiency of Contemporary HPAI H5N1 Virus Isolates in a Human Nasal Epithelium Model
- Tropism and Replication Competence of Cattle Influenza A(H5N1) Genotype B3.13 Virus in Human Bronchus and Lung Tissue
- Dr. Matteo Carpano: Bridging 20th Century Microbiology with One Health Principles
- Unmitigated Serial Interval and Intervention Efficiency in a School-Based Outbreak of Pertussis, South Korea, 2024
- Herpes Simplex Virus 1 (HSV-1) in Trigeminal Ganglia of Trafficked Neotropical Primates
- Genomic Epidemiology of Human Respiratory Syncytial Virus in Vaccinated and Unvaccinated Adults, Atlanta, Georgia, 2024–2025
- *Bartonella clarridgeiae* Prosthetic Valve Endocarditis and Aortic Root Abscess Presenting as Bilateral Tibioperoneal Trunk Mycotic Aneurysms in a Human Patient, 2020
- *Borrelia turicatae* in the City of Aguascalientes, Spirochete Isolation from Ticks and Antibody Detection in Wild Animals Captured in a Public Park
- Genomic Surveillance of Lassa Virus in Guinea through In-Country Sequencing
- Detection of Highly Pathogenic Avian Influenza (HPAI) H5N1 Viral RNA in Bovine Semen from a Bull Used for Natural Breeding on an Affected Dairy Farm, USA, 2024
- The Big One: How We Must Prepare for Future Deadly Pandemics

Complete list of articles in the May issue at
Complete list of articles in the April issue at https://wwwnc.cdc.gov/eid/#issue-331

Earning CME Credit

To obtain credit, you should first read the journal article. After reading the article, you should be able to answer the following, related, multiple-choice questions. To complete the questions (with a minimum 75% passing score) and earn continuing medical education (CME) credit, please go to http://www.medscape.org/journal/eid. Credit cannot be obtained for tests completed on paper, although you may use the worksheet below to keep a record of your answers.

You must be a registered user on http://www.medscape.org. If you are not registered on http://www.medscape.org, please click on the "Register" link on the right hand side of the website.

Only one answer is correct for each question. Once you successfully answer all post-test questions, you will be able to view and/or print your certificate. For questions regarding this activity, contact the accredited provider, CME@medscape.net. For technical assistance, contact CME@medscape.net. American Medical Association's Physician's Recognition Award (AMA PRA) credits are accepted in the US as evidence of participation in CME activities. For further information on this award, please go to https://www.ama-assn.org. The AMA has determined that physicians not licensed in the US who participate in this CME activity are eligible for AMA PRA Category 1 Credits™. Through agreements that the AMA has made with agencies in some countries, AMA PRA credit may be acceptable as evidence of participation in CME activities. If you are not licensed in the US, please complete the questions online, print the AMA PRA CME credit certificate, and present it to your national medical association for review.

Article Title

Pediatric Meningoencephalitis Cluster Caused by Snowshoe Hare Virus, Whistler, British Columbia, Canada, 2024

CME Questions

1. Which of the following statements regarding infection with snowshoe hare virus (SSHV) is most accurate?

A. Snowshoe hares are the only host
B. Most infections are reported between December and February
C. The incubation period before infection is 3 to 7 days
D. Snowshoe hare virus has previously only been associated with mild infections without hospitalization

2. How are most cases of SSHV infection successfully confirmed in the laboratory?

A. Reverse transcription-polymerase chain reaction (RT-PCR) testing during acute or subacute infection
B. IgM testing during acute infection
C. Neutralizing antibody titers during acute infection and the convalescent period
D. Viral cultures

3. Which of the following statements regarding the hospital presentation and outcomes of the 3 cases of SSHV infection in the current is most accurate?

A. The mean time from symptom onset to hospitalization was 10 days
B. 2 patients required care in the pediatric intensive care unit (PICU)
C. No patient died
D. 2 patients had a positive serum RT-PCR test for SSHV

4. What was the most common finding on cerebrospinal fluid (CSF) analysis in the current study?

A. Normal glucose; normal to slightly elevated protein
B. Low glucose; significantly elevated protein
C. Lymphocytic predominance
D. Neutrophilic predominance

EMERGING INFECTIOUS DISEASES®

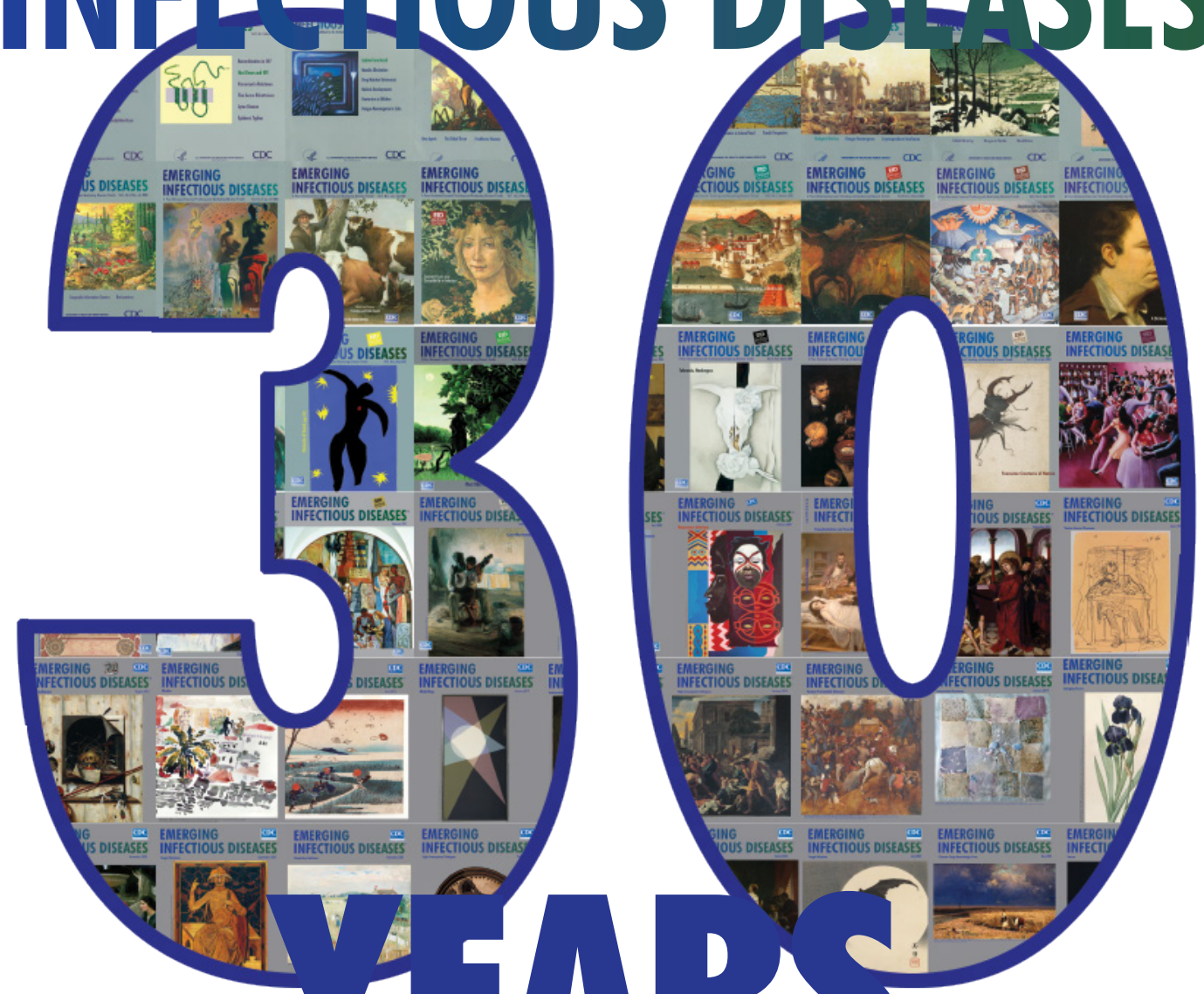

Presenting the ongoing challenges that emerging microbial threats pose to global health